Chin, Jhin Thiam

PhD 12 Mar 93

The University of Sydney

Copyright in relation to this thesis*

Under the Copyright Act 1968 (several provisions of which are referred to below), this thesis must be used only under the normal conditions of scholarly fair dealing for the purposes of research, criticism or review. In particular no results or conclusions should be extracted from it, nor should it be copied or closely paraphrased in whole or in part without the written consent of the author. Proper written acknowledgement should be made for any assistance obtained from this thesis.

Under Section 35(2) of the Copyright Act 1968 'the author of a literary, dramatic, musical or artistic work is the owner of any copyright subsisting in the work'. By virtue of Section 32(1) copyright 'subsists in an original literary, dramatic, musical or artistic work that is unpublished' and of which the author was an Australian citizen, an Australian protected person or a person resident in Australia.

The Act, by Section 36(1) provides: 'Subject to this Act, the copyright in a literary, dramatic, musical or artistic work is infringed by a person who, not being the owner of the copyright and without the licence of the owner of the copyright, does in Australia, or authorises the doing in Australia of, any act comprised in the copyright'.

Section 31(1)(a)(i) provides that copyright includes the exclusive right to 'reproduce the work in a material form'. Thus, copyright is infringed by a person who, not being the owner of the copyright and without the licence of the owner of the copyright, reproduces or authorises the reproduction of a work, or of more than a reasonable part of the work, in a material form, unless the reproduction is a 'fair dealing' with the work 'for the purpose of research or study' as further defined in Sections 40 and 41 of the Act.

Section 51(2) provides that 'Where a manuscript, or a copy, of a thesis or other similar literary work that has not been published is kept in a library of a university or other similar institution or in an archives, the copyright in the thesis or other work is not infringed by the making of a copy of the thesis or other work by or on behalf of the officer in charge of the library or archives if the copy is supplied to a person who satisfies an authorized officer of the library or archives that he requires the copy for the purpose of research or study'.

Keith Jennings
Registrar and Deputy Principal

*'Thesis' includes 'treatise', 'dissertation' and other similar productions.

AXIAL PILE RESPONSE

IN

CALCAREOUS SEDIMENT

Jhin-Thiam Chin, B.Eng., M.Eng.

A Thesis submitted for the
Degree of Doctor of Philosophy
School of Civil and Mining Engineering
The University of Sydney, Australia

March 1992

To my parents who have sacrificed so much in order to give me the opportunity of an education; for the never-ending love, care and understanding that came freely from them, my brother and sister which gave me the strength to overcome the many difficult times during this period —

To them, I dedicate this thesis to reflect on my deep appreciation and love

J T Chin
March 1992

CONTENTS

SYNOPSIS

Some studies of the axial response of piles in calcareous sediment have been conducted in this thesis. The experimental part of the work described in the present thesis is aimed towards further understanding the mechanisms governing the cyclic response of piles in calcareous sediments. For the present study, the axial cyclic response of piles in "Bass Strait" calcareous sediment is studied using a large model pile test facility. Model instrumented single piles of 50mm and 100mm diameters are utilised for the present test program. The cyclic response of the model piles when subjected to two-way displacement-controlled cyclic loading is investigated. The results of this series of tests are assessed in order to shed further light on the most appropriate model governing the degradation of skin friction capacity under cyclic loading conditions. It is found that the degradation of skin friction is governed by the normalised (to pile diameter) value of the "cyclic slip displacement".

For cyclic loading analysis, where repeated iterations are required, the use of a simple and computationally efficient approach is highly essential and desirable. To this end, the development of a simple and efficient "t-z" static and cyclic pile analysis approach is presented in the numerical part of the work undertaken in the present study. The utility of the analysis approach developed is demonstrated through some parametric solutions. In particular, the important parameters affecting the computed cyclic pile response are identified. The results of a comparative study of a few cyclic axial pile loading analyses further highlight the inconsistent predicted responses that can be obtained from the different analysis approaches. Overall, it can be concluded that our predictive ability for the static axial response of both single piles and pile groups is satisfactory. For cyclic loading analysis, it is shown that our predictive ability is far less satisfactory.

PREFACE

The work described in this thesis was carried out by the candidate during the period from September 1988 to March 1992. All of the work was conducted within the School of Civil and Mining Engineering, The University of Sydney.

The candidate was supervised by Professor H.G. Poulos, Professor of Civil Engineering (Soil Mechanics), during the entire period of his candidature.

The By-Laws of The University of Sydney require a candidate for the degree of Doctor of Philosophy to indicate which sections of the thesis are original. Where appropriate, the acknowledgement of information utilised from other sources and references is made in the text. In accordance with the above-mentioned By-Laws, the Author claims originality for the following work:

(i) the pile analysis approach outlined in Chapter 4. In particular, the development of the computationally efficient "t-z" analysis programs SPILE3 and SCPIL3;

(ii) the numerical solutions obtained using the analysis approach developed in Chapter 4, presented in Chapter 5;

(iii) the set-up of the large model pile test facility and the associated instrumentation, presented in Chapter 6;

(iv) the calibration and trial uninstrumented pile test results presented in Chapter 7;

(v) the planning, conduct and interpretation of the test results for the series of instrumented pile tests, presented in Chapter 8.

The following papers were prepared by the author and others during the period of the author's candidature. These papers are presented in support of his candidature.

- Chin, J.T., Chow, Y.K. and Poulos, H.G. (1990), "Numerical analysis of axially loaded vertical piles and pile groups", Computers and Geotechnics, vol.9, No.4, pp.273-290.
- Chin, J.T. and Poulos, H.G. (1991), "Axially loaded vertical piles and pile groups in layered soil", Int. Jnl. for Numerical and Analytical Methods in Geomechs., vol.15, No.7, pp.497-511.
- Chin, J.T. and Poulos, H.G. (1991), "A t-z approach for cyclic

axial loading analysis of single piles", Computers and Geotechnics, vol.12, No.3, pp.289-320.

- Chin, J.T. and Poulos, H.G. (1991), "Cyclic axial pile loading analyses: A comparative study", Accepted for publication in Computers and Geotechnics.
- Chin, J.T. and Poulos, H.G. (1992), "Tests on model jacked piles in calcareous sediment", under preparation.

ACKNOWLEDGEMENTS

I would like to acknowledge with gratitude the scholarship provided by the Centre for Geotechnical Research of the University of Sydney during the period of my candidature.

The technical support from the technical staff, in particular, Messrs. Ross Barker, Alex Farago, Wai Pong Li, Andrew Townsend, Phil Whitty and Rex Barry in the setting up of the experimental test facility are noted with appreciation. The help and suggestions readily given by Dr. Tim Hull in several aspects of the experimental work are also gratefully acknowledged.

Thanks are also due to my fellow research students for the many humorous moments together throughout this demanding period. In particular, I would like to thank Mr. Tony Chen for his assistance during the conduct of the experimental tests.

Finally, my deep appreciation and thanks to my supervisor, Prof. Harry Poulos, for giving me this privilege to work with him. I am also grateful for his continuous guidance, criticisms and encouragement that I received during this physically and mentally demanding period.

NOTATIONS

The following symbols are used in this thesis:

d = pile diameter

E_1 = Young's modulus of upper soil layer

E_2 = Young's modulus of lower bearing layer

E_{max} = initial tangent modulus at small strains

E_p = Young's modulus of pile

E_t = tangent modulus to stress-strain curve

$D_{\tau lim}$ = limiting capacity degradation factor for shaft elements

D_{blim} = limiting capacity degradation factor for base element

e = socket length of pile

f_{ij} = soil flexibility coefficient

G = shear modulus of soil

h = thickness of upper soil layer

K = pile-soil stiffness ratio (= E_p/E_1)

K_1 = stiffness of isolated single pile [= $P/(E_1 d\ w_t)$]

K_G = stiffness of pile group [= $P_G/(E_1 d\ w_t)$]

$[K_p]$ = assembled stiffness matrix of group piles

$[K_s]$ = soil stiffness matrix

$[K_T]$ = total assembled stiffness matrix of piles and soil

ℓ = pile length (= h+e)

m_s, n_s = accumulation parameters for shaft elements

m_b, n_b = accumulation parameters for base element

n = total number of nodes

N = number of cycles

N_p = number of piles in a pile group

P_b = mobilised base load

P_{bo} = pile base load at load reversal

P_c = cyclic load of loading parcel

P_f = initial static limiting base load

P_{fc} = limiting average (of tension and compression) base capacity applicable at a given cycle

P_o = mean applied load of loading parcel

P_z = axial load in pile at depth z

P_G = applied axial load on pile group

P_{max} = maximum applied load under cyclic loading

P_{min} = minimum applied load under cyclic loading

Q_c = ultimate compressive pile capacity for single piles

Q_{cg}	= ultimate compressive pile capacity for pile groups
Q_t	= tensile pile capacity for single piles
Q_{sus}	= maximum sustainable load level under cyclic loading
$\{P\}$	= vector of external applied load
$\{P_p\}$	= vector of pile-soil interaction forces acting on piles
$\{P_s\}$	= vector of pile-soil interaction forces acting on soil
r_o	= pile radius
r_m	= radial distance at which shear stress becomes negligible
R	= nonlinear Ramberg-Osgood parameter (program AXCAP)
R_c	= R_u or R_r as appropriate
R_{fs}	= hyperbolic constant for pile shaft elements (program SCPIL3)
R_{fb}	= hyperbolic constant for pile base element (program SCPIL3)
R_r	= curve-fitting constant for reloading curve
R_u	= curve-fitting constant for unloading curve
s	= spacing between group piles
$\{w_p\}$	= vector of pile deformation
w_t	= pile head settlement
z	= distance below ground level
z_3	= distance below ground level of the influenced node
z_4	= distance below ground level of the influencing node
ν_1	= Poisson's ratio of upper soil layer
ν_2	= Poisson's ratio of lower bearing layer
ρ	= inhomogeneity factor
ξ	= z_3/h
ξ_1	= z_3/ℓ
ζ	= z_4/h
ζ_1	= z_4/ℓ
ξ_b	= factor to account for stiffer underlying layer
ξ_y	= yield parameter (program RATZ)
τ	= shear stress
τ_o	= pile-soil interface shear stress
τ_c	= cyclic shear stress
τ_{cr}	= cyclic residual shear stress (program RATZ)
τ_f	= initial static limiting shear stress
τ_{fc}	= limiting average (of tension and compression) shear stress capacity applicable at a given cycle
τ_r	= residual shear stress
τ_u	= shear stress at load reversal
τ_{uo}	= pile-soil interface shear stress at load reversal
ε	= shear strain

ε_u = shear strain at load reversal

X = a representative stress level

ψ = accumulation rate parameter

λ_τ, λ_b = capacity degradation rate parameter for shaft and base elements respectively

η = strain-softening parameter (program RATZ)

α = nonlinear Ramberg-Osgood parameter (program AXCAP)

δ = secant modulus degradation value

ρ_c = cyclic displacement amplitude

ρ_{fs} = displacement required to mobilise peak static skin friction

ρ_{pp} = displacement from peak to residual value of skin friction

β_s = $(\tau_o r_o R_{fs}/\tau_f)$ for monotonic (static) loading

$= \dfrac{R_{fs}|\tau_o - \tau_{uo}|r_o}{2R_c\delta|\tau_{fc}|}$ for cyclic loading

β_b = $(P_b R_{fb}/P_f)$ for monotonic (static) loading

$= \dfrac{|P_b - P_{bo}|R_{fb}}{2R_c\delta|P_{fc}|}$ for cyclic loading

CHAPTER 1

INTRODUCTION

CHAPTER 1

INTRODUCTION

1.1 GENERAL INTRODUCTION

Pile foundations are one of the most commonly used foundation systems for both onshore and offshore structures. The increased oil and gas exploration and production activities in many parts of the world (see Fig. 1.1) over the last few decades have resulted in a substantial increase in the use of piles for supporting such offshore structures. Several regions of major petroleum activity are situated in those parts of the world where significant deposits of calcareous sediments (i.e. sediments with a significant amount of calcium carbonate mineral) are found (see Fig. 1.2). Experience (McClelland, 1974) has shown that these calcareous sediments offer inferior support to driven piles than silicate sediments. A considerable number of laboratory tests as well as a limited number of field tests have been conducted over the past ten years or so in order to gain a better understanding of the behaviour of calcareous sediments.

The low support capacity for pile foundations in calcareous sediments has been generally attributed to the high compressibility characteristic of the sediments (Poulos, 1988a). In the offshore environment, the effect of the cyclic nature of the loading acting on the piles further poses a problem to the available support capacity of the soil. Both laboratory and field tests results (for example, Poulos and Chan, 1986; Abbs *et al.*, 1988) have indicated the susceptibility to degradation (i.e. reduction) of the skin friction capacity of piles under cyclic loading conditions. It has also been shown by Poulos and Chan (1986), from model laboratory jacked pile tests, that piles in calcareous sand suffer more severe degradation of skin friction capacity than piles in silica sand.

Although it has been widely accepted that the effect of cyclic loading on piles can lead to a reduction of pile capacity, there is, at present, a lack of complete understanding of the main mechanisms governing the skin friction degradation of pile capacity. Laboratory model scale jacked pile tests in calcareous sediments (for example, Poulos and Chan, 1986; Lee and Poulos, 1987) have identified the importance of the cyclic displacement amplitude, and have revealed that significant degradation occurs when this cyclic displacement exceeds a certain threshold displacement value. This threshold displacement value has been found to be on the order of that required to fully mobilise the pile shaft capacity. The question then arises as to whether the degradation of skin friction is governed solely by the absolute value of the cyclic displacement amplitude or the normalised (usually with respect to the pile diameter) value (Poulos, 1989a). If the absolute criterion governs, then the implication is that prototype offshore piles can be expected to undergo severe degradation of shaft capacity even at low cyclic displacement amplitudes. If the normalised criterion governs then, for a given cyclic displacement amplitude, the prototype piles will be subjected to less degradation than the laboratory scale model piles. Preliminary results obtained by Lee (1988) (see also Lee and Poulos, 1991), from model grouted piles of 24mm, 50mm and 77mm diameters, suggest that the normalised (to diameter) value of the cyclic slip displacement (defined as the cyclic displacement amplitude less the displacement to mobilise the full shaft capacity) is the appropriate model governing the skin friction degradation under cyclic loading conditions. It is therefore the main objective of the experimental part of the work undertaken in the present study, using laboratory model jacked piles of 50mm and 100mm diameters, to shed further light on the most appropriate model governing the skin friction degradation of pile capacity.

The usefulness of an analysis approach in enabling "sensitivity" studies to be made of the influencing parameters cannot be over-emphasized. Such an analysis approach, if demonstrated to be of reasonable accuracy, can eliminate the need for a series of elaborate and often time-consuming laboratory and/or field tests required for a "sensitivity" study. However, to be of general use, such an analysis approach has to be "calibrated" first against laboratory and field tests results to ensure its applicability.

Methods of analysis for the static response of both single piles and pile groups developed over the past two decades or so have been well calibrated against laboratory and field tests results (for example, Poulos and Davis, 1980; Randolph and Wroth, 1979a). This is however not the case for the cyclic loading of piles. The difficulty of numerically modelling the cyclic loading effects, and the lack of good quality laboratory and field tests measurements, have both contributed to the present limited confidence in the available cyclic pile analysis methods. The two important effects of cyclic loading that have to be modelled are the possible degradation of the load capacity of the pile and the accumulation of permanent displacement, as cycling proceeds. Under such cyclic loading conditions, "failure" of the pile may occur either when the pile capacity has been degraded to a value less than the applied load, or when the pile experiences excessive permanent displacement without significant capacity reduction. At present, these effects of the complex pile-soil cyclic interaction response are simulated in a highly approximate manner by using simple empirical rules or criteria (for example, Poulos, 1981; Randolph, 1986; Trochanis *et al.*, 1987). Nevertheless, these analysis approaches provide a preliminary ability to assess the significance of each influencing parameter affecting the cyclic pile response. As the cyclic loading analysis requires repeated iterations, the use of a computationally economical method is highly essential and desirable, particularly, during the preliminary stage of assessing the significance of each influencing parameter. Accordingly, the development of a simple and computationally efficient load-transfer (t-z) approach for the cyclic axial loading analysis of single piles (and pile groups) forms one of the main objectives of the numerical part of the work undertaken in the present study.

A further main objective is to use the numerical results reported in the present study to highlight some of the pertinent parameters affecting the axial pile response under both static and cyclic loading conditions. In particular, the important parameters affecting the computed cyclic pile response are identified. The development of the computationally efficient "t-z" programs (SPILE3 and SCPIL3) in the present study is emphasized in the thesis.

1.2 OUTLINE OF THESIS

The following section gives a brief outline of the content of each chapter in the present thesis.

Chapter 1 gives a general introduction to the subject matter of the present thesis. It introduces the reader to the inferior support capacity for piles founded in calcareous sediments, the uncertainty as to the main mechanism governing the degradation of skin friction capacity under cyclic loading conditions, and the purpose of the experimental part of the work undertaken in the present study. The present limited confidence in the available cyclic pile analysis approaches is brought to the attention of the reader, together with the objectives of the numerical part of the work undertaken in the present study.

Chapter 2 presents a brief literature review on the existing state of knowledge, from both laboratory and field tests, of the behaviour of calcareous sediments. The review is divided into the following major sections: classification, engineering behaviour and properties of calcareous sediments, and design recommendations for pile foundations in such soil deposits. From the review, some remaining areas of uncertainty that need further research attention are identified.

A brief review of some numerical methods of analysis for the axial response of piles subject to a quasi-static cyclic loading condition is presented in Chapter 3. The review highlights the capabilities and limitations of these different approaches. It is emphasized that the use of a simple and computationally efficient cyclic pile analysis approach is highly essential and desirable, if the approach is to be of practical use.

Chapter 4 presents the method of analysis for the static response of axially loaded vertical single piles and pile groups embedded in homogeneous, two-layered or Gibson (soil modulus increasing linearly with depth) soil profiles. Three representations of the soil behaviour are utilised, namely, elastic-plastic continuum model, nonlinear hyperbolic continuum model, and nonlinear hyperbolic t-z "hybrid" model. Extensions of the static analyses to the cyclic axial response of single piles and pile groups are then presented. The development of the computationally efficient load-transfer (t-z) programs SPILE3 (static response analysis only) and SCPIL3 (static and cyclic response analysis) is discussed.

The results of parametric studies, using the analysis programs developed in Chapter 4, are presented in Chapter 5. The accuracy of elastic solutions obtained from the t-z program SPILE3 is assessed. Nonlinear solutions obtained from the static analysis programs, for three representative soil profiles, are also presented. Numerical results presented for the cyclic response of single piles and pile groups highlight the important factors affecting the computed response. A comparative study utilising different cyclic axial loading analysis programs is also undertaken. Finally, a comparison with a field cyclic pile load test measurements, using the t-z cyclic program SCPIL3, is presented.

Chapter 6 gives a detailed description of the design, construction and hydraulic loading system of a large test facility utilised for the present experimental work. The design, instrumentation and calibration of the diaphragm-type stress cells and model piles (50mm and 100mm diameters) are also described. Other necessary tasks, for example, sample preparation, data acquisition and loading control programs required for the conduct of a test, are detailed.

Some preliminary results and experiences with the use of the test facility (described in Chapter 6) are presented in Chapter 7. These include some typical calibration results for the diaphragm-type stress cells and the pile instrumented segments, the sand placement procedure adopted, pile testing procedure for the conduct of a test, and the results of preliminary uninstrumented model pile trial tests.

The test results obtained from a series of model instrumented jacked pile tests (using 50mm and 100mm aluminium pipe piles) in dry calcareous sand are presented in Chapter 8. Results are presented for the jacking (installation) response, initial static compression loading response, the cyclic displacement-controlled loading response, and the post-cyclic static compression loading response. The effect of cyclic loading on the degradation of skin friction capacity forms the main interest of the present experimental work. A comparison between theoretical solutions and measured results for the initial static compression loading response of the 100mm diameter model pile is also presented.

Chapter 9 summarises the main conclusions from both the experimental and numerical parts of the work undertaken in the present study. Suggestions for future research work to increase and further our understanding of pile behaviour in calcareous sediments are also included.

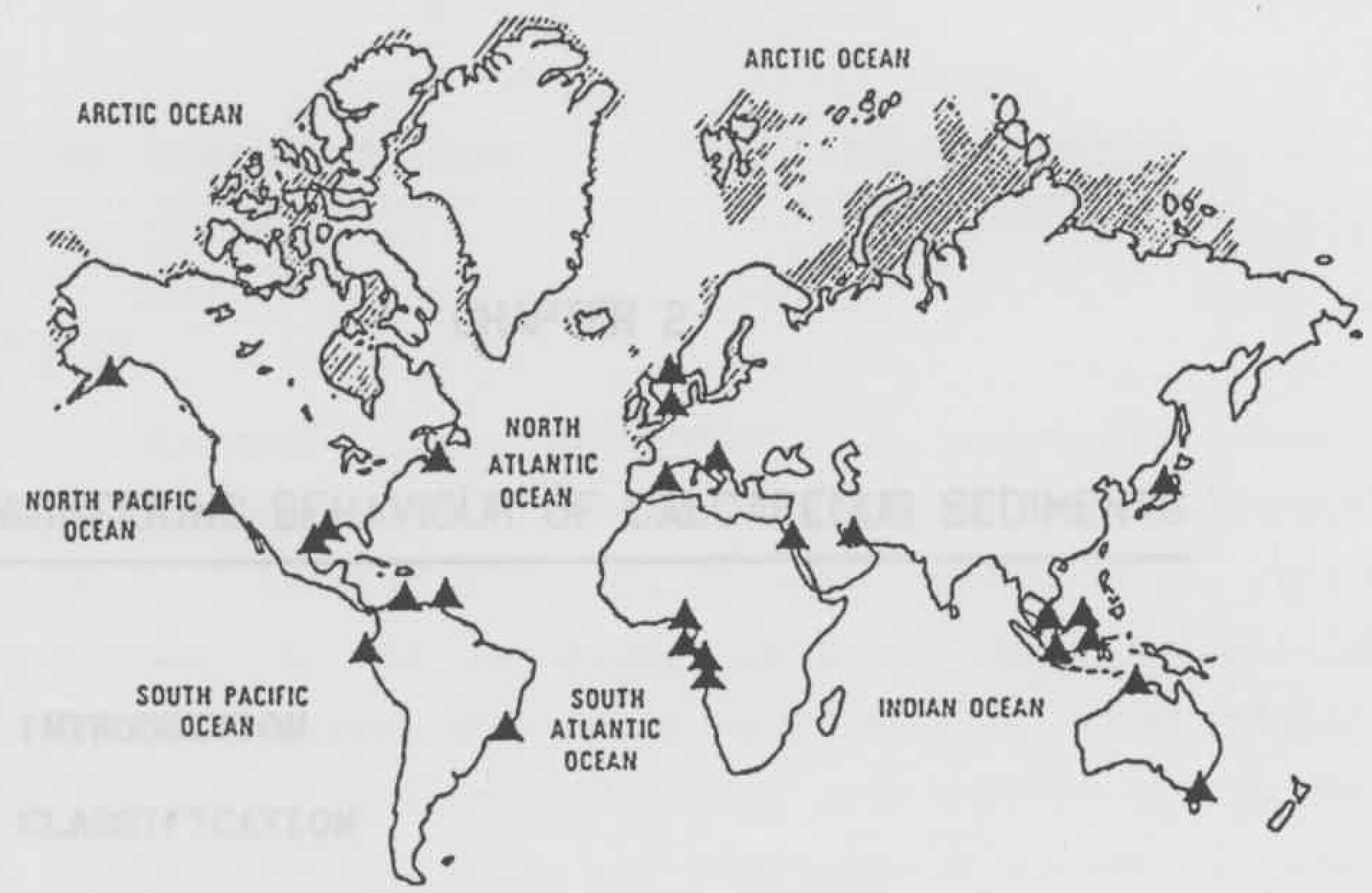

Fig. 1.1 Major regions of petroleum drilling activity in world oceans (after McClelland, 1974)

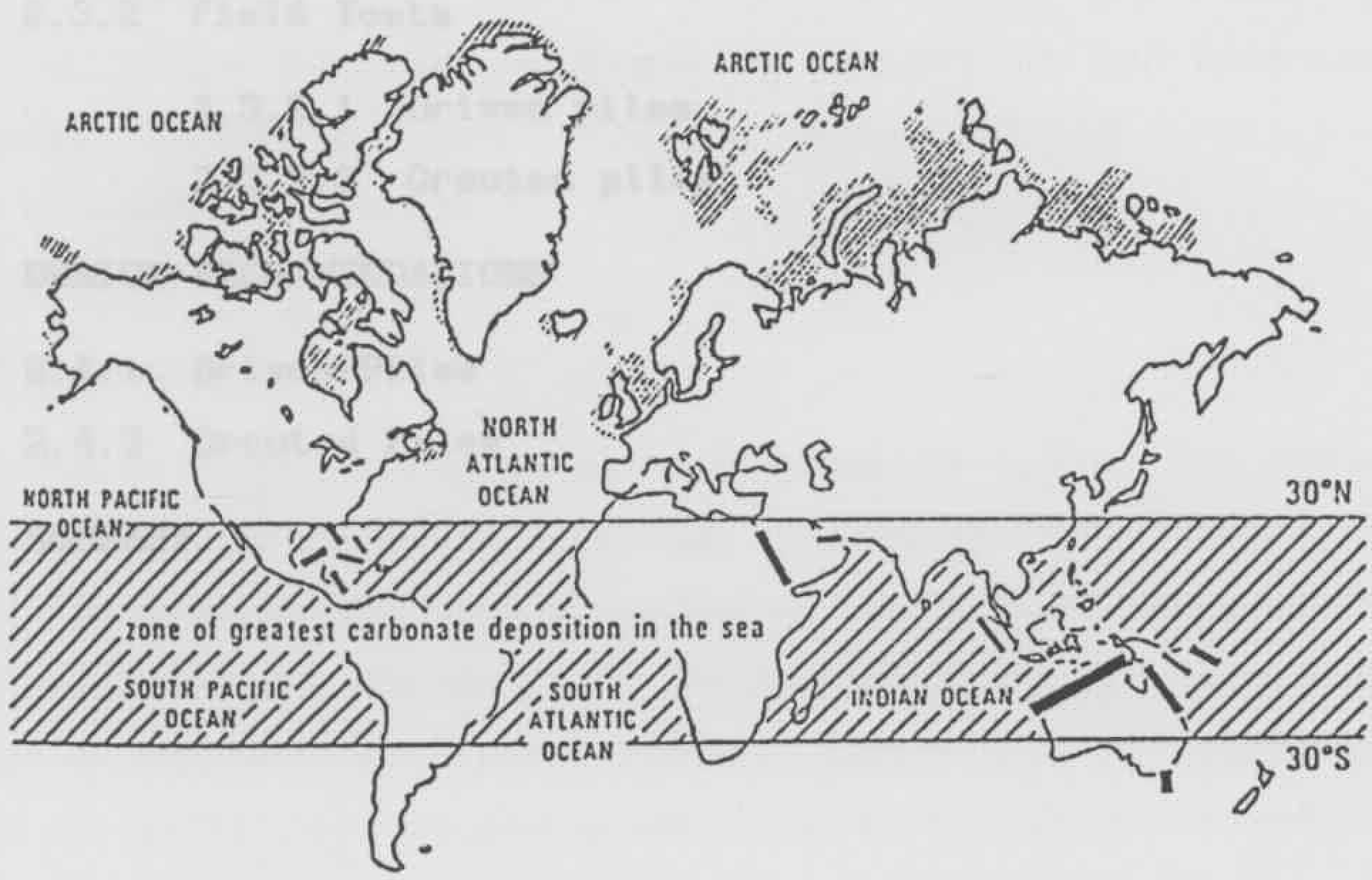

Fig. 1.2 Major deposits of carbonate sediments on continental shelves (after Rodgers, 1957)

CHAPTER 2

ENGINEERING BEHAVIOUR OF CALCAREOUS SEDIMENTS

CHAPTER 2

ENGINEERING BEHAVIOUR OF CALCAREOUS SEDIMENTS

2.1 INTRODUCTION

The term "calcareous" (or "carbonate") is generally used to describe those sediments, both onshore and offshore, that contain a significant amount of calcium carbonate mineral (Murff, 1987). Further detailed description of the sediments based on their depositional environment, mineral content and origin can also be made (Noorany, 1989). Unlike the more commonly encountered and studied silica sands and cohesive soils, the behaviour and characteristics of calcareous sediments affecting its engineering properties are far less understood. Such "awakening" to this unique class of sediments came mainly from offshore production work in the late sixties (McClelland, 1974). Surprisingly low skin friction resistances (generally less than 20 kPa) were encountered with driven piles in such soil deposits.

In this chapter, a brief review is presented on the existing state of knowledge, from both laboratory and field tests, of the behaviour of calcareous sediments. The review is divided into the following major sections: classification, engineering properties and behaviour of calcareous sediments, and design recommendations for pile foundations in such soil deposits.

2.2 CLASSIFICATION

The usefulness of an appropriate classification system for soils, in the field of geotechnical engineering, cannot be over-emphasized. Such a classification system should enable an estimate of the probable engineering behaviour of the soils to be made from simple laboratory tests. While an appropriate classification system for non-carbonate soils, based on particle size and plasticity index, is satisfactory, those for carbonate soils are at present only partially satisfactory. For such carbonate soils, other characteristics of importance like the susceptibility to crushing, carbonate content and the nature of cementation, if any, in the soil have to be included in any successful classification system (Datta *et al.*, 1982; Dutt and Ingram, 1990).

The classification system proposed by Fookes and Higginbottom (1975) was perhaps the first useful system for engineering purposes. Four criteria were used in their system of classification, namely, (i) carbonate content, (ii) degree of induration (or cementation), (iii) particle size, and (iv) origin of the carbonate material. Clark and Walker (1977) extended the system proposed by Fookes and Higginbottom to include the extremes of total carbonate and total non-carbonate sediments. Their system of classification was based on three parameters of engineering significance: grain size, carbonate content and strength. This system was further extended by King *et al.* (1980) and Beringen *et al.* (1982) by incorporating cone penetrometer tip resistance as a measure of cementation.

The importance of the carbonate content in affecting the engineering behaviour of a calcareous sediment has been shown by Demars *et al.* (1976). However, the carbonate content alone is not sufficient to enable a complete classification of the engineering behaviour of carbonate sediments. Factors like the susceptibility to crushing of the carbonate grains (Datta *et al.*, 1979a) and the cementation caused by the carbonate material (Noorany and Gizienski, 1970) have also to be included. Due to the absence of universally accepted procedures for characterization of the last two factors, a complete and universally accepted classification system for carbonate soils is still far from reality (Noorany, 1989; Dutt and Ingram, 1990).

2.3 ENGINEERING PROPERTIES AND BEHAVIOUR OF CALCAREOUS SEDIMENTS

The engineering properties of a soil that are of significance to a geotechnical engineer can be divided into two major categories: shear strength and compressibility characteristics of the soil. Available experience, from both laboratory and field tests, indicates vastly different behaviour of calcareous sediments from their terrigeneous counterparts (Poulos, 1980, 1985; Semple, 1987, 1988; McClelland, 1988; Randolph, 1988; Coop, 1990). Apart from their high carbonate content, these sediments exist at higher void ratios than silicate sediments, have angular particles that are highly susceptible to crushing with resultant significant volume reduction, and may exhibit variable amounts of cementation. This different behaviour of the sediment has resulted in costly "exposure" particularly for the offshore industry (Shinners *et al.*, 1988). As such, an attempt is made here to review some of the results from laboratory and field tests that have been conducted in such sediments.

2.3.1 Laboratory Tests

Due to limited field experience, extensive controlled laboratory tests have been conducted in the last decade or so to study the mechanics of behaviour of calcareous sediments. These tests, although at a small scale, are capable of providing valuable insight and understanding of the behaviour of this class of sediments. The tests can be divided into four major categories, namely, triaxial tests, interface shear tests, model jacked (or driven) pile tests, and model grouted pile tests. Each of these categories will be briefly reviewed in the following sections.

2.3.1.1 Triaxial tests

The conventional triaxial test, due to its well established and accepted procedures, has been used by many researchers (for example, Hermann and Houston, 1976; Datta *et al.*, 1979a, 1979b; Airey *et al.*, 1988) for determining the strength and compressibility characteristics of calcareous sediments. The cyclic triaxial test, which involves the application of repeated cycles of stress (or strain) loading, is used to study the response of the sediment under cyclic loading as is encountered in the offshore environment.

Demars *et al.* (1976) found that carbonate content has an important influence; in general, sediments with carbonate content greater than 40% exhibit granular behaviour while those less than 40% exhibit cohesive behaviour. As such, they suggested that the carbonate content be routinely determined and used as an index property for carbonate sediments.

The most notable early laboratory research on calcareous sediments was perhaps that reported by Datta and co-workers. Datta *et al.* (1979a), from results of drained triaxial tests, concluded that the susceptibility to crushing of the calcareous grains has an important effect on its behaviour. The drained angle of shearing resistance was found to decrease with increasing confining pressure as a result of increased particle crushing. This susceptibility to crushing was expressed in terms of a crushing coefficient, C_c defined as

$$C_c = \frac{\text{percentage of particles of the sand after being subjected to stress finer than } D_{10} \text{ of the original sand}}{\text{percentage of particles of the original sand finer than } D_{10} \text{ of the original sand}}$$

The coefficient increases with confining pressure as a result of the increased crushing of the sand grains. The material behaviour was also observed to alter from a brittle dilatant response to a more plastic response with volume reduction as crushing continues. Furthermore, they proposed an empirical relationship between the magnitude of crushing and the shear strength through the expression

$$K_c/K_{c1} = (C_c)^{-0.6} \qquad (2.1)$$

where K_c = maximum principal effective stress ratio

K_{c1} = value of K_c for confining pressure of 100 kPa.

C_c = crushing coefficient (as defined earlier)

It should be noted that, as mentioned earlier, there is still no single universally accepted procedure for quantitatively expressing the magnitude of crushing of the sand particles. Different definitions have been used by other investigators (Lee and Farhoomand, 1967; Dutt *et al.*, 1986).

The pore-water response, from undrained triaxial tests, has also been shown to be affected by the degree of particle crushing by Datta *et al.* (1979b). They observed that the pore-water pressure response under static loading changes from negative to positive as the magnitude of crushing increases, with resultant volume reduction. In contrast to that observed by Datta *et al.* (1979a) for the drained tests, the undrained angle of shearing resistance was found to be not significantly affected by the magnitude of crushing.

In a further paper, Datta *et al.* (1980a) reported the results of pore-water pressure development in undrained triaxial tests with repeated stress cycles. They found that the pore-water pressure increased with the number of stress cycles (Hermann and Houston, 1976) and that its development was more rapid for alternating (i.e with reversal) stress cycles than the compressive (i.e. biased) stress cycles. However, the development of permanent strain with increasing cycles was much larger with the compressive stress cycles than the alternating stress cycles. Furthermore, it was also suggested that crushing depends essentially on the permanent strain developed in the soil and is not influenced by the type of loading (i.e. whether static or cyclic). Their results indicate that cyclic loading has no significant influence upon subsequent static behaviour which is in contrast to that of Hermann and Houston (1976) where significant strength loss was observed. It may be noted that similar pore-water pressure generation studies of calcareous sediments under cyclic triaxial loading condition have also been reported by Dobry *et al.* (1988) and Kaggwa *et al.* (1988).

Frydman *et al.* (1980) reported results of static and cyclic triaxial tests on intact cemented calcareous specimens. They found that the degree of cementation has a significant effect on the stress-strain response of the specimens. Furthermore, break-down of the cementing bonds may occur at high stress with resulting high compressibility of the specimen. Tests conducted by Allman and Poulos (1988) on an artificially cemented calcareous soil further confirm the important influence of the degree of cementation on the response of calcareous sediments.

Further studies into this class of sediments (for example, Airey *et al.*, 1988; Hull *et al.*, 1988; Golightly and Hyde, 1988) have generally confirmed that their characteristics are vastly different from their terrigeneous counterparts.

2.3.1.2 Interface shear tests

In order to determine the frictional resistance that can be mobilised between the soil and some other material, an interface shear test is usually used. The direct shear (the more commonly used) and simple shear tests are appropriate for such determination. The relative merits of these two types of test are discussed by Matthews (1988). It should however be noted that this interface test may not satisfactorily simulate completely the actual complex mechanism of load mobilisation in an axially loaded pile.

Tests conducted by Noorany (1985) showed that the interface friction angles of the natural and crushed calcareous soils were about the same. The results therefore suggest that the frictional characteristics, which was thought to be influenced by the softness of the grains, may not fully account for the low shaft resistance of piles (Angemeer *et al.*, 1973). It is widely hypothesized now that the low resistance is due to a much lower than expected normal effective pile-soil interface stress, as a result of the more compressible nature of calcareous sediments (Nauroy and LeTirant, 1983). However, this hypothesis is yet to be conclusively confirmed from laboratory model and field scale pile tests with normal pile-soil interface stress measurements.

Static and cyclic direct shear tests by Poulos *et al.* (1982) show the significant detrimental effects of cyclic loading. The interface friction angle tends to decrease with cycling accompanied by significant volume reduction.

An improvement to the direct shear device has been made (Lam and Johnston, 1982; Boulon and Foray, 1986; Ooi and Carter, 1987) where the normal load (or stress) is no longer held constant but allowed to vary, in response to the dilating or contracting behaviour at the interface. This so called constant normal stiffness (CNS) direct shear device is capable of providing more representative simulation of the pile-soil/rock interface where the effect of the stiffness of the surrounding soil (or rock) mass on the interface behaviour is accounted for. A dilating interface would therefore increase the normal load acting on the specimen, thus increasing the frictional component of shear strength. The reverse applies for a contracting interface behaviour.

The use of the CNS direct shear device for monotonic and cyclic shearing of intact calcarenite core was reported by Ooi and Carter (1987). The significant influence of the normal stiffness condition on the calcarenite/calcarenite interface behaviour was evident. The results show that the calcarenite interface undergoes significant volume reduction accompanied by corresponding reduction in normal stress, as shearing continues. The further "damaging" effects of cyclic loading on the interface behaviour were also observed; increasing volume reduction, decreasing normal stress and increasing permanent shear displacement as cycling proceeds (Johnston *et al.*, 1988). Similar observations were also made by Boey and Carter (1988) from the monotonic shearing of an artificially cemented carbonate soil.

These tests therefore show the important influence of the interface behaviour on the mechanism of shaft friction mobilisation of, particularly, piles in calcareous sediments. The greater tendency of calcareous sediments to contract during shearing with corresponding normal stress reduction may well explain the much lower skin friction mobilised in such sediments.

2.3.1.3 Model jacked (or driven) pile tests

The interface shear tests mentioned earlier is useful for investigating the frictional force mobilisation characteristics between the soil and another interface material. It is however limited in its ability to fully simulate the complex friction mobilisation characteristics of an axially loaded pile. Ideally, an instrumented field scale pile test is the best method for studying the load mobilisation and performance characteristics of the pile. However, such field scale tests are not routinely done due to their prohibitive cost, particularly in the offshore environment. As such, laboratory scale model pile tests have been commonly used to investigate the performance characteristics of the pile embedded in the required soil medium. These laboratory tests can provide a controlled environment, in particular, eliminating the inherent variability of field deposits that makes interpretation of the results difficult. However, direct scaling of the model test results to the prototype may not usually apply and has to be used with caution (Meyerhof, 1983).

Laboratory scale model pile tests in calcareous sediments have been reported by, among others, Nauroy and LeTirant (1983), Nauroy *et al.* (1988), McCarel and Beard (1984), Lu (1986,1988), and Poulos and Chan (1986,1988). The major findings from this series of tests are presented below.

The tests of McCarel and Beard (1984) involved the driving of a 38mm (1.5in.) diameter model pile into a prepared sand bed. Two types of sand were used; silica and calcareous sands in order to study the different responses of both sands. For the calcareous sand, the parameters of significance are the density, cementation level and the carbonate content. Their results reinforced further the recent recognition of different behaviour between calcareous and silica sands. The calcareous sand, although generally exhibiting higher friction angles than silica sands, is however more susceptible to crushing with consequential much lower frictional capacity than that of the silica sand. Significant crushing of the calcareous sand grains was also observed at or near the pile wall. Their results also confirmed those of Noorany (1985) where the interface friction angles of the natural and crushed sands were found to be not significantly affected by the grain crushing. It was concluded that the frictional characteristics of a pile in calcareous sands are affected and depend on the inter-related effects of the parameters mentioned, and that none of these parameters alone can adequately explain its behaviour.

The tests of Nauroy and LeTirant (1983) further confirm the important influence of the compressibility of calcareous sand on its friction mobilisation characteristics. Their results, obtained using jacked and driven model piles of 50mm and 75mm diameter, show that the horizontal stress in the calcareous sand adjacent to the pile at the end of pile installation is less than its initial value (Fig. 2.1). The lower unit end-bearing capacity of calcareous sand as compared with silica sand was again attributed to its greater compressibility by the writers. The limiting compressibility index, defined as the slope of the e-log p curve (at an effective pressure of 800 kPa; e is the void ratio and p the applied pressure), was suggested by the writers to relate the influence of compressibility of the soil to its friction capacity (Fig. 2.2).

The important effects of grain crushing on axial pile behaviour were also observed by Lu (1988) who found an increase in grain crushing with increase in driving resistance. The extent of grain crushing was found to be greater for the higher density soil samples. The observed pullout resistance of the driven model piles in dense calcareous sand tends to decrease with increasing driving resistance and cement content. The test results also show that neither the extent of grain crushing nor the resistance to pile driving alone could satisfactorily explain the observed pullout resistance behaviour of piles in calcareous sands. Lu (1986) also reported the damaging effects of two-way displacement-controlled cyclic loading in reducing the friction capacity of the piles.

Poulos and Chan (1986) presented results of static and cyclic tests on 20mm diameter model piles embedded in calcareous sand. These tests excluded the development of end-bearing on the pile so as to enable the shaft friction development to be studied only. The effect of cyclic loading is presented as a degradation factor, first proposed by Poulos (1979a), which relates the value of a soil parameter after cyclic loading to the corresponding value for static loading. Their results show that significant cyclic degradation of skin friction will not occur unless the cyclic axial displacement exceeds the value required to cause static slip of the pile (Fig. 2.3). Therefore, the results suggest the presence of a "threshold" condition below which cyclic loading will have no significant influence. The effect of cyclic loading on skin friction was found to be more severe for soils of higher density and overconsolidation ratio (OCR). However, cyclic loading was found to have no significant effect on the soil modulus. The model jacked pile tests of Poulos and Chan (1988) further show the important influence of residual stresses due to pile installation. These residual stresses will have to be considered in order to obtain a more accurate interpretation of the test results (Holloway *et al.*, 1978). This test series (Poulos and Chan, 1988) seems to also suggest that cyclic loading has no significant effect on the end-bearing capacity. Another important observation was the accumulation of permanent displacement under non-zero mean load as cycling proceeds.

The influence of particle characteristics of calcareous sand, in particular, the uniformity of particle size, and the structure and composition of the grains, have been shown by Lee and Poulos (1987) to affect the static and cyclic model pile responses. The influence of the soil density has been further shown by Poulos and Al-Douri (1992) to have a significant effect on both the static and cyclic responses of the model jacked pile.

It is worthy of note that cyclic tests on laboratory scale model piles in sand (for example, Chan and Hanna, 1980; Gudehus and Hettler, 1981) and in clay (Holmquist and Matlock, 1976; Matlock *et al.*, 1982; Procter and Khaffaf, 1987; Hewitt and Poulos, 1988; Lambson and Craig, 1988) also show the detrimental effects of cyclic loading, although they may not be as severe as with calcareous sediments.

2.3.1.4 Model grouted pile tests

As mentioned in the previous section, the friction capacity of driven (or jacked) pile in calcareous sediments is much lower than that for silica soils. This lower capacity has been attributed to the crushing of the more compressible calcareous grains, particularly during the installation process with consequential volume reduction and resulting decrease in the normal pile-soil interface stress. Therefore, it appears that an installation method that subjects the calcareous grains to minimal "physical" stress would increase its friction capacity. To this end, the drilled and grouted pile seems to be a "better" foundation choice, although it may be more expensive and have more installation problems (McClelland *et al.*, 1969) than the driven pile foundation. As such, laboratory model pile tests have again been used to study the friction capacity characteristics of grouted piles in calcareous sediments.

The static model tests of Nauroy and LeTirant (1985) show that grouted piles always develop more friction capacity than driven piles (also evident from the laboratory model pile test results conducted by Young (1983) within the Soil Mechanics Laboratory of the University of Sydney). The skin friction capacity was found to be on the order of 5 to 100 times that of the driven piles, the "exact" value being dependent on the nature of the soil considered. The compressibility of the soil, an important factor for driven piles, was however found to be of less significance for grouted piles. The strength and nature of the soil-grout bond seem to be the predominant influencing factor.

The significant influence of the cementation level (by varying the cement content in artificially cemented samples) on the static skin friction of model grouted piles (23.3mm diameter) was evident from the test results of Allman *et al.* (1988) and Lee *et al.* (1989). The results also show that the static response of grouted piles, at higher cement content, exhibits greater post-peak strain-softening behaviour than jacked piles. It should be noted that these tests were essentially pile segment tests where the development of end-bearing resistance was excluded.

The results of cyclic tests were also reported further by Allman *et al.* (1988) which show the effect of cementation on the degradation of skin friction. The susceptibility to cyclic degradation appears to decrease and increase for pre-peak and post-peak load-controlled cycling respectively, with increase in the degree of cementation. The greater susceptibility to degradation for post-peak cycling, with increasing cementation level, may be due to the additional "degradation" as a result of the larger strain-softening response. This degradation due to strain-softening response, caused by the accumulated permanent displacement, should not be confused with the "physical" degradation of the calcareous sediments as a result of cyclic loading. It should however be noted that a clear distinction between the two different degradations is not easily established. The cyclic degradation used in this thesis refers to the "physical" degradation, unless otherwise specified.

As for driven piles, similar observations were made by Poulos and Lee (1988) of the beneficial effects of increasing overburden pressure, relative density and overconsolidation ratio on the static skin friction. The magnitude of the developed skin friction is however significantly greater than those of the model driven (or jacked) piles. The dependence of the static shaft capacity on the effective confining pile-soil stress was also shown experimentally by Lee and Poulos (1988a). For cyclic loading, Poulos and Lee (1988) found that severe degradation in skin friction occurs with increasing cyclic slip displacement (defined as the cyclic displacement in excess of that required to cause static failure).

An important observation was also made by Lee (1988) (also reported by Lee and Poulos, 1991) of the "scale effect" on the developed peak static skin friction. The model test results show that the peak skin friction decreases with an increase in the pile diameter (also observed by Nauroy *et al.* (1988) for driven piles). As pointed out by Poulos (1988a), caution must therefore be exercised in applying the results of such model tests to full-scale piles. Furthermore, the skin friction degradation due to cyclic loading was found to be also influenced by the pile diameter (Lee, 1988; Poulos, 1988a) as shown in Fig. 2.4(a). A plot of the degradation factor against the normalised (to diameter) cyclic slip displacement (Fig. 2.4b) however seems to be not significantly influenced by the pile diameter (Lee, 1988). This has important implications (Poulos, 1988a) for large scale piles; the skin friction degradation will be more severe if the degradation is dependent on the absolute value of cyclic slip displacement. However, more laboratory larger scale and/or full-scale tests are required to supplement the present limited data-base in order to confidently clarify this uncertainty.

It is interesting to note that test results reported by Turner and Kulhawy (1989), obtained from repeated axial loading tests on model drilled shafts in silica sand, also showed the degradation of skin friction capacity. This degradation of the skin friction depends primarily on the cyclic displacement magnitude and it appears to begin near the pile tip and progresses upward. Their results also indicate a greater proportion of the applied load being carried by the tip resistance in the compression phase of the repeated loading.

2.3.2 Field Tests

The considerable cost coupled with the difficult, if not sometimes impossible, procedures required for the conduct of field tests, particularly in the offshore environment, have contributed to the general lack of field test results. Such field results are required not only to substantiate and verify the laboratory test results but also to provide an assessment of the actual field response of the piles. In particular, more field results of piles in calcareous sediments are required to increase the present limited data-base on which empirical design recommendations are based.

Some of the field test results of both driven and grouted piles in calcareous sediments are briefly reviewed in the following sections.

2.3.2.1 Driven piles

Perhaps the first encounter with the unique behaviour of calcareous sediments came from offshore production work in Bass Strait, Australia (see Fig. 2.5) that culminated in a comprehensive load testing program being undertaken (Angemeer *et al.*, 1973). The unit static skin friction of the 20-inch. diameter driven steel conductor pipe piles was found to be significantly lower than the corresponding value normally used in conventional design in silica sands. However, the cyclic test results did not indicate a decrease in capacity with repetitive cycling and as noted by the writers (Angemeer *et al.*, 1973), the results were not conclusive. Conclusive results of the degrading effect of cyclic loading were however reported by Abbs *et al.* (1988) for another offshore carbonate site (North Rankin "A", Australia).

An interesting observation was also made between the skin friction values obtained from steel friction tests (SFT) and the driven conductor tests (Abbs *et al.*, 1988; Khorshid *et al.*, 1988). The steel friction tests involved pushing a 2.5m long by 60mm diameter steel tube into the soil at the required depth and measuring the skin friction on extraction (King *et al.*, 1980). Test results showed that the unit skin friction from the SFT's were much higher that those from the conductor tests. This indicates and suggests a diameter dependence of the developed skin friction for piles in calcareous sediments. It may be noted that, as mentioned in section 2.2.1.4, a similar "scale-effect" was also observed by Lee (1988) from laboratory model scale grouted piles. It is also of interest to note that a simple conceptual model, based on cavity expansion theory, has been suggested by Randolph (1988) to explain the "scale-effect" of the developed peak static skin friction.

Similar lower friction capacity of piles in offshore calcareous sediments have also been reported by, for example, Dutt and Cheng (1984), Dutt *et al.* (1985) and Puyuelo *et al.* (1983).

Onshore static tests have also been reported by Ismael and Al-Sanad (1986) for bored piles, and by Ismael (1989) for driven piles conducted at the same site consisting of a dense calcareous sand. The unit skin friction of the driven piles is lower than that developed by the bored piles (Ismael, 1989). This confirms the important influence of pile installation method on the developed skin friction capacity, particularly for piles in calcareous sediments.

It may also be noted that field tests conducted in clay (for example, Grosch and Reese, 1980; Karlsrud and Haugen, 1985; Karlsrud *et al.*, 1986; Bogard and Matlock, 1990a, 1990b) and in silty sand (for example, Puech and Jezequel, 1980; Puech *et al.*, 1982) also show similar "damaging" effects of cyclic loading.

2.3.2.2 <u>Grouted piles</u>

Field test results of offshore grouted piles are scarce compared to those of driven piles. This is due to the preferred use of driven piles because of the easier installation procedures than those of grouted piles.

Grouted section tests, which involve drilling a hole to a predetermined depth, lowering a short pipe section and then grouting the annular space between the hole and pipe, have been used in offshore field tests to determine the friction capacity of grouted piles (Angemeer *et al.*, 1975; King *et al.*, 1980; Withers *et al.*, 1986; William and Van der Zwaag, 1988). Like the steel friction tests, these tests only simulate the response of a segment of the pile shaft.

The field test results indicate higher friction capacity of grouted piles than driven piles. The further detrimental effects of cyclic loading in reducing the static friction capacity, and the accumulation of permanent displacement were reported by William and Van der Zwaag (1988).

Onshore model and full-scale field tests results have also been presented by Nauroy and LeTirant (1985) and Nauroy *et al.* (1985). Similar higher friction capacity was also observed as for the offshore tests. As reported by Nauroy *et al.* (1985), the movements of the pile under cyclic loading are influenced by the average mean load, maximum load level and the cyclic load component.

The series of laboratory and field tests that have been conducted serve to provide a better understanding of the mechanisms affecting the pile response in calcareous sediments. Of particular importance are the possible degradation of pile capacity and the accumulation of pile displacement under cyclic loading conditions. Based on these observations, pile analysis approaches have been developed to numerically simulate the two phenomena of capacity degradation and accumulation of pile displacement. Some of these analysis approaches will be briefly reviewed in Chapter 3.

2.4 DESIGN RECOMMENDATIONS

While design recommendations on the limiting skin friction and end-bearing capacities for non-carbonate sediments are probably adequate (API RP 2A, 1987), those for carbonate sediments are however based on site specific experience. This "inability" to suggest limiting resistance values that are general enough for calcareous sediments is due to their highly variable characteristics. In particular, the cementation level, although increasing the end-bearing capacity, may however result in a loss of lateral pressure and a corresponding decrease in the friction capacity (API RP 2A, 1987). For cyclic loading conditions, no specific design guidelines are available although the usual approach is to ensure that the response of the pile is "elastic" under the peak combined loading (Randolph, 1983a).

The data-base from both laboratory and field tests that have been conducted in the last decade or so serves to provide some guidelines for piles constructed in such sediments. It may be noted that the methods for estimating the skin friction and end-bearing capacities are similar to those used for the non-calcareous sediments, except that different lower limiting capacity values are applicable for the calcareous sediments. A comprehensive review of such design methods and the limiting capacity values applicable for different soil types can be found in Poulos (1988d). The reader is also directed to other related publications, for example, O'Neill (1983), Kraft (1991a) and Bea (1992), on the general subject of response of offshore piles.

2.4.1 Driven Piles

McClelland (1974), from limited field observations, has suggested limiting the unit skin friction and end-bearing capacities for calcareous sands to one-fifth (20 kPa) and one-half (5 MPa) of the corresponding values for non-calcareous sands, respectively. These recommendations however take no account of the amount of carbonate mineral present and the degree of cementation that may affect these limiting capacity values. Tables 2.1 to 2.4 show the different recommendations for the limiting skin friction and end-bearing capacities that have been suggested for driven piles in calcareous sands. As noted, these suggestions, except those of Agarwal *et al.* (1977), do not take into account the amount of carbonate present that may influence the response of the sand.

Agarwal *et al.* (1977) modified the suggestions of McClelland (1974) to take the carbonate content into account. It was suggested that the limiting values of McClelland (1974) be increased by 40% for carbonate content in excess of 45%. For calcareous sands with carbonate content less than 30%, the corresponding values for non-calcareous sands could be used while for carbonate content between 30% and 45%, it was suggested that a 60% increase of the value suggested by McClelland (1974) be adopted (Table 2.1). However, an appraisal of existing practice by Datta *et al.* (1980b) suggested the crushing susceptibility to be the relevant criterion for determining the magnitude of limiting capacity and not the carbonate content.

The series of laboratory and field tests (Nauroy and LeTirant, 1983, 1985) show that the limiting capacity values can be related to the limiting compressibility index of the soil (Nauroy *et al.*, 1986). These limiting capacity values are shown to decrease with an increase in the compressibility index (Tables 2.2 and 2.4). However, caution has to be exercised in using these limiting capacity values for calcareous soils other than those from which they were derived.

It is worthy of note that an empirical expression for the end-bearing resistance (obtained from model jacked pile tests) in cemented carbonate soils has been suggested by Houlsby *et al.* (1988). The suggested empirical expression relates the end-bearing resistance to the unconfined compressive strength of the cemented layer. Limiting end-bearing resistance values have also been suggested by Golightly and Nauroy (1990) based on the compressibility index of the soil (as opposed to the limiting compressibility index utilised by Nauroy *et al.* (1986)).

To illustrate the different ultimate design pile capacity that can be obtained, the hypothetical case of a closed-ended driven pipe pile in a uniform layer of calcareous sand is considered. The pile is 100m in length and has an external diameter of 1.0m. The computed ultimate pile capacities are shown in Table 2.5. Significant differences in the computed pile capacities are observed, with the carbonate content and the compressibility index having a major influence on the computed capacities. This example therefore shows the current uncertain and non-unified design guidelines with regard to pile capacity determination in such sediments.

2.4.2 Grouted Piles

Although grouted piles are shown to have much larger friction capacity than driven piles, there is still a general reluctance to adopt values far in excess of those recommended for driven piles in non-calcareous sands. This reflects the present lack of complete understanding of the mechanics of load mobilisation in grouted piles, and the need for further research and field test results to confidently adopt a larger limiting capacity value.

Nauroy *et al.* (1986) have adopted a limiting friction capacity value of 100 kPa while Hyden *et al.* (1988) suggested a limiting value of 200 kPa for grouted piles in uncemented calcareous sands. The end-bearing capacity is generally ignored in the design of long drilled and grouted piles under elastic conditions (Hyden *et al.*, 1988).

For grouted piles in cemented calcareous formations, a limiting friction capacity based on the unconfined compressive strength of the material has been proposed by, for example, Abbs and Needham (1985) as shown in Table 2.6.

The computed ultimate pile capacities of a hypothetical grouted pile, 100m in length and 1.0m in diameter, embedded in a uniform deposit of calacreous sand are shown in Table 2.7. For the uncemented case, the recommendation of Hyden *et al.* (1988) resulted in a pile capacity twice as much as that obtained by using the recommendation of Nauroy *et al.* (1986). For the cemented case, the only recommendations are those of Abbs and Needham (1985) whereby the computed ultimate pile capacity is dependent on the unconfined compressive strength. As mentioned earlier, more field test data are required to improve on the existing design recommendations.

2.5 SUMMARY

The response of calcareous sediments has been shown to be significantly different from those of the more commonly encountered terrigeneous sediments. This difference in response has been attributed to the particle characteristics, higher susceptibility to crushing, higher intraparticle voids, and the presence of cementation, if any, caused by the carbonate mineral, that are associated with calcareous sediments. It is worthy of note that a recent important observation by Semple (1988) seems to suggest that the responses of calcareous and silica soils, of similar initial void ratios, are comparable. More complete and detailed study is however required to fully confirm this significant observation.

Both laboratory and field tests results clearly show the lower friction capacity that can be derived from calcareous sediments. As compared to driven piles in such sediments, grouted piles are capable of offering greater capacity although it is generally more expensive and difficult to install. It may be noted that alternative conceptual pile systems to improve the load capacity of piles in calcareous sediments have also been suggested (The Earth Technology Corporation, 1983) and used (Barthelemy *et al.*, 1986, 1987). The further detrimental effects of cyclic loading, on both driven and grouted piles, are evident, in particular, the degradation of friction capacity and the accumulation of permanent displacement. With regard to the degradation of friction capacity, limited results at present seem to suggest a diameter dependence of the skin friction degradation factor. Furthermore, the effects of cyclic loading may be more severe for soils that exhibit greater post-peak strain-softening response, in particular the cemented carbonate sediments. The cyclic test results also seem to suggest a "threshold" condition below which cyclic loading will have no significant effect.

The design static capacity of piles in calcareous sediments is at present based on limiting capacity values that are significantly lower than those of non-carbonate sediments. The use of site specific design values, where available, particularly for piles in cemented carbonate formations, is emphasized and recommended (API, 1987). It is also worthy of note that correlations using in-situ tests to obtain the design parameters (Hagenaar, 1982; Dutt *et al.*, 1985; Ebelhar *et al.*, 1988, Dutt and Ingram, 1988) have been used with varying degrees of success. For piles subjected to combined static and cyclic loading conditions, the usual design approach at present is to ensure that the response of the pile is "elastic" under the peak combined loading.

From the review, the following remaining areas of uncertainty, in particular the pile response in the calcareous sediments, that need further research attention are listed below:

(i) Although different classification systems for calcareous sediments have been proposed, their use for engineering purposes has rather been limited. This is due to the absence of universally accepted procedures for characterization of the two important features of calcareous sediments; the susceptibility to crushing and the degree of cementation. A simple and universally accepted classification system, useful for engineering purposes, that incorporates universally accepted characterization procedures for the above mentioned factors is therefore needed.

(ii) It is widely accepted now that piles in calcareous sediments develop lower friction capacity than in silica soils. Some limited results seem to suggest that the lower capacity is caused by a lower than expected normal effective pile-soil stress. To this end, more laboratory model or field scale pile tests with normal pile-soil stress measurements are required to provide some quantitative data on the developed normal pile-soil stresses.

(iii) Although the "grouted driven pile" concept (Barthelemy *et al.*, 1987; Rickman and Barthelemy, 1988) looks promising in increasing the capacity of driven piles in calcareous soils, and is also more economically viable than the more expensive drilled and grouted pile option, more research efforts however should be directed towards quantifying the grout-penetration characteristics during the installation stage and also in assessing the long term cyclic performance of this "grouted driven pile" option.

(iv) Limited laboratory small scale model pile tests seem to indicate a "scale effect" of the developed peak static unit skin friction. Under cyclic loading condition, the degradation of pile shaft capacity seems to be governed by the "relative (to diameter) cyclic slip displacement" model. As such, tests conducted with larger scale model pile sizes (than those used thus far) are required to verify the above initial conclusions.

(v) Most of the research efforts expended thus far have concentrated on understanding the mechanics of pile shaft capacity degradation under cyclic loading. The degradation of pile base capacity under cyclic loading has however received far less attention. Some limited laboratory results from model footing tests have indicated no significant degradation of capacity with cyclic loading. This observation is encouraging in that for long friction piles, where the pile base load is negligible, the assumption of no degradation for the pile base capacity may be acceptable. However, for shorter piles, where the pile base load is greater, the degradation (if any) of the base capacity under the "violent" offshore cyclic loading condition may be a significant consideration. More research efforts into the mechanics and factors governing the degradation of pile base capacity is therefore clearly needed to supplement the present limited understanding of this base degradation effect.

(vi) It has been observed, from both laboratory and field tests, that accumulation of permanent pile displacement occurs particularly under one-way cyclic loading condition. This accumulation of pile displacement, if excessive, may lead to a "serviceability" problem for the superstructure. At present, this accumulation phenomenon is not clearly understood.

(vii) In practice, piles are seldom used as single isolated pile but rather in close proximity to other piles to form a pile group. The influence of this inter pile interaction (commonly known as pile-soil-pile interaction effect) due to cyclic loading on the two phenomena of capacity degradation and permanent pile displacement accumulation is a complex process and requires further research efforts to improve and substantiate the present limited understanding of the problem.

(viii) For the design of piles in calcareous sediments, different conservative design guidelines, based on limited laboratory and field tests data, have been suggested for determining the friction and end-bearing capacities. This conservative approach, in particular, the general reluctance to adopt larger friction capacity values for grouted piles, reflects the present uncertainty still associated with such sediments. The need to have a large data base of tests conducted in such sediments, interpretation of the tests data and the eventual recommendations of more unified design guidelines, is clearly evident. This will then lead to greater confidence in the adoption of such recommendations.

In this thesis, an attempt is made to study aspects (ii) and (iv) listed above. Aspect (iv) forms the major thrust of the experimental work undertaken in the present study, where laboratory-controlled model scale pile tests with different pile sizes are utilised. It is hoped that the experimental study will increase and improve our present limited understanding of pile behaviour in calcareous sediments.

Table 2.1 Limiting values of ultimate skin friction for driven piles in calcareous sand (after Poulos, 1988d).

limiting value of f_s (kN/m^2)	source
20	McClelland (1974)
28 (C.C.* > 45%)	Agarwal et al. (1977)
32 (C.C. 30-45%)	Agarwal et al. (1977)
100 (C.C. < 100%)**	Nauroy et al. (1986)

* C.C. = carbonate content

** see Table 2.2

Table 2.2 Limiting values of ultimate skin friction for driven piles in calcareous sand (after Nauroy et al., 1986).

limiting compressibility index, C_{pl}*	limiting value of f_s (kN/m^2)	
	open-ended pile	closed-ended pile
<0.02	100	120
0.02 - 0.03	50	100
0.03 - 0.04	20	50
0.04 - 0.05	10	50
0.05 - 0.1	5	20
0.1 - 0.2	0	10
0.2 - 0.3	0	5
0.3 - 0.5	0	2
>0.5	0	0

* Determined from isotropic triaxial compression test at effective pressure of 800 KPa.

Table 2.3 Limiting values of design bearing pressure for calcareous sand (extended from Poulos (1988d)).

Limiting value (MPa)	References
5	McClelland (1974)
3 - 5 (uncemented)	Datta et al. (1980)
6 (well cemented)	Datta et al. (1980)
10 (c.c. <30%)	Agarwal et al. (1977)
8 (c.c. 30-45%)	Agarwal et al. (1977)
7 (c.c. >45%)	Agarwal et al. (1977)
see Table 2.4	Nauroy et al. (1986)

Table 2.4 Limiting end-bearing pressure for driven piles in calcareous sands (after Nauroy et al. 1986).

Limiting compression index, C_{pl}	Limiting end-bearing pressure (MPa)
<0.02	≥ 20
0.02-0.03	15
0.03-0.04	10
0.04-0.05	8
0.05-0.1	4
0.1-0.2	1.5
0.2-0.3	1
0.3-0.5	0.5
>0.5	<0.5

Table 2.5 Computed ultimate pile capacities for driven pile in calcareous sediments based on different recommendations.

Recommendations of	Shaft capacity (MN)	End-bearing capacity (MN)	Total pile capacity (MN)	Remarks
McClelland (1974)	6.28	3.93	10.21	$f_s = 20\ kN/m^2$ $q_p = 5\ MN/m^2$
Agarwal et al. (1977)	8.79	5.49	14.28	c.c. >45%
	10.05	6.28	16.33	c.c. 30-45%
	31.42	7.85	39.27	c.c. <30%
				C_{pl} values
Nauroy et al. (1986)	37.69	15.71	53.40	<0.02
	15.71	6.28	21.99	0.04 - 0.05
	0.63	0.39	1.02	0.30 - 0.50

f_s = limiting unit skin friction

q_p = limiting unit end-bearing

c.c. = carbonate content

C_{pl} = compressibility index

Table 2.6 Limiting values of ultimate skin friction for grouted piles in cemented calcareous sand (after Abbs and Needham, 1985).

q_u^* (MPa)	a	b	Equation (MPa)
<1	0	0.375	$f_s = a + bq_u$
1-3	0.187	0.187	
>3	0.750	0	

* q_u = unconfined compressive strength

Table 2.7 Computed pile capacities for grouted piles in calcareous sediments based on different recommendations.

Recommendations of	Pile shaft* capacity (MN)	Remarks
Nauroy et al. (1986)	31.42	f_s = 100 kPa (uncemented)
Hyden et al. (1988)	62.83	f_s = 200 kPa (uncemented)
Abbs and Needham (1985)	$117.81q_u$ $58.75 + 58.75q_u$ 235.62	q_u < 1 MPa q_u 1 to 3 MPa — cemented q_u > 3 MPa

* — pile base capacity generally ignored; therefore total pile capacity taken as equal to pile shaft capacity.

q_u — unconfined compressive strength.

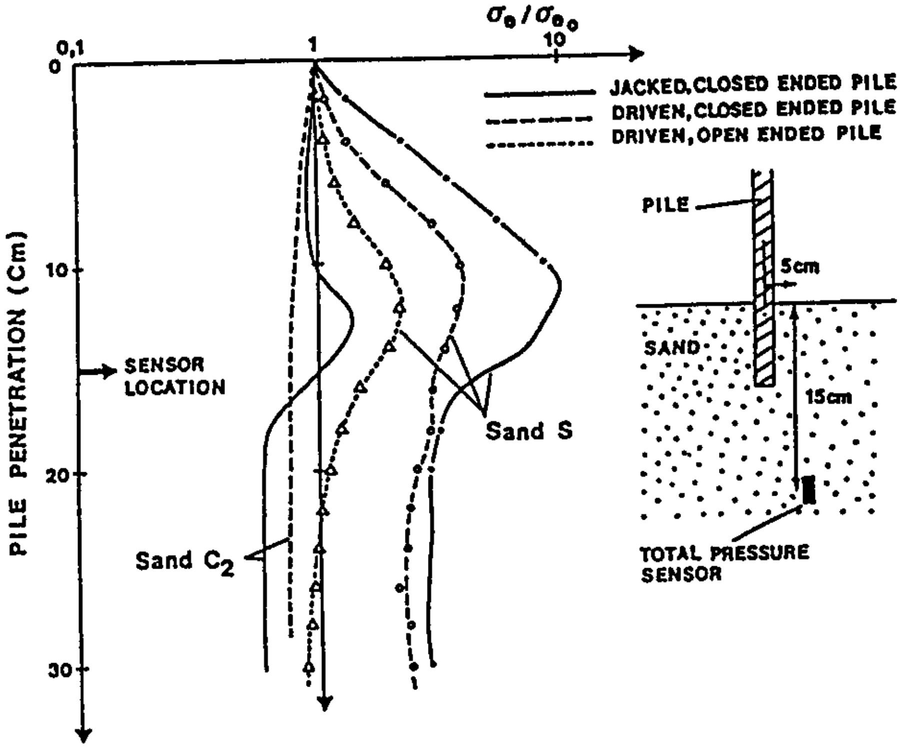

Fig. 2.1 Variations of lateral pressure in sand during pile penetration (confining pressure 200 kPa) - after Nauroy and LeTirant (1983)

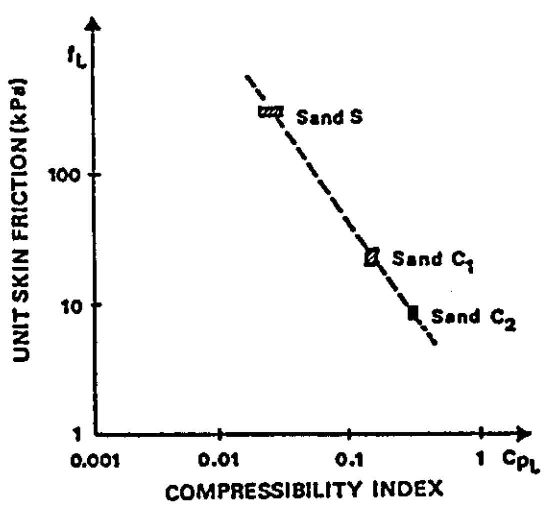

Fig. 2.2 Limiting unit skin friction versus limiting compressibility index (after Nauroy and LeTirant, 1983)

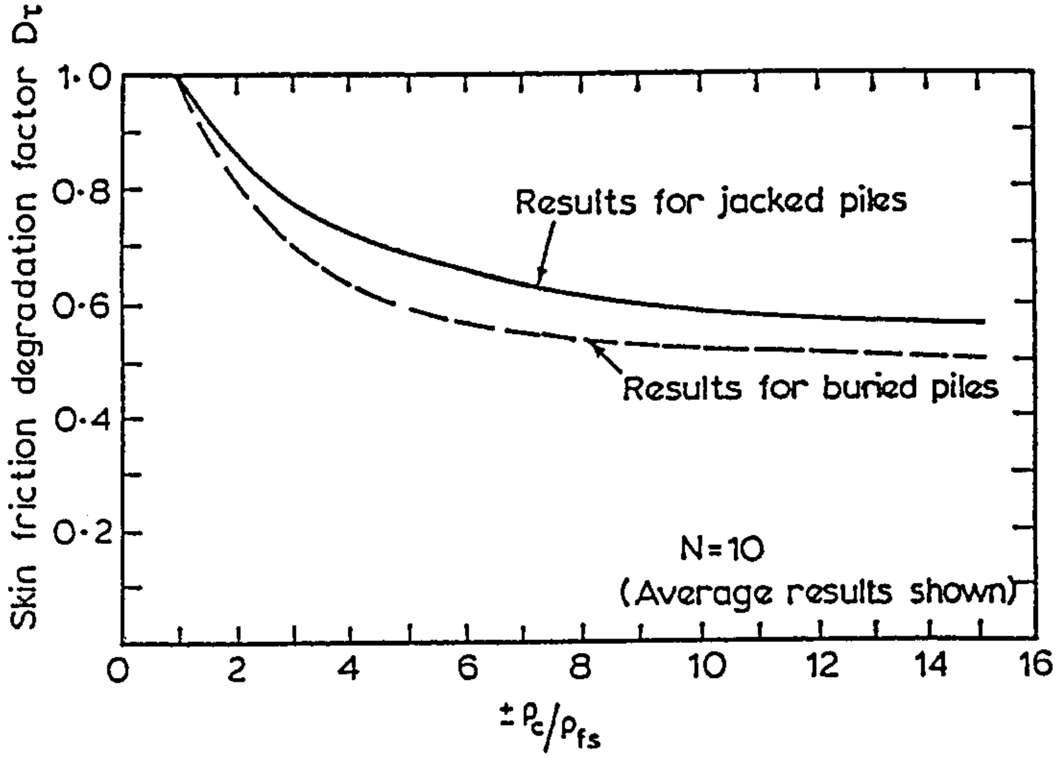

Fig. 2.3 Skin friction degradation factor as function of normalised cyclic displacement for piles in carbonate sand (after Poulos and Chan, 1986)

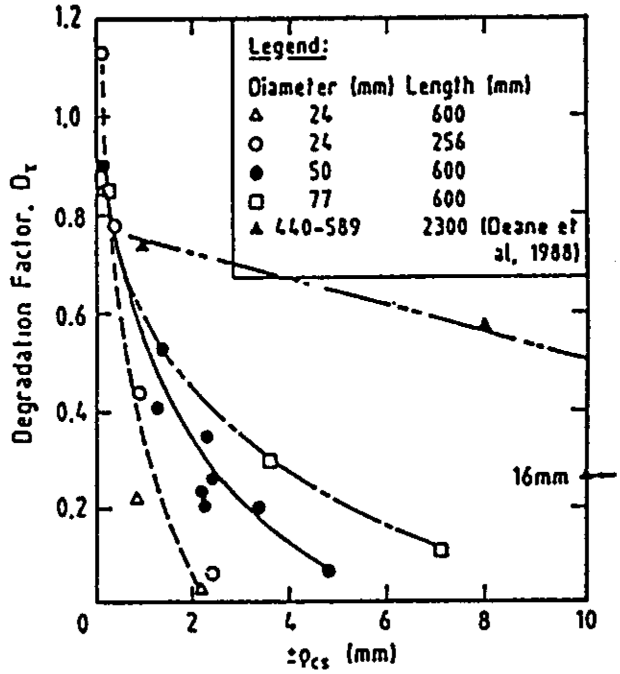

Fig. 2.4(a) Effect of cyclic slip displacement on D_τ with different pile diameters (after Lee, 1988)

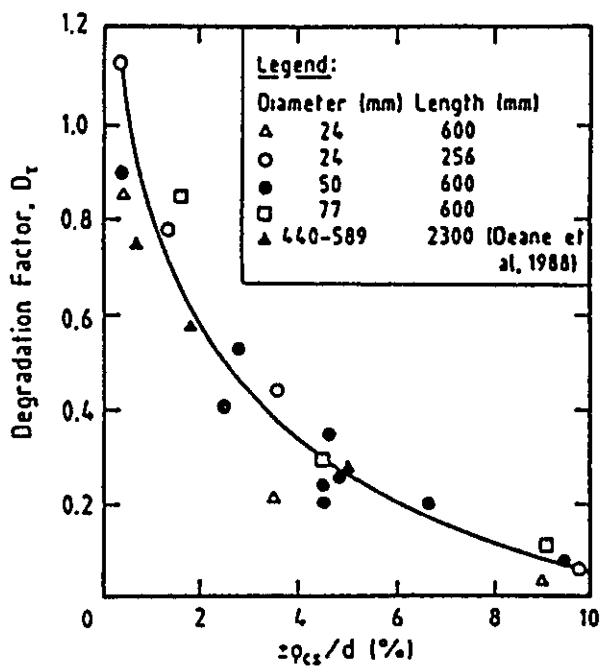

Fig. 2.4(b) Effect of normalised cyclic slip displacement on D_τ with different pile diameters (after Lee, 1988)

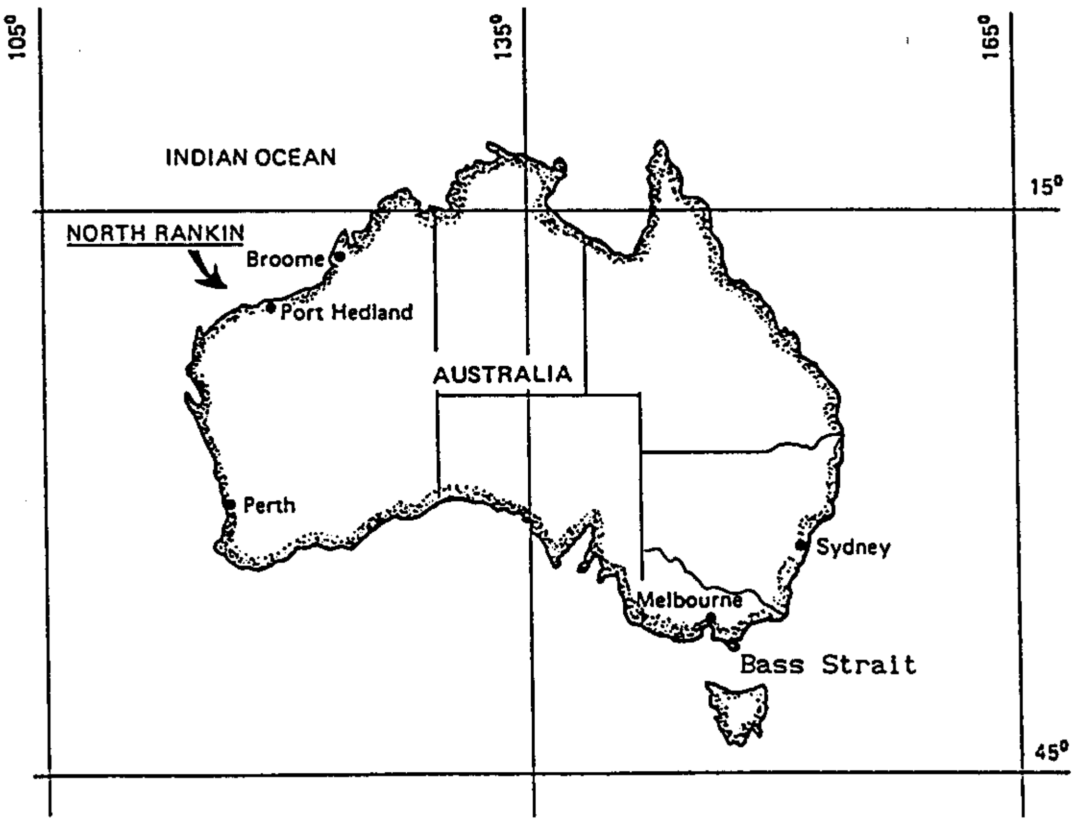

Fig. 2.5 Locations of Bass Strait and North Rankin production fields in Australia (after King et al., 1980)

CHAPTER 3

NUMERICAL MODELS FOR CYCLIC LOADING ANALYSIS

CHAPTER 3

NUMERICAL MODELS FOR CYCLIC LOADING ANALYSIS

3.1 INTRODUCTION

The main requirement of any analysis procedure is its ability to predict, with reasonable accuracy, the "output" response with changes in the "input" influencing parameters. This will enable "sensitivity" studies to be made of the influencing parameters without recourse to elaborate and often time-consuming laboratory and/or field studies. However, such analyses procedures have to be "calibrated" first against laboratory and/or field results to ensure its applicability.

While many methods of analysis are available for determining the static load-settlement response of single piles and pile groups (for example, Meyer *et al.*, 1975; O'Neill *et al.*, 1977; Randolph and Wroth, 1978; Poulos and Davis, 1980; Chow, 1986a; Armaleh and Desai, 1987; Kiousis and Elansary, 1987; Cheung *et al.*, 1988), those for response under cyclic loading condition are at present limited and far less satisfactory. As mentioned previously (chapter 2), cyclic loading may result in the degradation of the load capacity of the pile and the accumulation of permanent displacement, as cycling proceeds. Hence, any analysis method for the cyclic response of both single piles and pile groups must be able to model these two significant effects of cyclic loading. Failure may occur due to degradation of the pile capacity to a value less than the applied load value, or to excessive permanent displacement without significant capacity reduction.

This chapter will briefly review some of the numerical methods of analysis for the load-settlement response of piles subject to a quasistatic cyclic loading condition. These methods of analysis can be divided into two major groups, namely, the load-transfer approach and the continuum approach. The capabilities and limitations of these two different approaches will also be highlighted.

3.2 LOAD-TRANSFER APPROACH

The load-transfer (also known as "t-z") method of analysis, first proposed by Coyle and Reese (1966) for the static analysis of single piles, assumes the soil domain to behave as a "Winkler" soil. This "Winkler" soil concept assumes the soil domain to be represented by a series of independent discrete "springs". The response of each of these "springs" is further assumed to be affected only by the vertical displacement associated with that particular "spring". Therefore, the continuity of the soil domain, which results in the so-called interaction effect, has been ignored in the "Winkler" soil model. The term "Winkler" however is more commonly associated with laterally loaded pile analysis (also known as "p-y" analysis) while the term "load-transfer" (or "t-z") is commonly associated with axially loaded pile analysis. For the present axial pile problem, the soil domain surrounding the pile is thus represented by a number of such independent discrete "springs" acting along the length of the embedded pile. These "springs" define the shear stress-vertical displacement relationships ("t-z" curves) of the soil-pile system corresponding to a particular depth along the pile.

The main advantage of this load-transfer approach is the ability to ascribe any form of shear stress-vertical displacement relationship, whether linear or highly non-linear responses, to each of the "springs". These shear-displacement responses can be obtained from simple laboratory tests, such as the direct shear test or backfigured from an instrumented pile test. Empirical recommendations for such "t-z" curves have been suggested by, for example, Coyle and Reese (1966) and Holmquist and Matlock (1976) for piles in clay, and, for example, Coyle and Sulaiman (1967) for piles in sand. Simple semi-theoretical constructions for such "t-z" curves have also been suggested by Kraft *et al.* (1981a). Under cyclic loading, laboratory model cyclic pile test data (for example, Holmquist and Matlock, 1976) and cyclic shear test data (for example, Felio and Briaud, 1986) indicate the use of a "softened" (or "degraded") form of the "static" response is appropriate. However, the amount of "softening" required to account for such cyclic loading condition is, at present, highly empirical.

It is noteworthy that the t-z response obtained from a direct shear test represents a closer approximation to the no-interaction assumption utilised in the Winkler model, while the response backfigured from an instrumented pile test inevitably involves the interaction effect caused by the continuity of the soil medium. For analysis purposes, such recommended t-z curves, backfigured from instrumented pile tests, are utilised assuming they are specific to each particular depth along the pile. These recommended curves are preferred to those obtained from interface direct shear tests which are not capable of simulating many aspects of the complex pile-soil interaction response.

For pile group analysis, where continuity of the soil domain between the group piles has to be considered, the conventional load-transfer method proposed for single piles cannot be used. However, this limitation can be overcome by using a "hybrid" type of approach (O'Neill *et al.*, 1977; Chow, 1986a; Komaromy *et al.*, 1987) where the single pile response is represented by "t-z" curves while pile-soil-pile interaction is obtained using elastic continuum theory.

It is worthy of note that a modified load-transfer type of approach has been presented recently by Ooi *et al.* (1989), for the static analysis of single piles, where the influence of the normal pile-soil stress, due to a contractive or dilatant interface behaviour, is taken into account. The method is however numerically time-consuming and requires a number of empirical parameters to describe the yielding interface behaviour.

The extension of the load-transfer method to single piles that are subjected to quasistatic cyclic loading have been presented by, for example, Matlock and Foo (1980), Bea *et al.* (1984), Randolph (1986), Trochanis *et al.* (1987), Nadim *et al.* (1989), Abendroth and Greimann (1990) and Swinianski and Sawicki (1991). These methods are briefly reviewed in this section.

An extension of the numerical method developed by Matlock and Foo (1980), originally for analysing the driving of foundation piles by impact or vibration, is the ability to also analyse the quasi-static cyclic axial loading of piles. A hysteretic and degrading soil model (see equation 3.3 in section 3.3.1.2), in conjunction with an assemblage of "sub-elements" approach, is utilised by the writers. Although, theoretically, any desired nonlinear inelastic behaviour of the soil response could be simulated using the "sub-element" concept, the "prescriptions" for the sub-element responses are however highly empirical. This limitation increases as the number of sub-elements utilised in the numerical model increases.

The "sub-element" concept of Matlock and Foo (1980) has also been adopted by Bea *et al.* (1984) for the static and dynamic (or cyclic) response of both axially and laterally loaded single piles. In their approach (Bea *et al.*, 1984), any hysteresis or radiation damping associated with the dynamic pile-soil system can also be incorporated. However, no numerical solutions were presented by the writers for the cyclic axial response of cyclically-loaded piles.

The general form of the load-transfer curve as utilised in the computer program RATZ (Randolph, 1986) is shown in Fig. 3.1. It consists of three parts:

(i) an initial linear response up to a shear stress of $\xi_y \tau_p$, where τ_p is the peak skin friction and ξ_y is an empirical parameter between 0 and 1;

(ii) a non-linear parabolic response from $\xi_y \tau_p$ to τ_p;

(iii) a strain-softening response from τ_p to the residual value of skin friction τ_{res}, after an additional displacement Δw_{res} beyond the peak displacement, w_p.

This basic single pile load-transfer curve could be modified to approximately account for group piles effects by "softening" the elastic portion of the load-transfer curve, similar to that suggested by O'Neill *et al.* (1977). The influence of creep could also be approximately accounted for by "shifting" the load-transfer curve, with the amount of shifting obtained from the empirical expression suggested by Singh and Mitchell (1968).

Under cyclic loading, the accumulation of permanent displacement is simulated by the choice of the yield point on reloading (Randolph, 1986). The selection of this yield point, which is somewhat empirical and dependent on the parameter ξ_y, critically affects the amount of accumulated plastic displacement and degradation of the pile capacity. Furthermore, the accumulated plastic displacement is treated as equivalent to the plastic deformation under post-peak monotonic loading in assessing the amount of capacity degradation. It should be noted that under two-way symmetric loading, which causes yielding in both directions, the model predicts no net accumulation of permanent displacement, which is contrary to model laboratory test results (Lee, 1988). For such loading conditions, Randolph and Jewell (1989) have suggested that a plastic displacement equal to twice the width of the hysteresis loop be used to assess the degree of capacity degradation.

The cyclic loading analysis model adopted by Randolph (1986) is however limited to cases where the limiting resistance values in compression and tension are identical. Moreover, for a pile-soil system with a load-transfer curve that exhibits no post-peak strain-softening behaviour, the proposed model would suggest no degradation in pile capacity with cyclic loading. This is contrary to laboratory model test results where capacity degradation was observed for pile-soil interface that exhibits little or no post-peak strain-softening behaviour (Lee, 1988).

For the cyclic response of calcareous soil, the presence of very low resistance, under post-peak large displacement cycles or pre-peak cycles close to failure, has been observed (Fig. 3.2). This so-called "cyclic residual" response has been further modelled by Randolph and Jewell (1989) using a "gapping" approach, similar to that commonly used for laterally loaded pile analysis (for example, Swane and Poulos, 1982).

Trochanis *et al.* (1987) presented a load-transfer soil model, in conjunction with a finite element type solution procedure, for single piles subjected to quasistatic cyclic loading condition. The soil around the pile shaft is modelled by a number of bilinear elastic-plastic independent "springs" while the soil below the pile tip is modelled by a bilinear "spring" (Fig. 3.3). For cyclic or irregular loading and unloading , the soil model is governed by the well-known Masing (1926) rules. The degradation in strength or stiffness, as a result of cyclic loading, is incorporated by means of a simple empirical rule given by:

$$R_{i+1} = R_{ini} \left[1 - \phi \, (P_i - 0.5P_{ult})/P_{ult}\right] \tag{3.1}$$

where R = stiffness or strength of the "spring"; R_{ini} = the initial value of R; subscript i refers to the ith. cycle; ϕ = the degradation coefficient; $P_i \geq 0.5P_{ult}$ = the maximum load up to the ith. cycle; and P_{ult} = the ultimate yield load. It should be noted that the use of equation (3.1), whenever $P_i \geq 0.5P_{ult}$ in any cycle, is dependent on the arbitrary value of $0.5P_{ult}$ that has been adopted by the writers.

No results were presented by the writers for simulating the possible accumulation of permanent displacement under constant load cycling.

A more sophisticated multi-linear load-transfer soil model for cyclic loading has been adopted by Nadim *et al.* (1989), as shown in Fig. 3.4. The numerical model is conceptually similar to those used by Goulois (1982) for one-way cyclic loading, and Karlsrud *et al.* (1986) for the more general case of both one and two-way cyclic loading conditions. In all cases, the effects of cyclic loading are modelled through the use of "interaction diagram" and "degradation diagram" that relates the cyclic shear stresses and the amount of cyclic degradation respectively, to the number of load cycles. These interaction and degradation diagrams are however obtained from cyclic direct simple shear tests which may not truly simulate the actual complex pile-soil interface behaviour. The approach involves utilising these diagrams, in conjunction with the load-transfer analysis, iteratively until a "stable" solution is obtained. The possible accumulation of pile displacement, for cases where cyclic loading causes negligible pile capacity reduction, is not modelled by the writers.

Abendroth and Greimann (1990) utilised a nonlinear modified Ramberg-Osgood model to approximate the nonlinear soil resistance-displacement behaviour under axial and lateral loading conditions. The soil response is represented by a number of independent, uncoupled vertical and horizontal nonlinear Winkler "springs". The nonlinear "spring" response is obtained by curve-fitting the modified Ramberg-Osgood expression to the experimentally measured soil resistance-displacement relationships. For cyclic loading, the writers adopted the suggestions of Pyke (1979) for establishing the unloading and reloading curves. Limited results presented by the writers for the first cycle, under lateral loading alone, show similar trends between the numerical solutions and the experimental results. However, comparisons between numerical solutions and experimental results for greater numbers of cycles of loading are required to fully assess the numerical approach adopted. No results were presented by the writers for the cyclic axial pile response. The numerical approach suggested also does not model the degradation of pile capacity under cyclic axial loading conditions.

In the numerical approach of Swinianski and Sawicki (1991), the pile-soil interface response is governed by bilinear elastic-plastic load-transfer curves. The degradation (i.e. softening) of the load-transfer curves, as a result of cyclic loading, with increasing cycles is calculated based on a compaction theory for granular materials. The approach involves calculating the decrease in the normal pile-soil interface stress by using the compaction theory. This decrease in the normal pile-soil interface stress will in turn result in a reduction of the limiting value of the pile-soil interface shear stress. Any accumulation of permanent pile displacement is not explicitly modelled in the approach described by the writers, but may arise as a result of a softened (i.e degraded) load-transfer curves. Moreover, the empirical coefficients describing the compaction of a given granular material need to be obtained from a series of tests using the cyclic simple shear device. The approach is also limited to the quasistatic cyclic axial loading of piles in granular materials.

It may also be noted that a single element interface constitutive model, in conjunction with a Winkler-type model for the soil (or rock) domain, has been presented by Ooi *et al.* (1988) for the response of one-way pre-peak cyclic loading condition. This cyclic model, developed specifically for cemented material, takes into account the influence of the normal pile-soil stress, due to a contractive or dilatant interface behaviour, that is not accounted for in the conventional load-transfer analysis. The accumulation of shear displacement and the degradation of interface shear capacity are assumed to be caused by the degradation of the cohesive component of shear strength, with load reversal. This single element model has been used successfully, although it may be computationally time-consuming, by the writers for the static load-transfer analysis of a single pile (Ooi *et al.*, 1989). The extension of this single element cyclic model to the cyclic response of single piles, however, remains to be carried out.

3.3 CONTINUUM APPROACH

The elastic continuum methods of analysis includes the integral equation (also known as boundary element) methods and the finite element methods. Unlike the load-transfer approach mentioned earlier (section 3.2), the continuity of the soil domain is maintained in this continuum approach. Hence, the response at a particular node along the pile will affect, and is also affected by, the responses at all other nodes. The continuum approach, therefore, represents a more realistic simulation of the pile-soil system.

For static analysis, the finite element method (Desai, 1974; Valliappan *et al.*, 1974; Ottaviani, 1975; Pressley and Poulos, 1986) is very versatile but is however too expensive for routine analysis. Furthermore, for cyclic loading analysis, where repeated iterations are required, the use of a computationally economical method is highly essential and desirable. In this regard, the integral equation methods appear to be a "better" method particularly for problems of low surface to volume ratio (Banerjee, 1976).

The following sub-sections will briefly review the analysis methods that have been developed for determining the load-settlement response of a cyclically-loaded pile in both categories of the continuum approach, namely, the boundary element methods and the finite element methods.

3.3.1 Boundary Element Method

The static analysis of the load-settlement response of single piles and pile groups, using the boundary element methods, generally employ Mindlin's (1936) solutions for a homogeneous, isotropic elastic half-space (Poulos and Davis, 1968; Butterfield and Banerjee, 1971a). Approximate procedures utilising Mindlin's solutions to account for non-homogeneous soil profile have also been used (Poulos, 1979b; Poulos and Mattes, 1969; Yamashita *et al.*, 1987; Lee and Poulos, 1990). The use of Mindlin's solutions, which is strictly applicable to a homogeneous soil, for such non-homogeneous soil profiles is due to the non-availability of analytical solutions for a general multi-layered soil profile. However, an analytical solution for the particular case of a two-layered elastic soil profile is available and has been used for such static analysis (Banerjee and Davies, 1978, 1980; Lee *et al.*, 1987; Chow *et al.*, 1990).

While the static analysis of the load-settlement response of single piles and pile groups is well established, that for the cyclic response is however less satisfactory. The cyclic response analyses that have been developed are "extensions" of the static analyses, with empirical rules being generally used to model the interface behaviour due to cyclic loading (Poulos, 1988a).

The analysis models of Poulos and co-workers seem to be the only published simplified continuum boundary element approach for determining the cyclic load-settlement response of single piles and pile groups. This review is further divided into three sub-sections, namely, the effective and total stress methods for determining the cyclic degradation of pile capacity, and finally, the permanent displacement accumulation model.

3.3.1.1 Effective stress methods

Poulos (1979a) described an analysis procedure, with an "elastic-plastic" soil model, for the cyclic response of single piles using a simplified boundary element method (Fig. 3.5). The effects of cyclic loading are assumed to be caused by the generation of pore-water pressure, with increasing cycles. The analysis is based on an effective stress approach where the generation of pore-water pressure is related to the cyclic shear stress through the empirical expression obtained by Van Eekelen and Potts (1978) for Drammen Clay. The loading rate effects on the soil modulus, ultimate skin friction and ultimate base resistance are approximately accounted for by using the empirical expression suggested by Sangrey (1977). This rate effect is quantified by the factor D_r (= S_{ut}/S_{ur}; where S_{ut} = the soil parameter value at the actual loading rate, and S_{ur} = the corresponding soil parameter value at the reference "static" loading rate) as given below:

$$D_r = 1 + F_\rho \log_{10}(\lambda_m/\lambda_r) \tag{3.2}$$

in which λ_r = reference loading rate (e.g., for static load test); λ_m = actual loading rate; and F_ρ = rate factor (for example, typically 0.1 to 0.25 for piles in clay; Poulos, 1989a).

A "single step" approach is utilised where the behaviour of the pile after a specified number of cycles is determined. This approach therefore does not allow the response of the pile at the end of each cycle to be determined. Briefly, the "single step" approach proceeds as follows (Fig. 3.6):

— the pile is analysed for the maximum load and then the mininum load, as for a static analysis;
— the generated pore-water pressure is then obtained through an empirical expression, and the degradation of pile capacity and/or stiffness of the soil are calculated based on an effective stress method. The analysis is then repeated until the desired degree of convergence is attained.

The approach (Poulos, 1979a) is however limited to a given number of uniform load cycles, and the accumulation of permanent displacement (see section 3.3.1.3) is also not modelled.

A similar approach to that of Poulos (1979a) has also been presented by Lee and Poulos (1988b) where a more rigorous pore-water pressure generation and dissipation analysis, developed by Booker *et al.* (1976), is employed. The approach can cater for irregular cyclic loading condition through the use of an equivalent number of uniform stress cycles (Seed *et al.*, 1975), but is however limited to single friction piles with negligible end-bearing developed. It may be noted that other empirical pore-water pressure generation expressions with increasing cycles have also been proposed (for example, Dobry *et al.*, 1988; Kaggwa *et al.*, 1988) and can similarly be used in this approximate pile-soil cyclic response analysis.

In both methods mentioned above (Poulos, 1979a; Lee and Poulos, 1988b), the degradation of pile capacity with cyclic loading is caused by an increase in the pore-water pressure. The degradation in pile capacity due to mechanical (or "physical") degradation (for example, volumetric changes due to crushability of the material) is however not considered in both methods.

3.3.1.2 Total stress methods

To overcome the limitations of the effective stress approach, a total stress approach has been developed (Poulos, 1981, 1982a, 1983, 1984, 1989; Hewitt, 1988; Lee, 1988) where the degrading effects of cyclic loading on pile capacity are obtained through the use of empirical degradation factor "charts" and/or the "reverse-slip" degrading model of Matlock and Foo (1980). The degradation factor expresses the value of a soil parameter (for example, the pile-soil skin friction) after cyclic loading as a ratio of the corresponding value for static loading.

This degradation "chart" relates the degradation factor (for skin friction and/or base resistance) to the cyclic displacement, and is obtained from model test results. It is at present not conclusive as to whether the degradation factor is dependent on the absolute value or relative (to diameter) value of cyclic (or cyclic slip) displacement (Poulos, 1989a). As mentioned in section 2.3.1.4, limited results obtained by Lee (1988) seem to suggest dependence on the relative (to diameter) value of cyclic slip displacement (defined as the cyclic displacement in excess of that required to cause static slip). This "cyclic slip displacement" model is shown in Fig. 3.7.

The "reverse-slip" degrading model, developed by Matlock and Foo (1980), is given by the following expression:

$$D_{\tau} = (1 - \lambda)(D' - D_{lim}) + D_{lim} \tag{3.3}$$

where D_{τ} = current value of degradation factor; D' = degradation factor for previous cycle; D_{lim} = degradation factor for a large number of cycles; λ = degradation rate parameter. Equation (3.3) is used to calculate a new value of the degradation factor whenever slip occurs in both directions in a cycle; otherwise, the degradation factor remains unchanged at the value for the previous cycle. It may be noted that different values of D_{lim} and λ may be applicable for the shaft and base elements, although limited laboratory results indicate no significant degradation of end-bearing capacity with cyclic loading (Poulos, 1989a). Tentative values of D_{lim} and λ for piles in calcareous sediments are suggested by Poulos (1988a).

The soil modulus degradation due to cyclic loading can be approximately accounted for in the above analyses (Poulos, 1981, 1983; Hewitt, 1988) by using the empirical expression obtained by Idriss *et al.* (1978):

$$D_E = N^{-t} \tag{3.4}$$

in which D_E = modulus degradation factor; N = number of cycles; and t = degradation parameter depending on the cyclic strain. However, as pointed out by Poulos (1989a), results from model pile tests in calcareous sands suggest that there is no significant degradation of modulus during cycling, although it may be of some significance for piles in clay (see for example, Briaud and Felio, 1986).

The "cycle-by-cycle" approach is adopted in the above analyses where the degradation factors at the end of each cycle are obtained from the desired degradation model. The analysis is then repeated for the next cycle until the required number of cycles is simulated. Results from such analysis have been presented in the form of a "cyclic stability" diagram (Poulos, 1988b) which defines the response of the pile to various combinations of mean and cyclic loads. Such a "stability" diagram has great potential for use in assessing the cyclic pile response.

The analyses described thus far only model one aspect of cyclic loading; the degradation of pile capacity. The other important aspect of permanent displacement accumulation , particularly under non-zero mean load, is summarised in the next section.

3.3.1.3 Permanent displacement accumulation

There is as yet no reliable theory for predicting the permanent displacement of piles (Poulos, 1988a). However, approximate numerical procedures have been developed (Poulos, 1988a; Lee, 1988) to simulate this permanent displacement accumulation.

Poulos (1988a,1989a) presented an approach where the incremental permanent soil displacements, for both shaft and base elements, at the end of each cycle are calculated from an empirical expression obtained by Chua (1983), based on the work of Diyaljee and Raymond (1982), and is given by:

$$\delta S_p = S_{PN} \left[n\delta X + (m\delta N/N) \right] \tag{3.5}$$

where δS_p = increment in permanent soil displacement between cycles N and N+δN; δX = change in mean stress level between cycles N and N+δN; S_{PN} = permanent soil displacement at cycle N; m,n = experimentally determined parameters (different values applicable for shaft and base elements; Poulos, 1988a). These incremental permanent displacements are then treated as "external" soil movements, similar to that used for negative friction analysis due to a consolidating soil (Poulos and Davis, 1972), for the next cycle of analysis. Thus, the "imposed" external soil movements will result in increased permanent displacement of the pile. It may be noted that there is as yet no clear definition for the mean stress level, X (see equation 3.5). Based on limited experience, Poulos (1986) has assumed and adopted the stress level X as given by equation (3.6) below:

$$X = [(\tau_o \tau_c/2)^{0.5}]/\tau_f \tag{3.6}$$

where τ_o = the average stress at an element; τ_c = the elemental cyclic stress (half-amplitude). Different definitions for the stress level X have also been adopted by Poulos (1988c) and Poulos (1989c), as given by equations (3.7) and (3.8) respectively:

$$X = (\tau_o + 0.5\tau_c)/\tau_f \tag{3.7}$$

$$X = (P_o + 0.5P_c)/Q_c \tag{3.8}$$

where τ_f = the elemental static failure stress
P_o = mean load of loading parcel
P_c = cyclic load (half-amplitude) of loading parcel
Q_c = peak static pile capacity.

An alternative procedure (an extension of the basic pile analysis approach described by Poulos and Davis, 1980) for single piles has also been presented by Lee (1988), in conjunction with a non-linear Ramberg-Osgood soil model (Fig. 3.8), for simulating the accumulation of permanent pile displacement. The approach involves degrading the secant soil modulus on the reloading part of each cycle, similar to that used by Idriss *et al.* (1976) for computing the response of soft clay deposits under earthquake loading condition. The secant soil modulus after cycling, E_{sec}, is defined in terms of a secant modulus degradation factor, δ (Lee, 1988) given by:

$$\delta = E_{sec} / E_{ss} \tag{3.9}$$

in which E_{ss} = initial secant modulus. The value of δ for each cycle is then evaluated from the expression (Lee, 1988):

$$\delta = \delta_p - 0.5\psi X [\delta_p]^{(1+\psi X)/\psi X} \tag{3.10}$$

$$\text{and } X = (\tau_o + 2\tau_c)/2\tau_f \tag{3.11}$$

where δ = secant modulus degradation factor for the current cycle; δ_p = secant modulus degradation factor of previous cycle; X = the current normalised representative stress level, with the cyclic stress assumed to be twice as significant as the average stress; ψ = an accumulation rate parameter which is a function of soil and pile types, and all other parameters as defined earlier. It may be noted that the representative stress level X, as utilised by Lee (1988), is different from those adopted by Poulos (1986, 1988c, 1989c) mentioned earlier.

The approach (Lee, 1988) is however numerically more time-consuming than that of Poulos (1988a), as it involves an incremental analysis for each cycle of loading. The resulting non-uniform soil moduli along the pile are catered for by using the approximate approach of Poulos (1979b) in evaluating the soil influence coefficients.

It is worthy of note that both of the approaches mentioned (Poulos, 1988a, 1989a; Lee, 1988), for simulating the accumulation of permanent pile displacements, involve the use of empirical parameters (see equations 3.5 and 3.10) that have to be determined from model pile tests. Limited values for such parameters have been reported by Poulos (1988a) and Lee (1988).

The approach model developed by Poulos, as described previously, has been extended by Hewitt (1988) for the case of vertical pile groups consisting of dissimilar piles. Extension of the simplified boundary element method to a displacement softening interface behaviour (Fig. 3.9) has also been described by Poulos (1988a). For such interface behaviour, cyclic loading may result in "degradation" of pile capacity caused by the accumulated permanent displacement beyond that required for the peak static resistance. This degradation has been termed "static degradation" factor to differentiate between the "cyclic degradation" factor due to the effects of cyclic loading (Poulos, 1988b; Booker *et al.*, 1989). The lesser value (i.e. more degradation) from these two sources of degradation is used in the analysis (Booker *et al.*, 1989). For piles subjected to "storm loading" condition consisting of different parcels of cyclic loading, an approximate "equivalent number of cycle" approach, similar to that suggested by Van Eekelen (1977), is used (Poulos, 1988c)

3.3.2 Finite Element Method

The finite element method, which involves a discretization of the whole problem domain, is less attractive as a numerical tool compared to the boundary element method, particularly for problems involving a low surface to volume ratio. Furthermore, for cyclic loading, where repeated iterations are required, the cost of such analysis would be prohibitively expensive. These factors, coupled with the absence of a suitable simple constitutive model for the cyclic behaviour of soils, have limited the use of the finite element method for the cyclic response analysis of piles.

Boulon *et al.* (1980) have presented a finite element approach in conjunction with a simplified hyperbolic description of the accumulated permanent strains of the soil. These accumulated permanent strains in the soil, for a given number of cycles, are treated as an "initial strain" problem in the analysis. The effects of cyclic loading, on the limiting friction capacity of granular soils, is implicitly accounted for by the change in the computed normal pile-soil stress. For cohesive soils, where a total stress method is adopted for the computation of limiting friction capacity, it is however not clear with regard to the modelling of the effect of cyclic loading on pile capacity.

Although material models for cyclic behaviour of sands (for example, Ghaboussi and Momen, 1982) and those for clays (Carter *et al.*, 1982; Prevost, 1977) have been proposed, their incorporation into a finite element analysis for the cyclic response of piles are at present numerically complex and impractical, if not impossible. Because of this complexity, the finite element method is considered less "superior" than the simplified boundary element method described earlier where the effects of cyclic loading can be easily incorporated, albeit approximately.

3.4 SUMMARY

While the static analysis of single piles and pile groups is well established, the corresponding analyses for piles subjected to quasistatic cyclic loading conditions are far less satisfactory. The cyclic axial loading of piles is an interesting but difficult problem. This is due to the difficulty of accurately modelling the complex cyclic response of the pile-soil system. Each of the analysis methods reviewed has its own empirical or semi-empirical rules to model certain aspects of the cyclic response of the pile-soil system.

Two general approaches for the cyclic response analysis of single piles are available, namely, the load-transfer approach and the continuum approach (see Tables 3.1 and 3.2). The load-transfer approach is more "versatile" in that it can cater for highly non-linear t-z response, but however suffers from the disadvantages that the continuity of the soil domain is ignored, and group pile effects can only be approximately accounted for. The continuum approach, which considers continuity of the soil domain and where group pile effects are directly accounted, may however be computationally more time-consuming. In both approaches, the effects of cyclic loading can only be approximately modelled, particularly the accumulation of permanent displacement. In view of this, the use of a more refined method of analysis such as the finite element method, at present, may not be justifiable. Moreover, for such cyclic loading analysis, the use of a simple and computationally less time-consuming numerical approach is highly essential and desirable. To this end, a simple and efficient nonlinear load transfer (t-z) approach is presented in the present study, and will be described in Chapter 4.

The numerical approaches described are, in general, applicable to any soil type provided that the relevant input parameters, corresponding to the soil type considered, be used. Although constitutive cyclic soil models have been proposed, their incorporation into an efficient and "practical" pile-soil cyclic analysis remain a difficult and complex task.

Finally, as for any analysis approach, the empirical parameters describing the cyclic model have to be determined. Although a model with more parameters may give more flexibility in its use, the corresponding increased difficulty in obtaining these parameters may well defeat its use. The criterion then is to use a cyclic pile-soil model that has as few parameters as possible and at the same time is able to simulate satisfactorily the two cyclic phenomena of capacity degradation and accumulation of permanent displacement.

Table 3.1 Summary of some available cyclic analysis programs for axially loaded vertical piles.

Program name	Reference	Remarks
CYCESP	Poulos (1979a)	Continuum-based "single step" analysis. Effects of cyclic loading assessed from generated pore-water pressure response using an "effective stress" approach. Dissipation of generated excess pore-water pressure not considered. Permanent displ. accumulation not modelled.
DRIVE 7	Matlock and Foo (1980)	A discrete-element wave equation analysis originally developed for pile driveability analysis. Can cater for quasi-static cyclic axial loading of piles. Cycle-by-cycle approach in conjunction with a "reverse slip" capacity degrading model. Permanent displ. accumulation obtained as a result of capacity degradation.
RATZ	Randolph (1986)	Cycle-by-cycle "t-z" analysis. Capacity degradation and permanent displacement accumulation governed by choice of yield point on reloading. A "total stress" approach adopted.
CESPRAP	Lee and Poulos (1988b)	Continuum-based cycle-by-cycle analysis. "Effective stress" approach utilised in conjunction with a pore-water pressure generation and dissipation analysis. Permanent displacement accumulation not modelled.
SCARP	Poulos (1989c)	Continuum-based cycle-by-cycle analysis. "Total stress" approach utilised. Capacity degradation modelled using Matlock and Foo (1980) model or from empirical degradation "charts". Permanent displ. accumulation simulated using "external soil movements" approach.
AXCAP	Lee (1988)	Continuum-based cycle-by-cycle analysis. "Total stress" approach utilised. Matlock and Foo (1980) model or empirical degradation "charts" used to model capacity degradation. Permanent displ. accumulation simulated using a "degrading secant modulus" approach.

Table 3.2 Summary of input parameters required for cyclic axial loading analysis.

Program name	Input parameters required for cyclic loading analysis
CYCESP	- coefficient of earth pressure at rest, K_o - the initial vertical effective stress, σ'_{vo} - the initial overconsolidation ratio (OCR) of the soil - variation of the undrained modulus of the soil to the OCR value The generated pore-water pressure with increasing cycles is then determined from the empirical expression suggested by Van Eekelen and Potts (1978).
RATZ	- the parameter ξ_y which controls the initial static (monotonic) loading as well as the unloading-reloading response. Since the cyclic loading effect of capacity degradation is directly related to the post-peak strain-softening response, the following parameters are also required: - peak shear stress, τ_p - residual shear stress, τ_r - cyclic residual shear stress, τ_{cr} - displacement from peak to residual stress, Δw_{res}
CESPRAP	Similar to program CYCESP but with the use of a more rigorous pore-water pressure generation and dissipation analysis developed by Booker et al. (1976). Parameters required are: - variation of number of cycles to cause liquefaction, N_l, with cyclic stress level - equivalent number of uniform cycles, N_{eq} - time duration of cyclic loading, T_D - variation of soil empirical constant, Θ, with cyclic stress level - coefficient of volume compressibility, m_v - effective unit weight of soil - coefficients of permeability in radial and vertical directions (K_r, K_z respectively) - the cyclic soil parameters μ and α.

(Table 3.2 continues next page)

Table 3.2 (continued)

SCARP	- degradation rate parameter for soil modulus, λ_E - minimum degradation factor for soil modulus, D_{Elim} - standard (static) loading rate, ζ_r - peroid of cyclic loading, T_c - rate factors for shaft and base resistances ($F_{\rho s}$, $F_{\rho b}$) - rate factor for soil modulus, $F_{\rho m}$ If Matlock and Foo (1980) capacity degradation model utilised, the required parameters are: - degradation rate parameters, λ_τ (shaft) and λ_b (base) - the min. degrad. factors, $D_{\tau lim}$ (shaft) and D_{blim} (base) If empirical degrad. factors "charts" utilised, then - variation of relevant degrad. factors with the adopted cyclic displacement function (three options available). Note that a similar equation to that of Matlock and Foo (1980) model is utilised for determining the degrad. factor at any cycle. For permanent displacement accumulation, - parameters m_s, n_s for shaft elements - parameters m_b, n_b for base element. If reduction factors for skin friction, base resistance and soil modulus due to pore-water pressure generation required, - pore-water pressure parameters μ, α
AXCAP	- the nonlinear modified Ramberg-Osgood soil parameters R and α For capacity degradation, - Matlock and Foo (1980) model (as for "SCARP" above) in conjunction with a "cyclic displacement" empirical degradation factor "chart". For permanent displacement accumulation, - the accumulation rate parameter, ψ
DRIVE 7	At each node point, - initial nonlinear inelastic resistance-displacement relationship for the pile-soil system - maximum friction force which will be developed - minimum friction force which will be maintained after many reversals of plastic slip - degradation rate parameter, λ.

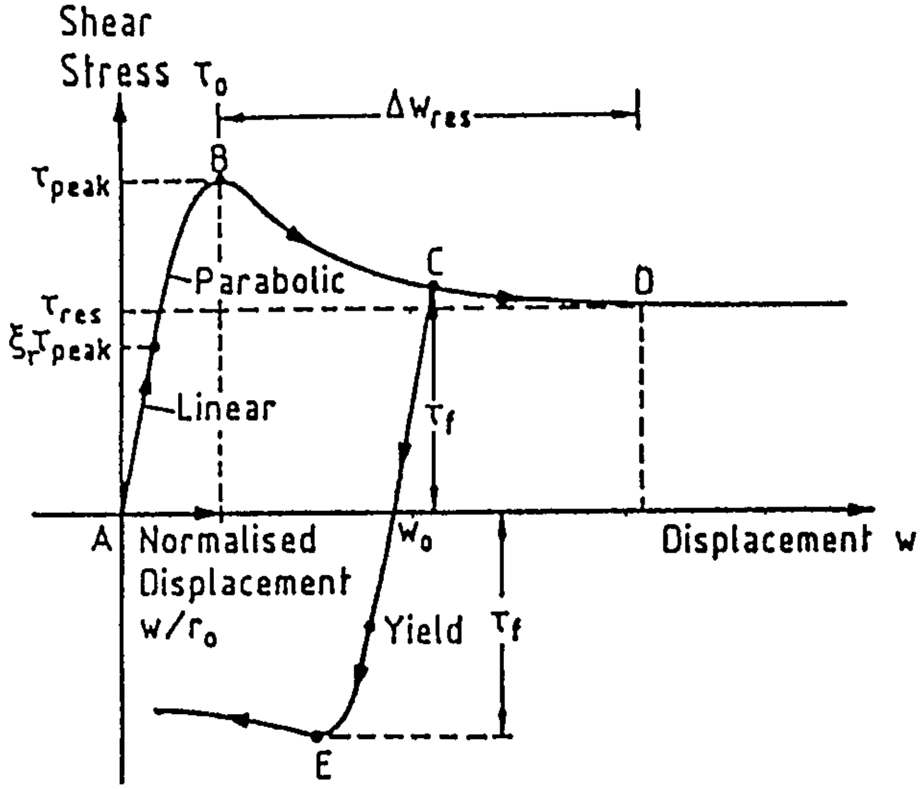

Fig. 3.1 Load transfer curve for program RATZ (after Randolph, 1986)

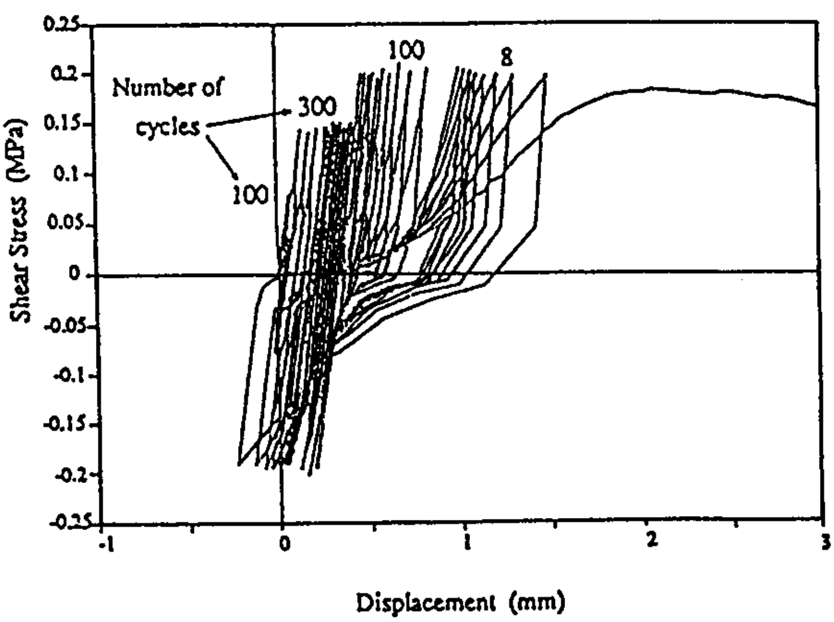

Fig. 3.2 Two-way cyclic rod shear test in calcarenite (after Randolph and Jewell, 1989)

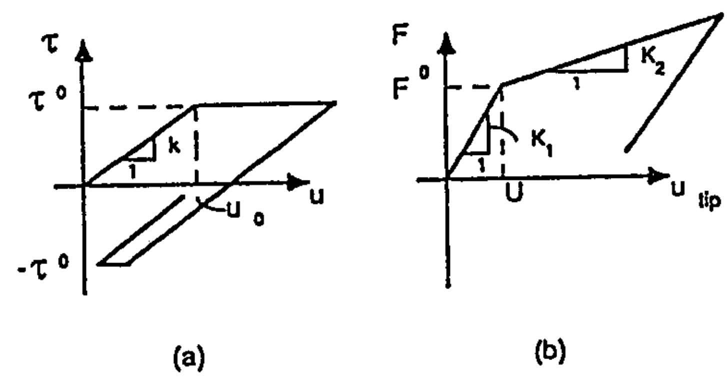

Fig. 3.3 Force-displacement relationships: (a) Shear layer; (b) Tip spring (after Trochanis et al., 1987)

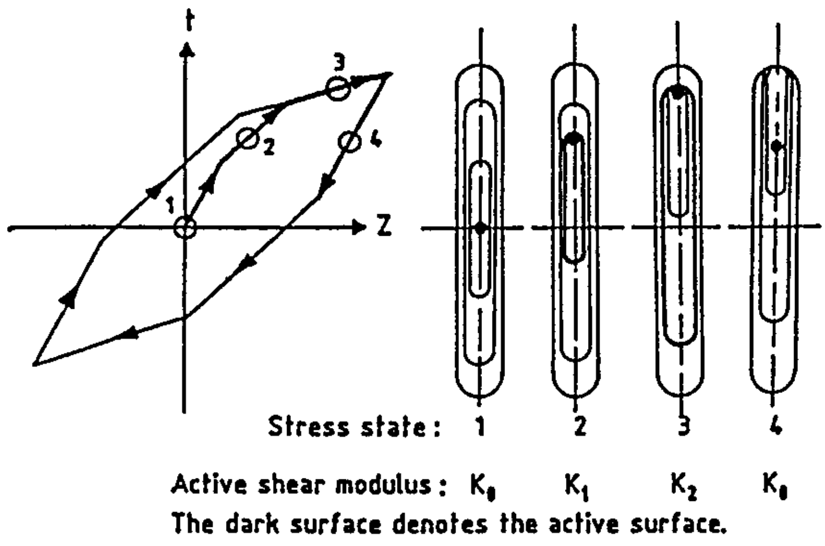

Fig. 3.4 Load transfer soil model as adopted by Nadim et al. (1989)

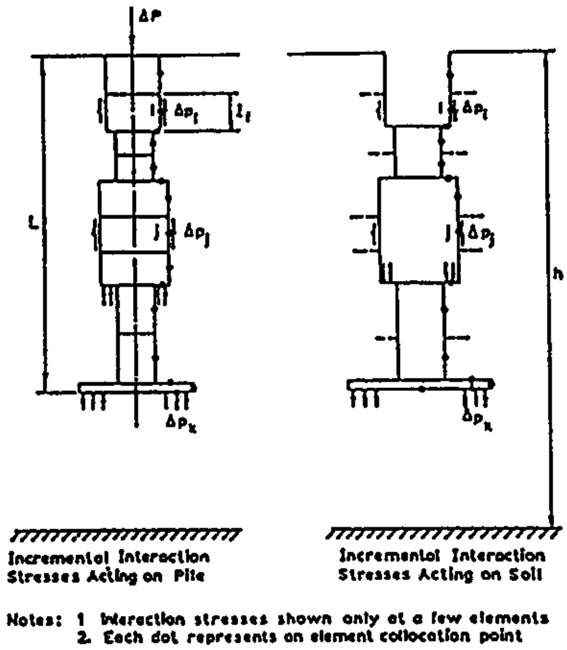

Fig. 3.5 Simplified boundary element method - division of pile into elements (after Poulos, 1979a)

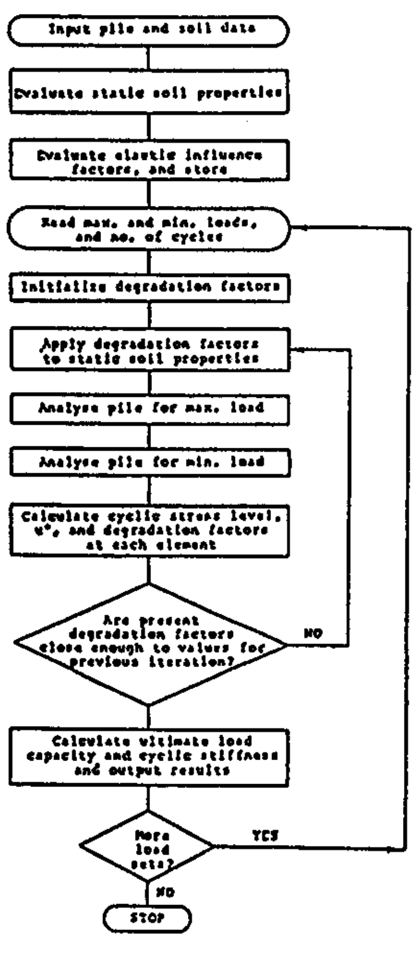

Fig. 3.6 Flow diagram for cyclic loading analysis (after Poulos, 1979a)

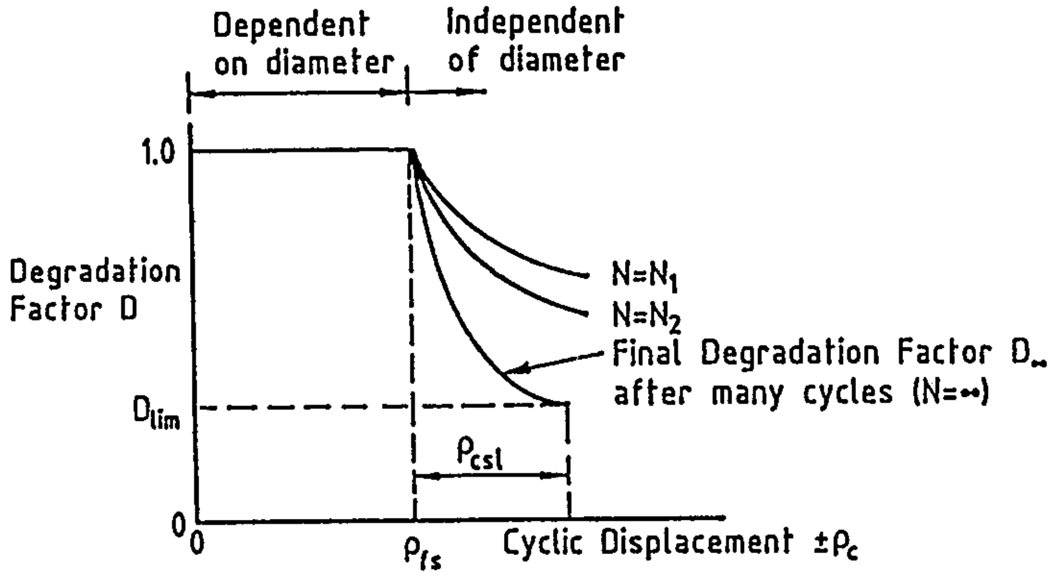

Degradation depends on cyclic slip displacement:

$$\rho_{cs} = \rho_c - \rho_{fs}$$

where ρ_{fs} = displacement required to cause static slip

Cyclic slip displacement required to cause maximum possible degradation = ρ_{csl} (independent of pile diameter)

Fig. 3.7 Model for cyclic degradation of skin friction (after Poulos, 1989a)

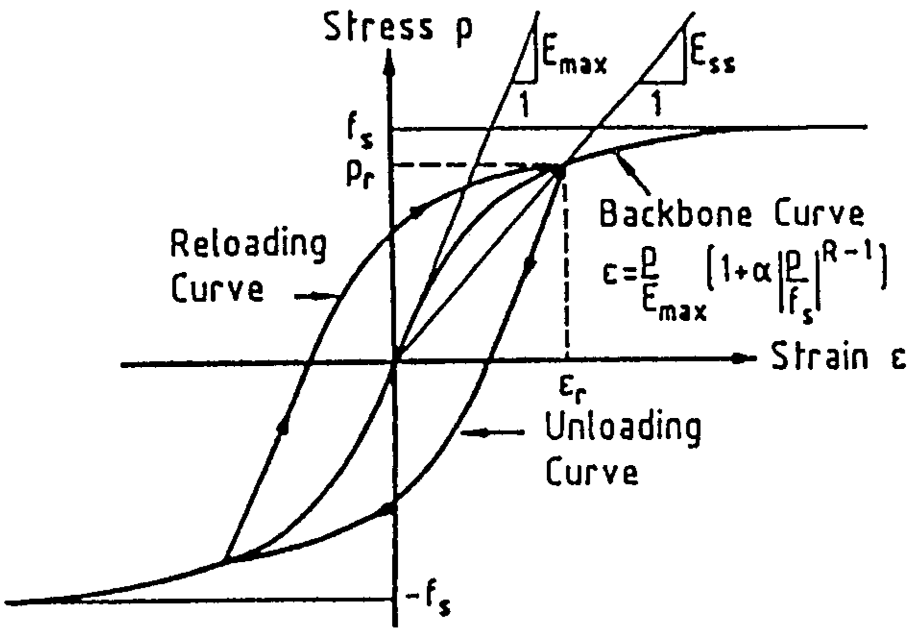

Fig. 3.8 Nonlinear Ramberg-Osgood interface model as utilised by Lee (1988)

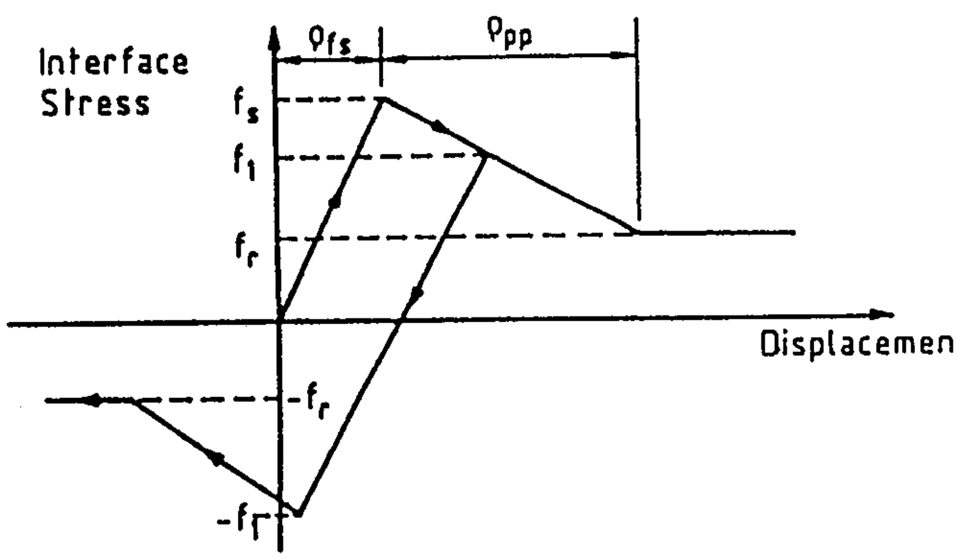

Fig. 3.9 Displacement-softening model of static interface behaviour (after Poulos, 1988a)

CHAPTER 4

METHOD OF ANALYSIS FOR AXIAL PILE RESPONSE

CHAPTER 4

METHOD OF ANALYSIS FOR AXIAL PILE RESPONSE

4.1 INTRODUCTION

As mentioned in Chapter 3, the static analysis of single piles and pile groups can be grouped into two broad approaches, namely, the load-transfer approach and the continuum approach. In the continuum approach, the boundary element method is more suited to problems of low surface to volume ratio (Banerjee, 1976).

The boundary element method generally employs Mindlin's (1936) solutions for a homogeneous, isotropic elastic half-space. For non-homogeneous soil profiles, approximate analyses using Mindlin's homogeneous solutions have been used. In practice, piles are usually used to penetrate a relatively homogeneous upper soil layer to socket into a stiffer underlying bearing stratum. For such a soil profile, the use of analytical solution for a layered soil is theoretically more correct than the approximate analyses utilising Mindlin's homogeneous solution.

This chapter therefore presents the method of analysis for the static response of single piles and pile groups embedded in a two-layered soil profile, with the homogeneous profile as a special case. The elastic analytical solution of Chan *et al.* (1974) for a two-layered soil profile is utilised in conjunction with a simplified boundary element method. The two-layered soil profile is particularly relevant to the case of a lightly overconsolidated clay overlying a heavily overconsolidated clay, or the case of a lightly cemented soil overlying a stronger cemented soil. For other soil profiles, such as a Gibson soil (where the soil modulus increases linearly with depth), an approximate approach is used. Finally, extension of the static analysis to the cyclic response of single piles and pile groups is presented. In particular, the development of the computationally more efficient nonlinear hyperbolic "t-z" programs (SPILE3 and SCPIL3) is presented.

4.2 STATIC RESPONSE ANALYSIS

The static response of axially loaded vertical pile groups embedded in a two-layered soil profile is formulated in the following sub-section. It should be noted that although the formulation is for a pile group, that for a single pile can similarly be analysed by considering one pile. Analyses involving different representations of the soil behaviour are presented; elastic-plastic (bilinear) continuum model, nonlinear hyperbolic continuum model and the nonlinear hyperbolic t-z "hybrid" model.

4.2.1 Elastic-Plastic Continuum Model (SPILE1)

The problem of an axially loaded vertical pile group embedded in a layered soil is shown in Fig. 4.1. The pile cap is assumed to be not in contact with the ground since a contacting cap has been shown to have non-significant effect on the group stiffness at normal working loads (Butterfield and Banerjee, 1971b; Chow and Teh, 1991).

The upper soil layer is of thickness h, with Young's modulus E_1, Poisson's ratio ν_1, overlying an infinite lower layer of modulus E_2 and Poisson's ratio ν_2. The pile socket length is e, making the total pile length ℓ = h+e. The decomposed system of the pile group problem results in the group piles being acted on by the pile-soil interaction forces $\{P_p\}$ and the external applied loads $\{P\}$ while the "extended" soil continuum is acted on by the pile-soil interaction forces $\{P_s\}$.

The group piles are divided into a finite number of elastic discrete bar elements with an axial mode of deformation. The stiffness matrices of the pile elements (see, for example, Smith, 1982) are assembled to give the following load-deformation relationship for the group piles (Chow, 1987):

$$[K_p]\{w_p\} = \{P_p\} + \{P\} \tag{4.1}$$

where $[K_p]$ is the assembled stiffness matrix (size nxn) of all elements of the group piles, $\{w_p\}$ is the vector (size n) of the nodal pile displacements, $\{P\}$ is the vector (size n) of external applied loads, $\{P_p\}$ is the vector (size n) of the pile-soil interaction forces acting on the pile, and n is the total number of nodes forming the pile.

For the extended soil continuum, the displacement at node i, w_{si} due to the pile-soil interaction forces $\{P_s\}$ (vector of size n) is given by:

$$w_{si} = \sum_{j=1}^{j=n} f_{ij} \, P_{sj} \tag{4.2}$$

where f_{ij} is the flexibility coefficient denoting the displacement at node i due to unit interaction force at node j, and n is the total number of nodes. The main difference between most of the boundary element continuum approaches available lies in the method adopted to evaluate the flexibility coefficient f_{ij}. As mentioned earlier, Mindlin's solution is generally used for the evaluation of f_{ij} (Poulos, 1979b; Butterfield and Banerjee, 1971a; Yamashita *et al.*, 1987). A rigorous approach for evaluating f_{ij} for a general soil profile, with elastic isotropic properties, using an axi-symmetric finite element procedure has also been suggested by Chow (1986b). This approach was further extended by Chow (1989) for the case of a cross-anisotropic elastic soil. The finite-layer numerical technique, applicable to an isotropic or cross-anisotropic elastic soil, has also recently been utilised by Lee and Small (1991) for these evaluations. For the present analysis, the analytical two-layered solution of Chan *et al.* (1974) is used for the evaluation of f_{ij}. Explicit expressions for the layered solutions are given in Appendix 4A.

For nodes on the same pile, f_{ij} is determined based on a uniformly distributed force over element node j using the Gaussian quadrature method. Details of the integration procedure are given by Chin (1988) and are reproduced in Appendix 4B. For normal pile spacings (3 to 5 diameters), f_{ij} can be obtained with sufficient accuracy by using a unit point load for interaction between nodes of different piles, resulting in considerable reduction in the computation time required without sacrificing the accuracy (Chin *et al.*, 1990).

Assembling equation (4.2) for all the nodes leads to the following flexibility equation for the soil continuum:

$$\{\mathbf{w}_s\} = [\mathbf{F}_s]\{\mathbf{P}_s\} \tag{4.3}$$

where $[\mathbf{F}_s]$ is the soil flexibility matrix (size nxn) and $\{\mathbf{w}_s\}$ is the vector (size n) of nodal soil displacements. Inverting equation (4.3) leads to the stiffness equation for the soil continuum:

$$\{P_s\} = [K_s]\{w_s\} \tag{4.4}$$

where $[K_s] = [F_s]^{-1}$ is the soil stiffness matrix (size nxn).

For elastic conditions, compatibility at the pile-soil interface requires $\{w_p\} = \{w_s\}$ and $\{P_p\} = -\{P_s\}$. From equations (4.1) and (4.4), the following global stiffness equation for the pile group problem is obtained:

$$[K_T]\{w_p\} = \{P\} \tag{4.5}$$

where $[K_T] = [K_p]+[K_s]$ is the assembled stiffness matrix (size nxn) of piles and soil.

Equation (4.5) can be solved for a prescribed load (i.e. flexible pile cap), or prescribed pile head displacement (corresponding to a rigid pile cap) using the "big-spring" technique (Smith, 1982). The pile group problem, under a prescribed axial load, with a rigid pile cap can similarly be simulated by "tying" the pile heads of the group piles with rigid bending elements of an arbitrary large stiffness. The bending element stiffness (Smith, 1982) is then assembled into the corresponding locations in the global stiffness matrix, $[K_T]$. This approach has the advantage that interaction between multiple pile groups under different prescribed axial loadings can be analysed at the same time.

Considerable saving in computation time is achieved by taking symmetry of the group piles into account in the nodal numbering scheme (Chow, 1986a) as shown in Appendix 4C. It may be noted that radial displacement compatibility at the pile-soil interface is not included as it has been found to have non-significant effect on the pile response (Mattes, 1969). Provision for pile-soil slip due to the elastic-plastic soil behaviour (Fig. 4.2a) is catered for by limiting the pile-soil interaction forces (Poulos and Davis, 1968) and is described in detail in section 4.4. It should be noted that an incremental approach is required for a non-elastic analysis.

The original program, based on the above formulation, developed by the author (Chin, 1988) has been modified to cater for group piles of unequal radii, moduli and lengths. For piles of equal radius and length, the single pile flexibility coefficients need be formed only once and copied into the global flexibility matrix corresponding to the identical piles. This reduces the computation time significantly in that the single pile flexibility coefficients need not be formed each time for the other identical piles. For group piles of unequal lengths, the analysis procedure is, at present, restricted to an identical number of nodes for the group piles. It should also be noted that for group piles of unequal radii, moduli or lengths, the "symmetry" effect (Appendix 4C) is not applicable. Provisions for a "strain-softening" pile-soil interface response (see section 4.5) and residual installation stress (see section 4.6) have also been incorporated in an approximate manner. The above modifications have been coded into the computer program SPILE1.

It is worthy of note that, as in any soil-structure interaction analysis, the numerical approach described in the present study requires a knowledge of representative values of the soil deformation parameters E_s and ν_s. Of these two parameters, the soil modulus E_s has been shown to be the most significant parameter. In situations where slip occurs at the pile-soil interface, the pile-soil shear strengths along the pile are also required for the nonlinear analysis (see section 4.4). Some representative values of these parameters can be found in Poulos and Davis (1980).

At present, there is no one unified method for determining the soil deformation parameter E_s. As such, a range of values for the soil modulus E_s is to be expected depending on the method used (see, for example, Poulos and Davis, 1980). The most satisfactory method appears to be to carry out a pile loading test in-situ and to back-figure the value of E_s from the measured settlements. The soil modulus value thus obtained can then be used for the settlement computations of other single piles and pile groups within the same general site.

In the numerical approach described in the present study, it has been assumed that the necessary soil modulus values required have been determined *a priori*.

4.2.2 Nonlinear Hyperbolic Continuum Model (SPILE2)

The elastic-plastic (bilinear) representation of the soil behaviour, although simple and frequently used, may not however be adequate, particularly, for soils that exhibit highly nonlinear response. For such a case, the use of a nonlinear soil model would be more appropriate and satisfactory.

The hyperbolic shear stress-shear strain model (Fig. 4.2b) has been found to adequately represent the nonlinear behaviour of most soils (Kondner, 1963; Kondner and Zelasko, 1963; Duncan and Chang, 1970). The hyperbolic tangent modulus, E_t, can be shown to be given by (Chow, 1986a):

$$E_t = E_{max}[1 - (\tau R_f/\tau_f)]^2 \tag{4.6}$$

where E_{max} = initial tangent modulus, τ = current shear stress, τ_f = limiting shear stress, and R_f = a curve-fitting constant between 0 and 1. It may be noted that the bilinear model is obtained for $R_f = 0$. The greater the value of R_f, the greater is the nonlinear response (Fig. 4.2b). Limited experience suggests that the R_f value for the shaft, R_{fs}, in the range 0 - 0.5 and for the base, R_{fb}, of about 0.9 may be appropriate (Poulos, 1989b). It should be noted that the stress-strain soil models mentioned in the present study (elastic-plastic response, nonlinear hyperbolic response) are strictly confined to a soil mass (i.e soil-soil response). Thus, in the present simplified boundary element analysis, it has been implicitly assumed that the response at the pile-soil interface is similar to that of the soil-soil response.

The analysis procedure is similar to that described in section 4.2.1 except in the evaluation of the flexibility matrix of equation (4.3). Due to the nonlinear model adopted, the flexibility coefficients have to be re-evaluated, corresponding to "new" values of the tangent soil modulus E_t, for each incremental step. Extensive computation time may therefore be required for such re-evaluations.

Ample evidence (for example, Robinsky and Morrison, 1964; O'Neill *et al.*, 1982b) however shows that large movements are confined to a narrow zone around the pile-soil interface. The bulk of the soil mass between the piles is therefore subjected to low strain levels and hence remains essentially elastic. The present analysis (computer program SPILE2) therefore utilises the initial tangent modulus for pile-soil-pile interaction. The interaction f_{ij} is evaluated once (using point load solution) and remains unchanged in the incremental nonlinear analysis. Hence, for each incremental step, the f_{ij} corresponding to the individual pile need to be evaluated only. The mean values of the tangent modulus in the upper and lower soil layers are then used, in conjunction with an approximate procedure (Poulos, 1979b), for evaluating the f_{ij}.

The necessary modifications to cater for the nonlinear hyperbolic continuum soil model described have been coded into the computer program SPILE2.

For piles embedded in a Gibson soil with modulus increasing linearly with depth, an approximate analysis is used in both programs SPILE1 and SPILE2. The modulus for the upper soil layer E_1 is obtained as the mean of the moduli at the influenced and influencing nodes (Poulos, 1979b).

ADDENDUM

Section 4.2.2 Nonlinear Hyperbolic Continuum Model (Spile2)

The extent of the narrow zone of significant soil movements (when a pile is loaded statically) is dependent on factors like the soil type, soil density and the level of the applied loading. For calcalerous sediments which exhibit greater compressibility characteristics (with consequential volume reduction under shearing), the extent of this zone may be increased locally around the pile. For normal practical pile spacings (2.5 to 5 pile diameters), it is felt that the assumption of elastic response (by the use of the initial tangent modulus) for the pile-soil-pile interaction effect is still reasonable, at least as a first approximation. In any case, when pile-soil slip occurs at a given node, the analysis assumes no further interaction between that node and other nodes. This analysis approach adopted is consistent with the nonlinear three-dimensional finite element numerical results presented by Trochanis et al. (1991), which shows the progress of pile-soil slip significantly reduces the amount of interaction between piles (pg. 83).

4.2.3 Nonlinear Hyperbolic t-z "hybrid" Model (SPILE3)

As mentioned previously, the nonlinear hyperbolic continuum model requires excessive computation time for the evaluation of the single pile flexibility coefficients. As such, a more efficient nonlinear numerical approach is needed. One such numerical model is the so-called t-z "hybrid" approach. This "hybrid" approach models the single pile response using load-transfer (t-z) curves, while pile-soil-pile interaction is obtained using elastic continuum theory. Fig. 4.3 shows a schematic representation of this "hybrid" approach.

In the present "hybrid" approach, the f_{ij} (equation 4.2) associated with the same pile for $i \neq j$ is set to zero; indicating no interaction between nodes of the same pile, which is the basis of the load-transfer analysis. The f_{ii} for nodes of a given pile is evaluated using load-transfer curves. The interaction f_{ij} between piles is obtained accurately using the analytical solutions of Chan *et al.* (1974) for a two-layered soil, and in an approximate manner for a Gibson soil.

Following the theoretical work of Randolph and Wroth (1978) and utilising the hyperbolic soil model as suggested by Kraft *et al.* (1981a) (see also Randolph, 1977), the coefficient f_{ii} for the pile shaft, using the tangent modulus approach, can be shown to be given by (Chow, 1986a):

$$f_{ii} = \frac{\ln\left[\dfrac{r_m - \beta_s}{r_o - \beta_s}\right] + \dfrac{\beta_s(r_m - r_o)}{(r_m - \beta_s)(r_o - \beta_s)}}{2\pi G_i L} \tag{4.7}$$

in which $\beta_s = (\tau_o r_o R_{fs}/\tau_f)$; G_i = initial shear modulus at node i, L = the pile segment length associated with the node, r_o = pile radius, r_m = some empirical distance at which the shear stress in the soil becomes negligible, R_{fs} = hyperbolic curve-fitting constant for the shaft, and τ_o = pile-soil interface shear stress. The flexibility coefficient at the base, f_{ii}^{base}, is assumed to be given by that of a rigid punch on an elastic half-space (Randolph, 1977). The resultant hyperbolic tangent flexibility is given by (Chow, 1986a):

$$f_{ii}^{base} = \frac{(1 - \nu)}{4G_i r_o [1 - \beta_b]^2} \tag{4.8}$$

in which $\beta_b = (P_b R_{fb}/P_f)$; P_b = mobilised base load, P_f = limiting base load, R_{fb} = hyperbolic curve-fitting constant for the base, and ν = Poisson's ratio at the pile base.

For single pile analysis, the nodal stiffness coefficients (equation 4.4) can thus be obtained as the reciprocal of equations (4.7) and (4.8). Considerable reduction in computation time is hence achieved as compared to the full continuum programs SPILE1 and SPILE2 where the flexibility matrix has to be inverted to obtain the stiffness matrix for each incremental step. For pile group analysis, f_{ii} for nodes on the same pile is obtained using equations (4.7) and (4.8) and the soil flexibility matrix inverted to give the soil stiffness matrix (as for programs SPILE1 and SPILE2). The advantage of the present procedure is that the computation time is reduced in forming the single pile flexibility coefficients.

It is also worthy of note that for the case of single piles, the total global stiffness matrix $[K_T]$ (equation 4.5) is banded with a semi-band width of 2. For pile group analysis using the "hybrid" approach, the stiffness matrix $[K_T]$ is however fully populated due to the interaction effects between piles.

The averaged value for r_m in equation (4.7) for a homogeneous soil is given by (Randolph and Wroth, 1978)

$$r_m = 2.5\ell\rho(1-\nu) \tag{4.9}$$

where ρ = inhomogeneity factor. For homogeneous soil, ρ = 1.0 while for nonhomogeneous soil ρ is the ratio of soil modulus at pile mid-depth to that at the pile base. Approximate expressions for r_m for a Gibson soil, and a Gibson soil overlying a stiffer base have also been suggested (Randolph and Wroth, 1979a). For other general soil profiles, the required r_m value may have to be determined from a more accurate finite element analysis.

For nonhomogeneous soil, Chow (1986c) has suggested that a suitable r_m value be obtained by arbitrarily varying the factor ρ so as to obtain comparable results with the full continuum solutions (Poulos and Davis, 1980). This approach is however limited in that a different ρ value may have to be used for different pile and soil parameters. In the present approach, a more rational procedure is suggested for the particular cases of two-layered and Gibson soil profiles.

The r_m value is given by:

for $\underline{h = 0}$ (i.e. homogeneous case),

$$r_m = 2.5\ell\rho(1-\nu_2) \tag{4.10}$$

for $\underline{h = \ell}$ (i.e. end-bearing case) and from Randolph and Wroth (1979a),

$$r_m = \ell\{0.25 + [2.5\rho(1-\nu_1)-0.25]\xi_b\} \tag{4.11}$$

where $\xi_b = E_1/E_2$ and h is defined in Fig. 4.1. The factor ρ is 1.0 (for this particular case) which is a measure of the homogeneity of the soil along the pile shaft. The influence of the underlying stiffer layer is accounted for by the factor ξ_b. For $0<h<\ell$ (i.e. socketed case), the present approach assumes a linear decrease of the r_m value from that for h = 0 to that for $h = \ell$. Hence, the required r_m value for $\underline{0 \le h \le \ell}$ can be shown to be given by:

$$r_m = h\{0.25 + [2.5\rho(1-\nu_1)-0.25]\xi_b\} + 2.5\ell\rho(1-\nu_2)[1-(h/\ell)] \tag{4.12}$$

For $\underline{h \ge 3\ell}$, the influence of the stiffer underlying layer is negligible (Randolph and Wroth, 1979a) and the r_m value is taken as that for the homogeneous case:

$$r_m = 2.5\ell\rho(1-\nu_1) \tag{4.13}$$

For $\ell<h<3\ell$, a similar linear increase in r_m value from that given by equation (4.11) to that of equation (4.13) is assumed. Hence, for $\underline{\ell < h \leq 3\ell}$, the r_m value is given by:

$$r_m = [(3\ell-h)/2]\{0.25 + [2.5\rho(1-\nu_1)-0.25]\xi_b\} + 2.5\ell\rho(1-\nu_1)[(h-\ell)/2\ell] \tag{4.14}$$

It is interesting to note that for the two-layered profile the r_m expression given by equation (4.12) involves the summation of two parts, corresponding to the portions of the pile embedded in both layers considered independently.

For the case of a Gibson soil overlying a stiffer bearing layer, the following approximate equations, similar to equations (4.12) and (4.14), may be utilised:

for $\underline{0 \leq h \leq \ell}$:

$$r_m = h\{0.25 + [2.0\rho(1-\nu_1)-0.25]\xi_b\} + 2.5\ell(1-\nu_2)[1-(h/\ell)] \tag{4.15}$$

for $\underline{\ell < h \leq 3\ell}$:

$$r_m = [(3\ell-h)/2]\{0.25 + [2.0\rho(1-\nu_1)-0.25]\xi_b\} + 2.0\ell\rho(1-\nu_1)[(h-\ell)/2\ell] \tag{4.16}$$

The constant 2.0, as utilised in the above equations for the Gibson soil profile, is based on the suggestion of Randolph and Wroth (1979a). The factor ρ is taken as the ratio $E(h/2)/E(h)$ and $\xi_b = E(h)/E_2$ where E_2 = Young's modulus of the underlying stiffer layer, $E(h/2)$ and $E(h)$ are the pile shaft Young's moduli at mid-depth and base of the upper Gibson soil respectively.

For pile groups embedded in Gibson soil, the single pile response is obtained using the approach outlined above while pile-soil-pile interaction is obtained using the analytical solutions of Chan *et al.* (1974), in conjunction with an approximate procedure, as described at the end of section 4.2.2.

It may be noted that the approximate averaged r_m values (equations 4.9 to 4.16) mentioned earlier have been obtained for the case of an isolated single pile. For pile groups, Randolph and Wroth (1979b) have suggested that the single pile r_m value be increased by an amount equal to the radius of the circle of equivalent area to that covered by the pile group. For pile group sizes normally encountered in practice, this additional increase in the r_m value (as suggested by Randolph and Wroth, 1979b) would not have a significant effect on the computed response (as it contributes mainly to a logarithmic term in equation 4.7). Some results reported by Randolph and Wroth (1979b), for a row of three piles, show that their analytical solutions tend to overpredict the extent of the zone of influence of the pile (i.e the r_m value) as compared to the measured results. Therefore, in the absence of more specific data, it has been assumed in the present study that the averaged single pile r_m values (equations 4.9 to 4.16) are equally applicable (as a first approximation) for the case of pile groups.

Modifications required for this nonlinear hyperbolic t-z "hybrid" model have been coded into the computer program SPILE3. Some results showing the accuracy of the present static analysis for single piles and pile groups embedded in two-layered and Gibson soil profiles are presented in Chapter 5.

4.3 CYCLIC RESPONSE ANALYSIS

For cyclic response analysis, the two phenomena of importance that need to be modelled are the degradation of pile capacity and the accumulation of permanent displacement. The extension of the static analysis programs mentioned earlier to approximately cater for such effects of quasistatic cyclic loading are described below. A "total stress" approach (see section 3.3.1.2) has been adopted where simple empirical rules are used to describe the capacity-degrading effect of cyclic loading (Poulos, 1989a).

4.3.1 Elastic-Plastic Continuum Model (SCPIL1)

The static elastic-plastic continuum program, SPILE1, has been substantially modified for cyclic loading analysis to form the static and cyclic analysis program SCPIL1. The assumed shear stress-shear strain representation of the pile-soil interface behaviour under cyclic loading condition is shown in Fig. 4.4.

The cyclic analysis approach adopted is similar to the analysis method of Poulos (1981, 1989a) except that the present approach uses an incremental analysis within each cycle of loading. The present incremental approach, although is computationally more time-consuming, is however able to "trace" the yielding (i.e. pile-soil slip) response of the pile elements. Hence, the order in which the pile elements slip is taken into account in the present approach. This ability to "trace" the yielding element, which influences subsequent load-transfer response of the remaining elastic elements with further applied loading, is essential, particularly, under cyclic loading conditions.

The capacity degradation model and the accumulation of permanent displacement (see sections 3.3.1.2 and 3.3.1.3) that have been incorporated into program SCPIL1 are described in sections 4.3.4 and 4.3.5, respectively. In the present version of the program (SCPIL1), the soil modulus has been assumed to remain constant during cyclic loading. The analysis could be modified, if required, to account for degradation in soil modulus (for example, using equation 3.4) where the soil flexibility matrix is re-evaluated, after each cycle, by using the approximate averaging procedure of Poulos (1979b). Both "1-way" and "2-way" cyclic loading conditions can be analysed. Briefly, the analysis proceeds as follows:

(i) The pile-soil system is analysed incrementally (equation 4.5) to reach the maximum cyclic load level, P_{max}. At each increment of loading, the pile elements are checked for any pile-soil slip. If pile-soil slip occurs, the flexibility matrix, corresponding to the slip element, is modified (see section 4.4) for the next increment of loading;

(ii) the analysis is similarly repeated for the unloading stage to reach the minimum load level, P_{min};

(iii) the load is then brought back to P_{max}, thus completing one cycle of loading. The effects of cyclic loading (capacity degradation and permanent displacement accummulation) are then incorporated (see sections 4.3.4 and 4.3.5), using the adopted cyclic response model at this stage;

(iv) steps (ii) and (iii) are then repeated for the next cycle of loading until the desired number of cycles is simulated.

Provisions have also been made in program SCPIL1 for cyclic loading under different "parcels" of non-uniform load amplitudes ("storm-loading" condition) as described in section 4.3.6.

4.3.2 Nonlinear Hyperbolic Continuum Model (SCPIL2)

The hyperbolic shear stress-shear strain model adopted for cyclic loading analysis is shown in Fig. 4.5. The initial or "backbone" curve is given by the following relationship (the interface response):

$$\tau = \frac{E_{max}\varepsilon}{[1 + (R_f E_{max}|\varepsilon/\tau_f|)]} \tag{4.17}$$

where E_{max} = the initial tangent modulus at small strains; τ_f = the initial static limiting shear stress; τ, ε = the current shear stress and shear strain, respectively; R_f = a curve-fitting constant (see section 4.2.2; = R_{fs} for shaft elements and R_{fb} for base elements). The tangent modulus, E_t (= $d\tau/d\varepsilon$) can be shown to be given by equation (4.6).

For cyclic loading condition, which involves load reversal, the unloading and reloading responses are usually governed by the Masing (1926) rules. These rules require that:

(i) the initial slope (or tangent) to the unloading and reloading curves be equal to E_{max}, the initial tangent modulus to the "backbone" curve;

(ii) the shape of the unloading and reloading curves be similar to that of the "backbone" curve, except that the scale is enlarged by a factor of 2.

A third rule, in addition to the original Masing's rules above, has been proposed by some researchers (for example, Jennings, 1965; Finn *et al.*, 1977) which requires that the unloading and reloading curves follow the "backbone" curve if the previous maximum shear strain is exceeded (points A and B in Fig. 4.5). An extension of this third rule for irregular loading condition has also been suggested and used (Jennings, 1965; Newmark and Rosenblueth, 1971; Finn *et al.*, 1977) which states that if the current loading or unloading curve intersects the curve described by a previous loading or unloading process, the stress-strain relationship follows that of the previous curve.

Ishihara *et al.* (1985) have shown that the conventional unloading curve, constructed using the Masing's rules, may not adequately represent the unloading stress-strain behaviour of soils. A slightly modified form of the "conventional" unloading curve, using the hyperbolic model, is utilised in the present approach as shown below:

$$(\tau - \tau_u) = \frac{E_{max}(\varepsilon - \varepsilon_u)}{[1 + (R_f E_{max}/2R_u)\left|(\varepsilon - \varepsilon_u)/\tau_{fc}\right|]} \tag{4.18}$$

where (τ_u, ε_u) is the current point of load reversal (see Fig. 4.5), R_u is a curve-fitting constant for the unloading curve, and τ_{fc} = the limiting shear stress after cyclic loading (= τ_f for the first cycle). It may be noted that for R_u = 1.0, equation (4.18) corresponds to the "conventional" unloading curve. A value of R_u can thus be obtained which best fits the experimental results. For values of R_u other than 1.0, the unloading curve given by equation (4.18) therefore corresponds to fictitious "initial" loading curves (Ishihara *et al.*, 1985). This fictitious "initial" loading curve has no physical meaning and should not be confused with the initial ("backbone") loading curve given by equation (4.17). The introduction of R_u into equation (4.18) is thus a convenient representation to give more scope to better match any available test data. The tangent modulus for the unloading curve can be shown to be given by:

$$E_t = d\tau/d\varepsilon = E_{max}[1 - R_f\left|(\tau - \tau_u)\right|/(2R_u\left|\tau_{fc}\right|)]^2 \tag{4.19}$$

The equation for the reloading curve in the present approach is given by:

$$(\tau - \tau_u) = \frac{E_{max}(\varepsilon - \varepsilon_u)}{[1 + (R_f E_{max}/2R_r\delta)\left|(\varepsilon - \varepsilon_u)/\tau_{fc}\right|]} \tag{4.20}$$

where (τ_u, ε_u) is as defined previously; R_r = curve-fitting constant for the reloading curve (assumed equal to R_u for the present analysis), and δ = a secant modulus degradation value due to cyclic loading (see section 4.3.5.2). The effects of different values of R_u and/or R_r (assuming δ = 1.0) are shown in Fig. 4.6. The tangent modulus is thus given by:

$$E_t = E_{max}[1 - R_f|(\tau - \tau_u)|/(2R_r\delta|\tau_{fc}|)]^2 \qquad (4.21)$$

Program SCPIL2 represents a substantial modification of the static analysis program, SPILE2, to incorporate the cyclic loading analysis described above. The analysis procedure is similar to that described in section 4.3.1 where an incremental approach is employed. The present nonlinear hyperbolic continuum model, however, requires that the flexibility matrix be re-evaluated at each incremental step (see section 4.2.2). The effects of cyclic loading are assessed at the end of each half-cycle. The new limiting capacity values and δ values (see sections 4.3.4 and 4.3.5) are then used for the reloading half-cycle. It should be noted that for any unloading or reloading event, as given by equations 4.18 and 4.20, the shear stress, τ, is limited to the limiting shear stress value applicable for that half cycle. Different initial limiting compressive and tensile capacities may be specified for each element, with the appropriate value, corresponding to any half-cycle of loading, being used. The value of τ_{fc} in equations (4.18) to (4.21) is then taken as the average of the absolute sum of the limiting compressive and tensile shear stresses applicable at a given cycle.

4.3.3 Nonlinear Hyperbolic t-z "hybrid" Model (SCPIL3)

The cyclic analysis procedure for the nonlinear hyperbolic t-z "hybrid" model is similar to that for the continuum model, SCPIL2. As mentioned in section 4.2.3., the difference lies in the evaluation of the single pile flexibility coefficients.

The flexibility coefficients, f_{ii}, for the shaft elements under cyclic loading can be shown to be given by equation (4.7), with the factor β_s given by:

$$\beta_s = \frac{R_{fs}|\tau_o - \tau_{uo}|r_o}{2R_c\delta|\tau_{fc}|} \qquad (4.22)$$

where τ_{uo} = pile-soil interface shear stress at load reversal, $R_c = R_u$ or R_r corresponding to the unloading or reloading curves respectively, and the other parameters as defined earlier. It may be noted that R_r has been assumed to be equal to R_u in the present analysis. Similarly, for the pile base element flexibility coefficient f_{11}^{base}, equation (4.8) applies with β_b given by:

$$\beta_b = \frac{|P_b - P_{bo}|R_{fb}}{2R_c\delta|P_{fc}|} \tag{4.23}$$

where P_{bo} = pile base load at load reversal, P_{fc} = limiting base load after cyclic loading (= P_f for the first cycle) and all other parameters as defined previously. It may be noted that, under cyclic loading conditions, δ (in equations 4.22 and 4.23) assumes a value of 1.0 for the unloading curve while a "degrading" δ value is adopted for the reloading curve (see section 4.3.5.2).

The advantage of the present nonlinear "hybrid" approach over the continuum model (SCPIL2) is the significant reduction in computation time required for re-evaluation of the single pile flexibility coefficients. The cyclic analysis procedure has been incorporated into program SPILE3 to form the static and cyclic analysis program, SCPIL3.

The cyclic analysis procedure is similar to that described previously (section 4.3.2) where the effects of cyclic loading are assessed at the end of each half-cycle. Obviously, the incremental nonlinear analysis becomes more accurate as the number of incremental steps is increased. However, for the same number of incremental steps, the present "t-z" analysis (program SCPIL3) is computationally more efficient than the single pile continuum analysis of Lee (1988) (also Lee and Poulos (1992)). At each incremental step, the nodal stiffness coefficients of the "springs" can be easily evaluated from the reciprocals of equations (4.7) and (4.8) with the appropriate values of β_s and β_b (equations 4.7, 4.8, 4.22 and 4.23). Note that it has been implicitly assumed that the cyclic loading condition has no significant effect on the "static" r_m value (as given by equations 4.12 to 4.16) in section 4.2.3.

4.3.4 Pile-Soil Resistance Degradation

As mentioned in Chapter 2, it has been observed from both laboratory and field tests (for example, Nauroy and LeTirant, 1983; Abbs *et al.*, 1988) that cyclic loading of piles can reduce the limiting pile-soil resistance values and hence, can result in a reduced pile capacity. At present, there is no satisfactory approach to model effectively this phenomenon. For the present study, any increase in pile capacity as a result of the loading rate effect has been ignored. This will lead to a more conservative assessment of the cyclic loading effect. However, this loading rate effect can be of particular significance for piles in clay (for example, Kraft *et al.*, 1981b; Dunnavant et al., 1990). If required, this loading rate effect can be approximately catered for using the simple approach suggested by Poulos (1979a, 1989a) (see section 3.3.1.1).

The approach adopted herein is similar to that utilised by Poulos (1981, 1989a) where the effect of cyclic loading on pile capacity is incorporated using simple empirical rules. The degradation of pile capacity (skin friction and/or end-bearing) is expressed as a degradation factor, which is defined as the ratio of the capacity after cyclic loading to the initial static capacity.

This degradation factor can be determined from the simple degradation model developed by Matlock and Foo (1980), or from degradation "charts" obtained empirically (see section 3.3.1.2). As pointed out by Poulos (1988a, 1989a), different hypotheses regarding the empirical skin friction degradation factor are possible at present. These include the following:

(i) the degradation factor, D_τ, is dependent on the absolute magnitude of cyclic displacement. The cyclic displacement is defined as the difference between the displacement at the maximum (P_{max}) and minimum (P_{min}) cyclic load levels;

(ii) D_τ is dependent on the relative (to diameter) value of cyclic displacement;

(iii) D_τ is dependent on the cyclic slip displacement; i.e., the cyclic displacement in excess of that required to cause static slip (ρ_{fs}). The ρ_{fs} values for each element can be determined from the analysis or can be input directly by the user.

(iv) D_τ is dependent on the normalised (to pile diameter) value of the cyclic slip displacement.

Limited results obtained by Lee (1988) seem to suggest that the skin friction degradation factor is dependent on the relative (to diameter) value of cyclic slip displacement. Clearly, more carefully controlled laboratory tests are required to further investigate this uncertainty. A number of these "degradation factor" relationships, corresponding to different numbers of cycles of loading, can be input into the program. Linear interpolation is utilised to obtain the intermediate values.

As compared to the skin friction degradation factor (D_τ) for the pile shaft, limited data are however available for the pile base resistance degradation factor, D_b. Limited results obtained by Poulos and Chua (1985), from model footing tests, indicate some reduction of capacity with cyclic loading. The model jacked pile tests of Poulos and Chan (1988) indicate no significant degradation of end-bearing capacity with cyclic loading. As suggested by Poulos (1989a), in the absence of other data, it will be assumed that the degradation of base resistance can be ignored (hence, $D_b = 1.0$).

The degradation models described above have been incorporated into the computer programs SCPIL1, SCPIL2 and SCPIL3. The choice of which capacity degradation model to use can be selected by the user. In the case where both the Matlock and Foo (1980) "reverse-slip" degrading model and the degradation "charts" approach are considered, the lesser degradation factor calculated is utilised. This will, with the present limited understanding of the capacity degrading effect of cyclic loading, result in a more conservative assessment of the cyclic loading effect on pile capacity.

The degradation factors are calculated for each element at the end of each cycle (half-cycle for programs SCPIL2 and SCPIL3) and multiplied with the initial limiting static capacities to obtain the "new" degraded limiting capacities. These "new" limiting capacities are then used for the next cycle (or half-cycle) of analysis.

4.3.5 Permanent Displacement Accumulation

The need to model the accumulation of permanent displacement, particularly under non-zero mean load (i.e. biased) cyclic loading condition, is essential in order to obtain a more realistic prediction of the pile response. As mentioned in section 3.3.1.3, two approaches are possible with the present simplified boundary element method; the "external imposed soil movements" approach (Poulos, 1989a) and the "degrading secant modulus" approach (Lee, 1988).

4.3.5.1 Elastic-plastic continuum model

In the elastic-plastic continuum model utilised in program SCPIL1, the soil modulus has been assumed to remain constant during cyclic loading. Any degradation in the soil modulus will result in a "softened" soil response and hence an increase in the pile displacement. It should also be noted that any degradation of the limiting capacity values due to cyclic loading will similarly result in an increased pile displacement. This accumulation of pile displacement, as a result of the degradation of soil modulus and/or limiting capacity values, is however not "satisfactory" as it results in a "rotation" of the cyclic load-settlement "loop" (see Fig. 4.7). The actual observed permanent displacement accumulation, particularly under non-zero mean load, involves a "progression" of the load-settlement "loop" with increasing number of cycles (Lee, 1988). An analysis procedure is therefore required to simulate this "progression" of the load-settlement "loop" under cyclic loading condition.

The approach adopted in program SCPIL1 is similar to that utilised by Poulos (1989a) whereby an "externally imposed soil movements" procedure is employed. The empirical incremental permanent soil displacement is given by equation (3.5) and is as shown below:

$$\delta S_p = S_{PN}[n\delta X + (m\delta N/N)] \tag{4.24}$$

where the parameters are as defined in equation (3.5). As mentioned in section 3.3.1.3, different definitions for the representative stress level X have been assumed and utilised (see equations 3.6 to 3.8, 3.11). As such, these different definitions for the stress level X have been included in the present program as possible options. Some results showing the influence of the adopted definition for the stress level X are presented in Chapter 5. The incremental permanent soil displacement at the end of each cycle is therefore calculated using equations (4.24) in conjunction with the adopted definition for the stress level X.

The load-deformation relationship for the case of a combined external applied load and external soil movements can be shown to be given by (Chin, 1988):

$$[K_T]\{w_p\} = \{P\} + [K_s]\{w_c\} \tag{4.25}$$

where $\{w_c\}$ = the vector (size n) of incremental permanent soil displacements at the end of each cycle, and all other parameters as defined in section 4.2.1. Equation (4.25) is similar to equation (4.5) except for the additional terms $[K_s]\{w_c\}$ which is the induced load on the pile due to the incremental permanent soil displacements. For the present cyclic loading analysis, equation (4.25) is solved incrementally during the unloading "leg" of each load cycle. The vector $\{w_c\}$ of incremental permanent soil displacements (positive downwards), calculated at the end of each cycle, is therefore further sub-divided into increments with the number of increments corresponding to that utilised for the unloading "leg".

It may be noted that the analysis described above, which will result in increased permanent pile displacement (positive downwards) with increasing cycles, caters for cases where the mean load of the applied loading parcel is greater than zero i.e. biased compression (positive) loading. For the case of a biased tensile (negative) loading (mean load less than zero), upward (negative) accumulation of pile displacements may occur with the pile eventually undergoing "pull-out" failure (Chan and Hanna, 1980). For such cases, the upward accumulation of pile displacements could be numerically simulated by introducing an incremental upward (i.e. negative) soil movements for the vector $\{w_c\}$. For the case of symmetric (or non-biased) loading, upward or downward accumulation of pile displacement is possible, although experimental results (Lee, 1988) tend to show a downward accumulation.

At this point, it is worthy to recall that simulations for the capacity degradation and permanent displacement accumulation for the present elastic-plastic program SCPIL1 are similar to that utilised by Poulos (1989a). The refinement introduced in the present study caters to the case of piles embedded in a two-layered soil profile where the soil flexibility coefficients are determined accurately through the analytical layered solutions of Chan *et al.* (1974). In the approach of Poulos (1989a), an approximate averaging procedure using Mindlin's (1936) homogeneous solutions has to be utilised for such a soil profile. Moreover, within each cycle of loading, the incremental analysis approach adopted in program SCPIL1 (although may be slightly computationally more time-consuming) enables the ability to "trace" the order of occurrence of pile-soil slip for the elements forming the pile.

4.3.5.2 <u>Nonlinear hyperbolic model</u>

For the nonlinear hyperbolic model (programs SCPIL2 and SCPIL3), the "degrading secant modulus" approach, as utilised by Lee (1988) in conjunction with a nonlinear Ramberg-Osgood soil model, has been adopted. Unlike the elastic-plastic model where a degradation of the soil modulus results in a "rotation" of the cyclic load-settlement "loop", a "progression" of the stress-strain "loop" (and hence the load-settlement "loop") is obtained by using a nonlinear soil model, such as the Ramberg-Osgood model (Lee, 1988) and the present hyperbolic model, in conjunction with the "degrading secant modulus" approach (see Fig. 4.8).

The permanent displacement accumulation due to cyclic loading can thus be simulated by "degrading" the value of δ (from 1.0), on the reloading curve (Fig. 4.8), in equation (4.21) for the continuum model (SCPIL2) and equations (4.22) and (4.23) for the "hybrid" model (SCPIL3). The degradation of δ is similar to a degradation of the secant modulus (see Fig. 4.7). Thus, the modified expression of Lee (1988) for the secant modulus degradation factor (equation 3.10) is adopted. Hence, δ is given by:

$$\delta = \delta_p - 0.5\psi X[\delta_p]^{(1+\psi X)/\psi X} \tag{4.26}$$

where δ_p = the δ value for the previous cycle; ψ = an accumulation rate parameter, and X is the current representative stress level (see section 3.3.1.3). In the absence of other data, the value of ψ of 0.02 obtained by Lee (1988), from model grouted pile tests, is adopted in the present analysis. It should be noted that for values of δ less than unity, permanent displacement will be accumulated with increasing cycles.

In this approach, the accumulation of permanent pile displacement is hence obtained by introducing and degrading the δ value on one "leg" of the load cycle, as cycling proceeds. As such, the upward or downward accumulation of pile displacement can thus be simulated by introducing and degrading the δ value on the appropriate "leg" of the load cycle. The programs (SCPIL2 and SCPIL3) have been coded to "choose" the appropriate "leg" of each load cycle based on the mean applied load of each loading parcel and the type of initial first cycle loading (i.e. whether tension or compression loading).

At this point, it is of interest to contrast the main similarities and differences between the present analysis (program SCPIL3) and that of Lee (1988) (see also Lee and Poulos, 1992). In both analyses, the simulation for capacity degradation follows that suggested by Poulos (1989a). The approach ("degrading secant modulus") utilised in both analyses for simulating the accumulation of permanent displacement is also similar. The main difference between both analyses lies in the adopted soil model. In the analysis of Lee (1988), the soil is treated as a continuum and the pile-soil interface response governed by the nonlinear modified Ramberg-Osgood model. Two empirical parameters (apart from the "standard" initial soil modulus and limiting friction values) are required to describe the soil model. The degree of nonlinearity is thus governed by the choice of these two parameters. At present, very limited data are available on these two parameters which are dependent on the soil type, amongst other factors. The solution of Mindlin (1936), which is strictly for a homogeneous soil, is utilised in conjunction with an approximate averaging procedure for determining the soil influence coefficients of a non-uniform soil modulus distribution along the pile. The greater computation time required to re-evaluate these influence coefficients for all the nodes (including inter-node interactions) at each incremental step within each cycle is a shortcoming of the analysis of Lee (1988). In the present analysis (program SCPIL3) however, the responses of the soil at a number of points along the pile are only considered without any interaction between them. The nonlinear soil response is governed by a hyperbolic relation, with the flexibility coefficients of these discrete "springs" at each incremental step easily evaluated from the simple form of equations (4.7) and (4.8). The present hyperbolic model requires one empirical parameter less than the Ramberg-Osgood model utilised by Lee (1988). Suggestions for the hyperbolic curve-fitting parameters (R_{fs} and R_{fb}) are also more readily available (Poulos, 1989b). Table 4.1 shows a summary of some tentative values available for the model parameters required in the present analysis using the nonlinear hyperbolic model (programs SCPIL2 and SCPIL3). These values have been assumed to be applicable in the absence of other specific values.

4.3.6 "Storm-Loading" Analysis

The analysis described thus far for cyclic loading condition involves a given number of cycles of constant loading amplitude. In actual field (particularly offshore) conditions, however, the piles are generally subjected to a "storm-loading" condition involving "parcels" of different number of cycles and different load amplitudes.

The static and cyclic analysis programs SCPIL1, SCPI12 and SCPIL3 have been coded to enable the "progression" from one parcel of loading to the next parcel. The total number of cycles is thus given by the sum of the number of cycles of each parcel of loading. In this approach, the different parcels of loading are thus treated as a "single parcel", with the number of cycles equal to the summation of number of cycles in each parcel, but with the appropriate load amplitude used at the corresponding cycle. The accumulation in permanent displacement is then modelled by using equation (4.24) for program SCPIL1, and equation (4.26) for programs SCPIL2 and SCPI13.

An alternative procedure has also been utilised by Poulos (1988c), in conjunction with the "externally imposed soil movements" approach (see section 4.3.5.1), whereby the different parcels of loading are "converted" into an equivalent number of cycles at the load level of the last parcel. The accumulated permanent soil displacement, corresponding to each load parcel, is calculated from the expression (Chua, 1983)

$$S_{PN} = B\, N^{m} e^{nX} \tag{4.27}$$

where S_{PN} = the accumulated permanent soil displacement after N cycles, B = an empirical parameter, and other parameters are as defined in equation (3.5). It may be noted that equation (3.5) represents the incremental form of equation (4.27). As shown by Poulos (1988c), the accumulated permanent soil displacement (from, for example, the first load parcel) calculated using equation (4.27) can be expressed in terms of an equivalent number of cycles of, for example, the load level of the last parcel, that gives the same accumulated displacement. This approximate procedure can be extended to the other parcels of loading, resulting in a total equivalent number of cycles at the load level of the last parcel. The different parcels of loading are thus reduced to a single parcel. This approach (Poulos, 1988c) therefore assumes that Miner's (1945) rule of superposition applies, which states that the cumulative effect is independent of the order in which the different parcels occur. It is worthy of note that a more rigorous semi-empirical procedure, based on cyclic triaxial test results on calcareous sands, has been suggested by Kaggwa *et al.* (1990) whereby the order of occurrence of prior parcels of loading are accounted for in determining the equivalent number of cycles of the present parcel. The approach (Kaggwa *et al.*, 1990) however requires that a series of cyclic triaxial tests be conducted to determine the necessary empirical parameters.

Some results showing the "storm-loading" effect on a hypothetical case are presented in Chapter 5. The "equivalent number of cycles" approach (Poulos, 1988c) can be easily implemented into program SCPIL1. Results obtained using this "equivalent number of cycles" approach (program SCPIL1) are also presented for comparison in Chapter 5. It may be noted that the static and cyclic analysis programs SCPIL1, SCPIL2 and SCPIL3 have provisions to enable a static analysis to be performed following different "parcels" of load-controlled cyclic loading.

4.4 PILE-SOIL SLIP

Satisfactory results cannot be obtained by using a purely elastic analysis when slip occurs at the pile-soil interface. A non-linear analysis using an incremental approach will have to be used. This non-linear analysis is particularly relevant to relatively compressible piles and piles embedded in soft ground conditions where significant pile-soil slip may occur.

In most finite element analyses, where the generally nonlinear interaction response of the structure-soil interface has to be modelled, some kind of interface elements have to be employed (for example, Desai *et al.*, 1984; Hermann, 1978). Simple or complex constitutive relations may be "assigned" to these interface elements to model the problem. It should however be noted that while a complex constitutive model may describe fully the relevant features of the interface response, the difficulty of obtaining the greater number of parameters required for the model may well defeat its use. In the present simplified boundary element approach, a fictitious interface element (with zero thickness) is utilised where an upper limiting resistance value is specified for each nodal point. Thus, pile-soil slip occurs when this limiting value is reached. While this approach may represent an over-simplification of the interface problem, it however avoids the difficulty of assigning appropriate properties required when employing interface/joint elements. This simplified approach has been shown to give acceptable results when utilised for a nonlinear pile-soil analysis (Poulos and Davis, 1980; Chow, 1986a).

At high soil strains, pile-soil slip will occur at the pile-soil interfaces of the individual piles in the group. When the pile-soil shear strength is fully mobilised at a particular node, full slippage takes place at that node. Any further increase in external applied loading will not increase the soil reaction at that node. Moreover, further increase in loads at other nodes (of the group piles) are assumed not to cause further increase in displacement at that particular node because of the discontinuity resulting from full slippage taking place. Thus, there is no further interaction through the soil between that node and the other nodes. It is worth noting that the results of a numerical study by Trochanis *et al.* (1991), utilising a nonlinear three-dimensional finite element approach, have shown that the progress of pile-soil slippage significantly reduces the amount of interaction between piles.

The numerical solution procedure adopted for the present analysis is similar to that utilised by Chow (1986a). For each load (or settlement) increment,

(i) for nodes at which the pile-soil shear strength is fully mobilised, set the corresponding rows and columns in the flexibility matrix to zero. Prescribe an arbitrary large value (say, $1x10^{12}$) for the coefficient at that node;

(ii) subsequent procedure is similar to that for the elastic analysis (equations 4.4 and 4.5) where the pile and soil stiffness matrices are assembled and solved to obtain the incremental settlement (or load).

Physically, the procedure in (i) means that there is no interaction between the node that has slipped and the other nodes. The use of an arbitrary large value for the flexibility coefficient at the node that has slipped corresponds to infinite soil displacement for that node (i.e zero stiffness condition). Provisions have also been incorporated within each load (or settlement) increment to iterate and redistribute any "excess loads" (elemental force (or stress) in excess of its limiting capacity), calculated from the present load (or settlement) increment, to other remaining elastic elements. The iteration is discontinued when the difference between the total pile load computed in the present and previous iteration is less than a specified tolerance (percentage of total pile load at present increment) input by the user. The procedures (i) and (ii) above are then repeated for the next load (or settlement) increment until the specified number of increments is attained.

As for any non-linear analysis, the resistance values (for both shaft and base elements) at which pile-soil slip occurs have to be estimated. These resistance values can be estimated using a "total stress" approach or an "effective stress" approach, as appropriate. Some of the available design methods for piles in different soil types have been summarised by Poulos (1988d).

The accuracy of the non-linear analysis depends on the accuracy in estimating the pile-soil resistance values, and the magnitude of the load increments used. The non-linear behaviour is modelled more accurately when smaller load (or settlement) increments are used. It should be noted that for a single pile analysis using the "t-z" approach (programs SPILE3 and SCPIL3), the nodal soil stiffness coefficients (reciprocal of equations 4.7 and 4.8) can be determined directly without the need to invert the flexibility matrix. In all programs, different limiting capacity values in compression and tension may be specified for each of the shaft and base elements.

4.5 "STRAIN-SOFTENING" RESPONSE

The present analysis described thus far assumes that the pile-soil interface behaviour does not "strain-soften", i.e. the pile-soil interface shear strength does not reduce to a lower residual value beyond a certain peak displacement. This assumption, however, may not be acceptable particularly for soils (for example, dense or cemented sand) that exhibit significant "strain-softening" response. This "strain-softening" pile-soil interface behaviour may significantly affect the static and cyclic pile response (Poulos, 1988e; Poulos *et al.*, 1988). Furthermore, it has been shown that, for long relatively compressible piles, this "strain-softening" pile-soil interface behaviour may significantly affect the developed pile shaft capacity and the load-settlement response of the pile (Murff, 1980; Poulos, 1982b; Randolph, 1983a, 1983b; Semple and Rigden, 1986).

As mentioned in section 3.3.1.3, the accumulated permanent displacement under cyclic loading condition, particularly under non-zero mean load, may result in the "static" degradation of pile capacity when the accumulated displacement exceeds that required to reach the peak static resistance. An analysis procedure is therefore required to incorporate this "strain-softening" behaviour into the pile response analysis.

The "softening" model adopted is similar to that utilised by Poulos (1988e) where the peak skin friction, τ_f, is assumed to decrease linearly to the residual skin friction, τ_r, over a displacement of ρ_{pp} (Fig. 4.9). Thus, the adopted "softening" model for program SCPIL1 is as shown in Fig. 4.9(a) while Fig. 4.9(b) shows the model utilised by programs SCPIL2 and SCPIL3. For static analysis, an incremental settlement approach is utilised (see section 4.4) where the applied load required to cause the additional incremental settlement is calculated. For load-controlled cyclic loading analysis, the "static" degradation factor due to "strain-softening" is calculated when the accumulated displacement exceeds ρ_{fs}, the displacement to reach the peak static skin friction. The "cyclic" degradation factor (section 4.3.4) is similarly determined, and the lesser value (i.e. more degradation) is used in the cyclic analysis (Booker *et al.*, 1989). Some results are presented in Chapter 5 showing the influence of the "strain-softening" behaviour on pile response.

4.6 RESIDUAL INSTALLATION STRESS EFFECT

The installation process for driven (or jacked) piles, as compared to bored piles, usually results in significant residual stresses being developed along the pile. These residual stresses generally do not affect the total ultimate capacity of the pile (see, for example, Hunter and Davisson, 1969). The analysis described thus far in the present thesis assumes an initially stress-free pile. As noted by, for example, Hunter and Davisson (1969), Vesic (1977) and Holloway *et al.* (1978), these residual stresses will have to be considered in order to obtain a more accurate interpretation or prediction of the pile response. Methods to account for these installation residual stresses have been suggested by, for example, Hunter and Davisson (1969) which involves an empirical procedure while Briaud and Tucker (1984) presented a semi-empirical procedure.

An approximate and simple approach has been suggested by Poulos (1987) for determining these residual stresses. The approach involves loading the pile (at final penetration) to failure in compression and then unloading back to zero load. As shown by Poulos (1987), and substantiated by Leonards and Darrag (1989), this procedure appears to be capable of giving a realistic prediction of the residual stress distribution along the pile. It may be noted that a more rigorous approach for simulating the installation stress would be to use a dynamic analysis, for example, as utilised by Holloway *et al.* (1978).

The simple approach suggested by Poulos (1987) has been adopted and incorporated into programs SCPIL1, SCPIL2 and SCPIL3. For pile groups analysis, two procedures are possible in the present analysis for determining the residual stresses:

(i) the group piles are considered independently; the residual stresses are hence obtained by considering each of the group piles as a single "isolated" pile.

(ii) the interactions between the group piles are considered. This can be achieved (for a rigid pile cap) by "tying" the heads of the group piles with rigid beam elements (see Appendix 4C). The whole group is then similarly analysed using the procedure of Poulos (1987).

Subsequent static and/or cyclic analysis proceeds as described in the earlier sections, except that the piles are no longer stress-free initially but have residual stresses. Some results showing the influence of the residual stresses on the pile response are presented in Chapter 5.

4.7 SUMMARY

A numerical approach, based on a simplified boundary element method, has been described for the static and cyclic response analysis of single piles and pile groups embedded in a two-layered soil profile, with the homogeneous profile as a special case. For other nonhomogeneous soil profiles, such as a Gibson soil, an approximate procedure is used. Three representations of the soil behaviour have been utilised, namely, elastic-plastic continuum model, nonlinear hyperbolic continuum model, and the nonlinear hyperbolic t-z "hybrid" model. For the nonlinear "t-z" approach (programs SPILE3 and SCPIL3), simple r_m expressions are suggested, for piles embedded in a two-layer and "Gibson" soil profiles, for determining the single piles t-z response.

For cyclic loading analysis, the two effects of importance that need to be modelled are the degradation of pile capacity and the accumulation of permanent pile displacement. The degradation of pile capacity, expressed as a degradation factor, is approximately modelled using simple empirical rules. The permanent pile displacement accumulation can be simulated by using the "external imposed soil movemenst" approach for the elastic-plastic continuum model, and the "degrading secant modulus" approach for the nonlinear hyperbolic models. A "cycle-by-cycle" approach has been adopted whereby the effects of cyclic loading are incorporated at the end of each cycle (program SCPIL1) or half-cycle (programs SCPIL2 and SCPIL3). The analysis described could be used approximately for the analysis under a general "storm-loading" condition. In particular, the development of the computationally more efficient cyclic nonlinear hyperbolic "t-z" program (SCPIL3) has also been described. Tables 4.2 and 4.3 give a summary of both the static and cyclic analysis programs that were developed and utilised in the present study.

Provisions for a "strain-softening" pile-soil response and the influence of residual installation stresses on the static and/or cyclic pile response have also been included in an approximate manner.

The non-linear analysis described is, in general, applicable to any soil type provided that the relevant input parameters, corresponding to the soil type considered, are used. For piles in calcareous sediment, there is at present very limited data on the cyclic empirical parameters required in the analysis approaches described. There is therefore a need for more laboratory and field tests data of piles in calcareous sediment in order to increase the data-base of these cyclic empirical parameters.

APPENDIX 4A

EXPLICIT EXPRESSIONS FOR LAYERED SOLUTIONS

(after Chin, 1988)

Chan *et al.* (1974) obtained an approximate closed form solution of a layered elastic half-space (as shown in Fig. 4.1) subjected to an interior point force. The expressions for the vertical displacement at a point $\bar{x}$ in the layered half-space due to a unit vertical point force acting in the interior of the layered half-space at a point $z_4\bar{e}_z$ are given by, respectively

$$
\begin{aligned}
w(\xi,\zeta) = {} & \frac{\gamma_1}{8\pi h \gamma_0 E_1}\Bigg[\gamma_3 G_0(\rho,f_{12}) + |\xi-\zeta| G_1(\rho,f_{12}) \\
& + \sum_{m=0}^{m=4} k_m \Big\{ (4\gamma_0\gamma_2 + 1)\, G_0(\rho,f_1+p_m) + \gamma_3(\xi+\zeta)\, G_1(\rho,f_1+p_m) \\
& + 2\xi\zeta G_2(\rho,f_1+p_m) - \tfrac{1}{2}(a+b\gamma_3^2)G_0(\rho,f_2+p_m) + b\gamma_3(2-\xi-\zeta)G_1 \\
& (\rho,f_2+p_m) - 2b(1-\xi)(1-\zeta)\, G_2(\rho,f_2+p_m) - ab\gamma_3 G_0(\rho,f_3+p_m) \\
& - ab(\xi-\zeta)G_1(\rho,f_3+p_m) + \tfrac{1}{2}\gamma_3(a+b)G_0(\rho,f_4+p_m) + [2b(4\gamma_0\gamma_2 \\
& +1)+a\xi-b\zeta]G_1(\rho,f_4+p_m) + 2b\gamma_3(1+\xi-\zeta)G_2(\rho,f_4+p_m) + 4b\xi(1 \\
& -\zeta)G_3(\rho,f_4+p_m) - ab\gamma_3 G_0(\rho,f_5+p_m) + ab(\xi-\zeta)\, G_1(\rho,f_5+p_m) \\
& + \tfrac{1}{2}\gamma_3(a+b)G_0(\rho,f_6+p_m) + [2b(4\gamma_0\gamma_2+1)-b\xi+a\zeta]G_1(\rho,f_6+p_m) \\
& + 2b\gamma_3(1-\xi+\zeta)G_2(\rho,f_6+p_m) + 4b\zeta(1-\xi)G_3(\rho,f_6+p_m) - ab(4\gamma_0 \\
& \gamma_2+1)G_0(\rho,f_7+p_m) + ab\gamma_3(\xi+\zeta)G_1(\rho,f_7+p_m) - 2ab\xi\zeta G_2(\rho,f_7+ \\
& p_m) + \tfrac{1}{2}(a+b\gamma_3^2)G_0(\rho,f_8+p_m) + b\gamma_3(2-\xi-\zeta)G_1(\rho,f_8+p_m) + 2b(1 \\
& -\xi)(1-\zeta)G_2(\rho,f_8+p_m)\Big\}\Bigg]
\end{aligned}
$$

$$(0 \le \xi_1 < h/\ell\ ,\ 0 \le \zeta_1 < h/\ell) \qquad \text{(4A.1)}$$

$$
\begin{aligned}
w(\xi,\zeta) = {} & \frac{\gamma_0}{4\pi h E_1}\sum_{m=0}^{m=4} k_m \Big\{ (c+d\gamma_3\gamma_4)G_0(\rho,f_1+p_m) + 2[\gamma_3(c-d+d\xi)+ \\
& d\zeta\gamma_4]G_1(\rho,f_1+p_m) + 4\zeta(c-d+d\xi)G_2(\rho,f_1+p_m) + (ac+bd\gamma_3\gamma_4)
\end{aligned}
$$

$$G_0(\rho,f_2+p_m) + 2bd\,[2(3-2\nu_1-2\nu_2)-\zeta\gamma_4-\gamma_3\xi]\,G_1(\rho,f_2+p_m) - 4bd(1-\zeta)(1-\xi)G_2(\rho,f_2+p_m) + (c\gamma_3+d\gamma_4)\,G_0(\rho,f_9+p_m) + 2[c(1-\zeta)-d(1-\xi)\,]\,G_1(\rho,f_9+p_m) + (ac\gamma_3+bd\gamma_4)\,G_0(\rho,f_4+p_m) + 2[ac\zeta+bd(\gamma_3\gamma_4+1-\xi)]\,G_1(\rho,f_4+p_m) - 4bd[\zeta\gamma_4+\gamma_3(1-\xi)]\,G_2(\rho,f_4+p_m) + 8bd\zeta(1-\xi)G_3(\rho,f_4+p_m)\Big\}$$

$$(h/\ell \le \xi_1 \le 1\ ,\ 0 \le \zeta_1 < h/\ell) \qquad (4A.2)$$

$$w\,(\xi,\zeta) = \frac{\gamma_0}{4\,\pi\,h\,E_1}\sum_{m=0}^{m=4} k_m\Big\{\,(c\gamma_3+d\gamma_4)\,G_0(\rho,f_{10}+p_m) + 2\,[c(1-\xi)+d(\zeta-1)\,]\,G_1(\rho,f_{10}+p_m) - (ac\gamma_3+bd\gamma_4)\,G_0(\rho,f_6+p_m) + 2\,[bd(\gamma_3\gamma_4-\zeta+1)+ac\xi]G_1(\rho,f_6+p_m) + 4bd[\gamma_3(\zeta-1)-\gamma_4\xi\,]G_2(\rho,f_6+p_m) - 8bd(\zeta-1)\xi\,G_3(\rho,f_6+p_m) + (c+d\gamma_3\gamma_4)\,G_0\,(\rho,f_1+p_m) + [2\gamma_3(c+d\zeta-d)+2d\gamma_4\xi]G_1(\rho,f_1+p_m) + 4(c+d\zeta-d)\xi G_2(\rho,f_1+p_m) - (ac+bd\gamma_3\gamma_4)G_0(\rho,f_2+p_m) + 2bd[\gamma_4(1-\xi)-\gamma_3(\zeta-1)]G_1(\rho,f_2+p_m) + 4bd(\zeta-1)(1-\xi)G_2(\rho,f_2+p_m)\Big\}$$

$$(0 \le \xi_1 < h/\ell\ ,\ h/\ell \le \zeta_1 \le 1) \qquad (4A.3)$$

$$w\,(\xi,\zeta) = \frac{1+\nu_2}{8\,\pi\,h\,\gamma_5 E_2}\Big[\gamma_4 G_0(\rho,f_{12}) + |\zeta-\xi|G_1(\rho,f_{12}) - \frac{\gamma_4}{2}\,[1 + (1-\mu_0)d\gamma_4]G_0(\rho,f_{11}) + (1-\mu_0)d\gamma_4(2-\zeta-\xi)G_1(\rho,f_{11}) + 2\,(1-\mu_0)d(\zeta-1)(1-\xi)G_2(\rho,f_{11}) + 2\mu_0\gamma_5\sum_{m=0}^{m=4} k_m\Big\{\gamma_3 cG_0(\rho,f_{11}+p_m) + (c-ac\gamma_3+4\gamma_0\gamma_4^2\,d^2)G_0(\rho,f_1+p_m) + 8\gamma_0\gamma_4 d[2c+d(\zeta+\xi-2)]G_1(\rho,f_1+p_m) + 4[c+4cd\gamma_0(\zeta-1)-4\gamma_0 d(c+d\zeta-d)(1-\xi)]\,G_2(\rho,f_1+p_m) - (ac+4\gamma_0\gamma_4^2\,bd^2)G_0(\rho,f_2+p_m) + 8\gamma_0\gamma_4 bd^2(2-\zeta-\xi)G_1(\rho,f_2+p_m) + 16\gamma_0 bd^2(\zeta-1)(1-\xi)G_2(\rho,f_2+p_m)\Big\}\Big]$$

$$(h/\ell \le \xi_1 \le 1\ ,\ h/\ell \le \zeta_1 \le 1) \qquad (4A.4)$$

where

$$\bar{x} = x\bar{e}_x + y\bar{e}_y + z_3\bar{e}_z \tag{4A.5}$$

$$\gamma_0 = 1-\nu_1 \tag{4A.6}$$

$$\gamma_1 = 1+\nu_1 \tag{4A.7}$$

$$\gamma_2 = 1-2\nu_1 \tag{4A.8}$$

$$\gamma_3 = 3-4\nu_1 \tag{4A.9}$$

$$\gamma_4 = 3-4\nu_2 \tag{4A.10}$$

$$\gamma_5 = 1-\nu_2 \tag{4A.11}$$

$$\mu_0 = \frac{E_2\gamma_1}{E_1(1+\nu_2)} \tag{4A.12}$$

$$a = \frac{\gamma_4-\mu_0\gamma_3}{\gamma_4+\mu_0} \tag{4A.13}$$

$$b = \frac{1-\mu_0}{1+\mu_0\gamma_3} \tag{4A.14}$$

$$c = \frac{1}{1+\mu_0\gamma_3} \tag{4A.15}$$

$$d = \frac{1}{\gamma_4+\mu_0} \tag{4A.16}$$

$$\rho = \frac{(x^2+y^2)^{1/2}}{h} \tag{4A.17}$$

$$\xi = z_3/h, \quad \xi_1 = z_3/\ell \tag{4A.18}$$

$$\zeta = z_4/h, \quad \zeta_1 = z_4/\ell \tag{4A.19}$$

$$G_n(\rho,\varphi) = \int_0^\infty \beta^n \exp(-\varphi\beta) J_0(\rho\beta)\partial\beta \quad \text{for } \varphi > 0 \tag{4A.20}$$

and $\bar{e}_x$, $\bar{e}_y$, $\bar{e}_z$ are the respective unit vectors along the x,y,z Cartesian coordinate system.

It can be shown that:

$$\left.\begin{aligned} G_0(\rho,\varphi) &= 1/s \\ G_1(\rho,\varphi) &= \varphi^3/s \\ G_2(\rho,\varphi) &= (-1/s^3)\,[1 - (3\varphi^2/s^2)] \\ G_3(\rho,\varphi) &= (-3\varphi\,/s^5)\,[3 - (5\varphi^2/s^2)] \\ \text{and} \qquad s &= (\rho^2+\varphi^2)^{1/2} \end{aligned}\right\} \tag{4A.21}$$

also,

$$
\left.\begin{aligned}
f_1 &= \xi + \zeta \\
f_2 &= 2 + \xi + \zeta \\
f_3 &= 4 + \xi - \zeta \\
f_4 &= 2 + \xi - \zeta \\
f_5 &= 4 - \xi + \zeta \\
f_6 &= 2 - \xi + \zeta \\
f_7 &= 4 - \xi - \zeta \\
f_8 &= 2 - \xi - \zeta \\
f_9 &= \xi - \zeta \\
f_{10} &= \zeta - \xi \\
f_{11} &= \xi + \zeta - 2 \\
f_{12} &= |\xi - \zeta|
\end{aligned}\right\} \qquad (4A.22)
$$

and k_m and p_m are constants (given at the end of the Appendix) and J_0 is the zero-order Bessel function of the first kind.

Equations (4A.1) to (4A.4) may be rewritten in the following forms

$$
w\,(\xi,\zeta) = \frac{\gamma_1}{8\,\pi\,h\,\gamma_0 E_1}\left\{ \gamma_3\, G_0(\rho, f_{12}) + |\xi-\zeta|\; G_1(\rho, f_{12}) + \sum_{m=0}^{m=4} k_m \left[\sum_{i=1}^{i=8} \sum_{j=0}^{j=3} A_{ij} G_j(\rho, f_i + p_m) \right] \right\}
$$

$$
\text{for } (0 \le \xi_1 < h/\ell \;,\; 0 \le \zeta_1 < h/\ell) \qquad (4A.23)
$$

$$
w\,(\xi,\zeta) = \frac{\gamma_1}{4\,\pi\,h\,E_1}\left\{ \sum_{m=0}^{m=4} k_m \left[\sum_{i=1}^{i=9} \sum_{j=0}^{j=3} B_{ij} G_j(\rho, f_i + p_m) \right] \right\}
$$

$$
\text{for } (h/\ell \le \xi_1 \le 1 \;,\; 0 \le \zeta_1 < h/\ell) \qquad (4A.24)
$$

$$
w\,(\xi,\zeta) = \frac{\gamma_1}{4\,\pi\,h\,E_1}\left\{ \sum_{m=0}^{m=4} k_m \left[\sum_{i=1}^{i=10} \sum_{j=0}^{j=3} C_{ij} G_j(\rho, f_i + p_m) \right] \right\}
$$

$$
\text{for } (0 \le \xi_1 < h/\ell \;,\; h/\ell \le \zeta_1 \le 1) \qquad (4A.25)
$$

$$w\,(\xi,\zeta) = \frac{1+\nu_2}{8\,\pi\,h\,\gamma_5 E_2}\Big[\gamma_4 G_0(\rho,f_{12}) + |\xi-\zeta|G_1(\rho,f_{12}) - (\gamma_4/2)[1+$$

$$(1-\mu_0)d\gamma_4]G_0(\rho,f_{11}) + (1-\mu_0)d\gamma_4(2-\zeta-\xi)G_1(\rho,f_{11}) + 2(1-$$

$$\mu_0)d(\zeta-1)(1-\xi)G_2(\rho,f_{11}) + 2\mu_0\gamma_5\Big\{\sum_{m=0}^{m=4} k_m\Big[\sum_{i=1}^{i=11}\sum_{j=0}^{j=2} D_{ij}G_j($$

$$\rho,f_i+p_m)\Big]\Big\}\Big]$$

$$\text{for } (h/\ell \le \xi_1 \le 1\ ,\ h/\ell \le \zeta_1 \le 1) \qquad (4A.26)$$

For all cases under consideration, p_m assumes the following values :

$$p_0 = 0,\ p_1 = 1,\ p_2 = 2,\ p_3 = 3,\ p_4 = 4 \qquad (4A.27)$$

The values of k_m, depending on the elastic properties of the layered half-space, are presented in Table 4A.1.

Table 4A.1 Values of k_m listed against arguments of μ_0, ν_1 and ν_2.

μ_0	ν_1	ν_2	k_0	k_1	k_2	k_3	k_4
1	0.25	0.25	1.000	0.000	0.000	0.000	0.000
5	0.25	0.25	1.000	-1.057	1.115	-1.138	0.422
10	0.00	0.25	1.000	-0.892	-0.312	0.668	-0.231
	0.25	0.25	1.000	-1.223	1.248	-1.203	0.459
	0.33	0.25	1.000	-1.412	1.955	-1.957	0.711
	0.45	0.25	1.000	-1.830	3.295	-3.249	1.107
	0.50	0.25	1.000	-2.079	3.999	-3.876	1.285
	0.25	0.00	1.000	-1.224	1.406	-1.401	0.522
	0.25	0.50	1.000	-1.225	1.069	-0.962	0.374
50	0.25	0.25	1.000	-1.364	1.328	-1.179	0.448
100	0.25	0.25	1.000	-1.382	1.337	-1.171	0.444
500	0.25	0.25	1.000	-1.397	1.344	-1.164	0.440
∞	0.00	-	1.000	-1.065	-0.261	0.851	-0.338
	0.25	-	1.000	-1.401	1.346	-1.162	0.439
	0.33	-	1.000	-1.613	2.158	-2.082	0.772
	0.45	-	1.000	-2.106	3.805	-3.818	1.367
	0.50	-	1.000	-2.409	4.719	-4.725	1.666

APPENDIX 4B

EVALUATION OF FLEXIBILITY COEFFICIENT

(after Chin, 1988)

The following numerical integration scheme has been utilised for the computations of the flexibility coefficients by the continuum programs described in Chapter 4.

Shaft Elements

The flexibility coefficient f_{ij} which denotes the vertical displacement at node i due to a uniformly distributed load of unit magnitude acting on shaft element j is given by:

$$f_{ij} = \frac{2}{A_S} \int_0^{\pi} \int_{z_1}^{z_2} I_w \, r_o \, dz \, d\theta \qquad (4B.1)$$

where z_1, z_2 = depth coordinates of ends of element j; r_o = radius of pile; $A_s = 2 \pi r_o(z_2 - z_1)$ = surface area of shaft element j; and I_w = coefficient of vertical displacement due to a unit vertical point load. The explicit expressions for I_w for a layered half-space are given in Appendix 4A.

The integrals given by Eq. (4B.1) can be efficiently evaluated using the Gaussian quadrature by transforming the z-θ coordinate system into the natural s-t coordinate system, as

$$f_{ij} = \frac{J^*}{\pi(z_2 - z_1)} \int_{-1}^{+1} \int_{-1}^{+1} I_w \, ds \, dt \qquad (4B.2)$$

where

$$\theta = \pi(s + 1)/2 \qquad (4B.3)$$

$$z = (z_1 + z_2)/2 + t(z_2 - z_1)/2 \qquad (4B.4)$$

$$J^* = \left(\frac{\partial\theta}{\partial s}\right)\left(\frac{\partial z}{\partial t}\right) - \left(\frac{\partial\theta}{\partial t}\right)\left(\frac{\partial z}{\partial s}\right) = \pi(z_2 - z_1)/4 \qquad (4B.5)$$

The integrals in Eq. (4B.2) may be evaluated numerically using the Gaussian quadrature (Zienkiewicz, 1977) as

$$\int_{-1}^{+1} \int_{-1}^{+1} I_w \, ds \, dt = \sum_{j=1}^{j=m} \sum_{i=1}^{i=m} w_i \, w_j \, I_w(s_i, t_j) \qquad (4B.6)$$

where w_i, w_j = weight constants; m = number of sampling points and $I_w(s_i,t_j)$ = value of function evaluated at sampling point (s_i,t_j).

Base Element

The flexibility coefficient due to the influence of the pile base is obtained as the displacement at node i due to a uniformly distributed circular patch load of unit magnitude acting at node j (the pile base) and is given by:

$$f_{ijb} = \frac{2}{A_b} \int_0^r \int_0^\pi I_w \; r \; dr \; d\theta \tag{4B.7}$$

where A_b = area of pile base. Hence Eq. (4B.7) in the natural s-t coordinate system is:

$$f_{ijb} = \frac{2J^*}{A_b} \int_{-1}^{+1} \int_{-1}^{+1} I_w \frac{r_o}{2} (t + 1) \; ds \; dt \tag{4B.8}$$

where $$\theta = \pi (s + 1)/2 \tag{4B.9}$$

$$r = r_o(t + 1)/2 \tag{4B.10}$$

$$J^* = (\frac{\partial\theta}{\partial s})(\frac{\partial r}{\partial t}) - (\frac{\partial r}{\partial s})(\frac{\partial\theta}{\partial t}) = \pi r_o/4 \tag{4B.11}$$

The integrals in Eq. (4B.8) can be evaluated efficiently using the Gaussian quadrature as in Eq. (4B.2). In performing the numerical integration of Eqs. (4B.2) and (4B.8) using Eq. (4B.6), the following scheme is found to be adequate for evaluating the flexibility coefficient, f_{ij}

(i) diagonal values of the flexibility matrix (i.e. i=j), m = 7 (see Eq. 4B.6)

(ii) off-diagonal values (i≠j) for the same pile, m=3, and

(iii) off-diagonal values (i≠j) for interaction between piles, m = 1. This is similar to using a point load for interaction computations between piles.

It may be noted that schemes (i) and (ii) were arrived at after extensive comparisons with solutions of Eqs. (4B.1) and (4B.7) evaluated by using Simpson's rule with very small increments of z-θ and r-θ coordinates. The use of Simpson's rule for such evaluations involves extensive computational time and is therefore less efficient than the Gaussian quadrature method.

APPENDIX 4C

EXAMPLES ON NUMERICAL PROCEDURES

(after Chin, 1988)

Incorporation of symmetry in pile group analysis

Consider, for example, the case of a row of three piles, as shown in Fig. 4C.1 with the nodal points numbered.

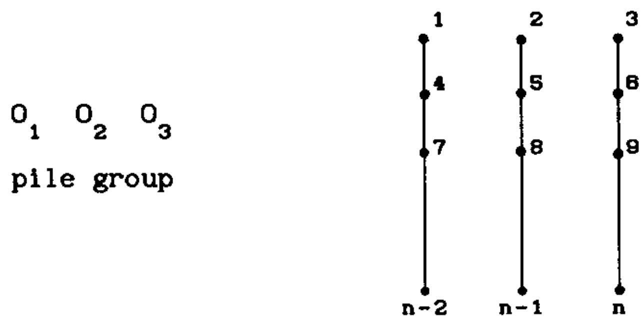

Fig. 4C.1 Row of three piles showing the numbering of the nodal points.

From Eqn. 4.2, the displacement at element i due to loads acting on the other elements is given by:

$$w_{si} = (f_{i1}P_{s1} + f_{i2}P_{s2} + f_{i3}P_{s3} + --- + f_{in}P_{sn}) \qquad (4C.1)$$

For pile groups with rigid (or flexible) caps under uniform vertical applied load, symmetry due to geometrical layout of the group piles results in Pile 1 and Pile 3 being subjected to the same loading conditions with $P_{s1} = P_{s3}$, $P_{s4} = P_{s6}$, $---$ $P_{s(n-2)} = P_{sn}$. Thus, there are two "different" pile types for the problem; Pile 1 and Pile 3 subjected to similar loading conditions and Pile 2 subjected to different loading conditions.

Eqn. 4C.1 can be rewritten as:

$$w_{si} = [(f_{i1}+f_{i3})P_{s1} + f_{i2}P_{s2} + (f_{i4}+f_{i6})P_{s4} + f_{i5}P_{s5} --- + (f_{i(n-2)}+f_{in})P_{s(n-2)}] \qquad (4C.2)$$

This implies that the problem can be re-analysed by considering only two piles; the influence of the third pile can then be considered by renumbering the nodal points as shown in Fig. 4C.2.

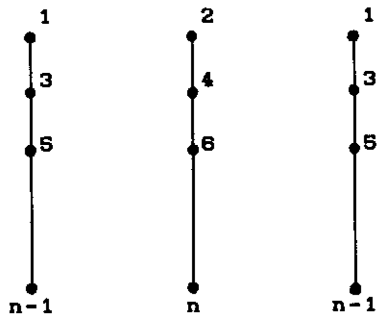

Fig. 4C.2 Node numbering for row of three piles with symmetry taken into account.

From Fig. 4C.2,

$$w_{s1} = (F_{11}P_{s1} + F_{12}P_{s2} + F_{13}P_{s3} + F_{14}P_{s4} + F_{1(n-1)}P_{s(n-1)} + F_{1n}P_{sn}) \qquad (4C.3)$$

Eqn. 4C.3 is similar to Eqn. 4C.2 with $F_{11} = (f_{11}+f_{13})$, $F_{12} = f_{12}$, $F_{13} = (f_{14} + f_{16})$, $F_{14} = f_{15}$, - - - - $F_{1(n-1)} = (f_{1(n-2)} + f_{1n})$ and $F_{1n} = f_{1(n-1)}$. These facts can be taken advantage of by numbering the nodal points of pile 3 equal to that as for pile 1, i.e 1, 3, 5, and so on while that for pile 2 is 2, 4, 6, and so on.

Therefore, the size of the flexibility matrix $[\mathbf{F_s}]$ (see Eqn. 4.3), particularly for large groups can be reduced by taking symmetry (due to geometrical layout of the group piles) into account by a proper sequence of numbering of the nodal points for the "different" pile types present. It should be noted that the influence of all the group piles are considered; the only difference being that the flexibility coefficient, f_{ij}, is accummulated in an efficient way in the flexibility matrix, $[\mathbf{F_s}]$.

Assembled stiffness matrix, $[K_p]$ of pile

The element stiffness matrix of a pile element under axial loading, K_{pe} is given by (see, for example, Smith 1982)

$$K_{pe} = \frac{E_pA}{L}\begin{bmatrix} 1 & -1 \\ -1 & 1 \end{bmatrix} \qquad (4C.4)$$

The assembled stiffness matrix of the group piles, $[K_p]$ for the case of the row of three piles with symmetry taken into account, can be analysed as that for two piles. Eqn. (4C.5) shows part of the stiffness matrix (until nodal point 6).

$$\frac{E_pA}{L}\begin{bmatrix} 1 & 0 & -1 & 0 & 0 & 0 & \\ 0 & 1 & 0 & -1 & 0 & 0 & \\ -1 & 0 & 2 & 0 & -1 & 0 & \\ 0 & -1 & 0 & 2 & 0 & -1 & \\ 0 & 0 & -1 & 0 & 2 & 0 & \\ 0 & 0 & 0 & -1 & 0 & 2 & \\ & & & & & & \\ & & & & & & \end{bmatrix} \qquad (4C.5)$$

<u>**"Big spring" technique**</u>

As mentioned in section 4.2.1, a specified prescribed displacement for piles can be most conveniently done numerically using the "big spring" technique (Smith, 1982).

From Eqn. (4.5), the load-displacement relationship for the pile group (or single pile) problem is:

$$[K_T]\ \{w_p\} = \{P\}$$

For the row of three piles, as shown in Fig. 4C.1, assume that a specified displacement at the pile heads (with a rigid pile cap) of w_t is desired. Taking symmetry into account, the numbering of the nodal points is as shown in Fig. 4C.2 for the two "different" pile types.

An arbitrary large value (say, $Y = 1\text{x}10^{12}$) is added to the total stiffness matrix, $[K_T]$ corresponding to the nodal positions 1 and 2. The value $(K_{T11}+Y)w_t$ (see Eqn. 4C.6) replace the value of the applied load in the appropriate nodal positions (1 and 2).

$$\begin{Bmatrix} K_{T11}+Y & K_{T12} & \cdots & K_{T1n} \\ K_{T21} & K_{T22}+Y & & \vdots \\ K_{T31} & K_{T32} & K_{T33} & \vdots \\ \vdots & & \ddots & \\ K_{Tn1} & \cdots & \cdots & K_{Tnn} \end{Bmatrix} \begin{Bmatrix} w_{p1} \\ w_{p2} \\ w_{p3} \\ \vdots \\ w_{pn} \end{Bmatrix} = \begin{Bmatrix} (K_{T11}+Y)w_t \\ (K_{T22}+Y)w_t \\ P_3 \\ \vdots \\ P_n \end{Bmatrix} \qquad (4C.6)$$

For w_{p1}, from Eqn. (4C.6), we obtain

$$(K_{T11}+Y)w_{p1} + [K_{T12}w_{p2} + K_{T13}w_{p3} + - - - - K_{T1n}w_{pn}] = (K_{T11}+Y)w_t \qquad (4C.7)$$

The terms within the square brackets can be considered very small compared to the term $(K_{T11}+Y)w_{p1}$. Evaluation of Eqn. (4C.7) will give:

$$w_{p1} = w_t \text{ (the prescribed pile head displacement)} \qquad (4C.8)$$

It can be similarly shown that w_{p2} is also equal to w_t.

Fictitious rigid members for equal pile head settlements

The use of fictitious members of large stiffness to ensure equal pile head settlements was mentioned in section 4.2.1 for the analysis of single pile groups or multiple pile groups under different prescribed axial loadings.

The stiffness matrix of these rigid members may be modelled using beam elements with high stiffness values (see, for example, Smith, 1982). In the present study, since there is no bending or rotation permitted in that element, an arbitrary large stiffness value (say, Y $= 1\times10^{12}$) is assumed for the elements of the stiffness matrix.

$$\text{i.e} \quad [K_b] = \begin{bmatrix} Y & -Y \\ -Y & Y \end{bmatrix} \qquad (4C.9)$$

Again, for the case of the row of three piles (Fig. 4C.1), with no symmetry taken into account, the bending stiffness matrix $[K_b]$ is assembled into the total stiffness matrix, $[K_T]$ of the load-displacement relationship (Eqn. 4.5) as shown below:

$$\begin{bmatrix} K_{T11}+Y & K_{T12}-Y & K_{T13} & K_{T14} & \cdots & K_{T1n} \\ K_{T21}-Y & K_{T22}+Y+Y & K_{T23}-Y & K_{T24} & & \vdots \\ K_{T31} & K_{T32}-Y & K_{T33}+Y & K_{T34} & & \vdots \\ K_{T41} & K_{T42} & K_{T43} & K_{T44} & \cdots & K_{T4n} \\ \vdots & & & & \ddots & \vdots \\ K_{Tn1} & \cdots & \cdots & \cdots & \cdots & K_{Tnn} \end{bmatrix}$$

The load-displacement relationship (Eqn. 4.5) is then solved; giving equal pile head settlements, i.e. $w_{p1} = w_{p2} = w_{p3}$. It may be noted that the procedure described above can also be used for the case of axially loaded pile groups with rigid caps; the difference being that the "big spring" technique imposed a desired displacement while the above procedure ensures equal pile head settlements for a given imposed load.

Table 4.1 Tentative values for model parameters required in present analysis using the nonlinear hyperbolic model (programs SCPIL2 and SCPIL3).

Model parameter	Remarks
ψ	= 0.02 (from model grouted pile tests in uncemented calcareous sediments, Lee (1988))
R_{fs}	= 0.5 (range 0 – 0.5, Poulos (1989b))
R_{fb}	= 0.9 (Poulos (1989b))
R_u, R_r	= 1.0 (assumed in present study)
D_{lim}, λ	see Poulos (1988a) for calcareous sediments

Table 4.2 Summary of the static analysis programs developed and utilised in the present study

Program name	Adopted soil model	Remarks
SPILE1	Elastic-plastic continuum model	Elastic or nonlinear analysis for axially loaded vertical single piles and pile groups (of any configuration). Provisions for "strain-softening" pile-soil response, and approximate residual stress determination.
SPILE2	Nonlinear hyperbolic continuum model	Elastic (by setting the hyperbolic constants $R_{fs} = R_{fb} = 0.0$) or nonlinear analysis for axially loaded vertical single piles and pile groups (of any configuration). For nonlinear analysis, approximate procedure for determining the flexibility coefficients. Provisions for "strain-softening" pile-soil response and approximate residual stress determination.
SPILE3	Nonlinear hyperbolic "t-z" hybrid model	Elastic ($R_{fs} = R_{fb} = 0.0$) or nonlinear analysis for axially loaded vertical single piles and pile groups (of any configuration). Elastic continuum solns. utilised for determining pile-soil-pile interaction flexibility coefficients. For nonlinear analysis of pile groups, only the single piles flexibility coefficients are evaluated in each incremental step. Provisions for "strain-softening" pile-soil response, and approximate residual stress determination.

Table 4.3 Summary of the static and cyclic analysis programs developed and utilsed in the present study

Program name	Adopted soil model	Remarks
SCPIL1	Elastic-plastic continuum model	As for static analysis (SPILE1). For cyclic loading analysis, "external soil movements" approach utilised for simulating permanent displ. accumulation. Capacity degradation modelled using either Matlock and Foo (1980) model or from empirical degradation "charts". Degradation of soil modulus and loading rate effect not considered but can be easily incorporated if required. Provision for "storm-loading" analysis.
SCPIL2 SCPIL3	Nonlinear hyperbolic continuum model Nonlinear hyperbolic "t-z" hybrid model	As for the corresponding static analyses (SPILE2 and SPILE3). For cyclic loading analysis, "degrading secant modulus" approach utilised for simulating permanent displ. accumulation. Capacity degradation modelled using either Matlock and Foo (1980) model or from empirical degradation "charts". Loading rate effect not considered but can be easily incorporated if required. Provision for "storm-loading" analysis. Note that the continuum model (SCPIL2) involves significant computation time in evaluating the single piles (i.e diagonal or f_{ii}) flexibility coefficients at each incremental step. The "t-z" hybrid model (SCPIL3) is however numerically more efficient.

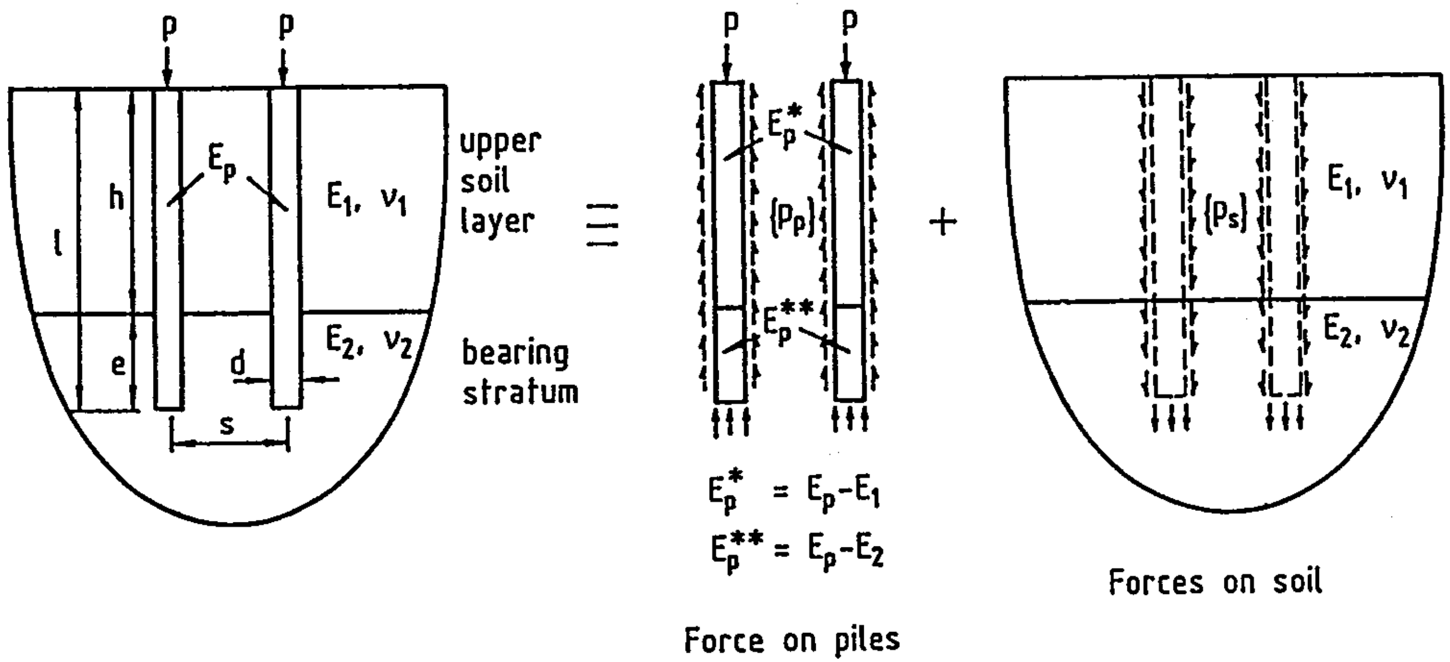

Fig. 4.1 Composition of pile group problem in a layered soil

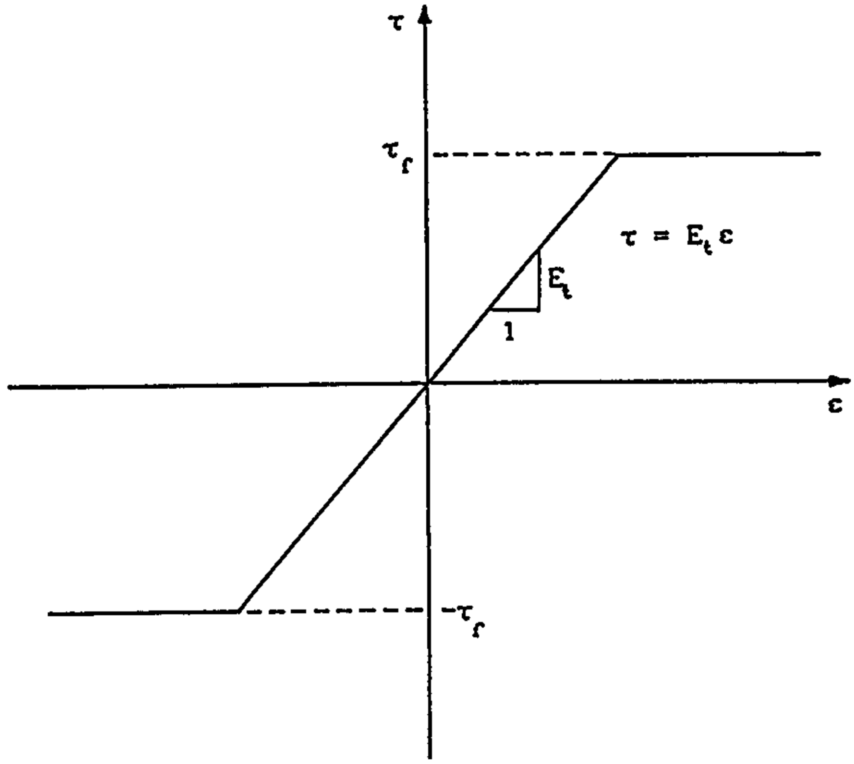

Fig. 4.2(a) Elastic-plastic interface model for static analysis

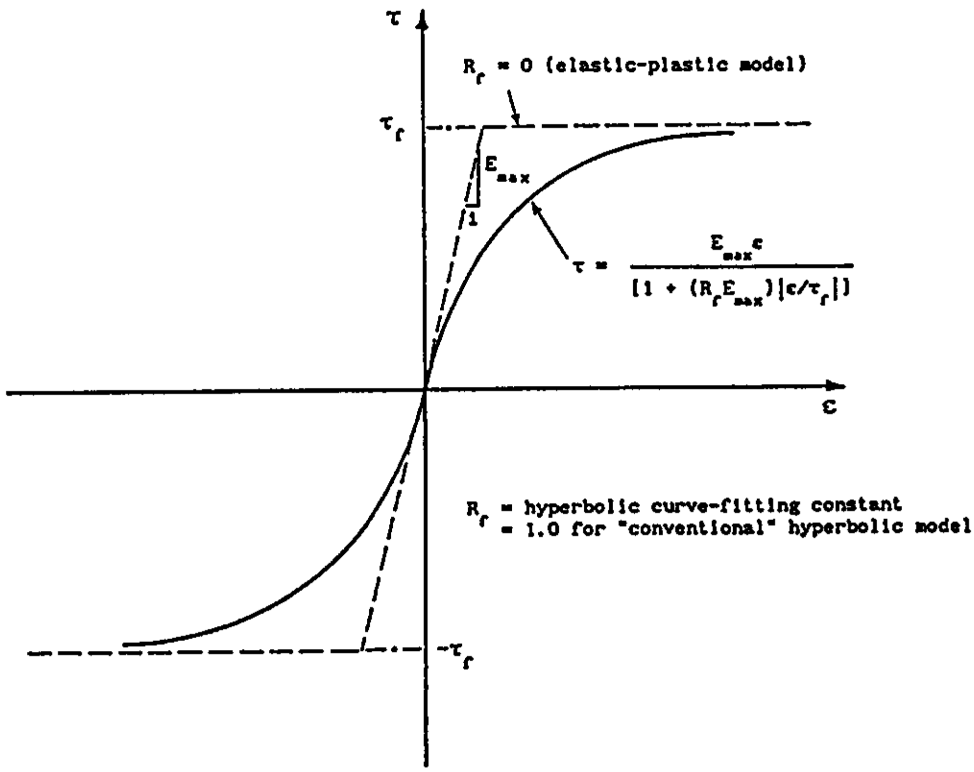

Fig. 4.2(b) Hyperbolic interface model for static analysis

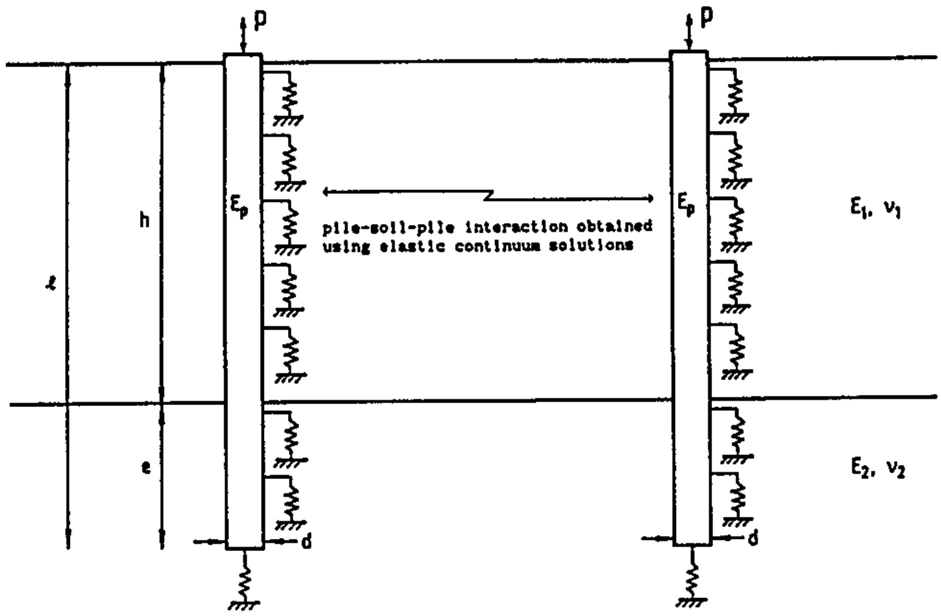

Fig. 4.3 "Hybrid" analysis approach for pile groups in layered soil

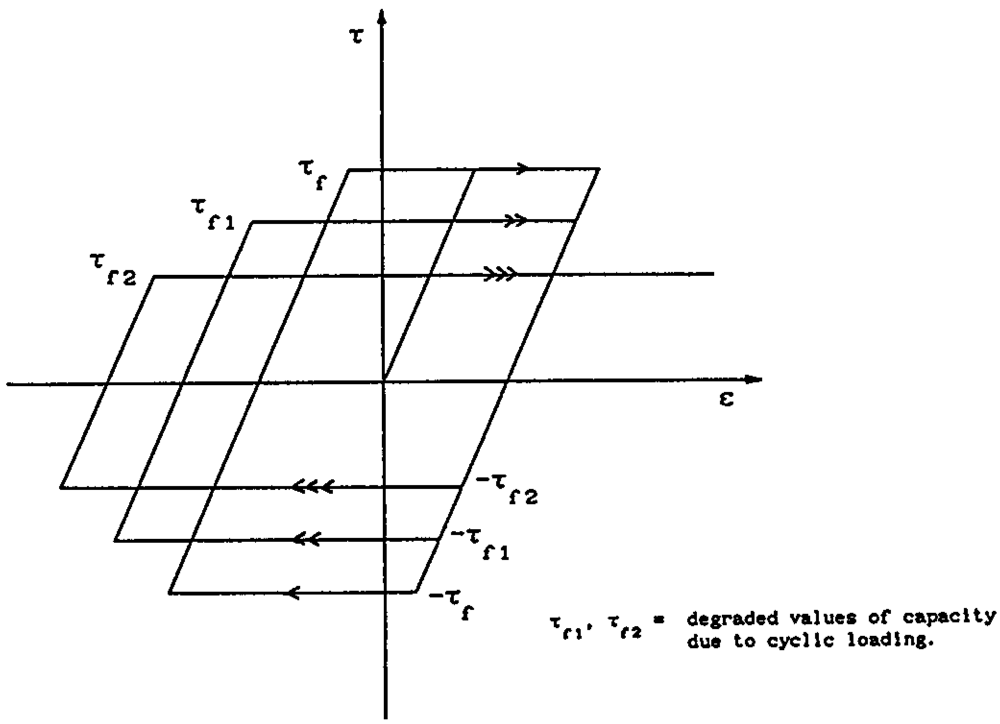

Fig. 4.4 Elastic-plastic (bilinear) interface model for cyclic loading analysis

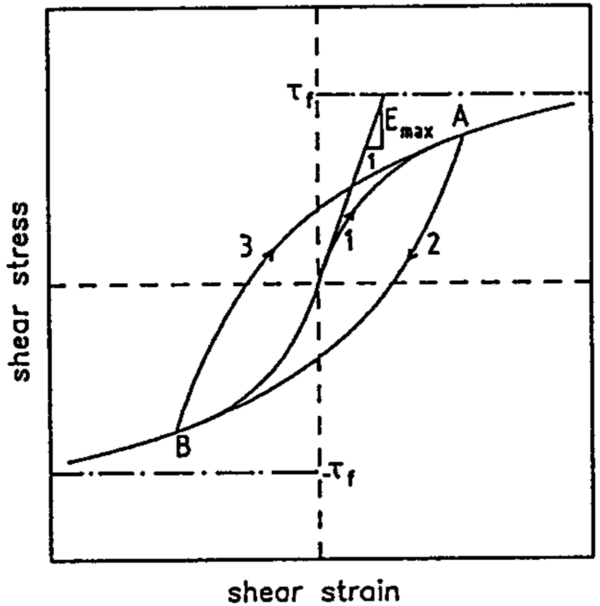

1: <u>initial "backbone" curve</u>

$$\tau = \frac{E_{max}\varepsilon}{[1 + (R_f E_{max})|\varepsilon/\tau_f|]}$$

2: <u>unloading curve</u>

$$(\tau - \tau_u) = \frac{E_{max}(\varepsilon-\varepsilon_u)}{[1 + (R_f E_{max}/2R_u)|(\varepsilon-\varepsilon_u)/\tau_{fc}|]}$$

3: <u>reloading curve</u>

$$(\tau - \tau_u) = \frac{E_{max}(\varepsilon-\varepsilon_u)}{[1 + (R_f E_{max}/2R_r\delta)|(\varepsilon-\varepsilon_u)/\tau_{fc}|]}$$

where (τ_u, ε_u) = point at which load reversal occurs,
τ_f = initial limiting static shear stress
τ_{fc} = limiting shear stress after cyclic loading

Fig. 4.5 Hyperbolic interface model for cyclic loading analysis

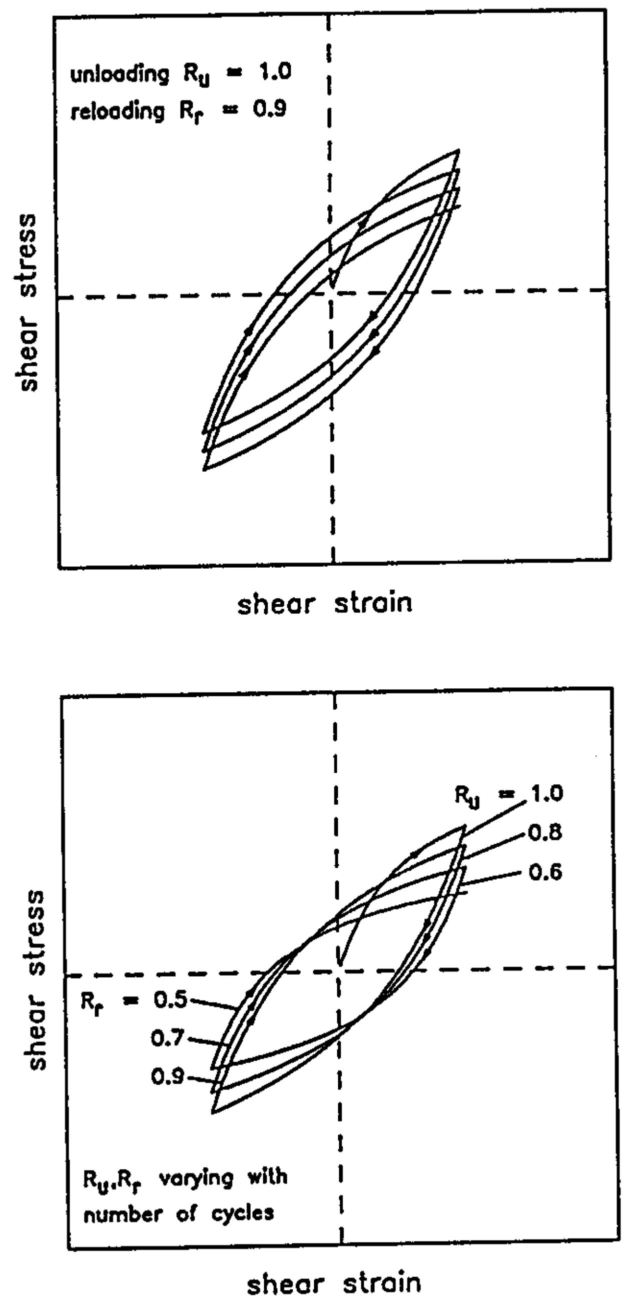

Fig. 4.6 Influence of hyperbolic curve-fitting constants R_u and R_r
(a) R_u = 1.0, R_r = 0.9; (b) varying R_u and R_r with cycles

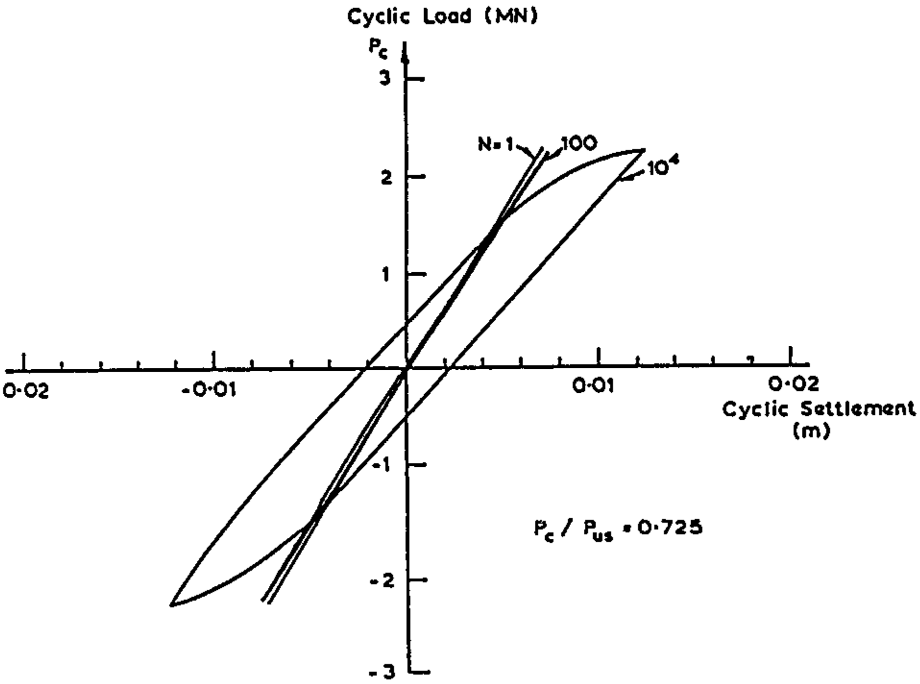

Fig. 4.7 Development of load-settlement "loop" (after Poulos, 1979a)

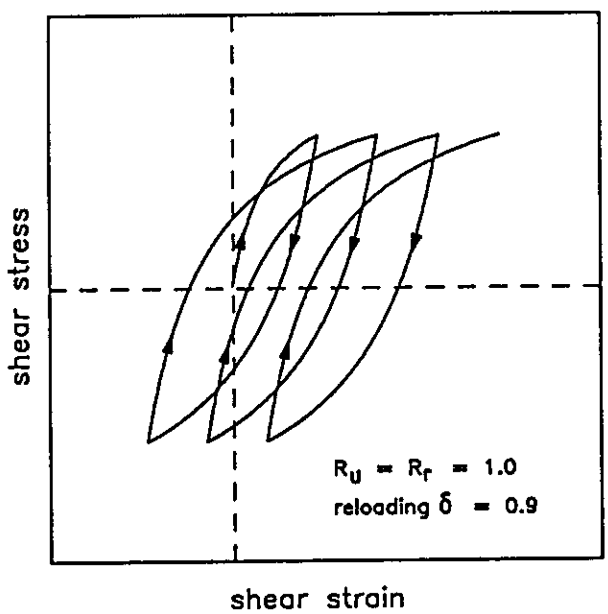

Fig. 4.8 Simulation of permanent displacement accumulation using the hyperbolic model (degrading δ value on reloading curve)

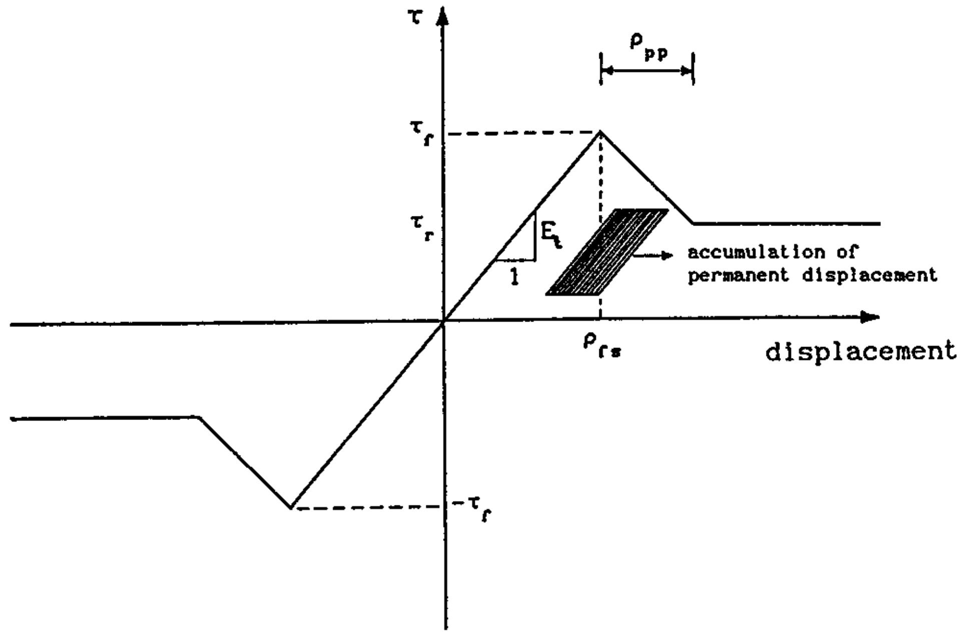

Fig. 4.9(a) Elastic plastic with "softening" model for cyclic loading analysis (program SCPIL1)

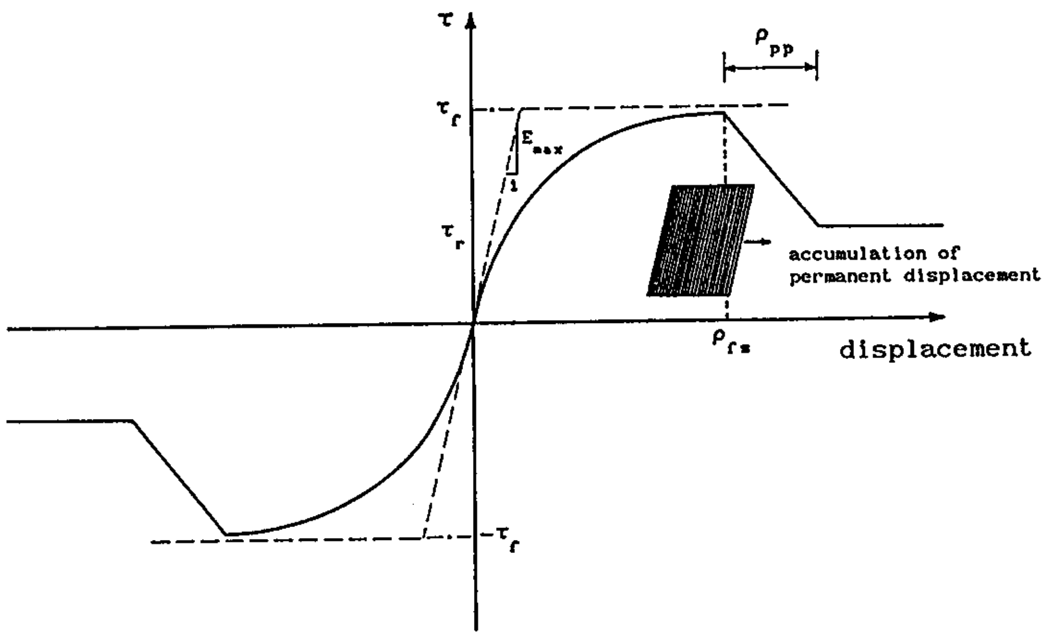

Fig. 4.9(b) Hyperbolic with "softening" model for cyclic loading analysis (programs SCPIL2 and SCPIL3)

CHAPTER 5

AXIAL PILE RESPONSE: SOME NUMERICAL RESULTS

CHAPTER 5

AXIAL PILE RESPONSE: SOME NUMERICAL RESULTS

5.1 INTRODUCTION

As mentioned in Chapter 3, one of the important uses of an analysis method for axial pile response is to enable "sensitivity" studies to be made of the influencing parameters. Such "sensitivity" studies will enable the relative importance of each of the influencing parameters to be assessed. The method of analysis, as described in Chapter 4, is used for the conduct of such "sensitivity" studies and some results of these studies are presented in this chapter.

Some static elastic solutions showing the accuracy of the t-z "hybrid" approach proposed (Chapter 4) are presented for both single piles and pile groups. The influence of the soil model adopted (elastic-plastic continuum model, nonlinear hyperbolic continuum model and nonlinear hyperbolic t-z "hybrid" model) on the static nonlinear pile response in three hypothetical soil profiles is also presented.

For the cyclic response of single piles, the influence of the following parameters are considered: the degradation of pile capacity, permanent pile displacement accumulation, effect of residual stresses, effect of strain-softening response, and a general "storm-loading" condition. Finally some numerical solutions for the cyclic response of pile groups are also presented.

It should be noted that it is not possible to present parametric results that will cater to all conceivable situations. As such, the numerical results presented in this chapter only serve to highlight some of the pertinent parameters that affect the pile response.

5.2 STATIC RESPONSE ANALYSIS

Some numerical results obtained using the static analysis programs SPILE1, SPILE2 and SPILE3 are presented in this section. In particular, the accuracy of elastic solutions obtained using the t-z "hybrid" approach (program SPILE3) is assessed. Some results showing the effect of residual stresses on both single piles and pile groups are also presented. Unless otherwise specified, between 10 and 20 elements are utilised to discretise the pile, with the larger number of elements being used for the longer piles.

5.2.1 Single Piles

Extensive parametric solutions for the elastic static response of single piles in a homogeneous soil deposit have been presented (for example, Poulos and Davis ,1980; Butterfield and Banerjee, 1971a) using the solutions of Mindlin (1936). Solutions for piles embedded in a two-layered soil profile have also been presented by Lee *et al.* (1987) and Chin (1988) where the analytical solutions of Chan *et al.* (1974) for a layered elastic half-space were employed.

In the following sub-section (section 5.2.1.1), some results obtained using the present analysis method, as outlined in Chapter 4, are compared with published solutions.

5.2.1.1 Elastic solutions

In the absence of analytical layered solutions at the time, Poulos and Davis (1968) utilised Mindlin's solutions in conjunction with the approximation of Steinbrenner (1934) for piles embedded in a finite soil layer overlying a rigid base. For the present elastic continuum analysis, the depth h of the finite soil layer is specified with the appropriate soil parameters E_1 and ν_1. The rigid base is obtained by specifying an arbitrary large value (say, 1×10^9) for the modulus ratio E_2/E_1. It may be noted that Poulos' method can only approximately account for a finite stiffness of the base layer while the present more rigorous formulation (program SPILE1) can easily cater by specifying an appropriate value for the modulus E_2.

Fig. 5.1 compares the single pile settlement influence value I_o obtained by Poulos (1974), Valliappan *et al.* (1974) and the present analysis (using program SPILE1). Close agreement is obtained between the present solutions and the finite element solutions of Valliappan *et al.* (1974). Poulos' approximate approach consistently gives stiffer solutions, particularly for smaller finite layer depths ($h/\ell < 2$) indicating the inadequacy of the approximation for such depths. For $h/\ell > 2$, better agreement is obtained and approaches the homogeneous solutions, indicating the lesser influence of the rigid base beyond such depths.

In practice, piles are commonly used to penetrate a relatively homogeneous upper layer to socket into a stiffer underlying bearing layer. Approximate analysis utilising Mindlin's solutions is commonly used to obtain the flexibility coefficients in such soil profiles (Poulos, 1979b). In the present formulation, the two-layered profile can be obtained by specifying appropriate parameters E_1, ν_1 and E_2, ν_2 for the upper and lower soil layers respectively.

Fig. 5.2 shows the influence of the soil stiffness ratio, E_2/E_1 on single pile settlements obtained by three different approaches. The approximate averaging procedure of Poulos and Davis (1980) consistently overestimates and underestimates the pile settlements for values of E_2/E_1 greater than unity and less than unity, respectively. The present solutions are in reasonable agreement with the infinite layer approach of Guo *et al.* (1987). Comparison of the load distribution (Fig. 5.3) along the pile shows good agreement except near the base where the present analysis (SPILE1) gives greater load transfer than that obtained by Guo *et al.* (1987).

For piles embedded in Gibson soil with modulus increasing linearly with depth, an approximate analysis using the present formulation is used (program SPILE1). The modulus for the upper soil layer E_1 is obtained as the mean of the moduli at the influenced and influencing nodes (Poulos, 1979b).

Fig. 5.4 shows that the present analysis consistently gives lower normalised stiffness compared to that obtained by Chow (1989) where an axi-symmetric finite element procedure is used to obtain the flexibility coefficients. The lower stiffness values are expected since the increasing modulus between the influenced and influencing nodes, and that below the pile tip, are not taken into account in the present approximate procedure. It may be noted that Yamashita *et al.* (1987), and Lee and Poulos (1990) proposed approximate procedures to take this intermediate increasing modulus (hence, stiffness) of the soil into account. The Banerjee and Davies (1977) solutions for square piles (Fig. 5.4) however show greater discrepancies particularly for ℓ/d = 10, and K (= $E_p/E_{v(l)}$) = 100 ($E_{v(l)}$ = soil Young's modulus at the level of the pile base in the Gibson soil profile).

Further comparisons showing the accuracy of the present elastic continuum analysis method, as outlined in Chapter 4, can be obtained from Chin (1988) and Chin *et al.* (1990). It may be noted that the nonlinear hyperbolic continuum model program (SPILE2) can similarly be used for an elastic analysis by setting the hyperbolic constants $R_{fs} = R_{fb} = 0$.

Fig.5.5 shows a comparison of the solutions for a single pile, which is embedded in a two-layered soil profile, obtained using the present t-z approach and the "conventional" approach. In the "conventional" approach, the solution procedure is as described in Chapter 4 but with the averaged r_m value calculated using equation (4.9). In the equation, the inhomogeneity factor $\rho = E_{ave}/E(\ell)$ where E_{ave} and $E(\ell)$ are the averaged pile shaft soil Young's moduli along the pile and pile base respectively, and the Poisson's ratio $\nu = \nu_1$ = the Poisson's ratio of the upper soil layer. As mentioned earlier, the linear elastic solutions, with no pile-soil slip, can be obtained by setting the hyperbolic constants $R_{fs} = R_{fb} = 0$. Solutions are presented showing the influence of the pile-soil stiffness ratio, K (= E_p/E_1) soil stiffness ratio, E_2/E_1 and the socketing length, e/d. As evident from the figure, quite significant differences occur between the present t-z solutions and the "conventional" solutions particularly for smaller h/d and e/d values, and greater E_p/E_1 and E_2/E_1 values.

To investigate further the accuracy of the t-z "hybrid" approach (program SPILE3), comparisons are made with the more rigorous elastic continuum solutions (Chin, 1988) for a layered soil.

Fig. 5.6(a) shows a comparison of solutions for the normalised single pile stiffness, $P/(E_1 d w_t)$ for various values of the distance, x, of the stiffer lower layer below the pile base. The present solutions are consistently stiffer than the continuum solutions (Chin, 1988) with a maximum difference of +12% for the case of x/d = 2.5 and $E_2/E_1 = \infty$. The stiffer solutions are expected since the soil continuity has been ignored in the present analysis for the single piles response. The influence of the pile length (ℓ/d) for two values of x/d = 5 and 30 is shown in Fig. 5.6(b).

The influence of the socketing length (e/d) is shown in Fig. 5.7(a) for e/d = 2 and 10. The case of e/d = 0 corresponds to that where the pile base rests at the interface of the two-layered profile. Stiffer solutions are again obtained using the present approach (SPILE3) with a maximum difference of +18% for the case of h/d = 5 and e/d = 0; the difference however decreases with increasing h/d. It is also interesting to note that the influence of the socketing length (e/d) decreases with increasing h/d, the pile behaving essentially as a friction pile with little load being transferred to the pile base. Also shown are the full continuum solutions (for e/d = 2 and 10) obtained using the analytical solutions of Chan *et al.* (1974) in conjunction with the averaging procedure of Poulos (1979b) where an average E value of the influenced and influencing nodes (with $\nu_1 = \nu_2 = 0.40$ and $E_1 = E_2$ = the average E value) is used in obtaining the flexibility coefficients. This is equivalent to utilising Mindlin's homogeneous solution with the average E value. Stiffer solutions are obtained using this averaging procedure particularly for the smaller h/d and e/d values. A comparison of the CPU time required by both methods is shown in Fig. 5.7(b). The present approach can be seen to be computationally more efficient than the continuum approach, particularly for longer piles where more elements are required for convergence of the solutions. This "saving" in CPU time makes the present approach (SPILE3) better suited for the cyclic response analysis of single piles and pile groups than the full continuum analysis (Poulos, 1983; Lee, 1988).

The effects of the pile-soil stiffness ratio, E_p/E_1 and the soil stiffness ratio, E_2/E_1 are shown in Figs. 5.8(a) and 5.8(b), respectively. Reasonably good agreement is obtained between the present solutions (SPILE3) and the continuum solutions (Chin, 1988) although, generally, stiffer solutions are obtained using the present analysis. The influence of e/d is less for the more compressible piles (Fig. 5.8a) while for $E_2/E_1 > 10$, the increase in pile stiffness becomes small when the socket length exceeds about 10 diameters (Chin, 1988; Chow *et al.* 1990). The full continuum solutions, obtained in conjunction with the averaging procedure of Poulos (1979b), again give stiffer solutions particularly for greater E_p/E_1 values (Fig. 5.7a) and E_2/E_1 values (Fig. 5.8b).

Fig. 5.9(a) shows the effect of increasing the socketing length, e/d on the normalised single pile stiffness. The continuum solutions (Chin, 1988) show that for e/d > 5 and 15 for $E_2/E_1 = 100$ and 10 respectively, there is marginal increase in stiffness for further increase in e/d. The present solutions (SPILE3), however, show a decrease in stiffness for such further increase in e/d; the decrease being more pronounced for $E_2/E_1 = 100$. As noted by Randolph and Wroth (1978) and Chow (1984, 1986c), the expression for r_m (equation 4.9) was found to be inadequate for long, very compressible single piles.

Therefore, the second expression of equation 4.12, corresponding to the socketed portion of the pile, may not be adequate for very compressible piles (i.e small E_p/E_2 ratios) and large socketing lengths, as noted from Fig. 5.9(a). A more accurate r_m value, if required, may have to be determined from a more refined numerical method such as the finite element method. However, for most practical problems, the use of equation 4.12 is probably adequate as shown by the comparisons of the previous figures. A comparison of the load distribution along the pile (Fig. 5.9b) shows reasonably good agreement between the present t-z solutions and the continuum solutions. The solutions obtained from the "conventional" r_m value show a greater load transfer in the upper soil layer as compared to the solutions from the other two approaches.

Table 5.1 shows a comparison of the settlement influence factor, I_ρ (= $w_t dE_{sl}/P$; E_{sl} = soil Young's modulus at the level of the pile base and w_t = pile head settlement) and the proportion of base load for single piles in Gibson soil. The present solutions (SPILE3) are in good agreement with the AXPIL5 (modified BEM; Poulos, 1979b) and ISOPE (FEM; Poulos, 1979b) solutions for the pile settlement. The Banerjee and Davies (1977) solutions, which are for a pile of square cross-section, also agree well with the other solutions except for ℓ/d = 10, K_b = 1000, and ℓ/d = 25, K_b = 100 where $K_b = E_p/E_{sl}$. The lack of agreement for these two cases is not clear and as noted by Poulos (1979b) could not be credibly attributed to the difference in pile cross-sections.

For the proportion of load transferred to the pile base, the Banerjee and Davies (1977) solutions are consistently lower than the other solutions. The present t-z solutions are in good agreement with the ISOPE solutions for ℓ/d = 10, and the AXPIL5 solutions for ℓ/d = 25.

Table 5.2 shows comparisons with the solutions of Randolph and Wroth (1979a) for single end-bearing piles in Gibson soil overlying a stiffer bearing layer. Generally good agreement is obtained between the present solutions (SPILE3) and the solutions of Randolph and Wroth (1979a). The simple analytical solution of Randolph and Wroth (1979a) significantly overpredicts the single pile stiffness for ρ = 0.5, ξ = 0.01 and ℓ/r = 40 and 80; the present solutions however are in good agreement with the finite element solutions.

The comparisons as shown previously (Figs. 5.6 to 5.9; Tables 5.1 and 5.2), for single piles in two-layered and Gibson soil profiles, show that the present t-z solutions (SPILE3) are in reasonably good agreement with the elastic continuum solutions. The advantage of the t-z approach is the significant reduction in computation time required. Further comparisons of the accuracy of the t-z approach (SPILE3) for pile groups are presented in section 5.2.2.1.

5.2.1.2 Nonlinear solutions

As shown in the previous section, elastic solutions obtained using the t-z approach (SPILE3) for single piles are in reasonably good agreement with the full continuum solutions. It may be noted that elastic solutions may not be applicable particularly for soils that exhibit significant nonlinear response and when the applied loading approaches the failure capacity of the pile. For such cases, an iterative nonlinear analysis is required in order to obtain a more realistic prediction of the pile response.

This section presents some comparisons of the load-settlement response of a single pile obtained using the full continuum elastic-plastic soil model (program SPILE1), the nonlinear hyperbolic continuum model (SPILE2) and the nonlinear hyperbolic t-z model (SPILE3).

A 50m long pile, of 1m diameter, embedded in three hypothetical but representative soil profiles (Poulos, 1987) are considered. The three soil profiles are a stiff overconsolidated clay, a soft normally consolidated clay, and a medium-dense sand. Fig. 5.10 shows the embedded pile, the variations of soil modulus and ultimate unit shaft resistance with depth. The relevant representative parameters for the three soil profiles, as suggested and utilised by Poulos (1987), are as shown in Table 5.3. The pile is discretised into 10 shaft elements and one base element, with a total of 11 nodal points.

The load-settlement response of the pile for three different pile moduli E_p = 2500 MPa, 25000 MPa and 250000 MPa are obtained. As noted by Poulos (1987), the modulus value of 25000 MPa is of practical relevance, and would apply to a concrete pile or a steel tube pile in which the steel section occupies about 12% of the gross cross-sectional area of the pile. The value of 2500 MPa and 250000 MPa would correspond to a extremely compressible and an extremely stiff pile respectively. For the nonlinear hyperbolic models (SPILE2 and SPILE3), some results showing the influence of the hyperbolic constants, R_{fs} and R_{fb}, are also presented.

Fig. 5.11 shows the influence of the soil model adopted, for three different pile moduli, on the nonlinear load-settlement response of the pile in stiff clay. As shown, the nonlinear behaviour is most significant for the more compressible piles (i.e. E_p = 2500 MPa), and the nonlinear hyperbolic continuum model adopted. For the practical pile modulus value of 25000 MPa, and at normal working load (safety factor of 2.0 to 3.0 based on ultimate load capacity), the computed load-settlement response is almost linear and is not influenced significantly by the soil model adopted. This further confirms the applicability of elastic solutions for determining the pile response under normal working load conditions (Poulos and Davis, 1980). For higher load values, particularly when the failure load is approached, significant nonlinearity results, the degree of nonlinearity being dependent on the soil model adopted. It is interesting to note that the computed nonlinear response using the nonlinear hyperbolic t-z model (with $R_{fs} = R_{fb} = 0.9$) is in reasonably good agreement with that of the elastic-plastic model. It should also be noted that the nonlinear t-z approach (SPILE3) is computationally more efficient than the nonlinear continuum approach (programs SPILE1 and SPILE2).

The effect of the hyperbolic constants R_{fs} and R_{fb} on the computed load-settlement response are shown in Figs. 5.12(a) and 5.12(b) for three different pile modulus values. Again, under normal working load conditions, the influence of R_{fs} and R_{fb} on the computed load-settlement response is insignificant. The effect is even less significant for the more compressible pile (E_p = 2500 MPa). For loads approaching the failure load, a stiffer response is obtained for a lower R_{fs} and R_{fb} values (corresponding to a lower degree of nonlinearity). As shown in Fig. 5.12(b) (curves 2 and 3), the effect of a more nonlinear pile base response (R_{fb} = 0.9) on the computed response is not significant. However, the effect of a lower R_{fs} value (curves 1 and 3), results in a stiffer response beyond the "working load" value. This shows that, for this particular soil profile and the adopted representative resistance values, the effect of R_{fs}, as compared to that of R_{fb}, has a more significant influence on the computed load-settlement response. This is so particularly for long friction piles where the shaft capacity forms a major proportion of the total pile capacity.

Further comparisons of the developed shear stress (normalised by the limiting resistance value) and load distributions, at an applied load of 50% of ultimate pile capacity, are shown in Figs. 5.13(a) and 5.13(b) respectively. A similar trend in the developed shear stress distributions is obtained from the three different approaches, the elastic-plastic model giving the largest normalised shear stress in the upper one-third of the pile, and the least in the lower two-thirds (Fig. 5.13a). As shown, the pile response is still elastic i.e. no significant pile-soil slip along the pile has occurred.

For the pile in soft clay (Figs. 5.14 to 5.16), generally similar observations as those for the stiff clay profile are obtained. The developed shear stress distributions (Fig. 5.16a), for the upper half of the pile, however show non-similar distributions between the continuum solutions (SPILE1 and SPILE2) and the t-z solutions (SPILE3). Nevertheless, reasonably good agreement is obtained for the load distributions along the pile (Fig. 5.16b).

Figs. 5.17 to 5.19 show the computed response for the pile in a medium-dense sand profile. As before, the influence of the soil model adopted is significant beyond the working load range (Fig. 5.17); the differences between the three nonlinear responses however are more pronounced as compared to those for the stiff clay profile (Fig. 5.11) and the soft clay profile (Fig. 5.14). Similar more pronounced responses are also observed for the effect of R_{fs} and R_{fb} values (Figs. 5.18a and 5.18b). As shown in Fig. 5.18(b) (curves 2 and 3), the effect of a more nonlinear pile base response has a major influence on the computed response as the failure load is approached. This is so because the pile base resistance forms a major proportion of the total pile capacity in the medium-dense sand profile. The developed shear stress (Fig. 5.19a), at a load of 50% of ultimate pile capacity, shows that the total shaft capacity is almost fully mobilised. Again, the load distributions along the pile, from the three different approaches, are in favourable agreement (Fig. 5.19b).

The following points are noted from the nonlinear static solutions presented in Figs. 5.11 to 5.19 for the three different representative soil profiles considered.

- : under normal working load conditions, the load-settlement response is essentially elastic for the pile modulus of practical relevance. The influence of the adopted nonlinear model is insignificant within the working load range.
- : beyond the working load range, the computed load-settlement response is influenced quite significantly by the nonlinear model adopted. In particular, where the total shaft capacity or pile base capacity forms a major proportion of the total pile capacity, proper modelling of the nonlinear response of the shaft or pile base response respectively is required in order to obtain a more "correct" response beyond the working load range.

Although the above conclusions are drawn from the three soil profiles that have been considered, it is felt that the conclusions are still valid for other soil profiles, for example, in a calcareous soil profile. It should be recalled that the conclusions drawn were based on the analyses conducted using an elastic-plastic model, and the nonlinear hyperbolic models. The use of a more nonlinear soil model is expected to cause an earlier deviation (of the load-settlement behaviour) from the linear elastic response even within the working load range (Jardine *et al.*, 1986). As mentioned in Chapter 4, the analysis procedure described (see Chapter 4) is applicable to any soil type provided that the relevant soil parameters corresponding to the soil type considered be utilised.

5.2.1.3 Effect of residual stresses

The numerical solutions that have been presented thus far assume an initially stress-free pile. However, in the actual practical situation, the pile is usually non stress-free initially i.e. some residual stresses exist along the pile. These residual stresses are influenced by the pile and soil type, and the method of pile installation. Significantly higher residual stresses are obtained for driven piles than bored piles where the effect of pile installation is less significant.

As noted by Poulos (1987), a more rigorous approach for determining the residual stresses, due to pile installation effects, is to use a wave equation analysis (Holloway *et al.*, 1978). However, as a first approximation, the simplified approach of Poulos (1987) may be adequate for most practical situations.

The simplified approach of Poulos (1987), as described in section 4.6, has been incorporated into the static analysis programs SPILE1, SPILE2 and SPILE3. Some results obtained using the elastic-plastic continuum program (SPILE1) and the nonlinear hyperbolic (with $R_{fs} = R_{fb} = 0$) t-z program (SPILE3) are presented for the three soil profiles (as used by Poulos, 1987) utilised in section 5.2.1.2 (see Fig. 5.10 and Table 5.3). It may be noted that more extensive solutions on the effects of residual stresses have been presented by Poulos (1987), and the limited results presented herein serves to verify the present residual stress incorporation and a comparison of the elastic-plastic continuum (SPILE1) and t-z (SPILE3) approaches.

Figs. 5.20 (a-b), 5.21 (a-b) and 5.22 (a-b) show the residual stress distributions in the stiff clay, soft clay and medium-dense sand profiles respectively. As shown, the magnitude of the residual stresses developed along the pile is more significant for the more compressible piles (E_p = 2500 MPa). Also, significant negative tensile slip may occur in the upper portion of the pile, particularly in the medium-dense sand profile, for the more compressible piles. The elastic-plastic t-z solutions (SPILE3) are in general agreement with those obtained using the elastic-plastic continuum program, SPILE1. It is found that the continuum solutions presented herein are in reasonably good agreement with those obtained by Poulos (1987), although the comparisons are not shown in the figures.

At this point, the discussion of Leonards and Darrag (1989) on the computed residual stress distributions obtained by Poulos (1987) is worthy of note. As noted by Leonards and Darrag (1989), for the medium-dense sand profile, the solutions of Poulos (1987) (also given by Fig. 5.22a for E_p = 25000 MPa) show that negative tensile slip occurs along almost the entire pile length, contrary somewhat to the field measurements reported by Rieke and Crowser (1987). This inconsistency has been partly attributed by Leonards and Darrag (1989) to the use of a "lower" soil modulus (as given by the linear modulus profile; see Table 5.3) at the pile base, as utilised by Poulos (1987).

As noted by Poulos (1989d), the use of a higher modulus at the pile base (than that given by the linear modulus variation profile) may be appropriate for piles in a sand profile. Although the analysis approach of Poulos (1987) is greatly simplified, it nevertheless provides a simple approximation for incorporating the effects of residual stresses, rather than assuming an initially stress-free pile.

Fig. 5.23 shows an example where the incorporation of an initial residual stress distribution results in a stiffer response, under subsequent compression loading, when the failure load is approached. This has important implications particularly for the case of long offshore piles with length to diameter ratio (ℓ/d) of about 100 or more. For such cases, where the influence of the pile base is not significant initially, a stiffer load-settlement curve is obtained when the residual stresses are included in the analysis. However, in situations where the pile base influence is significant (for example, short piles or when the pile tip is embedded in a relatively much stronger material) a less stiff response (under compression loading) may be obtained as a result of the residual compressive stress at the pile tip. As mentioned earlier, more extensive solutions on the effects of residual stresses can be obtained from Poulos (1987).

5.2.2 Pile Groups

As with the case of single piles (section 5.2.1), some results showing the accuracy of the present elastic method of analysis for pile groups are presented. In particular, the accuracy of the t-z "hybrid" approach for pile groups (SPILE3) is assessed. Finally, solutions obtained using the t-z "hybrid" approach are compared with field measurements of vertical pile groups embedded in a layered soil deposit.

5.2.2.1 Elastic solutions

For pile groups, the loading of adjacent piles will give rise to increased settlement compared to that of an isolated single pile. The interaction factor, first proposed by Poulos (1968), is used to quantify this additional increased settlement as a ratio of the isolated single pile settlement.

Fig. 5.24 compares the interaction factors, for two identical piles in a finite soil layer, using the present elastic continuum analysis

(SPILE1) and the solutions of Poulos (1968). As shown, the interaction effect is underestimated using Poulos' approximate approach for small finite layer depths ($h/\ell < 2$). Both solutions are however in close agreement as h/ℓ tends to infinity. It may be noted that (as shown in Fig. 5.1) the present elastic continuum solutions (SPILE1) for single piles have been shown to be in close agreement with finite element solutions.

For two identical piles embedded in a two-layered soil profile, reasonably good agreement (Fig. 5.25), except for s/d (pile spacing to diameter ratio) less than three, is obtained between the present continuum solutions and the infinite layer solutions of Cheung *et al.* (1988). For s/d less than three, the present continuum solutions give consistently lower interaction values. As mentioned in Chapter 4, the interaction between nodes of different piles is obtained using unit point load in the present method of analysis. As shown in Fig. 5.25, generally closer agreement is obtained for the smaller s/d ratios by using a distributed ring load for interaction between piles.

For pile groups in Gibson soil, comparisons are made with the more rigorous solutions of Chow (1989). Fig. 5.26 compares the stiffness reduction factors (Butterfield and Douglas, 1981), K_G/N_PK_1 where K_G and K_1 are the stiffnesses of the pile group and single pile respectively, and N_P is the total number of piles in the group. Lower stiffness reduction factors are obtained as compared to the solutions of Chow (1989) with a maximum difference of -15%. It may be noted that an approximate procedure, in conjunction with the analytical solutions of Chan *et al.* (1974), is used to calculate the flexibility coefficients in the present elastic continuum analysis (SPILE1) while Chow (1989) utilised a more refined axi-symmetric finite element procedure. Although the present analysis for a Gibson soil is approximate, it nevertheless can be used to give a preliminary conservative estimate of the group stiffness.

As with single piles, the accuracy of the t-z "hybrid" approach (SPILE3) for pile groups are compared to the elastic continuum solutions for a two-layered system and a Gibson soil profile.

The elastic interaction factor, α, for two equally loaded single piles socketed into the lower bearing layer is shown in Fig. 5.27. The present t-z "hybrid" solutions are in good agreement with the continuum solutions. As shown, the interaction effect is more significant for a less compressible pile and for decreasing pile spacing.

Fig. 5.28 shows the load distributions for a square 3x3 pile group obtained using the present approach (SPILE3), the continuum method (Chin, 1988; also from SPILE1) and the interaction factor approach (Poulos and Davis, 1980). Generally good agreement is obtained between the three different approaches.

For pile groups, it is convenient to present the group stiffness in terms of a stiffness reduction factor K_G/N_PK_1. Fig. 5.29 shows that the interaction factor approach (Poulos and Davis, 1980) consistently underestimates the group stiffness for a two-layered soil profile. The present t-z "hybrid" solutions are in good agreement with the layered continuum solutions (Chin, 1988) and the solutions of El-Sharnouby and Novak (1985). It may be noted that in the method of El-Sharnouby and Novak (1985), Mindlin's (1936) homogeneous solutions were utilised in conjunction with some averaging procedure to take into account the non-homogeneity of the soil continuum (Poulos, 1979b). The normalised pile group stiffness, for square groups of up to 36 piles, also are in good agreement with the continuum solutions, as shown in Fig. 5.30. It is of interest to note that, for the square groups of up to 36 piles considered in Fig. 5.30, analyses using the suggestion of Randolph and Wroth (1979b) (where the single pile r_m value is increased by an amount equal to the radius of the circle of equivalent area to that covered by the group) indicate a difference of less than -1% of the solutions obtained using the isolated single pile r_m value. Therefore, for practical pile group sizes, the use of the single pile r_m value, as utilised in the present study, is sufficient.

For two identical piles in a Gibson soil, an approximate procedure is utilised for the pile-soil-pile interaction where the modulus E_1 is taken as the average of the influenced and influencing nodes. Fig. 5.31 shows a comparison of the interaction factors obtained using the present analysis (SPILE3) and the solutions of Banerjee (1978) and Poulos (1979b). As shown, the present solutions are in better agreement with those of Banerjee (1978).

The previous comparisons (Figs. 5.27 to 5.31) therefore show that the present t-z "hybrid" approach (SPILE3) can be used for pile group analysis instead of the full continuum analysis. The advantage of the present t-z "hybrid" approach is the significant reduction in computation time required to form the single pile flexibility coefficients (see Fig. 5.7b).

5.2.2.2 A comparison with field results

To assess the applicability of the t-z "hybrid" approach proposed (program SPILE3), a comparison with the field measurements reported by Cole and Stroud (1977) is presented. Solutions obtained using the full continuum method are also presented for comparison. Elastic solutions are presented as under normal working load conditions, the pile response is essentially elastic (Poulos and Davis, 1980).

Cole and Stroud (1977) presented field measurements of rock-socketed bored pile foundations for two blocks of buildings. The plan in Fig. 5.32(a) shows the layout of the pile foundations while Fig. 5.32(b) shows the elevation of the two blocks of buildings. Table 5.4 tabulates the pile diameters and the corresponding dead loads acting on the piles.

The ground consisted of about 5m thick of fill and silty sandy clay overlying a bearing stratum of siltstones and sandstones. SPT blowcounts ranging between 10 and 50 in the upper layer and 100 and 350 in the bearing stratum were recorded.

The embedded lengths of the piles were 6.2m and 5.3m for Blocks A and B respectively, with the pile toes founded at 8.8m below ground level.

Based on the back-analysis of a test pile (Chin, 1988; Chow *et al.*, 1990), the deduced value of E_2 is 110000 kN/m^2 with E_1 taken as 10000 kN/m^2 (within the range recommended by Poulos and Davis (1980) for medium stiff clay). The Poisson's ratios ν_1 and ν_2 were taken as 0.4 and 0.3 respectively.

For the present elastic analysis, the bearing stratum extends from a depth of 5m and the soil parameters E_1, ν_1 and E_2, ν_2 are taken as those mentioned earlier. The Young's modulus of the pile material (concrete) was taken to be E_p = 25000 MN/m^2. All 55 piles of both Blocks A and B are analysed directly with the applied dead loads (Table 5.4) and with inter-group interactions. As noted by Chow *et al.* (1990), the interaction between piles determined by elastic theory will be experienced even at very large spacings. Thus, for large pile groups, the sum of this interaction effect can become significant.

Tests conducted in London Clay by Cooke *et al.* (1980) indicate that interaction is practically zero at a pile spacing of 12 pile diameters. Although the present soil profile is different, this limiting value would, perhaps, represent a satisfactory practical limit for pile interaction (Chow *et al.*, 1990). It is worthy to note that this limiting value for pile interaction depends on factors like the pile length to diameter ratio (ℓ/d) and the pile-soil stiffness ratio. Some solutions presented by Randolph and Wroth (1979b) show that the interaction factor (between two piles) approaches zero as the pile spacing to pile length ratio approaches unity.

Table 5.5 shows a comparison of the measured settlements with those obtained using the present t-z "hybrid" approach and the full continuum solutions (Chow *et al.*, 1990). Also shown are the present solutions obtained using the analytical solutions of Chan *et al.* (1974) in conjunction with the average E value of the influenced and influencing nodes procedure of Poulos (1979b) for determining the pile-soil-pile interaction. The flexibility coefficient, corresponding to pile-soil-pile interaction, is then obtained using the solutions of Chan *et al.* (1974) by setting $E_1 = E_2$ = the average E value and the Poisson's ratios ν_1 and ν_2 are taken as 0.40. This is equivalent to utilising Mindlin's homogeneous solution with the average E value. Stiffer solutions are obtained as compared to those where the pile-soil-pile interactions are obtained accurately (without averaging procedure of Poulos, 1979b) using the analytical solutions of Chan *et al.* (1974). The computed solutions tend to generally overpredict the settlements measured at the end of construction. Possible reasons for these discrepancies are discussed by Chow *et al.* (1990). The higher measured settlements $1^1/_2$ years after end of construction have been attributed to creep behaviour of the bearing stratum by Cole and Stroud (1977).

The present t-z "hybrid" solutions are also in close agreement to the full continuum solutions (Table 5.5). The smaller settlements predicted by the t-z "hybrid" approach are due to the "stiffer" t-z representations of the single pile response. Therefore, the computationally more efficient t-z "hybrid" approach proposed can be used as an analysis method instead of the more rigorous full continuum analysis.

5.3 CYCLIC RESPONSE ANALYSIS

This section presents some numerical results for both single piles and pile groups subjected to axial cyclic loading conditions. The numerical solutions have been obtained using the cyclic elastic-plastic continuum program, SCPIL1 and the cyclic nonlinear hyperbolic "t-z" program, SCPIL3.

It should be noted that numerous solutions, particularly for single piles under axial cyclic loading, have been presented elsewhere (for example, Poulos, 1979a, 1981, 1989a). These solutions are mainly for the case of a homogeneous soil profile, or for a Gibson soil where the soil modulus increases linearly with depth. Solutions for the case of a two-layered soil profile (relevant to the case of a lightly overconsolidated clay overlying a heavily overconsolidated clay, or a lightly cemented soil overlying a stronger cemented soil) are however not available. This section therefore presents some numerical solutions for the two-layered soil profile using the analysis approach as outlined in Chapter 4.

5.3.1 Single Piles

For the cyclic axial response of single piles, some numerical solutions showing the effects of the following factors on the cyclic response are presented in the following sub-sections. These factors include the pile capacity degradation, permanent displacement accumulation, effect of residual stresses, effect of a strain-softening pile-soil response, and the cyclic pile response under a general storm-loading condition.

It may also be noted that most of the numerical solutions presented in this section have been obtained using the nonlinear hyperbolic "t-z" static and cyclic analysis program, SCPIL3. As mentioned in Chapter 4, the use of the "t-z" approach for single piles, particularly for cyclic loading analysis, is computationally more efficient than the full continuum analysis (programs SCPIL1 and SCPIL2).

5.3.1.1 Pile capacity degradation

As shown by Poulos (1988b), the effects of cyclic loading on subsequent pile capacity can best be described through the use of a "cyclic stability" diagram. Three main regions are evident on such diagrams:

(i) a cyclically stable region in which cyclic loading has no influence on the axial capacity of the pile;

(ii) a cyclically metastable region in which cyclic loading causes some reduction of axial load capacity, but the pile does not fail within the specified number of cycles; and

(iii) a cyclically unstable region in which cyclic loading causes sufficient reduction of axial pile capacity, with the pile failing within the specified number of load cycles.

Note that in the definitions above, "failure" of the pile due to any excessive accumulation of permanent pile displacements has been ignored. If required, this "excessive permanent pile displacement" failure condition (the "serviceability loss" region; Lee and Poulos, 1992) could be included into the cyclic stability diagram above by further sub-dividing the metastable region.

In order to verify the computer coding for cyclic response analysis in programs SCPIL1 and SCPIL3, the hypothetical case of a driven steel tube pile in a normally-consolidated clay analysed by Poulos (1988b) was considered. Fig. 5.33 shows the relevant input parameters required for the analysis. It may be noted that the nonlinear hyperbolic continuum program SCPIL2 is not utilised due to the significantly greater running time required.

The influence of the soil modulus, pile stiffness, pile length and the number of cycles (Poulos, 1988b) on the cyclic response of the pile are considered. In general, the influence on the stable, metastable and unstable regions of the above mentioned parameters are of interest. "Failure" is defined as that due to excessive pile capacity degradation to a value below the applied loading.

Fig. 5.34(a) shows the influence of the soil modulus on the cyclic stability diagram. As the soil modulus increases, the stable zone shrinks, and the unstable zone and metastable zone grows. Hence, there is a more gradual transition from stable to unstable behaviour as the soil modulus increases (Poulos, 1988b). Note that the results obtained using program SCPIL1 (elastic-plastic model) are in reasonably favourable agreement (Fig. 5.34a) with those of Poulos (1988b). The results obtained using the nonlinear hyperbolic model (program SCPIL3) however show a larger metastable region as well as a larger cyclic load level to cause failure. It may be noted that contradictory results were obtained by Lee and Poulos (1992), in conjunction with a nonlinear Ramberg-Osgood model, which show that the cyclic load level to cause failure increases with increasing local soil modulus. This discrepancy will be discussed later. Further results for the influence of the pile wall thickness (Fig. 5.34b), pile length (Fig. 5.34c) and number of cycles (Fig. 5.34d) have also been obtained using the present less time-consuming nonlinear hyperbolic "t-z" program SCPIL3. In general, similar observations and conclusions to those of Poulos (1988b) are obtained:

(i) long compressible piles exhibit "ductile" cyclic behaviour with a large metastable zone, and hence a more gradual transition from stable to unstable response;

(ii) short stiff piles exhibit "brittle" cyclic behaviour with a small metastable zone, and hence an abrupt transition from stable to unstable response.

The results from the nonlinear hyperbolic "t-z" model, however, show a larger metastable zone and larger cyclic load level to cause failure, as compared to those obtained by Poulos (1988b). It, therefore, appears that the nonlinear soil model adopted, with the present Matlock and Foo (1980) capacity degradation model, may have a somewhat significant influence on the computed cyclic pile response; with a more nonlinear model resulting in an improved cyclic load carrying capacity.

Figs. 5.35(a) and 5.35(b) show the normalised shear stress (τ/τ_f) with depth, at 80% static compressive capacity, for three soil modulus distributions obtained by using programs SCPIL1 and SCPIL3, respectively. Both programs show that the degree of pile-soil slip increases with increasing soil modulus. Also, the region of pile-soil slip progresses down the pile as the soil modulus increases. Note that for the higher soil modulus values (E_s = 1.5 MPa/m and 10.0 MPa/m), program SCPIL1 (elastic-plastic continuum model) shows a slightly greater degree of pile-soil slip than those computed by program SCPIL3 (nonlinear "t-z" hyperbolic model). Under cyclic loading condition, the above observations, in conjunction with the Matlock and Foo (1980) "reverse-slip" degrading model, clearly explains the decrease in the cyclic load level to cause failure with increasing soil modulus (see Fig. 5.34a). For program SCPIL1, where the "external soil movements" approach (see section 4.3.5.1) is utilised, the negative shear stresses resulting from the induced soil movements are included in the overall pile analysis, thus, contributing to a more rapid occurrence of the "reverse-slip" stress condition. The results of Lee and Poulos (1992), obtained using a nonlinear Ramberg-Osgood model, however show that the degree of pile-soil slip (at 80% static compressive capacity) decreases as the soil modulus increases, hence, resulting in an increase in the cyclic load level to cause failure for increasing soil modulus. This discrepancy in the shear stress distributions (to those of Figs. 5.35a and 5.35b) may be due to the approximate procedure employed by the writers in evaluating the flexibility coefficients of a highly non-uniform soil modulus distribution arising from the nonlinear analysis. Therefore, in the absence of carefully controlled laboratory test results, the influence of an increase in the soil modulus on the maximum cyclic load level to cause failure remains questionable although both the elastic-plastic continuum model and the nonlinear hyperbolic "t-z" model show a decrease in the maximum cyclic load level.

As mentioned earlier, no numerical solutions are available for the particular case of a single pile embedded in a two-layered soil profile with a finite stiffness of the lower layer. As such, some numerical solutions, obtained using the nonlinear hyperbolic "t-z" program SCPIL3, are presented in this section for such a soil profile. Fig. 5.36 shows the "relevant" input parameters required for the analysis. To facilitate the parametric study, the following assumptions regarding the unit skin friction and base resistance have been made for the analysis:

(i) the unit skin friction resistance is a constant value within a given soil layer, and the ratio of the unit skin friction resistances of the lower layer to the upper soil layer (f_{s2}/f_{s1}) is equal to the ratio of the corresponding soil moduli (E_2/E_1);

(ii) the unit base resistance (q_b) is 100 times the corresponding unit skin friction resistance of the soil layer in which the pile base is founded. For the case when the pile base is resting at the interface of the two layers (i.e. $x = 0$ in Fig. 5.36), the unit skin friction resistance of the lower layer (i.e. f_{s2}) is utilised for determining the unit base resistance;

(iii) no tensile base resistance is assumed.

Furthermore, the pile is assumed to be subjected to a symmetric two-way load-controlled cyclic loading (i.e. with zero mean load). No accumulation of permanent pile displacement has been assumed, and the degradation of pile capacity is assumed to be governed by the Matlock and Foo (1980) degradation model. "Failure" of the pile is thus defined as when the pile capacity has been degraded to a value below that of the applied loading within a specified number of load cycles. For the present analysis, 10 load cycles has been used unless otherwise specified. The computer program SCPIL3 is utilised for the analysis with the corresponding hyperbolic constants $R_{fs} = 0.5$ and $R_{fb} = 0.9$. The pile is discretised into 15 shaft elements and one base element, with a total of 16 nodal points.

The numerical solutions are presented in terms of a maximum sustainable load level Q_{sus} (as a percentage of the initial total compressive pile capacity, Q_c) for the specified number of load cycles, before failure occurs. The influence of the pile length (ℓ/d), the distance between the pile base and the interface of the two layers (x/d), the pile-soil stiffness ratio (E_p/E_1), the soil stiffness ratio (E_2/E_1) and the number of load cycles (N) on the maximum sustainable load level (Q_{sus}) are investigated. It should be stressed however that the results presented are restricted to the assumptions that have been made.

Figs. 5.37(a) and 5.37(b) show the influence of the pile length, ℓ/d and the pile-soil stiffness ratio, E_p/E_1 respectively on the maximum sustainable load level, Q_{sus}. As the pile length increases, both the initial tensile and compressive pile capacities also increase. Fig. 5.37(a) shows more degradation of pile capacity occurs for the longer piles; the piles behaving as a friction pile with most of the applied loading being resisted by the pile shaft. For a given pile length, more capacity degradation occurs when the pile base is not resting at the interface of the two layers (i.e. $x/d > 0$); this is so particularly for the shorter piles (ℓ/d between 20 and 40; see Fig. 5.37a). This is because for $x/d = 0$, the influence of the lower stiffer layer, and hence on the pile base load developed (where no degradation is assumed), becomes more significant with a resulting higher sustainable load level. For the case of $x/d > 0$, the actual value of x/d is found to have an insignificant influence on the computed maximum sustainable load level. It may be noted that "failure" for the present problem is caused by the tensile capacity being exceeded. For the pile-soil stiffness ratio (Fig. 5.37b), as expected, more degradation occurs for the more compressible piles.

The influence of the soil stiffness ratio, E_2/E_1 (Fig. 5.38a) shows that the capacity degradation (for $x/d = 0$) is more severe for lower soil stiffness ratios. As explained earlier, a larger soil stiffness ratio, for the case of $x/d = 0$, results in a greater influence of the pile base where no degradation is assumed. Hence, in conjunction with the "reverse-slip" degrading model of Matlock and Foo (1980), a larger sustainable load level can be applied to the pile before failure occurs. The effect of the number of load cycles is shown in Fig.5.38(b) where Q_{sus} is shown to decrease with an increase in the number of load cycles. The decrease in Q_{sus} is also greater for the longer piles. It may be noted that for the case of $\ell/d = 20$ and 40, the corresponding Q_{sus} appears to be not significantly affected by the number of load cycles. This is because, for both cases, failure occurs within 10 cycles of loading.

The above examples (Figs. 5.37 and 5.38) show that an increase in the compressive pile capacity, Q_c can be obtained by founding the pile base at the interface of the two layers. The greater influence of the pile base thus results in a greater developed pile base load. Since no degradation of the pile base resistance is assumed, a larger maximum sustainable load can be applied before failure occurs. It should be noted that this conclusion reached is restricted to cases where no (or little) degradation of pile base resistance applies.

In practice, however, piles are rarely designed to rest at the interface of both layers, but are usually socketed into the lower stiffer layer. Some numerical solutions obtained for the socketed pile are presented next where the assumptions and input parameters of the previous example are utilised (see Fig. 5.36). In addition, the socketed length of the pile in the lower stiffer layer is denoted by the symbol e.

The influence of the thickness of the upper soil layer (h/d), soil stiffness ratio (E_2/E_1), and pile-soil stiffness ratio (E_p/E_1), for three different socketing lengths (e/d), are shown in Figs. 5.39(a), 5.39(b) and 5.39(c) respectively. More capacity degradation occurs for the longer piles (i.e. larger h/d values), the more compressible piles (i.e smaller E_p/E_1 values) and smaller soil-stiffness ratio, E_2/E_1. Although increasing h/d increases the maximum sustainable load level (Fig. 5.39a), more capacity degradation also occurs. Note that the percentage difference between the initial tensile capacity before cycling and the Q_{sus} value indicates the amount of capacity degradation that has occurred with the pile failing in the specified number of cycles. For a given value of h/d, increasing the socketing length (e/d) results in more degradation (Fig. 5.39a). This is due to the lesser influence of the pile base for greater socketing lengths. More capacity degradation is also observed with increasing e/d for smaller E_2/E_1 ratios (Fig. 5.39b) and smaller E_p/E_1 ratios (Fig. 5.39c). It should be noted that these initial numerical results remain to be verified by carefully controlled laboratory testing.

In order to have a better appreciation of the progression of capacity degradation along the pile, the normalised elastic shear stress distribution along a socketed pile is shown in Fig. 5.40(a). Greater shear stresses are observed to develop in the lower stiffer layer. Note that reasonably good agreement is obtained for the elastic shear stress distribution from both the elastic continuum program, SCPIL1 and the "t-z" program, SCPIL3. The shear stress distributions (from program SCPIL3) for a particular load level (10% Q_c), normalised by the initial limiting unit skin friction resistance assumed, are shown in Fig. 5.40(b) for two E_p/E_1 ratios. As shown, the normalised shear stresses are greater along the upper soil layer particularly for the more compressible piles. Although Fig. 5.40(a) shows greater shear stresses are developed along the pile in the lower stiffer layer, the normalised value (Fig. 5.40b) shows that, for the more compressible pile (E_p/E_1 = 1000), any capacity degradation (using Matlock and Foo model) will commence from the top of the pile downwards. For the more rigid pile (i.e. E_p/E_1 = 10000; Fig. 5.40b), the normalised shear stress distribution is more uniform. Hence, the important points to be noted from Fig. 5.40(b) are:

(i) for the more compressible piles, capacity degradation occurs gradually from the top of the pile downwards, and hence a more gradual transition from stable to unstable behaviour is expected;

(ii) for relatively rigid piles, capacity degradation occurs simultaneously everywhere along the pile; leading to an abrupt transition from stable to unstable behaviour.

The distributions of the degradation factor (defined as the post-cyclic elemental skin friction to the initial static elemental skin friction resistance) along the pile for different E_p/E_1 ratios are shown in Figs. 5.41(a) and 5.41(b) for the case of $E_2/E_1 = 1$ and 10, respectively. For the homogeneous profile i.e E_2/E_1 (Fig. 5.41a), significantly greater degradation occurs along the pile shaft for the more compressible piles. For the relatively rigid piles i.e. $E_p/E_1 =$ 10000 (Fig. 5.41a), some degradation occurs at both ends of the pile with a major portion of the pile shaft undergoing no degradation yet for the specified number of load cycles. For the case with a stiffer lower layer (Fig. 5.41b), again the more compressible piles are subjected to a greater degree of degradation along the pile shaft. However, for the specified number of load cycles, minimal or no degradation of the pile shaft resistance in the lower stiffer layer is observed.

The solutions presented thus far are obtained for a two-way cyclic loading condition. Some results showing the influence of the type of loading condition, i.e. whether one-way or two-way loading, are presented in Figs. 5.42(a) and 5.42(b) for different values of E_p/E_1 and E_2/E_1, respectively. As shown, utilising the same Matlock and Foo capacity degradation model, a significantly greater load level can be applied to the pile under one-way cyclic loading condition (from zero to Q_{sus}) before failure occurs. This is in accord with experimental and field observations (for example, Lee, 1988; Bogard and Matlock, 1990a, 1990b) that two-way cyclic loading (about zero mean load) has a more severe effect on piles than one-way loading (minimum load is zero).

The development of the stable, metastable and unstable regions, under two-way cyclic loading about zero mean load, is shown in Figs. 5.43(a), 5.43(b) and 5.43(c) as a function of h/d, E_p/E_1 and E_2/E_1 respectively. The effects of E_p/E_1 (Fig. 5.43b) and E_2/E_1 (Fig. 5.43c) are obtained for the particular case of h/d = 60 and e/d = 5. As h/d increases (i.e. longer piles), the stable and unstable regions decrease in size while the metastable region increases (Fig. 5.43a).

Note that although the tensile capacity increases as h/d increases, the amount of degradation of pile capacity also increases. For the more compressible piles (Fig. 5.43b), a larger metastable zone is observed with a gradual transition from stable to unstable response. It may be noted that although the more compressible piles give a "better" cyclic response in terms of a gradual transition from stable to unstable behaviour, the larger magnitude of settlements associated with more compressible piles also have to be considered. On the other hand, a relatively rigid pile gives less settlement but its cyclic response is less favourable, being characterized by an abrupt transition from stable to unstable response. The influence of E_2/E_1 (Fig. 5.43c) shows that as E_2/E_1 increases, the stable zone decreases in size while both the metastable and unstable zones increase in size. It should be noted that this observation is similar to that for a Gibson soil profile (Fig. 5.34a) considered earlier. The solutions therefore show that a more "ductile" behaviour of the pile is expected as the soil stiffness ratio E_2/E_1 increases.

Some results showing the influence of the hyperbolic constants R_{fs} and R_{fb}, and the degradation rate parameter, λ, on the cyclic pile response are shown in Figs. 5.44(a) and 5.44(b) respectively. As shown in Fig. 5.44(a), a more nonlinear soil model (i.e. $R_{fs} = 0.5$, $R_{fb} = 0.9$) results in a slightly larger stable zone. The maximum sustainable load level, Q_{sus}, also increases slightly. It may be noted that the above results are obtained based on the "reverse-slip" degrading model of Matlock and Foo (1980). Fig. 5.44(b) shows the influence of the degradation rate parameter, λ (see equation 3.3) on the maximum sustainable load level. A more severe capacity degradation model, i.e. larger λ value, results in a lower Q_{sus} for the same specified number of load cycles. However, the λ effect is not particularly significant; with a variation of Q_{sus} of about 5% Q_c for the three λ values considered (Fig. 5.44b). The effect of λ for different E_p/E_1 values is further shown in Fig. 5.45. The influence of λ is more significant for the more compressible piles and smaller soil stiffness ratio, E_2/E_1.

As mentioned in Chapter 3, the effects of cyclic loading on the pile response are best represented by the "cyclic stability" diagram (Poulos, 1988b) which shows the different combinations of mean load and cyclic load levels to cause failure of the pile within a specified number of load cycles. Two such stability diagrams (capacity degradation only) for the case of h/d = 60 and e/d = 5 are shown in Figs. 5.46(a) and 5.46(b) for different values of E_p/E_1 and E_2/E_1 respectively. As the pile-soil stiffness ratio E_p/E_1 increases (Fig. 5.46a), the cyclic load level required to cause failure, at any given applied mean load level, also increases. The stability diagram therefore grows in size for increasing E_p/E_1 ratios. The reverse however is observed for increasing soil stiffness ratio, E_2/E_1 (Fig. 5.46b). Note also that the stability diagram is symmetrical about the peak point "F" (Fig. 5.46a) whereby load combinations to the left of point "F" causes the pile to fail in tension while combinations to the right causes the pile to fail in compression. As noted by Poulos (1988b), the peak point "F" represents the maximum cyclic load that can be sustained without failure at the corresponding optimum mean load level. This optimum mean load level is given by $(Q_c - Q_t)/2$ where Q_c and Q_t are the compressive and tensile pile capacities respectively. For larger E_2/E_1 ratios (Fig. 5.46b), the peak point "F" is observed to move to the right and, hence, increasing the optimum mean load level. This is due to the larger compressive capacity (Q_c) as compared to the tensile capacity (Q_t) for increasing E_2/E_1 ratios.

The solutions presented thus far, for the degradation of pile capacity, have been obtained using the "reverse-slip" degrading model of Matlock and Foo (1980). As mentioned in section 4.3.4, different hypotheses regarding the degradation of skin friction are possible at present. Some results are presented next to show the effect of adopting a different skin friction degradation model.

The hypothetical example problem of Poulos (1989a) is utilised for the present analysis to assess the effects of different capacity degradation models. Fig. 5.47(a) shows the hypothetical driven steel tube pile 100m long, 1.0m diameter with a 37.5mm wall thickness, embedded in a deep uniform calcareous sand deposit. The equivalent Young's modulus of the pile is taken as 28.9×10^3MPa based on the ratio of the actual cross-sectional area of the pile to that of a solid pile, with the modulus of steel taken as 200×10^3MPa. The other relevant input soil parameters are also shown in the figure. The base resistance and soil modulus are assumed to undergo no degradation under cyclic loading. For the degradation of skin friction, the degradation factor "chart" as shown in Fig. 5.47(b) is utilised. Four possible skin friction degradation models are considered:

(i) the "absolute cyclic displacement" model. This means that the absolute cyclic displacement (ρ_c) values in Fig. 5.47(b) are directly applicable;

(ii) the "relative (to diameter) cyclic displacement" model. For this case, the normalised values (ρ_c/d) in Fig. 5.47(b) are utilised;

(iii) Matlock and Foo degradation model. The corresponding degradation parameters for the shaft elements are:

$$D_{\tau lim} = 0.25, \ \lambda = 0.60$$

(iv) the "cyclic slip displacement" model. For this model, the displacement to cause static slip (ρ_{fs}) is first subtracted from the cyclic displacement (ρ_c) calculated by the program before utilising the absolute horizontal scale of Fig. 5.47(b) to determine the corresponding degradation factor. Note that the ρ_{fs} values for the shaft elements are determined directly from the analysis.

Zero permanent displacement accumulation for shaft elements is assumed while for the base, the accumulation parameters adopted are m_b = 0.12 and n_b = 5.9 (Poulos, 1989a). Note that the elastic-plastic continuum program SCPIL1 is utilised for the present example problem.

Fig. 5.48(a) shows the post-cyclic shaft capacity under different cyclic load amplitudes (with zero mean load) in conjunction with the different skin friction degradation models mentioned above. As shown, the absolute cyclic displacement model gives the most severe shaft capacity degradation while the cyclic slip displacement model gives the least severe degradation. The mormalised (to diameter) cyclic displacement model also gives less severe degradation as compared to the absolute cyclic displacement model. Both the Matlock and Foo (1980) model and the "cyclic slip displacement" model result in no shaft capacity degradation until a cyclic load of about 4.7 MN and 4.8 MN respectively is reached whereby a sudden significant reduction in shaft capacity occurs with resulting failure of the pile. However, the reduction in shaft capacity is more gradual for both the absolute and normalised cyclic displacement models. It is also shown (Fig. 5.48a), using the absolute cyclic displacement model, that one-way cyclic loading (0 to P_c) gives a less severe shaft capacity degradation than two-way cyclic loading.

The above example therefore shows the important influence of the skin friction degradation model utilised on the computed post-cyclic shaft capacity. There is as yet no absolute evidence to suggest which skin friction degradation model is the "correct" one, in particular, the dependence on the absolute or normalised cyclic displacement. Limited experimental model grouted pile test results obtained by Lee (1988) however seem to suggest the normalised (to pile diameter) value of the "cyclic slip displacement" model is the likely governing skin friction degradation model. The model jacked pile tests conducted in the present study, as will be described in Chapter 8, were carried out with the aim to shed further light on the most appropriate degradation model.

Some solutions showing the accumulation of permanent pile displacements are shown in Fig. 5.48(b) under one-way cyclic loading condition. The accumulation in pile displacement increases as the cyclic load level increases (0 to P_{max}). For relatively low load levels (P_{max}/Q_c = 0.1 and 0.2), no significant accumulation is observed while at a load level of P_{max}/Q_c = 0.28, significant accumulation occurs with the pile failing at the 18th. cycle. This accumulation of permanent pile displacement will be dealt with in more detail in the next section.

It may be noted that the above observations on the shaft capacity degradation and permanent pile displacement accumulation are consistent with those of Poulos (1989a).

5.3.1.2 Permanent pile displacement accumulation

As mentioned in Chapter 4 (section 4.3.5), two general approaches are possible to simulate the accumulation of permanent pile displacement. These are the "external soil movements" approach and the "degrading secant modulus" approach. In the present section, no degradation of pile capacity has been assumed so that the simulation of permanent pile displacement accumulation by both approaches can be assessed. Some results obtained using both approaches are presented in the following sub-sections.

5.3.1.2.1 "External soil movements" approach

The elastic-plastic continuum program SCPIL1 utilises the "external soil movements" approach (see section 4.3.5.1) to simulate the permanent pile displacement accumulation under cyclic loading condition. Some results are presented for a hypothetical case of a pile embedded in a two-layered soil profile (see Fig. 5.49). The "relevant" input parameters required for the analysis are also shown in Fig. 5.49. The pile is subjected to one-way cyclic loading (i.e applied load from 0 to P_{max}/Q_c value unless otherwise specified). Note that the input soil parameters utilised are within the range recommended by Poulos (1988a) for lightly cemented, and highly cemented calcareous soils. Thus, the two-layered soil profile considered here is relevant to the case of a lightly cemented calcareous soil overlying a highly cemented calcareous soil.

Figs. 5.50(a) and 5.50(b) show the computed maximum pile head settlement after 10 cycles for different values of the pile modulus, E_p and lower soil modulus, E_2 respectively. As expected, larger pile head settlements are observed for the lower pile modulus E_p (Fig. 5.50a) as the load level (0 to P_{max}) increases. On the other hand, increasing the lower soil modulus (E_2) decreases the maximum pile head settlements (Fig. 5.50b). Note that for the increasing E_2 values (500 MPa and 1000 MPa), the unit skin friction distribution for the lower layer, as shown in Fig. 5.49, has been conservatively utilised (i.e using the "standard" f_{s2}= 100 kN/m^2 even though the soil modulus E_2 is increasing).

The influence of the number of cycles (N), for different load level (P_{max}/Q_c), is shown in Fig. 5.51(a). The accumulated maximum pile head settlement increases as the number of cycles increases. Failure due to excessive accumulation of pile displacement may occur eventually under a sufficiently high load level. Fig. 5.51(b) shows the influence of the permanent displacement parameters m_s, n_s and m_b, n_b on the accumulated maximum pile head settlement. As shown, significantly less permanent pile displacement is obtained for the case where no permanent displacement accumulation for the pile shaft elements was assumed (i.e. m_s, n_s = 0). Hence, a significantly larger load level (P_{max}/Q_c) could be sustained by the pile before failure occurs if this assumption were made. On the other hand, the assumption of no accumulation for the pile base (i.e. m_b, n_b = 0) has only a minor influence on the accumulated pile displacement (see Fig. 5.51b). This example therefore demonstrates, particularly for long offshore piles, the importance of proper modelling of the permanent displacement accumulation for the shaft elements which may significantly affect the computed pile response. Some tentative guidelines, obtained from limited laboratory tests, on the accumulation parameters m_s, n_s and m_b, n_b have been reported by Poulos (1988a). It may be noted that the permanent displacement accumulation parameters adopted in the present example problem are the lower end values suggested by Poulos (1988a). For larger values of the parameters, a more severe permanent displacement accumulation can be expected.

As mentioned in section 3.3.1.3, there is as yet no clear definition for the stress level X. Hence, some results showing the influence of the adopted definition for X, on the computed pile response, are required so as to enable the significance of each definition be appreciated.

Fig. 5.52(a) shows the accumulated maximum pile head settlements obtained using four different definitions for the stress level, X. As shown, significant differences in the computed pile responses are obtained with definition (2) (equation 3.7) and definition (4) (equation 3.8) giving the most severe and least severe responses, respectively. The "failure" of the pile due to excessive pile accumulation , using X given by equation (3.7), after 41 cycles at the low load level of $P_{max}/Q_c = 0.03$ appears unrealistic and, hence, the numerical results have to be treated with caution. This "premature" failure is due to the rapid accumulation of the incremental external soil movements obtained from equation (3.5) in conjunction with the adopted stress level X (equation 3.7).

Therefore, at present, in the absence of a single absolute definition for X, the computed pile response is expected to vary depending on the adopted choice of X (see Fig. 5.52a). Fig. 5.52(b) shows that significantly larger accumulated pile displacement is obtained under one-way cyclic loading than two-way cyclic loading (with zero mean load). This trend is consistent with the experimental model test results obtained by Lee (1988).

Some results showing the shear stress distributions (at P_{max}) along the pile shaft as cycling proceeds are shown in Fig. 5.53(a). The shear stress distribution changes as cycling proceeds; the shear stress becoming more negative in the upper portion of the pile while at the same time becoming more positive in the lower portion. These changes are caused by the additional stresses induced on the pile due to the incremental external soil movements. The shear stress distribution at failure (N = 41 cycles) shows that almost two-thirds of the pile is subjected to negative shear stresses while the lower one-third under positive shear stresses. Note that for large incremental external soil movements and low applied load levels, the shear stress distribution along the pile may be dominated by the larger induced stresses due to the external soil movements. It should be noted that the above numerical results showing the shear stress distributions, as cycling proceeds, may not give a realistic representation of the actual stress distributions and hence must be treated with extreme caution and suspicion. The results thus obtained are a consequence of the adopted "external soil movements" approach. Fig. 5.53(b) further shows the displacements of the pile head at both the minimum (i.e zero applied load for this case) and maximum (i.e $P_{max}/Q_c = 0.03$) ends of each loading cycle, as cycling proceeds. The accumulation of permanent displacement is somewhat gradual up until cycle number 18, after which increasing accumulation occurs with the pile eventually failing at N = 41 cycles.

It is worth noting that the above solutions have been obtained assuming no degradation of pile capacity. A more severe response (i.e. larger accumulated displacement) would be obtained if the effect of any capacity degradation is included.

5.3.1.2.2 "Degrading secant modulus" approach

The "degrading secant modulus" approach is utilised in the nonlinear hyperbolic programs SCPIL2 and SCPIL3. Some results obtained using the nonlinear hyperbolic "t-z" program SCPIL3, for the same example problem as considered in section 5.3.1.2.1 (Fig. 5.49), are presented. As before, no degradation of pile capacity is assumed.

Fig. 5.54(a) shows that negligible accumulation of pile displacement is obtained even for a relatively high load level $P_{max}/Q_c = 0.50$ (i.e one-way cycling from 0 to P_{max}/Q_c value). Note that the accumulation rate parameter, ψ of 0.02, obtained from model grouted pile tests by Lee (1988), has been assumed to be applicable and utilised for the present analysis. The results thus obtained (Fig. 5.54a) contrast with those obtained in the previous section where significant accumulation occurs with increasing load level (see Fig. 5.51a). The significant influence of the accumulation rate parameter

ψ, on the permanent displacement accumulation, is further shown in Fig. 5.54(b). The larger the value of ψ, the greater is the accumulated displacement with increasing cycles. Therefore, it appears that a larger ψ value may be appropriate at higher load levels. Indeed, the averaged value of ψ (= 0.02) obtained by Lee (1988) was based on model tests with stress level X (= $[\tau_o+2\tau_c]/2\tau_f$) between 0.2 and 0.6. In the absence of controlled laboratory or field test data, again the above numerical results shown must be treated with caution and suspicion.

The influence of the choice of the stress level X on the accumulated pile settlement for ψ = 0.02 and 0.6 are shown in Figs. 5.55(a) and 5.55(b) respectively. As shown, the choice of X seems to have a more significant effect for greater ψ values.

Some results showing the influence of the hyperbolic constants R_{fs} and R_{fb} for ψ = 0.02 and 0.2 are shown in Figs. 5.56(a) and 5.56(b), respectively. As expected, the more nonlinear model (R_{fs} = R_{fb} = 0.9) results in greater accumulated displacements. The effect of the nonlinear model is also more significant for the larger ψ value (Fig. 5.56b). Note that a more nonlinear pile base response (compare curves 1 and 2 in Figs. 5.56a and 5.56b) seems to have almost no effect on the computed pile response at a load level of P_{max}/Q_c = 0.50. However, at higher load levels, where the pile base load mobilised is greater, the effect of a more nonlinear pile base response may have a more significant influence on the computed accumulated pile settlements.

Overall, the present section (section 5.3.1.2) has shown that our ability at present to model the accumulation of permanent pile displacement appears to be very poor. As shown, conflicting results with regard to the magnitude of the computed permanent pile displacement are obtained from the two different approaches. The question of which is the correct and satisfactory approach is highly debatable and the adoption of a particular approach at present is based mainly on personal preference and experience.

5.3.1.3 <u>Effect of residual stresses</u>

Some results showing the influence of residual stresses on the post-cyclic shaft capacity are presented in this section. The example problem, with the relevant input pile and soil parameters, as shown in Fig. 5.49 is utilised. In addition, zero permanent displacement accumulation has been assumed. The degradation of pile capacity is further assumed to be governed by the Matlock and Foo (1980) model with $D_{lims} = 0.25$, $\lambda_s = 0.6$, and $D_{limb} = 1.0$, $\lambda_b = 0.0$ (i.e. no base capacity degradation). Note that the results presented have been obtained using the nonlinear hyperbolic "t-z" program SCPIL3 (with $R_{fs} = 0.5$ and $R_{fb} = 0.9$).

Fig. 5.57 shows the computed residual stress distribution along the pile. Significant negative (tensile) slip occurs over the top three-fifths of the pile while the lower two-fifths are similarly subjected to negative residual stresses. These residual stresses are then included in the subsequent pile analysis instead of an initially "stress-free" pile.

Fig. 5.58(a) shows the computed post-cyclic shaft capacity with increasing cycles, for different P_{max}/Q_c values, under one-way compressive cyclic loading. As shown, more rapid degradation of shaft capacity occurs when the residual stresses are included, this effect being more significant for larger P_{max}/Q_c values. This more rapid degradation, in conjunction with the Matlock and Foo model, is due to "reverse-slip" being initiated more rapidly. The effect of the residual stresses however decreases with increasing cycles. Note that for $P_{max}/Q_c = 0.7$, failure due to excessive capacity degradation occurs after 6 cycles of loading. For two-way cyclic loading (Fig. 5.58b), the reverse trend is however observed where less shaft capacity degradation is obtained with the residual stresses included. This result is not unexpected since "reverse-slip" (with residual stresses) occurs less rapidly at the lower cyclic load level $\pm P_c/Q_c$.

It may be noted that the numerical results obtained showing less detrimental effect of residual stresses under two-way cyclic loading (Fig. 5.58b) is dependent on the occurrence of "reverse-slip" during cyclic loading. The inclusion of residual stresses however results in greater reduction of the cyclic stiffness of the pile with increasing cycles (Poulos, 1987). Therefore, the adoption of the "cyclic displacement models" (section 4.3.4) would result in a more severe degradation of pile capacity. This contradictory results, for two-way cyclic loading, again highlight the importance of the adopted capacity degradation model on the computed response. There is as yet no conclusive evidence to suggest which (if any) of the models considered here is the "correct" governing capacity degradation model.

5.3.1.4 Effect of strain-softening response

The numerical results presented thus far assume no "softening" of the elemental limiting pile shaft capacities for displacements greater than those required to develop the peak elemental shaft capacities. This assumption is not entirely true as it has been observed (for example, Kraft *et al.*, 1981c; Chandler and Martins, 1982) for certain soils that once the peak limiting value is reached, the developed friction capacity reduces to a residual value with further displacements. Some results, obtained using programs SCPIL1 and SCPIL3, are presented in this section to illustrate this "softening" effect.

The pile and soil parameters of the example problem as shown in Fig. 5.49 are again utilised. Any degradation of pile capacity is further assumed to be caused solely by the "softening" effect. As mentioned in section 4.5, the "softening" is assumed to decrease linearly from the peak value, τ_f, to the residual value, τ_r, over a displacement of ρ_{pp}. The displacement ρ_{fs} to reach the peak value, τ_f, for each element is calculated from the analysis.

Fig. 5.59(a) shows the post-cyclic shaft capacity, for different P_{max}/Q_c values, with increasing cycles under one-way cyclic loading. The "softening" effect is shown to be more significant for the larger load levels. This is due to the larger accumulated pile displacements at higher load levels. Note that the whole pile shaft has been degraded to its residual value after 17 cycles under a load level $P_{max}/Q_c = 0.30$. The influence of the magnitude of ρ_{pp} (displacement from peak to residual values) on the post-cyclic shaft capacity is shown in Fig. 5.59(b). The smaller the value of ρ_{pp}, the more rapid (and hence larger) degradation is observed.

The influence of the ratio of the residual to peak friction values, τ_r/τ_f, is shown in Fig. 5.60(a). In general, the smaller the ratio of τ_r/τ_f (i.e. greater softening effect) the more significant the degradation of pile shaft capacity. Fig. 5.60(b) shows further the influence of the adopted stress level X on the post-cyclic shaft capacity. As shown, definition (2) (equation 3.7) gives the most severe degradation of shaft capacity. This is due to the larger accumulated displacements computed using definition (2) (see Fig. 5.52a).

Some results obtained using the nonlinear "t-z" program SCPIL3 are further shown in Figs. 5.61(a) and 5.61(b) for different P_{max}/Q_c values and different ψ (accumulation rate parameter) values, respectively. Note that the computed response shows negligible degradation of shaft capacity, at a load level of $P_{max}/Q_c = 0.30$ (with $\psi = 0.02$), as compared to that obtained using program SCPIL1 (see Fig. 5.59a). The larger the value of ψ (Fig. 5.61b), the greater is the degradation of shaft capacity due to the "softening" effect.

5.3.1.5 "Storm-loading" analysis

In actual field conditions, the pile foundations, particularly in the offshore environment, are frequently subjected to a sequence of cyclic loading of different load amplitudes and number of cycles. This "storm-loading" condition may have a significant effect on the cyclic degradation of pile capacity and the accumulation of permanent pile displacement. Some results are presented in this section to show the "storm-loading" effect on the accumulated pile displacement.

Fig. 5.62 shows the storm-loading condition consisting of four different "parcels" of one-way cyclic loading amplitudes. Each "parcel" is assumed to consist of 200 cycles of loading. For the present analysis, no "softening" effect and degradation of pile capacity have further been assumed. Results have been obtained using both the elastic-plastic continuum program (SCPIL1) and the nonlinear hyperbolic "t-z" program (SCPIL3).

The influence of the accumulation rate parameter ψ and the adopted stress level X (using program SCPIL3), on the computed pile displacements, are shown in Figs. 5.63(a) and 5.63(b) respectively. As shown in both figures, a "step" increase in the pile displacement is observed at the transition from a lower amplitude load parcel to a higher amplitude parcel. Within each load parcel, the accumulated displacement is greater for the larger ψ values (Fig. 5.63a); with the pile failing (i.e. excessive pile displacement) at the end of the third load parcel at N = 600 cycles for $\psi = 0.6$. The adopted stress level X also significantly affects the magnitude of the computed pile displacements (Fig. 5.63b) with definition (4) (equation 3.8) giving the least accumulated displacement.

Some results have also been obtained using the elastic-plastic program (SCPIL1) with the relevant parameters as shown in Fig. 5.62.

The influence of the adopted stress level X is shown in Fig. 5.64(a) where again the choice of X was found to significantly affect the computed accumulated pile displacements. Definition (2) (equation 3.7) results in the pile failing after only 14 cycles of loading under the first load parcel. As discussed in section 5.3.1.2.1, this result seems unrealistic in view of the low applied load level of P_{max}/Q_c = 0.10.

As shown by Poulos (1988c), the different parcels of cyclic loading could be "converted" into an equivalent number of cycles, N_{ke}, of the last load parcel by using the equation

$$N_{ke} = \sum_{j=1}^{k} N_j \, e^{\alpha(X_j - X_k)} \qquad (5.1)$$

where N_j is the number of load cycles of parcel j, X_j and X_k are the stress levels of parcels j and k respectively, and α = n/m (n,m are the displacement accumulation parameters; see section 3.3.1.3). For the present analysis, definition (4) (equation 3.8) has been adopted for the stress level X and the value of α = 3.0/0.055 = 54.5. Note that both the m and n values adopted for the shaft and base elements were based on the lower end of the tentative recommendations of Poulos (1988a). Using the above equation, the computed N_{ke} equals 203.4 cycles. However, N_{ke} of 204 cycles has been utilised for the present analysis.

Fig. 5.64(b) shows the accumulated pile displacements obtained when the order of occurrence of the load parcels is changed, and that obtained by using N_{ke} of the last load parcel (4). Load sequences (a) and (b) (see Fig. 5.64b) gave similar final computed pile displacements while load sequence (c) gave a larger final pile displacement. In general, the order of occurrence of the loading parcels has a major influence on the final computed pile displacements. It may be noted that some results obtained from cyclic triaxial tests by Kaggwa *et al.* (1990) show the final accumulated displacements to be affected by the order of occurrence of the loading parcels. As mentioned in section 4.3.6, the use of equation (5.1) implicitly assumes that Miner's rule of superposition applies whereby the N_{ke} value (of the last load parcel) is not affected by the order of occurrence of prior parcels. The final computed pile displacement using N_{ke} (see Fig. 5.64b) is greater than those of the other load sequences (a) to (c). However, the computation time is significantly reduced whereby 204 cycles need be analysed instead of the total 800 cycles of loading. It may be noted from equation (5.1) that α (= n/m) is a significant factor in determining the equivalent number of cycles, N_{ke} (Poulos, 1988c).

5.3.2 Pile Groups

The cyclic analysis of single piles (section 5.3.1) highlights the difficulty of proper modelling of the effects of cyclic loading, in particular, the accumulation of permanent pile displacement. For pile groups, the additional effect of cyclic loading on pile-soil-pile interaction (and hence on the pile group response) is far less understood and as such a satisfactory approach to model the cyclic response of pile groups is not available at present.

An approximate approach, as outlined in Chapter 4, follows the procedure adopted by Poulos (1982a, 1983, 1984) where pile-soil-pile interaction is obtained using elastic-continuum theory and the effects of cyclic loading modelled in a similar manner as for the single piles. Some limited numerical results obtained using program SCPIL1 are presented to show the cyclic response of pile groups.

The hypothetical soil profile as shown in Fig. 5.47(a) is utilised for the present pile group analysis. The following assumptions have been adopted unless otherwise specified. The degradation of pile shaft capacity for the individual group piles is assumed to be governed by the "relative (to diameter) cyclic displacement" model as shown in Fig. 5.47(b). No degradation of base resistance and soil modulus are also assumed. For permanent displacement accumulation, the following parameters are adopted:

$$m_s = n_s = 0 \quad \text{(i.e. no shaft accumulation)}$$

$$m_b = 0.12,\ n_b = 5.9 \text{ (Poulos, 1989a)}$$

$$X = (\tau_o + 0.5\tau_c)/\tau_f$$

The analysis is carried out for 10 cycles of uniform amplitude loading.

Fig. 5.65(a) shows the post-cyclic shaft capacities developed under two-way cyclic loading for square 2-pile and 4-pile groups. Note that the results have been obtained by assuming that each of the group piles is subjected to the same applied cyclic load given by the value $\pm P_c/Q_c$. As compared to that for the single pile, lower post-cyclic shaft capacities (i.e. more capacity degradation) are obtained for the larger pile groups. The greater capacity degradation, in conjunction with the capacity degradation model adopted, is due to the increased pile displacement as a result of greater pile-soil-pile interaction. It should be noted that the adoption of a different capacity degradation model, for example, the "cyclic slip displacement" model may lead to a less severe capacity degradation for pile groups.

Some results presented by Poulos (1984), in conjunction with the "cyclic slip displacement" capacity degradation model, have concluded that group effects should not have a significant effect on the cyclic degradation of pile capacity. This conclusion could be explained in terms of two counterbalancing effects of pile-soil-pile interaction (Poulos, 1984):

(i) the cyclic displacement is increased due to interaction between the piles, thus tending to increase the cyclic degradation of pile capacity

(ii) the static displacement for full slip, ρ_{fs}, is also increased, thus tending to reduce the amount of cyclic degradation.

The ρ_{fs} value is therefore shown to be a significant parameter affecting the cyclic degradation of pile groups. It should however be noted that this is valid only when the "cyclic slip displacement" model is adopted.

Fig. 5.65(b) shows the accumulated pile displacements under one-way cyclic loading for the single pile, 2-pile and 4-pile groups. The results have been obtained using the "absolute cyclic displacement" model, as utilised previously in obtaining Fig. 5.48(b) for the single pile. Under the applied cyclic loading of $P_{max}/Q_c = 0.2$, little accumulation of pile displacement is observed. The 4-pile group however shows greater accumulation over the first four cycles of loading and little accumulation thereafter. The greater magnitude of pile displacement for larger pile groups is due to the increased pile-soil-pile interaction effect.

The influence of the pile spacing s/d, on the post-cyclic shaft capacity, is shown in Figs.5.66(a) and 5.66(b) for the 2-pile and

4-pile groups respectively. The degradation of pile capacity, using the "relative (to diameter) cyclic displacement" model, is more significant for the closely spaced (i.e. smaller s/d value) pile groups. As before, this is due to the increased pile displacement as a result of greater pile-soil-pile interaction. The spacing effect also appears to be more significant for the larger (i.e. 4-pile) group (see Fig. 5.66b).

Some numerical results are also shown for the case of a 9-pile group under two-way cyclic axial loading. The analysis under a prescribed axial load with a rigid pile cap can be simulated by "tying" the pile heads of the group piles with rigid bending elements (see section 4.2.1 and Appendix 4C). Fig. 5.67(a) shows the post-cyclic shaft capacities (after 10 cycles of loading) of the three "different" pile types obtained in conjunction with the "absolute cyclic displacement" model (given by Fig. 5.47b) for shaft capacity degradation. The results show that the innermost pile (pile type 3) is subjected to the most severe capacity degradation while the outermost pile (pile type 1) the least. As before, the amount of degradation increases with increasing cyclic load level P_c/Q_{cg} where Q_{cg} is the ultimate compressive capacity of the pile group. For P_c/Q_{cg} of about 0.10, almost full degradation (with the adopted capacity degradation model) occurs in all the group piles. The shear stress distributions for the three "different" pile types, at P_c/Q_{cg} of 0.02 and 0.10, are further shown in Fig. 5.67(b).

It should be noted that the above numerical results obtained for pile groups, as for the single piles, are dependent on the adopted capacity degradation model. Furthermore, it has been assumed that the effect of pile-soil-pile interaction due to cyclic loading does not affect the adopted capacity degradation "chart" (as shown in Fig. 5.47b) for the single piles. As for any analysis approach, the numerical results presented above for pile groups remain to be verified by laboratory and field tests data. In particular, the conclusion reached by Poulos (1984) that group effects should not have a significant effect on the cyclic degradation of pile shaft load capacity remains to be fully verified. It may be noted that preliminary model test results obtained by Al-Douri (1992), for 2-pile and 4-pile groups consisting of 25mm diameter model piles, seem to show no significant group effects in affecting the degradation of pile shaft load capacity.

5.4 A COMPARATIVE STUDY OF CYCLIC AXIAL LOADING ANALYSES

As reviewed in Chapter 3, the cyclic loading analysis of piles can be categorised into the load-transfer (i.e Winkler-type) approach or the continuum approach. The assumptions and limitations inherent in both approaches have also been described in Chapter 3. Thus far, no attempt has been made to assess the predictions obtained from these different approaches. Therefore, in this section, a comparative study of a hypothetical pile problem is undertaken using selected cyclic pile analysis computer programs. The computer programs utilised are "RATZ" (Randolph, 1986), "SCARP" (Poulos, 1989c), "AXCAP" (Lee, 1988) and the present t-z program "SCPIL3".

It is recognised that in each program the soil model and/or cyclic approach utilised are different and hence, different sets of empirical parameters may be relevant to each program. It has been found necessary in the present comparative study to adopt "representative" values of these parameters that have been reported in the literature. Although the present hypothetical soil profile may not be similar to that from which these parameters were derived, it nevertheless is of interest to compare the predictions obtained from these programs.

The hypothetical problem utilised is that described by Randolph and Jewell (1989) for an offshore drilled and grouted pile. The hypothetical pile consists of a steel tube pile 1.7m in external diameter with a 50mm wall thickness grouted into a 50m long by 2m diameter hole (Fig. 5.68). For simplicity, the soil profile utilised for the present hypothetical problem is assumed to be homogeneous with the soil properties as shown in Table 5.6. The static displacement ρ_{fs} required to mobilise the peak skin friction is calculated within each analysis approach. No base resistance is assumed for the present problem. The equivalent pile modulus E_p is taken as 23.44×10^3 MPa. The pile is discretised into 10 shaft elements and one base element, with a total of 11 nodal points. The pile is further assumed to be subjected to the storm-loading pattern shown in Table 5.7. In addition, the cyclic loading parameters required for each of the individual programs are listed below:

RATZ (Randolph, 1986):

Yield parameter, ξ_y	= 0
Cyclic residual shear stress, τ_{cr}	= 10 kPa
Strain-softening parameter, η	= 0.7

Parameter δ = 4 and no creep effect

SCARP (Poulos, 1989c):

Accumulation parameters:

$m_s = 0.06$, $n_s = 3.0$

$X = (P_o + 0.5P_c)/Q_c$ —— equation (3.8)

"Reverse-slip" capacity degrading model:

$D_{\tau lim} = 0.033$, $\lambda_\tau = 0.25$ for shaft elements

$D_{blim} = 1.0$, $\lambda_b = 0.0$ i.e. no base degradation

No permanent displacement accumulation for the pile base element and no degradation in soil modulus are allowed for. The accumulation parameters m_s and n_s adopted are the lower end values for drilled and grouted pile in weakly cemented soil recommended by Poulos (1988a). The minimum degradation factor, $D_{\tau lim}$, for the shaft elements is 0.033, and reflects the possible degradation of the shaft capacity to the cyclic residual value of 10 kPa used in program RATZ.

AXCAP (Lee, 1988):

Nonlinear Ramberg-Osgood parameters:

$R = 3.2$, $\alpha = 9.0$

Accumulation rate parameter, $\psi = 0.02$

Stress level, $X = (\tau_o + 2\tau_c)/2\tau_f$ —— equation (3.11)

The "reverse-slip" capacity degrading model is adopted with the relevant parameters similar to those utilised for program SCARP. No capacity degradation and displacement accumulation for the pile base element are assumed. Note that program AXCAP is not able to account for the "strain-softening" pile-soil response adopted in the present example problem. However, preliminary analyses using programs SCARP and SCPIL3 indicated that, with the present storm-loading condition, the post-peak strain-softening response had an insignificant influence on the computed results.

The parameters R, α and ψ used were based on model grouted pile test results obtained by Lee (1988).

SCPIL3 (present method):

Nonlinear hyperbolic parameters:

$R_{fs} = 0.5$, $R_{fb} = 0.9$

Accumulation rate parameter, $\psi = 0.02$

Stress level, $X = (P_o + 0.5P_c)/Q_c$ —— equation (3.8)

The "reverse-slip" capacity degrading model adopted as for program SCARP. No capacity degradation and accumulation for the pile base element are assumed (similar to programs SCARP and AXCAP).

The nonlinear hyperbolic curve-fitting parameters R_{fs} and R_{fb} utilised for the shaft and base elements respectively were based on the recommendations of Poulos (1989a).

In the present hypothetical problem of a drilled and grouted pile, the base resistance has been assumed to be zero. This assumption actually reflects the present conservative design guidelines where the end-bearing capacity of a drilled and grouted pile is generally ignored even though some resistance may be developed (Hyden *et al.*, 1988). For situations where the pile base capacity is significant (for example, with driven piles) the proper modelling of the pile base response under cyclic loading is required.

The solutions from the individual programs are presented to show the load-settlement response of the pile under the "storm-loading" sequence. Furthermore, where possible, the variations of the shear stress distributions along the pile, and the pile head settlement against number of cycles are also presented. Finally, the results thus obtained from the different programs are compared and any discrepancy highlighted and discussed.

Figs. 5.69(a) to 5.69(c) show the RATZ solutions (after Randolph and Jewell, 1989) for the load-settlement response, shear stress variations (at depth of 1.0m) with cycling and the post-cyclic shaft capacity of the pile respectively. It can be observed that as the mean and cyclic loads increase during the loading sequence, accumulation of permanent pile displacement occurs (Fig. 5.69a) while the pile-soil shear stress (at 1.0m below top of pile) decreases (Fig. 5.69b). The RATZ solutions further show that some degradation of the shaft capacity occurs (Fig. 5.69c) over the top 20m of the pile following the cyclic loading sequence. This capacity degradation is expected as it has been assumed in the RATZ analysis that any accumulated displacement is equivalent to the post-peak "softening" response (see section 3.2).

The SCARP solutions obtained are shown in Figs. 5.70(a) to 5.70(c) for the load-settlement response, shear stress variations for the first element, and the shear stress distributions along the pile respectively. The load-settlement response (Fig. 5.70a) shows similar trend to the RATZ solutions; the SCARP solutions however show a greater displacement accumulation under the first load parcel. It should be noted that, as mentioned in section 5.3.1.2.1 (see also Fig. 5.52a), the stress level X (= $[P_o + 0.5P_c]/Q_c$) adopted in program SCARP tends to give the least accumulation of displacement. Larger accumulated displacements are to be expected when utilising a different definition for the stress level X. For the shear stress variations (Fig. 5.70b) of the first element (at an average depth of 2.5m below ground level), negligible degradation of the limiting unit elemental shaft capacity occurs following the cyclic loading sequence. This is in contrast to the RATZ solutions (see Fig. 5.69b) where degradation of the limiting unit elemental shaft capacity occurs over the top 20m of the pile. Indeed, in conjunction with the capacity degradation model adopted, the SCARP solutions show the post-cyclic pile shaft capacity to be negligibly affected by the cyclic loading sequence. Fig. 5.70(c) shows the normalised (to initial "static" value) shear stress distributions (at the maximum load ends) along the pile, as cycling proceeds. It is interesting to compare the distributions at N = 1 cycle and 400 cycles within the first load parcel. As shown, the pile-soil shear stress decreases over the top one-third of the pile while the shear stress on the lower two-thirds increases from N = 1 cycle to N = 400 cycles. As explained in section 5.3.1.2.1 (see also Fig. 5.53a) this variation is due to the inclusion of the pile-soil shear stresses from the "external soil movements" in the overall pile analysis.

Figs. 5.71(a) to 5.71(c) show the AXCAP solutions obtained for the load-settlement response, shear stress variations for the first element, and the shear stress distributions along the pile respectively. Due to restrictions of the program, only limited points at the end values of the cyclic loading sequence for the load-settlement response (Fig. 5.71a) and shear stress variations of the first element (Fig. 5.71b) were plotted. As shown in Fig. 5.71(a), significantly larger accumulated displacements (than the RATZ and

SCARP solutions presented earlier) are obtained from the individual load parcels. Also, the shear stress variations (Fig. 5.71b) at the first element (average depth of 2.5m below ground level) show a rapid progression from positive shear stresses to negative shear stresses as cycling proceeds. For most part of the cyclic loading stage, the shear stress (of the first element) remains at the negative limiting value (-0.3 MPa) at the corresponding minimum load ends. As for the SCARP solutions, negligible reduction in the post-cyclic pile capacity is obtained using the "reverse-slip" capacity degrading model. The shear stress distributions along the pile, as shown in Fig. 5.71(c), are in contrast to those obtained by program SCARP (see Fig. 5.70c). The AXCAP solutions show greater negative shear stresses developed over the top one-third of the pile while greater positive shear stresses are developed in the lower two-thirds of the pile. At the end of the cyclic loading sequence (i.e. N = 1191 cycles), the AXCAP solutions show that slip occurs over the lower one-third of the pile. This observed discrepancy may be due to the approximate procedure employed in program AXCAP (Lee, 1988; Lee and Poulos, 1992) for evaluating the flexibility coefficients of a highly non-uniform local soil modulus distribution arising from the nonlinear analysis. A separate analysis of the problem using a smaller value for the Ramberg-Osgood parameter α of 3.0 shows similar variations as the case with α = 9.0, except that the total accumulated displacement is almost halved.

The present solutions obtained using program SCPIL3 are shown in Figs. 5.72 and 5.73 for the case of ψ = 0.02 and 0.08 respectively. The analysis with ψ = 0.08 was performed in order to have an appreciation of the influence of ψ on the computed response. The variations of the computed responses are similar for both cases, except that larger accumulated displacement is obtained for the larger ψ value. A total accumulated displacement of 6.4mm and 10.3mm are obtained for ψ = 0.02 and 0.08 respectively. Also, a more rapid progression of the shear stress at average depth of 1.25m below ground level (calculated from the lumped force at node 1) from positive to negative shear stresses is observed (compare Figs. 5.72b and 5.73b) for the case with ψ = 0.08. Note that in the present analysis (also those of programs SCARP and AXCAP) the cyclic residual shear stress utilised in program RATZ is not explicitly modelled. As for programs SCARP and AXCAP, the SCPIL3 solutions show negligible reduction in the post-cyclic pile capacity. Figs. 5.74(a) and 5.74(b) further show the normalised shear stress (τ/τ_f) distributions for ψ = 0.02 and ψ = 0.08 respectively. Both distributions are somewhat similar except for the top one-fifth of the pile where, for the case of ψ = 0.08, the shear stresses progress towards the negative end as cycling proceeds. Larger positive shear stresses are also obtained for the lower four-fifths of the pile. Note that the general trend is similar to that obtained by program SCARP (see Fig. 5.70c).

As a matter of interest, some additional analyses were performed (using program SCPIL3) to assess the influence of adopting a different stress level X, a more nonlinear soil model, and larger ψ value. Each of these parameters was varied in turn while maintaining the remaining parameters at the "standard" values mentioned at the beginning of this section.

Fig. 5.75(a) shows the results obtained for the total accumulated displacement. By far, the accumulation rate parameter ψ has the greatest influence on the accumulated displacement. The more nonlinear model (i.e. $R_{fs} = R_{fb}$ = 0.9) resulted in a slightly larger accumulated displacement. The use of the stress level $X = (\tau_o + 2\tau_c)/2\tau_f$, similar to that utilised by program AXCAP, gave almost identical results to those obtained using the "standard" stress level $X = (P_o + 0.5P_c)/Q_c$. However, as shown in section 5.3.1.2.2, the adoption of a different stress level X (see section 3.3.1.3) may have a significant effect on the computed accumulated displacement, particularly for larger ψ values. Fig. 5.75(b) shows the variations of the shear stress (at average depth of 1.25m below ground level) for the case of $R_{fs} = R_{fb}$ = 0.9. Comparing Figs. 5.72(b) and the present figure 5.75(b), a greater progression of the shear stresses to negative values is observed for the more nonlinear model.

In the preceding paragraphs, the individual results obtained from each program were presented and discussed. The important parameters affecting the computed response were also highlighted. In the following paragraphs, summarised comparisons of the results from the different analyses are presented. The comparisons are restricted to the initial static displacement (at 50 MN load), the total accumulated pile displacement following the cyclic loading sequence, the initial and final pile cyclic stiffness, and the pile-soil shear stress distributions during the cyclic loading. Note that the "standard" parameters mentioned for each program are relevant unless otherwise specified.

Fig. 5.76(a) shows the initial computed static displacements, at an applied load of 50 MN, obtained from the different programs. The solutions obtained from programs RATZ, SCARP and SCPIL3 show good agreement. Larger static displacement is however obtained from the nonlinear Ramberg-Osgood continuum program AXCAP. The more nonlinear model (i.e with the Ramberg-Osgood parameters R = 3.2, α = 9.0) resulted in about 28% increase in the computed static displacement as compared to the case for the less nonlinear model (R = 3.2, α = 3.0). The computed static displacements shown in the figure (for the "standard" parameter cases) are found to vary between -14% and +36% of the average displacement value from the four programs. Overall, the computed static displacements from the different programs are in reasonably good agreement except for program AXCAP where a larger computed displacement is to be expected.

The total accumulated displacements as a result of the cyclic loading parcels obtained from the different programs are shown in Fig. 5.76(b). Again, the results from program RATZ, SCARP and SCPIL3 are in generally good agreement giving the same order of magnitude in the computed total accumulated displacement. The AXCAP solutions however gave a significantly larger total accumulated displacement. The total accumulated displacements obtained with R = 3.2, α = 9.0, and R = 3.2, α = 3.0 are respectively about 845% and 338% greater than the average computed displacement (for the "standard" cases) from the other three programs. The SCPIL3 solution with ψ = 0.08 gave an increase of about 60% in the computed total accumulated displacement as compared to the case with ψ = 0.02. It is of interest to note that separate analyses using program RATZ, with ξ_y = 0.5, and program SCARP, with m_s = 0.12 and n_s = 6.0 (i.e twice the "standard" values), resulted in a total accumulated displacement of about 64% and 156% of the corresponding values for the "standard" case respectively. Although programs AXCAP and SCPIL3 utilised the same "degrading secant modulus" approach to simulate the accumulation of permanent displacement, the results obtained from both programs are however vastly different. These results show the important influence of the adopted soil model for the present cyclic analysis. It should be noted that it is at present not known which (if any) is the correct computed solution for the total accumulated displacement. The comparison here serves to highlight the possible magnitudes of accumulated displacement that can be obtained depending on which program is utilised for the analysis. In contrast to the computed static displacements (see Fig. 5.76a), a much greater degree of uncertainty is associated with the determination of the total accumulated pile displacement as a result of cyclic loading. Table 5.8 further shows the accumulated displacements obtained for each of the loading parcels from the four programs. As shown, significant discrepancy is observed in the computed accumulated displacements for each loading parcel, with programs AXCAP and SCPIL3 giving the largest and least computed values respectively.

Fig. 5.76(c) shows the initial (at N = 1 cycle) and final (at N = 1191 cycles) cyclic stiffness values of the grouted pile computed from the different programs. The cyclic stiffness utilised here is defined as the ratio of the cyclic load to the cyclic displacement. Both programs SCARP and SCPIL3 show very negligible reduction in the computed cyclic stiffness. However, programs RATZ and AXCAP both gave a reduction in the cyclic stiffness of about 22% as compared to their respective initial cyclic stiffness values. The initial cyclic stiffness values from the four different programs are found to vary between -6% and +8% of the average initial stiffness value obtained from the four programs. A larger variation of ±17% of the average final stiffness value is however obtained for the final stiffness values computed by the four programs.

It is worthy of note that a field cyclic tensile test of a pile in glacial till reported by McAnoy *et al.* (1982) showed no degradation in the cyclic pile stiffness (i.e no change in the cyclic displacement) with increasing cycles, for a given cyclic load level, even though the pile was approaching "failure". Their results also indicate a decrease in the cyclic pile stiffness with increasing cyclic load level. Laboratory model pile test results in clay reported by Poulos (1981) and Hewitt (1988) also showed a similar general decrease in the cyclic pile stiffness with increasing cyclic load level. Both results also showed a small decrease of the cyclic pile stiffness with increasing cycles under a given cyclic load level. Clearly, more carefully controlled laboratory test data are required to supplement the present limited data on this "cyclic pile stiffness degradation" question. Only then can a confident assessment be made as to which program gives a more appropriate general predicted response under the cyclic loading condition.

Fig. 5.77 shows the normalised shear stress (τ/τ_f) distributions along the pile computed by the different programs, as cycling proceeds. Generally, the shear stress distributions from programs RATZ, SCARP and SCPIL3 compare favourably except for the final cycle (N = 1191 cycles), although program RATZ gives a somewhat more uniform distribution along the pile. For the first cycle (Fig. 5.77a), program AXCAP gives a more uniform distribution as compared to the other three programs where greater shear stresses are obtained towards the top of the pile. This discrepancy between the AXCAP solutions and the other solutions may be due to the approximate procedure employed in program AXCAP for evaluating the flexibility coefficients of a highly non-uniform local soil modulus distribution arising from the nonlinear analysis. Significant differences between the AXCAP solutions and the other solutions are also evident during the cyclic loading stage (see Figs. 5.77b to 5.77d). At the end of the cyclic loading sequence (Fig. 5.77d), both programs SCARP and SCPIL3 show favourable agreement with pile-soil slip occurring over the upper-half of the pile. Contradictory results obtained by program AXCAP indicate pile-soil slip occurring over the bottom one-third portion of the pile while the RATZ solutions indicate no pile-soil slip at all. In addition, program AXCAP even indicates the existence of negative shear stresses over the upper top portion of the pile.

Some general comments are relevant at this stage on the present comparative study using the four selected cyclic axial loading analysis programs.

It is gratifying to observe that the computed initial static displacements from the four programs compare favourably in general, thus reinforcing and increasing confidence in the present available static analysis approaches. For cyclic loading analysis however, the present level of confidence is far lower. There is a lack of understanding of the mechanisms causing the two observed phenomena of capacity degradation and accumulation of permanent pile displacement under cyclic loading. Moreover, the extent of occurrence of these two phenomena is dependent on many factors, for example, the applied mean and cyclic load levels, and the characteristics of the soil type used (Poulos, 1988a). Because of these complexities, highly empirical or semi-empirical approaches have been utilised to simulate these two observed effects of cyclic loading. Obviously, these simplified approaches have limitations and the solutions obtained are dependent on the assumptions and the parameters adopted in each analysis approach. There is, at present, a limited data-base on the cyclic empirical parameters required in each analysis approach. Therefore, there is a need for more laboratory and field scale pile tests data in order to increase the data-base of these cyclic empirical parameters. It is also worthy to note that cyclic element tests (for example, triaxial and shear tests) can provide useful insight into the mechanisms causing the capacity degradation and accumulation of permanent displacement affecting piles under cyclic loading condition.

The comparisons presented in Figs. 5.76(b), 5.76(c) and 5.77 show the inconsistent predicted responses that can be obtained from different cyclic axial loading analysis programs. This inconsistency is due to the different approaches adopted to model the effects of cyclic loading. Therefore, in the absence of complete understanding of the mechanisms causing the capacity degradation and accumulation of permanent displacement under cyclic loading and its proper numerical modelling, the solutions obtained from any existing cyclic axial loading analysis programs have to be treated with caution. Although the simplified approaches adopted in the four selected programs may not be fully satisfactory, they nevertheless provide an ability where the cyclic loading effects are approximately catered for. They also enable the significance of each influencing parameter to be assessed. The difficulty of accurately modelling the complex pile-soil cyclic effects is reflected in the present practical design approach where, for piles subjected to combined static and cyclic loading, the usual approach is to ensure that the response of the pile is "elastic" under the peak combined loading (Randolph, 1983a). At present, the choice of which program to use is still a matter of preference based on experience.

5.5 A COMPARISON WITH A FIELD CYCLIC PILE LOAD TEST

There is generally a lack of good quality field cyclic pile test measurements reported in the literature. In order to assess the present numerical approach, the static and cyclic field loading tests of a drilled and grouted pile reported by Nauroy *et al.* (1985) are considered for the present comparison. The computer program SCPIL3 developed in the present study is utilised for obtaining the predicted response.

Nauroy *et al.* (1985) reported the static and cyclic field loading tests results of a drilled and grouted pile embedded in calcareous sand. The pile consisted of a steel tube of 0.22m external diameter, and 10mm wall thickness, grouted into a calcareous sand formation between depths of 7.15m and 15m. The final dimension of the grouted section is 7m long by 0.35m average diameter, as quoted by Nauroy *et al.* (1988). The pile was subjected to the loading "parcels" as shown in Table 5.9 while Fig. 5.78 shows the measured load-settlement response of the pile.

For the present analysis, the soil parameters as suggested by Randolph and Jewell (1989) are utilised. The shear modulus of the soil is taken to increase linearly from 50 MPa at the top of the grouted section to 100 MPa at the pile tip while the peak skin friction is assumed to also increase linearly from 110 kPa to 220 kPa over the 7m interval. The residual capacity of the pile is taken as 65 kPa after a post-peak movement of 200mm. Note that this "strain-softening" response can be incorporated into the present analysis using the procedure suggested by Poulos (1989a). The Poisson's ratio of the soil is taken as 0.5 while R_{fs} = 0.5 and R_{fb} = 0.9 are utilised for the present analysis. Under cyclic loading, the "reverse-slip" capacity degrading model is utilised with D_{lim} = 0.05 and λ = 0.4 (lower end of values suggested by Poulos (1988a) for drilled and grouted piles in uncemented calcareous soils). No base resistance is assumed while the accumulation parameter, ψ, is taken as 0.02 with the stress level X = $(\tau_o + 2\tau_c)/2\tau_f$ (equation 3.11). The pile is discretised into 10 elements with a total of 11 nodal points.

Fig. 5.79(a) shows the computed load-settlement response, with ψ = 0.02, under the sequence of loading parcels. Loading parcels C2 and C4 contribute the major proportion of the accumulated displacement, with a total displacement (at the end of parcel C5) of about 5.5mm. The total measured pile displacement at the end of parcel C5 (neglecting the static test S_{12}), is about 13mm. Although the accumulated pile displacements (from the individual load parcels) are not matched precisely, the analysis does show the significant contributions of loading parcels C2 and C4 to the total pile displacement. Load parcel C4 is by far the most significant loading parcel, as only 138 cycles of this load parcel results in an accumulated displacement of almost half that due to parcel C2 of 1000 cycles. This shows the important influence of the cyclic load level on the computed pile response. The measured results indicated that parcel C4 contributed the major proportion of the accumulated displacement while the present numerical results show parcel C2 to contribute the most. The present analysis, in conjunction with the adopted capacity degrading model, shows minimal degradation of pile capacity resulting from the cyclic loading sequence. This result is in general agreement with the field measurements.

In order to have an appreciation of the influence of the accumulation rate parameter ψ, the results of the analysis using ψ = 0.08 is shown in Fig. 5.79(b). Table 5.10 tabulates the computed accumulated displacements for each of the individual load parcels obtained from both analyses. As expected, larger accumulated pile displacement is obtained from the loading sequence with ψ = 0.08. The total pile displacement at the end of load parcel C5 of about 12mm is in good agreement with the measured value of about 13mm. However, this agreement may have been fortuitous. Although the computed total pile displacement (with ψ = 0.08) is in good agreement with the measured value, discrepancies still exist between the computed and measured values for the individual load parcels. The accumulation rate parameter ψ is therefore an important parameter affecting the amount of computed accumulated displacement. Clearly, more research work and test data are required to further define this rate parameter, ψ.

5.6 SUMMARY

In this chapter, some numerical results have been presented for both single piles and pile groups, subjected to either static or cyclic applied loading, using the analysis approach described in Chapter 4. The following general conclusions can be drawn from the numerical results obtained from both the static and cyclic analyses conducted.

For static loading, the influence of the adopted soil model is not particularly significant within the working load range. However, beyond the working load range the computed response is influenced quite significantly by the nonlinear model adopted. In particular, the efficiency and accuracy of the "t-z" program SPILE3 for both single piles and pile groups analysis have been demonstrated. Overall, our present ability to model the static response of both single piles and pile groups is quite satisfactory.

For cyclic loading, the computed response is influenced by a greater number of parameters. In particular, the two major phenomena of capacity degradation and accumulation of permanent displacement have to be modelled. Some parametric results presented in the present chapter highlight the more important parameters affecting the predicted cyclic pile response. A comparative study of a hypothetical single pile problem, using different cyclic axial loading analysis programs, further highlights the inconsistent predicted responses that can be obtained. This inconsistency is due to the different analysis approaches utilised to simulate the two cyclic loading phenomena. Moreover, the adopted soil model also has an influence on the computed cyclic response. There is therefore a need for good quality laboratory test data in order to understand fully the mechanisms causing these two cyclic loading phenomena. Only then can a confident assessment be made as to which analysis approach gives a more appropriate predicted cyclic response. The comparison with the results of a field cyclic pile load test shows that the general trends from the numerical solutions and field measurements are generally consistent, even though the results for the individual load parcels are not matched precisely. For pile groups, much less is known at present on the influence of pile-soil-pile interaction on the cyclic response of the group. Simple analysis approaches for pile groups have been suggested but have yet to be fully "calibrated" against good quality laboratory and field tests results. Some numerical results presented in this chapter show that, depending on the capacity degradation model adopted, group effects can lead to either a more severe or less severe computed degradation response as compared to the corresponding single pile solutions. Overall, our ability at present, as compared to the static loading case, to model the cyclic axial response of both single piles and pile groups appears to be very poor, in particular, with regard to the predicted accumulated permanent pile displacement.

Table 5.1 Comparison of settlement influence values and relative base load for single piles in Gibson soil

	sett. influence factor, I_ρ				rel. base load, P_b/P			
	ℓ/d = 10		ℓ/d = 25		ℓ/d = 10		ℓ/d = 25	
K_b	100	1000	100	1000	100	1000	100	1000
AXPILS	0.249	0.176	0.274	0.122	0.242	0.270	0.088	0.126
ISOPE	0.231	0.184	0.250	0.118	0.180	0.220	0.120	0.200
Banerjee & Davies	0.241	0.233	0.204	0.116	0.113	0.140	0.047	0.078
Present	0.226	0.161	0.259	0.115	0.183	0.202	0.087	0.124
Note: $h/\ell = 2$; $\eta = E_{so}/E_{sl} = 0$; $\nu_s = 0.5$								

Table 5.2 Comparison of load-settlement ratio for end-bearing piles

	load - settlement ratio ($P/G_l r w_t$)						
	soil type	ξ = 1	0.5	0.25	0.1	0.01	
ℓ/r = 20	ρ = 1.0	41.5	51.7	64.8	88.6	158.5	(1)
		41.6	52.1	66.1	90.3	156.9	(2)
		41.6	52.2	66.2	90.4	157.1	(3)
	ρ = 0.5	25.0	33.3	45.3	69.4	142.4	(1)
		28.5	36.7	48.4	71.6	150.2	(2)
		28.5	36.5	47.4	68.4	136.6	(3)
ℓ/r = 40	ρ = 1.0	53.6	65.1	73.2	84.6	104.2	(1)
		54.5	62.6	71.8	84.3	106.3	(2)
		54.5	62.7	71.9	84.5	106.6	(3)
	ρ = 0.5	34.8	43.3	51.0	62.8	84.1	(1)
		34.5	41.0	49.5	64.5	101.2	(2)
		34.8	40.4	46.9	57.6	80.9	(3)
ℓ/r = 80	ρ = 1.0	65.3	69.3	72.4	75.5	78.8	(1)
		62.1	67.1	71.8	76.9	82.8	(2)
		62.3	67.3	72.1	77.3	83.3	(3)
	ρ = 0.5	35.8	39.0	42.1	45.6	49.8	(1)
		37.2	42.0	48.0	58.0	78.7	(2)
		36.7	39.4	41.9	45.2	50.3	(3)

E_p/G_l = 1000 for all piles, ν_s = 0.4

(1) Finite element solutions
(2) Analytical solutions
— Randolph and Wroth (1979a)

(3) Present solutions

Table 5.3 Soil parameters utilised for static nonlinear analyses of single piles (after Poulos, 1987).

Soil type	Soil modulus parameters		Ult. shaft resistance parameters		Ultimate toe resistance
	E_s (MPa)	N_v (MPa/m)	τ_{ao} (kPa)	β_V (kPa/m)	τ_{bu} (MPa)
stiff clay	50	0	75	0	1.35
soft clay	0	1.0	0	1.5	0.675
silica sand	0	1.5	0	2.0	10.0

Table 5.4 Pile diameters and dead loads (after Cole and Stroud, 1977)

Pile	Diameter, d (mm)	Dead load per pile (kN)
A	1220	5031
B	760	885
C	760	1470
D	760	1430
E	1060	3061
F	1220	4975
J	760	1835
K	760	1079
L	560	713
N	760	711
P	1060	1423

Table 5.5 Comparison between theoretical and measured settlements of pile groups at Coventry Point

	Settlement (mm)				
Pile group	Computer soln.			Measured, end of construction	Measured, $1^1/2$ yrs. after end of construction
	(1)	(2)	(3)		
1	17.1	16.9	15.2	10 - 15	15 - 21
2	17.2	16.9	15.7		
3	23.2	22.5	20.2		
4	23.0	21.8	20.0		
5	22.5	21.2	19.7		
6	14.8	14.5	13.2		
BLOCK B	30.9	29.5	27.6	19 - 21	27 - 30

(1) full continuum solutions
(2) present solutions (with solutions of Chan et al. (1974) for pile-soil-pile interaction)
(3) present solutions (with averaging procedure of Poulos (1979b) for pile-soil-pile interaction)

Table 5.6 Soil parameters for hypothetical offshore drilled and grouted pile (after Randolph and Jewell, 1989).

Shear modulus, G	200 MPa
Poisson's ratio, ν	0.50
Peak skin friction, τ_f	300 kPa
Residual skin friction, τ_r	30 kPa
Post-peak displ. to residual	1000 mm

Table 5.7 Storm-loading parcels for hypothetical offshore drilled and grouted pile (after Randolph and Jewell, 1989).

Wave height (m)	Number of cycles	Average load (MN)	Cyclic load (MN)
10	500	45.0	5.0
11	300	45.5	5.5
12	180	46.0	6.0
13	100	46.5	6.7
14	50	47.0	7.5
15	30	47.5	8.3
16	15	48.0	9.2
17	8	48.5	10.2
18	5	49.0	11.5
19	2	49.5	13.0
20	1	50.0	15.0

Table 5.8 Computed accumulated displacements for individual load parcels obtained from the four programs

Loading parcel	Computer program			
	RATZ	SCARP	AXCAP	SCPIL3
1	1.44	2.64	7.02	0.36
2	0.41	0.34	5.06	0.34
3	0.43	0.19	3.10	0.26
4	0.58	0.13	2.78	0.19
5	0.76	0.09	1.42	0.12
6	0.82	0.07	0.84	0.09
7	0.75	0.05	0.54	0.05
8	0.63	0.04	0.58	0.03
9	0.48	0.04	0.78	0.02
10	0.24	0.02	0.10	0.01
11	–	–	0.07	0.01

Accumulated displacement values in millimetres

Note: accumulated displacement calculated from difference between last cycle and first cycle displacement values in each loading parcel.

Table 5.9 Cyclic loading parcels (after Nauroy *et al.*, 1985) for drilled and grouted pile.

Load parcel	Average Load (kN)	Cyclic Load (kN)	Number of cycles
C_1	300	100	1000
C_2	300	200	1000
C_3	500	100	1000
C_4	300	300	138
C_5	500	100	500

Table 5.10 Comparison between measured and predicted accumulated pile displacements for individual load parcels.

Load parcel	Accumulated displacement (mm)		
	measured	ψ = 0.02	ψ = 0.08
C_1	0.31	0.15	0.51
C_2	0.93	0.95	4.00
C_3	0.53	0.27	1.19
C_4	7.78	0.39	1.83
C_5	0.57	0.15	0.70

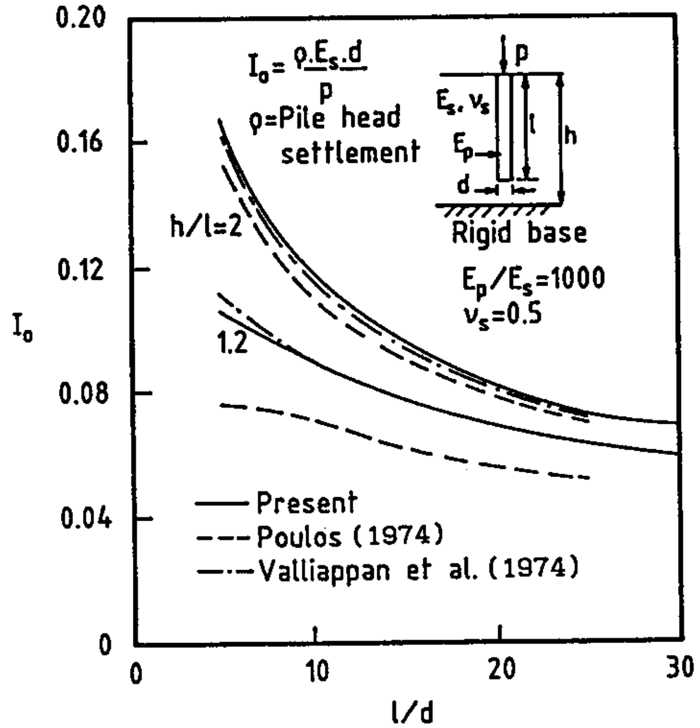

Fig. 5.1 Comparison of solutions for single piles in finite soil layer (program SPILE1)

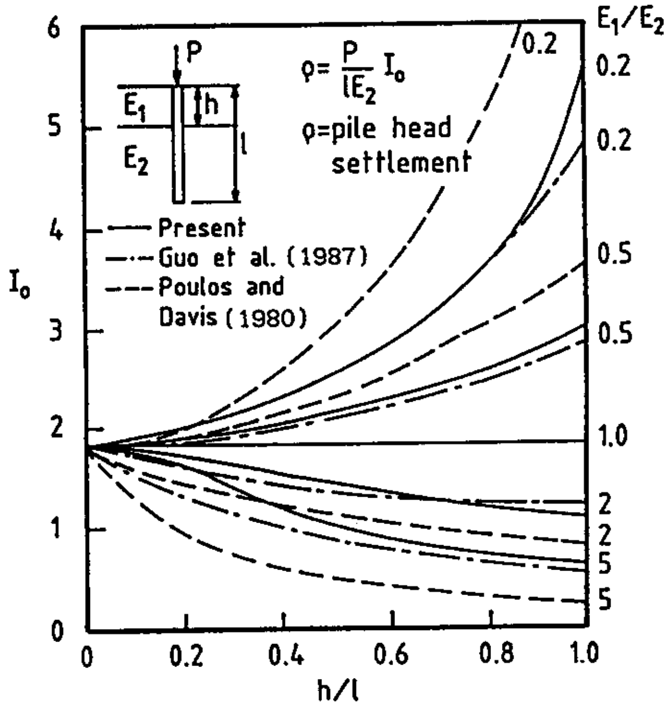

Fig. 5.2 Comparison of socketed single piles solutions for effect of E_2/E_1 ratio (program SPILE1)

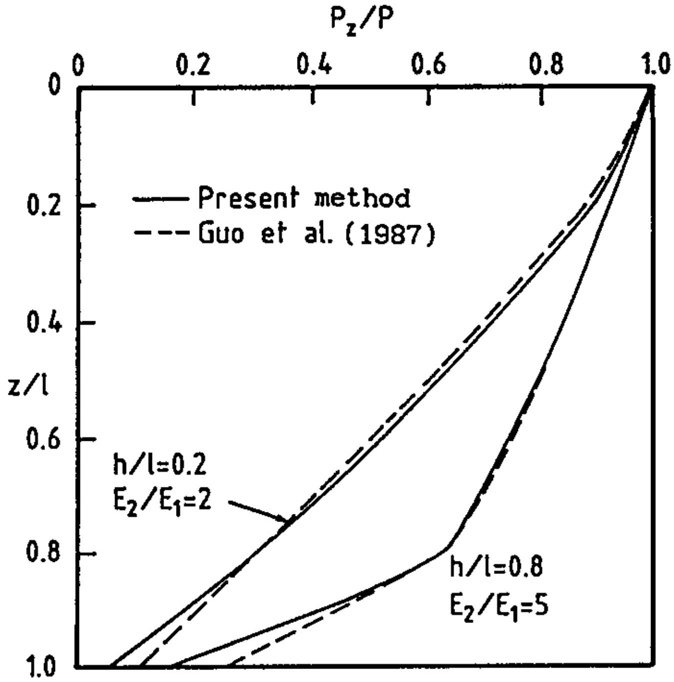

Fig. 5.3 Comparison of load distributions for a socketed pile (program SPILE1)

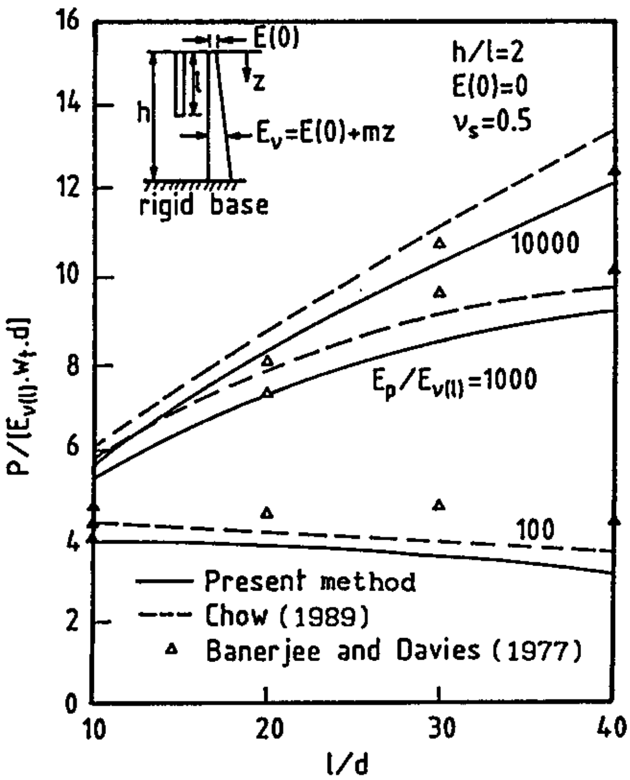

Fig. 5.4 Comparison of normalised stiffness values for single piles in Gibson soil (program SPILE1)

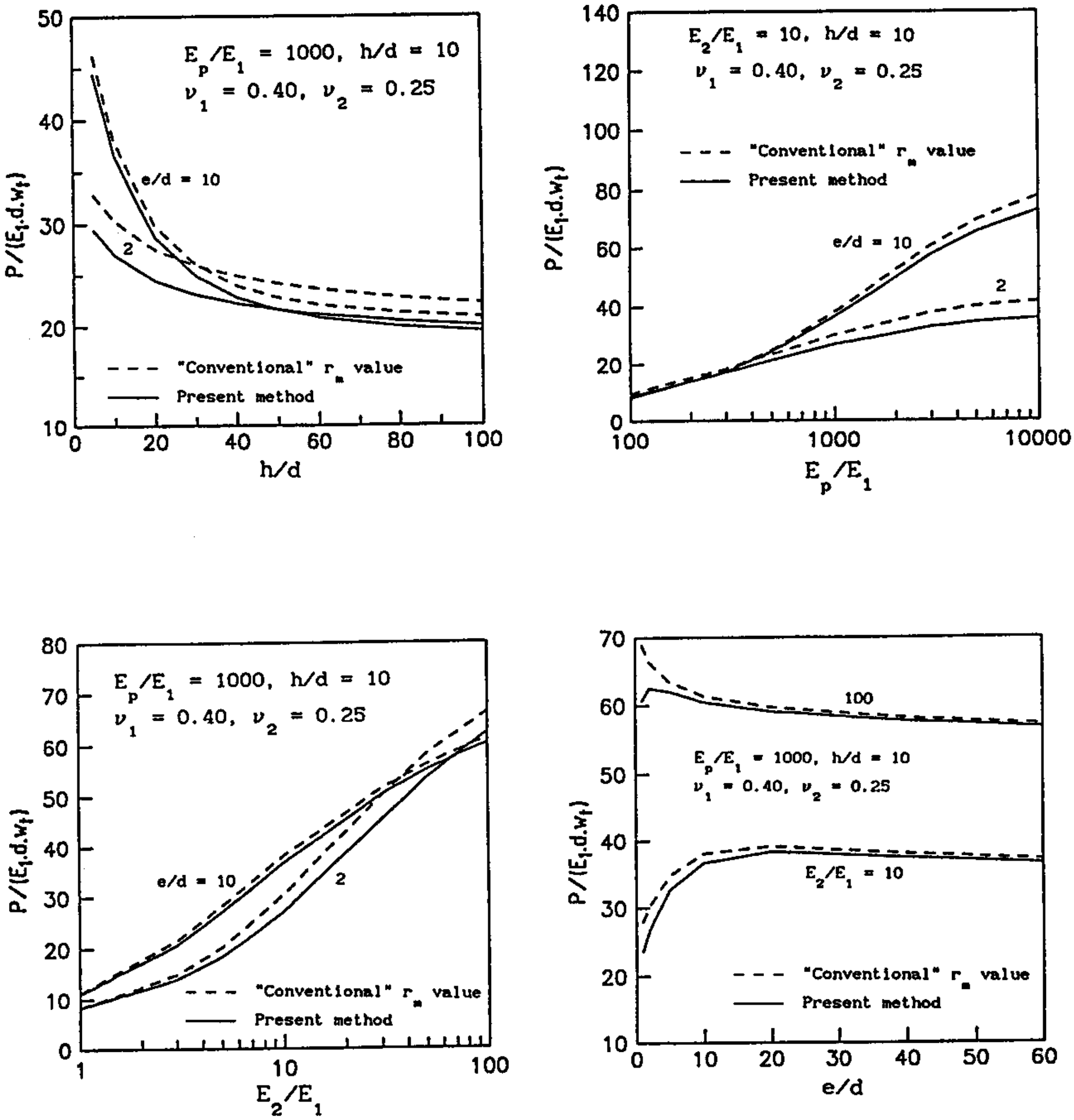

Fig. 5.5 Comparisons between single piles solutions obtained using the "conventional" r_m value and the present method (program SPILE3)

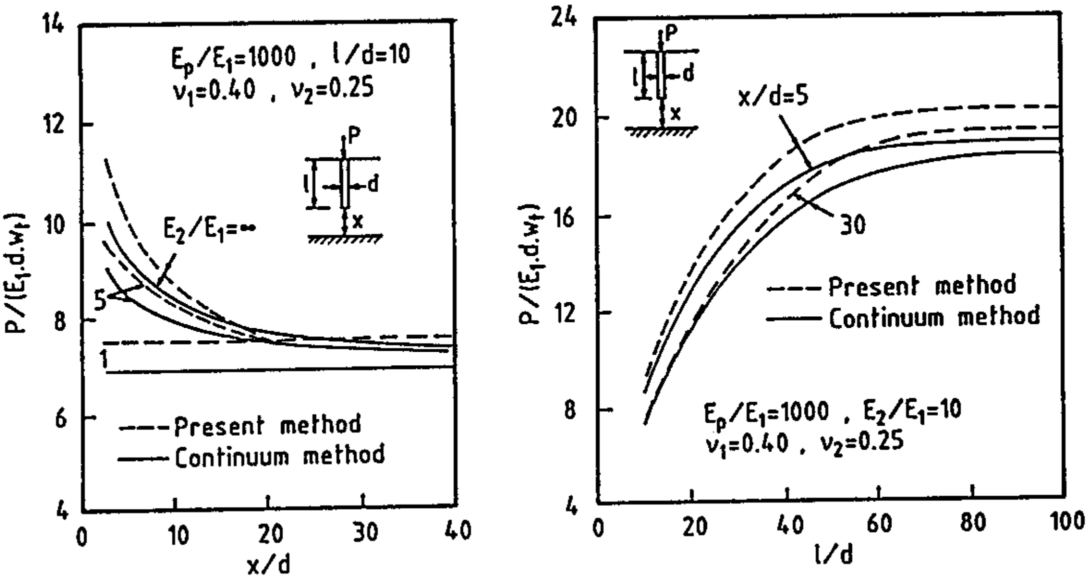

Fig. 5.6 Comparisons of solutions for single piles in finite soil layer (using program SPILE3): (a) effect of x/d; (b) effect of ℓ/d

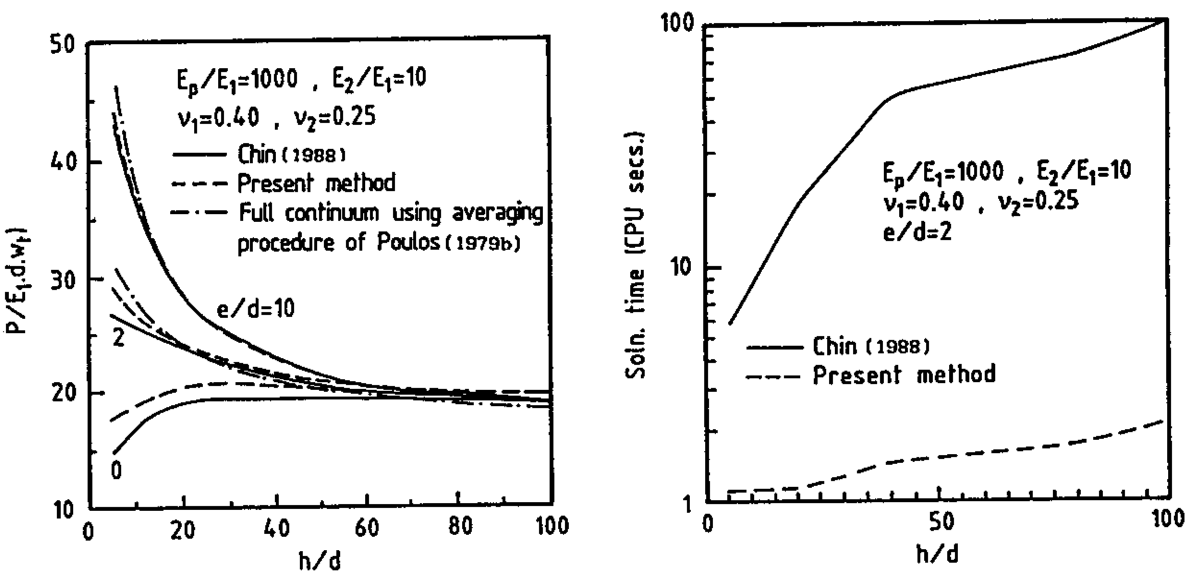

Fig. 5.7 Comparisons of solutions for socketed single piles (using program SPILE3): (a) effect of h/d; (b) solution time

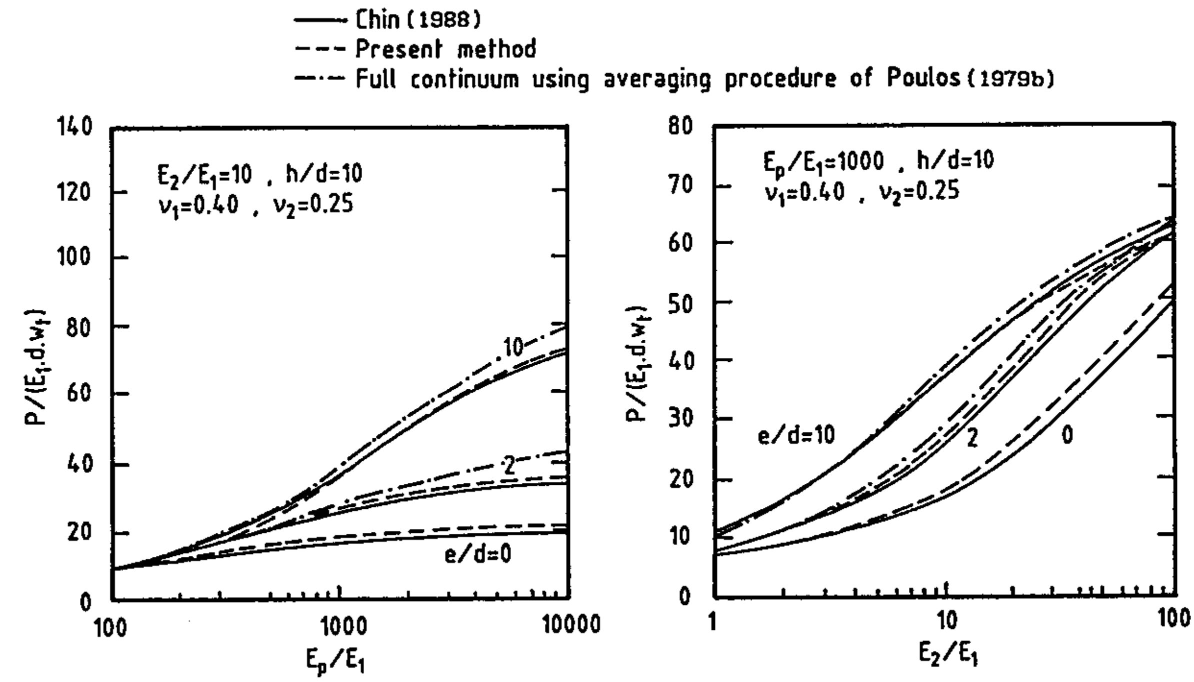

Fig. 5.8 Comparisons of solutions for socketed single piles (using program SPILE3): (a) effect of E_p/E_1; (b) effect of E_2/E_1

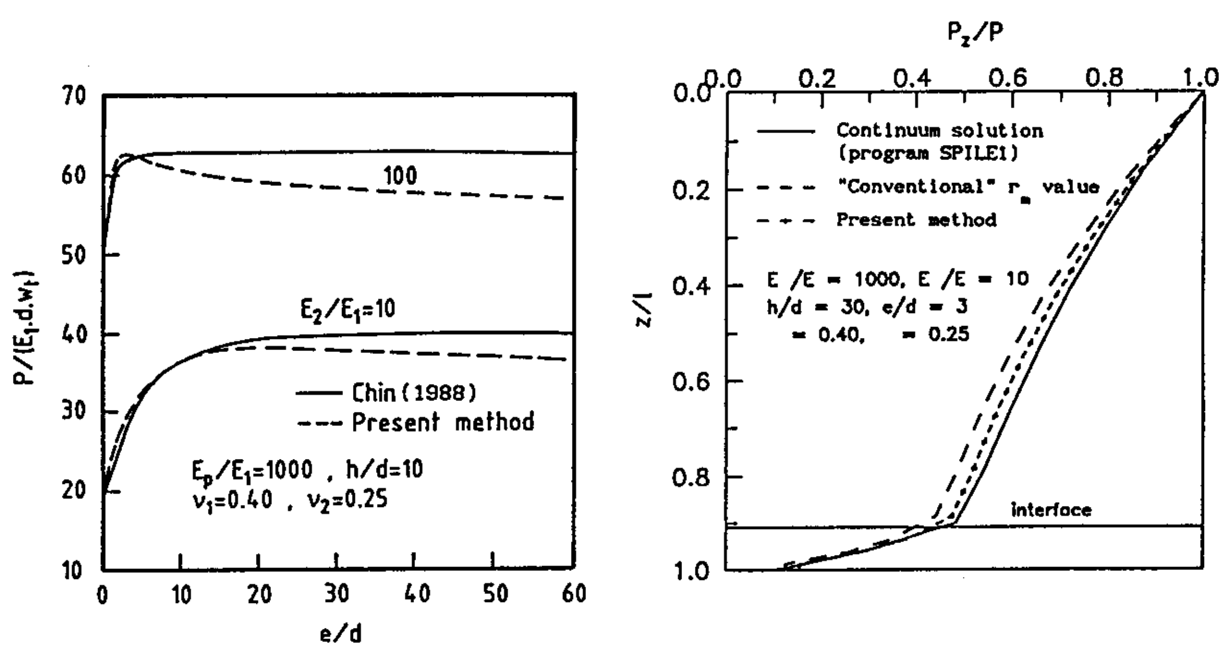

Fig. 5.9 Comparisons of solutions for socketed single piles (using program SPILE3): (a) effect of e/d; (b) load distribution

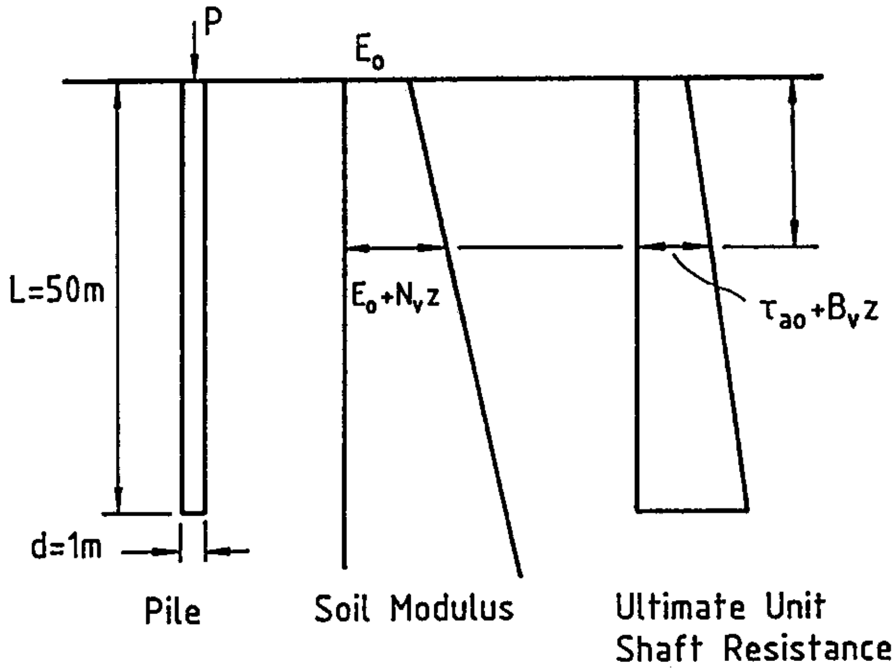

Fig. 5.10 Example problem utilised for static nonlinear analysis of single piles; see Table 5.3 for soil parameter values (after Poulos, 1987)

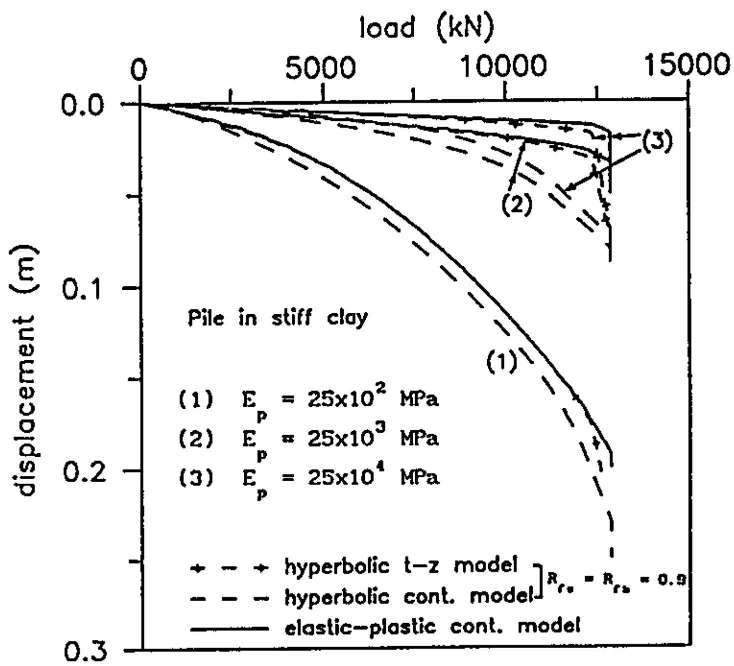

Fig. 5.11 Influence of adopted soil model on computed load-settlement response for single piles in stiff clay

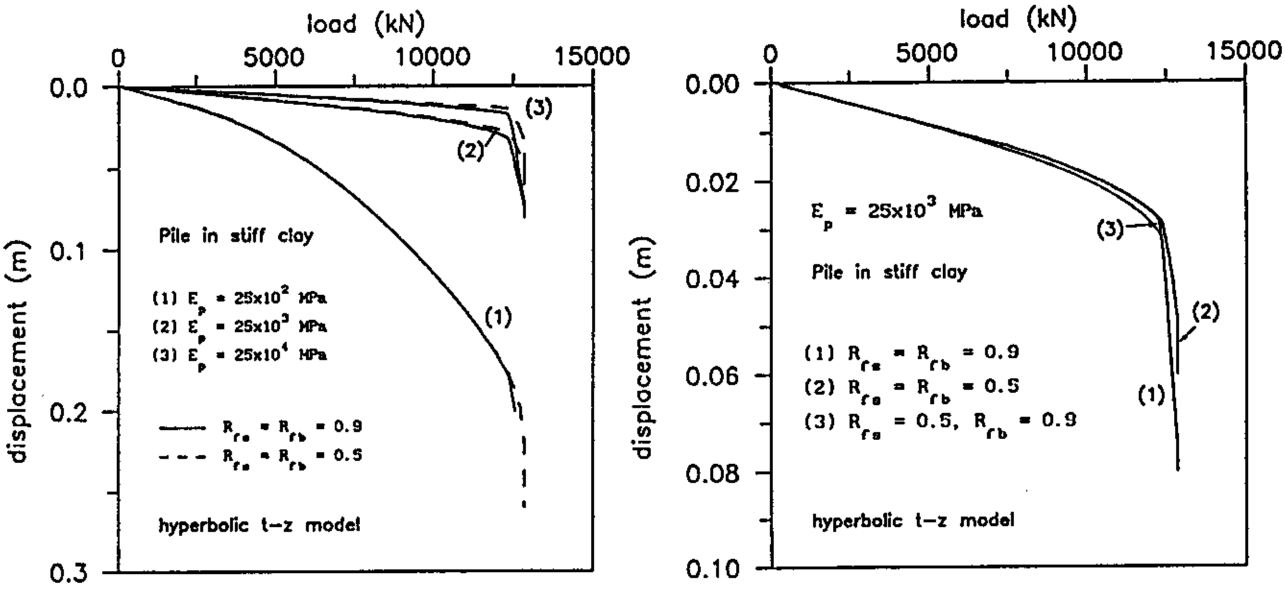

Fig. 5.12 Pile in stiff clay (using program SPILE3): (a) influence of pile modulus; (b) influence of R_{fs} and R_{fb}

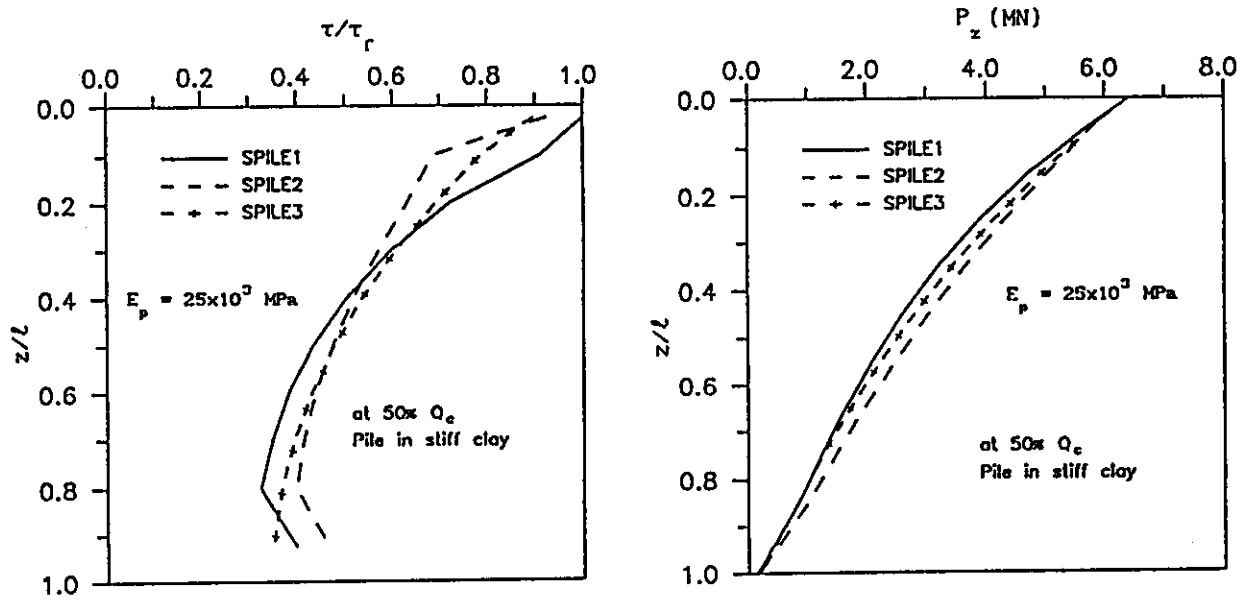

Fig. 5.13 Influence of adopted soil model for pile in stiff clay: (a) shear stress distributions; (b) load distributions

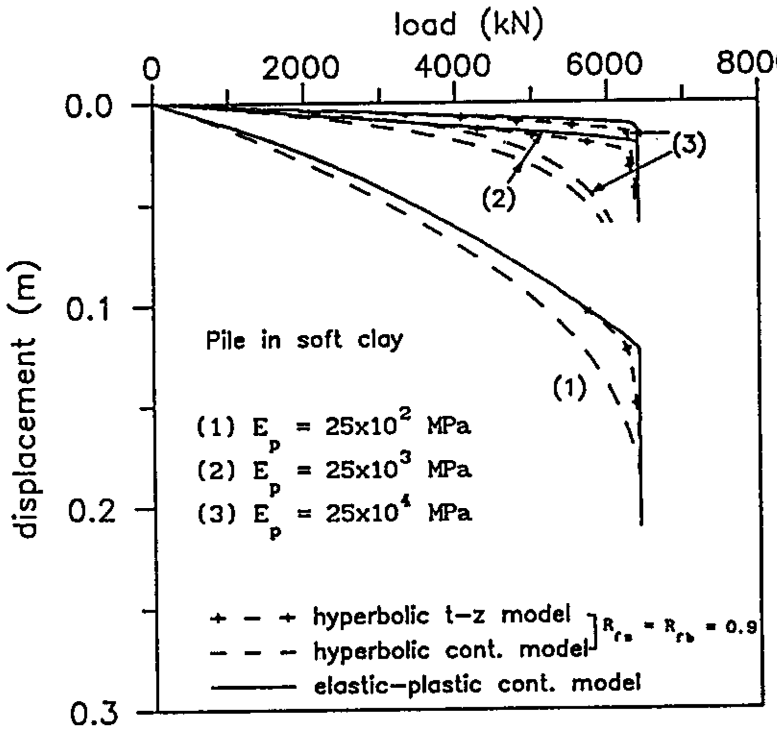

Fig. 5.14 Influence of adopted soil model on computed load-settlement response for single piles in soft clay

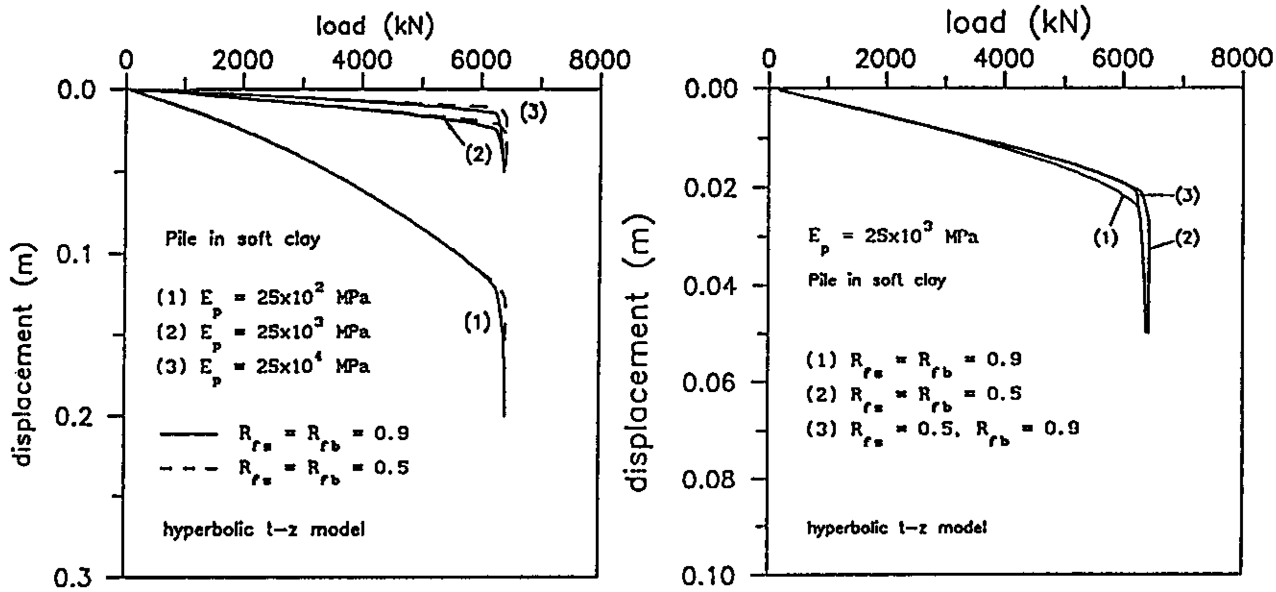

Fig. 5.15 Pile in soft clay (using program SPILE3): (a) influence of pile modulus; (b) influence of R_{fs} and R_{fb}

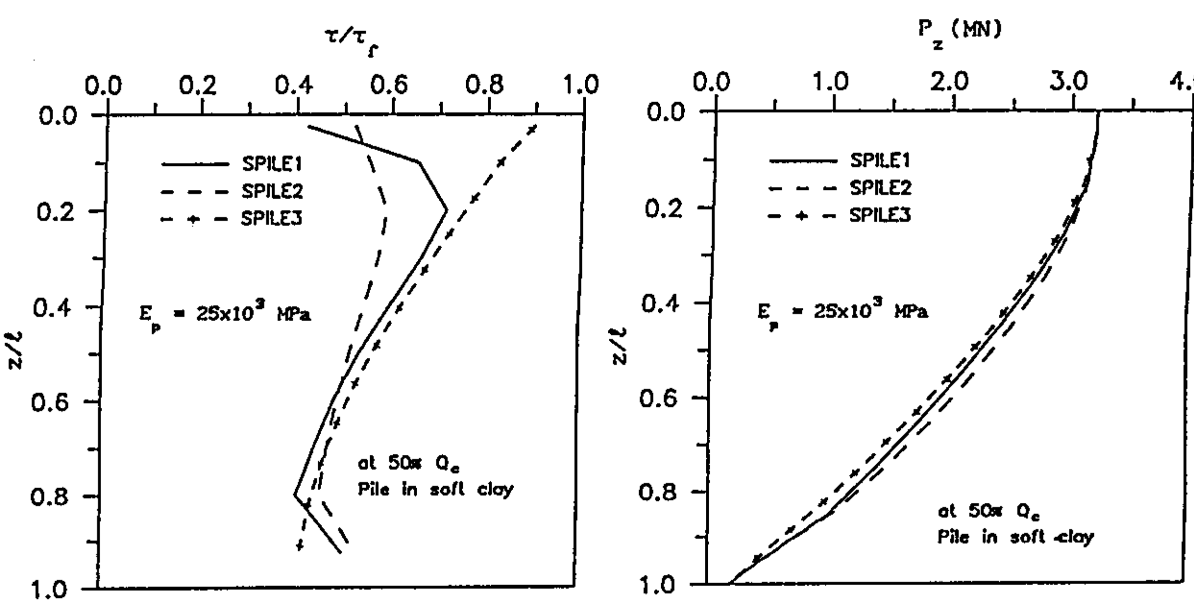

Fig. 5.16 Influence of adopted soil model for pile in soft clay: (a) shear stress distributions; (b) load distributions

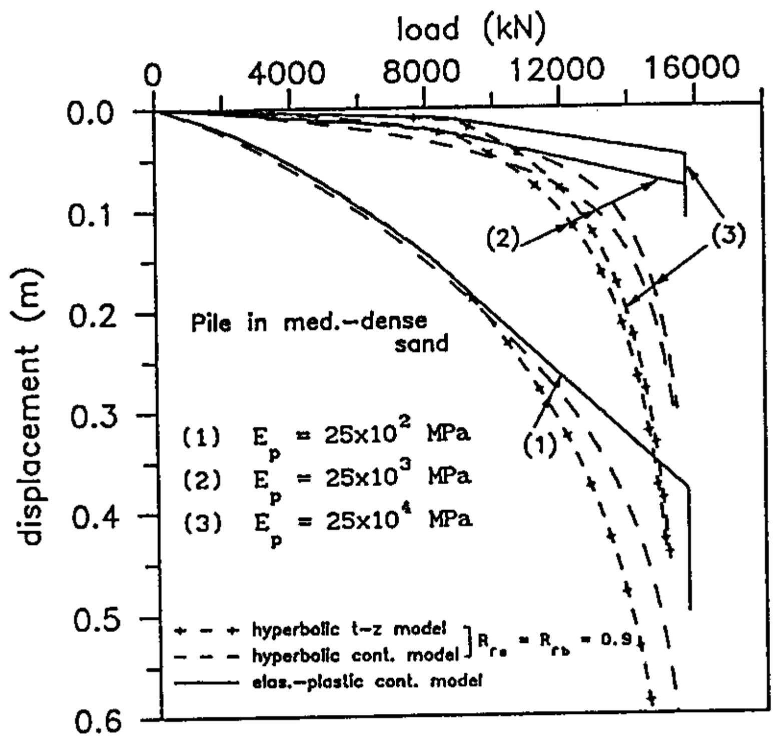

Fig. 5.17 Influence of adopted soil model on computed load-settlement response for single piles in medium-dense sand

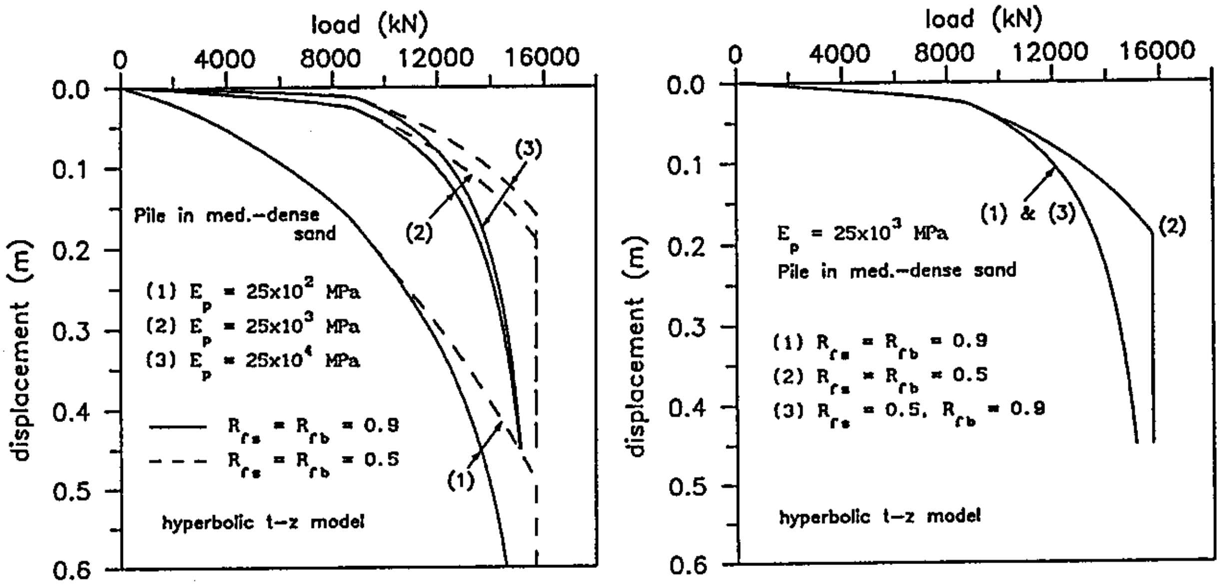

Fig. 5.18 Pile in medium-dense sand (using program SPILE3): (a) influence of pile modulus; (b) influence of R_{fs} and R_{fb}

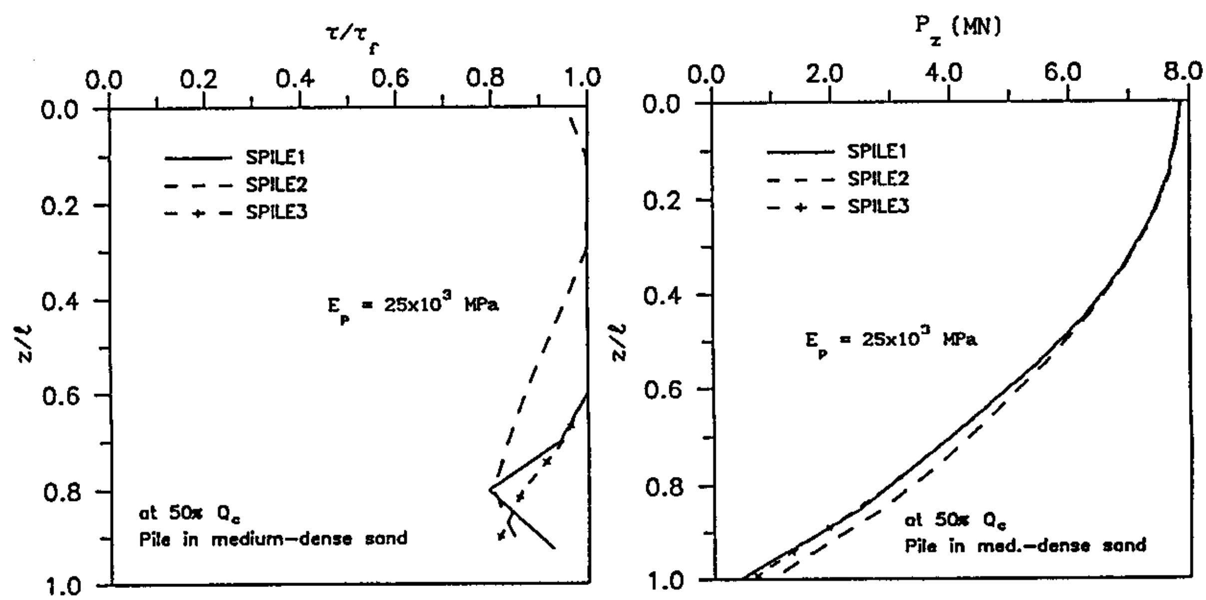

Fig. 5.19 Influence of adopted soil model for pile in medium-dense sand: (a) shear stress distributions; (b) load distributions

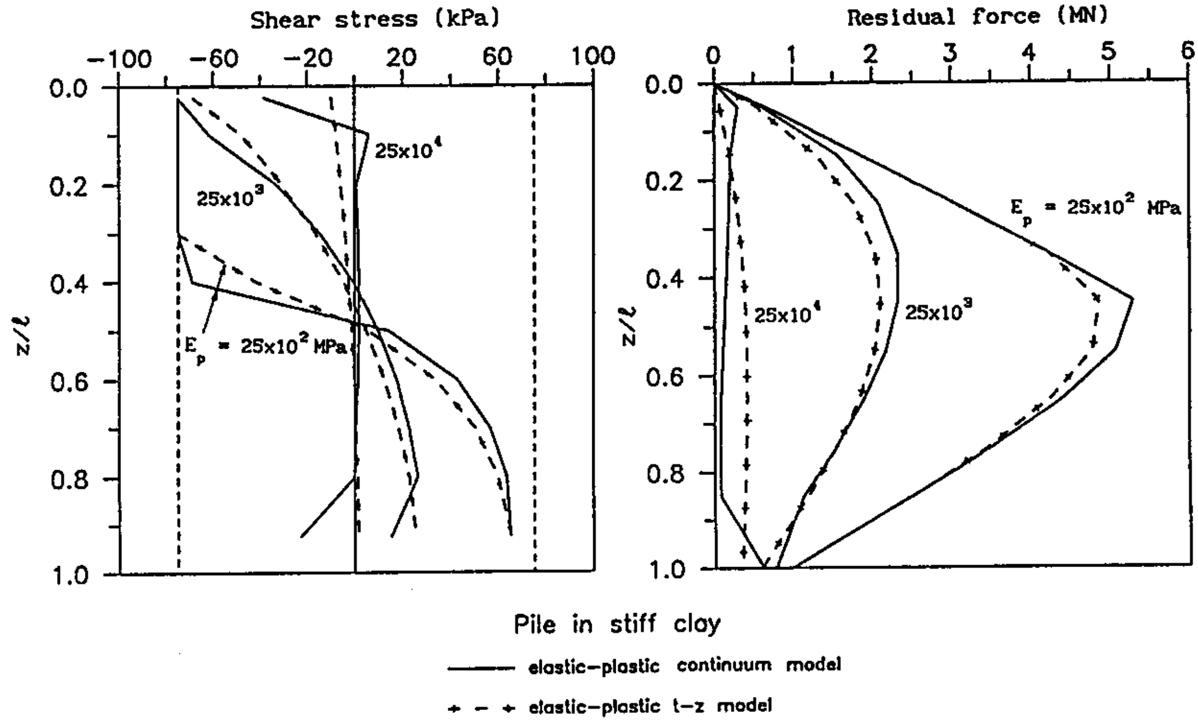

Fig. 5.20 Pile in stiff clay: (a) residual shear stress distributions; (b) residual force distributions

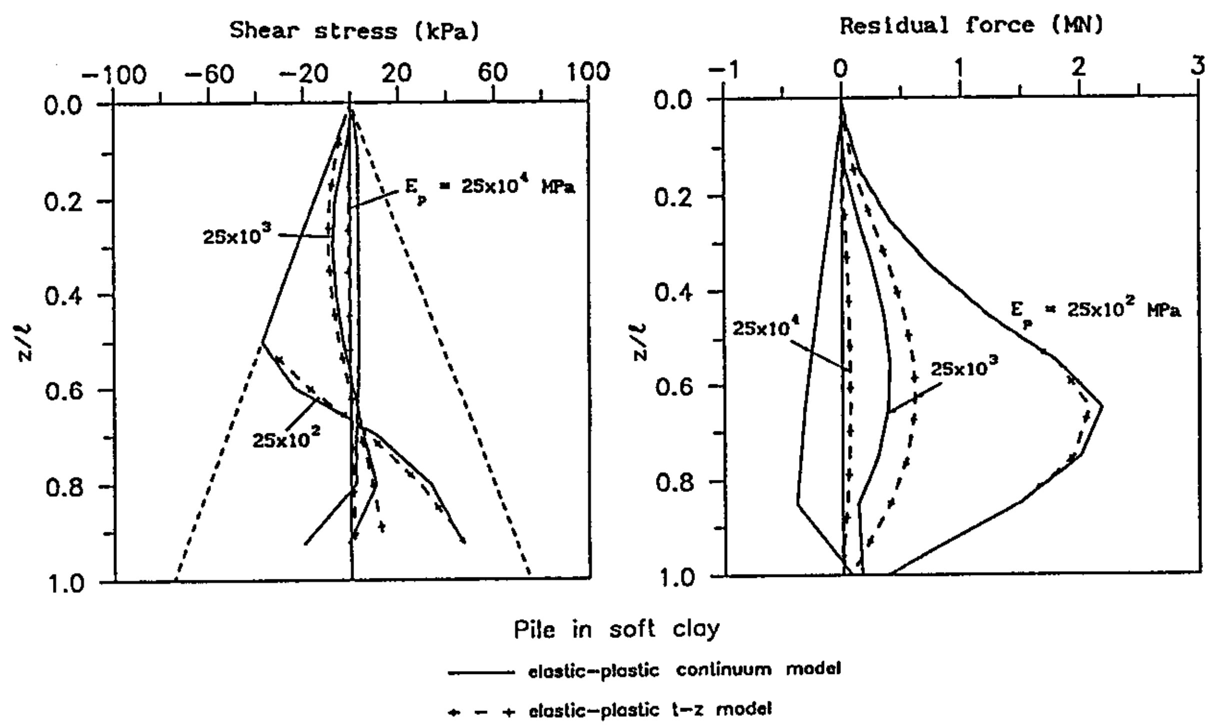

Fig. 5.21 Pile in soft clay: (a) residual shear stress distributions; (b) residual force distributions

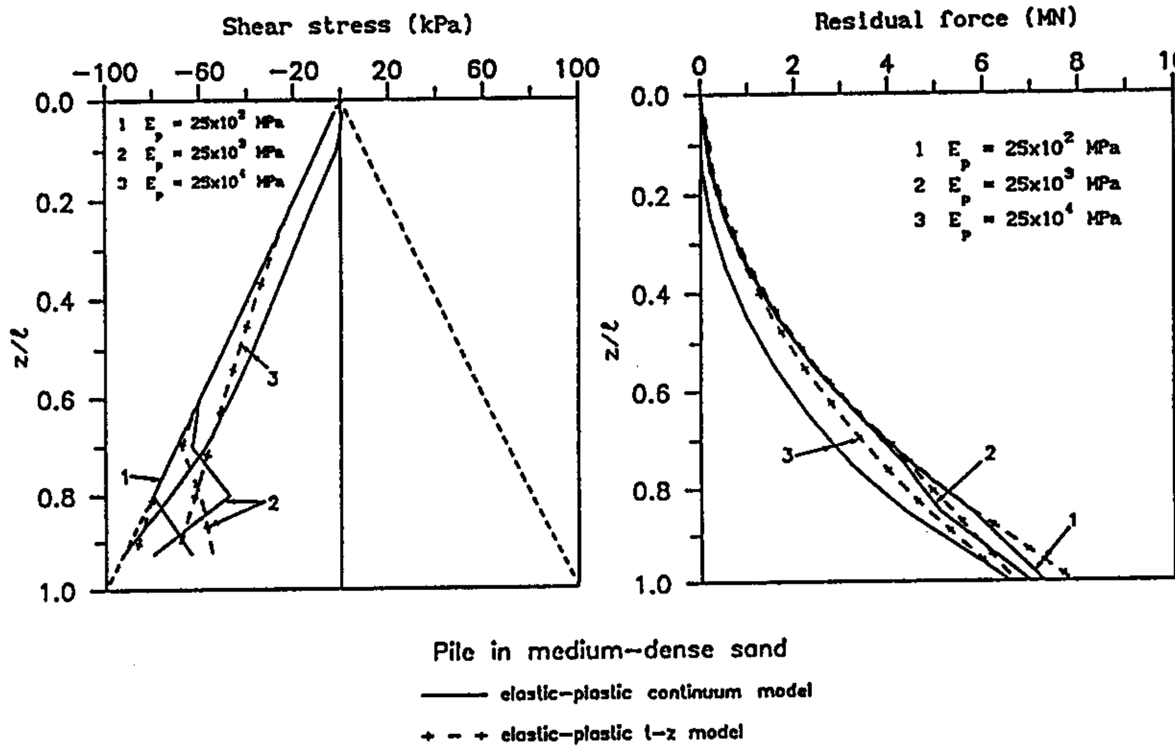

Fig. 5.22 Pile in medium-dense sand: (a) residual shear stress distributions; (b) residual force distributions

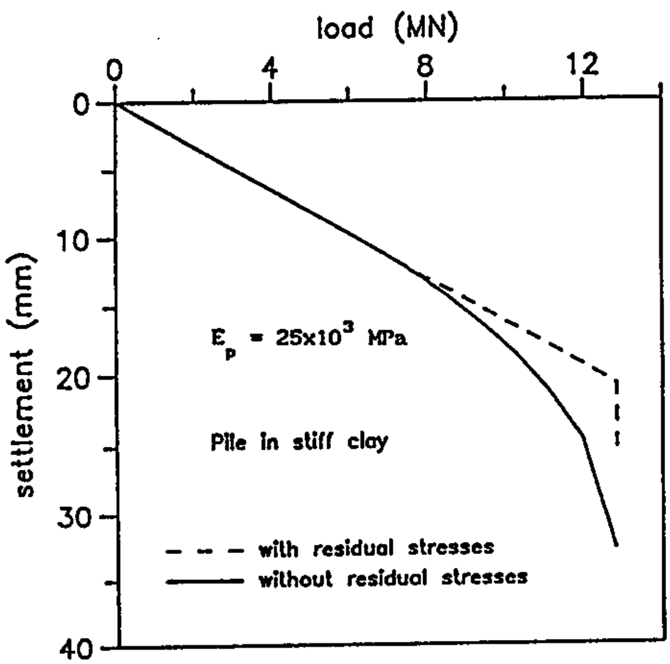

Fig. 5.23 Influence of residual stresses on compression load-settlement response

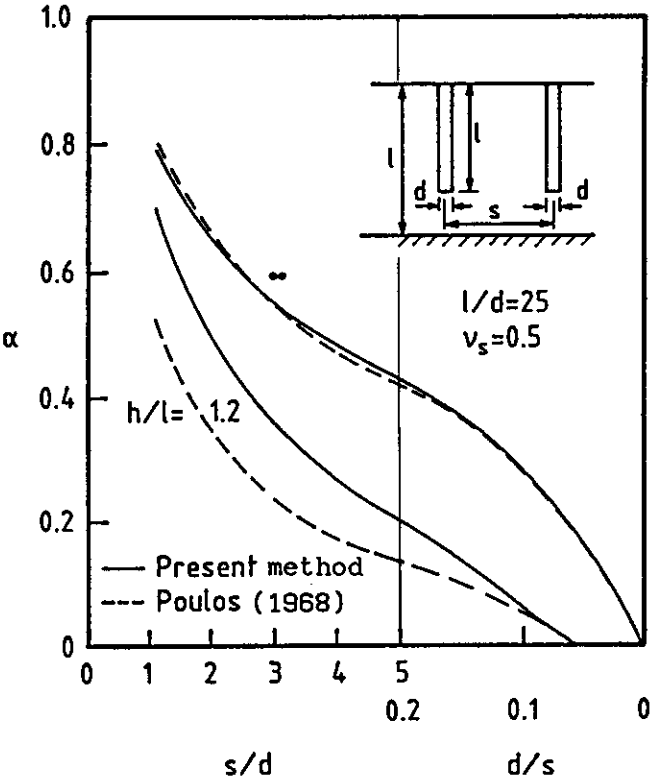

Fig. 5.24 Comparison of elastic interaction factors for pile groups in finite soil layer (program SPILE1)

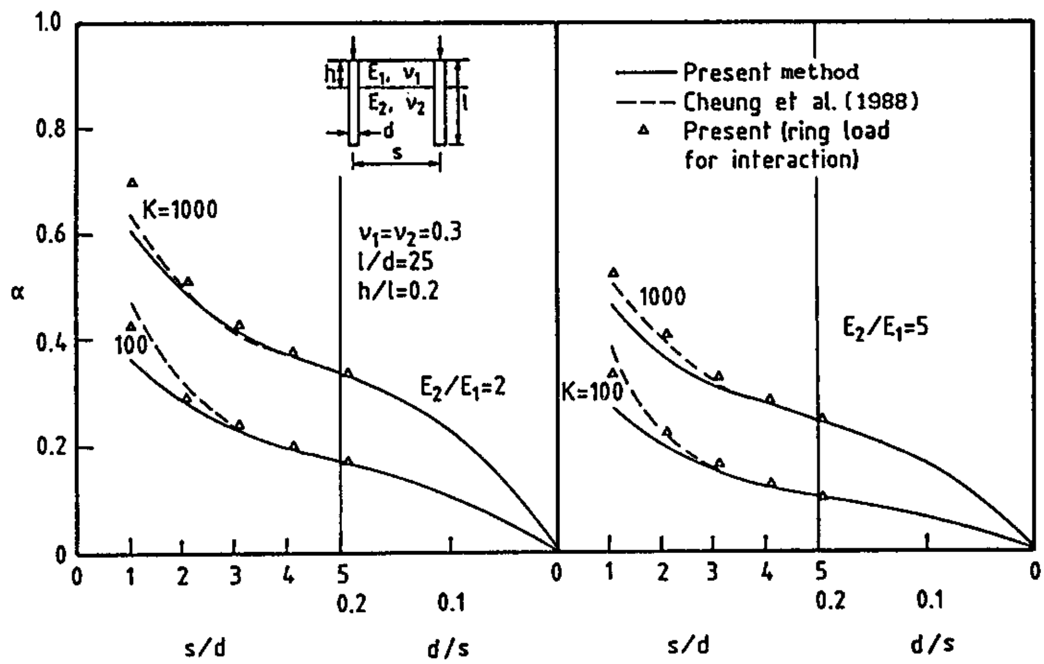

Fig. 5.25 Comparison of elastic interaction factors for socketed pile groups (program SPILE1)

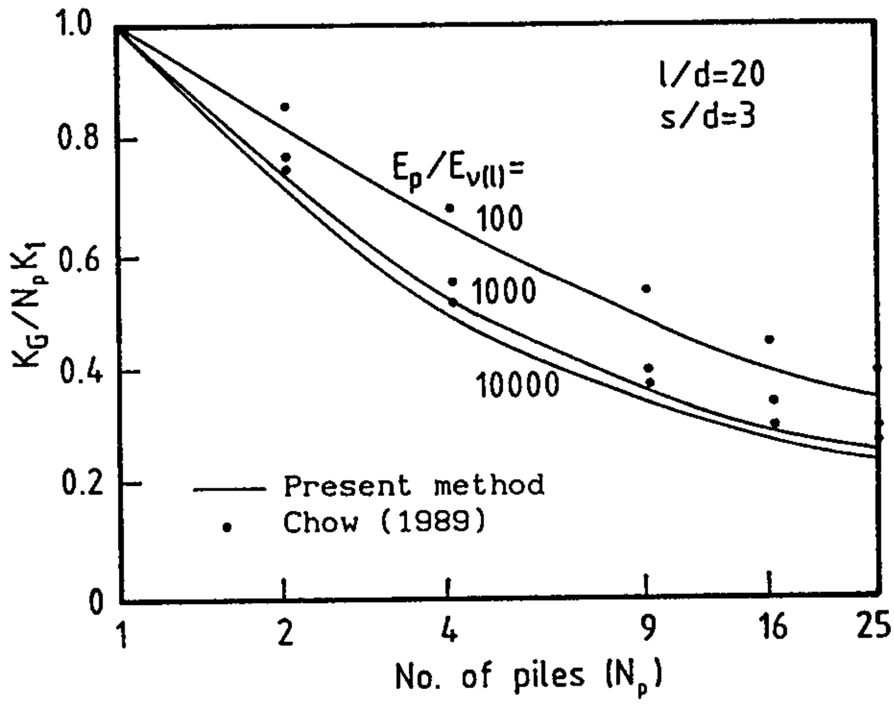

Fig. 5.26 Comparison of elastic stiffness reduction factors for pile groups in Gibson soil (program SPILE1)

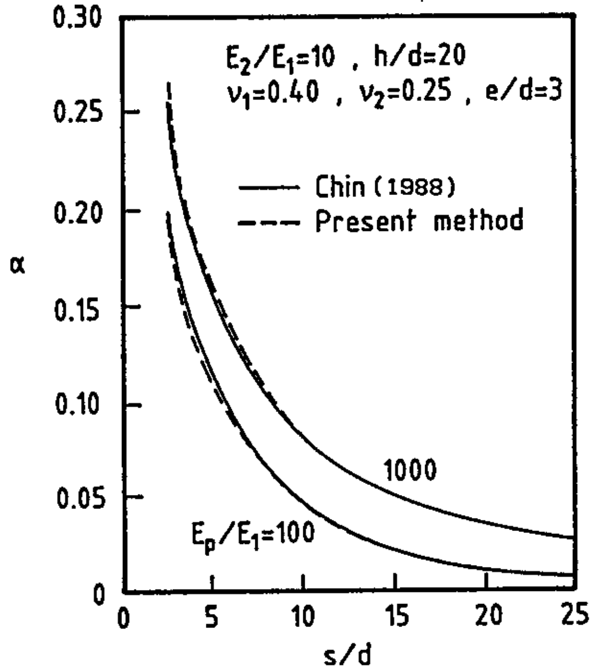

Fig. 5.27 Comparison of elastic interaction factors for socketed pile groups (program SPILE3)

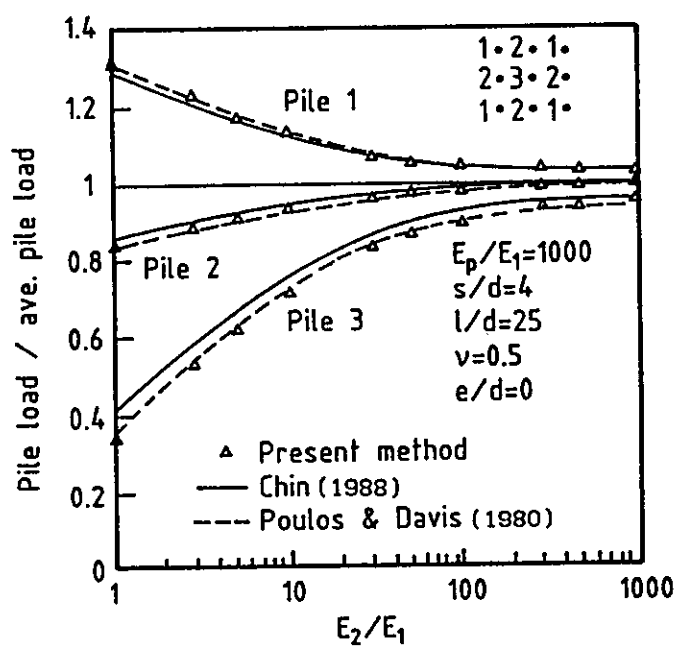

Fig. 5.28 Comparison of elastic load distributions for end-bearing pile groups (program SPILE3)

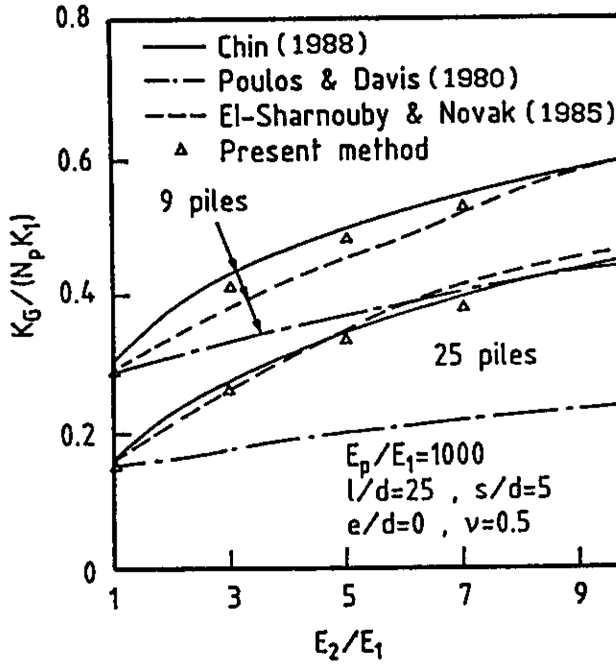

Fig. 5.29 Comparison of elastic stiffness reduction factors for end-bearing pile groups (program SPILE3)

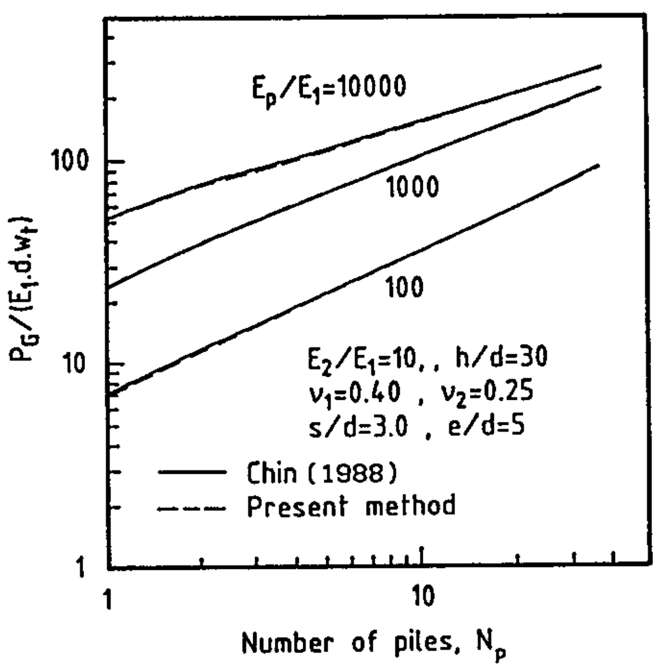

Fig. 5.30 Comparison of elastic normalised group stiffness for socketed pile groups (program SPILE3)

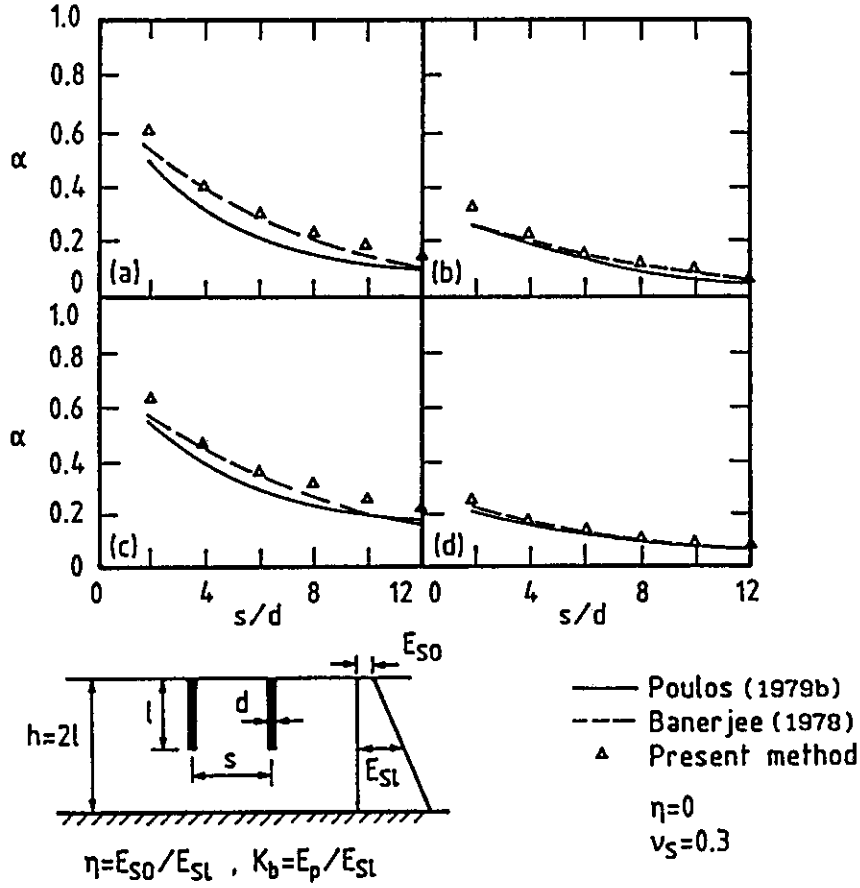

Fig. 5.31 Elastic interaction factors for pile groups in Gibson soil: (a) ℓ/d = 20, K_b = 10000; (b) ℓ/d = 20, K_b = 100; (c) ℓ/d = 40, K_b = 10000; (d) ℓ/d = 40, K_b = 100

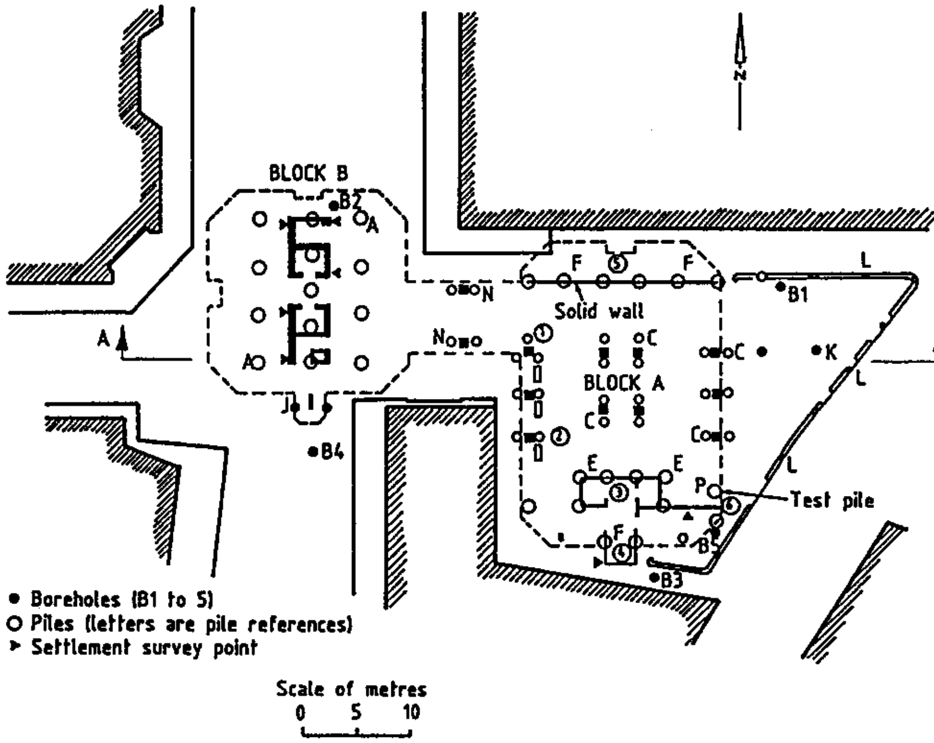

(a)

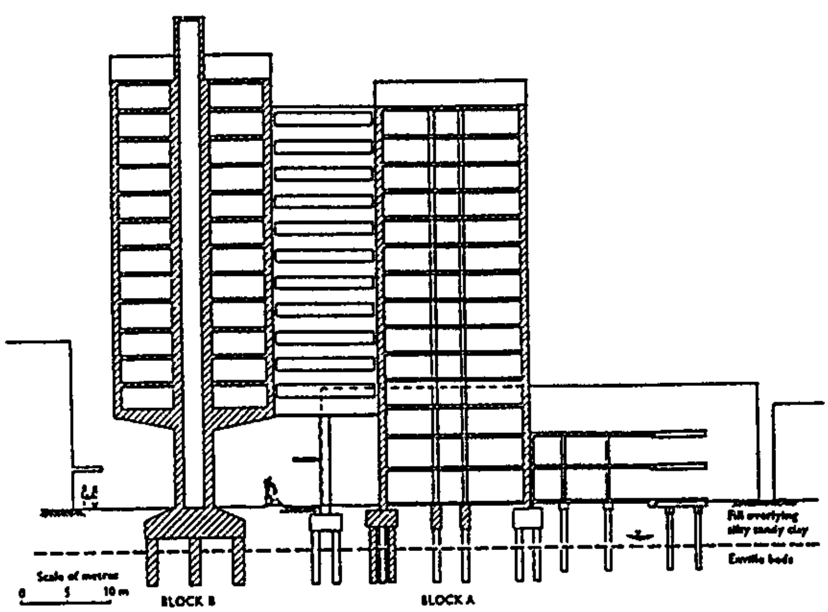

(b)

Fig. 5.32 Details of a highrise construction with socketed pile groups reported by Cole and Stroud (1977): (a) pile foundations layout plan; (b) elevation view through A-A

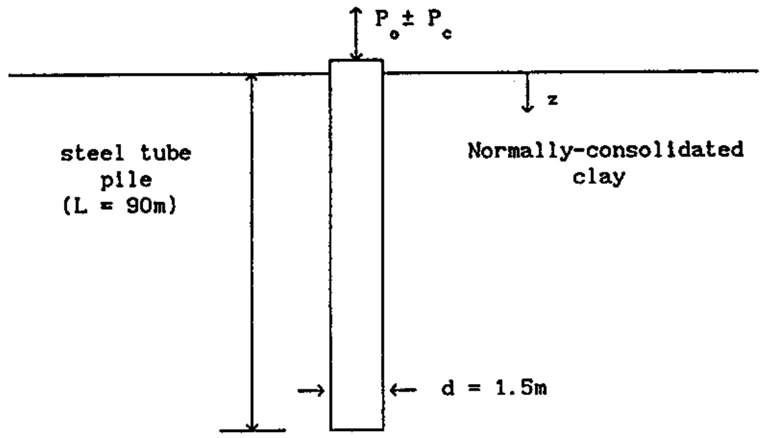

<u>Pile parameters</u> :

wall thickness, t = 60 mm
E_p (equivalent) = 30720 MPa

<u>Soil parameters</u> :

soil modulus, E_s = 1.5z MN/m^2

Poisson's ratio, ν_s = 0.5

limiting shaft capacity, τ_{fs} = 2.5z kN/m
(with no "strain-softening")

limiting base resistance, τ_{fb} = 2.025 MN/m^2
(no tensile base resistance)

<u>For cyclic loading analysis</u> :

(a) two-way cyclic loading (i.e $P_o = 0$)

(b) Matlock and Foo (1980) capacity degradation model

$D_{\tau lim} = 0.30$
$\lambda = 0.25$

(c) no degradation for base resistance and soil modulus

(d) no loading rate effects included

(e) permanent displacement accumulation parameters

program SCPIL1 : $m_s = 0.1$, $n_s = 2.0$
$m_b = 0.1$, $n_b = 2.0$

program SCPIL3 : $R_{fs} = 0.5$, $R_{fb} = 0.9$
$\psi = 0.02$

representative stress level X utilised in both programs
$= (\tau_o + 2\tau_c)/2\tau_f$

(see section 3.3.1.3 for definitions of parameters)

Fig. 5.33 Parameters adopted for hypothetical driven pile in normally-consolidated clay (after Poulos, 1988b)

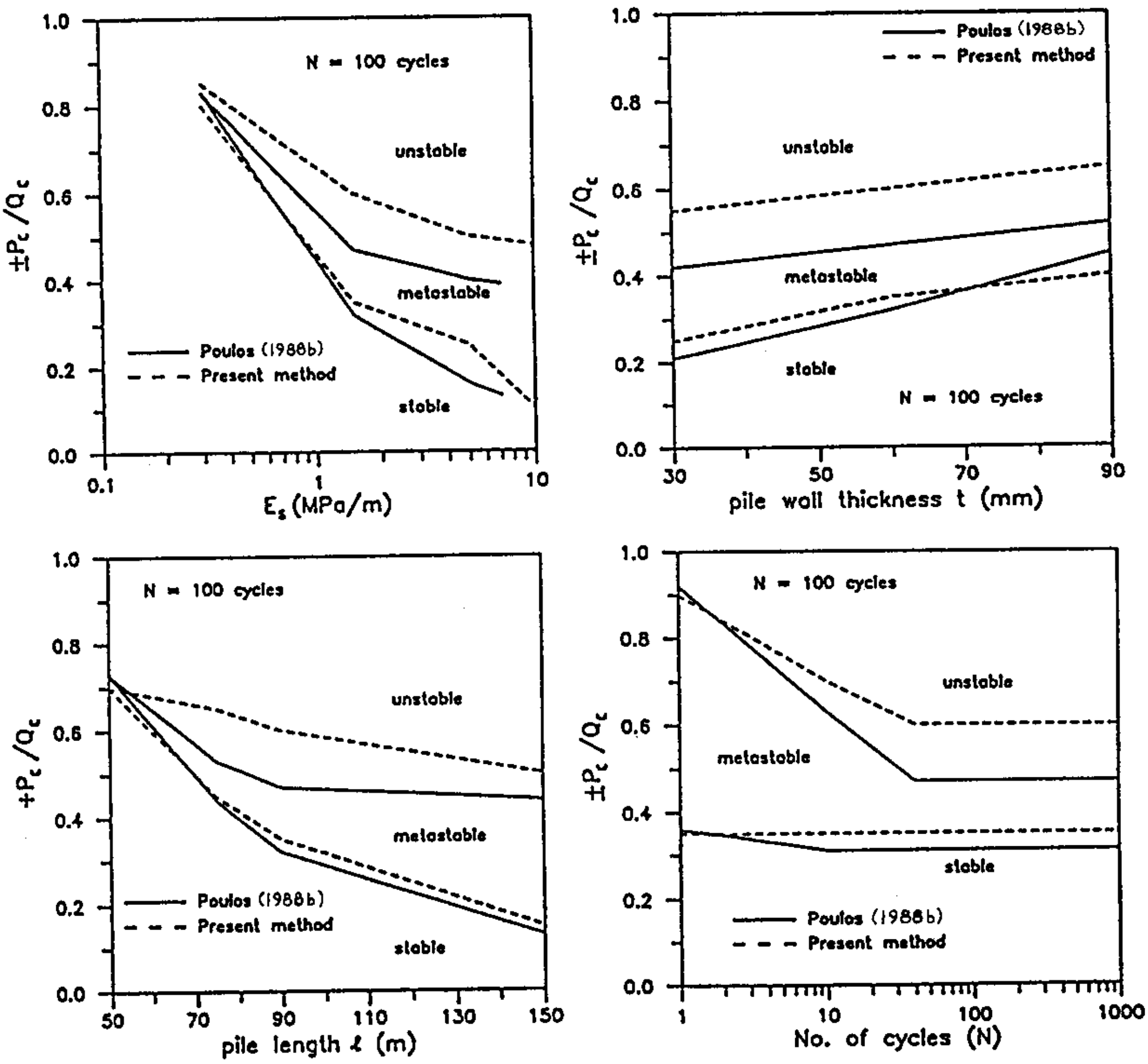

Fig. 5.34 Comparisons of solutions for hypothetical pile in normally-consolidated clay: (a) influence of soil modulus; (b) influence of pile wall thickness; (c) influence of pile length; (d) influence of number of cycles

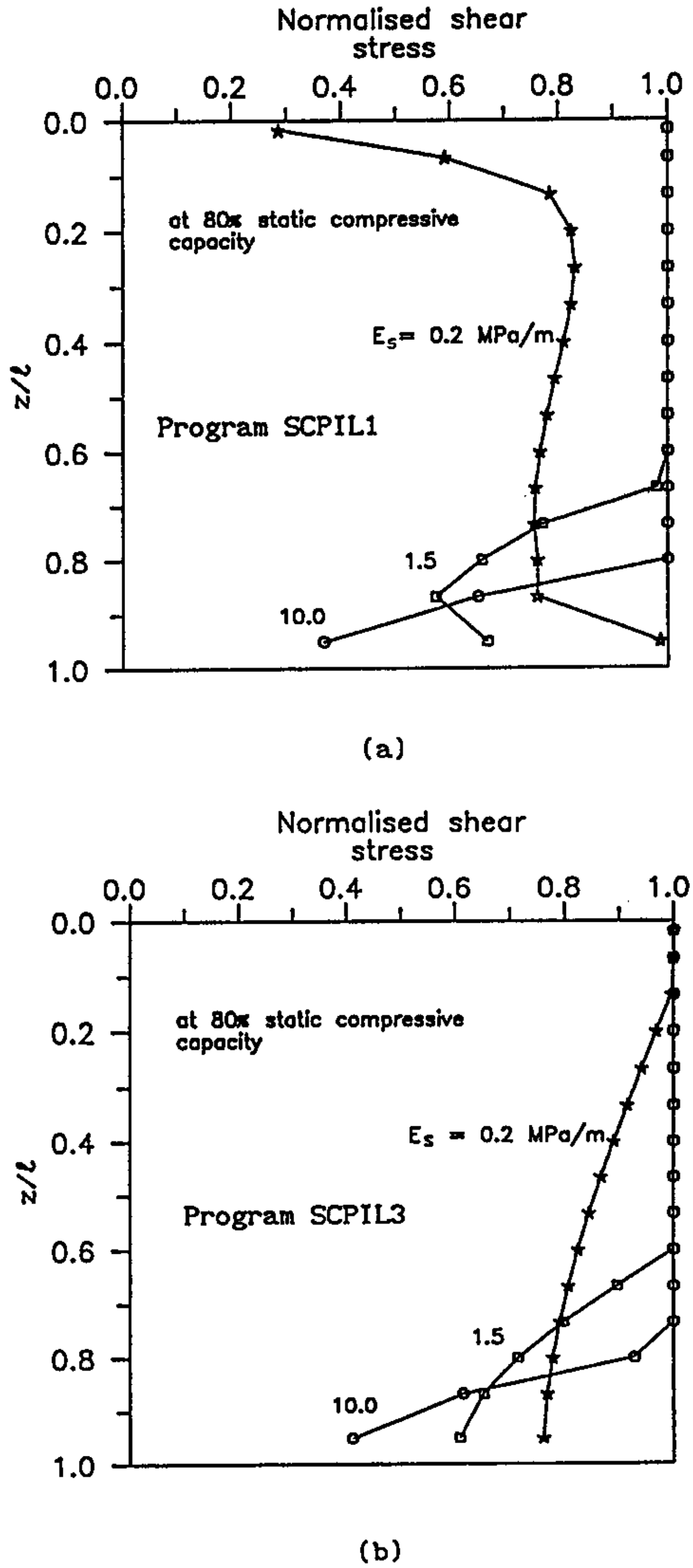

Fig. 5.35 Normalised static shear stress distributions obtained from (a) program SCPIL1; (b) program SCPIL3

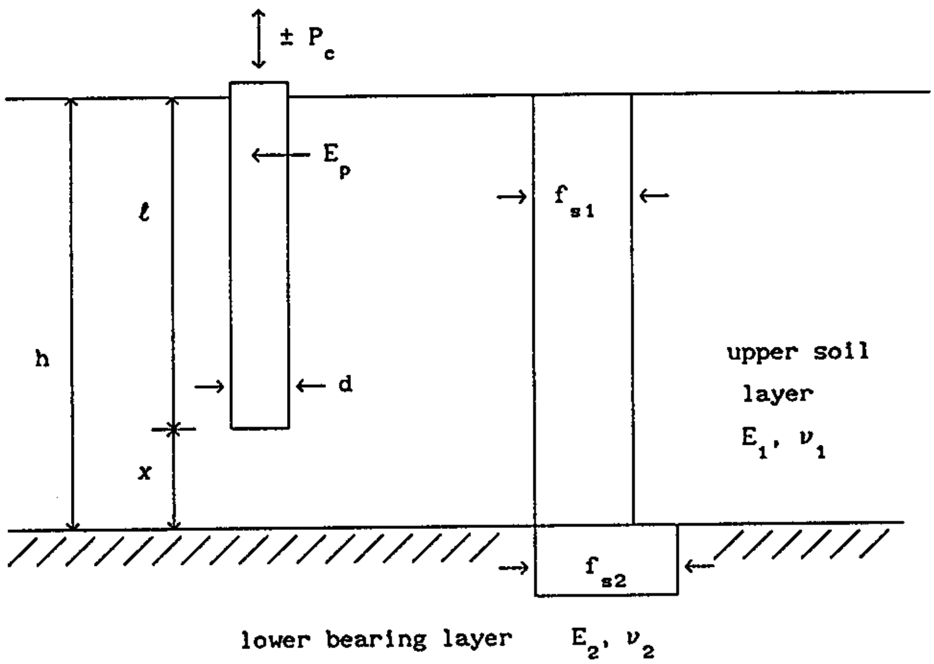

unit resistance values

skin friction : $f_{s2}/f_{s1} = E_2/E_1$

base resistance : $q_b = 100\ f_{s1}$ (for $x > 0$)

$= 100\ f_{s2}$ (for $x = 0$)

- no tensile base resistance assumed
- shaft resistance identical under tension and compression

capacity degradation model

Matlock and Foo (1980) model : $D_{\tau lim} = 0.30$

$\lambda_\tau = 0.25$

no base resistance degradation assumed

Fig. 5.36 Example problem and parameters adopted for parametric study of piles embedded in two-layered soil profile

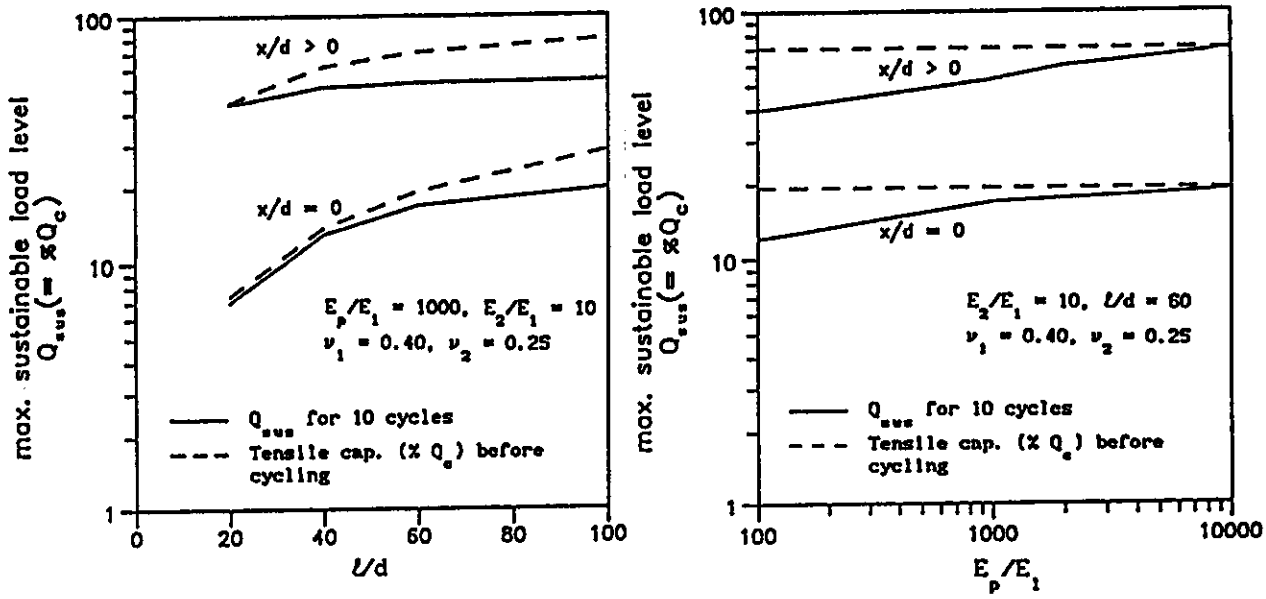

Fig. 5.37 Q_{sus} for non-socketed pile in two-layered soil profile: Influence of (a) ℓ/d; (b) E_p/E_1

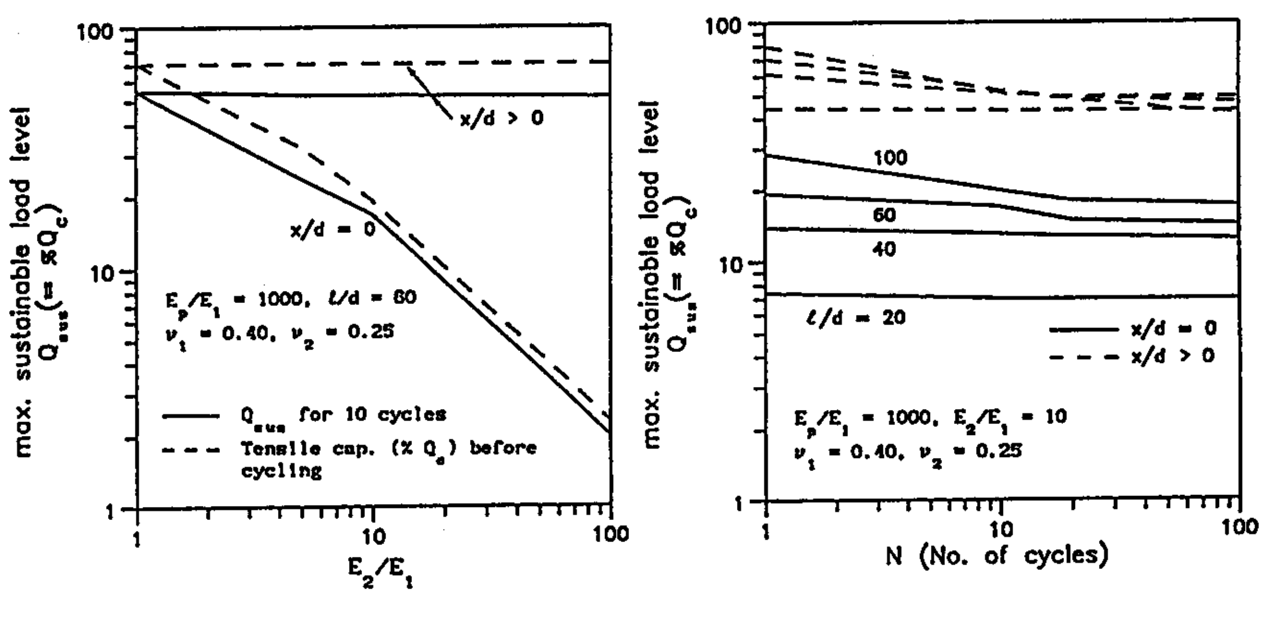

Fig. 5.38 Q_{sus} for non-socketed pile in two-layered soil profile: Influence of (a) E_2/E_1; (b) number of cycles, N

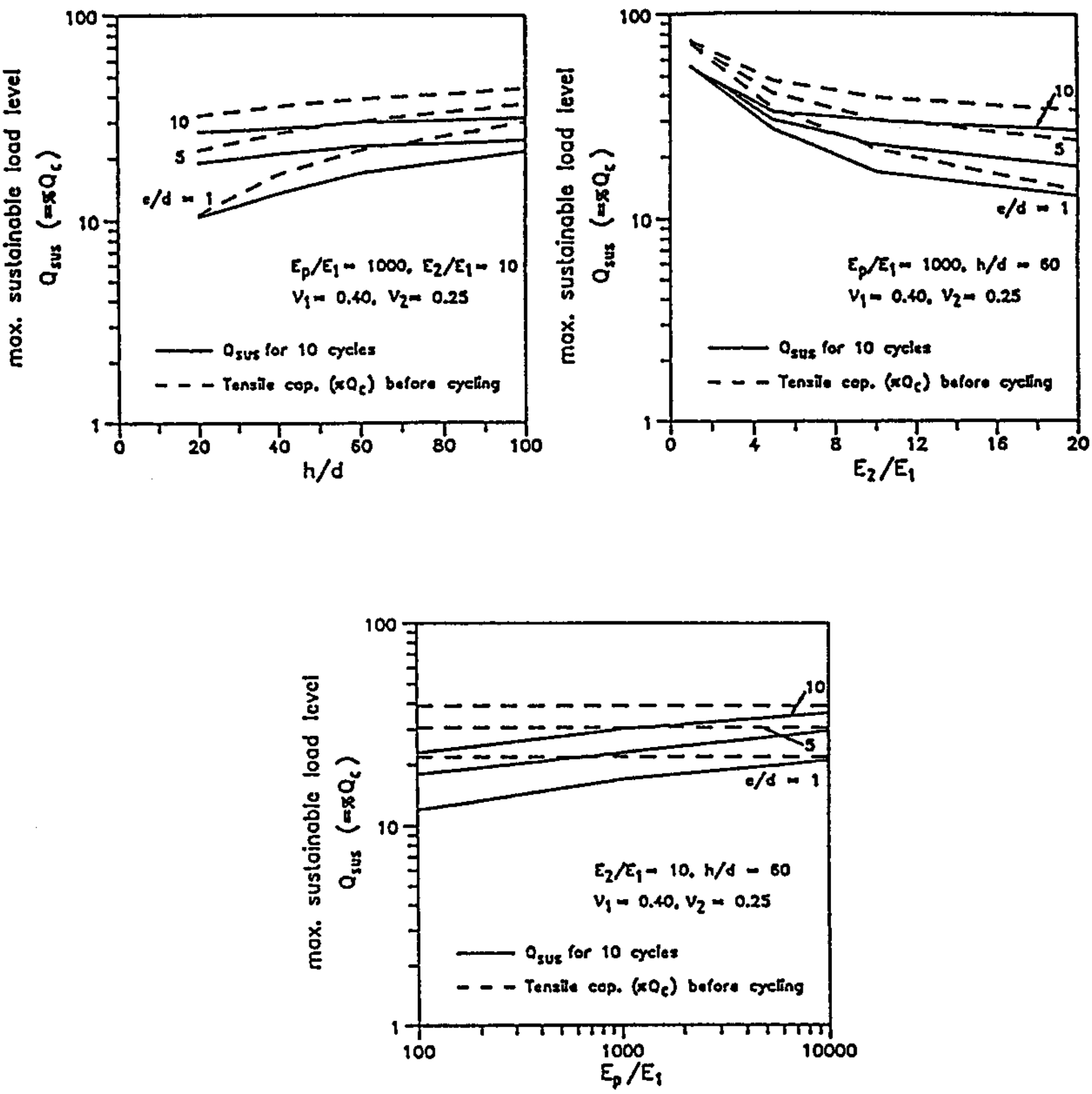

Fig. 5.39 Q_{sus} for socketed pile in two-layered soil profile: Influence of (a) h/d; (b) E_2/E_1; (c) E_p/E_1

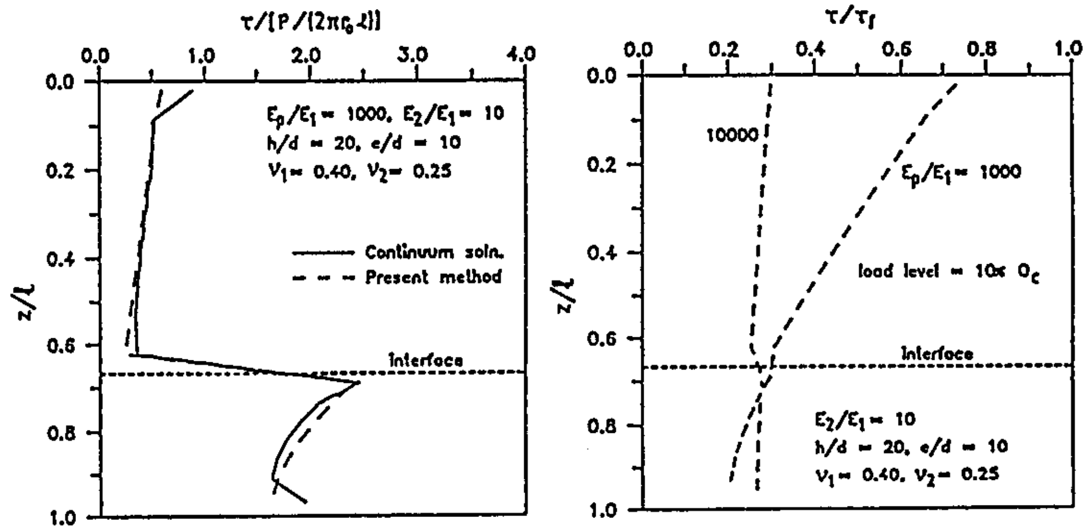

Fig. 5.40 Solutions for a socketed pile: (a) elastic pile-soil shear stress distribution; (b) normalised distribution at load of 10% Q_c

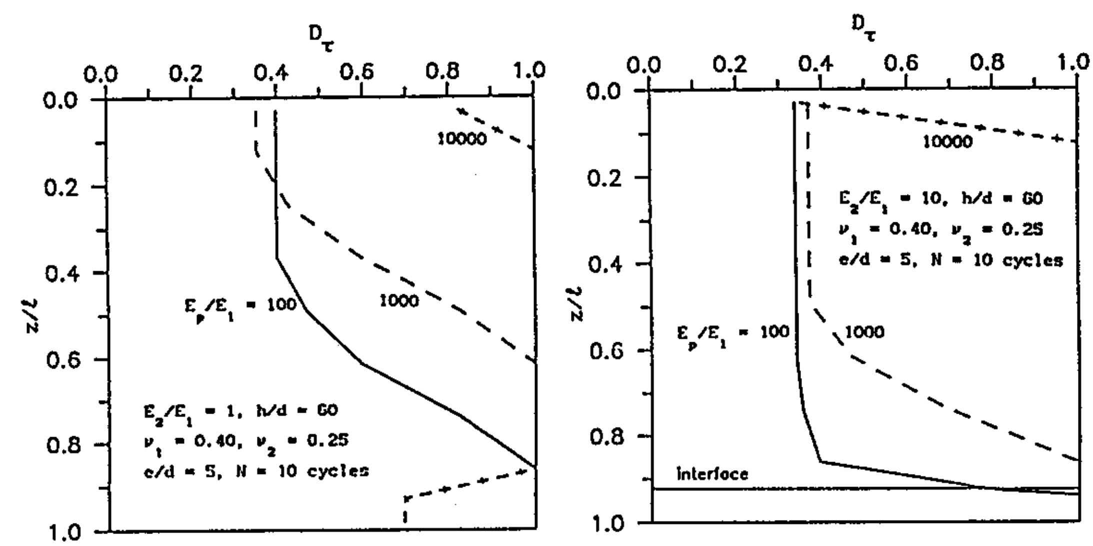

Fig. 5.41 D_τ distributions at corresponding maximum sustainable load level for (a) $E_2/E_1 = 1$; (b) $E_2/E_1 = 10$

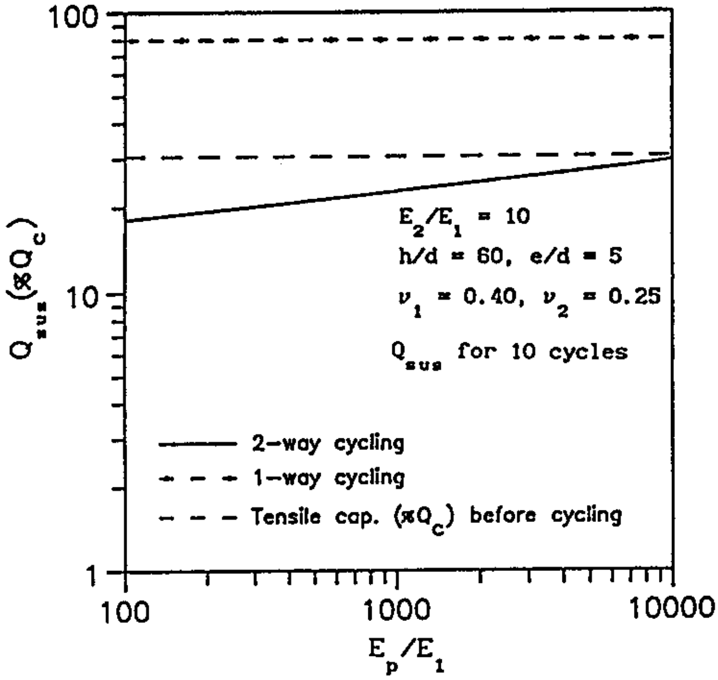

(a)

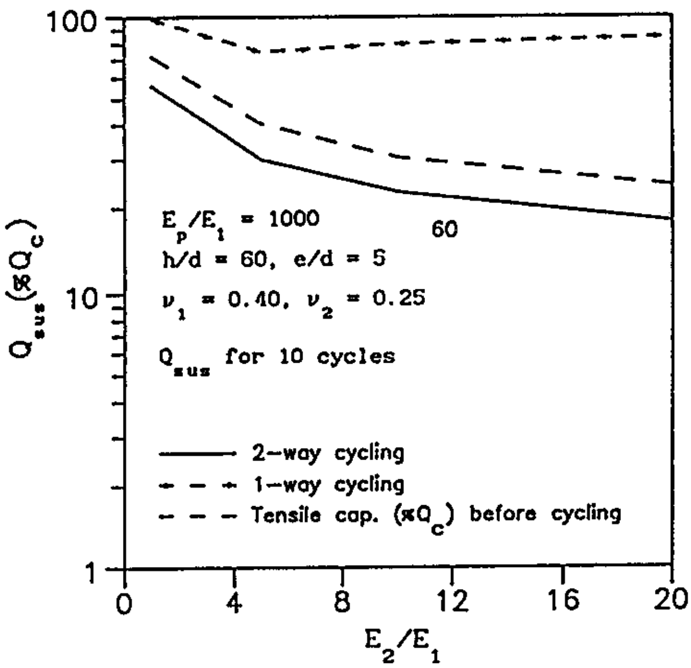

(b)

Fig. 5.42 Influence of type of loading condition on Q_{sus} for different (a) E_p/E_1 ratios; (b) E_2/E_1 ratios

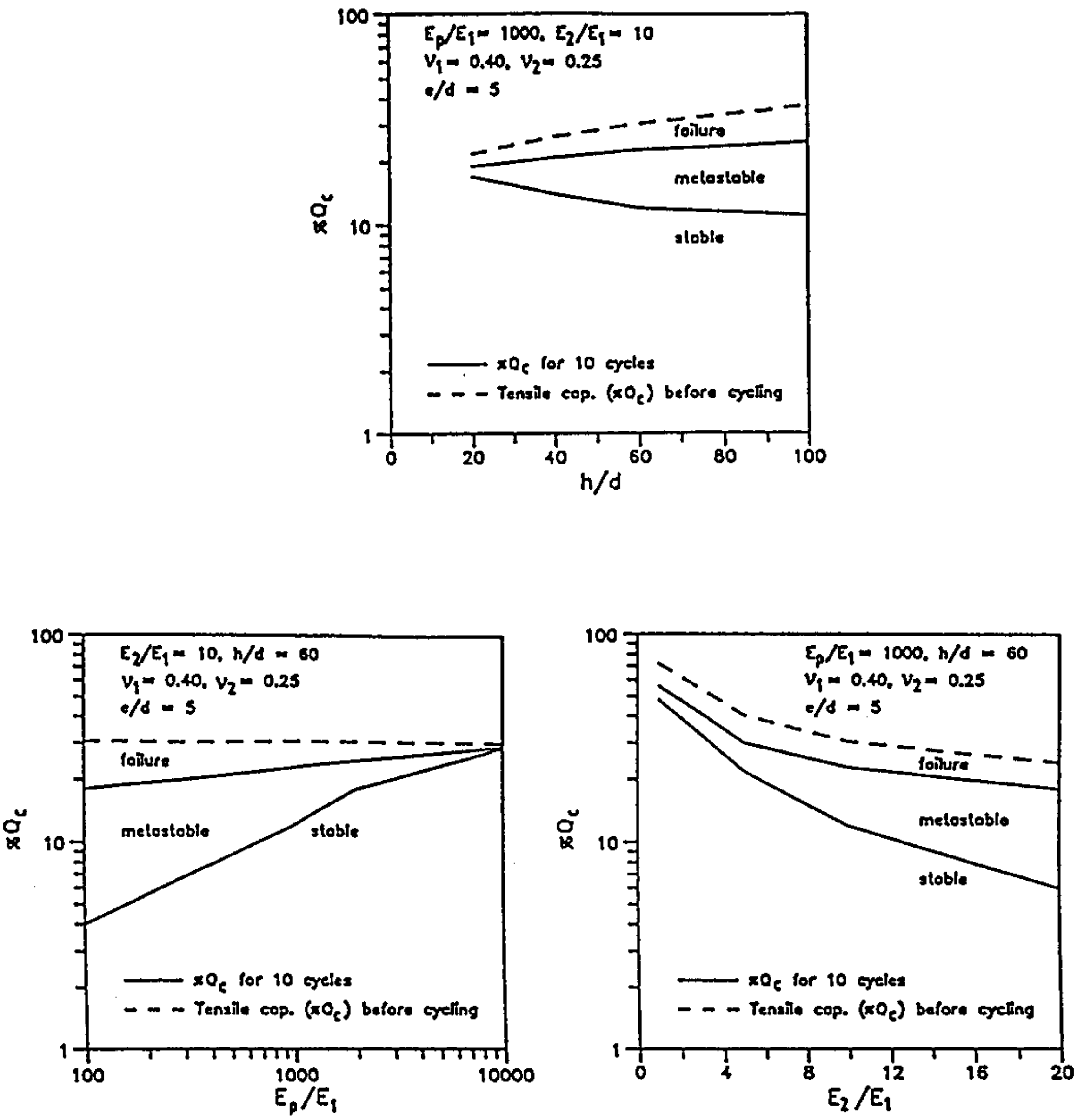

Fig. 5.43 Cyclic response of a socketed pile: Influence of (a) h/d; (b) E_p/E_1; (c) E_2/E_1

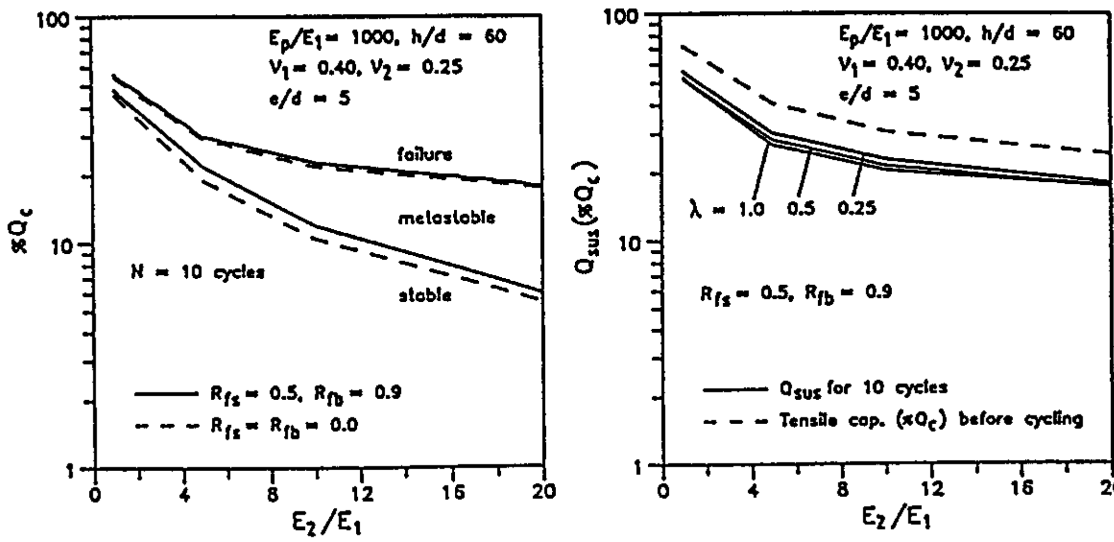

Fig. 5.44 Cyclic response of a socketed pile: Influence of (a) hyperbolic constants for different E_2/E_1 ratios; (b) degradation rate parameter λ on Q_{sus} for different E_2/E_1 ratios

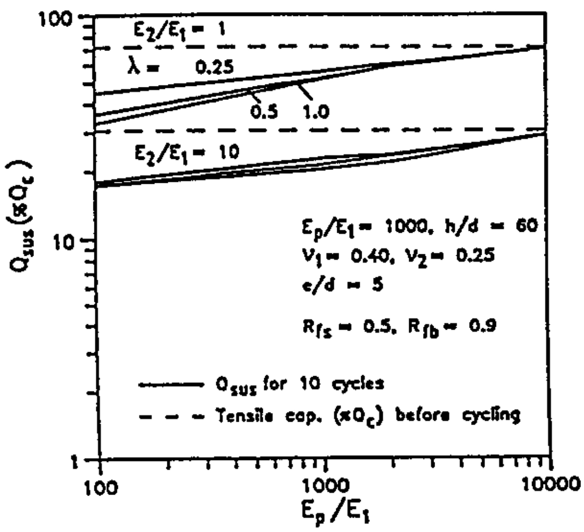

Fig. 5.45 Influence of degradation rate parameter λ on Q_{sus} of a socketed pile for different E_p/E_1 ratios

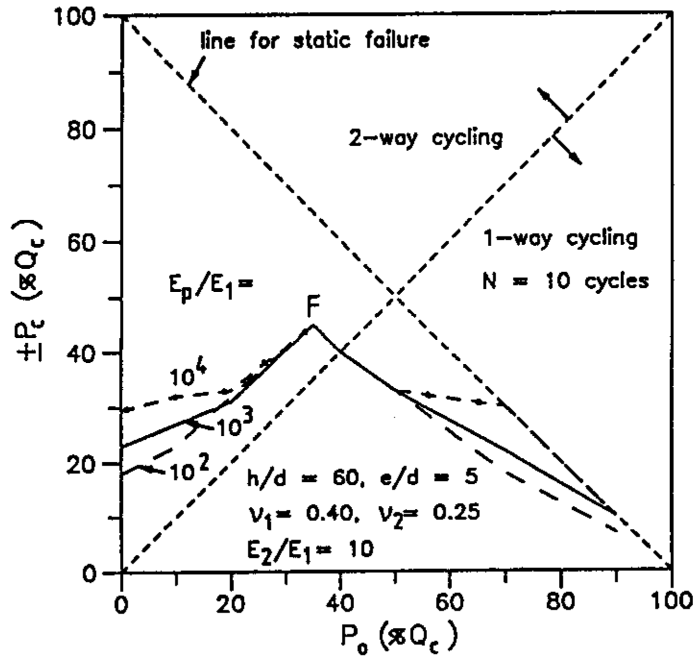

(a)

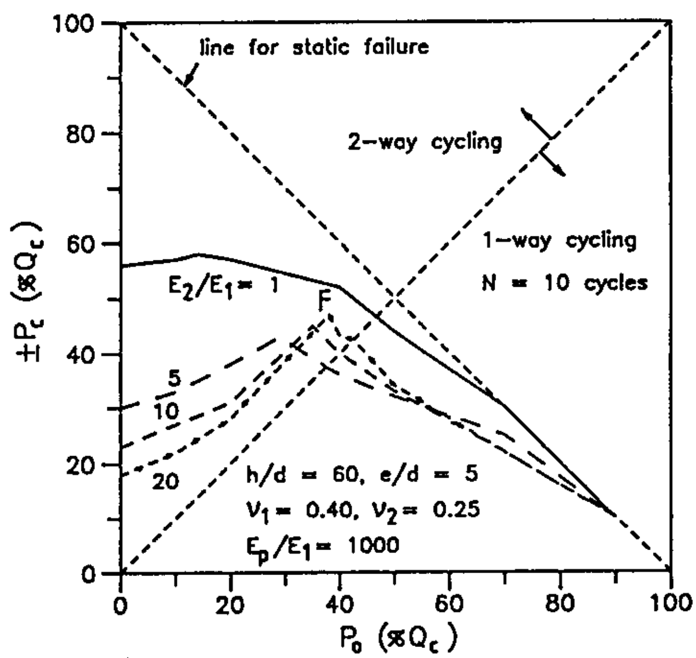

(b)

Fig. 5.46 Cyclic stability diagrams for a socketed pile: Influence of (a) E_p/E_1 ratio; (b) E_2/E_1 ratio
(lines shown are upper limits of metastable zone)

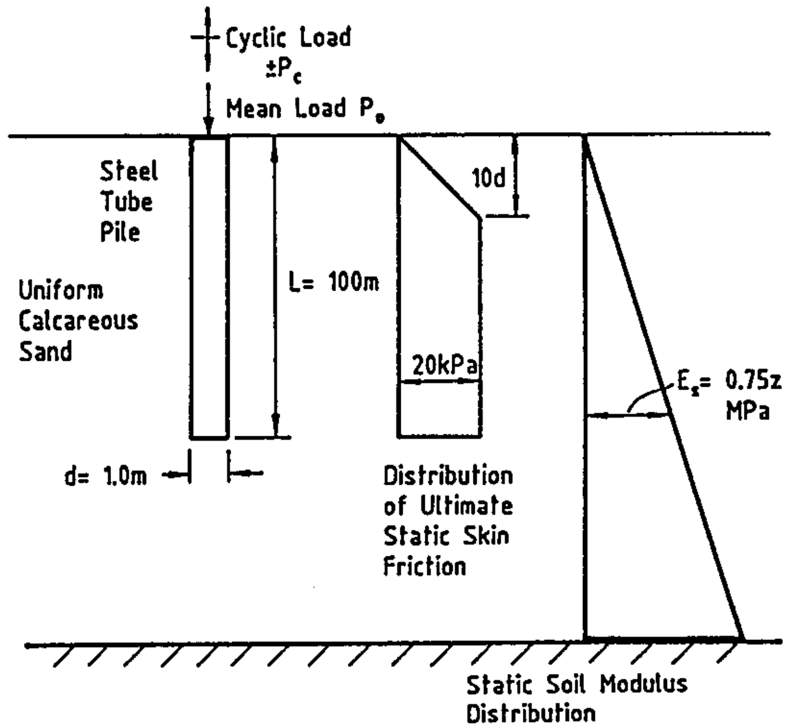

Fig. 5.47(a) Hypothetical driven pile in Gibson soil (after Poulos, 1989a)

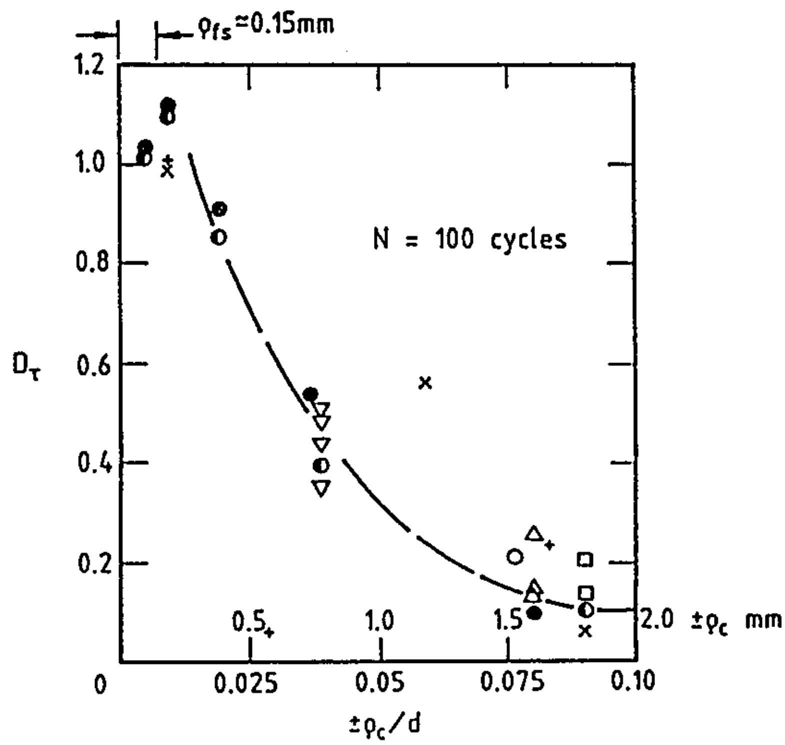

Fig. 5.47(b) Skin friction degradation factors - model jacked piles in calcareous sand from Bass Strait (after Poulos, 1989a)

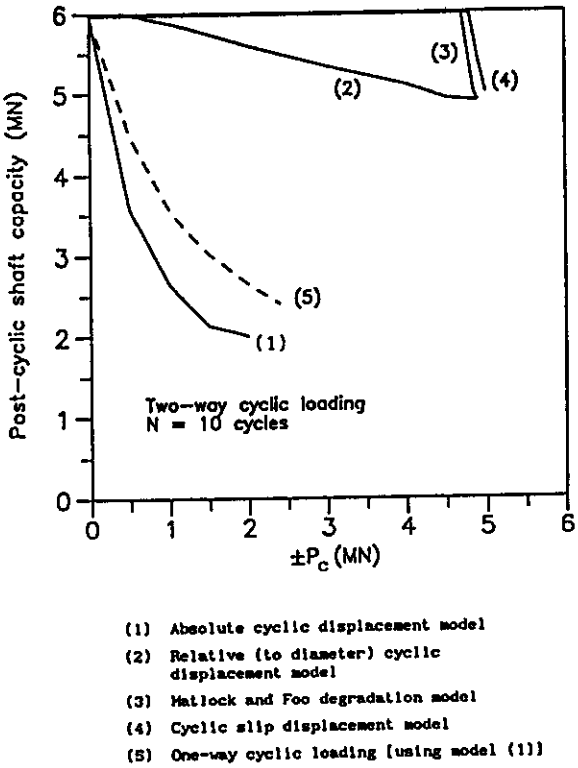

Fig. 5.48(a) Computed post-cyclic shaft capacity using different capacity degradation models

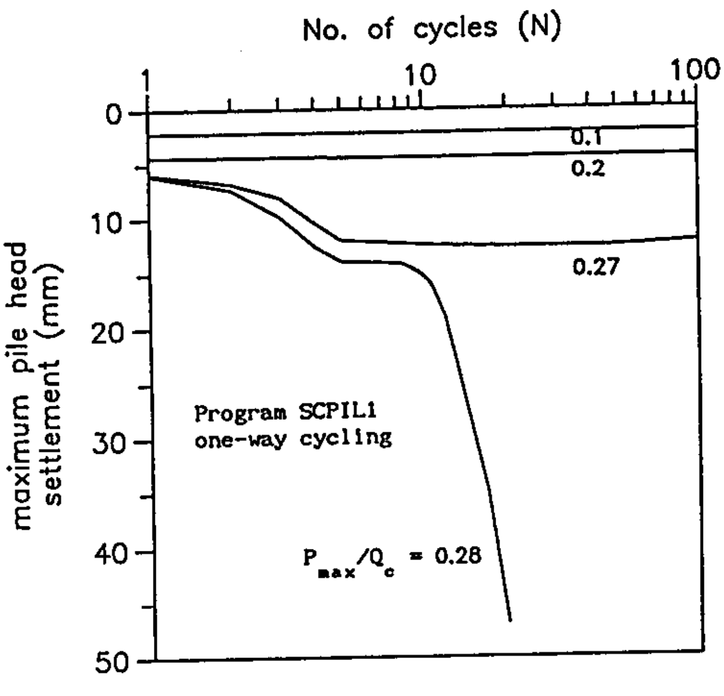

Fig. 5.48(b) Computed pile displacements for different P_{max}/Q_c values with increasing cycles

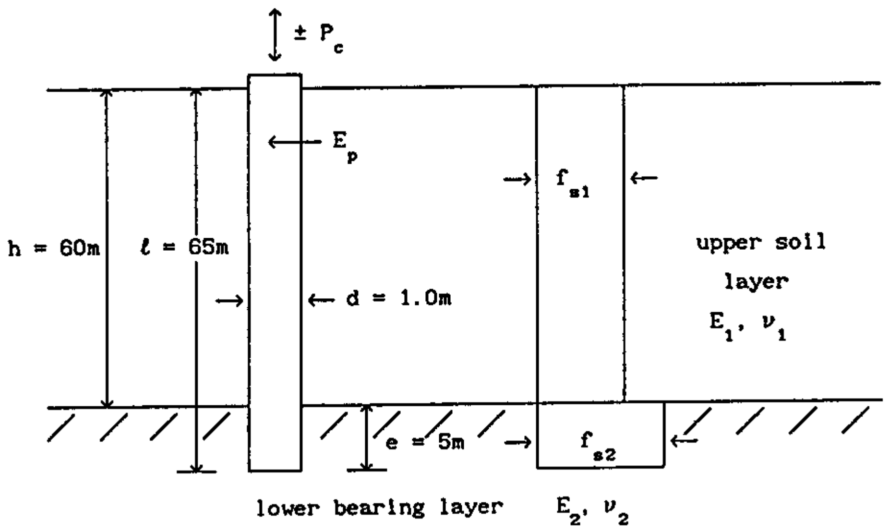

E_p = 25000 MPa (unless otherwise specified)

Soil parameters :

f_{s1} = 40 kN/m^2] [upper end of values for weakly and
f_{s2} = 100 kN/m^2] strongly cemented soil (for driven piles) - Poulos (1988a)]

E_1 = 100 MPa] [lower and upper end of values for weakly
E_2 = 250 MPa] and strongly cemented soils respectively (for driven piles) - Poulos (1988a)]

q_p = $100f_2$ = 10 MPa; use 9 MPa [extreme end for strongly cemented calcareous soils - Poulos (1988a)]

$\nu_1 = \nu_2 = 0.50$

For cyclic loading analysis :

The following have been adopted unless otherwise specified

N = 10 cycles

No degradation of pile capacity assumed

No base resistance in tension assumed

Permanent displacement parameters (program SCPIL1) :

$m_s = 0.06$, $n_s = 3.0$ — lower end of values for drilled and grouted piles (Poulos, 1988a)

$m_b = 0.05$, $n_b = 3.0$ — lower end for driven piles (Poulos, 1988a)

representative stress level $X = (\tau_o + 0.5\tau_c)/\tau_f$

Fig. 5.49 Hypothetical pile in two-layered soil profile utilised for permanent displacement accumulation analysis

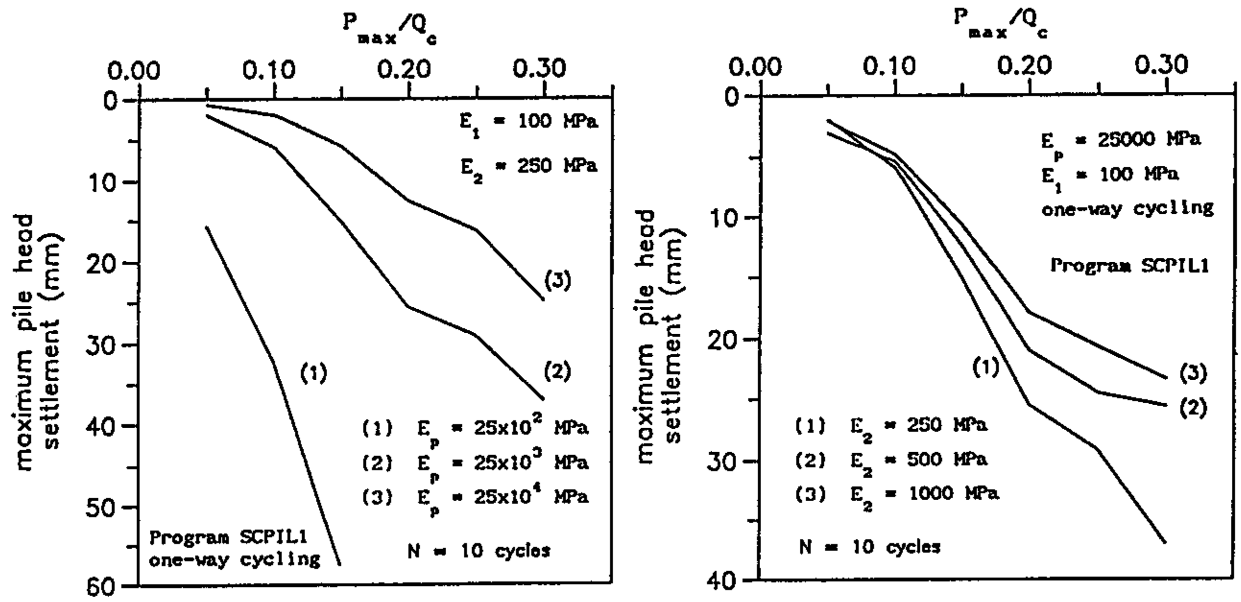

Fig. 5.50 Influence of (a) E_p/E_1 ratio and (b) E_2/E_1 ratio on maximum pile displacement (program SCPIL1)

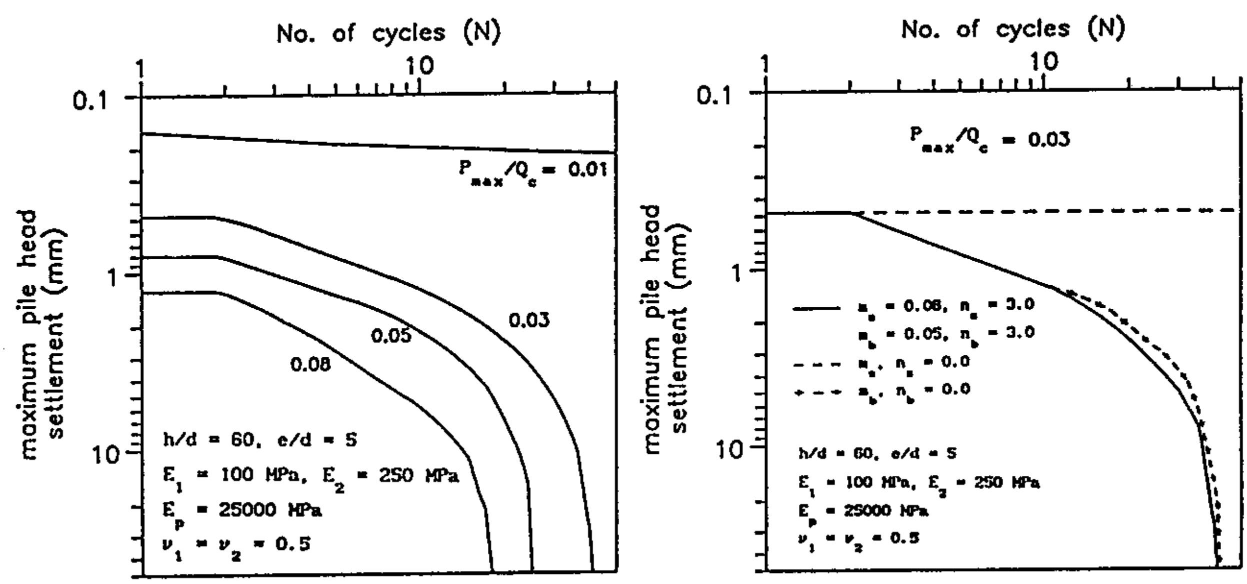

Fig. 5.51 Maximum pile displacement computed using program SCPIL1: Influence of (a) P_{max}/Q_c values; (b) accumulation parameters m_s, n_s and m_b, n_b

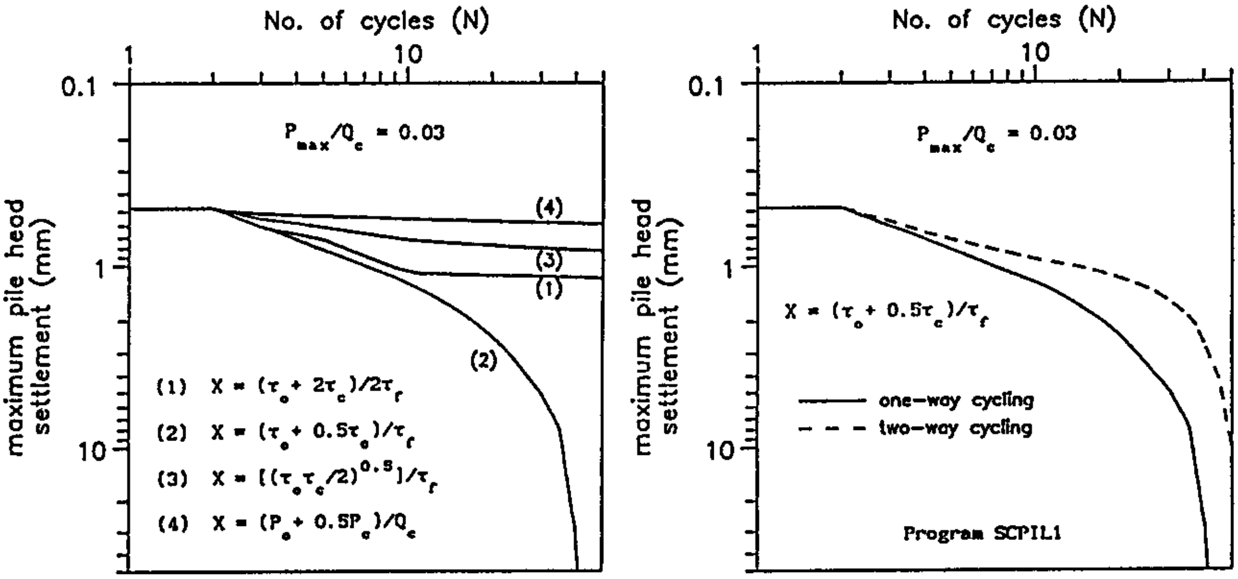

Fig. 5.52 Maximum pile displacement computed using program SCPIL1: Influence of (a) adopted stress level X; (b) type of loading

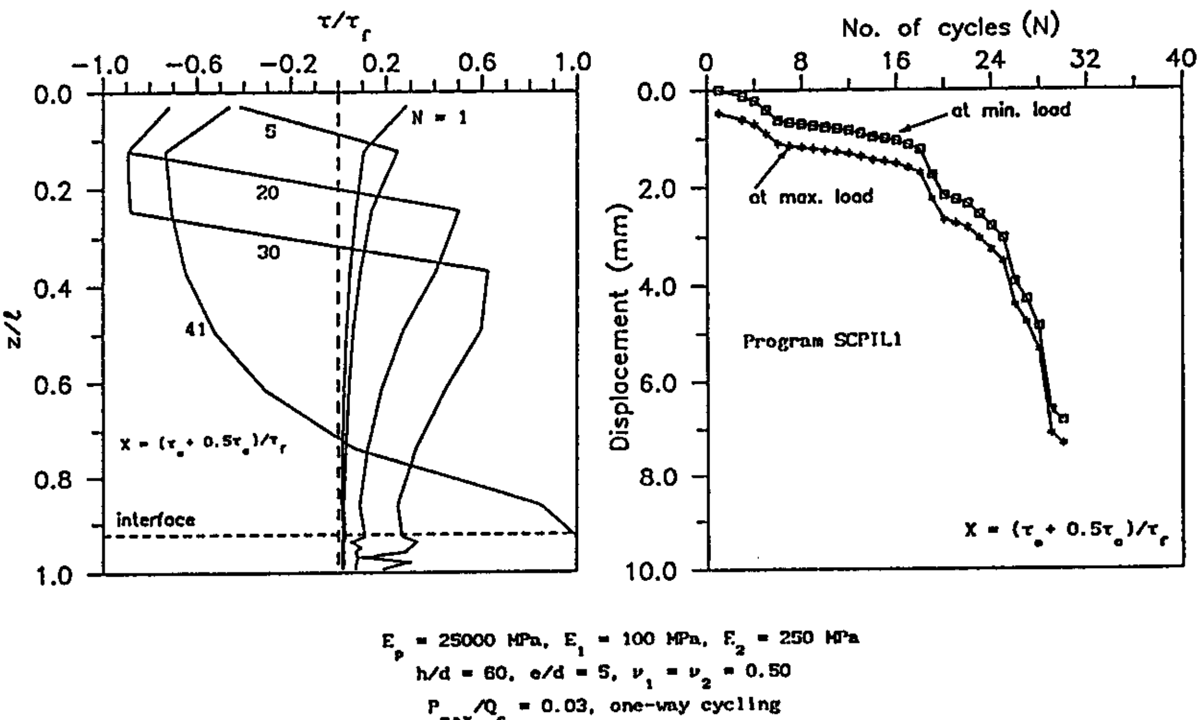

Fig. 5.53 (a) Shear stress distributions along pile at maximum load end; (b) pile head displacement at minimum and maximum load ends

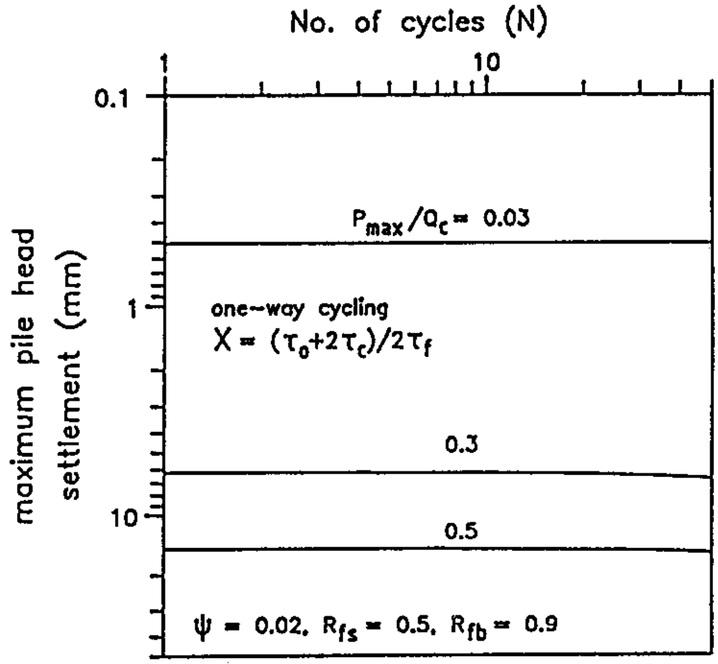

Fig. 5.54(a) Influence of P_{max}/Q_c values on maximum pile displacement (program SCPIL3)

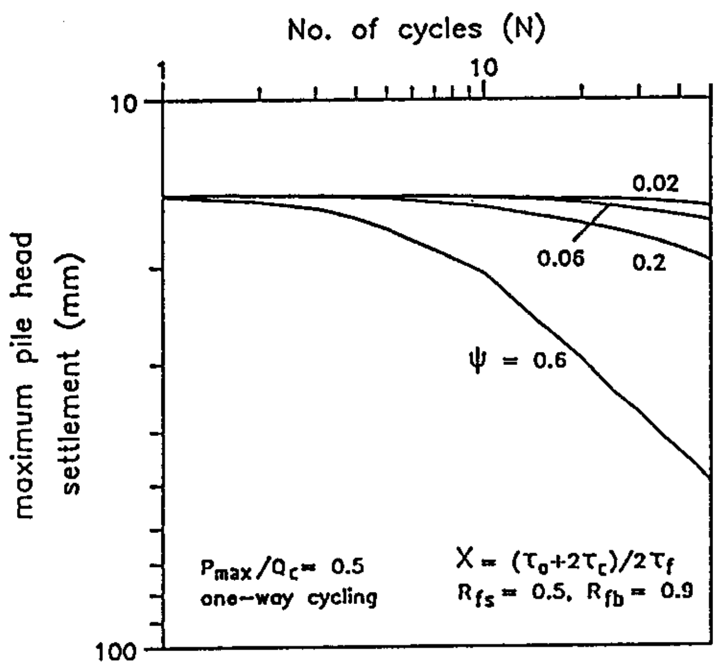

Fig. 5.54(b) Influence of accumulation rate parameter ψ on maximum pile displacement (program SCPIL3)

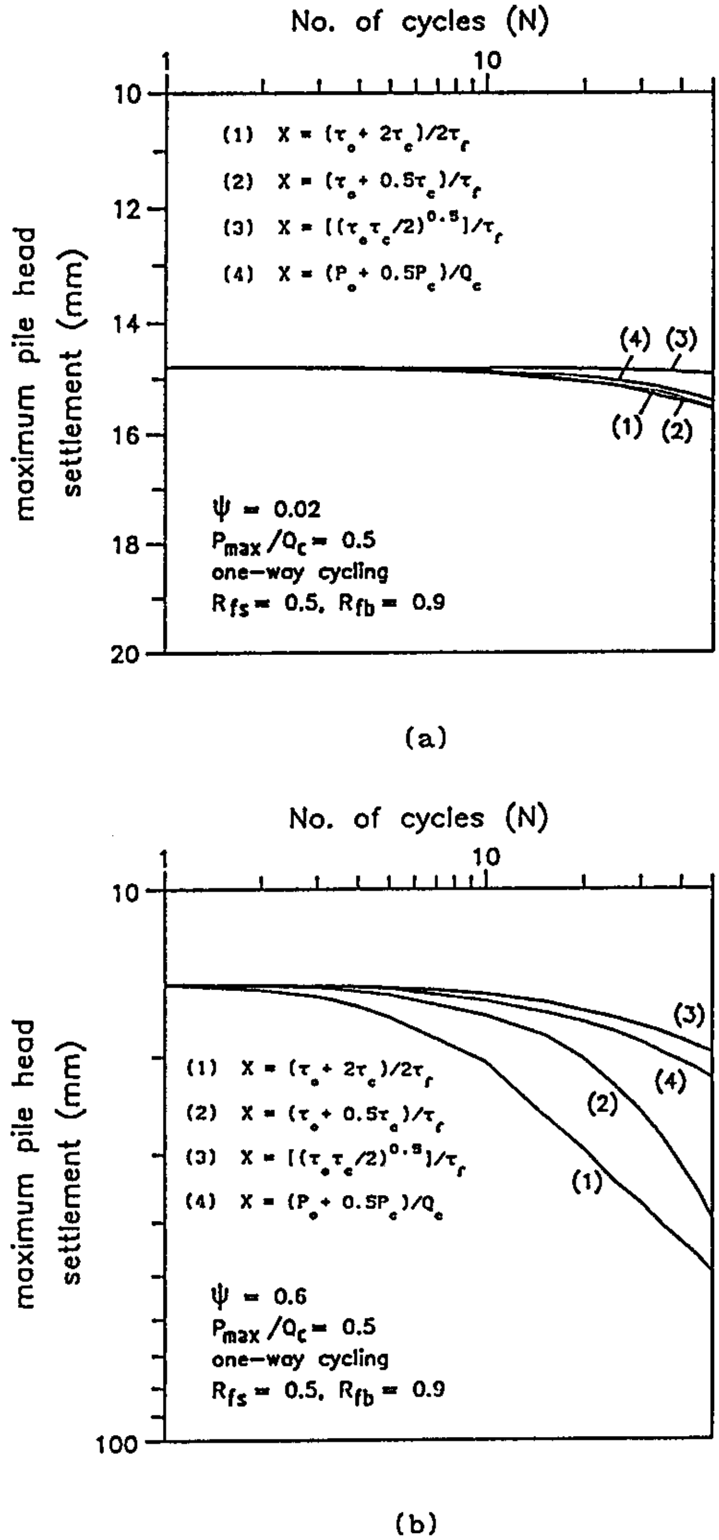

Fig. 5.55 Influence of adopted stress level X on maximum pile displacement (program SCPIL3): (a) $\psi = 0.02$; (b) $\psi = 0.6$

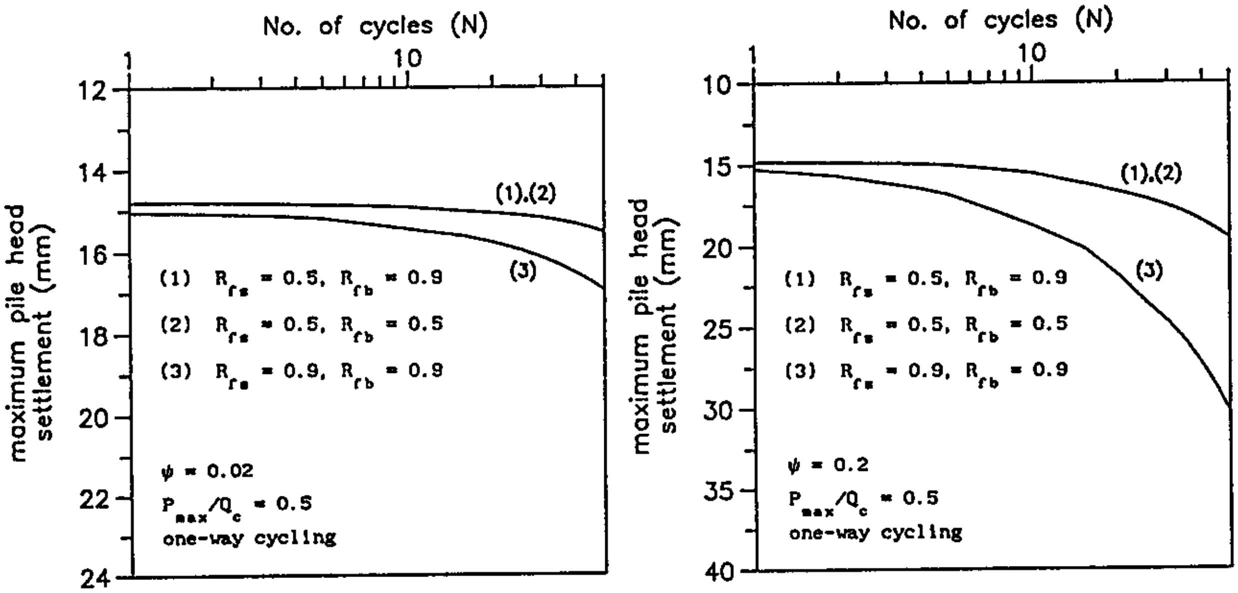

Fig. 5.56 Influence of hyperbolic constants R_{fs} and R_{fb} on the maximum pile displacement (program SCPIL3): (a) ψ = 0.02; (b) ψ = 0.2

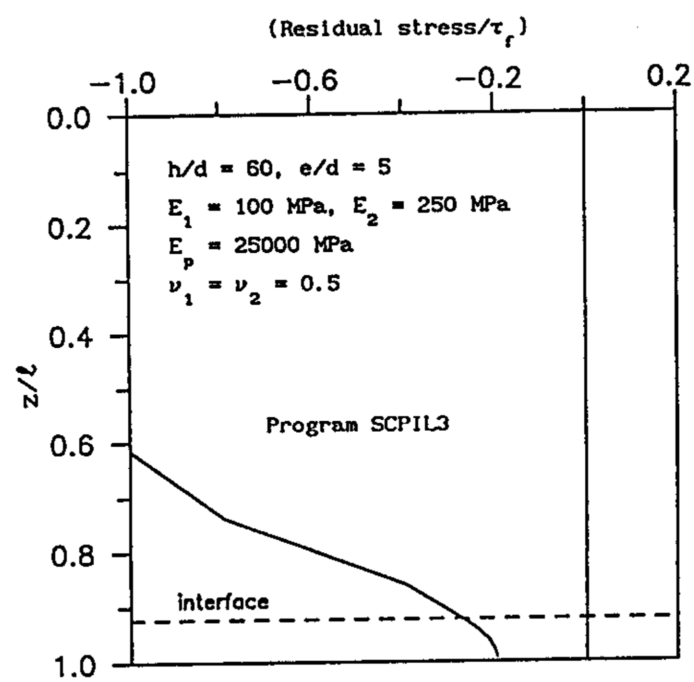

Fig. 5.57 Computed residual stress distribution for hypothetical pile in two-layered soil profile

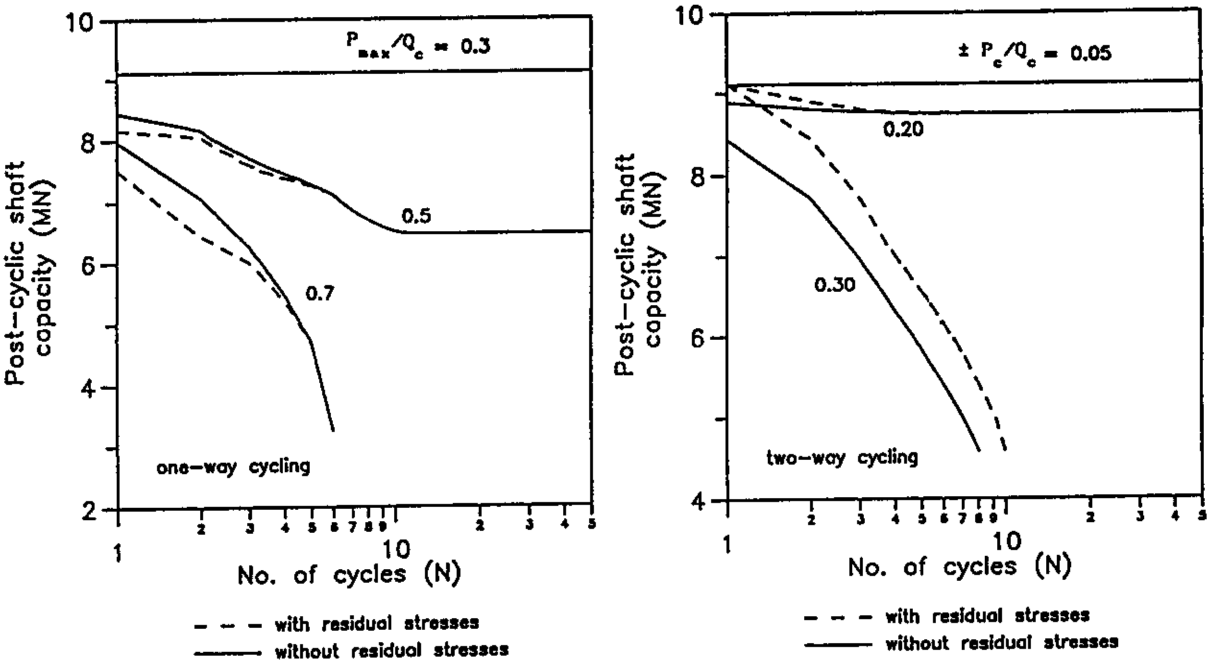

Fig. 5.58 Influence of residual stresses on post-cyclic shaft capacity computed using program SCPIL3: (a) one-way cyclic loading; (b) two-way cyclic loading

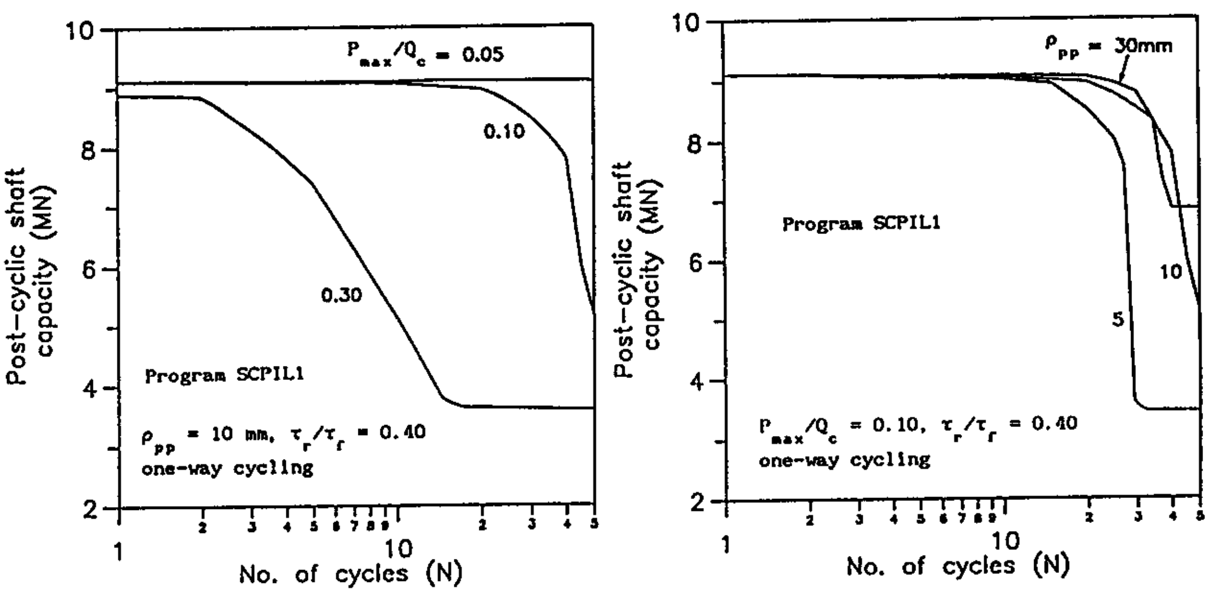

Fig. 5.59 Post-cyclic shaft capacity with "strain-softening" response (Program SCPIL1): Influence of (a) P_{max}/Q_c values; (b) ρ_{pp} values

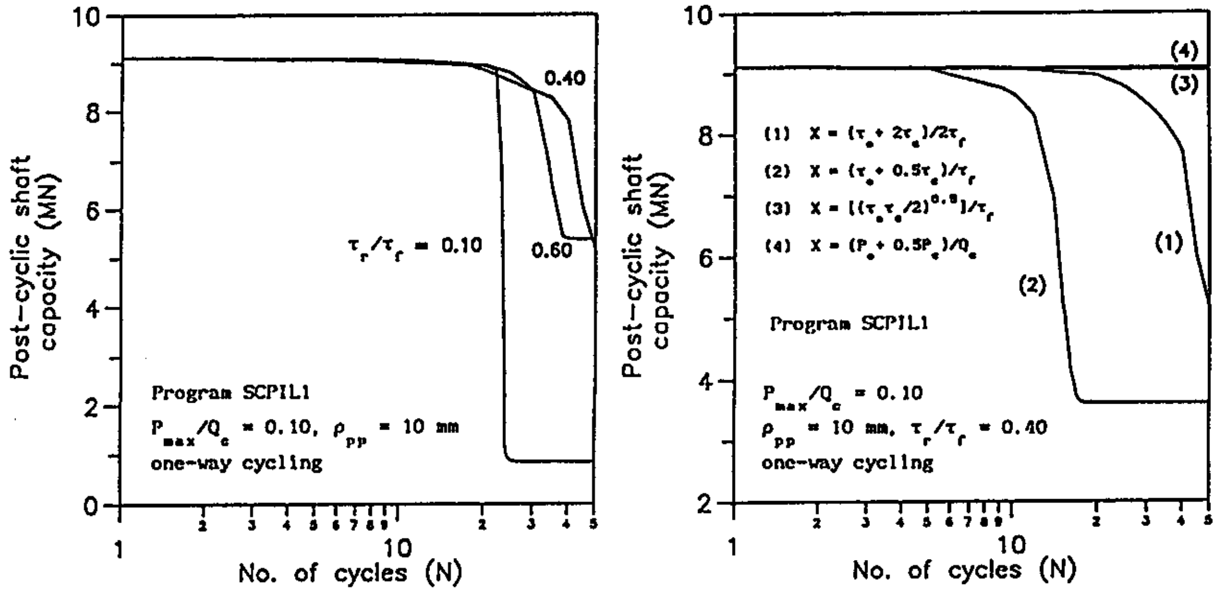

Fig. 5.60 Post-cyclic shaft capacity (Program SCPIL1): Influence of (a) "strain-softening" pile-soil response; (b) stress level X with "strain-softening" pile-soil response

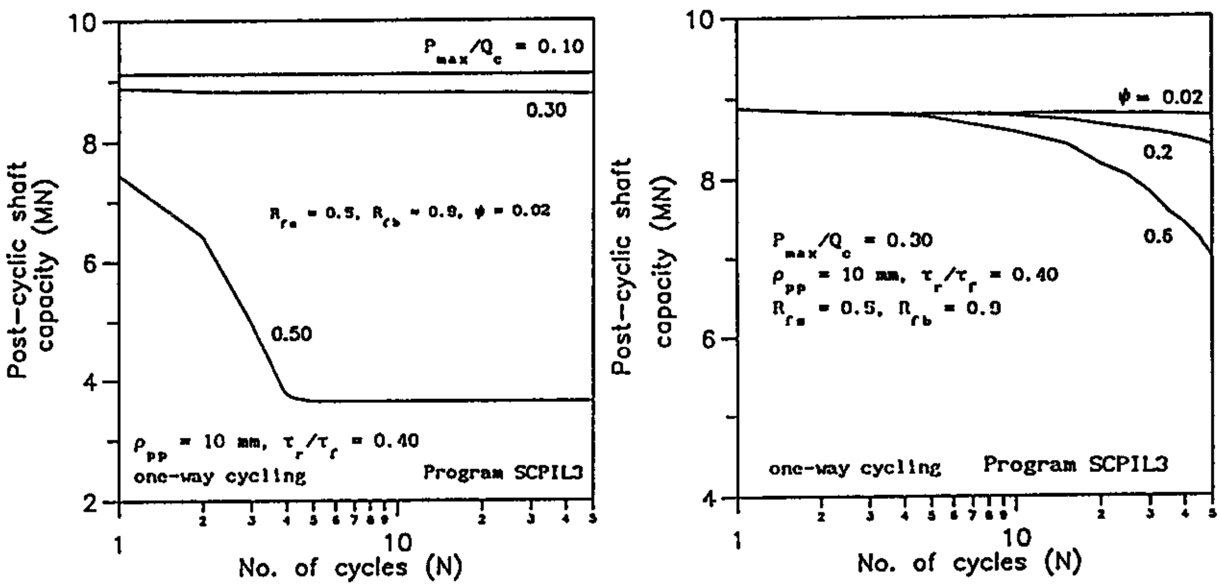

Fig. 5.61 Post-cyclic shaft capacity with "strain-softening" response (Program SCPIL3): Influence of (a) P_{max}/Q_c values; (b) accumulation rate parameter ψ

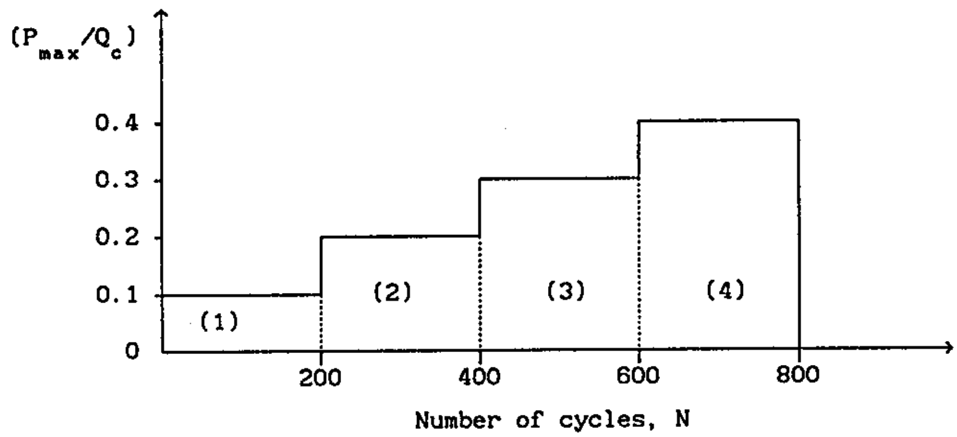

Load sequence (a) : (1)→ (2)→ (3)→ (4)

(b) : (1)→ (3)→ (2)→ (4)

(c) : (3)→ (2)→ (1)→ (4)

<u>program SCPIL1</u>

$m_s = m_b = 0.055$

$n_s = n_b = 3.0$

<u>program SCPIL3</u>

$R_{fs} = 0.5$

$R_{fb} = 0.9$

Fig. 5.62 Loading parcels utilised for "storm-loading" analysis

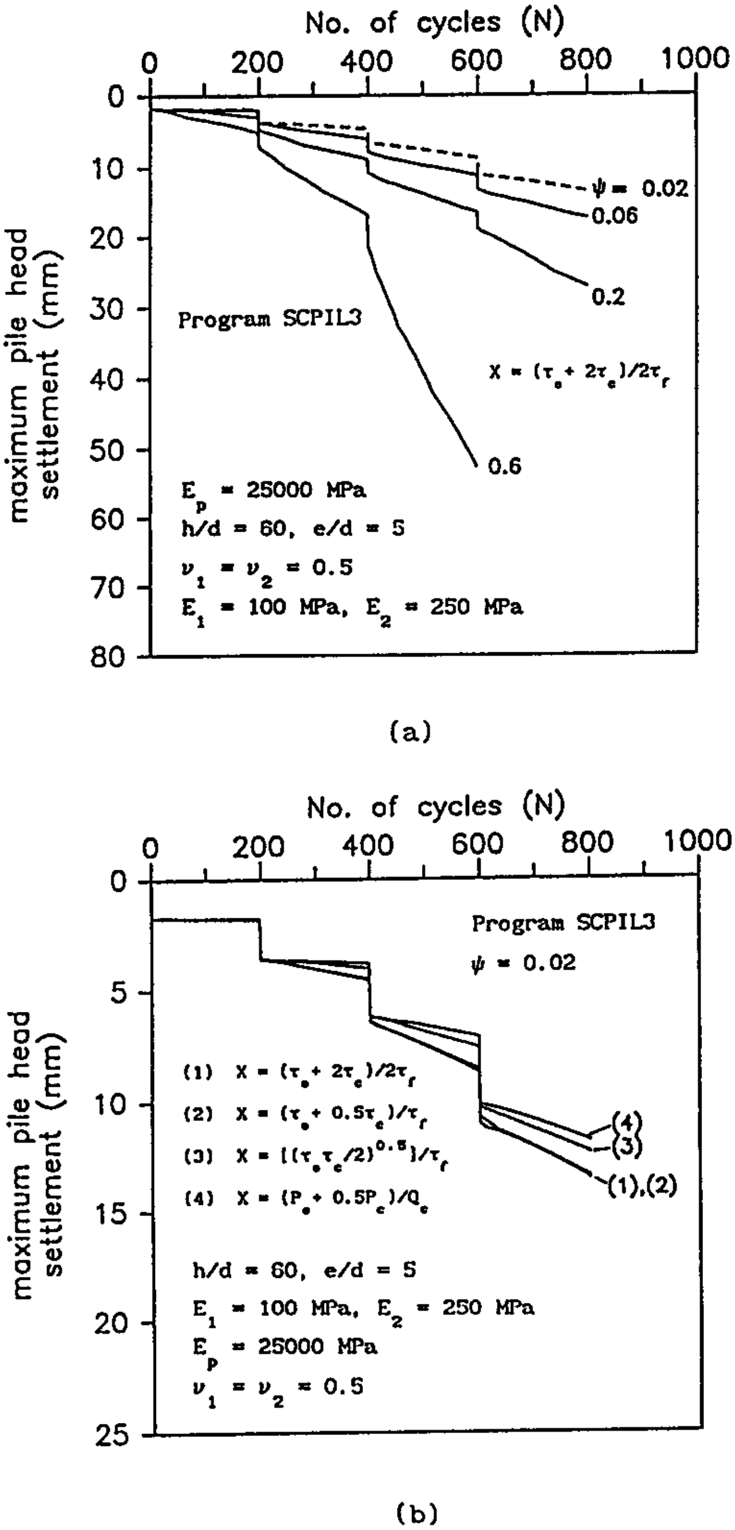

Fig. 5.63 Maximum pile displacement under "storm-loading" using program SCPIL3: (a) influence of accumulation rate parameter ψ; (b) influence of stress level X

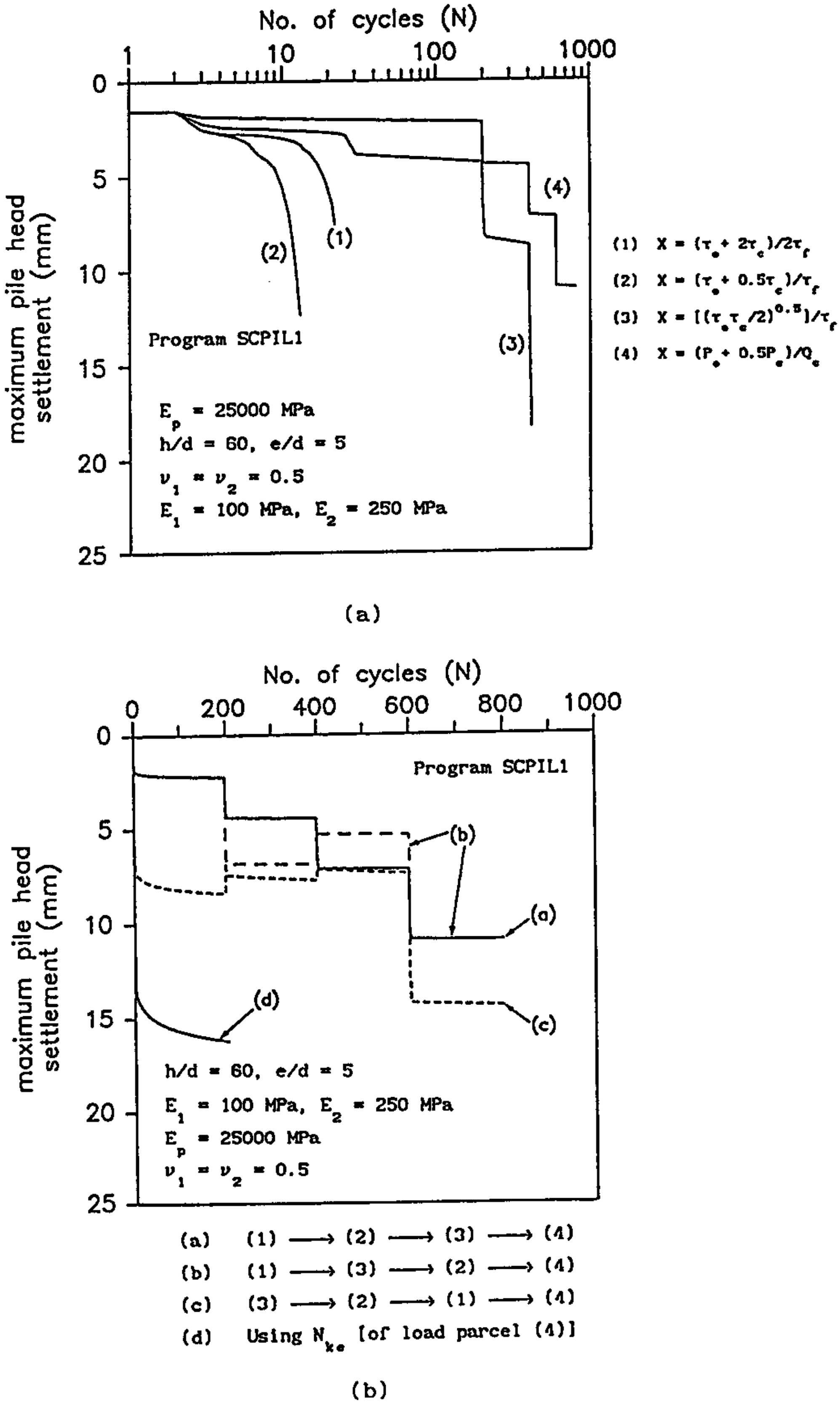

Fig. 5.64 Maximum pile displacement under "storm loading" (Program SCPIL1): Influence of (a) stress level X; (b) order of loading parcels

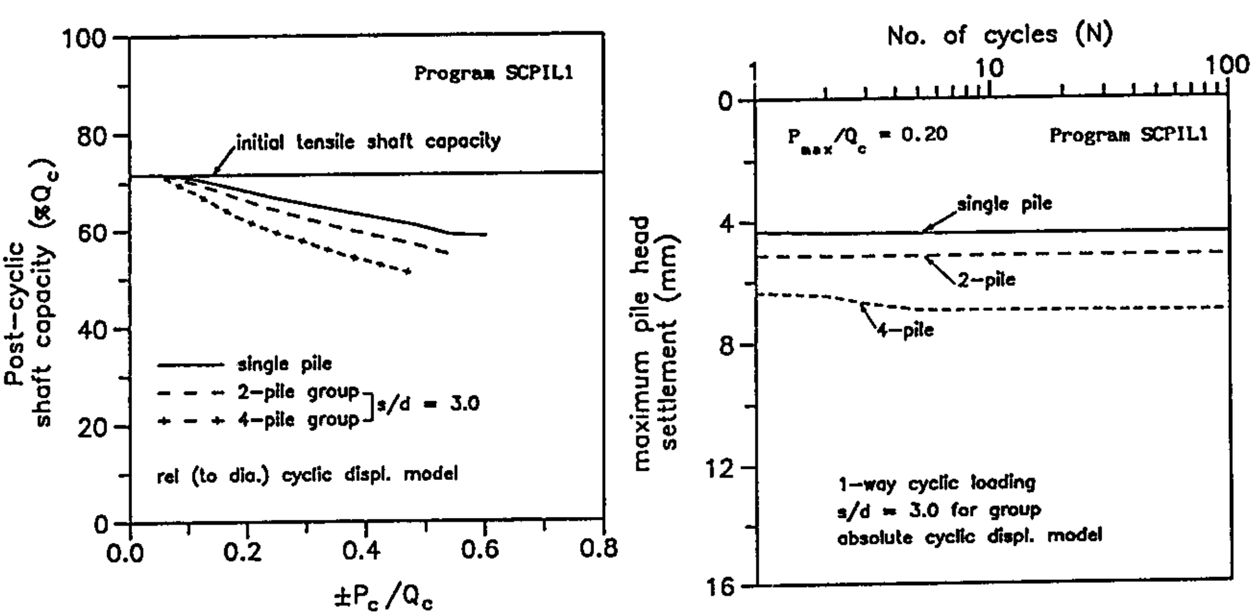

Fig. 5.65 (a) Influence of cyclic load level on post-cyclic shaft capacity for pile groups; (b) Influence of group effect on maximum pile head settlement

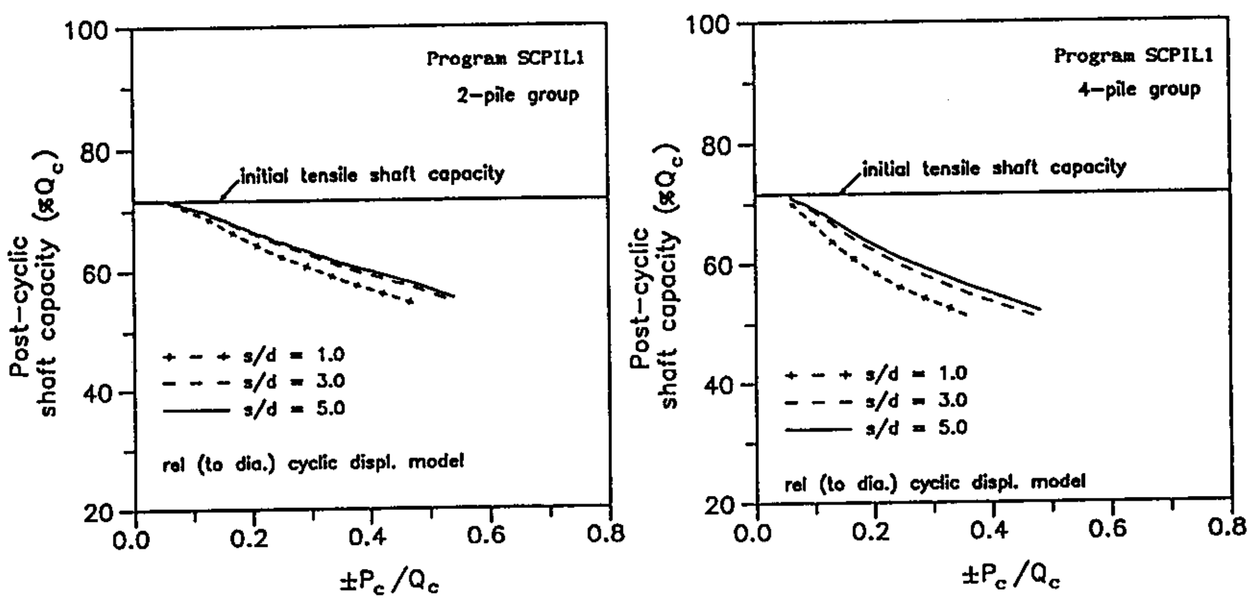

Fig. 5.66 Influence of pile spacing s/d on post-cyclic shaft capacity: (a) 2-pile group; (b) 4-pile group

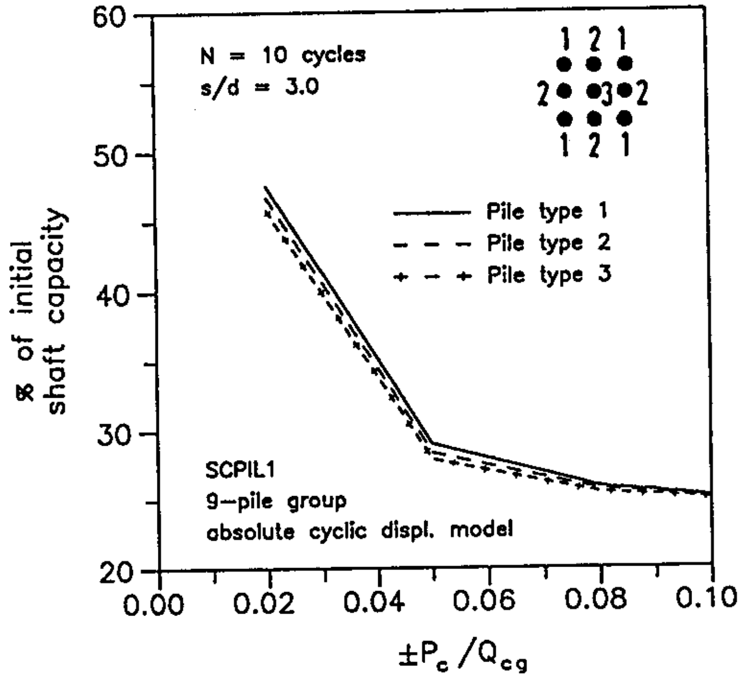

(a)

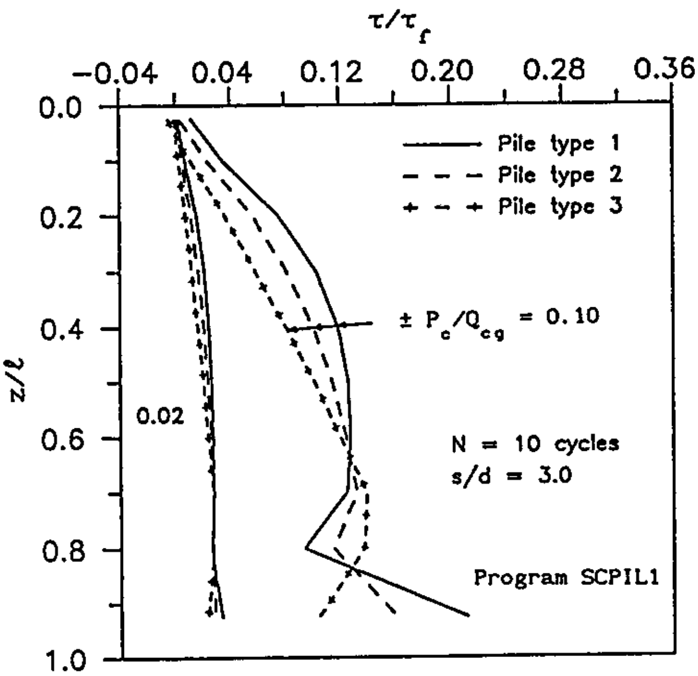

(b)

Fig. 5.67 Solutions for 3x3 pile group: (a) post-cyclic shaft capacities of the group piles; (b) normalised shear stress distributions for the group piles

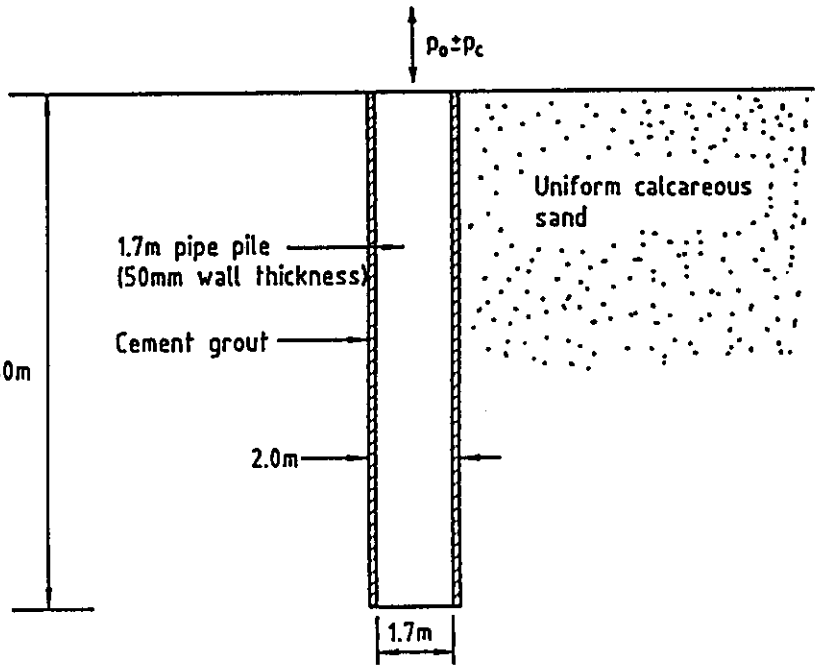

Fig. 5.68 Hypothetical drilled and grouted pile utilised for comparative study of cyclic axial loading analyses

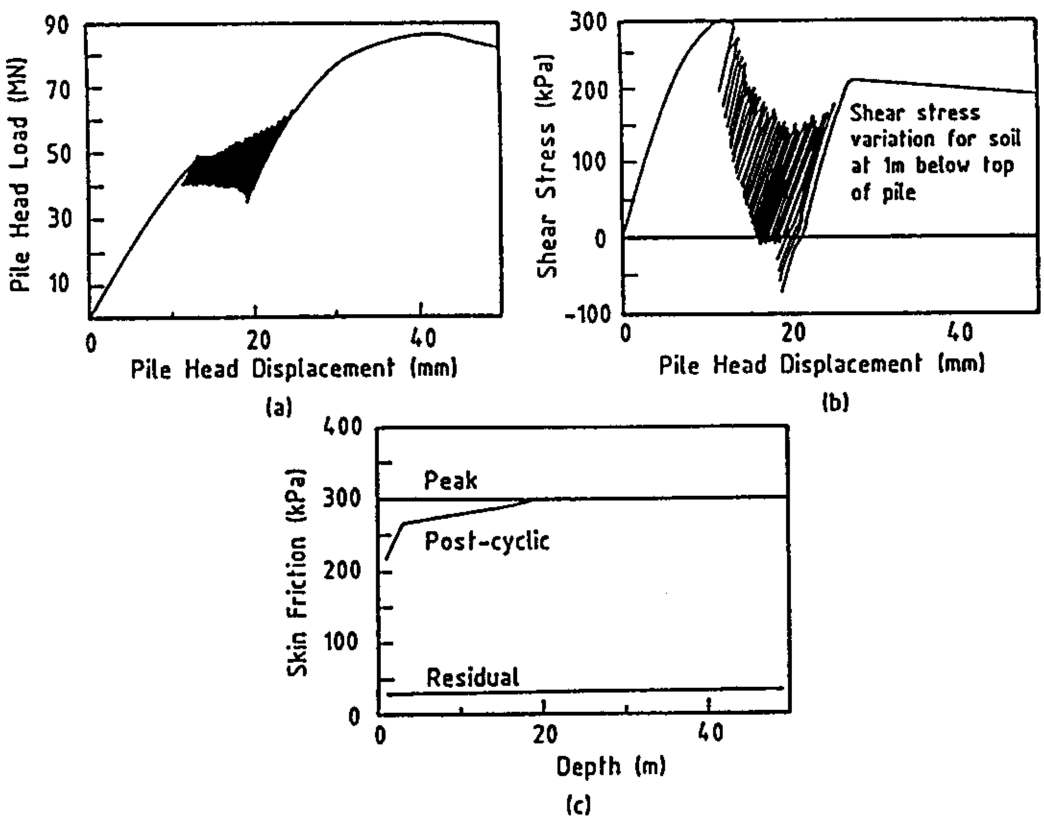

Fig. 5.69 RATZ solutions: (a) load-settlement response; (b) shear stress response; (c) variations of post-cyclic skin friction with depth

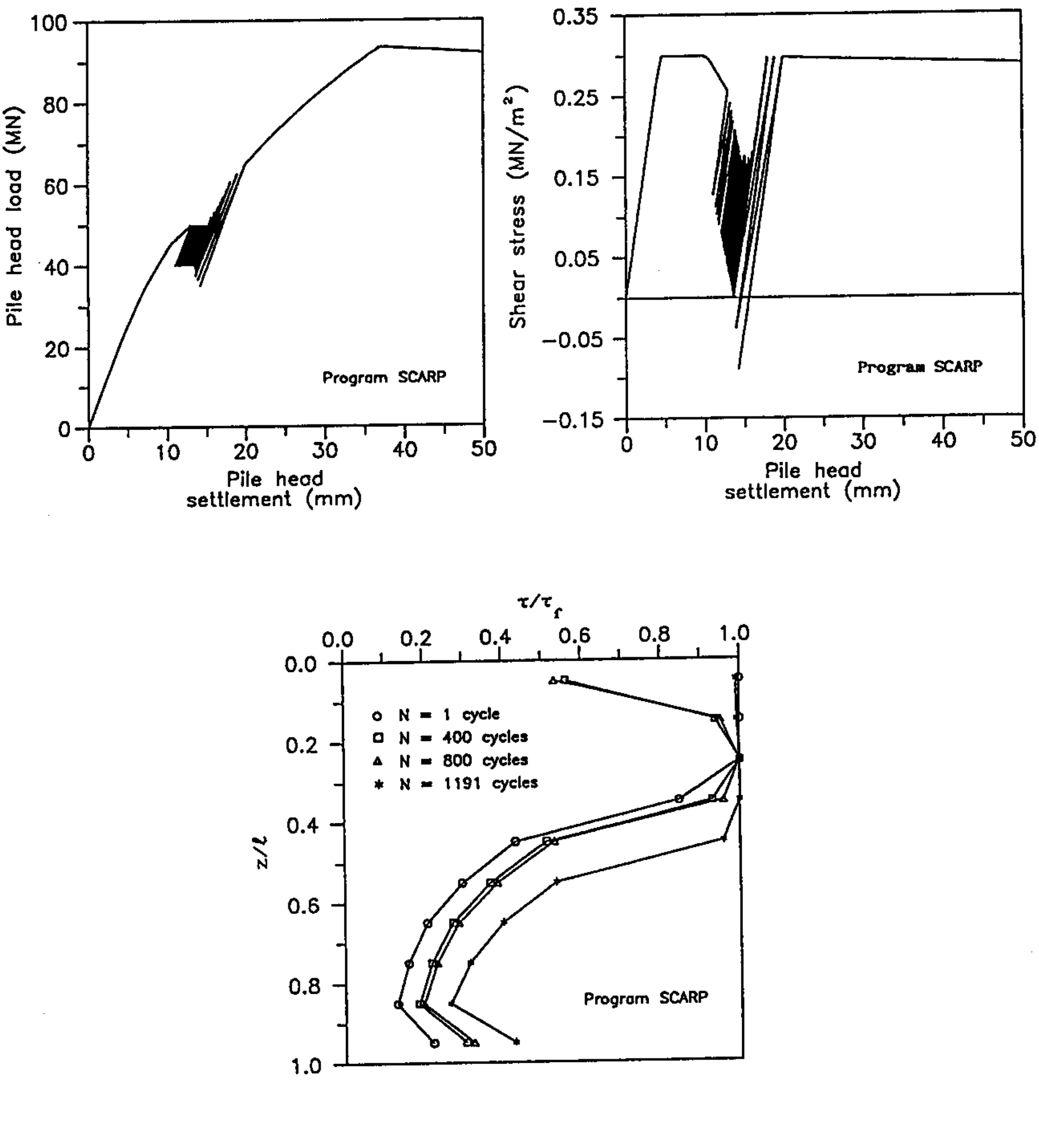

Fig. 5.70 SCARP solutions: (a) load-settlement response; (b) shear stress variation at average depth of 2.5m; (c) shear stress distributions along pile with increasing cycles

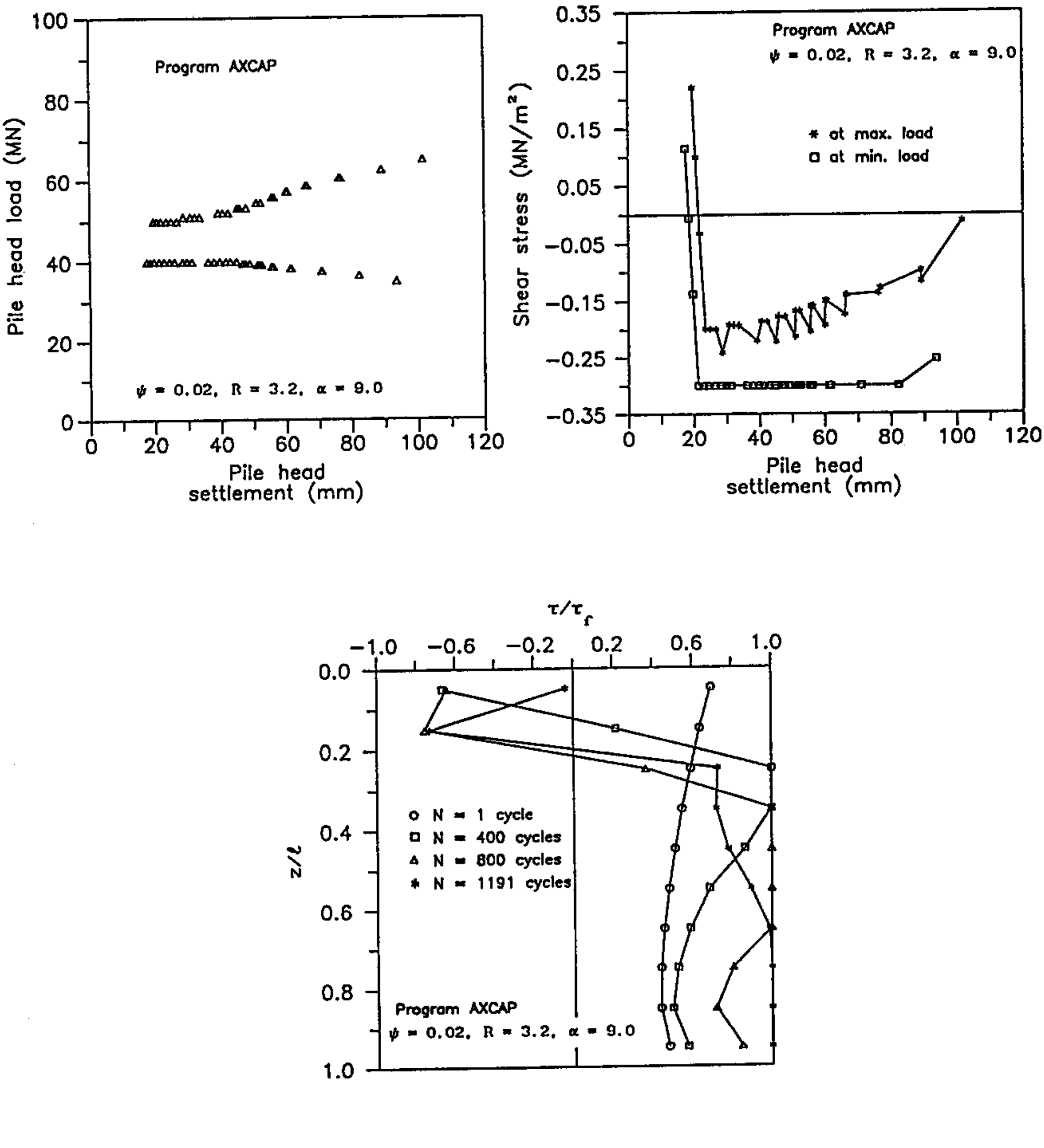

Fig. 5.71 AXCAP solutions: (a) load-settlement response; (b) shear stress variation at average depth of 2.5m; (c) shear stress distributions along pile with increasing cycles

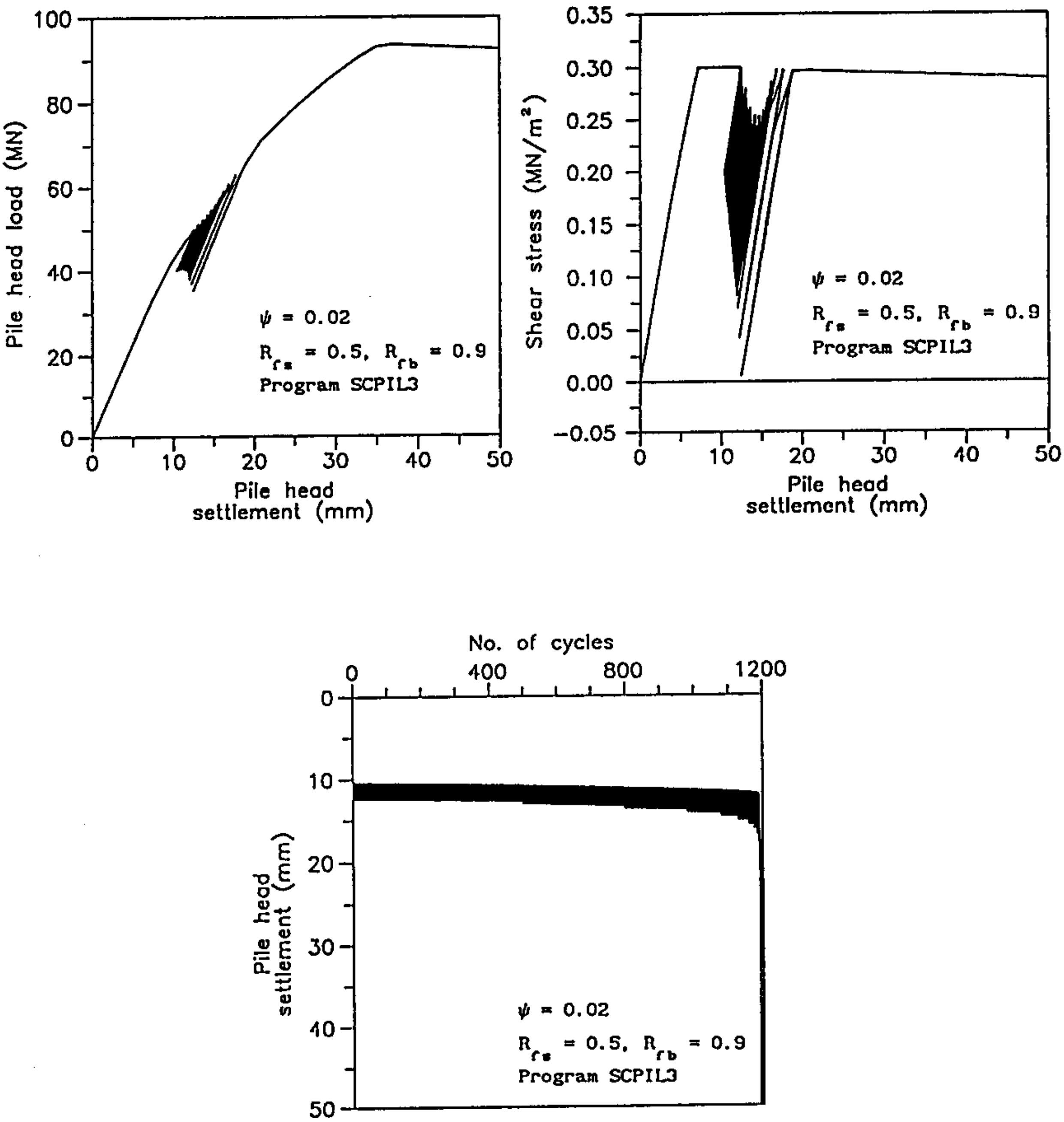

Fig. 5.72 SCPIL3 solutions with $\psi = 0.02$: (a) load-settlement response; (b) shear stress variation at average depth of 1.25m; (c) pile head settlement with increasing cycles

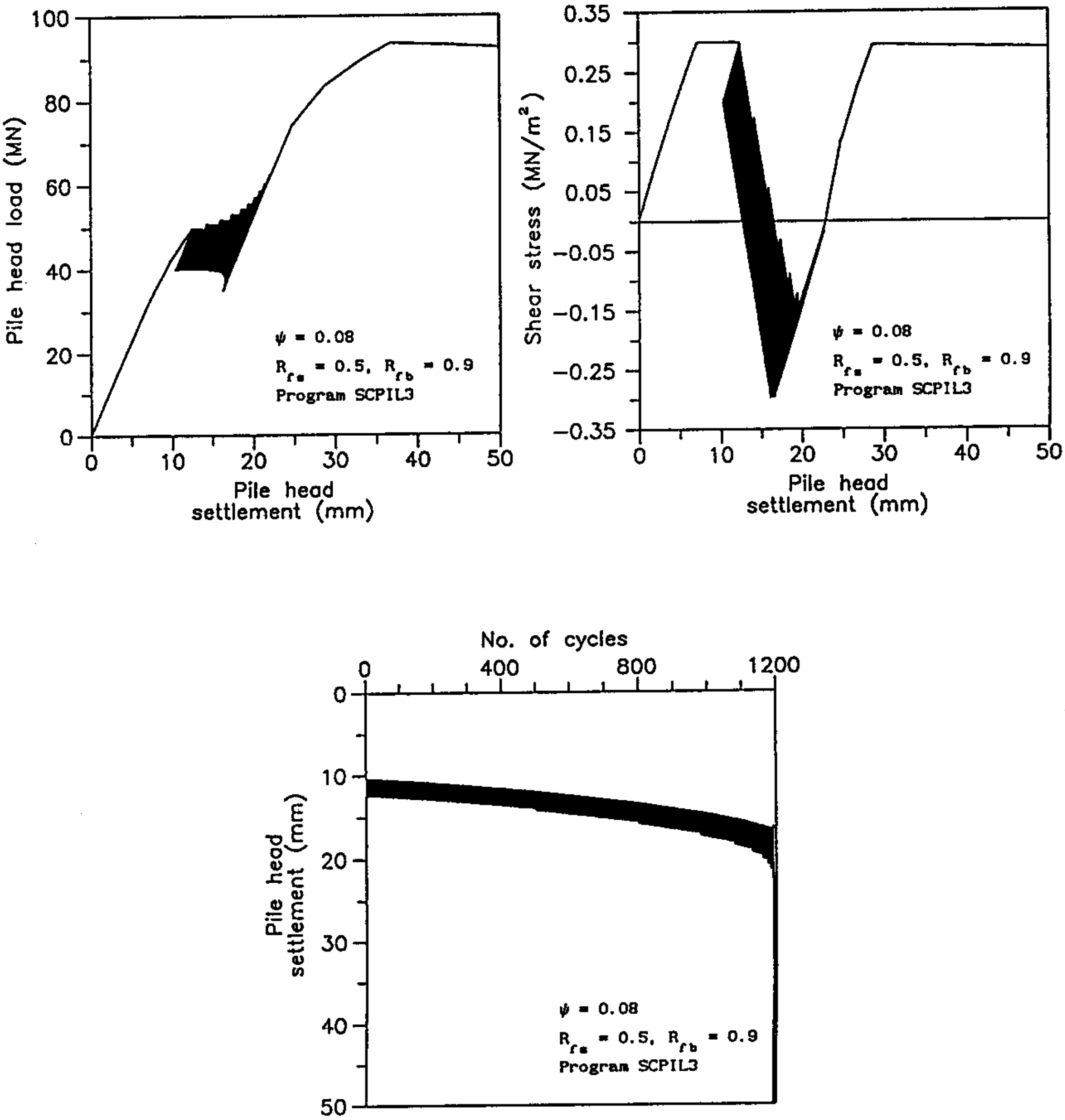

Fig. 5.73 SCPIL3 solutions with ψ = 0.08: (a) load-settlement response; (b) shear stress variation at average depth of 1.25m; (c) pile head settlement with increasing cycles

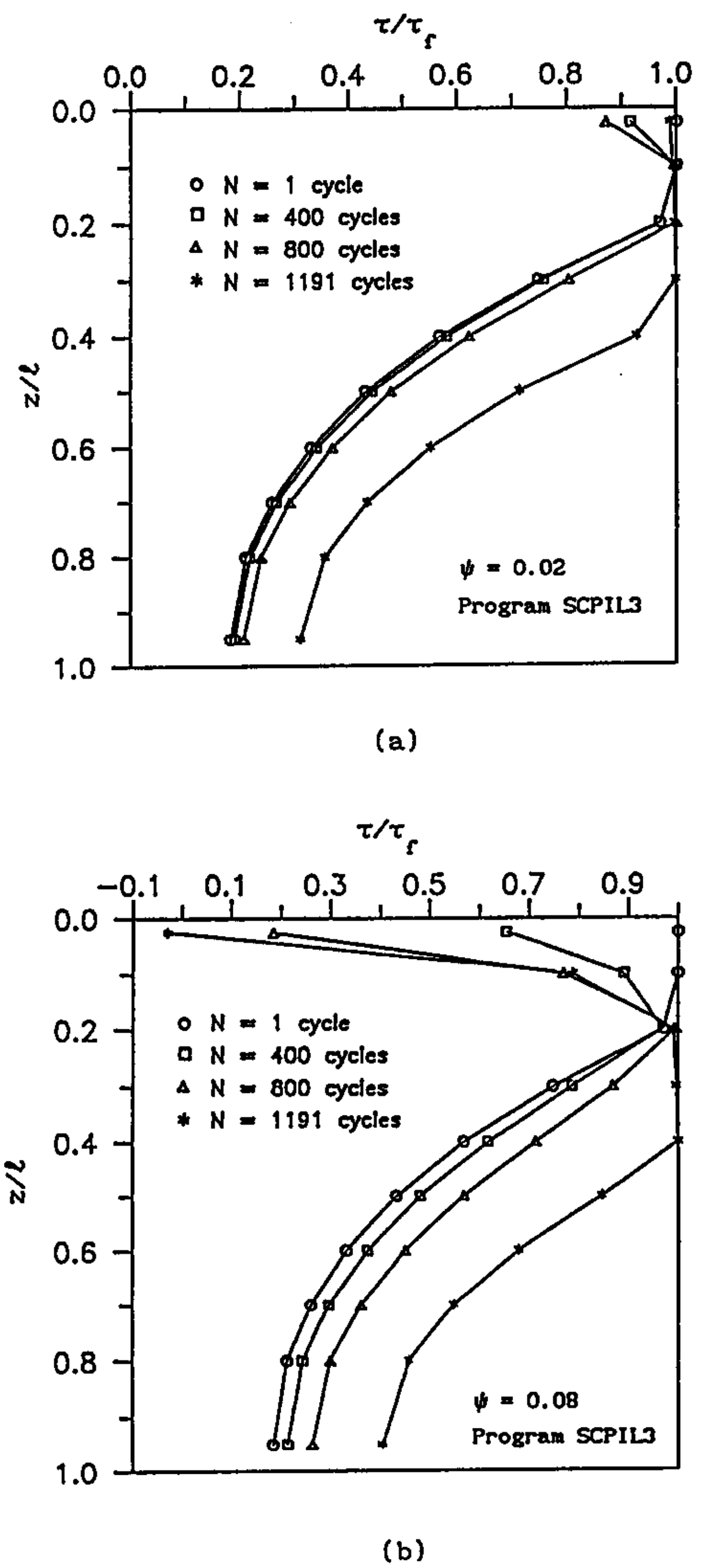

Fig. 5.74 SCPIL3 solutions: (a) shear stress distributions along pile for $\psi = 0.02$; (b) shear stress distributions for $\psi = 0.08$

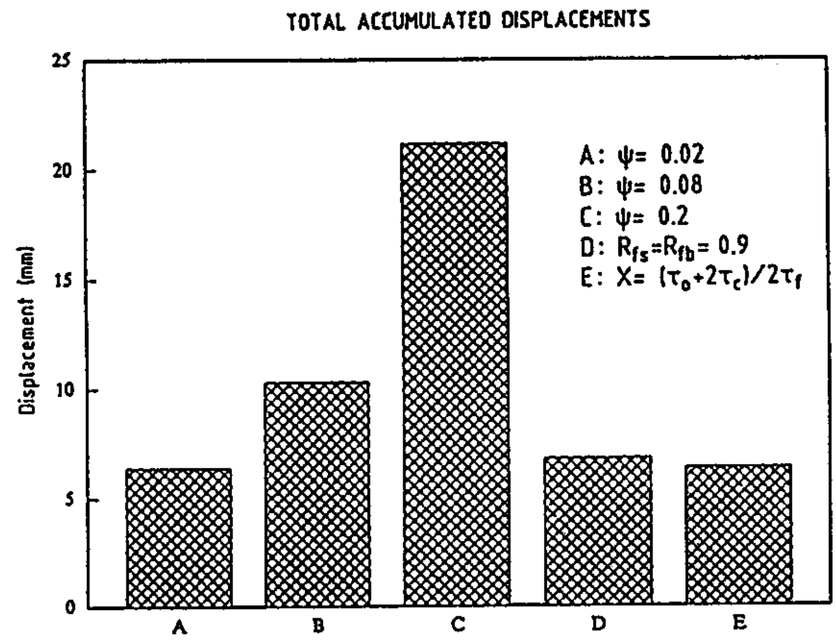

Fig. 5.75(a) SCPIL3 solutions: effect of parameter variation on computed total accumulated displacement

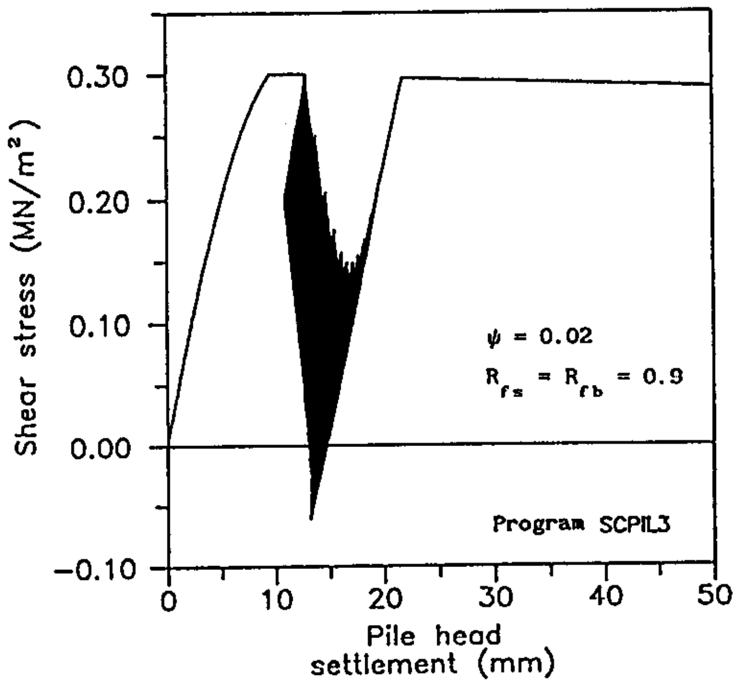

Fig. 5.75(b) SCPIL3 solutions: shear stress variation at average depth of 1.25m obtained using R_{fs} = R_{fb} = 0.9

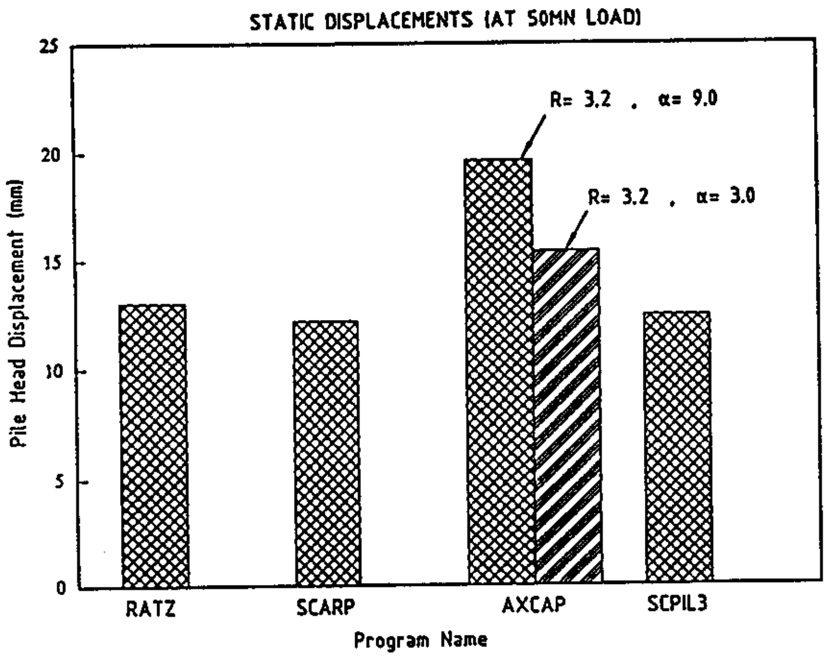

Fig. 5.76(a) Comparison of the static displacements obtained from the different programs

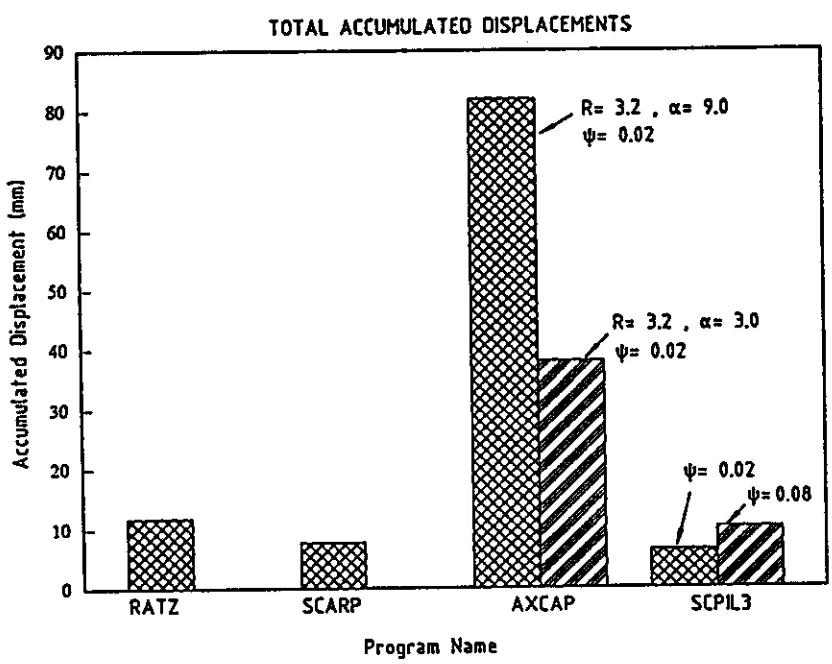

Fig. 5.76(b) Comparison of total accumulated displacements obtained from the different programs

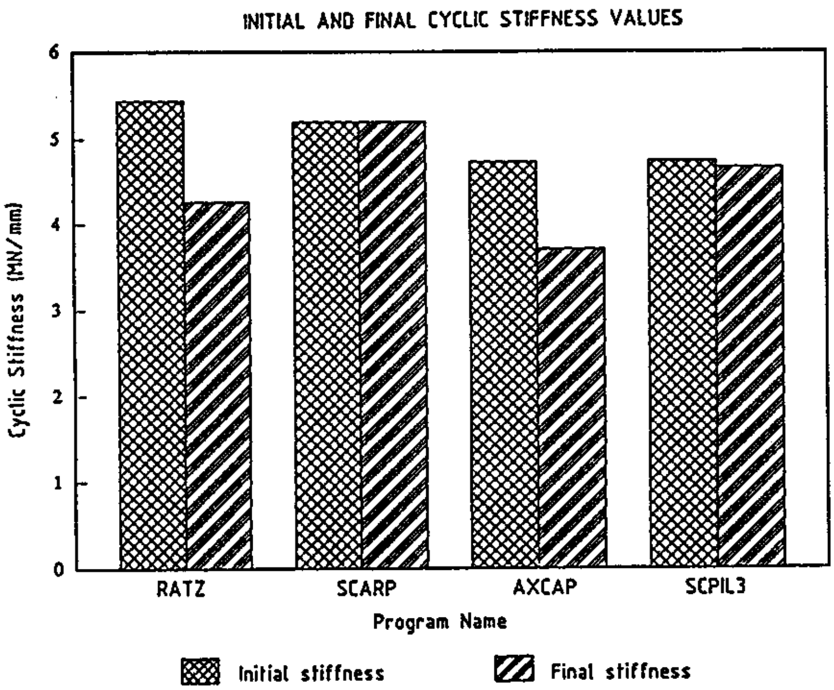

Fig. 5.76(c) Comparison of initial and final cyclic stiffness values obtained from the different programs

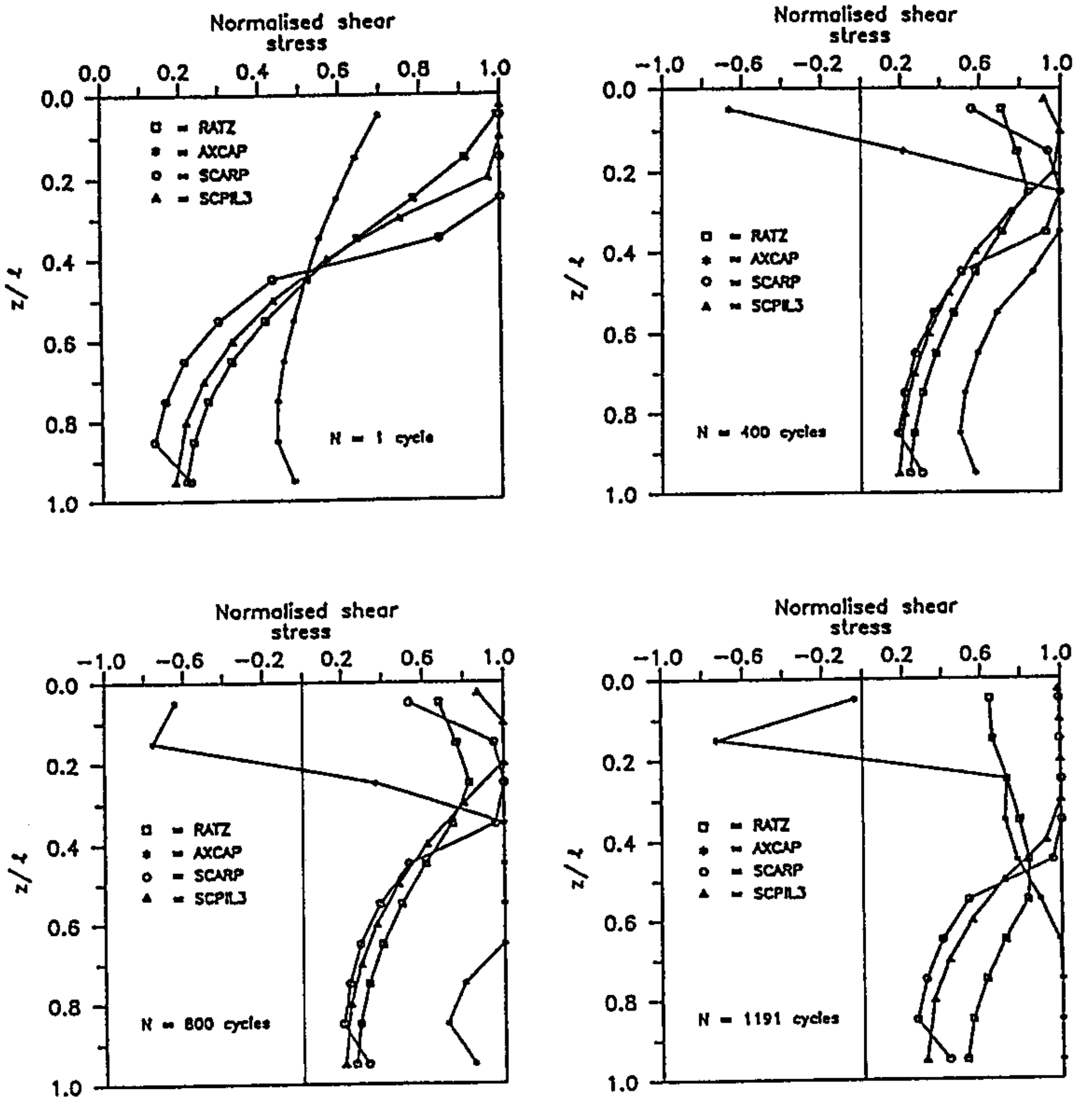

Fig. 5.77 Comparisons of the normalised shear stress distributions from different programs: (a) at N = 1 cycle; (b) at N = 400 cycles; (c) at N = 800 cycles; (d) at N = 1191 cycles (final)

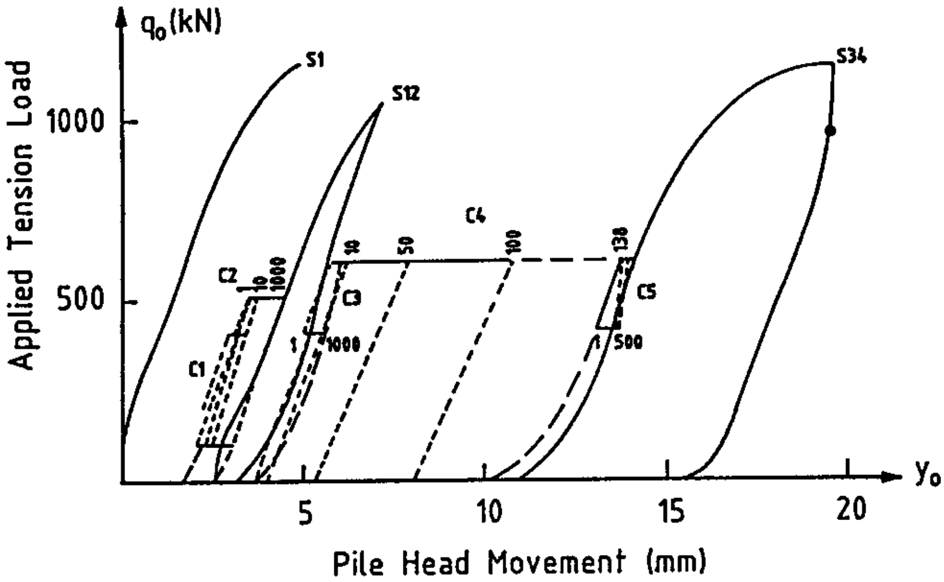

Fig. 5.78 Measured results of field cyclic pile test reported by Nauroy et al. (1985)

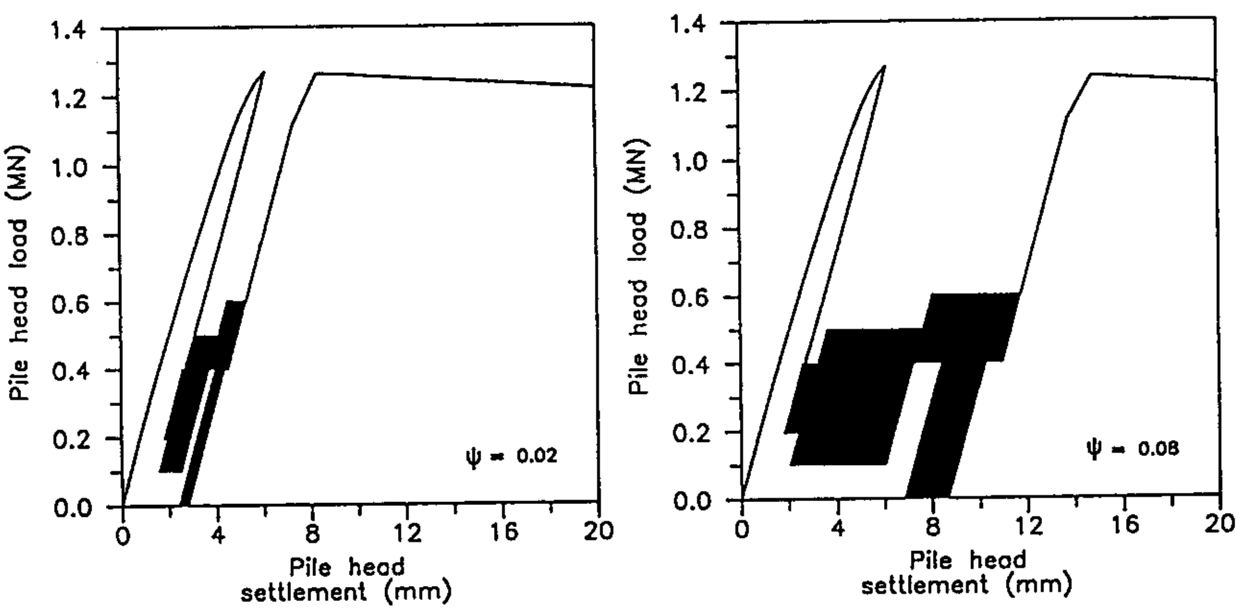

Fig. 5.79 Computed load-settlement response of field cyclic test: (a) with $\psi = 0.02$; (b) with $\psi = 0.08$

CHAPTER 6

MODEL PILE TEST FACILITY

CHAPTER 6

MODEL PILE TEST FACILITY

6.1 INTRODUCTION

As mentioned in Chapter 2, more laboratory model scale and/or field scale pile tests in calcareous sediments are required to substantiate and increase the present limited database of tests in such sediments. In particular, there seems to be a "scale effect" on the developed peak static unit skin friction and the degradation of skin friction under cyclic loading (section 2.3.1.4).

The major thrust of the experimental work in the present study was to investigate this "scale effect" phenomenon using laboratory scale instrumented model piles of different diameters. The model pipe pile sizes used were of a size greater than those used previously (< 50mm diameter) in this laboratory. An attempt was also made to instrument these model piles to approximately measure the normal pile-soil interface stress. For the case of "wet" soil tests, these model piles were also instrumented with miniature pore-water pressure transducers to measure the pore-water pressure response at the pile-soil interface.

In this chapter, the design, construction and hydraulic loading system of a large test facility for the conduct of these larger laboratory model pile tests are described. The design, instrumentation and calibration of the diaphragm-type stress cells and model piles are then described. Finally, all other necessary tasks, for example, sample preparation, data acquisition and load control programs required for the conduct of a test, are detailed.

6.2 LARGE TEST FACILITY

The idea of a large test facility, to be constructed within the School of Civil and Mining Engineering, was first mooted by Prof. H.G. Poulos in 1984. The reason behind the idea then was that the facility would enable larger model pile sizes (and of greater length too) to be tested which represents a more realistic simulation of the actual practical situation. The need for such a test facility was further reinforced later when model test results conducted with calcareous sediment seem to show a "scale effect" on the developed peak static unit skin friction and the degradation of skin friction under cyclic loading (Lee, 1988).

In the following sub-sections, the design of the test equipment (section 6.2.1) and the load control systems (section 6.2.2) are described in detail.

6.2.1 Test Equipment

The construction and fabrication of the necessary components of the test facility stretched over the period 1986 through 1991. However, most of these components were constructed and installed during the period of the author's candidature beginning from September 1988. The whole test facility was finally completed in August 1991 when the first trial test with a 50mm diameter uninstrumented model pile was made.

This section describes the design requirements and construction of the components of the test facility.

The design requirements for the test facility were as listed below:

1. As it was decided to locate the test facility on the upper floor of an existing workshop, the maximum permissible height of the test chamber was restricted to 1.5m after taking into account all other necessary components.
2. In anticipation of "wet" soil tests to be carried out, an above-level pedestal for supporting the test chamber was needed. This allows the necessary drainage connections to be fixed to the base plate of the test chamber. For the case of "dry" soil tests, the pedestal would facilitate the removal of sand from the base of the chamber (by using a "shutter" unit attached to the drainage hole instead of the drainage fitting). Also, the pedestal should be sufficiently robust to support the total dead load of the test chamber when filled with sand, estimated at about 2000 kg.
3. The diameter of the test chamber was decided at 1.0m after taking into account the fabrication capability of the engineering workshops and load limitation on the existing floor beams. For testing with a maximum pile size of 100mm diameter, the test chamber will have a distance from the walls to the test pile of

4.5 pile diameters. To avoid the influence of the side wall of the test chamber, this distance should preferably be as large as possible so as to avoid the zone of influence of the penetrating pile. However, this zone of influence of the penetrating pile is dependent on the soil type (amongst other factors) and with calcareous sediments, which are compressible, this distance of 4.5 pile diameters (assuming 100mm diameter model pile) will perhaps be sufficient to avoid any major effect from the side wall. It may be noted that some experimental tests conducted by Williams (1979) with 30mm diameter model jacked piles in silica sand indicate no significant effect at a distance of about 6.8 diameters from the tank wall. To obtain some qualitative indication of this effect, the author had decided to install diaphragm-type boundary stress cells along the side wall of the test chamber. As such, holes (4 Nos.) had to be drilled along a vertical plane on the side wall of the chamber and properly sealed, with the boundary stress cells in position, to avoid any possibility of leakage occurring. The design and calibration of the diaphragm-type stress cells are described in section 6.3.

4. In order to obtain a realistic simulation of field conditions, the "overburden" effect has to be reproduced in the laboratory. This can be achieved by a system of pressure regulator supplying a certain known air pressure onto the top surface of the sand in the test chamber. As such, a leak-proof condition has to be maintained around the top lid and the pile guide which guides the pile into the sand bed. An overburden pressure of between 100 kPa and 200 kPa is expected to be the desirable test pressure. To have some indication of how effective is the overburden pressure transfer to the base of the chamber, it was decided to position two of the diaphragm-type cells on the base plate of the chamber.

5. The top lid of the test chamber should be as light as possible to facilitate handling and at the same time to be capable of resisting the applied overburden pressure. To achieve this, a dome-shaped lid working on the principle of a stretched membrane was adopted. The dome-shape was fabricated by pressurizing a thin (4mm thickness) flat piece of mild steel sheet (with its edges rigidly clamped down) until a central deflection (with respect to the edge) of about 80mm was attained.

6. As the top of the test chamber would be about 2.2m above existing

floor level, a handling facility was required to facilitate the handling of the top lid, top rim for bolting and particularly during the placement of sand into the test chamber. An L-shaped gantry crane was chosen as the most suitable facility for the present case. The crane should be of sufficient height and rigidity and securely bolted to the existing floor beams.

7. A working platform was considered a necessity during the conduct of a test. This platform was set at 1.2m above the existing floor level and surrounds the test chamber. It enables one to move freely around the test chamber. A 1.0m railing around the platform was required to ensure safety while on the platform.

8. In order to avoid having more dead load loadings on the existing floor beams, a rigid reaction frame over the test chamber was ruled out. A self-equilibrating loading system, which is of minimal dead load and capable of not transmitting any applied testing load to the floor beams, was thought to be the most suitable loading system for the present facility. Furthermore, this loading system should be capable of controlling the rate of penetration of the test pile during the pile installation stage. As cyclic model pile tests are expected to be conducted using the test facility, the loading system should also be able of applying a cyclic load onto the test pile. To this end, it was envisaged that a servo-controlled hydraulic loading system, with two side rams attached to the test chamber while the pistons of the side rams were attached to the rigid crosshead above the test chamber, would form the loading system during the pile installation stage. For cyclic loading tests, a dual-flow servo-controlled hydraulic jack seated into the central part of the crosshead would provide the cyclic loading required. Although the preliminary required load capacity of the hydraulic loading system was calculated based on a 50mm diameter model pile, allowance had however been made in the chosen system for the case of a greater model pile size. The as-adopted system is capable of providing a total combined load (from the two side rams) of about 180 kN during the pile installation stage which requires the most jacking force. This maximum jacking force is more than sufficient to install a 100mm diameter model pile under the expected effective test overburden pressure of 100 kPa to 200 kPa. This hydraulic loading system is described further in section 6.2.2.

9. The crosshead above the test chamber had to be of sufficient rigidity and properly aligned and connected to the pistons of the two side rams. After the pile installation stage, and prior to testing using the inner central jack, it was required that the crosshead be rigidly held in position. Although the "locking-off" of the two side rams would hold the crosshead in position, an independent locking system connected to the test chamber was required as an additional safety feature in the event that the hydraulic system malfunction.

10. Finally, it was envisaged that a system of coupling pieces would connect the model pile and the load cell unit to the central jack on the crosshead. The coupling system should enable the connection between the model pile and the central jack be disconnected, if required, after the installation of the pile. It was also required that the coupling system should ensure accurate vertical alignment of the model pile so as to obtain a smooth movement of the pile through the pile guide prior to subsequent penetration into the sand bed.

All the above design requirements of the test facility had been considered and incorporated, resulting in the final completed facility as shown schematically in Fig. 6.1 (and as photographed in Plate 6.1).

The construction details of each of the components of the test facility are described briefly hereafter.

Component 1:

Fig. 6.2(a) shows the elevation and plan views of the test chamber. The chamber was fabricated by rolling a 5mm thick mild steel sheet to the required diameter (1.0m) and welding the two vertical joints together. Two 255x85mm channels were then welded to two diametrically opposite sides of the test chamber so as to provide a flat surface for fixing the two side rams of the hydraulic loading system. In order to enable the top lid and the base plate be bolted to the test chamber, two annular rings (with 30 bolt-holes) were welded to both the top and base of the test chamber. In addition, both the annular rings were provided with a 10mm circular groove for housing the "O"-ring required to ensure an air-tight condition. Four holes were then drilled in a vertical plane, on one side of the test chamber, at the positions shown in Fig. 6.2(a) to accommodate the diaphragm-type stress cells (see section 6.3). As the test chamber was of insufficient wall thickness, mild steel "seats" (Fig. 6.2b) had to be fabricated and welded to the outside surface of the chamber at the hole positions. The diaphragm-type cells were then housed within these "seats" and tightened adequately by a "capturing" nut at the end.

Component 2:

The top lid (Fig. 6.3) was designed to work on the principle of a stretched membrane. It was fabricated by clamping the edges of a 4mm thick mild steel sheet rigidly and subsequently "blowing" it to the required shape through the use of hydraulic pressure. Bolt holes were provided on the top lid for bolting to the top rim of the test chamber. In order to ensure that the circular edge of the top lid was rigidly clamped down and also to avoid any leakage through the "O"-ring, another annular ring over the edge of the lid (see Fig. 6.3) was thought to be desirable. To facilitate proper alignment of the three different components for bolting purposes, four locating-pin holes were drilled in the three components.

The central fixed pile guide attachments (Fig. 6.3) were required to be leak-proof as well as providing a smooth guiding surface for the sliding pile guide that was attached to a rubber membrane. Since the experimental program involved different model pile sizes, the attachment details for the top lid were designed to take this requirement into account economically. The as-adopted design, as shown in Fig. 6.3, required only the component marked "A" to be fabricated for each model pile diameter size. The maximum model pile size that could be tested using the adopted details was limited to 150mm diameter. "O"-rings were again used to ensure an air-tight condition. During application of the overburden test pressure, the sand bed, which was separated from the direct overburden pressure by a rubber membrane, would settle as a result of compression (or consolidation in the case of "wet" soil tests) taking place. At this stage, it was required that the sliding pile guide be able to move freely downwards together with the settlement of the top sand surface. "O"-rings on the internal surface of the sliding guide should ensure no leakage between the guide and the model pile. Finally, an inlet pressure fitting and a drainage fitting (for drainage purposes in the case of "wet" soil tests) were installed on the top lid.

Component 3:

As mentioned earlier, a self-equilibrating loading system was necessary to ensure no test loading being transferred to the existing floor beams. The adopted design involved attaching the two side rams of the hydraulic system to diametrically opposite sides of the test chamber, as shown in Fig. 6.4. The side rams of 1.2m maximum extension were bought from Lucas Industries Australia Limited. Both rams were bolted to the channels that were welded to the test chamber. During this assembly stage, it was required that both rams be aligned as vertical as possible. Two inlet/outlet ports, one at the top part and one at the bottom part of each ram, were connected to the hydraulic pump which was in turn connected to a control system which controls the upward or downward movement of the piston within the rams.

Component 4:

A circular mild steel base plate (Fig. 6.5a), of 31mm thickness, was fabricated to form the base of the test chamber. The base plate serves, in addition to containing the sand inside the chamber, as housing for a drainage connection and two diaphragm-type stress cells. Note that the two holes for accommodating the stress cells were located in the same vertical plane as the four holes on the side wall of the test chamber. In the case of "wet" soil tests, the drainage connection at the base plate and drainage ports on the rubber membrane at the top sand surface act as two-way drainage, and hence, reduce the time required to achieve full consolidation of the sand deposit. A 10mm groove for an "O"-ring was provided on the base plate to ensure no leakage. The drainage fitting on the base plate is also shown in Fig. 6.5(a). In order to facilitate the removal of dry sand from the test chamber at the end of a test, a "shutter" unit, as shown in Fig. 6.5(b), was fabricated to fit onto the drainage hole on the base plate. Thus, for dry sand tests, this "shutter" unit was used instead of the drainage fitting.

Component 5:

The crosshead (Fig. 6.6) over the test chamber serves to connect the two side rams and also as housing for the inner servo-controlled hydraulic jack. The side arms of the crosshead were fabricated by welding together 12mm and 15mm thick mild steel sheets. A 37mm diameter pin slot was provided at the bottom end of each arm for the locking-pins (see component 10) which were required to ensure that the crosshead was held rigidly. The central portion of the crosshead consists of a box-frame to accommodate the servo-controlled jack. Two

50mm diameter holes were provided on the rear side of the box-frame to allow for the necessary inlet/outlet connections to the central jack. Finally, a slotted cylindrical section was welded to the end of each side arm for connecting the crosshead to the pistons of both side rams by an internally threaded "holding" nut (see Fig. 6.6). It is imperative that the crosshead, when seated on both side rams, ensures that the threaded head of the servo-controlled jack is in proper alignment with the pile guide on the top lid. This is necessary to ensure that the model pile that is attached to the central jack will be in a truly vertical position and in alignment with the pile guide.

<u>Component 6</u>:

To ensure access to the drainage connection and the diaphragm stress cells on the base plate, it was thought necessary that the test chamber be raised above the existing floor level. A pedestal support, as shown in Fig. 6.7, was built onto the existing transfer beams which in turn rested on the floor beams below. The four legs of the pedestal support utilised were 102x102mm box-section members which were bolted onto the transfer beams. The top of the pedestal was made up of four 98x98x7mm "I" channels welded together to form a rectangular frame which was then welded to the four supporting legs. To increase the rigidity of the support, lateral braces were welded to the four support legs and bolted onto the transfer beams.

<u>Component 7</u>:

An L-shaped gantry crane (Fig. 6.8) was next erected for the test facility. The main body of the crane consisted of 200x200mm mild steel box-section. To facilitate erection of this member, the 5m long section was split into two-halves of 2.5m each. The lower-half was positioned over the transfer beam by using a mobile hoist and then bolted in place to the transfer beam. The positioning of the top-half posed more problems as there was no handling facility at the location capable of reaching the necessary height required to lift the top-half into position. An elegant lifting solution was devised whereby one edge of the base of the top-half was positioned against one top edge of the bottom-half. The two edges were held together by a pin-joint while the top end of the top-half rested against the transfer beam. A pulley system was then devised to lift the inclined top-half into a vertical position and then bolting its base to the bottom-half. The arm of the gantry crane was next lifted into place using a similar procedure. The 30mm diameter rod attached to the side arm and to the main vertical member ensured that the arm was held in a horizontal position. The movement of the arm in a horizontal plane was achieved through the use of movable, rotating joint connections attached to the main vertical member. Bracings for the vertical member were positioned by welding 76x40mm channels at right-angles to an existing floor beam and to one end of the transfer beam, as shown in the plan view of Fig. 6.8. A "roller and pulley" hanger on the side arm allowed the necessary lifting required. The test chamber was lifted to sit on the supporting pedestal upon completion of the gantry crane.

Component 8:

A working platform was considered a necessity to enable the top of the test chamber be within reach and to allow unobstructed access around the chamber. As such, a circular platform (Fig. 6.9) which enclosed the test chamber was adopted. The inner (1.1m radius) and outer (2.6m radius) rings of the platform were rolled from 50x20mm mild steel box-section members. Braces were welded in between both rings to link the two rings together, as shown in Fig. 6.9. The platform was fabricated as a whole before "splitting" into two-halves along the centreline C-C to facilitate subsequent work and its transfer from workshop to the test chamber location. At the positions of the two side rams and the gantry crane, the platform was detailed to accommodate these components. The "legs" of the platform, three on each half-circle of the platform, were fabricated using 25x25mm mild steel box-section members cut to the required lengths and welded to the platform. These "legs" supported the platform at an elevation of 1.25m above the existing floor level. The completed two-halves of the platform were brought to the test chamber location and assembled by pulling them together and bolting along the centreline C-C. Plywoods of 15mm thickness were then cut to match the platform and utilised as the platform floor cover. A 1.0m railing around the platform was next fabricated in two-halves using 25x25mm mild steel box-section members. The two halves were then welded to the outer ring of the platform. A door at one end of the railing, together with a simple staircase, were also fabricated to complete the working platform for the test facility.

Component 9:

The hydraulic power unit for the test facility was supplied, installed and commissioned by Lucas Industries Australia Limited. Prior to the installation of the hydraulic unit, the necessary power requirements were installed by the Buildings and Grounds Division of the University of Sydney.

The power unit consisted of a pressure compensated variable displacement pump bell-house mounted to an electric motor of 9 kW via a flexible coupling. This assembly was mounted vertically on and protruding through the deck, but outside the oil compartment, of the 150 litres reservoir. This facilitate access to the pump at all times for maintenance purposes. Also mounted on the deck were a filtered filler breather, an adjustable pressure relief valve, a pressure filter (10 micron nominal), the side rams electro-proportional control valve and the return line filter (10 micron nominal). The hydraulic assembly is capable of providing a maximum system pressure of 8000 kPa.

The hydraulic servo-valve to control the inner central jack in the crosshead assembly was mounted on the side arm of the crosshead. All the necessary pipework and hoses required to connect both side rams and the central jack to the hydraulic pump unit were then installed.

<u>Component 10</u>:

A locking-pin system was required, during the testing stage using the inner central jack, in order to hold the crosshead in a rigid position. The adopted design, as shown in Fig. 6.10, involved "anchoring" the crosshead to both side channels on the test chamber through a system of bolted plates. These "anchoring" plates were cut to the required shapes from 10mm thick mild steel sheets. The bottom-half, with a plate on each side of the channel, was bolted rigidly to the channel. Five sets of bolt holes (11mm diameter), three on each row, were drilled on the plates forming the top-half. At any time, only three consecutive sets of bolt holes were utilised for connection to the bottom-half. As such, the distance of the pin holes (on the top plates) to the top of the test chamber can be varied by changing the three sets of bolt holes utilised. The as-adopted design (see Fig. 6.10) was based on an estimated maximum pile penetration, with all necessary pile coupling pieces (see component 11) to the central jack in place, of 860mm. At this maximum penetration position, the pin holes on the crosshead are 338mm above the top of the test chamber. The bolt holes as provided on the top plates could be utilised for two other pile penetrations of 830mm and 800mm, i.e. with 30mm lifts. However, allowance had been made on the top plates to cater for pile penetrations of less than 800mm, if required, by drilling additional rows of bolt holes with 30mm spacing centre-to-centre. Two 37mm diameter mild steel rods were then machined to fit smoothly through the pin holes on the top plates and the crosshead. In order to ensure that the crosshead would be always on the right final penetration position and to facilitate the placing of both locking-pins, mild steel "seats" of the required height were fabricated and utilised.

Component 11:

A system of coupling pieces (Fig. 6.11) was required to connect the model pile head to a load cell unit which was in turn connected to the threaded end of the inner central jack. The coupling system should be able to allow the model pile to be disconnected from the central jack, if required, after the pile installation stage. The adopted design accomplishes this requirement by releasing the "capturing" nut that holds the parts marked "A" and "B" (see Fig. 6.11) together. To economise on the design, so as to cater for model piles of different diameters, only part marked "C" need be fabricated for each diameter size. The coupling pieces were fabricated from mild steel blocks and properly machined to ensure good alignment of the model pile and load cell unit.

Component 12:

Ideally, for the present study, a truly uniform sand mass of constant density everywhere within the test chamber is desirable. Due to the size of the test facility, the placement of sand into the test chamber involves a significant amount of effort. This consideration, coupled with the limitations of the present test facility, had resulted in the adoption of the "single hose" method of sand placement. The method involved placing an equal amount of sand into the 600x600x600mm discharge box (see Fig. 6.12) which had a 35mm diameter hole at the centre of the base plate. A shutter unit welded to the base plate, directly below the hole on the base plate, allowed the discharge of the sand to be controlled. A 700mm length of flexible hose was then attached to the shutter unit. The discharge box could be lifted to the required height above the test chamber by the gantry crane that had been erected. A similar smaller discharge box

(380x380x380mm) was also fabricated for the sand placing task. The sand placement procedure adopted will be described further in Chapter 7.

It may be noted that this method of sand placement has been shown by Bieganousky and Marcuson (1976) to be capable of producing homogeneous deposits in the medium-dense range.

Component 13:

In order to gauge the effectiveness of the sand placement method adopted, it was intended that two small diameter model piles (24mm diameter) acting as "penetrometers" be jacked into the prepared sand bed. The variation of the jacking force required with depth of penetration would give an indication of the uniformity of the sand bed. Since the end-bearing component contributes a significant proportion of the jacking force required, these small diameter piles will give a jacking force versus penetration response that is somewhat similar to an actual cone penetrometer. A jacking force versus penetration response that is not characterised by a sudden significant increase or decrease in the jacking force will therefore show that the sand bed is fairly uniform.

The adopted design, as shown in Fig. 6.13, involved attaching the two existing solid Aluminium piles (of length 470mm each) to two solid "extension" rods (24mm diameter) of 830mm length each. These two assembled pile "penetrometers" were then connected to a stiff horizontal plate. A threaded coupling piece allowed the horizontal plate (30mm thickness) to be connected to the threaded end of the central jack on the crosshead. A load cell unit attached between one of the pile "penetrometers" (as only a single 5 kN capacity "SHOWA" load cell was available) and the horizontal plate allowed the jacking force required with pile penetration to be recorded. The jacking force required for the other pile "penetrometer" could then be deduced from the difference between the "HSI" and "SHOWA" load cell readings. An additional pair of threaded holes were provided on the horizontal plate to enable the distance between the penetrometer and the centre of the test chamber be varied, if required.

It is interesting to note that Sweeney and Clough (1990) presented brief reviews of some of the existing large scale calibration chambers (see, for example, Bellotti *et al.*, 1982) and describe the design of a large calibration chamber at Virginia Polytechnic Institute (VPI), Blacksburg, USA. Although such chambers have been constructed mainly for the purpose of calibrating cone penetrometers and other in-situ devices, they could be easily adapted for conducting model pile test. Provisions have been made in the VPI calibration chamber to independently apply lateral confining stress and vertical stress to the specimen within the chamber. The application of a (known) lateral confining stress would result in a "flexible" lateral boundary condition for the specimen, as opposed to the "rigid" boundary condition where the specimen is in direct contact with the (rigid) side walls of the chamber. Model pile tests using a test chamber, in conjunction with a "flexible" lateral boundary condition, have been conducted by, for example, Evans (1987), Vipulanandan *et al.* (1989), Parkin *et al.* (1990) and O'Neill and Raines (1991).

Although the initial design of the present test facility did not provide for an independent lateral confining stress application, the necessary modifications to achieve this "ability" could be incorporated at a future date if desired. It may be noted that in actual field conditions, the surrounding soil mass may very well impose a "constant lateral stiffness" boundary condition intermediate of the two extremes of perfectly "flexible" and "rigid" conditions.

6.2.2 Hydraulic Loading System

The hydraulic loading system of the test facility should be capable of satisfying the model pile test requirements which generally comprise the following stages:

(a) initial jacking (or installation) stage,
(b) actual testing stage.

The initial jacking stage (a) requires control to be based upon achieving a constant rate of penetration (with respect to time) of the pile. It should be noted that during this "constant rate of penetration" stage, the developed resistance to penetration may vary. This requirement of a constant penetration rate can be achieved through the use of an electro-proportional valve. The side rams to raise and lower the crosshead can be controlled by varying the control signal to the amplifier control unit, which in turn controls the direction and speed of travel in direct proportion to the input signal strength and polarity. The "flow" loop of the installed control system for both side rams is shown in Fig. 6.14. The control panel was provided with two rates of penetration of about 48 cm/minute and 77 cm/minute, corresponding to the slow ("S") and fast ("F") operation modes respectively. For the selected rate of penetration, two additional push-buttons provide the choice of an upward or downward movement of both side rams. The control system also allows for any pauses during this initial pile installation stage.

At the desired final penetration, the crosshead will be mechanically locked (using both locking-pins) and the two hydraulic side rams isolated from further testing until required to withdraw the pile at the end of each test. The withdrawal of the pile would be a reversal of the pile jacking stage procedure.

The actual testing stage (b) of the total pile test consists of two types of test with either load or deflection being controlled, with respect to time, by using the 100mm stroke hydraulic jack located within the crosshead. The control system for this stage is more complicated than that of the first stage (a) described above.

The first type of test involves loading the model pile, either load-controlled or deflection-controlled, to any desired final value of the controlling variable. At present, this is achieved by manually controlling the input command signal to the "Moog" control unit which in turn controls the "Moog series 62" servovalve that was mounted on the crosshead. The ultimate pile load capacity, after the initial pile installation stage, can be determined by loading the model pile to "failure" (defined as increasing excessive settlement at almost constant applied load) using this control process. Fig. 6.15 shows the basic "flow" loop of the control unit for the "Moog" servovalve that was installed for the inner central jack.

The "Moog" control unit is fed by two voltage signals, one is the "input" command signal while the other is the "feedback" signal that can be either from the load cell unit or from the LVDT (Linear Variable Displacement Transformer) that are attached to the model pile. At the present stage, the system was wired-up to work on a "feedback" signal from the LVDT. This "feedback" signal is then compared to the "input" command signal, the resulting output from the servo-amplifier control unit then drives the servovalve accordingly until the "feedback" signal matches the "input" command signal. Hence, any changes to the "input" command signal will generate an immediate response from the central hydraulic jack.

The second type of test subjects the installed pile to a specified number of cycles (sine-wave based) of either load-controlled or displacement-controlled loading. The "Moog" servo-amplifier control unit installed is capable of catering for a maximum frequency of operation of 11.8 cycles per minute. The expected frequency of testing is about 3 cycles per minute, i.e. with a period of about 20 seconds, typical of the offshore loading condition. As mentioned earlier, only the displacement-controlled cyclic loading option was provided at the present stage. The required sine-wave "input" voltage command signal, of the desired frequency, can be generated through a voltage generator.

To generate the voltage required for the "input" signal needed to drive the "Moog" servovalve, a 12-bit 2-channel D/A (Digital to Analog) converter board (model CIO-DAC02, supplied by Computer Boards, Inc.) was utilised for the present test facility. The D/A board was installed in a separate micro-computer different from the one required to control the data acquisition process (as described in section 6.5). A control program was written to control the voltage generation required for the different stages in the model pile testing process (see Chapter 7). The required sine-wave "input" voltage command signal, of the desired frequency, can therefore be easily generated and fed to the servo-amplifier control box (see Fig. 6.15).

Fig. 6.16(a) shows the three different tests, with zero or non-zero mean value, that can be carried out using the servo-controlled jack. The expected variation of the developed load during a deflection-controlled test is shown in Fig. 6.16(b) while Fig. 6.16(c) shows the deflection variation under a load-controlled test. For deflection-controlled tests, the developed load generally tends to decrease with time, i.e., with increasing cycles of the controlled variable. Under load-controlled tests (not incorporated at the present stage), the deflection of the pile head tends to accumulate with increasing cycles. It should be noted that this accumulation of displacement at the pile head should not exceed the travel limits of the attached LVDT, otherwise damage to the LVDT will occur. It is envisaged that the computer program controlling the whole test procedure will have the "ability" to terminate the test when either end of the travel limits of the LVDT is approached.

At present, the installed control unit for the servo-controlled jack only allows one controlling variable, the pile deflection, to be utilised throughout a test. However, the ability to change from one controlling variable to another controlling variable (from load to deflection, or vice-versa) during a single test is desirable and can be incorporated into the present control unit at a future date.

After some preliminary trial tests of the hydraulic system, additional modification work to the existing power unit had to be incorporated. In order to prevent the sudden build-up of pressure during the initial starting of the pump, two solenoid valves were included into the pipework assembly for the central crosshead jack. These solenoid valves (models SV-1-16-C and SV-3-16-O) enabled the fluid to be returned to the pump reservoir when the pump was first switched on (see Fig. 6.17). Subsequent fluid flow to the connecting pipework was achieved by closing (or opening) the two solenoid valves through two push-buttons provided on the control box.

A major problem noticed during the trial tests was the uneven movement of both side rams, particularly near the extreme end (last 100mm movement) of the upward stroke. The problem was more significant towards the extreme end of the upward stroke when the stability of the side ram-crosshead assembly was least. This situation was undesirable since it would result in a tilted (non-horizontal) crosshead. This in turn may result in significant bending of the model pile which was connected to the crosshead and was restrained laterally at the other end by the pile guide assembly on the top lid. Fortunately, for the downward stroke, both side rams showed much less differential movement as compared to the upward stroke. A trial test with an uninstrumented model pile, with no overburden pressure applied on the sand mass, showed that the small differential movement (about 4mm) initially was quickly reduced to zero when sufficient force developed during the pile jacking process. This observation was encouraging in that the larger pile jacking force expected with an applied overburden pressure would contribute positively to negating any initial differential movement rapidly. Moreover, the stability of the side ram-crosshead assembly was increased due to the reaction provided by the model pile during the jacking stage.

As designed, both side rams should move with the same rate proportional to a given constant flow rate from the pump. This equal movement of both side rams could be achieved if the fluid flow from the pump was "split" equally at the pipework junction which branches to both side rams. It was concluded that this designed condition was not achieved from the differential movements observed. To investigate the problem further, the crosshead (see Fig. 6.6) was removed from both side rams. This allowed the independent movements of both side rams to be monitored. It was found that significant differential movement occurred with one ram trailing the other (in the upward stroke) of about a maximum of 700mm! Almost half the value was obtained for the downward stroke. The magnitude of this differential movement was also found to be affected by the movement mode adopted (i.e "slow" or "fast" mode), with the faster mode resulting in greater differential movement. Therefore, it was clear that significantly more friction was encountered in one of the side rams. However, these internal friction values of both side rams were considered insignificant when compared to the dead weight of the crosshead. It was thought that the much greater dead weight of the crosshead, together with its rigidity, would ensure equal movements of both side rams. This was however not the case and the question remains that unequal amount of fluid flow was going into both side rams, particularly during the upward stroke. Note that measurements taken showed that the internal pistons of both side rams were of identical length and diameter.

A simple and cheap solution was suggested by Lucas Hydraulics (the supplier of the hydraulic power unit) where a flow-control valve was incorporated into the pipework assembly corresponding to the faster side ram (see Fig. 6.17). By adjusting the flow-control valve, a setting was found where the upward stroke of both side rams (without the crosshead) was almost identical. For the downward stroke however differential movement still existed. More trial runs showed that the flow-control valve installed was only able to match the movements of both side rams either in the upward stroke or downward stroke, but not both. The "best" compromise setting that was chosen resulted in a differential movement of about 200mm for both the upward and downward strokes. The crosshead was then reassembled back onto both side rams. Trial runs conducted by the author showed that an improved condition was obtained than without the flow-control valve. The optimum condition (for a given flow rate) was obtained by subsequent minor "tuning" of the flow-control valve. This optimum condition confined, but did not eliminate, the tilting problem to the last 90mm of the upward stroke. It may be noted that a more expensive and better solution consisting of a flow-divider valve was also looked into. This flow-divider valve can physically divide the fluid flow from the pump into almost identical amount going into both side rams. However, due to the small fluid flow of the present facility, the best available commercial flow-divider valve (suggested by Lucas Hydraulics, Australia) can perform the task but with an "error" in the fluid flow of between 2% and 4%. It was concluded that this option would make the problem worse than its present condition and, hence, was not considered further.

The present facility, with the flow-control valve, therefore excludes the last 90mm, of the maximum possible extension of the side ram-crosshead assembly of 1.2m, as useful for testing purposes. A micro-switch unit will be incorporated (at a later stage) to automatically switch off the crosshead movement when that limit is reached.

6.3 DIAPHRAGM-TYPE STRESS CELLS

As mentioned earlier, during the penetration of the model pile into the prepared sand bed, zones of stress increases and displacements will be generated in the soil mass around the penetrating pile. Ideally, these stress increases and deformations should be allowed to "dissipate" into the surrounding soil medium. To achieve this ideal dissipation would require a much larger test chamber than that which has been fabricated for the present test facility. Conversely, too small a test chamber, with its rigid side boundaries, will tend to "obstruct" this dissipation resulting in a "reflecting" effect which may affect the response of the penetrating pile. This phenomenon becomes more significant as the ratio of the model pile diameter to the test chamber diameter increases.

It was decided that instrumented diaphragm-type stress cells be installed on the test chamber to provide some qualitative indication of the "rigid boundary" effect. The design and calibration of these stress cells are described hereafter.

6.3.1 Design Requirements

The accurate measurement of soil stress, through the use of an embedded stress cell, is a complex task and has been the subject of extensive research over the past few decades (for example, U.S. Waterways Experimental Station, 1944; Trollope and Lee, 1957, 1961; Weiler and Kulhawy, 1978). Ideally, the embedded stress cell should be of the same stiffness as the soil that it replaces so as not to affect the response of the soil mass. As this requirement is virtually impossible to satisfy completely, the soil stress measured will be affected by the characteristics of the embedded stress cell.

The diaphragm-type stress cell forms one of the more commonly used type of stress cells for measuring soil stresses. When subjected to stresses, the instrumented diaphragm face of the cell will undergo deflection with a maximum deflection occurring at the centre of the diaphragm face. Clearly, the deflection of the diaphragm face will result in some local redistribution of soil stresses around the embedded cell. It is not intended here to give a comprehensive review of the factors affecting the performance of such diaphragm-type cells. A comprehensive assessment of such factors can be found in the publications by Krizek *et al.* (1974) and Weiler and Kulhawy (1982).

For the present study, the diaphragm-type cells are to be utilised as "boundary" cells along the side wall (4 Nos.) and on the base plate (2 Nos.) of the test chamber.

The general guidelines, established by the U.S. Waterways Experimental Station (1944), for such "boundary" diaphragm-type cells are as listed below:

(i) the projection of the cell body outside the boundary surface should not exceed 1/30th of the cell diameter;

(ii) the maximum central deflection of the diaphragm face should not exceed 1/1000th of the cell diameter.

The adopted design for the diaphragm-type cells in the present study is shown in Fig. 6.18. Requirement (i) above is satisfied as the cells are to be installed flush with the inside surface of the side wall. Some finite element analyses of the stress cell showed that the diaphragm diameter (30mm) to the central deflection ratio (with thickness of diaphragm face = 1.3mm), under a maximum pressure of 200 kPa, is 2206, satisfying requirement (ii) above. Fig. 6.19 shows the axisymmetric finite element mesh utilised for determining the central deflection of the diaphragm cell. The adopted design is simple but yet capable of providing a qualitative indication of the "rigid boundary" effect during the pile installation stage.

The stress cells can be easily installed onto the test chamber by tightening the cells against the housings provided (see Fig. 6.2b and Fig. 6.5) through "capturing" nuts on the threaded face of the cells. The calibrations of the stress cells are described in the next section.

6.3.2 Calibration

Before the stress cells could be utilised, their responses had to be calibrated against known applied pressure acting over the instrumented diaphragm face of the cells. Strain-gauges are normally used for measuring such responses of the diaphragm face. Some preliminary work on the present diaphragm cell indicated that 350 ohms gauges (with better heat dissipation characteristic at higher excitation voltage) were preferred than the more common 120 ohms gauges. The aluminium temperature-compensated strain-gauges, type 3/350LY13A (manufactured by HBM, Germany) of 350 ohms and 3mm gauge length, utilised were arranged in a full Wheatstone bridge circuit with two "active" and two "dummy" gauges, as shown in Fig. 6.18. The instrumentation of the cells were carried out solely by the author.

In order to calibrate these "boundary" diaphragm-type cells, the small calibration chamber (Fig. 6.20) was designed and fabricated. Note that provisions had been incorporated in the calibration chamber design for its use in the calibration of the instrumented segments of the model pile shaft, as described later in section 6.4.2.2 The internal diameter to depth ratio of the mild steel chamber was 1.7. Rubber "O" rings were used to ensure proper sealing of the chamber. Any pressure loss, due to friction over the relatively smooth internal side surface of the chamber, was thought to be minimal and acceptable for the present usage. Each cell was seated in turn into the housing on the base plate while the fluid (air) pressure was applied through a pressure hole on the top plate. The face of the cell was flush with the base plate to be consistent with the "boundary" condition of the cell when installed on the test chamber. Any changes in the applied fluid pressure will cause corresponding changes in the deflected shape of the diaphragm face, which in turn will result in a change in the output voltage of the strain-gauge arrangement measured by a HP 3458A multimeter. A calibration "chart" can thus be obtained which relates the known fluid pressure to the output voltage of the cell.

It has been shown (for example, Trollope and Lee, 1957; Selig, 1980; Weiler and Kulhawy, 1982) that a fluid-calibrated diaphragm cell may not usually give a representative measurement when embedded within, or in contact with, a sand mass. This is because stress redistribution may occur around the cell when the diaphragm face deflects, resulting in an "under registration" or "over registration" as compared to the fluid-calibrated response. As noted by, for example, Weiler and Kulhawy (1978), the most reliable approach would be to calibrate the cells under the same conditions that the cells would most likely be subjected to in their applications.

For the present study, it was decided that "in sand" calibrations be also conducted on the stress cells to obtain some indication of the behaviour of the cells in contact with a sand mass. The "in sand" calibration was also thought to give a more representative response when considering the present usage of the cells.

The calibration chamber was filled with sand in a systematic procedure to simulate three different sand densities of a relatively loose state, a medium-dense state (relative density = 66%) and a relatively dense state (relative density = 86%). After the filling-up of the calibration chamber, the sand mass was isolated from the applied fluid pressure by placing a piece of rubber membrane over its top. For known applied fluid pressures, the responses of the cells were measured as for the "fluid-calibration" case. Some typical results obtained from the calibration of these diaphragm-type cells are presented and discussed in Chapter 7.

6.4 INSTRUMENTED MODEL PILE

In order to obtain information on the behaviour of the pile during installation and the subsequent load-deformation and load-distribution characteristics of the embedded pile, some form of instrumentation has to be employed on the pile. In almost all pile loading tests, the pile head load and pile head displacement are measured since the necessary measuring equipment can be easily installed. More complex and elaborate instrumentation has to be employed if detailed responses of the pile in terms of load-distribution, normal pile-soil interface stress, pile-soil interface shear stress and pile-soil interface pore-water pressure (if any) are required.

Instrumented model piles utilised for laboratory testing have been reported by, for example, Chan and Hanna (1980) and Steenfelt *et al.* (1981). Large scale instrumented model piles for field testing have also been reported by, for example, Cooke and Price (1973), Butterfield and Johnston (1973), Baligh *et al.* (1985), Ponniah (1989), Bond and Jardine (1989), and Coop and Wroth (1989). It should be noted that any instrumentation employed on the model pile shaft will inevitably result in a "non-uniform" pile which may in turn affect its response. The greater the amount of instrumentation introduced, the more "non-uniform" the pile will be. However, this is a necessary sacrifice that is required in order to obtain information on the response of the pile over its entire length.

In the following sub-sections, the instrumentation provided on the model pipe piles for the present study are described. These include the measurements of the pile head load and pile head deflection (section 6.4.1), axial load and normal pile-soil interface stress along the pile shaft (section 6.4.2) and pore-water pressure response (if required) along the pile shaft (section 6.4.3). It must be emphasized that pile instrumentation for accurate measurement of the pile response is a complex task which is being continuously improved from the experience gained over many years of instrumented pile testing (for example, Bogard *et al.*, 1985). As such, it should be noted that the instrumentation of the first large scale model piles (at the University of Sydney), in particular, for the measurements of the normal pile-soil interface stress (if possible) and pile-soil interface pore-water pressure response, were attempted within the constraints of the present test facility, manpower and financial availability, and the time available for the present study remaining in the author's period of candidature. However, any experience gained from the present instrumentation can be utilised to further improve on the subsequent instrumented model piles.

6.4.1 Pile Head Instrumentation

The pile head load was measured by a "HSI model 3100-0030" universal tension and compression load cell, of 30000 lbs. (134 kN) capacity, that could be attached to the model pile through the coupling pieces as shown in Fig. 6.11. The other end of the load cell was connected to the threaded end of the central jack. The load cell has a sensitivity of about ±2mV/V at full scale. A 126mm stroke LVDT (Linear Variable Displacement Transformer) attached to the crosshead assembly, which provided a reference support, was utilised to measure the pile head displacement. A "twisted" plate, as shown in Fig. 6.21, was fabricated to connect the tip of the movable extension rod of the LVDT to the upper threaded end of the central jack. Therefore, any movement of the central jack, as measured by the LVDT, was assumed to be equal to the pile head displacement since the intermediate coupling pieces and load cell unit were relatively much stiffer elements contributing very negligible influence to the assumption.

6.4.2 Axial Load and Normal Pile-Soil Interface Stress Measurements

Instrumentation provided along the pile shaft is generally more complicated than those employed for the pile head. In this section, the instrumentation details adopted in the present study for the measurements of the axial load and the normal pile-soil interface stress (if possible) along the pile shaft are described.

6.4.2.1 Axial load

The measurements of axial load in tubular piles are usually accomplished by means of strain-gauges mounted on the internal pile walls to form the so-called axial load cells. These cells are calibrated by applying an axial load and monitoring the output response of the strain-gauge arrangement (see, for example, Hunter and Davisson, 1969; Vesic, 1970; Yazdanbod *et al.*, 1984). As such, the calibration process does not take into account the effect of a confining lateral soil pressure that is present during actual pile testing. This inconsistency in the calibration process becomes more significant, resulting in under-registration of the axial load, in cases where large lateral confining soil pressures are encountered.

An approach which takes into account the effect of this lateral confining soil pressure on the axial load measurement has been suggested by Chan (1976) (see also Chan and Hanna, 1980). It involves separate measurements of the axial and tangential (hoop) strains at each load cell location. The approach however does not allow the lateral (or normal) pile-soil confining pressures along the pile to be determined.

For the present study, the test pile (Fig. 6.22) was formed from smaller segments threaded together. The use of threaded segments is to enable the test pile be disassembled, if required, to correct any faulty segments although this task is by no means easily accomplished. The threaded connections were designed to be capable of resisting the full anticipated design load of the test pile applied in tension. A trial tension test of the threaded connection confirmed the "ability" to resist the full anticipated design load.

Five of the segments were instrumented with strain-gauges to form the load cell units for the pile shaft of the present test pile. The strain-gauged segments (Fig. 6.23) were machined to a smaller wall thickness (1.5mm) at the strain-gauge locations so as to increase the sensitivity (i.e output response) of the strain-gauge arrangement. Two sets of two "active" strain-gauges (type HBM 3/350LY13A), one on each diametrically opposite sides, measure the axial and circumferential (hoop) strains independently. The two sets of strain-gauges were connected to two other sets of gauges (installed on an aluminium plate) acting as "dummies" to form two independent Wheatstone bridge circuits. The adopted strain-gauge arrangements would be self-compensating for any bending or torsion that may develop, particularly during the pile installation stage, and introduced as minimum as possible the amount of wiring inside the test pile. A preliminary trial test of using a single set of "dummies" and a "switching" mode, in conjunction with the two active sets of gauges, showed an unstable drift response in the measured voltage readings. As such, it was decided that an individual set (2 Nos.) of "dummies" have to be used for each of the individual set of active gauges. Altogether, five such sets of "dummies" for the pile shaft instrumentation together with the necessary wirings were prepared by the author. It may be noted that these sets of "dummies" can be similarly used for the instrumentation of the other model pile sizes.

For calibration under axial load alone, the instrumented pile shaft segments were subjected to incremental applied vertical loads, using an Amsler tension and compression testing machine, until the expected design load of the test pile size was reached. At each incremental load, the axial and cicumferential strains occurring at the instrumented section were recorded separately as voltage changes by the HP 3458A multimeter.

It may be noted that during the initial design for the instrumented segments, the effects of the thickness of the instrumented section were recognised. These were:

(i) The thinner the instrumented section of the segment, the greater the responses of both bridges under axial load alone and under horizontal applied stress alone (described further in section 6.4.2.2).

(ii) The thicker the instrumented section, the smaller the responses of both bridges, particularly the response under horizontal applied stress alone.

The output responses of both bridges under the applied axial load alone were considered to be of measurable magnitudes (based on an initial range for the thickness of the instrumented section) and therefore did not pose much problem. The main problem lies with the output responses under the applied horizontal stress alone. A thickness for the instrumented section had to be chosen such that the output responses, under the applied horizontal stress alone, were of sufficient sensitivity and at the same time not too flexible with respect to the uninstrumented section. Moreover, the greater load that could be expected during the initial pile installation (jacking) stage also had to be taken into account. Based on some axisymmetric finite element analysis of the instrumented segment, under the anticipated applied horizontal stress, a thickness of 1.5mm (for 50mm diameter model pile) was adopted for the instrumented section. The corresponding adopted thickness for the 100mm diameter model pile was 2.0mm. In all cases, the maximum tensile stress in the instrumented section was limited to less than 60% of the yield stress of the pile material (aluminium).

The theory behind this "axial load and normal pile-soil interface stress" load cell is described further in the following section.

6.4.2.2 <u>Normal pile-soil interface stress</u>

Compared to the measurement of axial load along the pile shaft, the normal pile-soil stress measurement over the pile length constitutes a more difficult task. As mentioned in section 6.3.1, this difficulty is mainly due to the tendency for stress redistribution within the soil medium in contact with the measuring component.

Perhaps the first early satisfactory version of the contact earth pressure cells developed came from the work of Arthur and Roscoe (1961) conducted at Cambridge University. Since then, numerous designs and improvements over the basic cell of Arthur and Roscoe (1961) have been built at Cambridge University (see, for example, Bransby, 1973; Maddocks, 1983). Such Cambridge cells have been utilised in laboratory model pile testing (for example, Williams, 1979) and in field tests (for example, Bond and Jardine, 1989, 1991). Other types of cells have also been developed or utilised by other investigators for measuring the normal pile-soil interface stress, for example, Johnston (1983) (adaptation of Cambridge model), Baligh *et al.* (1985), Rowlands *et al.* (1989) and Ponniah (1989). It should be noted that the question of which type of cell is "better" is still highly debatable at present. Hence, a qualitative interpretation of the cell's response can at best be attempted only.

The basic concepts of the Cambridge contact stress cells, based on the initial design of Arthur and Roscoe (1961), are presented briefly hereafter as these are of relevance to the present study.

The forces acting on the stress cell consist of a normal load (N) at an eccentricity, e (from the central axis of the cell) and a shear load (S), as shown in Fig. 6.24. The three strain-gauge circuits installed on the cell are not independent and the application of any load gives rise to voltage outputs V_N, V_e and V_S from the normal, eccentricity and shear circuits respectively (see, for example, Williams, 1979). Thus, by varying each of the load components separately in the calibration process and recording the corresponding voltage outputs from the three circuits, the following matrix relationship can be obtained (Williams, 1979):

$$\begin{Bmatrix} V_N \\ V_e \\ V_S \end{Bmatrix} = \begin{bmatrix} a_{11} & a_{12} & a_{13} \\ a_{21} & a_{22} & a_{23} \\ a_{31} & a_{32} & a_{33} \end{bmatrix} \begin{Bmatrix} N \\ e \\ S \end{Bmatrix} = [Z] \begin{Bmatrix} N \\ e \\ S \end{Bmatrix} \qquad (6.1)$$

where the coefficients of the matrix [Z] can be obtained from the above calibration process. Equation (6.1) is then inverted to obtain the load components given by:

$$\begin{Bmatrix} N \\ e \\ S \end{Bmatrix} = [C] \begin{Bmatrix} V_N \\ V_e \\ V_S \end{Bmatrix} \tag{6.2}$$

where $[C] = [Z]^{-1}$ is the calibration matrix (order 3x3) of the load cell. Hence, in the actual usage of the cell, the loads acting on the cell can be obtained by simply multiplying the calibration matrix [C] with the three voltage outputs (with respect to initial zero load values) as given by equation (6.2). It may be noted that although the working concept of the cell is theoretically sound and simple, absolute proper care has to be exercised in the manufacture of the cell and, particularly, during the tedious calibration process.

For the present study, the basic theoretical concept of the Cambridge contact stress cells described earlier was adopted. A number of considerations were taken into account before reaching the final adopted method for determining the normal pile-soil interface stress. These considerations were:

(i) If some form of contact stress cell (similar to the Cambridge model) were employed, the necessary packing of the cell, onto the pile shaft, capable of effectively sealing the assembly (in the case of "wet" soil tests) would result in a somewhat highly "non-uniform" pile shaft. The packing pieces for such cells would be in addition to those required for the pore-water pressure probes (see section 6.4.3)

(ii) Even if the Cambridge - type cell were adopted, the necessary manpower availability and technical skills required to fabricate and instrument a successful cell within a satisfactory time period was considered a problem. The question of manpower availability, lacking during the period of the author's candidature, was an important factor that had to be taken into account.

Based on the above considerations, the use of contact stress cells that need to be installed on the pile shaft was ruled out for the present study. Instead, a simpler approximate approach was adopted which relied on the separate measurements of the axial and circumferential (hoop) strains under the applications of axial load alone and normal horizontal stress alone.

As mentioned in section 6.4.2.1, the voltage outputs of the axial and circumferentially orientated strain-gauge circuits under axial loading alone can be obtained by subjecting the instrumented segment to known applied axial loads. Similarly, the responses of both strain-gauge circuits, under an applied horizontal stress alone, can be obtained by subjecting the segment to known applied horizontal stress. To achieve this, the calibration chamber (see section 6.3.2) was utilised.

The top and bottom ends of the chamber were modified to accommodate the instrumented segment by attaching the three plates marked "A", "B" and "C" to the chamber body (Fig. 6.25). A pressure inlet valve on a side of the chamber body enabled the necessary required pressure to be applied. Note that to cater for a different pile segment size, only the components marked "A" and "B" need be fabricated to accommodate the new size. "O" rings have again been used to prevent any leakage along the surface of the pile segment. By varying the applied pressure, the responses of both strain-gauge circuits, measured by the HP 3458A multimeter, can be obtained.

Note that the design details of the instrumented segments of the pile shaft, for the measurements of both axial load and normal pile-soil interface stress, have been described earlier in section 6.4.2.1.

The relationship relating the applied loads (or stresses) to the voltage outputs of the two strain-gauge circuits is given by :

$$\begin{Bmatrix} V_A \\ V_N \end{Bmatrix} = \begin{bmatrix} a_{11} & a_{12} \\ a_{21} & a_{22} \end{bmatrix} \begin{Bmatrix} A \\ N \end{Bmatrix} = [Z] \begin{Bmatrix} A \\ N \end{Bmatrix} \qquad (6.3)$$

where A is the applied axial load, N is the normal pile-soil horizontal stress, V_A and V_N are the voltage outputs from the axial and circumferential circuits respectively, and [Z] is a matrix (order 2x2) of coefficients obtained from the calibration process. By varying the applied axial load alone (i.e with no applied horizontal stress), the coefficients a_{11} and a_{21}, which represent the axial and circumferential strain-gauge circuits responses (per unit of applied load) respectively, can be obtained. Similarly, by varying the applied horizontal stress alone (i.e with no applied axial load), the coefficients a_{12} and a_{22} (which are the responses per unit horizontal stress) can be obtained. Equation (6.3) is then inverted to give the following equation:

$$\begin{Bmatrix} A \\ N \end{Bmatrix} = [C] \begin{Bmatrix} V_A \\ V_N \end{Bmatrix} \tag{6.4}$$

where $[C] = [Z]^{-1}$ is the calibration matrix (order 2x2) of the instrumented segment.

It is worth noting that such an approach involving the independent measurements of the axial and circumferential (hoop) strains, for determining the axial loads and normal pile-soil interface stresses, has also been utilised in the model tests of Steenfelt *et al.* (1981). It is however not known how effective was the normal pile-soil interface stress measurement procedure as no results were presented by the writers. A somewhat similar approach has been adopted by Huntsman *et al.* (1986) for determining the in-situ lateral stresses using cone penetrometers. Their method involves measuring the circumferential strains only (caused by the lateral stress) over a thinned-section of the cone penetrometers. The technique of measuring the circumferential strains using strain-gauges has also been utilised by Lade *et al.* (1981) in a series of model centrifuge tests of deep vertical shafts in dry sand.

It should be emphasized, as in any soil stress measurements, absolute quantitative measurement of the lateral stresses acting on piles (or penetrometers) are most difficult to obtain. A qualitative interpretation of the results is thus considered to be more appropriate. Some preliminary test results from an initial trial instrumented segment showing the applicability of the adopted approach are presented in Chapter 7.

In the approximate approach adopted for the present study, as outlined earlier, the following points can be noted:

(i) Calibration simulating the shear stresses over the pile shaft was omitted. It was assumed that the effects of the shear stresses (on the strain-gauged section) were identical to those of an axial load. Thus, the difference in the axial loads measured between any two adjacent load cells was assumed to be distributed uniformly over the pile shaft surface area between the two cells (i.e as shear stresses). Therefore, any actual non-uniform distribution of the shear stresses was assumed to have identical effect (as the uniformly distributed case) on the resultant response of the load cell unit.

(ii) While the Cambridge contact stress cell gave the measured lateral stress response at a particular "point", the present adopted approach gave an averaged response of the lateral stresses acting over and along the circumferential area of the instrumented segment. Any non-uniform lateral stress distribution was hence measured as an averaged response and interpreted as a uniform lateral stress distribution over the instrumented segment.

(iii) "In-sand" calibration of the instrumented segment, under an applied horizontal stress, to cater for a pile that is subjected to a cyclic load, is highly complex and difficult for interpretation. As such, it was not attempted in the present study.

Therefore, based on the above points, the normal pile-soil interface stress measurement using the present instrumented segment can only be interpretated qualitatively whereas an absolute (quantitative) interpretation of the axial load measurement can be made. It must be emphasized that the simplified procedure adopted in the present study for deducing the normal pile-soil interface stress was attempted in order to maximise the information that could be obtained from each strain-gauged segment. Although preliminary results from a trial instrumented segment (see section 7.4.2) showed the applicability of this simplified procedure, the performance of the model instrumented pile, consisting of a number of these instrumented segments, remains to be assessed. The satisfactory or non-satisfactory interpretation of the deduced normal pile-soil interface stress, obtained from tests using the model instrumented pile, will be discussed further in Chapter 8.

6.4.3. Pore-Water Pressure Measurement

The instrumented segments of the pile shaft are also required to measure the pore-water pressure response (in the case of "wet" soil tests) at the pile-soil interface. This task can be achieved by attaching miniature pore-water pressure transducers (Druck PDCR81 model) to the thicker section (2.5mm) of the instrumented segments.

The final adopted attachment details for the pore-water pressure transducer are shown in Fig. 6.26. A backing piece, machined to fit the internal surface of the segment, provided the necessary support to which the pressure transducer housing was attached. This backing piece was held in position to the pile shaft segment by four screws positioned 90° apart. "O" ring grooves were further machined on the backing piece to ensure a leak-proof condition for the assembly. The pressure transducer housing was connected to the backing piece support through a threaded connection. A small "O" ring groove was provided on the internal surface of the housing to ensure no leakage occurring at the housing-transducer interface. All the necessary attachments were fabricated and machined to ensure that the installed assembly was flush with the external pile surface.

Note that the present adopted attachment method enables the pore-water pressure transducer to be removed, if required, from the pile shaft. This can be easily achieved by releasing the transducer housing from the backing piece. This "ability" to remove the pore-water pressure transducer is required to enable the transducer to be utilised in other model piles. However, the necessary attachment pieces have to be fabricated to suit the new pile size.

Trial tests during the initial development stage were mainly confined to eliminating the leakage problem from the back of the housing-transducer interface. The leakage was finally eliminated by using an "O" ring at the housing-transducer interface. Plate 6.2 shows an instrumented segment with the miniature pore-water pressure transducer.

Calibration of the pore-water pressure transducer on each of the instrumented segment was easily carried out using the small calibration chamber. This was done simultaneously with the calibration for the response of the strain-gauged section under an applied horizontal stress. An air pressure system, in conjunction with an air-water pressure pot, was utilised for creating the necessary hydrostatic pressure required. A typical calibration response of the pore-pressure transducers is presented in Chapter 7.

It is worthy of note that pore-water pressure measurements along the pile shaft have been conducted in laboratory model tests (for example, Matlock *et al.*, 1982) and in the field (for example, Puech and Jezequel, 1980; McAnoy *et al.*, 1982; O'Neill *et al.*, 1982a).

6.5 DATA ACQUISITION

In this section, the necessary data acquisition equipment utilised for the conduct of the model pile testing program is described. The computer control programs written to cater for the different stages required in each individual model pile test are also detailed. The different stages of the model pile test are described further under the section "Test Procedures" in Chapter 7.

There are altogether a total maximum number of 23 channels of readings that have to be monitored during each model pile test. These consist of two channels for the load cell and displacement transducer required for monitoring the pile head load and pile head displacement respectively, ten channels for the five instrumented strain-gauged segments of the pile shaft, one channel for the pile base strain-gauged tip, six channels for the six diaphragm-type pressure cells along the side wall and base of the test chamber, and four channels (if required) for the pore-pressure transducers attached to the pile shaft strain-gauged segments.

The digital data acquisition system consists of a scanning digital voltmeter together with a portable micro-computer system. The digital voltmeter utilised for the present test facility was a Hewlett-Packard HP 3458A multimeter in conjunction with a switch/control unit model HP 3488A. A total of 40 channels (for two wires DC voltage measurements) from four "Relay Multiplexer" option assemblies (model 44470A), installed on the switch/control unit, form the maximum data acquisition capability of the present installed system. Since the present digital multimeter system has a measurement accuracy of one microvolt, both the strain-gauged and transducer output responses can be read and recorded directly without the use of amplifiers or other bridge-balancing circuitry. Thus, the use of this system eliminates the need for signal-conditioners and amplifiers (which inherently magnify the "noise" level as well) often associated with drift and uncertainty in strain-gauge measurements. Another micro-computer system, with the D/A board CIO-DAC02 installed in it, was utilised to generate the required "input" loading command signal. Fig. 6.27 shows the "flow" of the adopted data acquisition system as well as the separate control for generating the displacement-controlled cyclic loading necessary for the present test facility.

Two control programs were written for the test facility, one for the data acquisition (program DAQ.BAS) and another for the input loading command signal (program DLOAD.BAS). Both programs were written using "QuickBasic" language and utilised within a "QuickBasic" environment.

It is essential and desirable that the load-displacement response at the pile head be monitored and displayed to the user during the different stages of the test. To this end, a graphic display showing the pile head load versus pile head displacement response was incorporated into the data acquisition program DAQ.BAS. Provisions were also made for the corresponding values to be tabulated and displayed on the monitor screen. As will be described in Chapter 7 (under the section "Test Procedures"), this graphic option is used to assist in the loading control required at certain stages of the test. Also, this option enables any irregularity during the testing stage to be visibly detected. During the cyclic loading stage, the channel readings specific to selected cycle numbers can be stored in a specified file instead of storing the readings for all cycles. This will reduce the amount of core-storage required from the micro-computer system.

The program DLOAD.BAS is utilised to control the D/A voltage converter for generating the required voltage "input" magnitudes necessary for the different stages of the test. As mentioned earlier, this program is used in conjunction with the graphic option (of program DAQ.BAS) for controlling the direction of loading of the servo-controlled hydraulic jack, to which the model pile is attached.

6.6 SAND PREPARATION PROCEDURE

In this section, the necessary tasks that have been performed by the author in preparing a large volume of calcareous sand are described. The detailed sand placement procedure that was adopted for filling the test chamber is further described in Chapter 7.

Due to the large size of the test chamber, a considerable amount of calcareous sand specimen was required to fill up the test chamber (volume of test chamber about $1.22m^3$). As such a large volume of prepared calcareous sand sample was not available in the laboratory, a large volume of such sand had to be prepared from the "raw" sand (from Bass Strait, Australia) that was supplied by Esso, Australia.

In deciding the amount of sand required, consideration was given to the case where "wet" soil tests are to be conducted. For such "wet" soil tests, the need of being able to carry on a test, while the wet sand from the previous test is being dried, is highly essential. It should be emphasized that for such "wet" soil tests, the process of drying and preparing the sand back to a "condition" suitable for sand placement for a test is time-consuming and needs considerable effort. A total of about $3.1m^3$ of sand was prepared by the author over a continuous period of about $3^1/_2$ months, from early August 1989 to mid November 1989.

Altogether 136 bags of wet "raw" sand were transferred to the "sand preparation" room next to the test facility. The bags were cut open to allow the necessary ventilation while the contents of three bags of sand were spread out each time onto 64x64x8cm deep trays prior to placement into a drying oven. A Qualtex forced-convection oven (model OM36SE3D) of 286 litres ($0.286m^3$) internal volume was purchased for the necessary drying process. The sand from the 64x64x8cm trays were then placed onto six smaller 52x38x7cm deep trays which were in turn placed into the oven. Each "batch" of sand took between 12 hours and 14 hours, at an oven temperature of 120°C, for complete drying.

After complete drying, the trays were removed from the oven and the sand sieved to remove the large shelly components present in the "raw" sand. The sand was sieved using a 3/16" (4.75mm) sieve of the BS410/86 sieve sizes. Due to the powdery nature of calcareous sediments, considerable amount of dust was present during the sieving process and protective mask had to be worn at all times. The sieved sand was placed into cylindrical bin containers (38cm diameter by 53cm height) with a total of 55 such containers required to contain the approximately $3.1m^3$ of sand prepared.

Although the "raw" sand was obtained from the same general site in Bass Strait, Australia, two somewhat "different" types of sand were evident from the prepared sand. 20 containers of the prepared sand were of a more powdery type while the rest (35 containers) had a more silica-like colour and less powdery. In order to have a "uniform" sand for the present study, it was decided that the two "different" types of sand be mixed in a certain ratio. The required proportions of both sand types were placed on the covered floor and mixed as thoroughly as possible by using a spade. The "mixing" was carried out solely by the author over a continuous two weeks period. The so-called "uniform" sand thus prepared was stored back into the bin containers.

A number of tests were conducted to obtain the averaged index properties of the "uniform" sand, and are as shown in Table 6.1. The tests (except the carbonate content test) were conducted in accordance with the recommendations of the Australian Standard AS1289 (1977). For the carbonate content test, the "acid-soluble weight loss" method, as described by Chaney *et al.* (1982), was adopted. It may be noted that the index tests were conducted for the 12 sand samples obtained randomly from the 55 containers of sand. Generally, the results vary within ±7% of the averaged values shown in Table 6.1. These averaged values are also found to be consistent with those reported by Poulos (1985) for the Australian Bass Strait calcareous sand deposits. Detailed general characteristics of the Bass Strait calcareous sand are reported in this reference (Poulos, 1985). The grain-size distribution curves of the prepared sand samples were found to vary within the band shown in Fig. 6.28.

6.7 SUMMARY

This chapter has described in detail the design requirements and construction of a large test facility for model pile testing. Some of the problems encountered during the construction of the test facility, in particular those concerned with the hydraulic loading system, are also highlighted and discussed together with the remedial solutions adopted.

The parallel development of other related tasks required for the conduct of a model pile test are also presented. These include the design of the model pile and its related instrumentation, the design of the diaphragm-type stress cells, the preparation of a large volume of calcareous sand for the present facility, and the computer control programs required for data acquisition and loading application.

Table 6.1 Some relevant properties of the calcareous soil utilised in the present study

Minimum density	12.06 kN/m^3
Maximum density	14.48 kN/m^3
Specific gravity	2.69
Carbonate content	70.0 %
ϕ_p (R.D. = 48%)*	45°

ϕ_p = peak friction angle

R.D. = relative density

* Al-Douri (1991)

Plate 6.1 A view of the model pile test facility

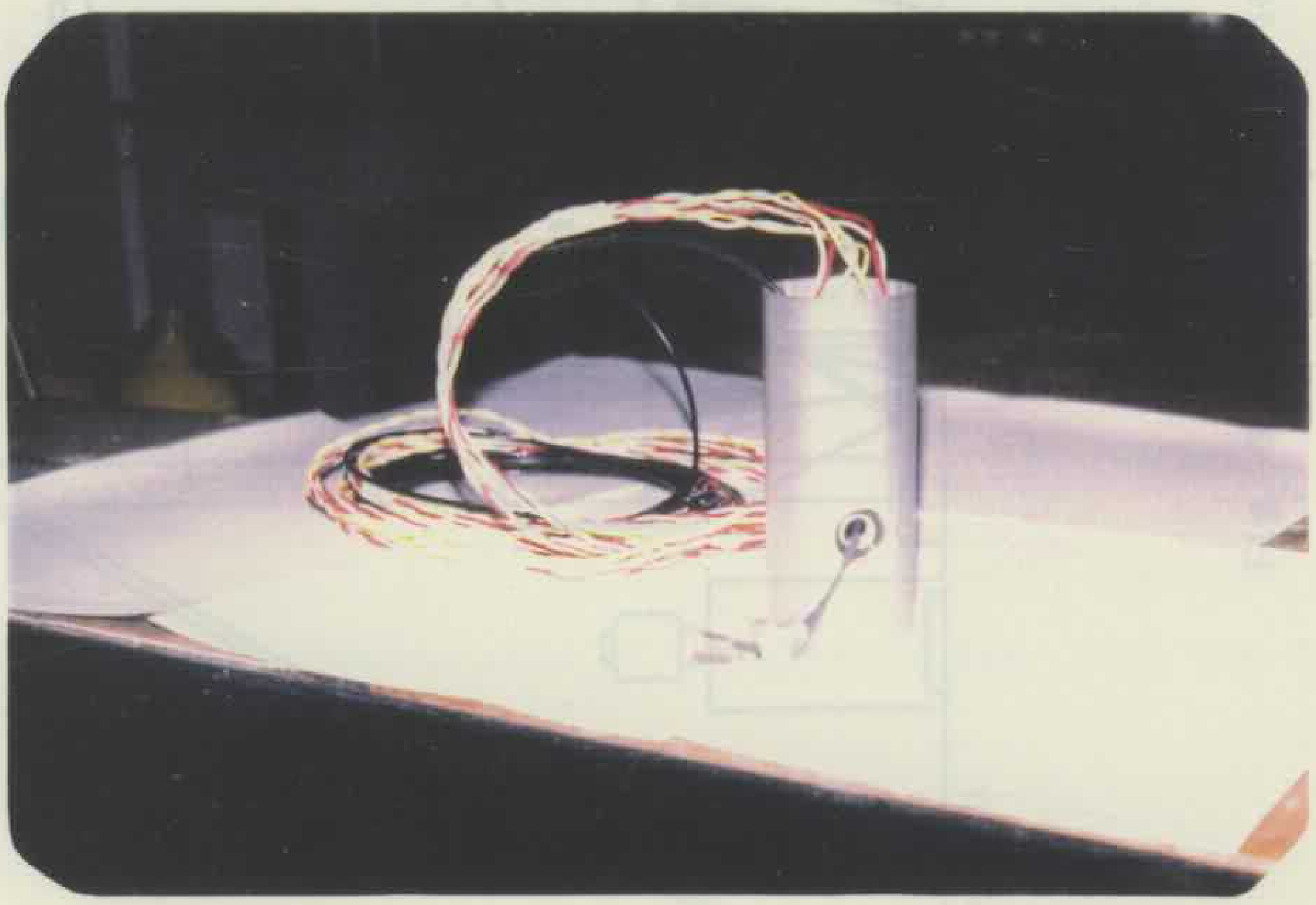

Plate 6.2 50mm diameter instrumented segment showing the miniature pore-pressure transducer

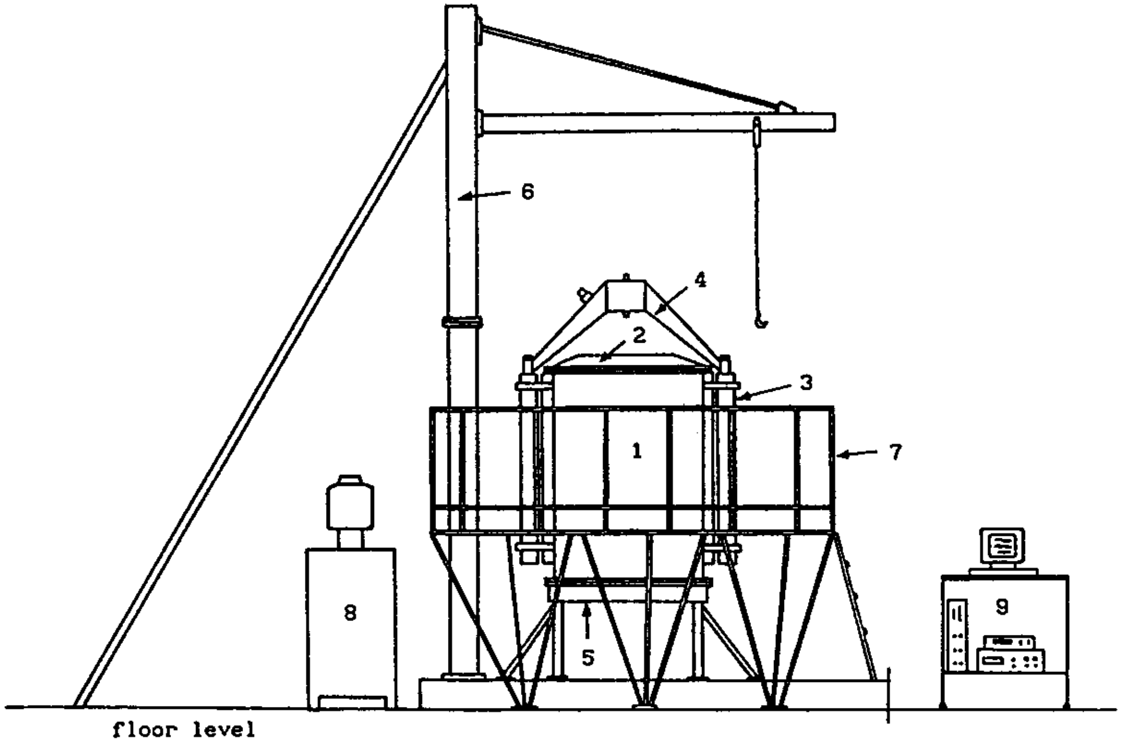

1 test chamber
2 top lid
3 side ram
4 crosshead
5 pedestal
6 gantry crane
7 working platform
8 hydraulic pump
9 data acquisition system
10 locking-pin*
11 discharge box*
12 couplings for model pile*
13 pile "penetrometer"*

* not shown on figure

Fig. 6.1(a) A schematic view of the model pile test facility

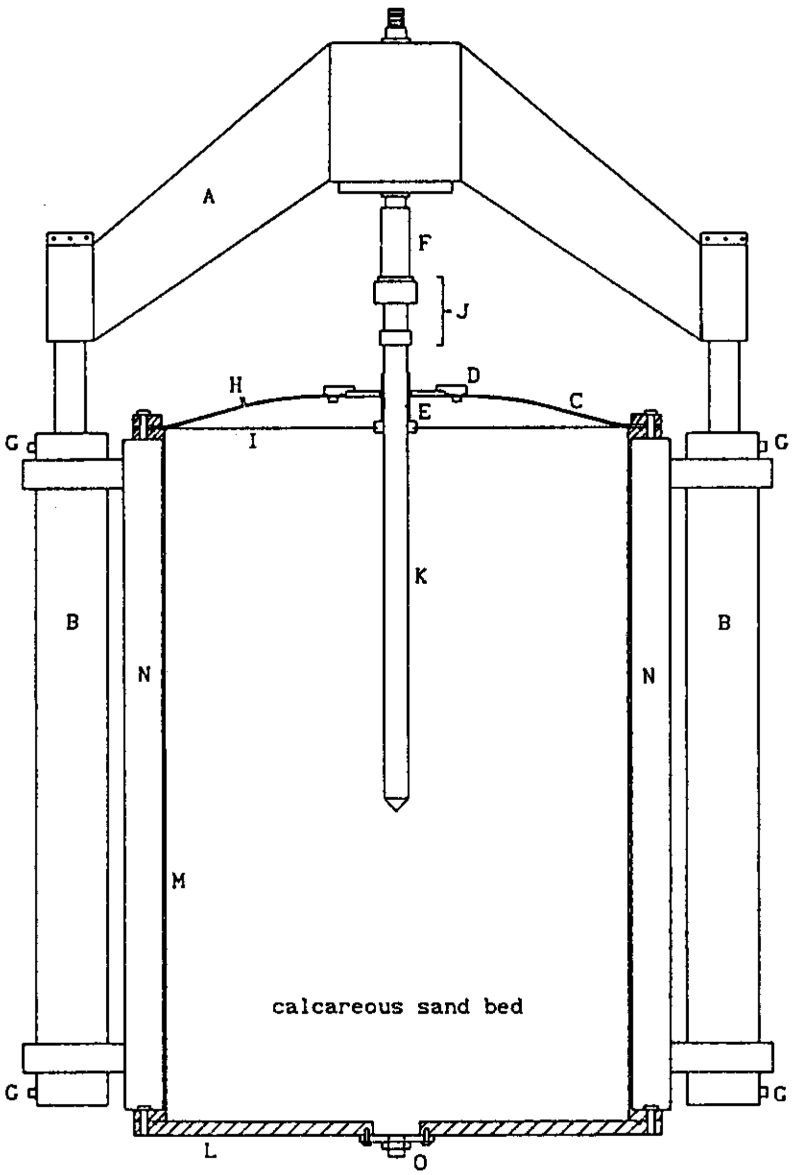

A crosshead of test facility
B hydraulic side rams
C top lid
D fixed collar on top lid
E sliding collar
F "HSI" load cell
G hydraulic inlet/outlet ports of side rams
H air pressure inlet
I rubber membrane
J couplings for model pile
K instrumented model pile
L base plate of test chamber
M side wall of test chamber
N channel for attaching side rams
O "shutter" unit on base plate

Fig. 6.1(b) A schematic view of the test chamber with the model pile in place

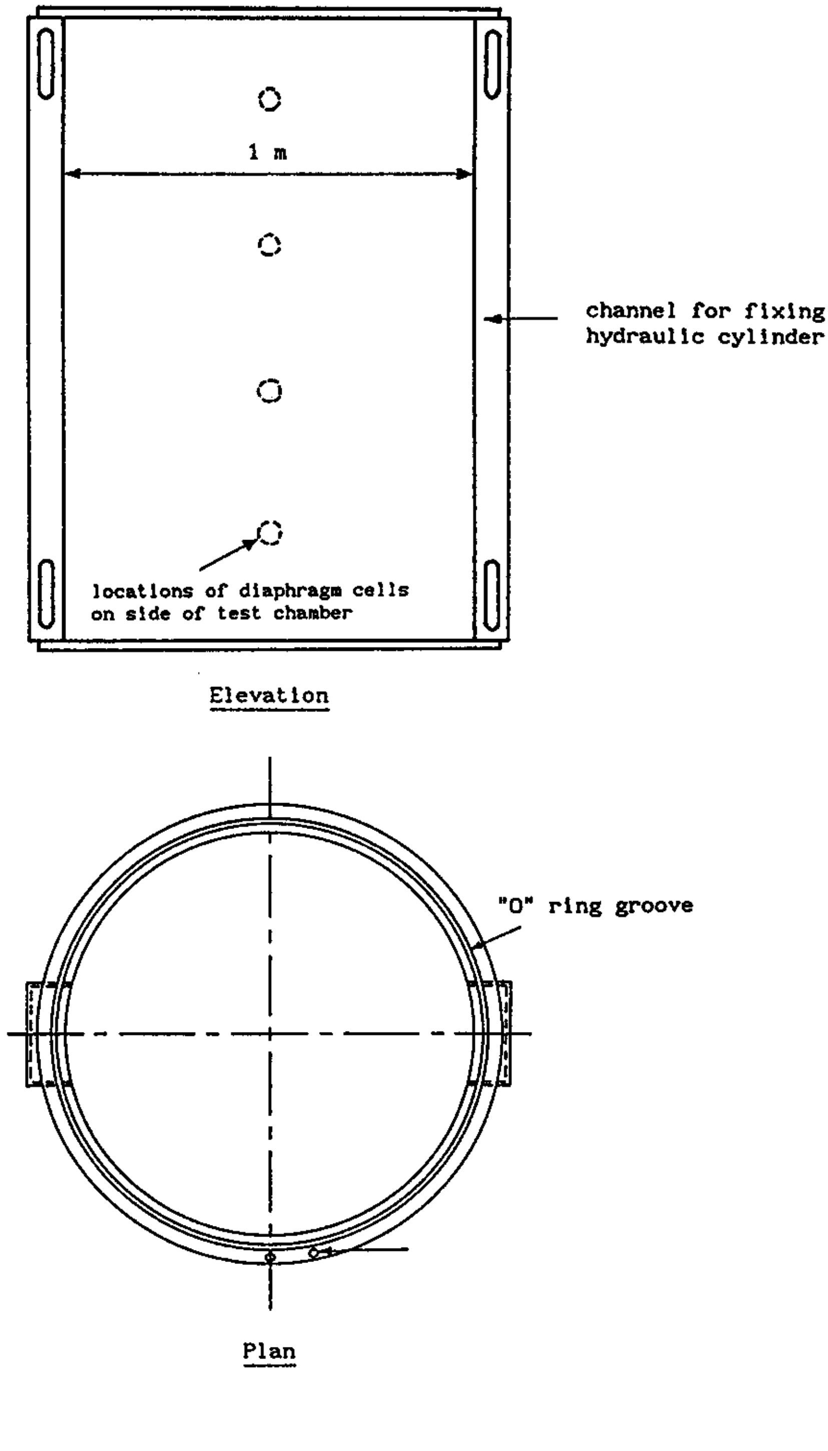

Fig. 6.2(a) Test chamber showing locations of diaphragm stress cells

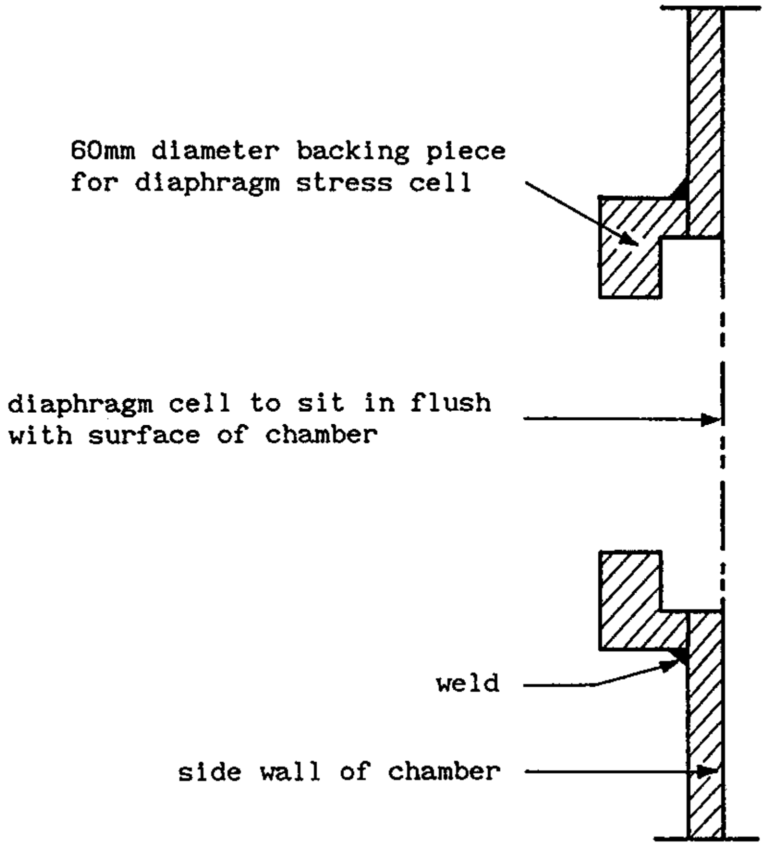

Fig. 6.2(b) Attachment details for diaphragm cells on test chamber

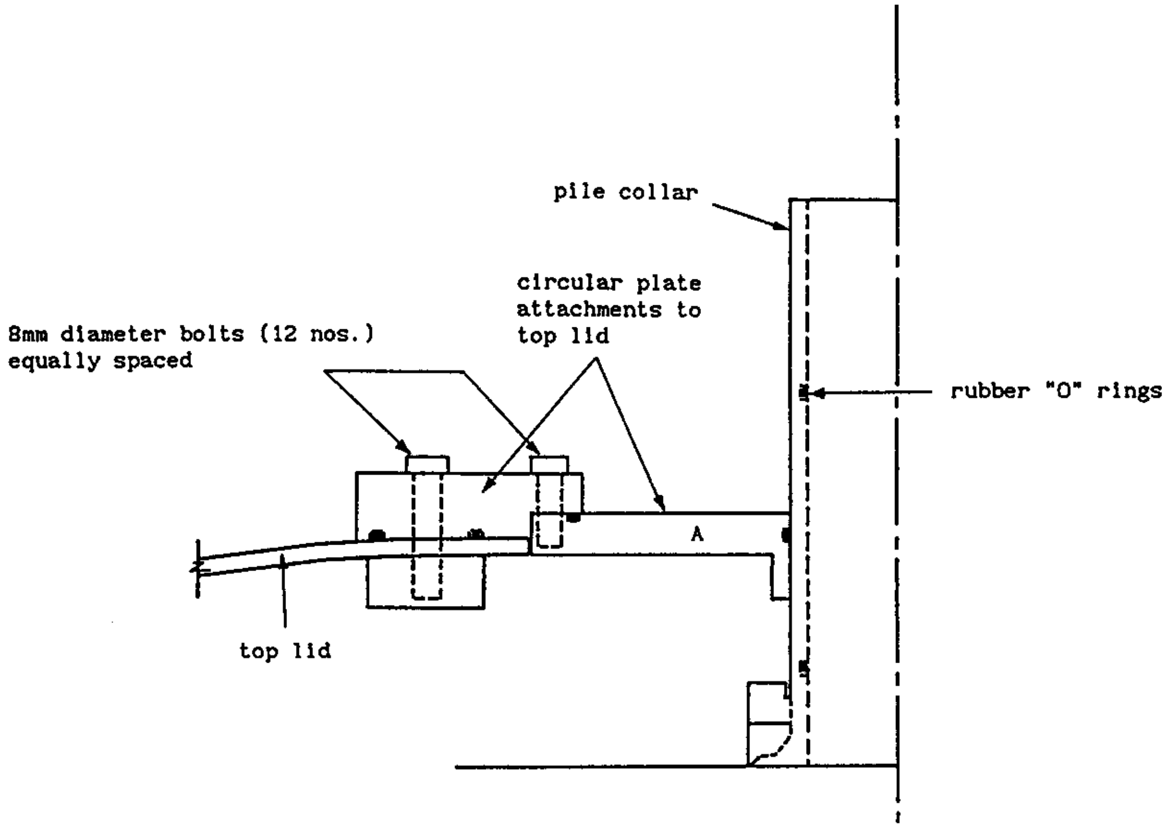

(a)

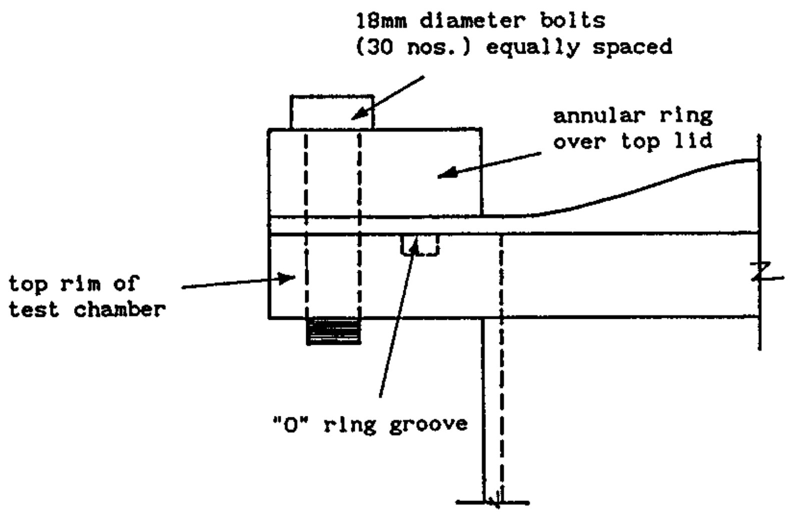

(b)

Fig. 6.3 (a) Details of fixed pile guide collar attachment to top lid; (b) details of top lid attachment to test chamber

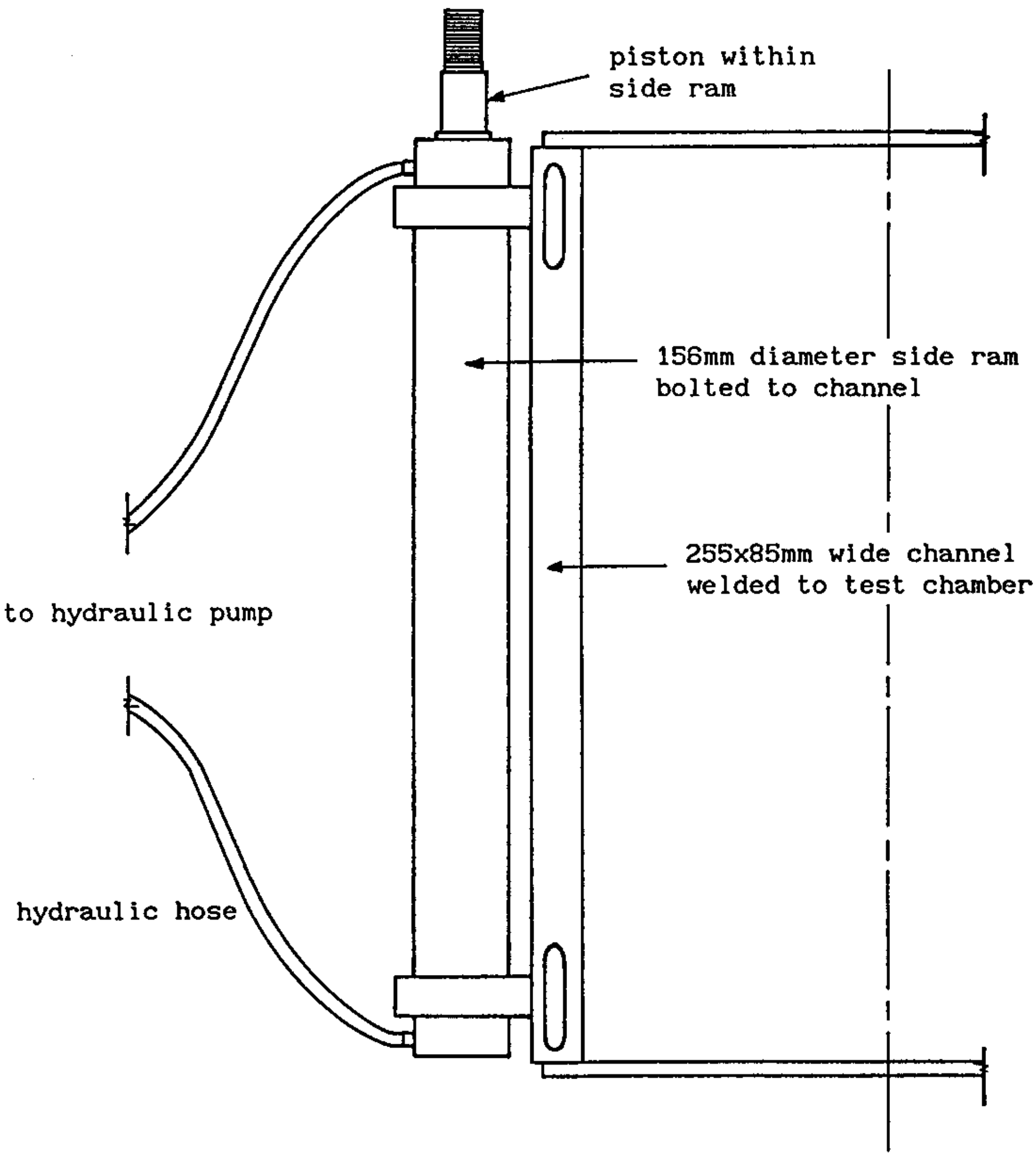

Fig. 6.4 Hydraulic ram attachment to the test chamber

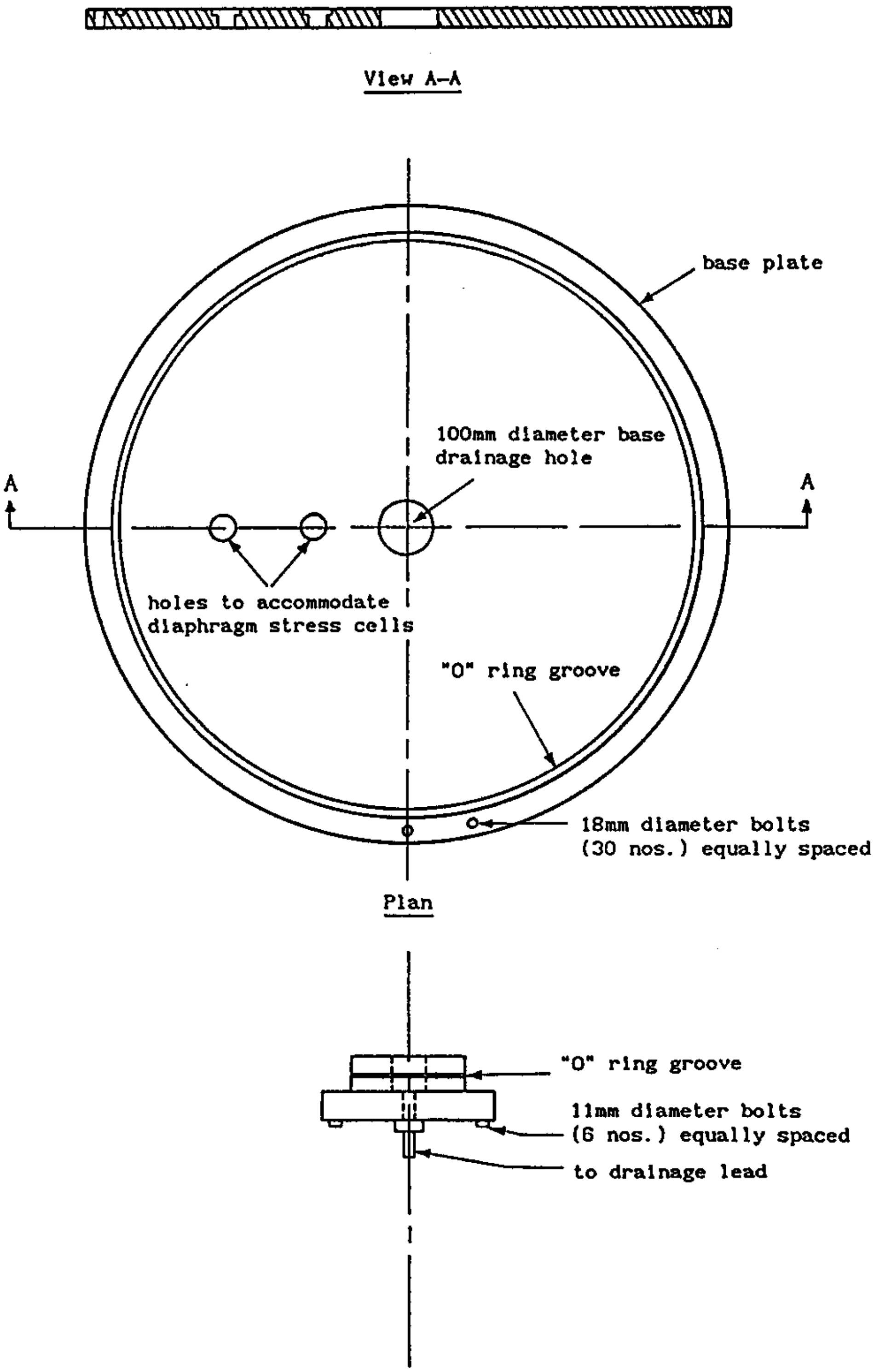

Fig. 6.5(a) Details of base plate showing locations of diaphragm cells, drainage outlet and drainage fitting

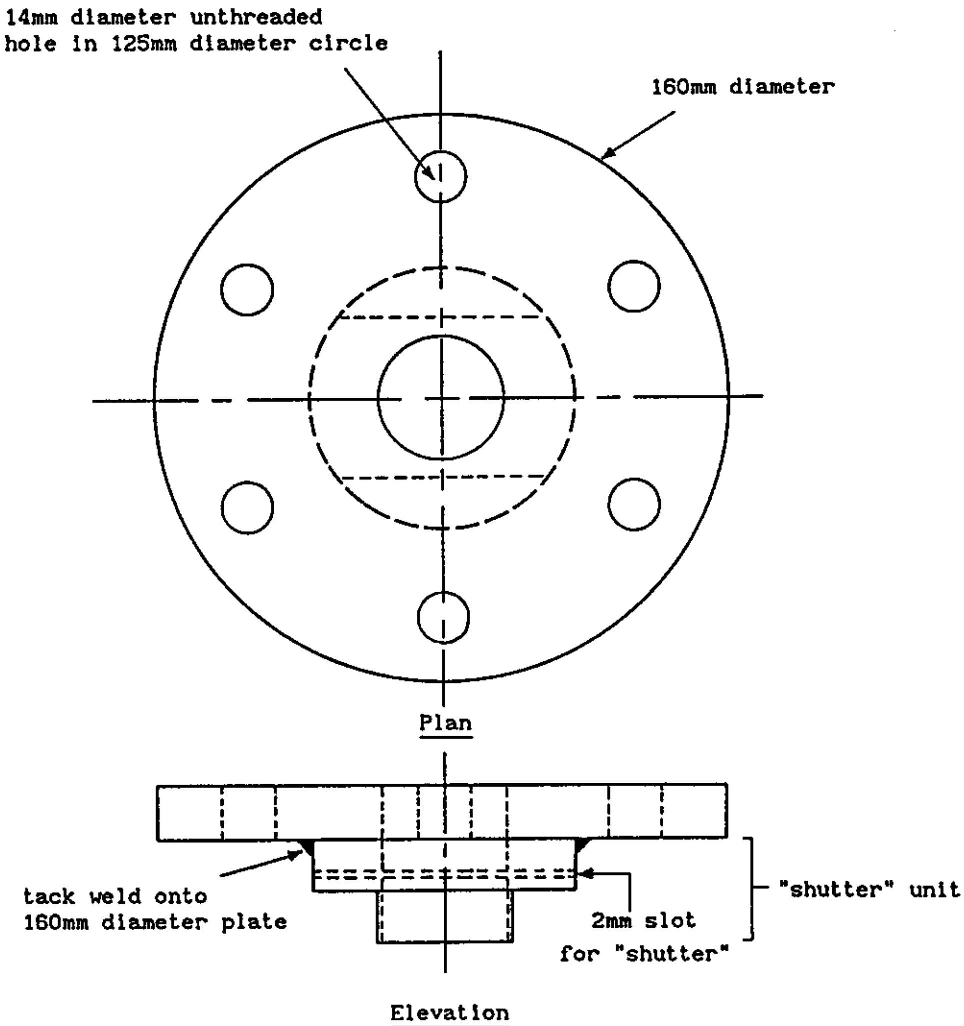

Fig. 6.5(b) Details of "shutter" unit attachment to base plate for sand discharge in the case of dry tests

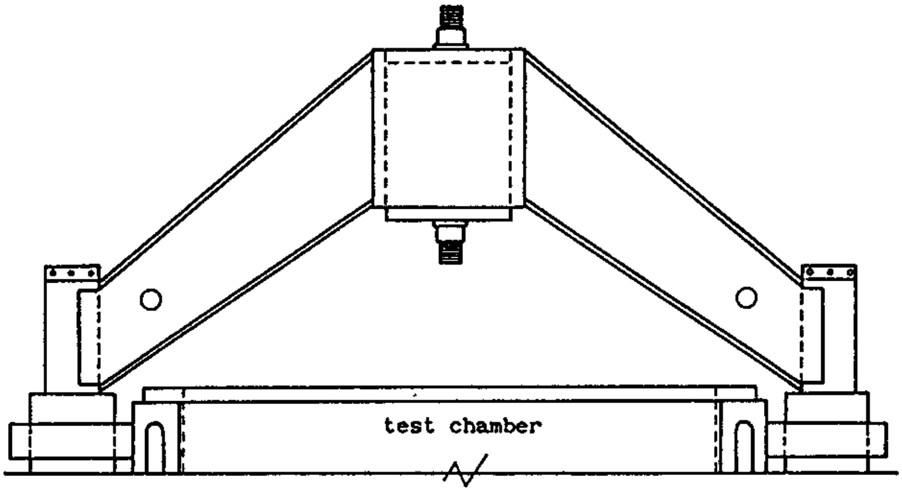

Elevation

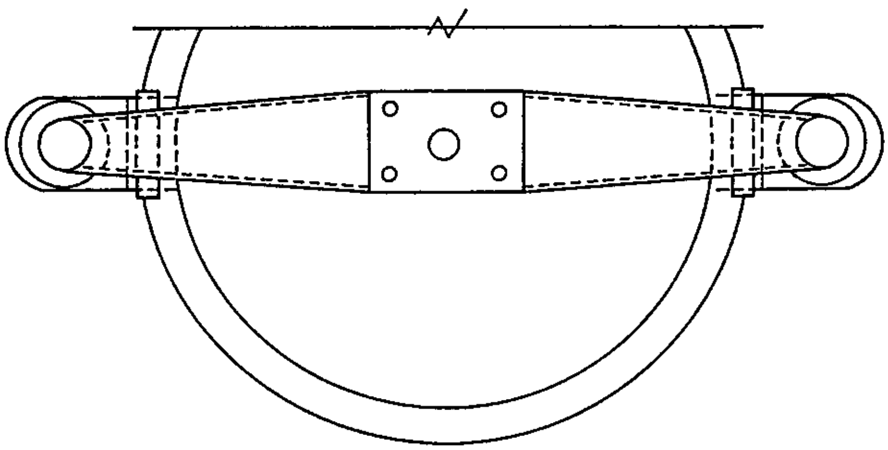

Plan

Fig. 6.6 Crosshead details of test facility showing attachment to the hydraulic side rams

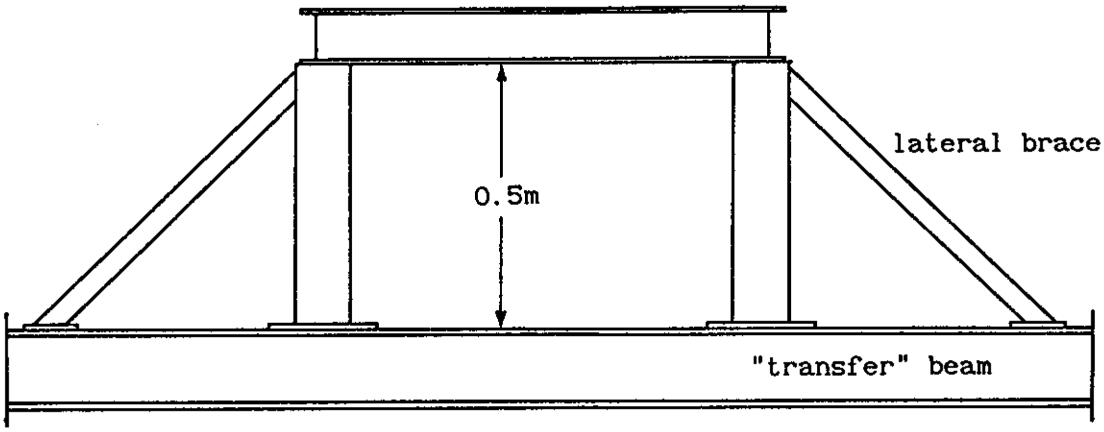

Elevation

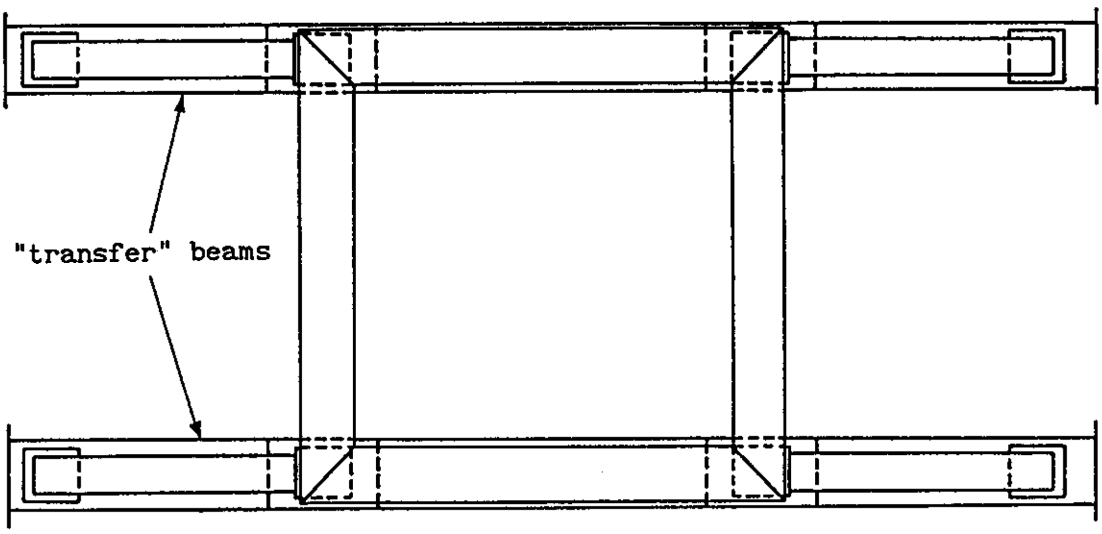

Plan

Fig. 6.7 Details of base support pedestal for the test chamber

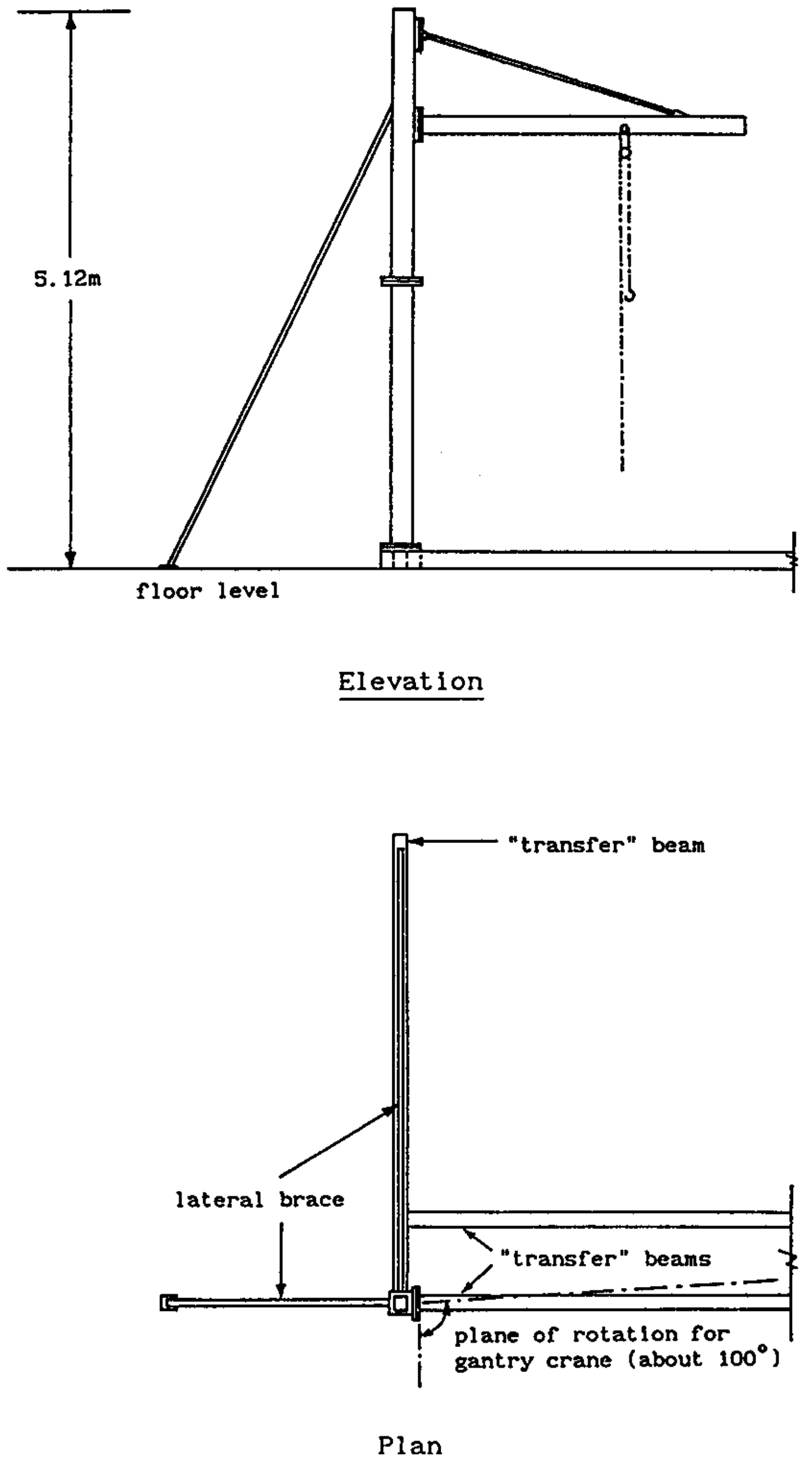

Fig. 6.8 Schematic view of gantry-crane for test facility

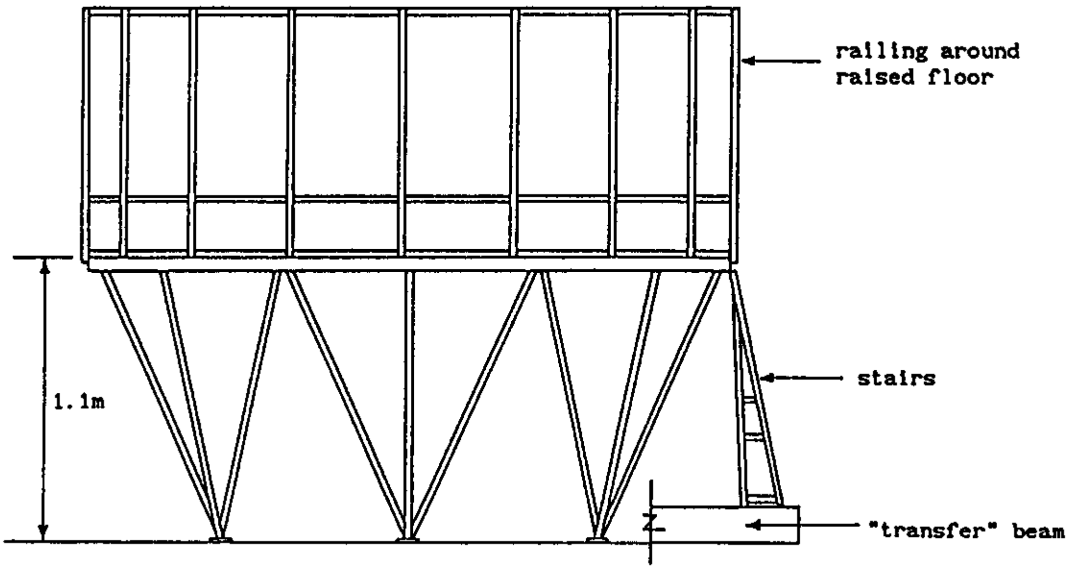

Elevation

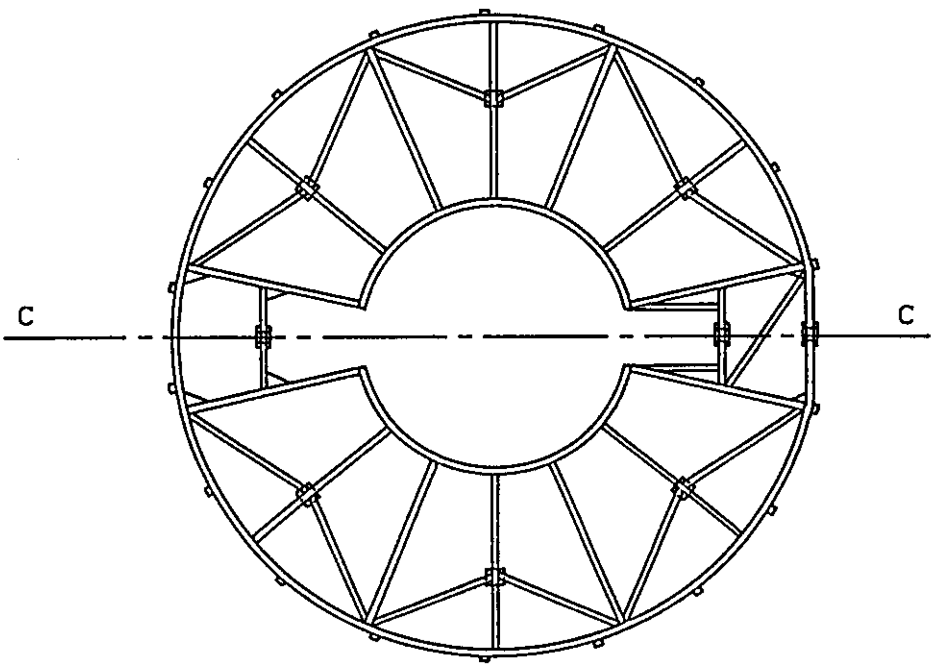

"Skeletal" Plan of raised floor

Fig. 6.9 Details of elevated working platform around test chamber

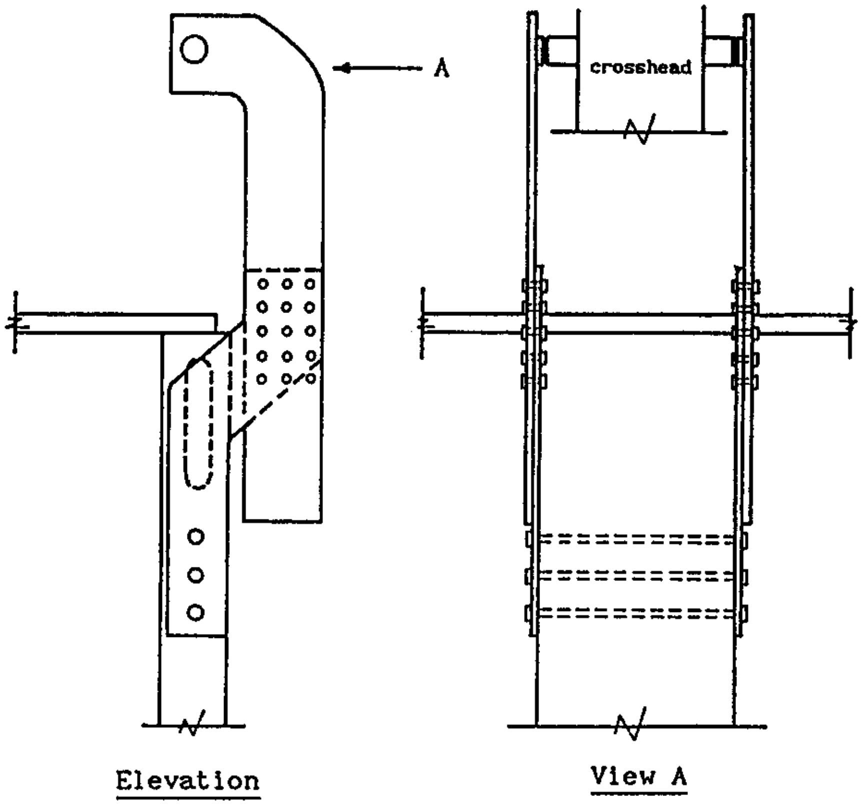

Fig. 6.10 Attachment details for "locking" of the crosshead

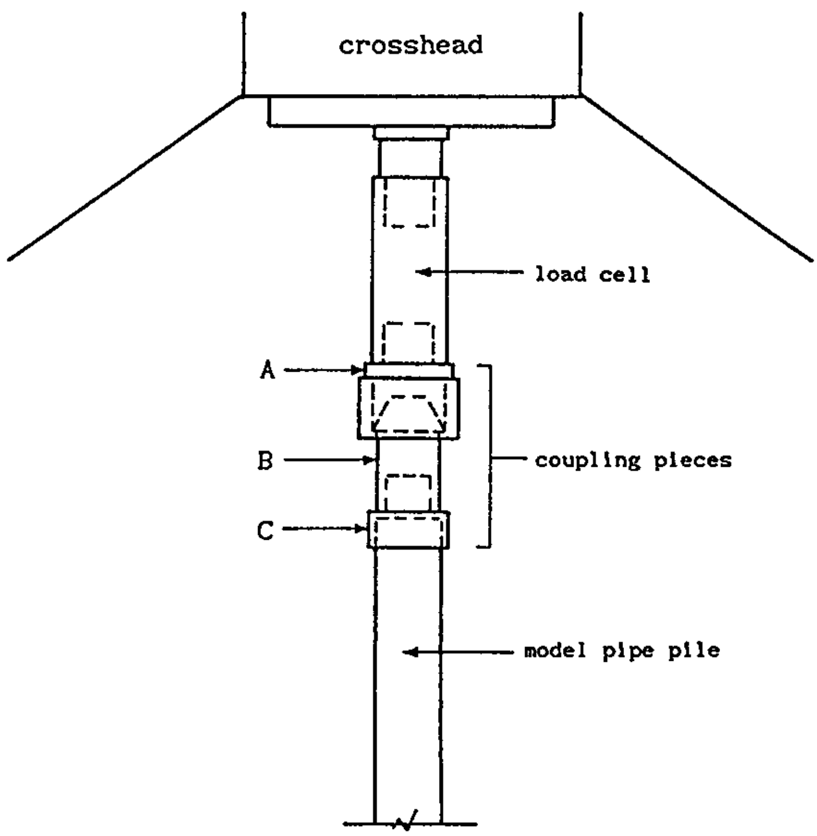

Fig. 6.11 Details of model pile attachment to the central crosshead servo-controlled hydraulic jack

Note: A similar smaller box (380mm sides) with "roller" legs was also fabricated to facilitate placement of sand into the test chamber

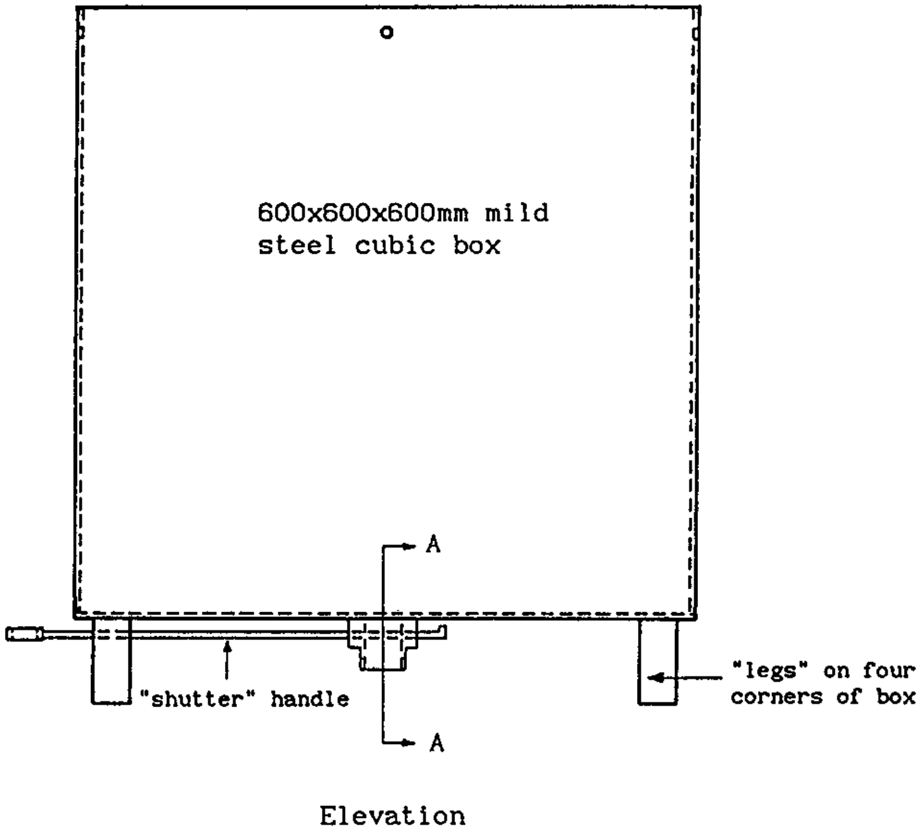

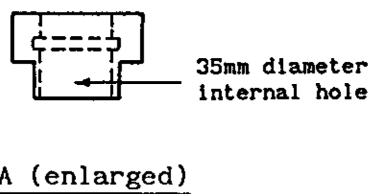

Fig. 6.12 Discharge-box utilised for the sand placement task

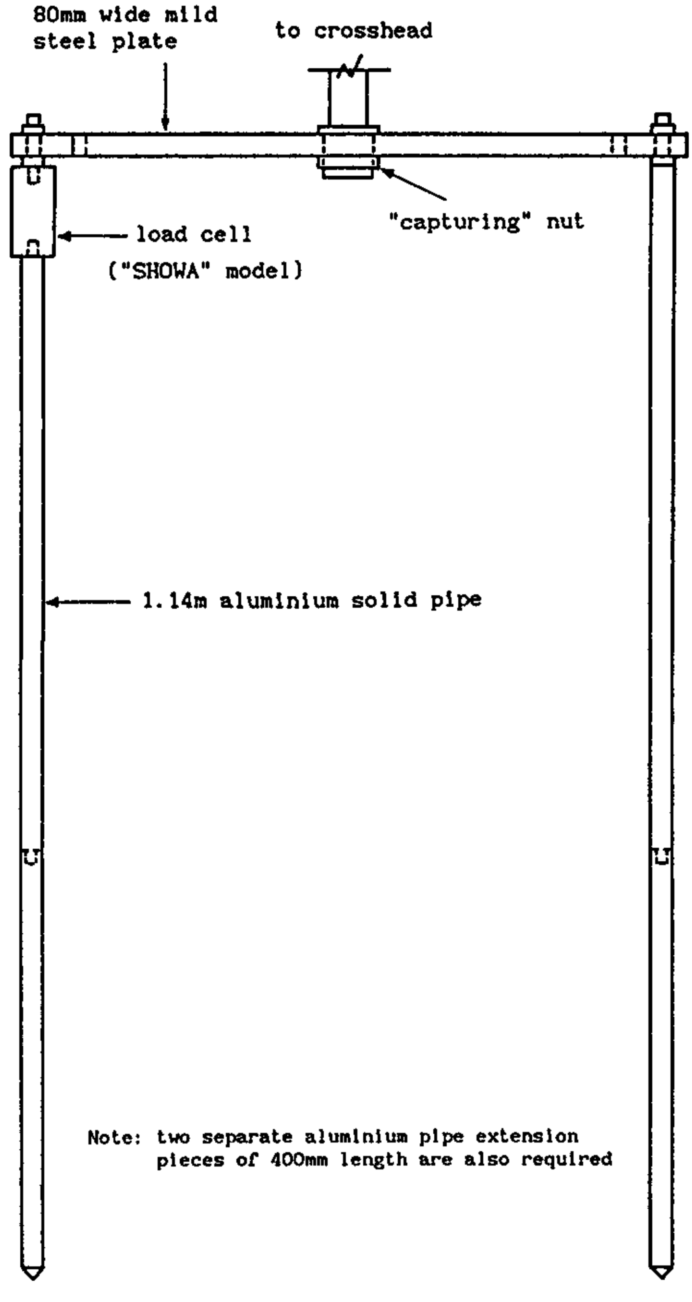

Fig. 6.13 Details of pile "penetrometer" attachment to the central hydraulic jack on crosshead

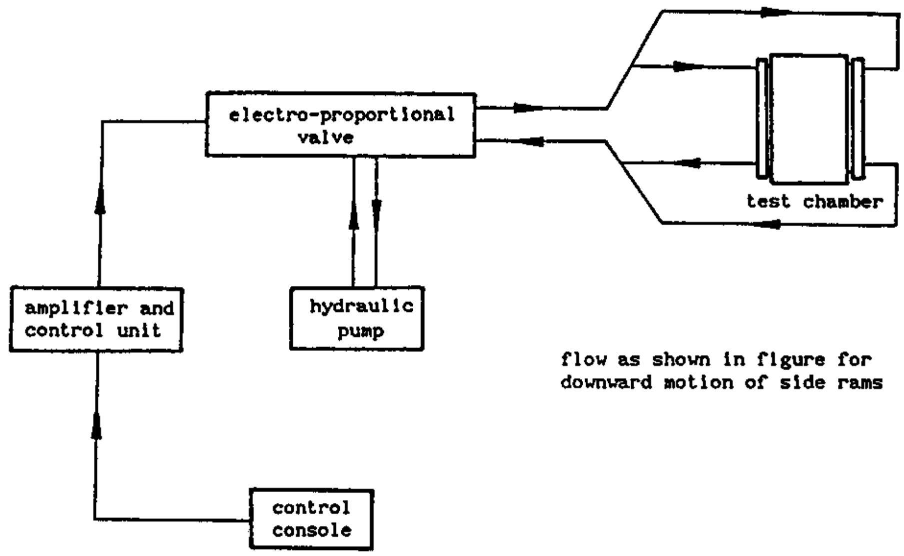

Fig. 6.14 "Flow-loop" of control system for both side rams of test facility

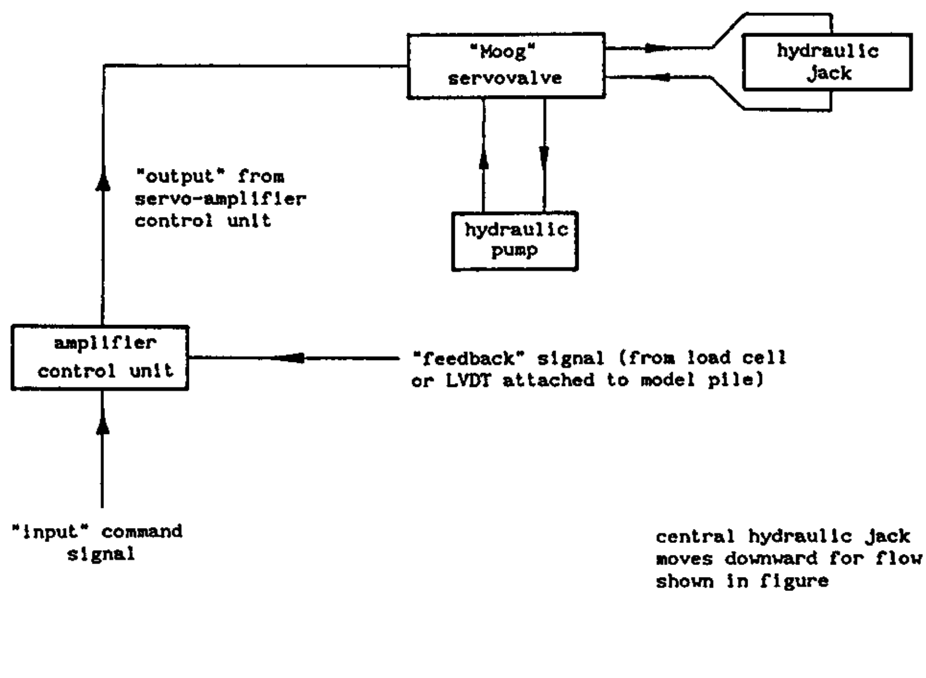

Fig. 6.15 "Flow-loop" of control system for the central servo-controlled hydraulic jack

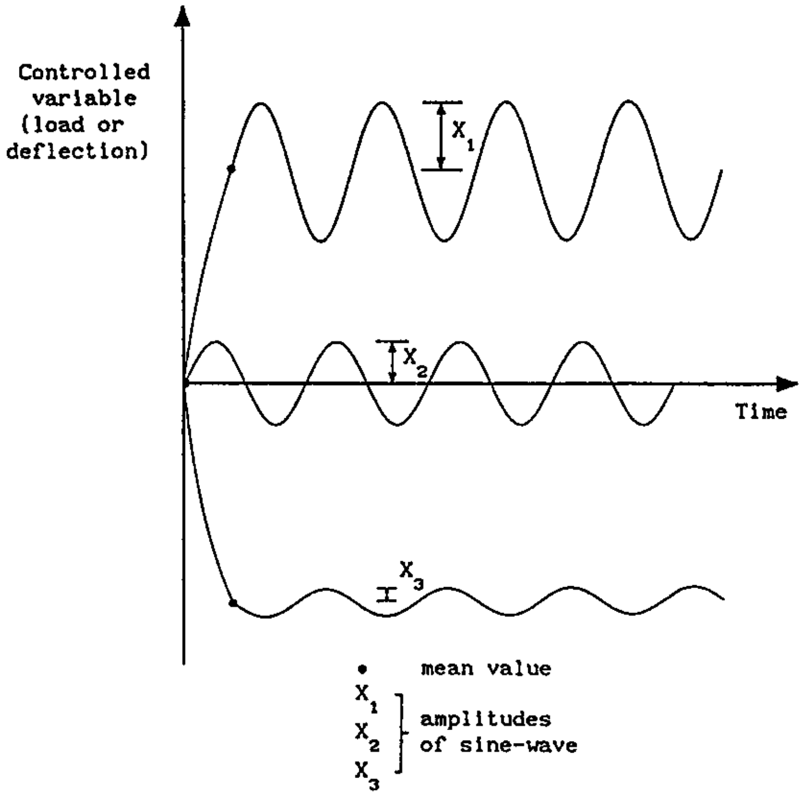

Fig. 6.16(a) Tests under a controlled variable with different mean values and cyclic amplitudes

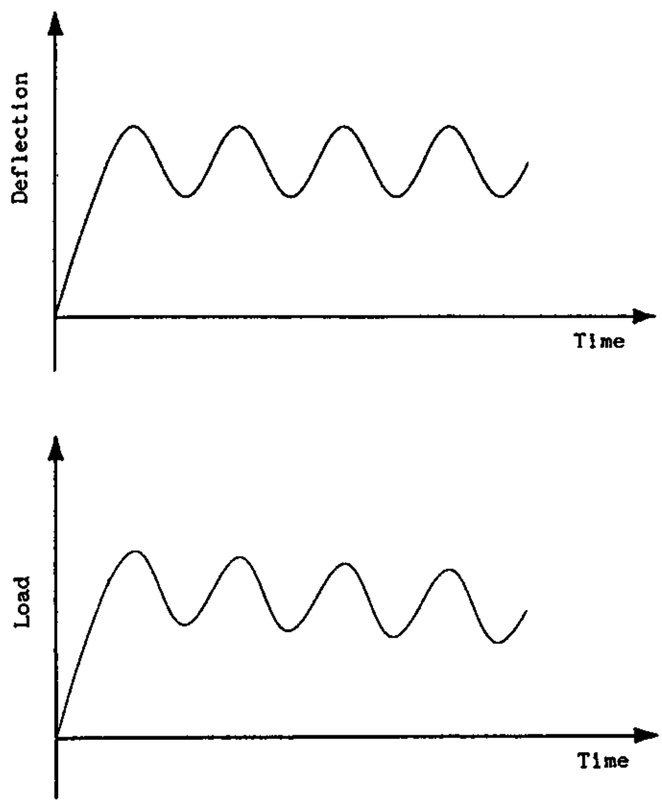

Fig. 6.16(b) Expected load variation during deflection-controlled test

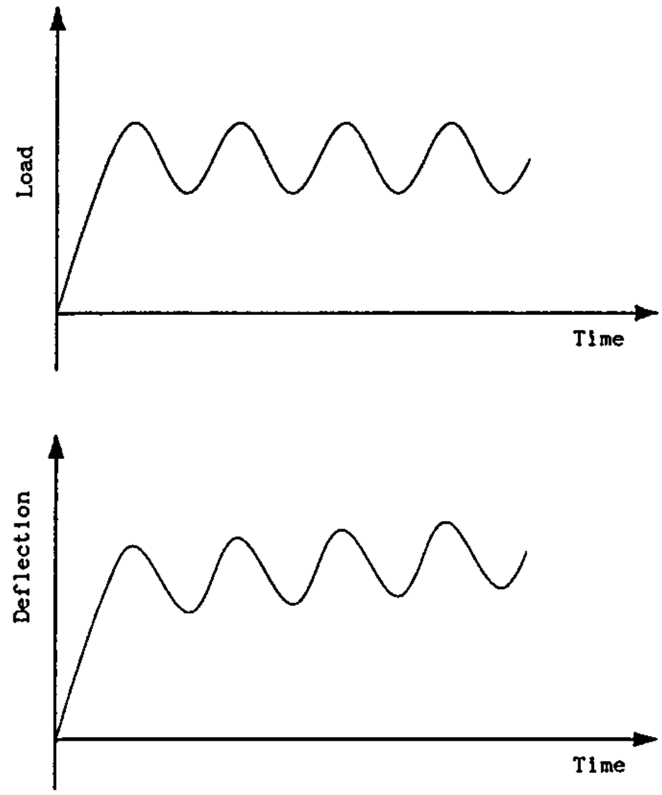

Fig. 6.16(c) Expected deflection variation during load-controlled test

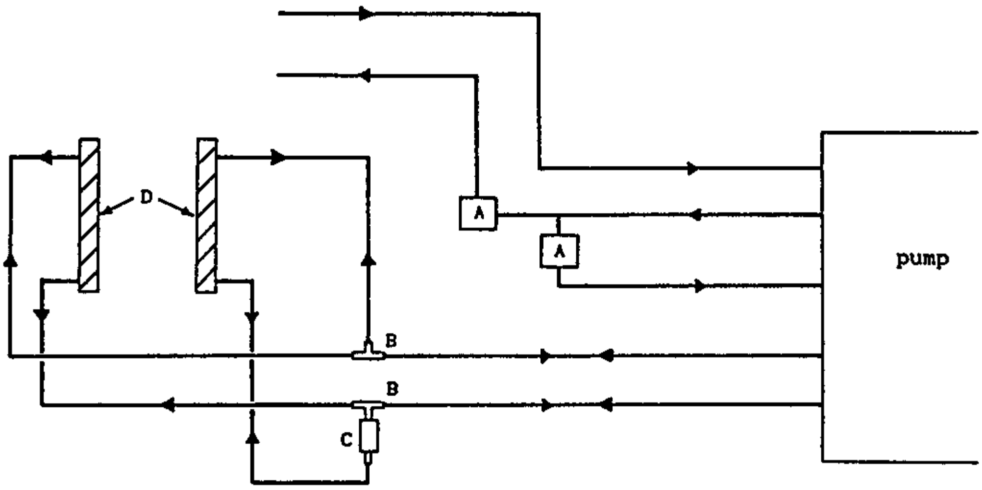

A solenoid valves

B "T" joint

C flow-control valve

D side rams of test chamber

Fig. 6.17 Piping details of the test facility

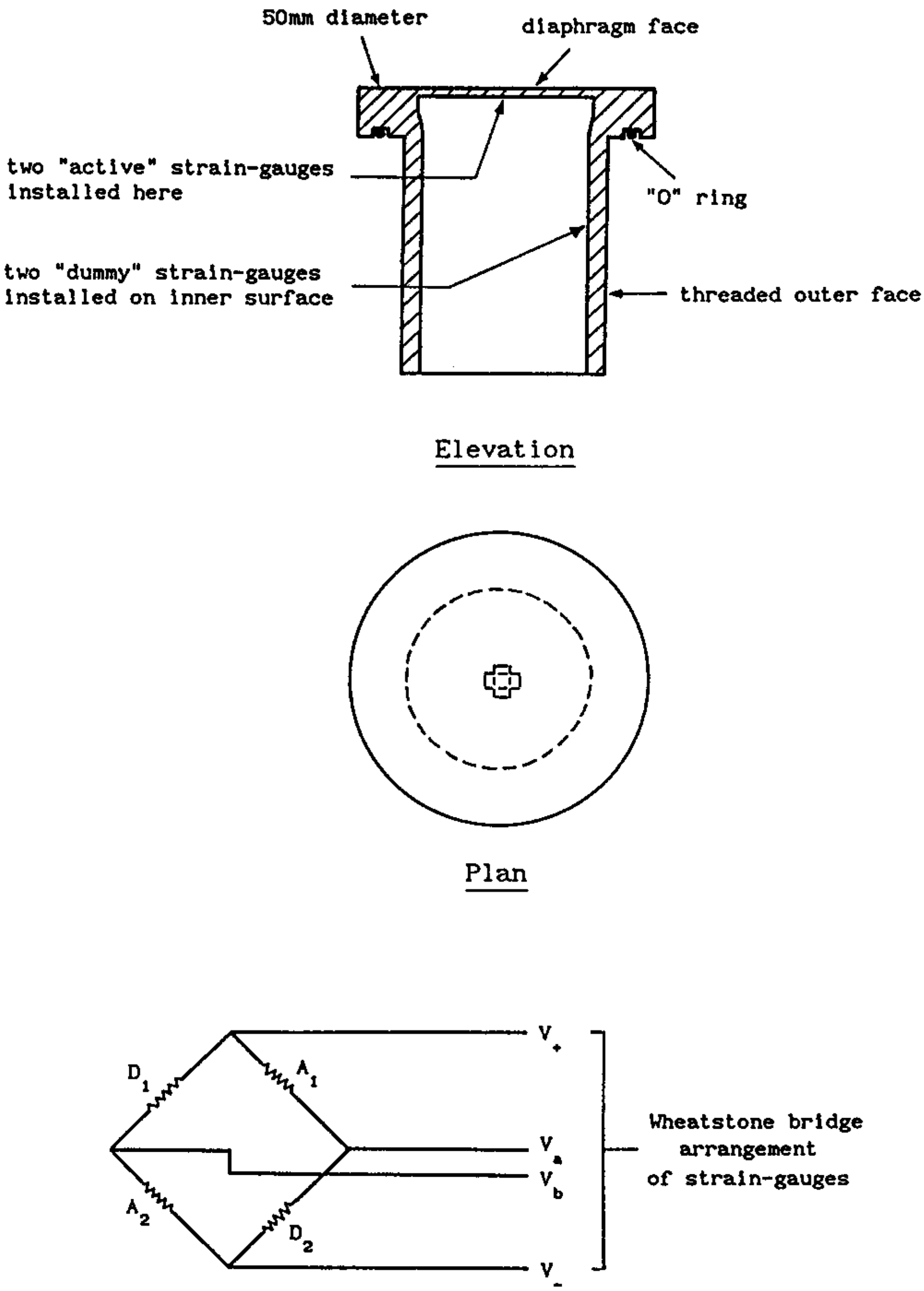

D_1, D_2 = "dummy" gauges

A_1, A_2 = "active" gauges

V_+, V_- = excitation voltage

V_a, V_b = output response voltage

Fig. 6.18 Schematic view of diaphragm stress cell showing strain-gauges arrangement

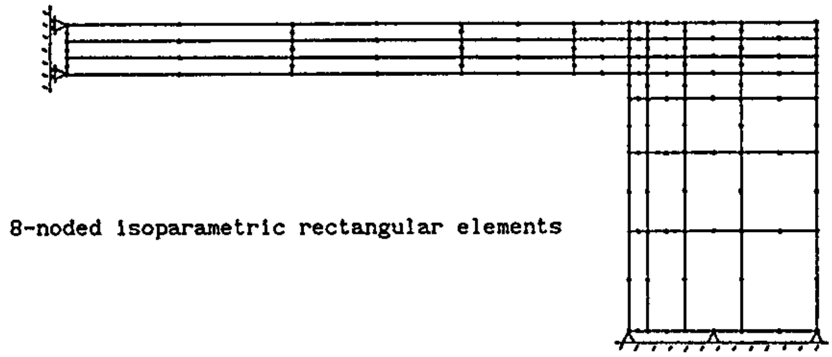

Fig. 6.19 Axisymmetric finite element mesh of diaphragm stress cell

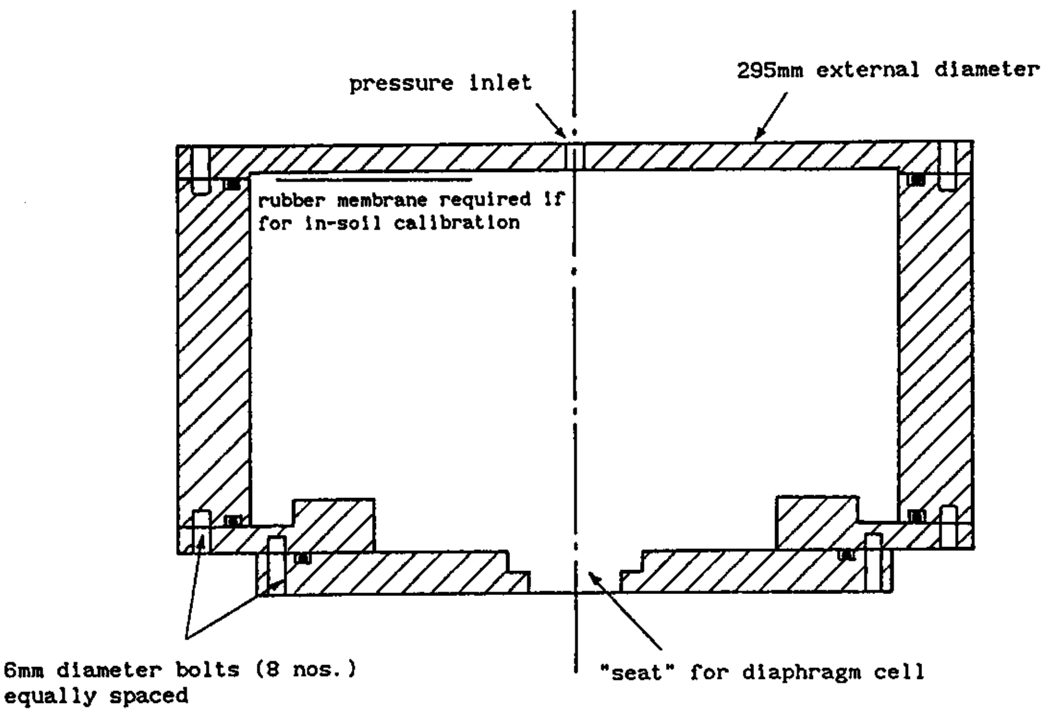

Fig. 6.20 Details of small calibration chamber for calibration of diaphragm stress cells

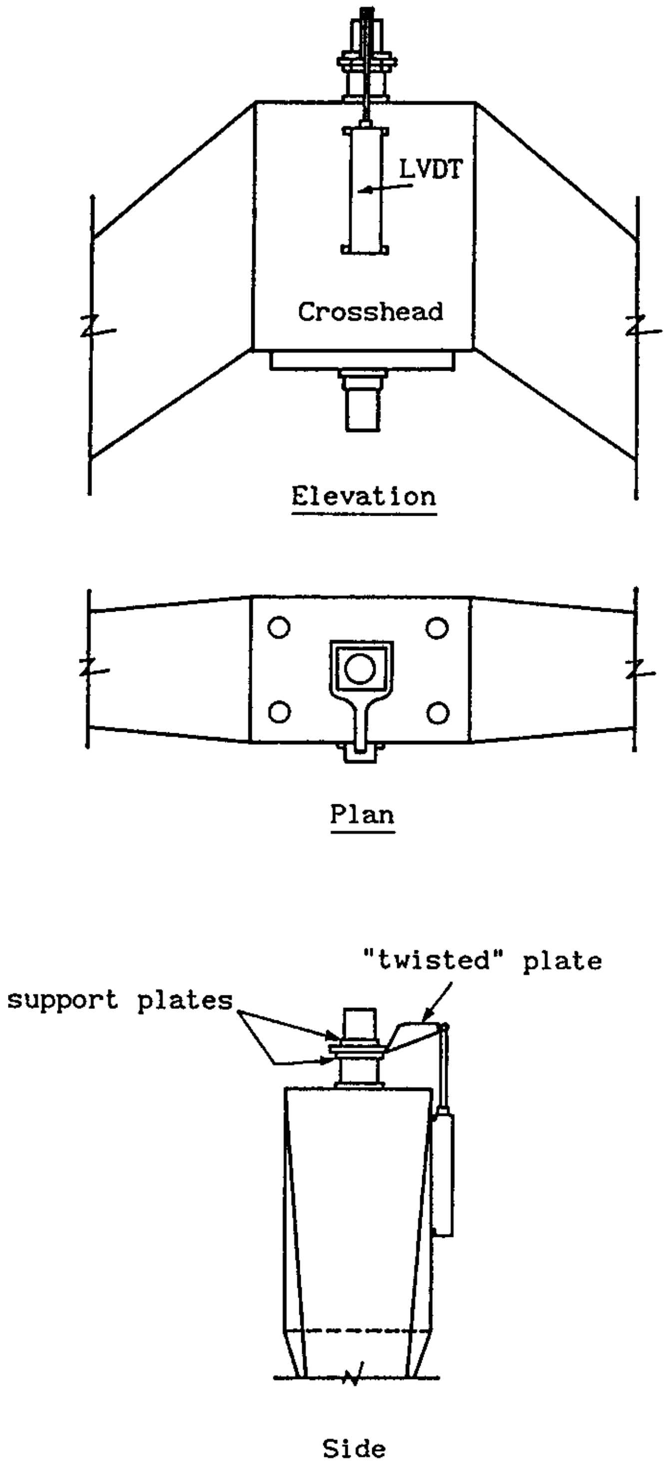

Fig. 6.21 Details of displacement transducer attachment to the central hydraulic jack on crosshead

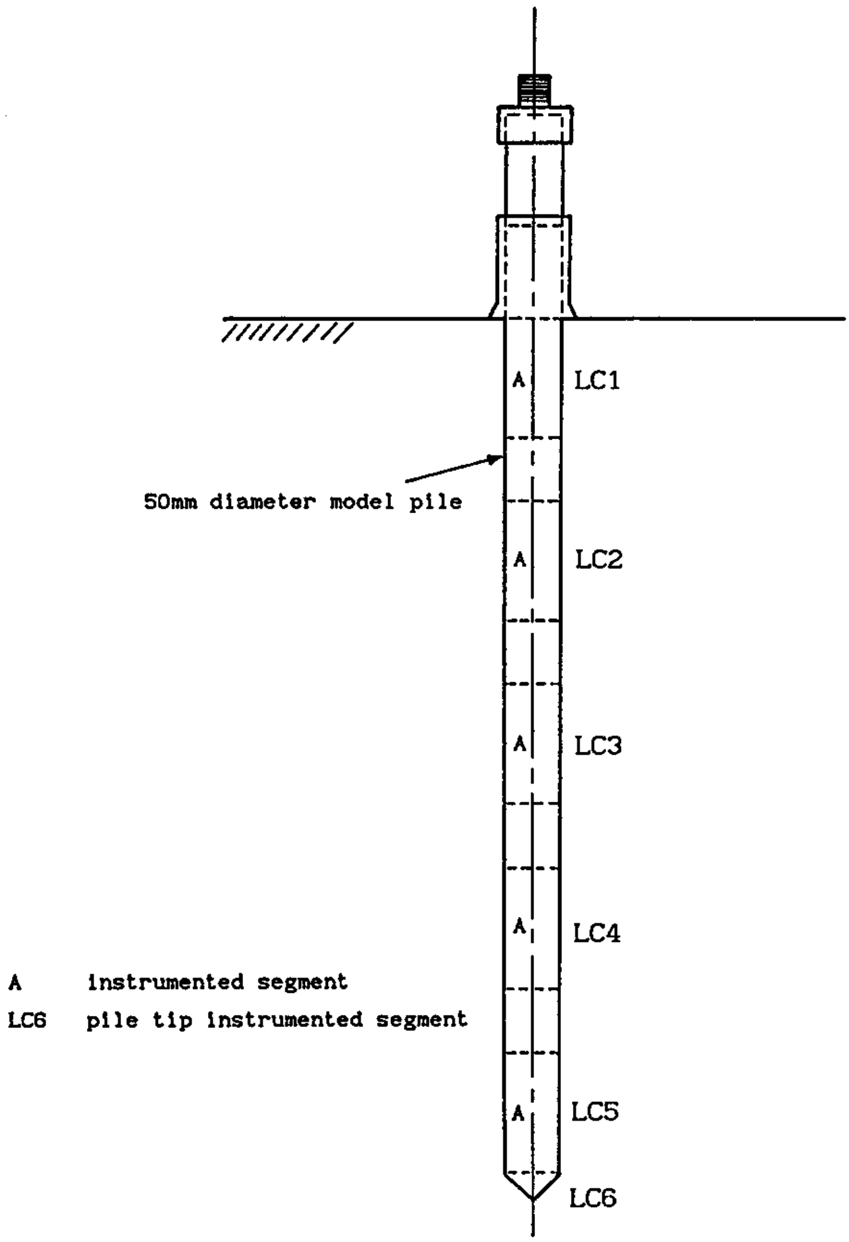

Fig. 6.22 Schematic view of instrumented model pile showing numbering of the instrumented segments

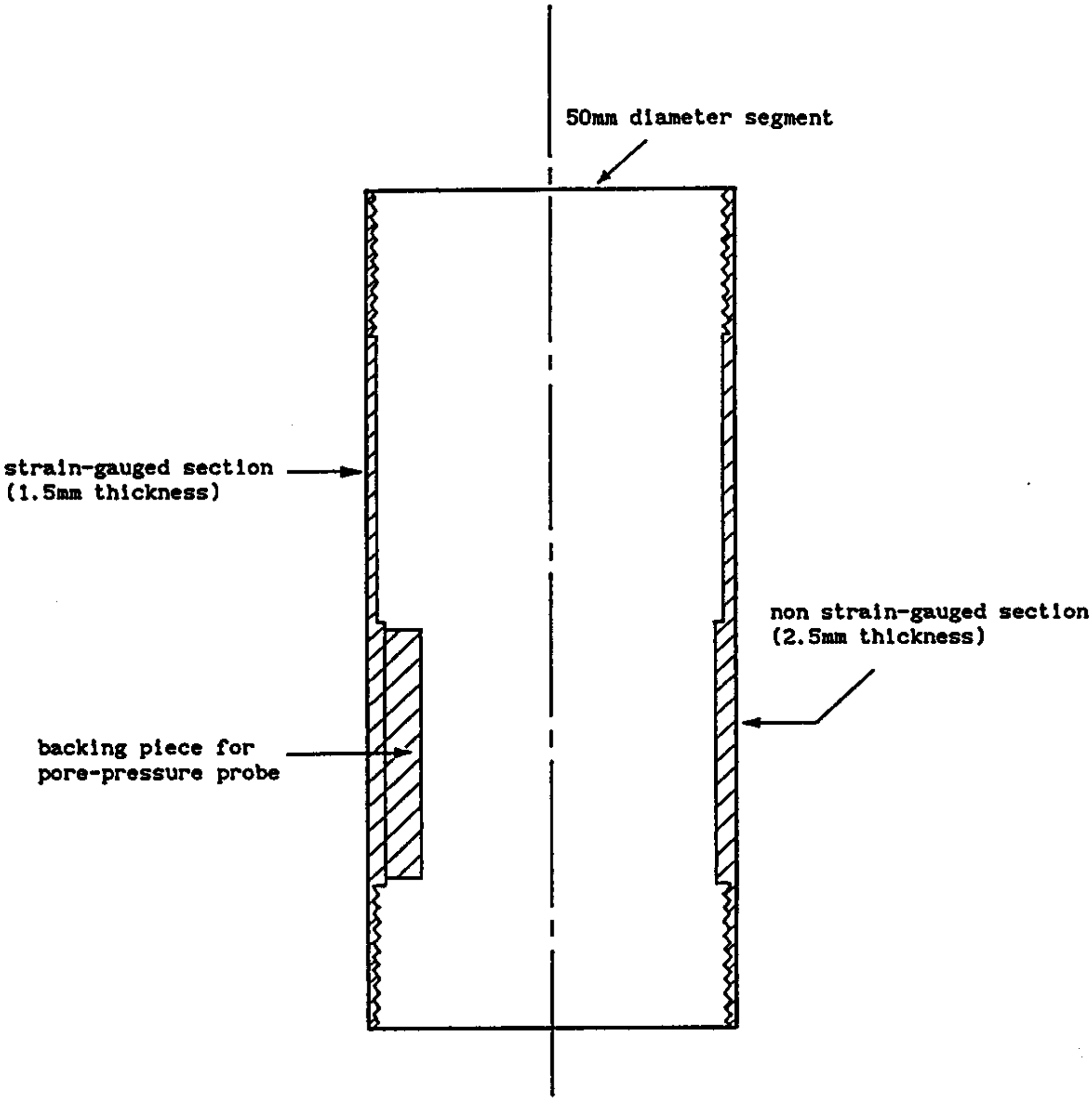

Fig. 6.23 Details of instrumented segment of model pile

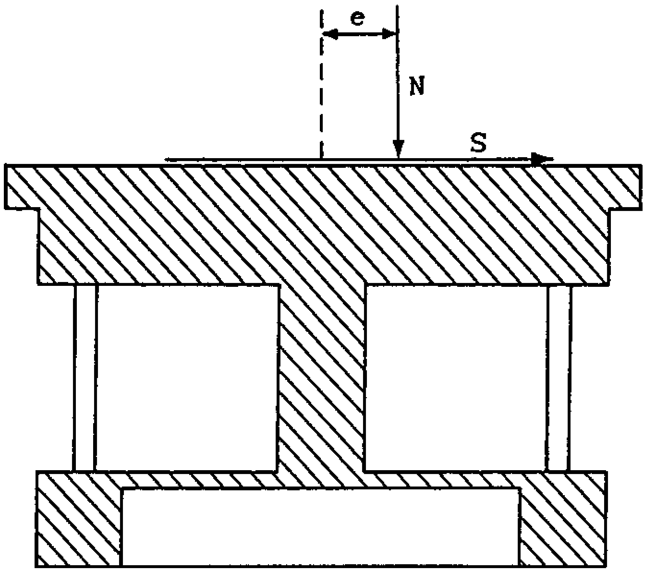

Fig. 6.24 Cross-section of Arthur and Roscoe (1961) transducer showing normal load (N), shear load (S) and eccentricity (e) of axial load

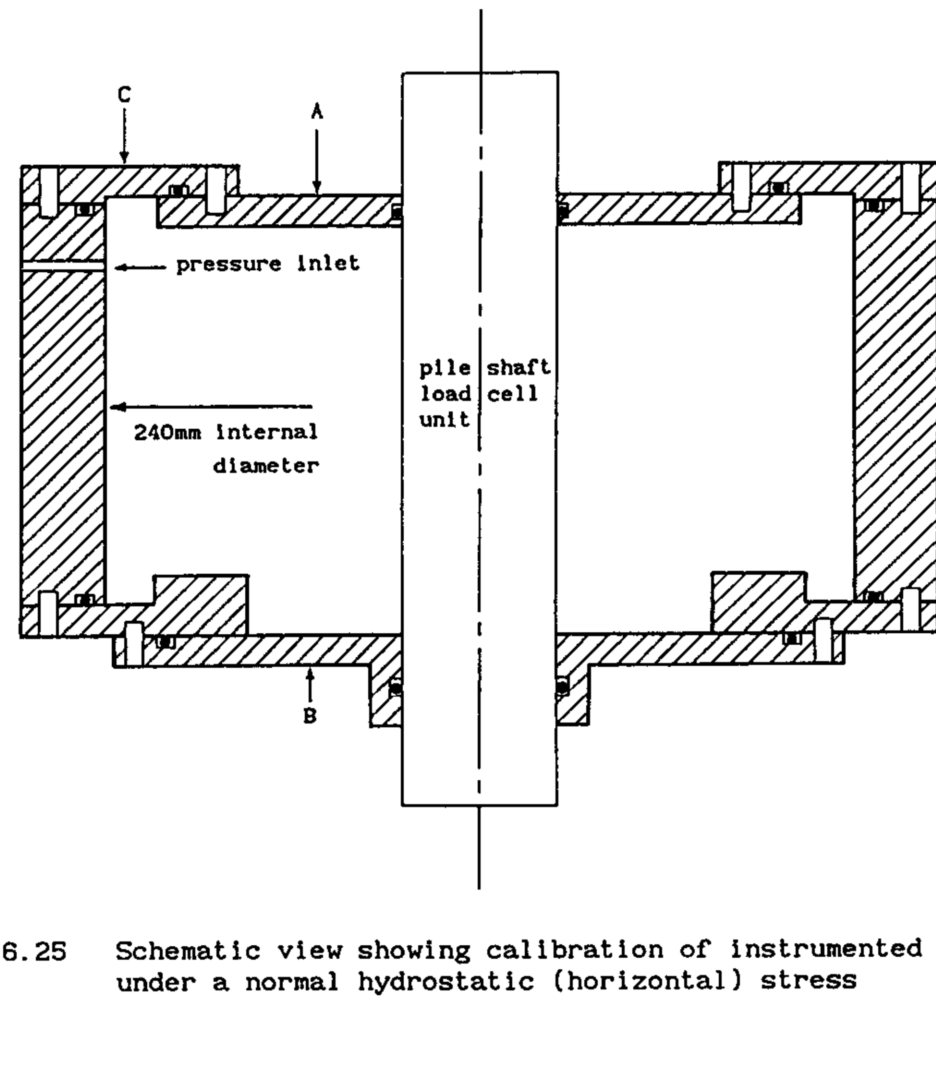

Fig. 6.25 Schematic view showing calibration of instrumented segment under a normal hydrostatic (horizontal) stress

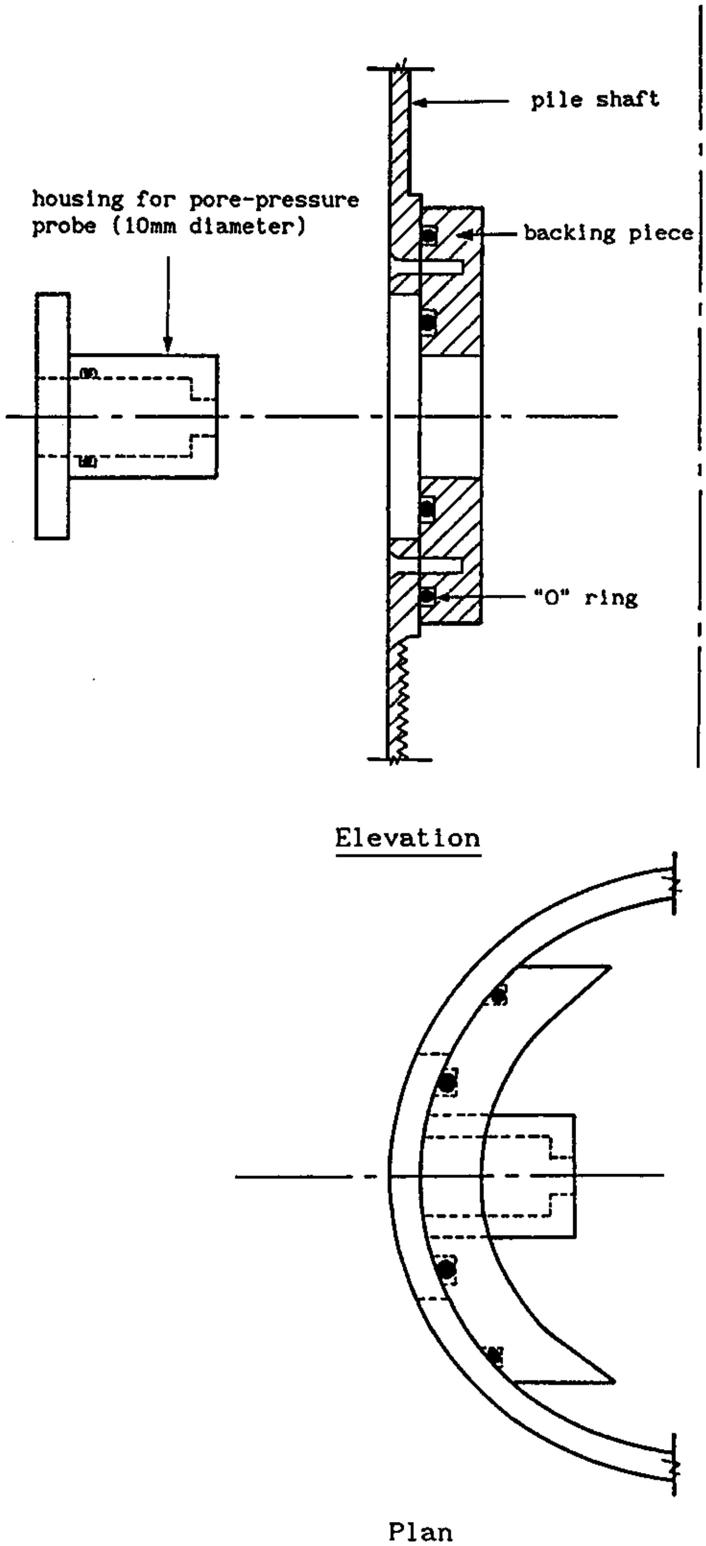

Fig. 6.26 Details of miniature pore-water pressure transducer attachment to instrumented segment of model pile shaft

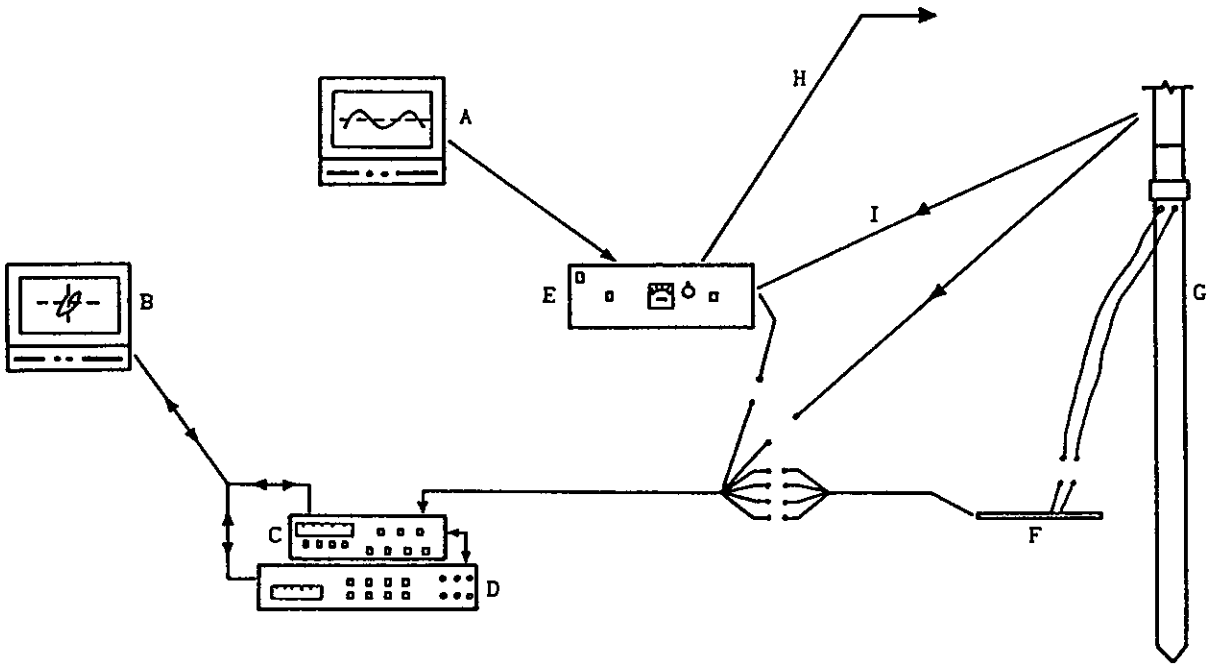

A microcomputer for generating input command signal

B microcomputer for data acquisition and graphic display

C HP 3488A switch/control unit

D HP 3458A multimeter

E "Moog" control box

F "dummy" strain-gauges

G model instrumented pile

H command signal to "Moog" servovalve on crosshead

I "feedback" signal to "Moog" control box from either load or displacement transducer

Fig. 6.27 "Flow-loop" of loading control and data acquisition of the present test facility

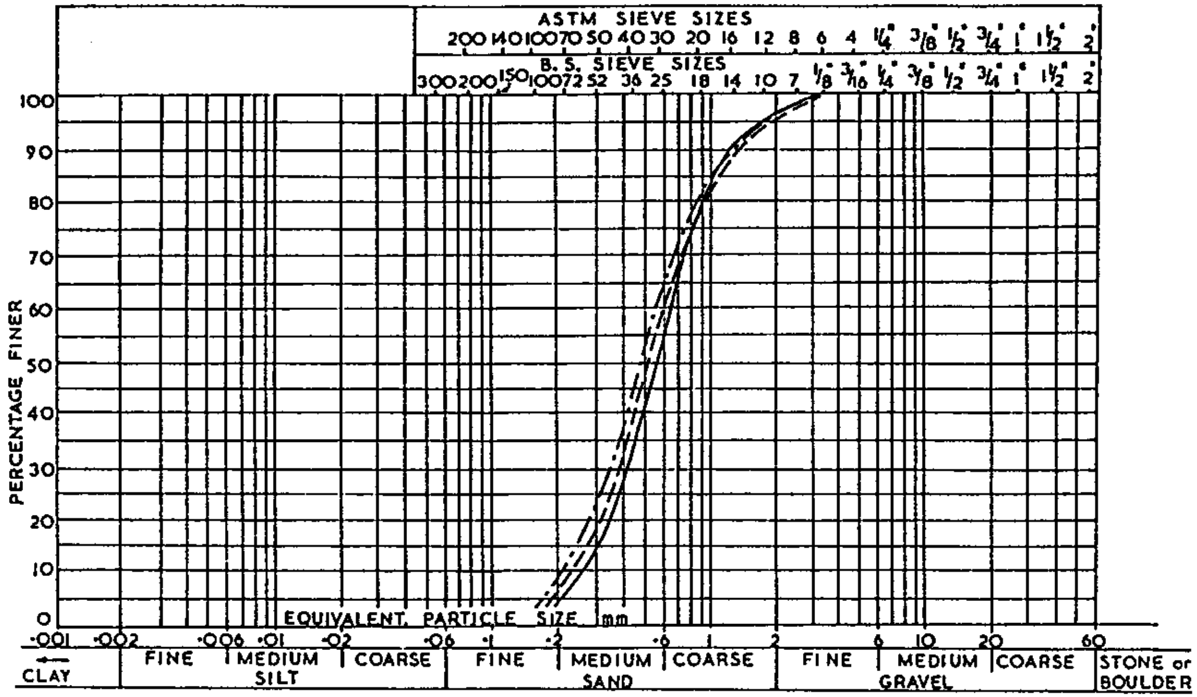

Fig. 6.28 Grain size distribution of prepared calcareous sand

CHAPTER 7

SOME CALIBRATION AND TRIAL MODEL PILE TEST RESULTS

CHAPTER 7

SOME CALIBRATION AND PRELIMINARY TRIAL MODEL PILE TEST RESULTS

7.1 INTRODUCTION

In the preceding Chapter, the design requirements and construction of the model pile test facility as well as the necessary instrumentation required have been described in detail. In the present chapter, some initial preliminary results and experiences with the use of the test facility are presented. These include:

- some typical calibration results for the diaphragm-type stress cells;
- some calibration results for the pile instrumentation;
- the sand placement procedure adopted;
- the pile testing procedure for the different stages required;
- the results from trial uninstrumented model piles of 50mm and 100mm external diameters.

The experience gained from these initial preliminary trial tests is utilised to improve on the test procedures for the actual instrumented model pile tests, the results of which are presented in Chapter 8.

7.2 SOME CALIBRATION RESULTS FOR DIAPHRAGM-TYPE STRESS CELLS

The calibration of the diaphragm-type stress cells was carried out using the small calibration chamber as described in section 6.3.2. Some typical results from the calibration process are presented in this section.

Fig. 7.1(a) shows the "fluid" calibration response for a typical cell W1 subjected to a maximum pressure of 200 kPa. The results have been plotted to show the incremental output signal voltage change for changes in the applied pressure. An almost linear response was obtained up to the maximum pressure under a strain-gauge excitation voltage of 6 volts. As expected, the unloading response is identical to the loading response, thus, exhibiting no hysteretic behaviour.

Fig. 7.1(b) shows the responses of a typical cell, for the three different density states, under the first cycle of loading. Note that the "in sand" calibration responses and the "fluid" calibration response are almost identical for applied pressures of less than 50 kPa. For higher pressures (>50 kPa), the "in sand" responses differ significantly, depending on the density state, from the "fluid" calibration response. This may be due to significant stress redistribution, due to "arching" of the sand mass over the deflected diaphragm face of the cell, for the higher applied pressures. Thus, for the higher pressure values (>50 kPa), the deduced soil stress, from the output response of the cell, if based on the "fluid" calibration chart would give a lower stress value than the "true" value - an "under-registration" case (Weiler and Kulhawy, 1982). Upon unloading, significant "arching" behaviour occurs resulting in a "locked-in" stress state over the cell, thus, contributing to the slow response of the cell to the reduced applied pressure. This hysteretic observation is consistent with those reported by, for example, Selig (1980). The responses of the cell, after four unloading-reloading cycles, are further shown in Fig. 7.1(c) and Fig. 7.1(d) for the relatively loose and relatively dense states respectively. Cycling appears to have no significant influence on the general shape of the response curve of the cell.

As the major use of the stress cells is to provide an indication of the "rigid boundary" effect during the initial installation of the model pile, the "unloading" and "cycling" effects noted from the calibration process would not be of major concern. It should be noted that a qualitative indication of the "rigid boundary" effect is sought in the present study and any stress values interpreted from the present study should not be treated as absolute quantitative values. It must be emphasized again that the accurate measurement of soil stress is a most difficult and complex task dependent on many factors. It still remains a challenging task for the engineering profession to improve on the current available methods of measurement.

7.3 CALIBRATION RESULTS FOR PILE INSTRUMENTED SEGMENTS

The calibration of the pile shaft instrumented segments required the separate application of a normal pressure and an axial load. As described in section 6.4.2.2, calibration under a normal pressure alone enables the coefficients a_{12} and a_{22} of the calibration matrix [Z] to be determined (see equation 6.3). Similarly, the coefficients a_{11} and a_{21} can be obtained by calibrating for the axial load alone.

7.3.1 Normal Stress Calibration

For the normal stress calibration, a hydrostatic pressure was applied to the pile shaft instrumented segment installed on the small calibration chamber. Plate 7.1 shows the pile segment inserted into the water-filled calibration chamber prior to attaching the top plate of the chamber. The use of a hydrostatic pressure is to also enable the pore-pressure transducer, which is attached to the pile segment, to be calibrated simultaneously. The responses of both sets of gauges (vertical and horizontally oriented gauges) and the pore-pressure transducer (where available) were independently monitored using the HP3458A multimeter. The two sets of "active" gauges had to be connected to corresponding sets of external "dummy" gauges to form a complete circuit.

Fig. 7.2(a) shows a typical measured response of the two sets of "active" gauges with increasing hydrostatic pressure to a maximum of 100 kPa. As expected, an almost linear response of the gauges was obtained. Note that the sign (+ve or -ve) of the voltage change is opposite for the two sets of gauges although Fig. 7.2(a) only shows the absolute voltage change. The coefficients a_{12} and a_{22} can hence be obtained from the slopes of the vertical and horizontal gauges responses respectively. The ratio of the response of the vertical gauges to the corresponding horizontal gauges was found to vary between 0.38 and 0.44 for the five instrumented segments. The variation of this ratio can be attributed to the slight differences in orientation of the gauges in the different segments. The coefficients a_{12} and a_{22} for the instrumented segments are given in Appendix 7.

A typical calibration response of the miniature pore-pressure transducer is shown in Fig. 7.2(b). Notice that the "true" response of the transducer is obtained for pressures greater than about 10 kPa. The reduced response of the transducer for pressures less than about 10 kPa may be due to the yet incomplete saturation of the transducer. Indeed, as noted by, for example, Hansen *et al.* (1990), complete saturation of the pore-pressure porous filter is required to ensure accurate and fast response of the transducer. However, the ability to ensure complete saturation of the porous filter at all times is a difficult task and is not attempted in the present study. It was felt that, for the present study, the additional accuracy that could be gained did not justify the additional significant effort required to overcome this "saturation" problem.

7.3.2 Axial Load Calibration

The calibration for the axial load effect was carried out by subjecting the 50mm diameter instrumented segments to increments of applied loading to a maximum of 10 kN. Plate 7.2 shows the axial load calibration using an "Amsler" tension and compression testing machine. The instrumented segment was "protected" at both ends by attaching two "dummy" segments to it. The necessary connections to the two external sets of "dummy" strain-gauges were carried out as for the normal stress calibration case.

Fig. 7.3 shows the responses of the vertical and horizontal gauges for incremental compression load to a maximum of 10 kN. As expected, within the elastic range, an almost linear response was obtained. The responses (voltage change) of both sets of gauges are also much greater than the normal stress calibration case. The segment was also subjected to an applied tension load (maximum of 5 kN) and Fig. 7.3 shows that the responses under tension and compression loadings are almost identical. The coefficients a_{11} and a_{21} can hence be determined from the slopes of the two responses. The coefficients for the different segments are given in Appendix 7.

The validity of the approach using equation (6.4) was checked for an instrumented segment. Under a given applied horizontal stress, the applied axial load was varied and compared to the backfigured values obtained from the measured voltage responses of the vertical and horizontal strain-gauges. Similarly, under a given applied axial load, the applied normal horizontal stress was varied and compared to the backfigured values. In both cases, satisfactory comparisons were obtained, thus, indicating the validity of the approach. As mentioned in Chapter 6, the satisfactory or non-satisfactory performance of these instrumented segments forming the model pile in the actual pile tests will be discussed further in Chapter 8.

From the calibration responses under normal pressure and axial load presented earlier, it is evident that, for large applied load and low confining normal pressure, the normal pressure has an insignificant effect on the measured axial load. However, for cases of high normal pressure and at low applied load levels, failure to take this normal pressure effect into account would result in an under-estimation of the measured axial load distribution along the pile.

7.4 SAND PLACEMENT PROCEDURE

The filling-up process of the test chamber involves a considerable amount of effort due to the large volume of calcareous sand required. As mentioned in section 6.2.1, in view of the constraint of the present test facility, the "single hose" method of sand placement was adopted for the present study.

The procedure involved putting a given quantity of sand into the large discharge-box, then moving it to the gantry crane position and subsequently lifting it up to the required position. Due to the limited head-room available between the level of the top of the test chamber and the horizontal arm of the gantry crane, a single stationary position for the discharge-box was selected corresponding to the maximum attainable height. This maximum position of the discharge-box resulted in a distance of about 400mm between the top of the test chamber and the base of the discharge-box. A 35mm diameter flexible hose was connected to the bottom face of the discharge-box through a "shutter" unit (see Fig. 6.12). The box was then manoeuvred as close as possible to the test chamber. Due to the obstruction provided by the crosshead of the test chamber, it was not possible to position the box directly above the test chamber. The top of the test chamber had to be covered up at all times during the placement process to prevent the powdery calcareous sand from contaminating the surrounding areas. This was achieved by covering the top of the test chamber with a piece of cloth. A small cut-out hole on the cloth provided an opening through which the flexible hose was accommodated. The discharge of the sand can be commenced by pulling on the handle connected to the "shutter" unit.

The influence of the height of fall of the discharged sand on the attainable density (using this "single hose" method) was investigated. The sand within the large discharge-box was allowed to "free fall" from the end of the flexible hose into a small cylindrical container (50mm diameter by 47mm height). By varying this "free fall" height, the different attainable densities were determined and are as shown in Fig. 7.4. It is observed that a "free fall" height greater than about 500mm results in negligible increase in the attainable density. The maximum attainable dry density corresponds to a relative density of about 40%. Indeed, as noted by Bieganousky and Marcuson (1976), the "single hose" method of sand placement is only capable of achieving a formed sand in the medium-dense range.

A "free fall" height of at least 500mm was thus adopted for the present sand placement process. As shown schematically in Fig. 7.5, the discharged sand, with the flexible hose positioned at the centre of the test chamber, forms a cone-shaped mass at the deposited end. During the first trial placement conducted, some difficulties were encountered in discharging the sand effectively for the last one-third volume of the test chamber. This was due to the restriction of being not able to raise the discharge-box as the level of the deposited sand in the test chamber increased.

The problem above led to a modified improved procedure that was adopted for the sand placement of the actual pile tests. This modified procedure required the fabrication of another similar, but smaller (380x380x380mm), discharge-box. The procedure involved using the large discharge-box, as described earlier, to fill the bottom-half of the test chamber. The upper top-half was then filled by using the small discharge-box. This was done by attaching the discharge-box to the crosshead of the test facility, which enabled the discharge-box to be positioned at the necessary elevation as the deposited sand level in the test chamber increased.

In order to have some indication of the uniformity of the placed sand, a "pile penetrometer" test was conducted (see Fig. 6.13). A typical plot of the jacking load-penetration response is shown in Fig. 7.6. This jacking load-penetration response of the "pile penetrometer" was obtained for the placed sand of every test. A consistent jacking load-penetration response therefore gives an indication of consistency in the placement procedure adopted. It may be noted from Fig. 7.6 that the jacking load-penetration responses of both the pile penetrometers are generally in reasonably good agreement. The response, as measured by the "SHOWA" load cell (of 5 kN capacity), should be considered as the more accurate measured response of the penetrometer. The response of the other penetrometer was then obtained as the difference between the load readings of the central load cell ("HSI" model) and the

"SHOWA" load cell. Since the "HSI" load cell utilised was of 30000 lbs. (134 kN) capacity, its sensitivity at the low load levels was greatly reduced. This may have contributed to the generally lower load response (obtained as the difference between the "HSI" and "SHOWA" load cells readings) for the other pile penetrometer. The increasing jacking load response with penetration reflects the effect of the increasing effective confining overburden pressure with depth.

It is interesting to observe that the jacking load versus penetration response does not seem to reach a limiting value (i.e a limiting tip resistance since the skin friction along the pile "penetrometer" is negligible). The presence of such a "critical" depth, below which the unit end-bearing and unit skin friction remain approximately constant, was first suggested by Vesic (1963) based on experimental model pile test results. This "critical" depth concept is widely adopted in most piling codes for estimating the capacity of pile foundations. For the present case, however, no such "critical" depth was observed even for a total penetration of about 55 pile diameters. As pointed out and discussed by, for example, Kulhawy (1989) and Kraft (1991b), the existence of such suggested "critical" depth is questionable. Clearly, more research work is required in this interesting area. For the present study, the jacking load versus penetration response of the pile "penetrometer" is utilised solely to gauge the consistency of the placed sand for each of the different tests conducted.

It is of interest to note that results obtained from the instrumented pile tests (as will be described in detail in Chapter 8), under an applied overburden pressure of 100 kPa, show that a "softening" response (after an initial peak) is obtained with pile installation depth for the 50mm diameter model piles. For the 100mm diameter model instrumented piles, this "softening" effect is not evident. The "softening" observed is caused by the reduced effective overburden pressure (from the applied pressure of 100 kPa at the top of the sand mass) in the sand mass with depth. In the case of the 100mm diameter model pile, the measured response is influenced by the reduced effective overburden pressure in the sand mass as well as the "rigid boundary" effect of the test chamber. Therefore, under the present test conditions, it is not possible to assess further this "critical" depth phenomenon, in particular for the developed end-bearing resistance with pile penetration.

7.5 TEST PROCEDURES

In this section, the complete test procedures required for the conduct of a model pile test are described. As mentioned in section 6.5, the model pile testing stage requires the simultaneous use of a data acquisition program (DAQ.BAS) and the loading control program (DLOAD.BAS) on two separate micro-computer systems. Figs. 7.7 and 7.8 show the flow-charts for both programs DAQ.BAS and DLOAD.BAS respectively that were written by the author.

There are altogether a total of five stages in the model pile testing process. These stages are:

(1) Pile installation (or jacking) stage;

(2) Unloading to zero load (after stage 1) to obtain the residual installation stress condition;

(3) Static compression loading to "failure" and subsequent unloading to zero load;

(4) Specified number of cycles of displacement-controlled cyclic loading;

(5) Post-cyclic static compression loading to "failure".

The "input" voltage command signal required in each of these stages can be generated by the loading program DLOAD.BAS in conjunction with the DAC02 D/A voltage converter. Both programs DAQ.BAS and DLOAD.BAS were written and utilised within the "QuickBasic" environment.

Due to time restriction remaining in the author's candidature, only "dry" sand tests were conducted in the present study although the pile instrumentation was originally designed to cater also for "wet" soil tests. The details of the test program are presented in Chapter 8.

The procedures that were adopted for the conduct of each model pile test are detailed below:

(a) The filling-up of the test chamber was carried out using the sand placement procedure as described in the previous section 7.4;

(b) The "pile penetrometer" test (see Fig. 6.13) was performed next in order to assess the uniformity of the placed sand from the measured jacking force-penetration response. At this stage, the sand mass was not subjected to any applied overburden pressure;

(c) The rubber membrane with the attached pile guide was then placed in position over the sand mass. This was followed by placing and positioning the top lid over the rubber membrane. The top rim was then placed over the top lid and the assembly bolted into position (see Fig. 6.3b). The pile collar guide was next bolted into position onto the top lid (Fig. 6.3a).

The required test overburden pressure of 100 kPa was then applied to the sand mass for about half an hour before reducing it to zero. The resulting compaction of the sand mass caused a settlement at the top of about 40mm. The pile guide collar attached to the top lid was then removed followed by the pile guide collar attached to the rubber membrane. The sand level in the test chamber was then topped-up through the central hole on the top lid. After that, the pile guide collar was re-attached back to the rubber membrane followed by the larger collar for the top lid;

(d) Before switching on the hydraulic pump, the null-indicator on the "Moog" control box was set to zero. The two push-buttons corresponding to the solenoid valves were also set to an "off" mode. After switching on the hydraulic pump, the two solenoid valves push-buttons were turned to the "on" mode. The crosshead of the test facility was raised to the required height with the side rams extended a distance of about 1.1m. The threaded end of the crosshead central jack was moved to its uppermost extreme end by using the "manual" control. The model pile was then slid into the pile guide and connected to the central jack through the coupling connections (see Fig. 6.11);

(e) The necessary instrumentation connections to the "dummy" strain-gauges and to the HP3458A multimeter system were made. Program DAQ.BAS was next "activated" and the initial readings for the diaphragm-type stress cells taken. An overburden air pressure of 100 kPa was then applied to the sand mass through a pressure inlet line on the top lid. Checks were made to ensure that there was no leaking of the air pressure. The diaphragm-type stress cell readings were again taken after that to obtain an indication of the stress transfer within the test chamber;

(f) The crosshead assembly was then moved down until the tip of the model pile was in contact with the sand bed. Next, the initial readings for all channels were taken following the next "block" routine in program DAQ.BAS (see Fig. 7.7). Note that the readings taken corresponding to the diaphragm-type stress cells were "reset" to the initial readings taken in step (e). The weight of the model pipe pile was accounted for through the initial load cell reading taken at this stage. Program DLOAD.BAS was then "activated" and ready for the next pile installation stage;

(g) The pile installation stage was controlled by pushing on the appropriate button on the "mobile" control console for the side rams. Markings on the model pile provided an indication of the amount of penetration into the sand mass. During this installation stage, the channel readings were continuously taken by the multimeter and displayed on the monitor screen. At each required penetration depth, the readings were saved to a specified file by pressing the "S" key. The crosshead was continuously moved down until it came in contact and stopped by the two "seats" on the side rams. The two "seats" were made to the required height to ensure that the locking-pins could then be inserted into position (see Fig. 6.10) to hold the crosshead in a rigid position. The crosshead central jack was next moved to its mid-position, a movement of about 50mm from its extreme upper end position, by either using the "manual" or "automatic" control. The "automatic" control involves using program DLOAD.BAS to generate the required input voltage signal incrementally through the DAC02 D/A voltage converter. The "manual" control however involves offsetting the null-indicator in the appropriate direction to obtain a downward motion of the central jack. The "manual" control was adopted at this stage to incrementally advance the central jack to about its mid-position. This was achieved by referring to the movement of the central jack measured by the displacement LVDT and displayed on the monitor screen by program DAQ.BAS. The channel readings were saved to file when required by pressing the "S" key. After this installation stage, program DAQ.BAS was advanced to the next stage;

(h) Stage 2 involved unloading the pile to zero load in order to obtain the residual installation stress condition. The "prompt" option in program DLOAD.BAS was utilised to increase or decrease the "input" voltage command signal, generated by the DAC02 converter, when required in order to control the movement of the central servo-jack. At this stage, graphics option 1 in program DAQ.BAS was utilised to show the pile head load versus pile head displacement response. Also, the channel readings were saved to file when required. Hence, by referring to the graphics option (and tabulated values too) of the pile head response the unloading process was controlled by using the "prompt" option in program DLOAD.BAS. The unloading stage was stopped when the pile head compressive load was reduced to almost zero;

(i) Stage 3 involved loading the pile to "failure" in compression and subsequent unloading to zero load. Graphics option 2 (with different axes scales than option 1) was utilised in program DAQ.BAS. The procedure was similar to that for stage 2 where the pile head load versus pile head displacement response was plotted on the monitor screen. "Automatic" control was utilised for the loading stage while the "prompt" control was used for the unloading stage, through program DLOAD.BAS. For the "automatic" loading stage, the total final "input" voltage (corresponding to the final specified pile head displacement to reach) required was output incrementally over a time of about one minute, that is, about one minute displacement rate of loading to "failure". An option was provided in program DLOAD.BAS to control on a "prompt" basis if found necessary to reach "failure" after the end of the "automatic" control. The unloading stage to zero pile head load was similar to that for stage 2;

(j) The cyclic loading stage 4 was more complicated than the other stages. The "step" sine-wave voltage input for a specified number of cycles was generated and controlled by program DLOAD.BAS. For the present study, a period of about 20 seconds was utilised with a total of 50 cycles of loading unless otherwise specified. In program DAQ.BAS, the graphics option 2 from stage 3 was utilised. A routine incorporated into DAQ.BAS was able to "track" the number of cycles that the pile had been subjected to as well as to save the channel readings to file for specified cycle numbers. Options were provided in both programs DAQ.BAS and DLOAD.BAS to do more number of cycles (after the initial 50 cycles) if required;

(k) The final stage 5 involved loading the pile to "failure" in compression to obtain the post-cyclic pile capacity. The loading control utilised in program DLOAD.BAS was similar to the loading stage in stage 3 described earlier. After the unloading part of stage 5 was completed, a further set of different amplitude displacement-controlled loading (of 50 cycles) was applied followed by another post-cyclic static compression loading (i.e. steps j and k repeated);

(l) After completion of testing, the "capturing" nut (see Fig. 6.11) holding the model pile to the central jack was disconnected, and the crosshead moved up to its uppermost position. Next, the bolts on the pile guide collar attached to the top lid were released. The model pile was then removed from the sand bed by slowly pulling it up manually;

(m) Finally, the sand within the test chamber was removed through a 35mm diameter hole "shutter" unit attached to the base plate of the test chamber. The removed sand was stored back into containers ready for placement for the next test.

7.6 PRELIMINARY UNINSTRUMENTED MODEL PILE TRIAL TESTS

In order to test the overall system, trial uninstrumented model pile tests were conducted using the procedure as detailed in section 7.5. For these uninstrumented pile tests, the pile head load and pile head displacement were measured by the "HSI" load cell and the displacement LVDT respectively. These preliminary tests provided valuable experience with the use of the test facility and also enabled improvements to be made to the control programs and test procedures.

In this section, some of the trial test results from both the 50mm and 100mm diameter uninstrumented model piles are presented.

7.6.1 50mm Diameter Model Pile

The first trial sand placement procedure adopted to fill the test chamber for the trial test led to an improved procedure as described in section 7.4. A relative density of about 14% was obtained for the placed sand (based on average density calculated from total mass of sand of about 1490 kg divided by volume of test chamber). This attained average density is rather low as compared to that of about 40% for a height of fall of about 500mm (see Fig. 7.4) obtained from discharging the sand into a small cylindrical container. The reason for this discrepancy is not clear and may be due to the increased difficulty of proper deposition within the test chamber. The low relative density obtained with calcareous sediments was also observed by Parkin *et al.* (1991) during sample preparation using a sand spreader for a test chamber of 1.2m diameter and 1.8m height. Considerable scope therefore exists in future work for developing an effective sand placement procedure for calcareous sediments that is capable of attaining a wide range of relative densities. An overburden air pressure of 100 kPa was utilised for the trial model pile tests. Upon application of the overburden pressure, the soil surface settled about 40mm. Thus, the effective average relative density of the sand mass (after application of the overburden pressure) increased to about 30% prior to the pile test.

Fig. 7.9 shows the responses of the diaphragm-type stress cells when the overburden pressure of 100 kPa was first applied to the top of the sand mass. Cells W1 to W4 along the side wall of the test chamber measure the total horizontal stress at each depth while cells B1 and B2 measure the total vertical stress at the level of the base plate. As shown, cell W4, being the lowest along the side wall, measured a horizontal stress value of about 14 kPa while cells W1 to W3 measured a larger value between 24 kPa and 27 kPa. The vertical total stress increases at the level of the base plate were about 20 kPa and 30 kPa, as measured by cells B1 and B2 respectively. The deduced total vertical stress increase in the vicinity of the cells along the side wall indicated a stress value of about 70 kPa for cells W1 to W3, and about 40 kPa for cell W4. Note that these deduced vertical stress values were obtained by using a conservative value for the friction angle (ϕ) of 40° for the calcareous sand, and assuming the coefficient of lateral earth pressure to be given by $K_o = 1-\sin\phi$. The stress cell measurements therefore indicate quite significant reduction in the vertical stress within the test chamber for depths below that of cell W3. The vertical stress along the central axis of the test chamber and at the level of cell W3 was estimated to be between 50 kPa and 60 kPa. It is reasonable to assume that the applied overburden pressure of 100 kPa decreases linearly from the top to a value of between 50 kPa and 60 kPa (along the central axis of the test chamber) at the level of cell W3. Note that the maximum embedment depth of the model pile in the actual pile tests is about 850mm i.e. almost at the level of cell W3.

It is interesting to note that Smits (1982), using lateral stress transducers along the side wall of a 1.9m diameter chamber, found that the initial lateral stresses due to the applied overburden pressure of 100 kPa decreased with depth as a result of wall friction. The responses obtained from the diaphragm stress cells in the present study are in agreement with those of Smits (1982).

Upon unloading to zero overburden pressure (after first application of the overburden pressure of 100 kPa), residual stress values were recorded by the diaphragm cells, particularly cells B1 and B2. Cells W1 to W4 registered residual stress values of between 6% and 12% of the corresponding stress values at 100 kPa overburden pressure. A larger percentage of about 50% and 40% was obtained for cells B1 and B2 respectively. The presence of such residual stress values upon unloading indicate a "locked-in" stress state within the sand mass. This "locked-in" stress state is commonly attributed to "arching" behaviour of the soil. This "arching" behaviour is particularly significant in the vertical direction (i.e. direction of overburden pressure application) as evident from the residual stress values measured by cells B1 and B2.

It is believed that the reduction in the vertical stress within the central part of the test chamber, particularly below the level of cell W3, is caused more by "arching" behaviour in the sand mass rather than the loss due to friction along the side wall. This "arching" behaviour becomes more significant as the height to diameter ratio of the test chamber increases. Although an axisymmetric finite element analysis of the problem would give some indication of the stress transfer within the test chamber, its results however are influenced by the adopted soil parameter values, in particular the friction characteristics at the soil-chamber interface. Moreover, the volume reduction response of calcareous sediments under shearing as well as the "arching" phenomenon may not be readily accounted for in the finite element analysis. Nevertheless, some elastic axisymmetric finite element analyses of the test chamber were conducted to obtain some indication of the stress transfer within the chamber. It was also decided that diaphragm-type "boundary" stress cells be utilised in the present study to provide some quantitative indication of the stress transfer within the test chamber. As mentioned in section 7.2, the stress measurements from these "boundary" cells should not be treated as absolute quantitative values since such diaphragm cells have their own limitations as well.

The elastic finite element analyses of the stress transfer within the test chamber were conducted using an existing axisymmetric program (J.M. Rotter, private communication). The sand within the test chamber was modelled by using 36 numbers of 8-noded isoparametric elements. As it is an elastic analysis, the calculated stress values will not be affected by the adopted Young's modulus for the soil. For the present case however the soil Young's modulus adopted was 10000 kPa with the Poisson's ratio taken as 0.35. The influence of the Poisson's ratio was also investigated whereby a value of 0.45 was utilised for the analysis. Three "boundary" conditions were analysed:

(i) a completely "free" condition along the side wall,
(ii) a completely "fixed" condition along the side wall, and
(iii) "free" condition for the top two-fifths of the chamber and "fixed" condition for the bottom three-fifths along the side wall.

Table 7.1 shows the computed stress distributions, under an applied overburden pressure of 100 kPa, at the vicinity of the locations of the diaphragm-type stress cells. Also shown are the measured values as indicated by the stress cells. The calculated stress values are shown to be influenced significantly by the adopted "boundary" condition along the side wall. The actual relevant boundary condition in the test chamber is intermediate between the two extremes of a completely "free" and "fixed" conditions. The allowance of some "free" condition over the top two-fifths of the chamber (i.e condition (iii) above) was found to also significantly alter the stress distribution. The influence of the soil Poisson's ratio was also significant, with greater stress transfer for the larger value (ν = 0.45). It is also interesting to note that the finite element elastic solutions at the location of cell B1 (nearer to the central axis of the test chamber) show a greater stress value than that at cell B2. This trend is contradictory to the measured values where cell B2 (nearer to the side wall) showed a greater stress value than cell B1. This discrepancy may be due to the complex stress transfer response within the sand mass which is not readily modelled in the simple elastic finite element method.

The trial model pile testing involved a learning and improvement process and as such it was not necessary to perform the tedious task of removing the sand from the test chamber and refilling it following each trial test. In order to slightly compact the softened central zone due to the extraction of the pile, a higher overburden pressure of 130 kPa was applied to the sand mass. The overburden pressure was then reduced to 100 kPa prior to the next trial test. The results of a fully successful (involving all the five stages) trial test, after three earlier trial tests ahich were not fully successful, are presented next.

Fig. 7.10 shows the responses of the "boundary" stress cells during the initial model pile installation stage to a depth of about 910mm. This installation stage involved lowering the crosshead, to which the model pile was attached to, at a constant rate. The difference between the stress cell readings at any penetration depth and the initial (zero penetration depth) readings gives the measured stress increases due to the installation of the model pile. Generally, the responses of the stress cells were not significantly affected by the installation of the 50mm diameter model pile (maximum stress increase of between 7% and 10% of the applied overburden pressure of 100 kPa). A slight increase in the stress measurement of a particular cell was obtained as the pile tip approached the level of that cell. This was due to the radially outward and downward displacement of the sand caused by the penetrating pile tip. A reduction of the measured stress was observed as the pile tip penetration passed the level of that particular cell. Note that this observation is consistent with the results obtained from an embedded total pressure sensor reported by Nauroy and LeTirant (1983). From the stress cell results shown in Fig. 7.10, it is reasonable to conclude that, at the expected penetration depth of about 850mm, the "rigid boundary" effect of the side wall and base of the test chamber is not significant. It should be noted that for a denser sand and at higher overburden pressures, this "rigid boundary" effect may be of greater significance.

It is interesting to note that Baligh (1984) has described an approach, using the strain-path technique, to determine the stresses and strains in the surrounding incompressible clay soil as a result of the vertical penetration of a sperical-nosed object (simulating a pile). The analysis results indicate that the zone of strain greater than 2%, which is assumed by Baligh (1984) to represent the boundary between elastic and plastic soil behaviour, extends to about 4.5 pile radii horizontally from the pile shaft and about 2.5 pile radii below the pile tip. It is desirable therefore to ensure that this plastic zone (which represents the zone of permanent soil deformation) of the penetrating pile be contained within the soil mass, so as to reduce any significant effect from the rigid boundaries of the test chamber.

Although the soil utilised in the present study is different from that (clay soil) where the above results were obtained by Baligh (1984), it nevertheless is of interest to adopt these values as general guidelines for the present study. For the 50mm diameter model pile utilised in the present study, the horizontal distance between the pile shaft and the side wall of the test chamber is about 19 pile radii while the vertical distance between the pile tip and base of the test chamber is about 26 pile radii. In the case of a 100mm diameter model pile, these two corresponding distances are 9 pile radii and 13 pile radii.

The jacking load-penetration response of the model pile is shown in Fig. 7.11. As shown, the jacking load mobilised to penetrate the first 100mm movement increased rapidly. This was due to the larger confining overburden pressure at the top. For depths between 100mm and 700mm, the jacking load increased gradually. However, for depths between 700mm and 910mm, the jacking load increased quite rapidly. This could be due to the greater compacted soil around that region from the earlier trial tests carried out. For the present uninstrumented trial test, the mobilised pile tip load response cannot be assessed at this stage. At the end of the installation stage, a "stress relief" situation was observed where the measured pile head load reduced from its previous peak value to an "equilibrium" value. This phenomenon is not clearly understood although it has been attributed to a creep response of the soil, which in turn causes a redistribution of stresses around the pile.

Fig. 7.12(a) shows the complete load-settlement response of the pile for the subsequent stages 2 to 5 forming a single test. The pile was subjected to 62 cycles of displacement-controlled cyclic loading with a cyclic displacement amplitude of ±2.64mm. As shown, successive cycles of loading reduces the tension and compression loads at both ends of the cyclic "loop". Fig. 7.12(b) shows the responses for specific cycles N = 1, 2, 10 and 62 (final cycle). The initial averaged maximum unit skin friction over the pile shaft (obtained from the maximum tension load at N = 1) was found to be about 6 kPa, which is consistent with the recognised low unit friction values associated with driven (or jacked) piles in calcareous sediments. It may be noted that this initial average maximum unit skin friction value obtained is in general agreement with the static friction values reported by

Poulos and Chan (1988) from model jacked pile tests in calcareous sand. The post-cyclic peak static compression load was also affected by the cyclic loading sequence, with a reduction of about 19% of the initial pre-cyclic peak static load and mobilised at a much greater displacement magnitude.

Fig. 7.13 shows the diaphragm stress cell responses during the initial static compression loading and subsequent unloading to almost zero load (stage 3). Cells W1 to W3 along the side wall seem to be either not affected or only marginally affected (reduced stress cell readings) by the initial loading stage. The compression loading thus had little effect on the measured horizontal stress for positions above the level of the pile tip. Cells W4, B1 and B2, being closer to the higher stressed regions at and below the level of the pile tip, showed an increase in the stress readings notably during the initial 2.5mm of downward movement of the pile. These stress measurements increase of between 5% and 8% of the applied overburden pressure are not considered significant in view of the increased compaction of the underlying soil from the earlier trial tests. Upon unloading of the pile, all cells except W1 registered a decrease in the stress readings. Cell W1 seems to be not affected by the unloading stage, indicating its position to be far from the zone of influence of the pile during unloading. It may be noted that these observations of the responses of the diaphragm stress cells are in qualitative agreement with the observations reported by O'Neill and Raines (1991) obtained from stress cells embedded within the sand mass.

The responses of the diaphragm-type stress cells are further shown in Fig. 7.14(a) at the compression end of cycles N = 1 and 62. The cells along the side wall show a general decrease in the measured stress value following the cyclic sequence, the reduction being greater for the lower cells. Cells B1 and B2 on the base plate also indicate a decrease. The reduced values measured by both cells B1 and B2 are expected in view of the reduced compression load at the compression end of the cyclic loading stage. The detailed responses of the stress cells W4, B1 and B2 are shown in Fig. 7.14(b) for cycles N = 1 and 62. In general, the cyclic loading stage caused a continuous volume reduction of the soil surrounding the pile as inferred from the stress cell readings.

In practice, the static load testing of a pile may be any one of these three methods: the maintained load test (ASTM D1143-81), the constant rate of penetration (CRP) test (Whitaker and Cooke, 1961) or the method of equilibrium test (Mohan *et al.*, 1967). Of these three methods, the maintained load test is the most commonly used method although it is the most time-consuming method. The static load testing method employed in the present study (unless otherwise specified) is similar to that of the CRP test. The developed pile head load caused by the given rate of penetration of the pile head is therefore continuously measured during the test. In order to have some indication of the rate effect (if any) on the developed peak static load capacity, a trial static test was carried out. Fig. 7.15 shows the static load-settlement response for three cycles of loading where the time to reach a given displacement limit (loading stage of about 6.5mm) varied from 30 seconds to two minutes. A slight decrease in the peak load was observed for the slower rate of penetration. In general, the rate effect is not particularly significant and, for the present study, a rate of penetration of about 6.5mm per minute was adopted as the reference "static" loading rate.

An inherent objective of the static loading test, apart from determining the load-deformation response of the pile, is to also determine the ultimate static capacity of the pile. However, this ultimate capacity condition corresponding to "failure" of the pile (i.e. increasing large displacement at constant load) is usually not reached in a normal pile load test in practice due to cost considerations and/or equipment limitations. For such cases, a practical equivalent "failure" condition of the pile has been suggested for determining the ultimate capacity of the pile. For example, Whitaker (1970) and ISSMFE (1985) recommended that the ultimate capacity be taken as the load corresponding to a pile head movement of 10% of the pile diameter. Therefore, in the present study the ultimate static capacity of the pile is taken as the load corresponding to a pile head movement of 10% of the pile diameter.

7.6.2 <u>100mm Diameter Model Pile</u>

Following the earlier 50mm diameter model pile trial tests, a 100mm diameter model pile trial test was then conducted. The procedure adopted was similar to that used for the 50mm trial model pile tests. A similar applied overburden pressure of 100 kPa was used for the present trial test.

Fig. 7.16 shows the responses of the diaphragm-type stress cells during the initial installation stage of the model pile. As compared to the 50mm diameter case, a more pronounced increase in the normal stresses measured by the stress cells was obtained (measured stress increase of between 40% and 60% of the applied overburden pressure of 100 kPa). This indicates the more significant influence of the lateral restraint of the side wall to the penetrating pile. A similar observation was also obtained whereby a decrease in the stress cell readings was evident as the pile tip approached and passed the individual level of the top three cells.

The jacking load-penetration response is shown in Fig. 7.17 where a maximum load of about 38 kN was mobilised at the final penetration depth of about 950mm. Below a penetration depth of about 400mm, a gradual increase in the jacking load was observed with further penetration. This increase was also consistent with the observed increase in the measured stress readings of cells B1 and B2 (see Fig. 7.16) below that level, thus indicating the greater influence of the bottom base plate as compared with the 50mm diameter case.

Fig. 7.18 shows the complete static and cyclic loading test results conducted subsequent to the initial pile installation. Under cyclic loading, 62 cycles of displacement-controlled loading with a cyclic displacement amplitude of about ±5.28mm (i.e cyclic displacement amplitude to diameter ratio of 0.053, similar to that for the 50mm diameter case) was applied to the model pile. As shown in the figure, the initial static loading indicated an ultimate static capacity of about 30 kN which was lower than the jacking load mobilised (of about 38 kN) at the final penetration depth. The difference between these two load values could therefore be attributed to the more significant influence of the "rigid-boundary" of the test chamber (particularly the influence of the base plate of the test chamber at this final penetration depth) during the jacking stage. It may be noted that, for the 50mm diameter case, these two load values were almost identical, thus indicating non-significant influence of the "rigid-boundary" effect. The responses of the stress cells during this initial static loading stage are further shown in Fig. 7.19. Cells W1 and W2 appear to be not affected by this loading stage. The maximum increase in the stress readings for cells W4, B1 and B2 was approximately 50% of the corresponding maximum increase during the pile jacking stage. For cell W3 however, a smaller maximum increase of about 8% was obtained. These readings therefore indicate the smaller influence of the "rigid-boundary" effect as compared to the initial jacking stage.

The initial average peak unit skin friction, obtained from the measured tensile force at N = 1 cycle (see Fig. 7.18), was found to be about 8 kPa. This unit skin friction value obtained is thus slightly greater than the 6 kPa value for the 50mm diameter case. This initial preliminary result is therefore contradictory to the observed reduction of the unit static skin friction value with increasing diameter reported by Poulos (1988a) (see also Lee, 1988) from model grouted pile tests. It may be noted that the laboratory and field driven pile tests reported by Nauroy *et al.* (1988) also indicated a decrease in the peak unit skin friction with increasing diameter. This discrepancy between the present preliminary results and those reported earlier could have been caused by the increased compaction of the confined sand mass by the penetrating pile. The general increased "confining" stresses in the sand mass for the 100mm diameter pile, as deduced from the stress cell readings, may have also contributed to the increased average unit peak skin friction value measured. This preliminary result will be further assessed in the actual pile tests described in Chapter 8.

The pile head load versus pile head displacement responses for the specific cycles N = 1, 2, 10 and 62 (final) are shown in Fig. 7.20. As shown, a reduction in the pile head load on both extreme ends of the cyclic loop was observed for cycles N = 1, 2 and 10. This observation is similar to that for the 50mm diameter case. However, for N greater than 10 cycles, as shown in the figure for N = 62, an increase in the pile head load towards the compression end of the cyclic loop was observed. This increase was probably not due to an increase in the pile tip load since the diaphragm stress cell readings indicated a general decrease (particularly those of cells W4, B1 and B2) following the cyclic loading sequence (see Fig. 7.21). As noted by Turner and Kulhawy (1989), it is possible that cyclic loading may cause degradation of the ultimate tip resistance, and it is also possible that the tip resistance could increase, for example, due to sand densification around the pile tip under repeated compression loadings. For the present uninstrumented pile trial test, it was not possible to evaluate whether the measured increase in the pile head load (beyond the first ten cycles) was due to an increase in the pile tip resistance mobilised. It was suspected that the increase could be due to some sand particles getting "stuck" in the space between the pile body and the pile guide collar. This suspicion was later reinforced in view of the "stuck" condition of the model pile to the pile collar when trying to remove the model pile upon completion of the test. Some scratch marks were noticed on the body of the model pile. A slight modification to the pile collar was adopted to try to eliminate this problem in the actual pile tests. Again, the trend of these preliminary cyclic loading results will be further assessed in the actual pile tests. The post-cyclic static ultimate capacity was about 28 kN, a reduction of about 7% of the initial pre-cyclic capacity value.

7.7 SUMMARY

This chapter has presented some calibration results for the diaphragm-type stress cells as well as for the model pile instrumented segments. The sand placement procedure adopted and the complete test procedures for the conduct of a model pile test have also been described in detail. The preliminary test results from the 50mm and 100mm diameter model uninstrumented trial piles were also presented and discussed.

Under the application of an overburden test pressure of 100 kPa, the side wall diaphragm stress cells W1 to W3 recorded a stress value of between 24 kPa and 27 kPa while cell W4 recorded a value of about 14 kPa. For the diaphragm cells B1 and B2 (on the base plate of the test chamber), vertical stress values of about 20 kPa and 30 kPa were measured respectively. These measured stress values of the diaphragm cells reflect the effect of friction loss (along the side walls of the test chamber) as well as "arching" behaviour in the sand mass. The responses of the stress cells showed a more significant influence of the "rigid boundary" effect during the installation of the 100mm diameter (uninstrumented) model pile. The measured stress increases of the stress cells were found to be between 4 and 6 times the corresponding values for the 50mm diameter model pile. The side wall cells indicated a maximum stress increase as the penetrating pile approached the level of each cell.

These preliminary trial tests also enabled some improvement corrections to be made to some components of the test facility, the loading control and data acquisition programs, and the overall test procedures.

APPENDIX 7

The calibration constants for the load cells, displacement transducer, diaprragm-type stress cells and the instrumented segments of the model piles utilised are listed below:

Load cell (SHOWA DB-500K model, 5 kN capacity)	134.844 kN/volt
Load cell (HSI 3100-0030 model, 134 kN capacity)	6352.433 kN/volt
Displacement transducer (MOOG A04955-005, 126mm stroke)	319.124 mm/volt

Diaphragm-type stress cells:

Cell W1:	< 245.3 μV change	= 203832.042 kPa/volt
	> 245.3 μV change	= 468530.376 kPa/volt
Cell W2:	< 213.2 μV change	= 234558.249 kPa/volt
	> 213.2 μV change	= 415474.102 kPa/volt
Cell W3:	< 169.9 μV change	= 278233.033 kPa/volt
	> 169.9 μV change	= 501896.052 kPa/volt
Cell W4:	< 176.2 μV change	= 283714.772 kPa/volt
	> 176.2 μV change	= 495922.416 kPa/volt
Cell B1:	< 212.5 μV change	= 276238.767 kPa/volt
	> 212.5 μV change	= 536960.802 kPa/volt
Cell B2:	< 162.5 μV change	= 307629.204 kPa/volt
	> 162.5 μV change	= 346366.995 kPa/volt

50mm diameter model pile instrumented segments:

Segment LC1:
$a_{11} = 3.6436\times10^{-4}$ volt/kN
$a_{12} = -6.1301\times10^{-7}$ volt/kPa
$a_{21} = -1.2806\times10^{-4}$ volt/kN
$a_{22} = 1.4329\times10^{-6}$ volt/kPa

Segment LC2:
$a_{11} = 3.1840\times10^{-4}$ volt/kN
$a_{12} = -4.5639\times10^{-7}$ volt/kPa
$a_{21} = -1.0595\times10^{-4}$ volt/kN
$a_{22} = 1.1962\times10^{-6}$ volt/kPa
Pore-pressure transducer = 7963.286 kPa/volt

Segment LC3:
$a_{11} = 3.1599\times10^{-4}$ volt/kN
$a_{12} = -5.4104\times10^{-7}$ volt/kPa

$a_{21} = -1.2135\times10^{-4}$ volt/kN
$a_{22} = 1.3826\times10^{-6}$ volt/kPa
Pore-pressure transducer = 5587.993 kPa/volt

Segment LC4:
$a_{11} = 3.4009\times10^{-4}$ volt/kN
$a_{12} = -6.1546\times10^{-7}$ volt/kPa
$a_{21} = -1.0237\times10^{-4}$ volt/kN
$a_{22} = 1.3879\times10^{-6}$ volt/kPa
Pore-pressure transducer = 7505.711 kPa/volt

Segment LC5:
$a_{11} = 3.2974\times10^{-4}$ volt/kN
$a_{12} = -4.8634\times10^{-7}$ volt/kPa
$a_{21} = -1.2500\times10^{-4}$ volt/kN
$a_{22} = 1.2919\times10^{-6}$ volt/kPa
Pore-pressure transducer = 7203.508 kPa/volt

Cone tip segment = 1747.103 kN/volt

100mm diameter model pile instrumented segments:

Segment LC1: 4.9541 kN/mV

Segment LC2: 5.6604 kN/mV

Segment LC3: 4.8783 kN/mV

Segment LC4: 5.7662 kN/mV

Segment LC5: 5.8982 kN/mV

Cone tip segment: 3.6788 kN/mV

Table 7.1 Stress values within test chamber calculated from elastic axisymmetric finite element analysis.

Location	ν = 0.35			ν = 0.45			
	(1)	(2)	(3)	(1)	(2)	(3)	(4)
W1	53.8	40.5	54.7	81.8	61.9	83.4	26.9
W2	53.8	23.1	44.2	81.8	43.4	74.5	24.8
W3	53.8	11.4	36.4	81.8	27.8	62.9	23.9
W4	53.8	4.5	16.3	81.8	16.9	37.4	14.1
B1	100	6.3	26.1	100	19.7	47.6	20.2
B2	100	4.6	19.4	100	17.0	41.3	30.4
middle of pot	100	24.7	65.9	100	39.4	75.9	–

Applied overburben pressure on sand mass = 100 kPa

(1) "free" condition along side wall

(2) "fixed" condition along side wall

(3) upper two-fifths "free" and bottom three-fifths "fixed" along side wall

(4) measured values by stress cells

All values shown in kPa

Plate 7.1 Normal stress calibration of instrumented segment (50mm diameter)

instrumented segment

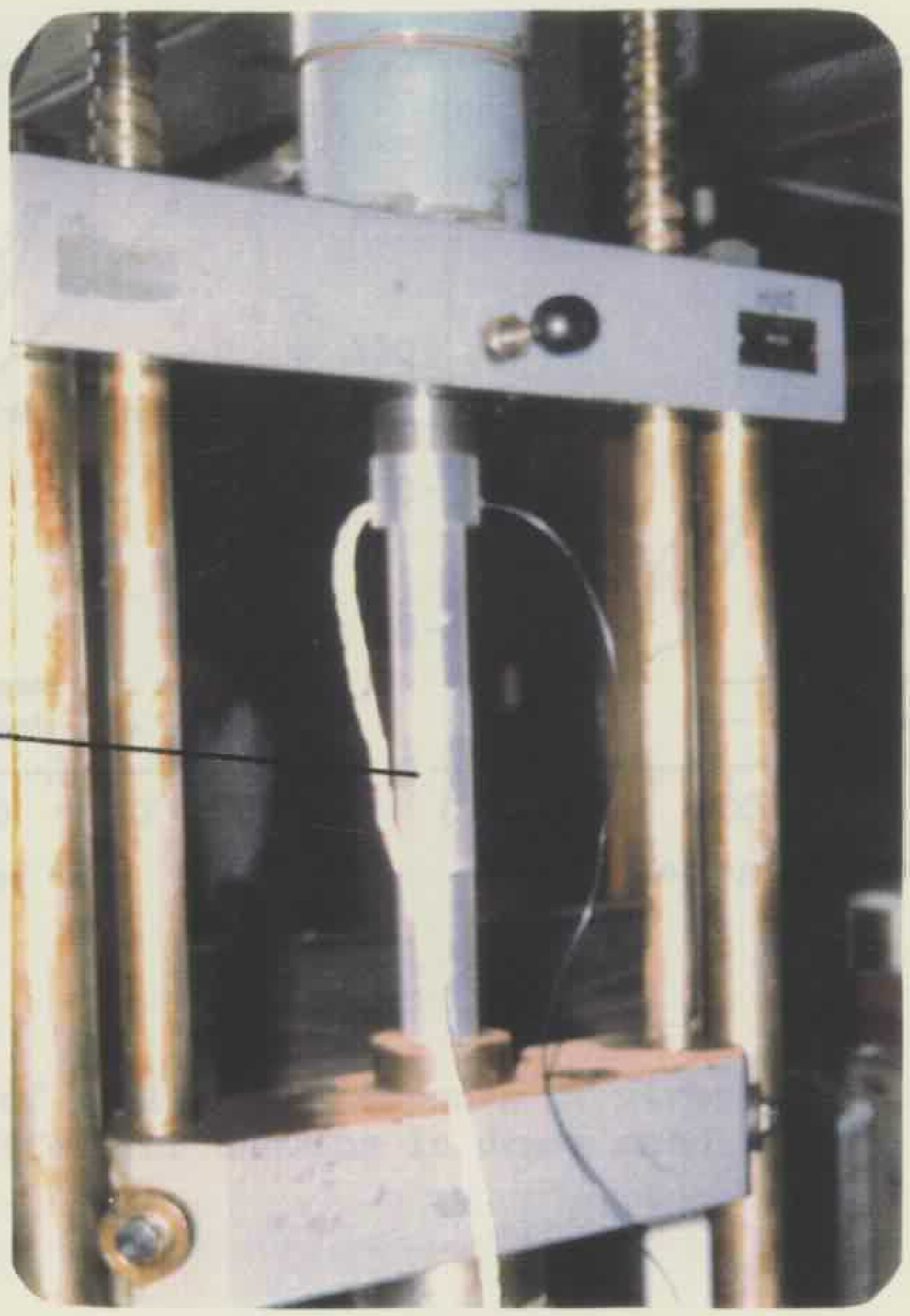

Plate 7.2 Axial load calibration of instrumented segment (50mm diameter)

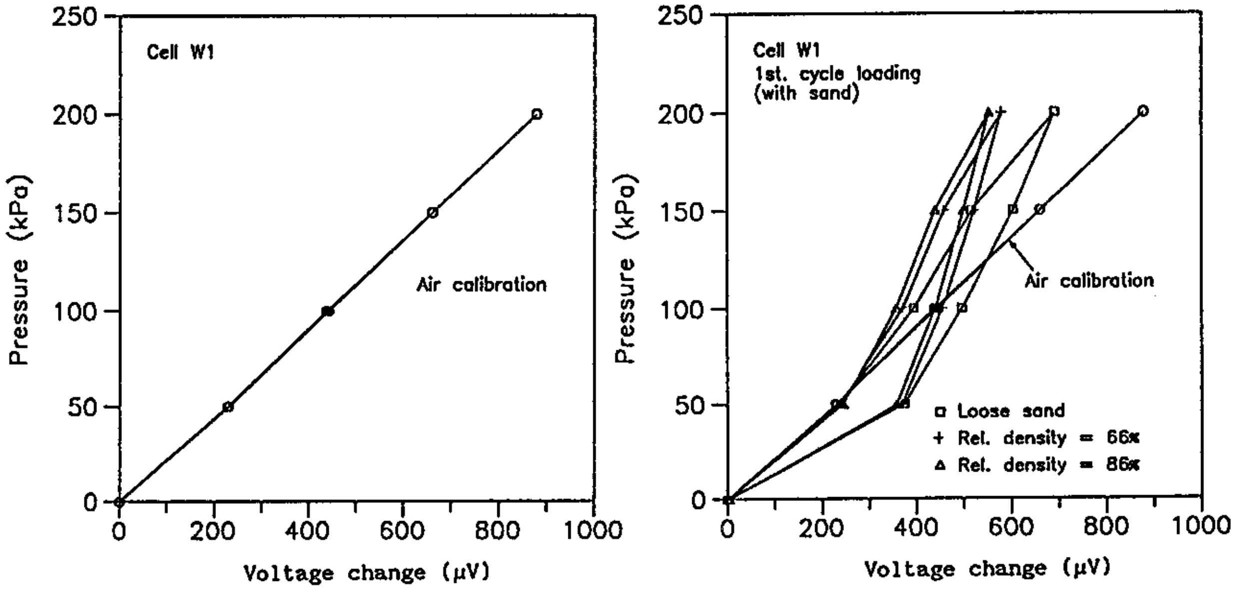

Fig. 7.1 (a) Air calibration response of stress cell; (b) Response of stress cell in sand for three different density states

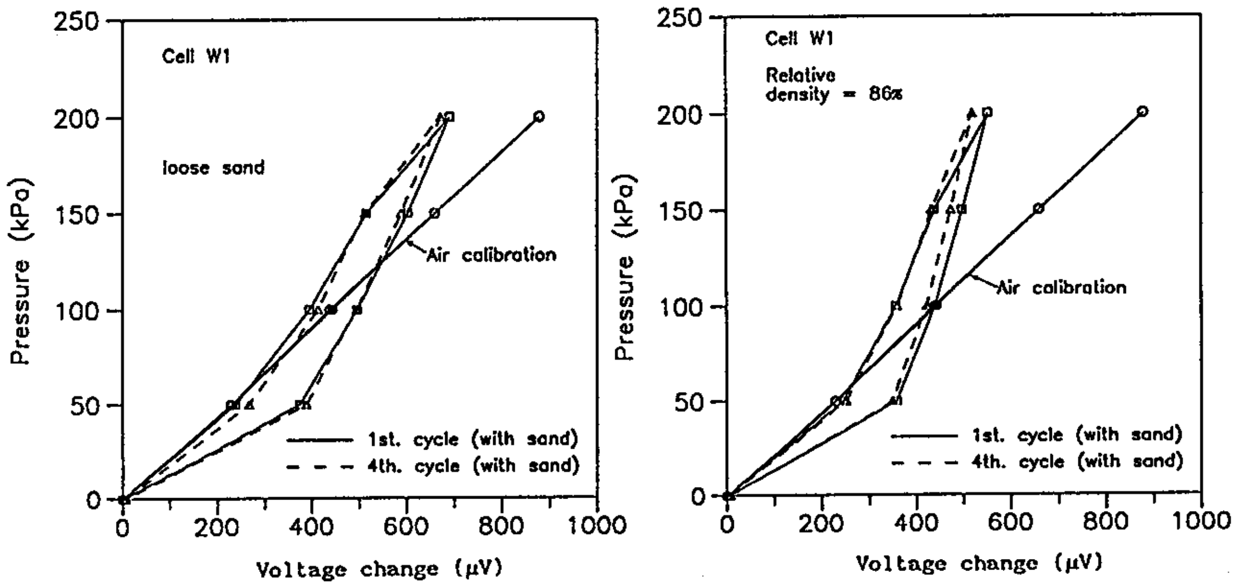

Fig. 7.1 (c) Effect of cycling on response of stress cell in loose sand; (d) Effect of cycling in dense sand

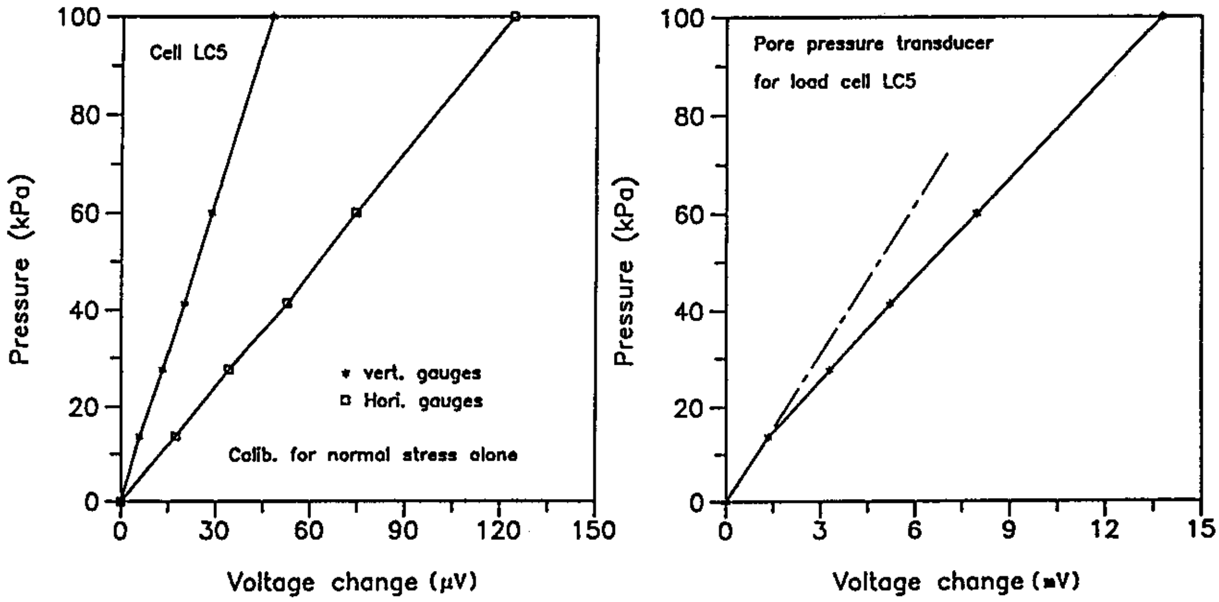

Fig. 7.2 Calibration of instrumented segment under applied horizontal (hydrostatic) stress: (a) vertical and horizontal gauges responses; (b) pore-water pressure transducer response

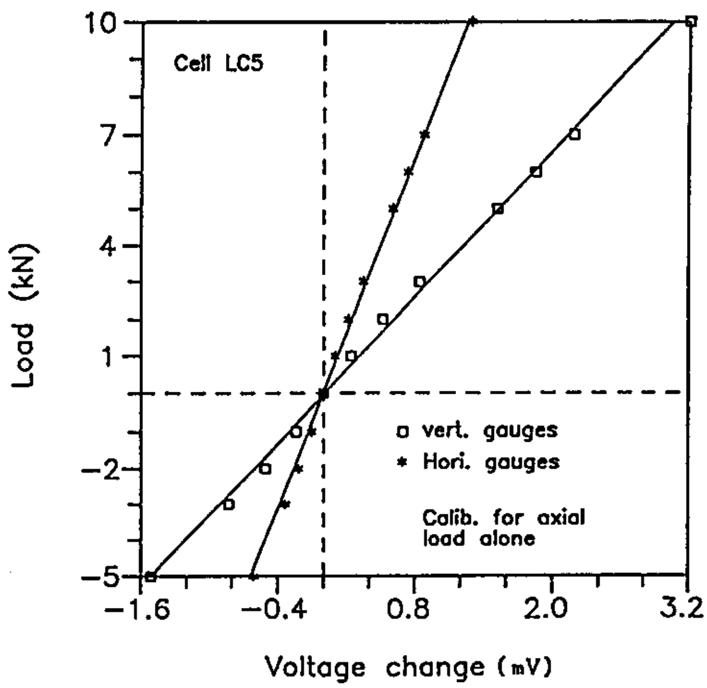

Fig. 7.3 Typical calibration response of instrumented segment under tension and compression axial load alone

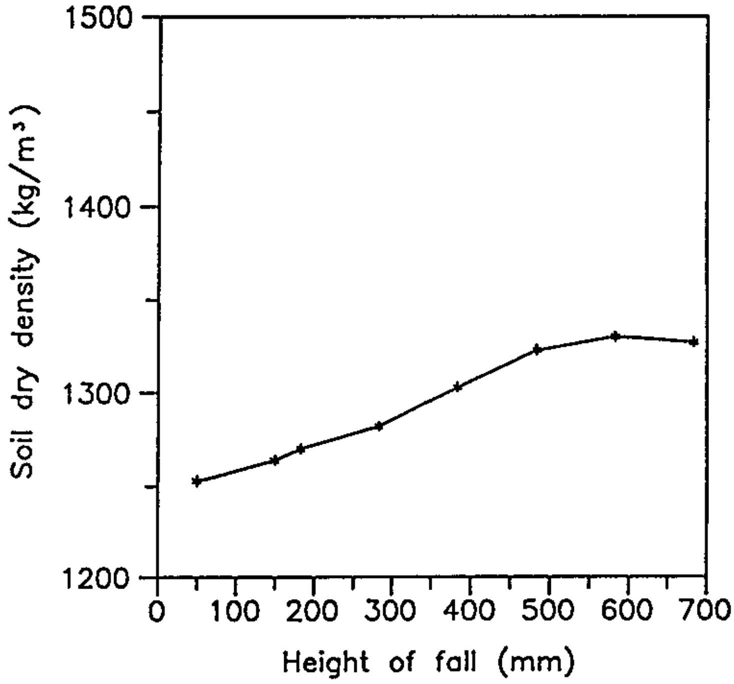

Fig. 7.4 Calibration results for height of falling sand against density

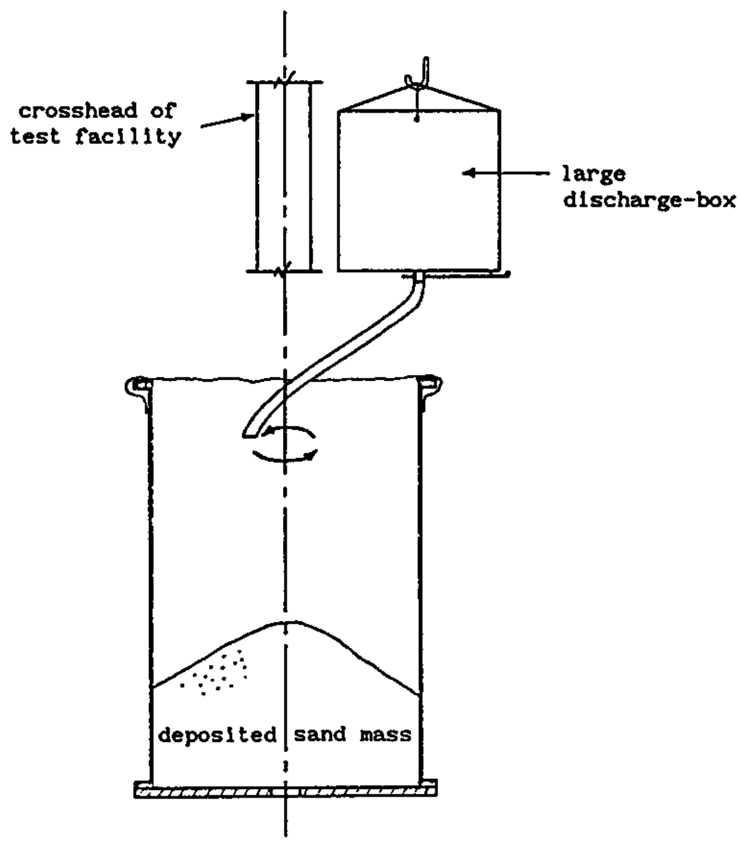

Fig. 7.5 Schematic diagram showing the sand placement procedure for filling the bottom-half of test pot

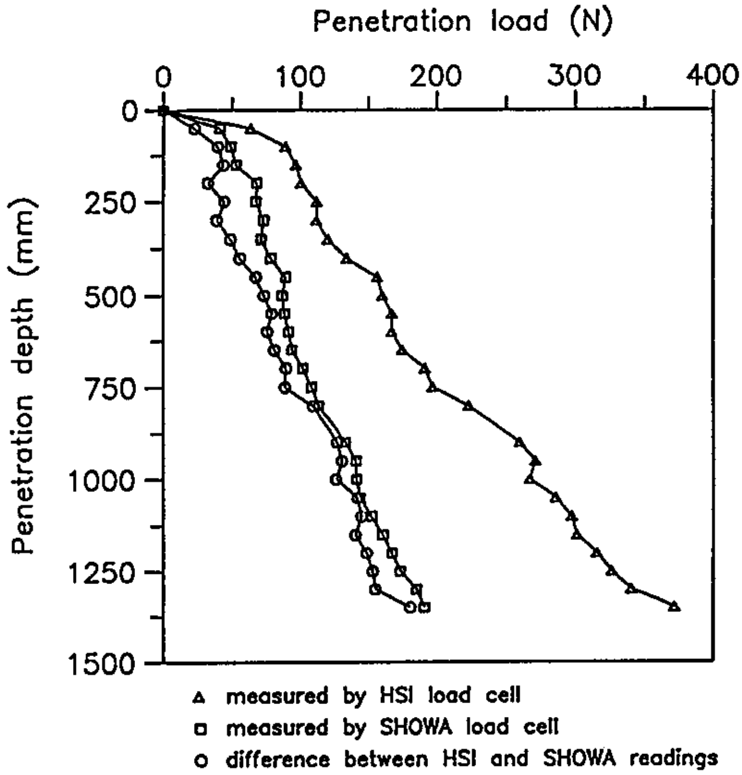

Fig. 7.6 Jacking load-penetration response obtained from pile "penetrometer" test

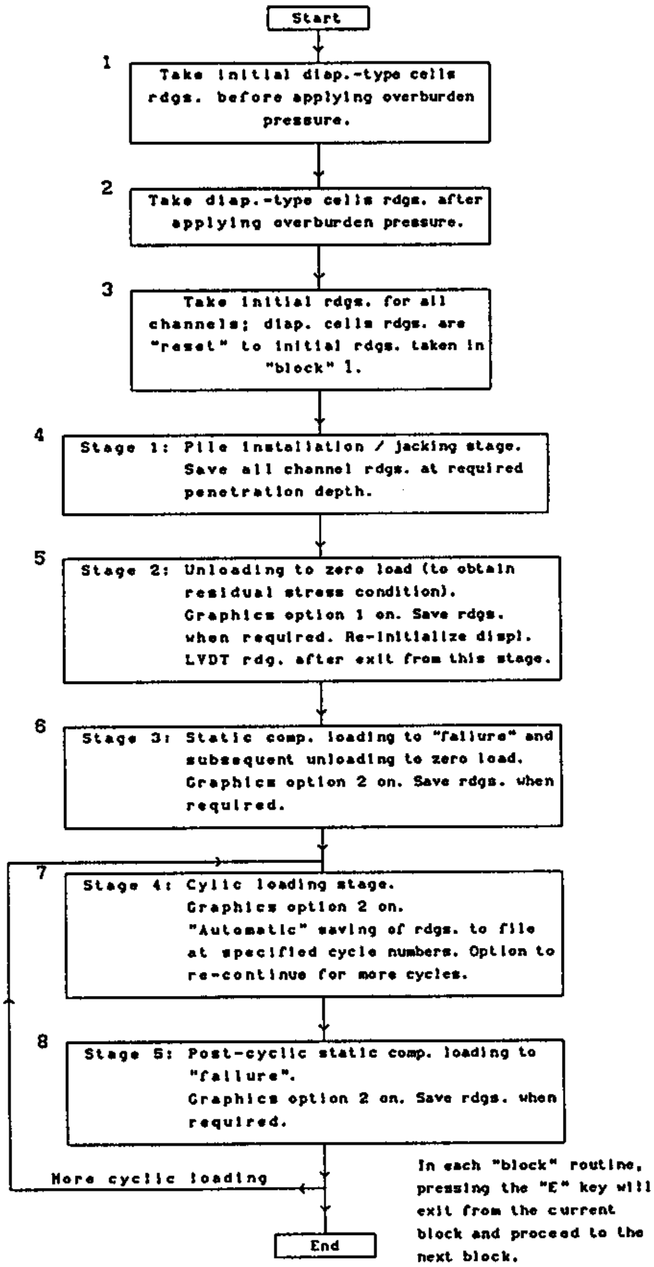

Fig. 7.7 Flow-chart for program DAQ.BAS

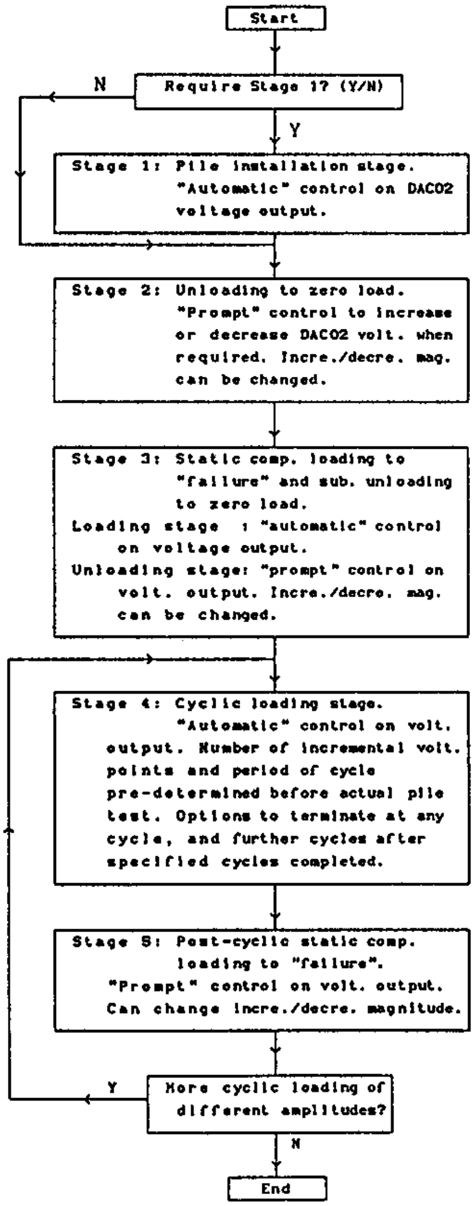

Fig. 7.8 Flow-chart for program DLOAD.BAS

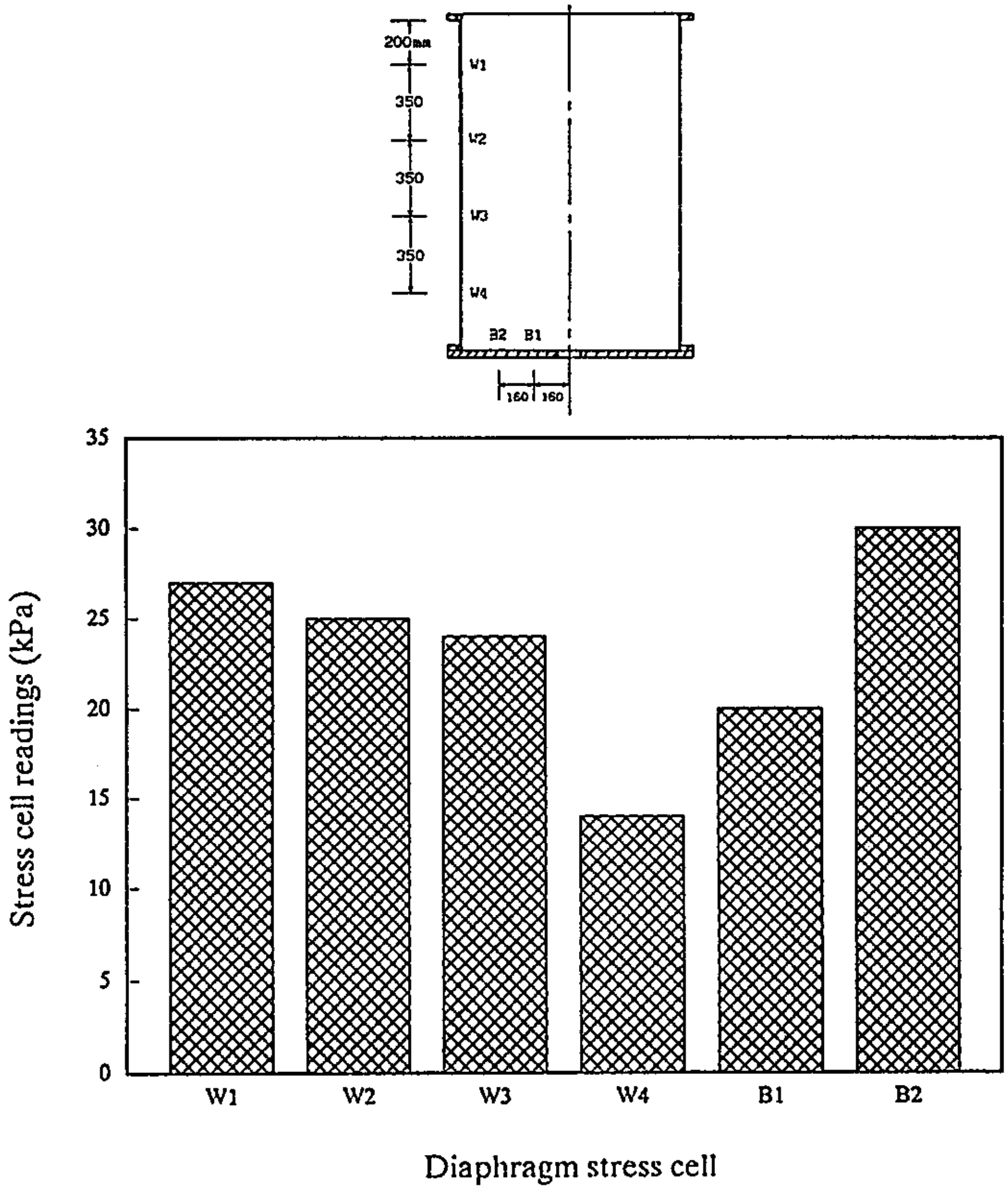

Fig. 7.9 Diaphragm stress cell responses after application of overburden pressure (100 kPa)

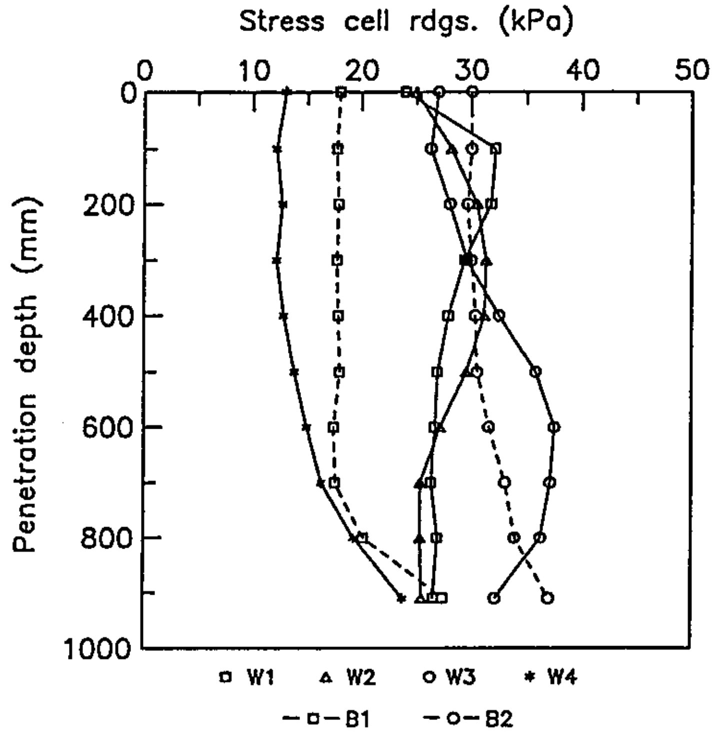

Fig. 7.10 Diaphragm stress cell responses during installation of 50mm diameter uninstrumented model pile

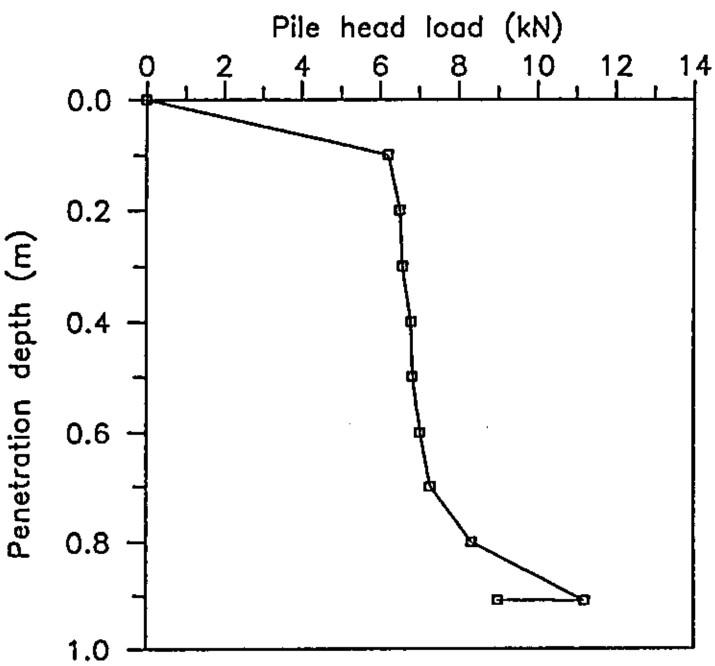

Fig. 7.11 Jacking load-penetration response during installation of 50mm diameter uninstrumented model pile

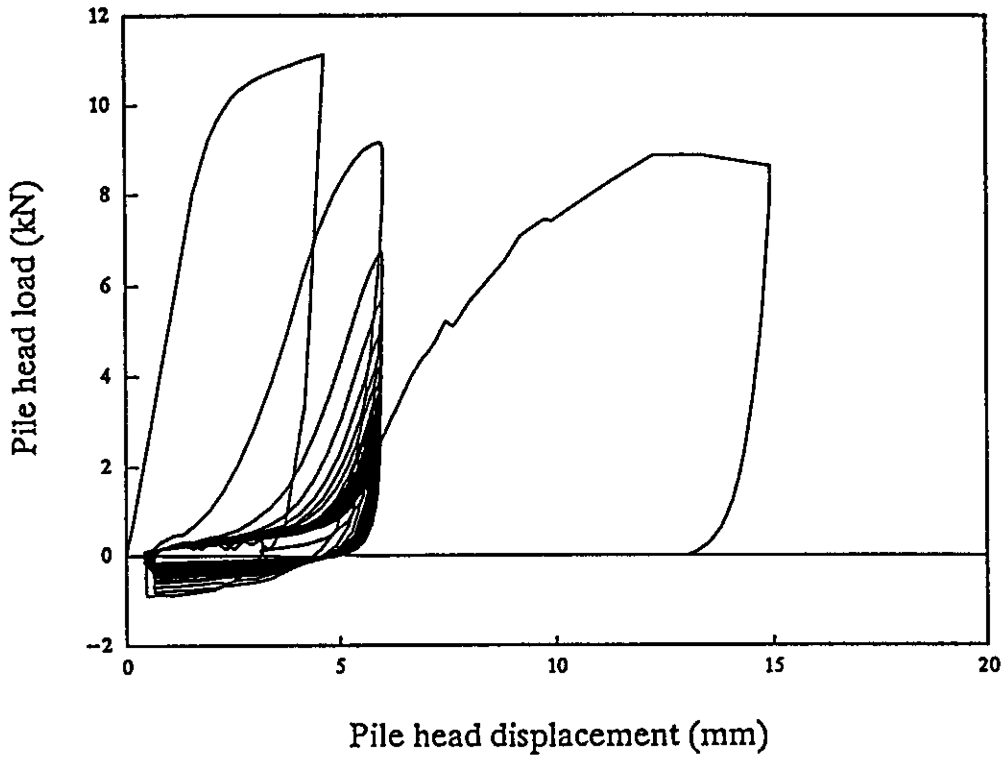

Fig. 7.12(a) Complete load-settlement response for 50mm diameter uninstrumented model pile: – initial static loading, cyclic loading and post-cyclic static loading responses

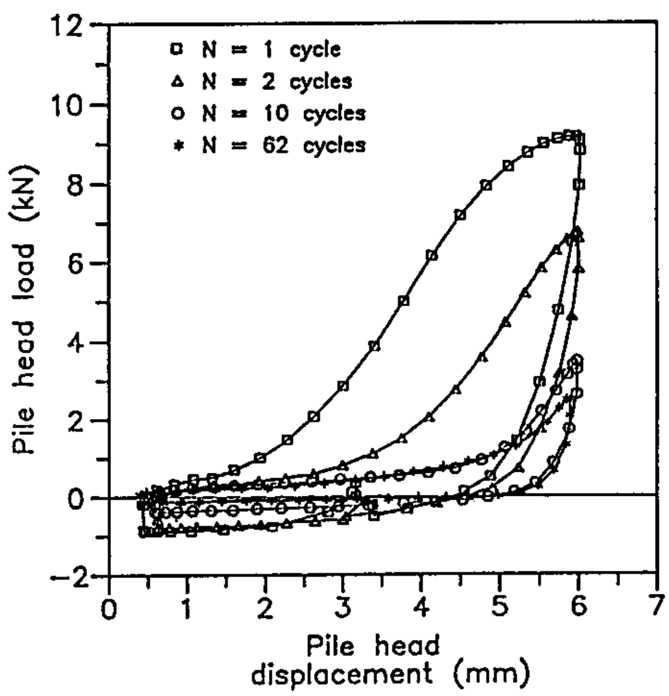

Fig. 7.12(b) Load-settlement response at specific cycles for 50mm diameter uninstrumented model pile

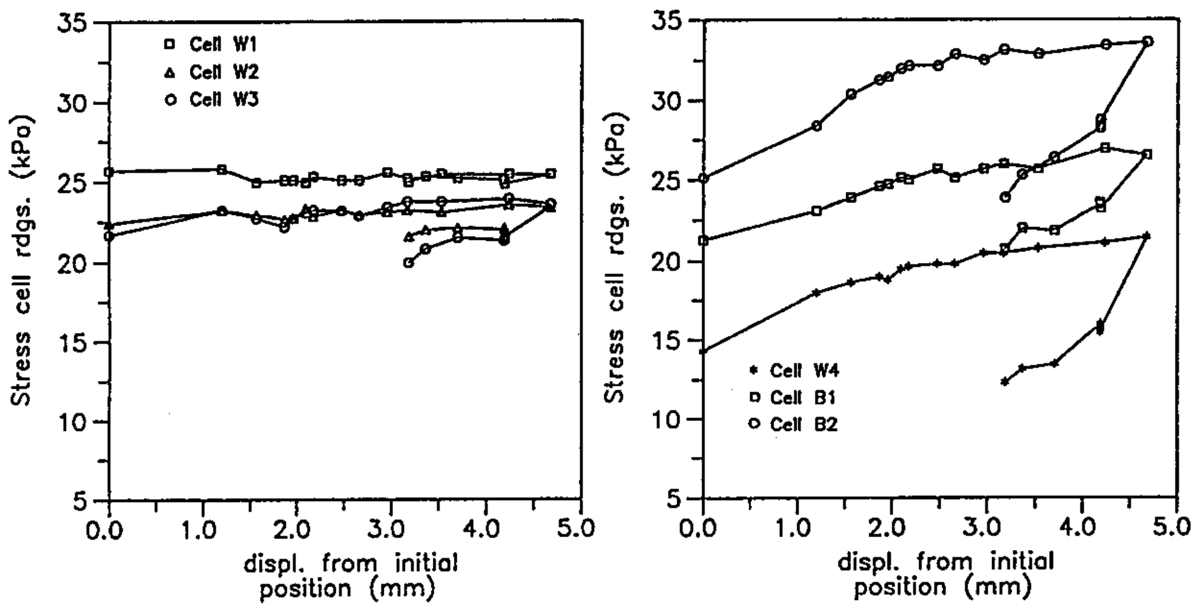

Fig. 7.13 Diaphragm stress cell responses during initial static loading of 50mm diameter uninstrumented model pile

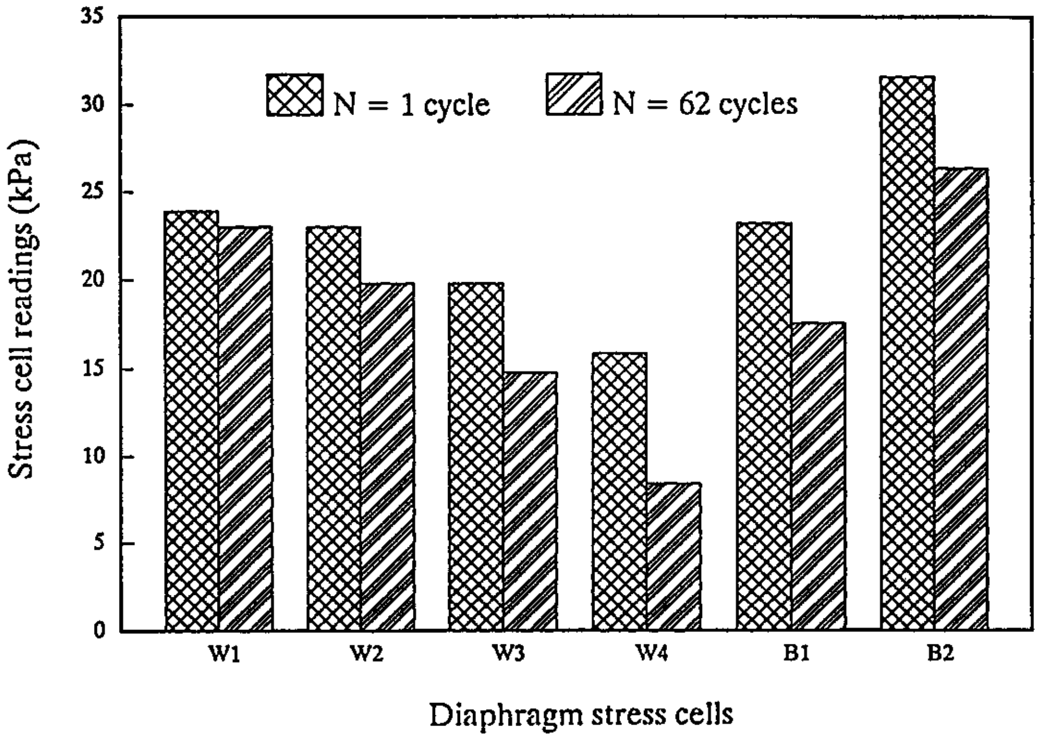

Fig. 7.14(a) Diaphragm stress cell responses before and after cyclic loading stage (50mm diameter model pile)

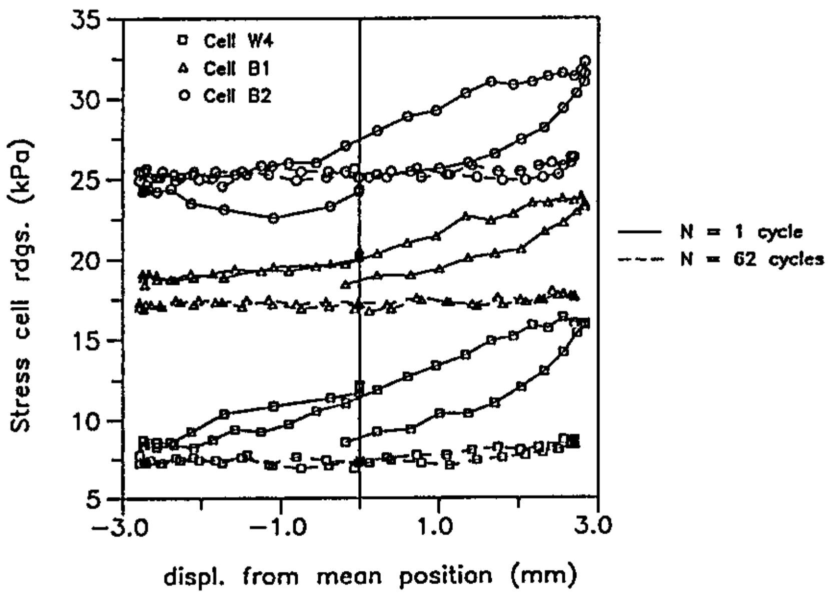

Fig. 7.14(b) Complete responses of cells W4, B1 and B2 at cycles N = 1 and 62 (50mm diameter model pile)

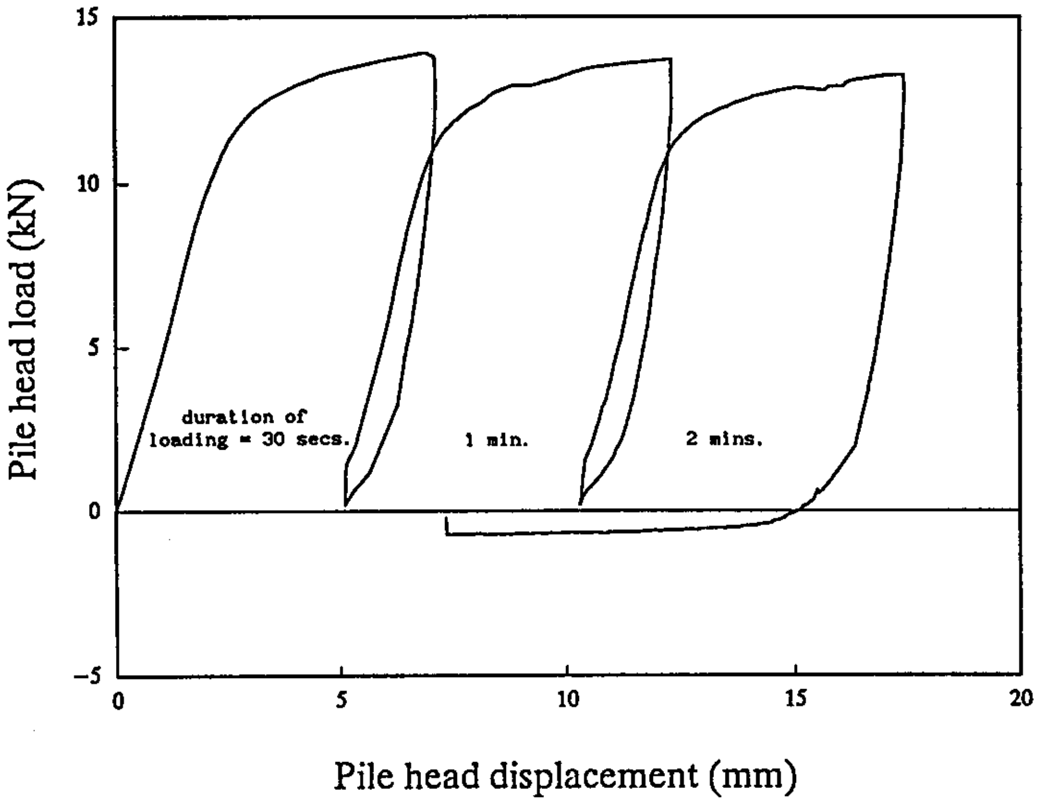

Fig. 7.15 Effect of loading rate on ultimate "static" compressive pile capacity

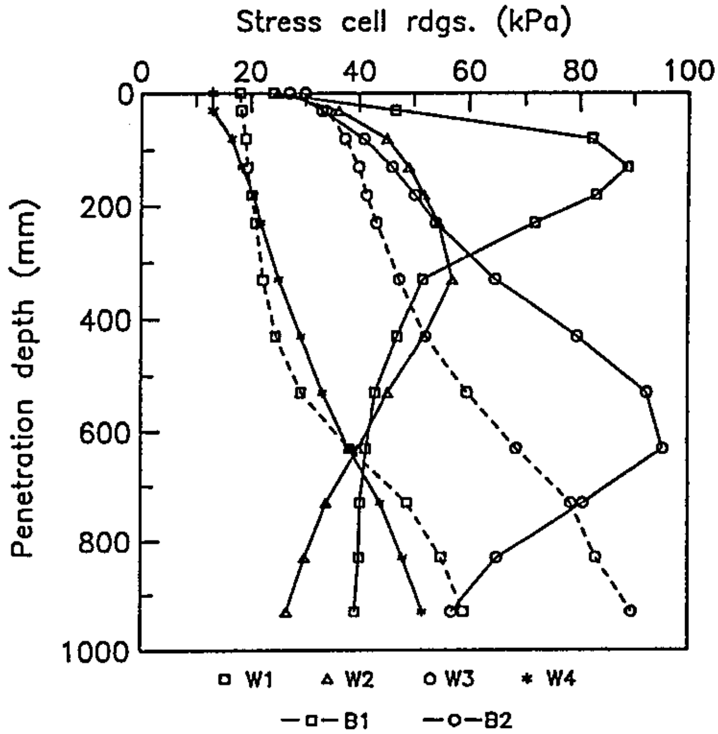

Fig. 7.16 Diaphragm stress cell responses during installation of 100mm diameter uninstrumented model pile

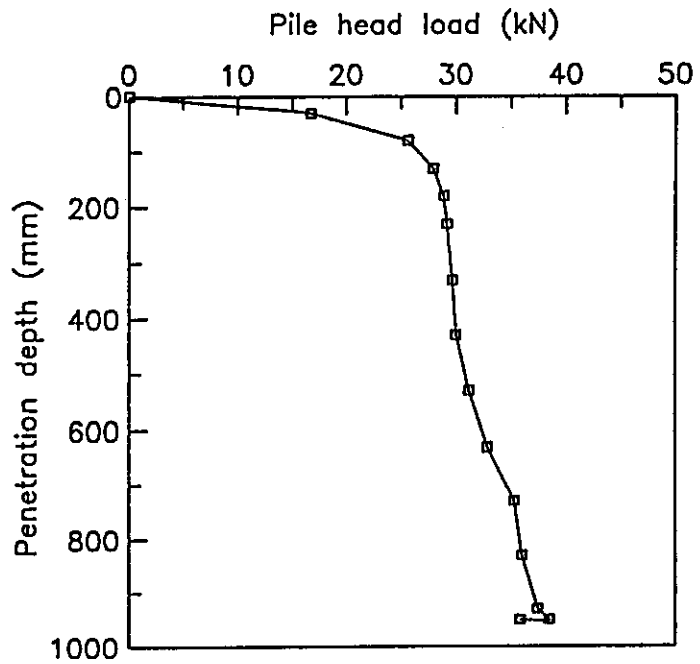

Fig. 7.17 Jacking load-penetration response during installation of 100mm diameter uninstrumented model pile

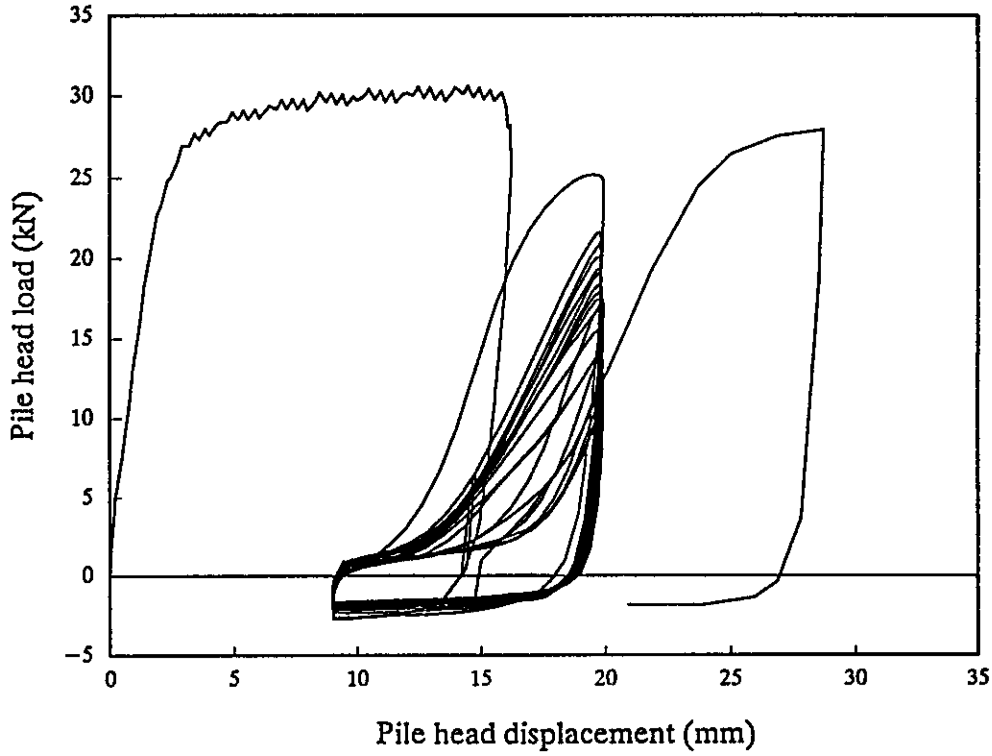

Fig. 7.18 Complete load-settlement response for 100mm diameter uninstrumented model pile:- initial static loading, cyclic loading and post-cyclic static loading responses

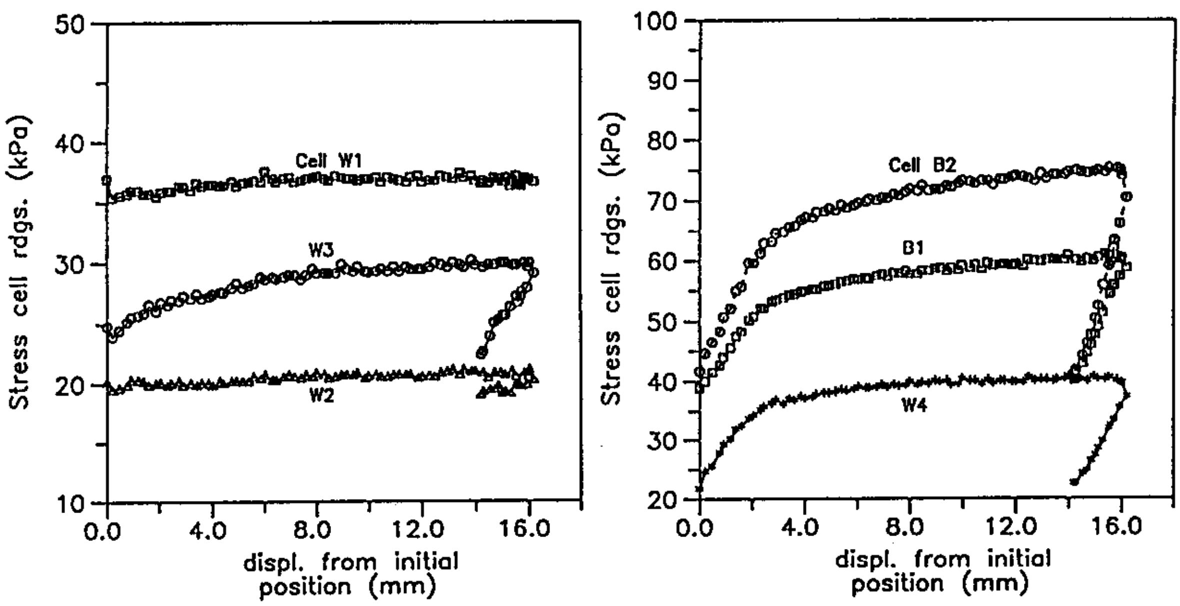

Fig. 7.19 Diaphragm stress cell responses during initial static loading of 100mm diameter uninstrumented model pile

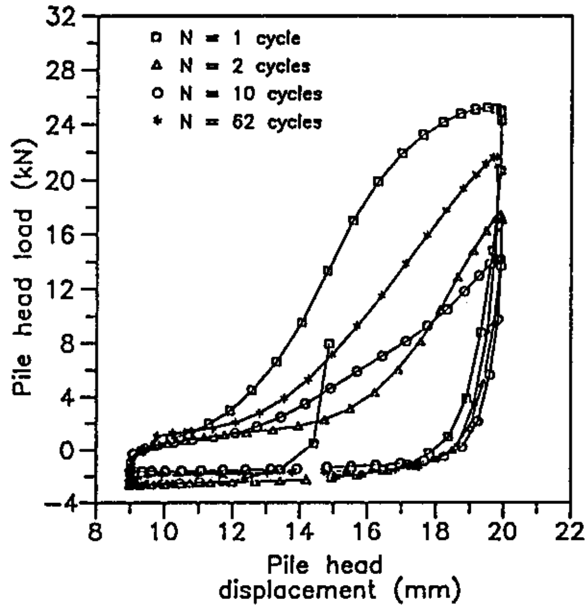

Fig. 7.20 Load-settlement response at specific cycles for 100mm diameter uninstrumented model pile

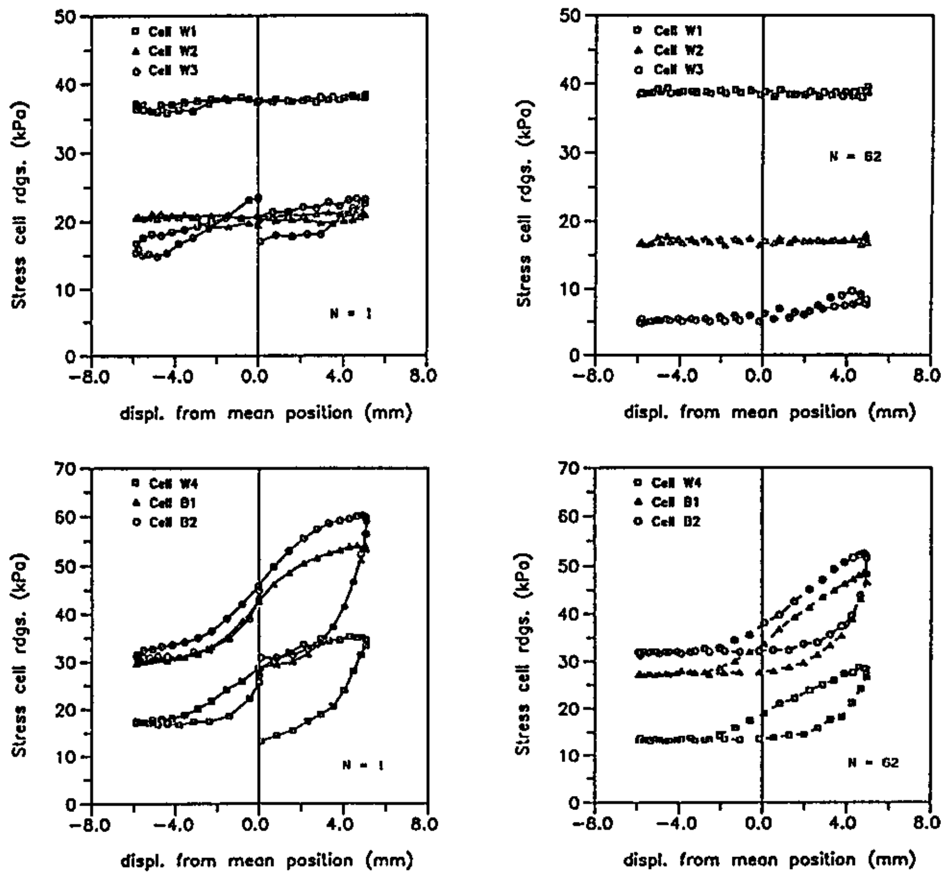

Fig. 7.21 Diaphragm stress cell responses at N = 1 and 62 (final) cycles of cyclic loading stage for 100mm diameter model pile

CHAPTER 8

INSTRUMENTED JACKED MODEL PILE TEST RESULTS

CHAPTER 8

INSTRUMENTED JACKED MODEL PILE TEST RESULTS

8.1 INTRODUCTION

In this chapter, the test results obtained from a series of model instrumented jacked pile tests in dry calcareous sand are presented and discussed. The model jacked pile tests were conducted using 50mm and 100mm external diameter instrumented aluminium pipe piles.

The test procedures adopted for the conduct of each test are as described in detail in Chapter 7. The influence of the pile diameter on the jacking (installation) response, initial static compression loading response, the cyclic displacement-controlled loading response, and the post-cyclic static loading response are assessed from the test results obtained. In particular, the effect of cyclic loading on pile capacity forms the main interest of the present experimental work.

8.2 TEST PROGRAM

For the present study, a total of six tests were conducted using both the 50mm and 100mm diameter closed-ended instrumented model piles. Table 8.1 shows the loading details adopted for each of the tests conducted. All six tests were carried out under a two-way displacement-controlled cyclic loading condition, with different cyclic displacement amplitudes being utilised. "Parcel" A (see Table 8.1) forms the main cyclic loading parcel of interest while the subsequent parcel or parcels were carried out to determine the effect (if any) of pre-cycling on the current parcel.

All tests were conducted using dry calcareous sand under a "standard" overburden pressure of 100 kPa. The embedded length of the pile was about 800mm for all the tests conducted. Thus, the length to diameter (ℓ/d) ratios for the 50mm and 100mm diameter model piles were 16 and 8 respectively. The model piles utilised were considered to exhibit a relatively "rigid" response under the present test conditions. Even though the pile instrumentation (for the 50mm diameter model pile) was designed initially with miniature pore-water pressure transducers to cater for the case of "wet" soil tests, only "dry" soil tests were conducted due to time restrictions in the author's candidature. It should also be noted that, due to the size of the test facility, a considerable amount of effort was required in the preparation for each test.

For all the tests conducted, the internal wall of the test chamber was greased and separated from the sand mass by a layer of polythene sheet. The responses of the diaphragm stress cells for the "greased" condition under the application of the overburden pressure (100 kPa) are compared to the "non-greased" responses presented in section 7.6.1.

This series of instrumented pile tests should provide a more detailed information on the pile response, and the general trends obtained are compared to the preliminary trends observed in the trial tests.

8.3 50mm DIAMETER MODEL PILE TEST RESULTS

Three tests were conducted using the 50mm diameter instrumented model pile, with the relevant loading details given in Table 8.1. The test results are presented and discussed in this section for the following loading stages: - installation (jacking) response, static loading response, and the cyclic loading response.

As mentioned earlier, the internal wall of the test chamber was greased for the actual instrumented pile tests. Fig. 8.1(a) shows the averaged responses of the diaphragm stress cells for the "greased" and "non-greased" conditions. Generally, under the "greased" condition, an increase in the stress cell measurements was recorded except that of cell B1. The side wall cells W1 to W4 recorded an increase of between 33% and 75% of the corresponding stress values for the "non-greased" case. The base cell B2 registered an increase of about 84% (of the corresponding stress value for the "non-greased" case) while cell B1 seems to be only marginally affected by the "greased" condition along the side wall. This observation therefore suggests the presence of some "arching" behaviour within the sand mass over the lower central portion of the test chamber.

Fig. 8.1(b) further shows the incremental responses of the stress cells for incremental increase in the applied overburden pressure. Generally, a quite linear response was obtained for all the stress cells. The "greased" condition was adopted for the present instrumented model tests as it resulted in a generally improved vertical stress transfer within the test chamber.

Fig. 8.2 shows the pile "penetrometer" responses obtained for the three tests (with zero applied overburden pressure) in order to gauge the consistency of the placed sand. In general, the agreement between the three responses appears to be quite satisfactory, thus indicating that the placement procedure adopted was adequate for the present study. Plates 8.1 and 8.2 show the pile "penetrometers" prior to, and after, installation into the sand bed respectively.

8.3.1 Installation (Jacking) Response

Fig. 8.3 shows a typical plot of the stress cell responses during the installation of the 50mm diameter model pile. Generally, the "rigid boundary" of the test chamber had an insignificant effect on the installation of the pile. The greater effective confining pressure (due to the applied overburden pressure) over the upper half of the chamber was reflected in the measured increase in the readings of cells W1 and W2 during the first 200mm of penetration. At the final penetration of about 800mm, the lower cells W4, B1 and B2 seem to be not affected by the penetrating pile. This is in contrast to the observed increase in the measured readings (for cells W4, B1 and B2) obtained in the trial test (see Fig. 7.10). This observed increase in the trial test was due to the greater sand density in the lower portion of the chamber caused by repeated compactions (from the trial penetration tests) and the use of a larger overburden pressure of 130 kPa for compacting the "used" sand. This observation therefore shows the important influence of the sand density in affecting the stress transfer within the test chamber during the installation of the pile.

The variations of the jacking load at the pile head and pile tip during the pile installation stage for the three tests are shown in Figs. 8.4(a) and 8.4(b) respectively. In general, the measured responses for the three tests were found to agree quite well. As shown, the maximum jacking force was mobilised at a penetration of about 100mm (i.e two pile diameters). Beyond this depth, the jacking force required reduced with further penetration until the "ultimate" condition was reached when the penetration depth exceeded about 500mm. The tip load mobilised during this installation stage constituted a major proportion of the jacking load required. The "softening" response of the jacking load required was due mainly to the corresponding decrease in the pile tip load mobilised (since the developed skin friction along the pile shaft forms only a small proportion of the total jacking load). This reduction in the mobilised pile tip load could be attributed to the contractive volume change characteristics of the calcareous sand, and to the fact that the effective confining pressure in the sand mass (as a result of the applied overburden pressure) decreased with depth. It is not possible to state conclusively at this stage which one of these two factors contributes most to the "softening" observed, although it is likely that, under the present test condition, the reduced effective confining pressure in the sand mass was the dominant factor which contributed to the observed "softening".

It may be noted that the "softening" response in the jacking load obtained in these actual instrumented pile tests was not observed in the trial test results presented in section 7.6.1. This discrepancy could have been caused by the compacted sand mass due to repeated usage of the "same" sand during the trial testing stage.

Figures 8.4(c) and 8.4(d) further show the developed average unit skin friction and end-bearing pressure respectively during the model pile installation stage for the three tests conducted. The peak average skin friction values (Fig. 8.4c) show greater variation and generally occur within a penetration of about 100mm (i.e two pile diameters). Beyond this depth, the average skin friction decreased with further penetration and became more or less constant when the penetration depth exceeded about 10 diameters. Test A3 registered an initial peak value of about 67 kPa while values of about 32 kPa and 13 kPa were obtained for Tests A2 and A1 respectively. The reason for the large variation obtained between the three tests, particularly the low value registered for Test A1, is not clear but may be due to the difficulty of accurate measurement of the low shaft resistance (obtained from the difference between the measured pile head and pile tip load readings) at shallow penetration depths. All three tests however showed consistent trends with the 25mm model jacked pile test results reported by Poulos and Chan (1988). Even though the peak average skin friction values vary significantly for the three tests, the "ultimate" values (at final penetration depth) of about 9 kPa however were in good agreement. The mobilised end-bearing pressure (Fig. 8.4b) decreased with penetration and reached an "ultimate" value of between 1.99 MPa and 2.17 MPa for the three tests.

Plates 8.3 and 8.4 show the 50mm diameter instrumented model pile prior to, and after, installation into the sand bed respectively.

After completion of the installation stage, the load on the pile head was reduced to almost zero in order to obtain the residual stress condition along the pile. Considerable scatter was observed in the measured strain-gauged load cells readings along the pile for the three tests. It was not clear what could have contributed to this inconsistency, but it might have been due to some drift in the strain-gauges and the reduced accuracy at such low load levels. This difficulty in obtaining consistent residual force distribution was also observed in the field test results reported by, for example, O'Neill *et al.* (1982a) and Rieke and Crowser (1987). Fig. 8.5(a) shows the residual force values as measured by the load cells along the pile for Test A3. The results for the other two tests were too scattered to provide any reasonable interpretation. Based on our understanding of the physical aspects of the problem (Rieke and Crowser, 1987; Leonards and Darrag, 1989), the curve shown was fitted to the data points (excluding the "circled" data point). The residual force was observed to increase (due to the presence of negative downward-directed pile-soil shear stresses) along the pile to a depth of about 90% of the pile length, and thereafter decreased (because of the presence of positive pile-soil shear stresses) to the residual compressive pile tip load. The peak compressive residual force was about 6% of the total static compressive capacity of the pile. The residual shear stress distribution, based from the fitted residual force profile, is further shown in Fig. 8.5(b). The transition from negative shear stresses to positive shear stresses is evident at the vicinity of the pile tip.

It was a disappointment (as is usually inevitable in any instrumentation system) that the deduced normal pile-soil interface stresses, from the measured strain-gauge readings at each load cell segment (see section 6.4.2), were erratic for any consistent interpretation of the deduced values. These deduced values tend to alternate between positive (i.e compressive pressure) and negative values during jacking. It was not known why this inconsistent response occurred but might be caused by any slight off-vertical alignment of the pile during penetration. Even though the strain-gauge arrangement would theoretically cancel out any bending effect, this bending effect might not have been completely nullified due to the possibility of some slight misalignment of the installed strain-gauges. Moreover, the low developed average pile-soil normal stress expected (under the applied overburden pressure of 100 kPa), as deduced from the strain-gauge readings, would be affected more by any slight bending present. For situations where large normal pile-soil interface stresses are developed (for example, under higher applied overburden pressures), any slight bending effect would probably be less significant.

It should be noted that it is not possible to know whether the embedded pile shaft is perfectly vertical during penetration. Although increasing the rigidity of the pile (i.e larger thickness of the pipe pile) would reduce any bending of the embedded pile shaft, it would also result in a less "sensitive" pile.

The deduced normal pile-soil stress values during the subsequent stages of the pile test also showed a similar inconsistent response. Therefore, no useful interpretation could be obtained for these stages as well. Although the calibration of each segment showed the applicability of the approach, the actual instrumented pile tests however indicated this simplified procedure for deducing the normal pile-soil interface stresses to be affected by the factors mentioned above. It is hoped that future attempts to measure the normal pile-soil interface stress could be directed at the more complicated method of installing Cambridge-type contact stress cells along the pile shaft.

8.3.2 Initial Static Response

The complete pile head load-settlement responses for the three 50mm diameter model pile tests are shown in Figs. 8.6(a)-(c). Note that not all cycles of the cyclic loading stage are shown as only the data from specific cycles were saved to file during the conduct of the tests. This section will look in more detail at the response of the pile during the initial static loading stage.

Fig. 8.7 shows the initial static loading responses for the three tests. Table 8.2 further summarises the initial static loading results obtained. The maximum "static" compressive load (at about 10% pile diameter movement) mobilised was found to vary between about 4.8 kN and 5.4 kN. The shaft capacity on the other hand was found to vary between 0.86 kN and 1.25 kN, forming less than between 17% and 23% of the total pile capacity. The end-bearing capacity thus provided the major component of the total developed pile capacity. Although the developed static capacity for Test A1 was lower than the other two tests, the agreement among the three tests was considered reasonably good within experimental accuracy, in view of the scale of the test. It may also be noted that the maximum static load values obtained are in good agreement with the corresponding values obtained during the installation stage at the final penetration depth.

Figs. 8.8(a) and 8.8(b) further show the developed average unit skin friction (over the embedded length of the pile shaft) and end-bearing pressure during the initial static loading. In general, the developed average unit skin friction varied from about 6.8 kPa to 10 kPa and was mobilised fully at a displacement of about 1.5mm to 2.0mm (i.e between 3% and 4% of the pile diameter). The "up and down" nature of the data points was due to the hydraulic loading system where a "relax" condition of the pile was obtained between points of downward (i.e compression) movement of the central jack. The end-bearing pressure developed varied between 2.01 MPa and 2.12 MPa, with a slightly greater displacement of about 3.5mm (i.e 7% of pile diameter) required to fully mobilise it.

It is of interest to note that the maximum unit average skin friction (over the embedded pile shaft) under tension loading (obtained from the measured pile head tension load at the first cycle of Test A3) is about 59% of the averaged maximum unit skin friction value (about 8.3 kPa) under compression loading. The lower skin friction under tension loading, as compared to that under compression loading, has also been observed in other model scale (for example, Yazdanbod *et al.*, 1984) and field scale (for example, Hunter and Davisson, 1969; Rieke and Crowser, 1987) driven pile tests.

The load distributions along the pile at failure for the three tests are shown in Fig. 8.9. The results from Tests A2 and A3 seem to be in good agreement, generally indicating greater load transfer over the top 400mm of the pile and in the vicinity of the pile tip. The reason for the discrepancy obtained in the load distribution for Test A1 is not clear.

8.3.3 Cyclic Loading Response

In this section, the cyclic responses of the three 50mm diameter model piles under the sequence of displacement-controlled loading parcels are presented and discussed.

The complete load-settlement responses of the three tests have been shown earlier in Figs. 8.6(a) to 8.6(c). The normalised values (with respect to the corresponding values at N = 1 cycle) of the measured pile head load, at both the tension and compression ends of each cycle, are shown in Figs. 8.10(a) to 8.10(c) for the three tests. Table 8.3 further tabulates the measured pile head load at the beginning and end of each displacement-controlled parcel.

As shown (Fig. 8.10), there is generally a continuous decrease in the mobilised skin friction (given by the measured pile head load at the tension end of each cycle) as cycling proceeds. The magnitude of decrease (i.e degradation) in the mobilised skin friction was found to be dependent on the magnitude of the cyclic displacement to which the pile was subjected. Table 8.4 tabulates this reduction in terms of a degradation factor (defined as the ratio of the measured pile head tension loads of the last cycle to the first cycle within each load parcel) for each of the loading parcels. As expected, for the primary loading parcel A, more significant degradation was obtained for the larger cyclic displacement tests (see Fig. 8.11). The results appear to indicate that for normalised cyclic displacement, ρ_c/d, of less than ±0.025, minimal degradation in skin friction is to be expected. It is of interest to note that this cyclic displacement amplitude (ρ_c/d = ±0.025), where minimal degradation in skin friction was obtained, is of the order of that required to fully mobilise the shaft resistance. The rate of reduction in the degradation factor value decreased with increasing cyclic displacement values (see degradation values for parcel A of Table 8.4). For Test A1, the influence of the subsequent larger displacement loading parcels B and C resulted in further degradation of the skin friction resistance. This observation was also obtained for Test A2 where further degradation occurred under load parcel B. It may be noted that the degradation in skin friction, under the cyclic displacement ρ_c/d of ±0.10 (i.e load parcels C and B for Tests A1 and A2 respectively) for Test A2 was more significant than for Test A1. It was not clear what could have contributed to this discrepancy. For Test A3 (with load parcels details the reverse of those in Test A2), the smaller cyclic displacement parcel B had an insignificant effect in causing further degradation of the skin friction. This shows that application of smaller displacement loading parcels, following a larger displacement loading parcel, should not result in any further significant degradation of the skin friction since most degradation would have occurred within the larger displacement loading parcel. It is interesting to note that the final normalised values of the tension pile head loads for Tests A2 and A3 (see Figs. 8.10b and 8.10c) are almost identical (a value of about 0.2). This suggests the presence of a minimum (or limiting) degradation factor corresponding to maximum possible degradation for the pile-soil system. This limiting degradation factor is thought to be primarily a function of the soil type, soil density and the characteristics of the pile-soil interface. This observation also appears to indicate that the total degradation in skin friction is independent of the order of occurrence of the displacement-controlled loading parcels.

The cyclic test results (see Figs. 8.10a to 8.10c) also revealed an interesting observation at the compression end of the cyclic loading parcels. The results indicated that, depending on the magnitude of the cyclic displacement, it was possible to obtain an increase in the measured compression load following an initial reduction. This increase in the measured pile head load was due to a corresponding increase in the measured pile tip resistance which, in turn, was caused by the compaction of the sand mass under the pile tip (see Figs. 8.12a to 8.12c). Table 8.5 tabulates this pile tip "magnification" factor (defined as the ratio of the measured pile tip resistances of the last cycle to the first cycle within each displacement parcel) for the three tests. As noted by Turner and Kulhawy (1989) (and mentioned in section 7.6.2), the pile tip resistance may degrade or increase under repeated compression loading. The present results appear to indicate a threshold cyclic displacement (ρ_c/d) value of ±0.025 (parcel A of Test A1; Fig. 8.10a) below which, a reduction in the pile tip resistance is expected to occur while an increase is expected for larger cyclic displacement values. It may be noted that the trial 50mm diameter model test (see section 7.6.1), under a cyclic displacement ρ_c/d of ±0.053, indicated a continuous reduction in the measured pile head compression load. This is contrary to the observed increase (after an initial reduction) obtained in the actual test under the same cyclic displacement value (see parcel A of Test A2, Fig. 8.10b). This discrepancy could have been caused by the "stiffer" sand mass in the trial test, with minimal flow of sand into the vicinity of the pile tip required for compaction under the pile tip to occur. Based on this reasoning, it is hypothesised that for cemented sand (or dense sand) no increase in the pile tip resistance would be obtained. Table 8.6 further tabulates the estimated initial and post-cyclic static capacities (at 10% pile diameter movement) for the three tests. The post-cyclic static capacities were estimated as the pile head load at a pile head displacement of about 10% pile diameter from the compression end of the relevant displacement parcel. The influence of the larger displacement parcel in increasing the static pile capacity is clearly evident. The final static capacity values for Tests A2 and A3 were found to be in good agreement.

The present cyclic results therefore indicate that although the skin friction capacity degrades under cyclic loading, the total post-cyclic compressive static pile capacity can increase if the pile tip is subjected to sufficiently large cyclic displacement amplitudes. For tension piles however, which rely solely on the mobilised skin friction, any increase in the pile tip resistance as a result of cyclic loading provides no contribution to the tensile capacity of the piles.

8.4 100mm DIAMETER MODEL PILE TEST RESULTS

Three tests were conducted, with the loading details as shown in Table 8.1, using the 100mm diameter instrumented model pile. As mentioned in section 8.3.1, the deduced normal pile-soil interface stresses using the 50mm diameter instrumented model pile were not satisfactory for any consistent interpretation. As such, the 100mm diameter model pile had been instrumented to measure solely the axial load along the pile. For Tests B2 and B3, a loading period of about 40 seconds was utilised for the two-way displacement-controlled loading parcels. The test results are presented and discussed in the following sub-sections.

8.4.1 Installation (Jacking) Response

The typical responses of the diaphragm stress cells during the installation of the 100mm diameter model pile are shown in Fig. 8.13.

The top three cells W1, W2 and W3 (along the side wall) registered quite significant increases as the penetrating pile approached the level of the cells. The maximum increase registered by these three cells was about five times greater than the corresponding maximum increase recorded during the installation of the 50mm diameter model pile (compare Figs. 8.3 and 8.13). At the final embedded penetration of about 800mm, the influence of the bottom rigid base plate was considered not significant from the measured readings of the base cells B1 and B2. Again, the denser sand mass in the trial test (see Fig. 7.16) resulted in an earlier larger increase in the stress readings of cells B1 and B2.

The jacking-load penetration responses for the three tests that were measured at the pile head and pile tip are shown in Figs. 8.14(a) and 8.14(b) respectively. Good consistent agreement was obtained for the three tests. As compared to the case of the 50mm diameter model pile (see Figs. 8.4a and 8.4b), no "softening" was observed in the jacking load except near the final embedded depth of the pile. This absence of the "softening" effect could be attributed to the larger increased effective confining stresses in the sand mass (as indicated by the diaphragm stress cells) caused by the penetrating pile. The maximum jacking load was reached after a penetration of about four diameters into the sand bed. Figs. 8.14(c) and 8.14(d) further show the developed average unit skin friction and end-bearing pressure respectively with pile penetration. Good agreement is obtained for both responses. The developed average skin friction at final penetration for the three tests was found to be about 13.8 kPa (Fig. 8.14c). This value of 13.8 kPa is greater than the 9 kPa value obtained from the 50mm diameter model pile tests. It may be noted that the developed average unit skin friction values at shallow penetrations show less variation among the three tests as compared to the 50mm diameter case (compare Figs. 8.4c and 8.14c). For the developed end-bearing pressure, again larger values of between 2.91 MPa and 3.0 MPa (as compared to between 1.99 MPa and 2.17 MPa for the 50mm diameter case) were obtained for the three tests. As mentioned earlier, the larger values obtained for the developed average unit skin friction and end-bearing pressure could be attributed to the larger effective confining stresses in the sand mass caused by the penetration of the 100mm diameter model pile.

As with the 50mm diameter tests, the installation residual force distributions for the present 100mm diameter tests also show considerable scatter (Fig. 8.15). Due to the erratic nature of the as-measured values of the residual force along the pile, no attempt was made to fit a curve to the data points. Nevertheless, the results showed that the embedded pile shaft was subjected to a net compressive force as a result of the residual stresses. The peak compressive residual force values (at the pile tip) for the three tests were found to vary between 7% and 8% of the averaged value of the total static compressive capacities for the three tests.

8.4.2 Initial Static Response

The complete pile head load-settlement responses for the three tests are shown in Figs. 8.16(a) to 8.16(c). For Tests B2 and B3, only 25 cycles and 10 cycles of parcel B respectively were managed during testing due to excessive settlement of the sliding collar. The present section will however confine attention to the initial static loading responses of the three tests.

Fig. 8.17 shows the total mobilised pile head load and shaft load capacity with increasing static pile head displacement. Table 8.7 further summarises the results obtained for the three tests. As compared to the 50mm diameter pile test results, the present 100mm diameter test results show very good agreement. The total static compressive capacity was found to vary between 26.3 kN and 26.8 kN while the shaft capacity was in the range 3.2 kN to 3.4 kN. The shaft capacity therefore forms a minor proportion (about 13%) of the total static capacity of the pile. It may also be noted that the total static capacity mobilised is in good agreement with the corresponding value obtained during the installation stage at final penetration. This agreement is in contrast to that obtained in the trial test (see section 7.6.2) which showed the jacking load at final penetration to be greater than the mobilised static load value. This again indicates the greater influence of the "rigid boundary" of the test chamber for the denser sand mass that was associated with the trial test.

A displacement of about 2mm (i.e 2% pile diameter) was required to fully mobilise the pile shaft capacity. This magnitude of movement was also found to fully mobilise the shaft capacity for the 50mm diameter pile tests (see Fig. 8.7). The test results (from both the 50mm and 100mm diameter piles) therefore appear to indicate that the static diaplacement required to fully mobilise the pile shaft capacity is practically independent of pile diameter. It may be noted that the model and field scale pile test results reported by Nauroy *et al.* (1988) also showed that the displacement to mobilise the full shaft capacity was practically independent of the pile diameter. This trend was also noticed in the model drilled shaft tests in cohesionless soil reported by Turner and Kulhawy (1987). For the pile tip, a larger static displacement of about 5mm (i.e 5% pile diameter) was required to mobilise fully the end-bearing resistance.

Figs. 8.18(a) and 8.18(b) further show the developed average unit skin friction and end-bearing pressure during the initial static compressive loading test. Good agreement among the three tests is obtained for both cases. The developed maximum unit skin friction values of between 12.6 kPa and 13.5 kPa were found to be greater than the corresponding values (between 6.8 kPa and 10 kPa) obtained for the 50mm diameter pile (see Fig. 8.8a). The average maximum unit skin friction value under tension loading (obtained from the measured pile head tension loads at the first cycle of parcel A for Tests B2 and B3) was about 10.7 kPa, forming about 82% of the averaged unit compressive skin friction value of 13 kPa. The results of model grouted pile test reported by Lee and Poulos (1991) indicate a reduction of the maximum unit skin friction with increasing pile diameter (model grouted pile diameters tested were 24mm, 50mm and 77mm). The larger maximum unit skin friction obtained for the present 100mm diameter jacked pile tests (as compared to the 50mm diameter jacked pile tests) is considered to be a result of the greater compaction and increased effective confining stresses in the sand mass caused by the installation of the jacked pile. It is also worthy to note that an assessment of field pile test results by Meyerhof (1983) suggest that the ultimate unit skin friction, of both bored and driven piles, in sand (of a given density) or clay (of a given shear strength) is practically independent of the pile diameter. Therefore, the reduction of the maximum unit skin friction with increasing diameter observed in model pile test by Lee and Poulos (1991) (also Nauroy *et al.*, 1988) can be attributed to the particular characteristics of calcareous sediments. The mobilised end-bearing pressures of between 2.93 MPa and 2.99 MPa (at 10% pile diameter movement) for the three tests were also greater than the corresponding values (between 2.01 MPa and 2.12 MPa) for the 50mm diameter pile. Again, the larger value for the 100mm diameter pile was felt to be a result of the greater compaction and larger effective confining stresses in the sand mass mentioned earlier. It is of interest to note that Meyerhof (1983) suggest a reduction of the ultimate end-bearing pressure with increasing diameter, for piles greater than about 0.5m diameter.

The load distributions along the pile at failure for the three tests are shown in Fig. 8.19. Reasonably good agreement is obtained for the three tests. There seems to be a quite linear reduction of the load distribution down the pile, indicating a reasonably constant skin friction along the pile shaft.

8.4.3 Cyclic Loading Response

The responses of the three model tests under the sequence of displacement-controlled loading parcels are presented and discussed in this section. As mentioned earlier, Tests B2 and B3 had to be terminated before the complete number of cycles for parcel B (50 cycles) was attained. Test B2 was terminated after 25 cycles of parcel B while for Test B3 only 10 cycles were managed. The termination was necessary due to excessive settlement of the sliding collar which, if exceeded the "O"-ring level on the fixed collar (see Fig. 6.3), would result in the leakage of air pressure.

The complete load-settlement responses for the three tests have been shown earlier in Figs. 8.16(a) to 8.16(c). The normalised values at the tension and compression ends of each cycle for the three tests are shown in Figs. 8.20(a) to 8.20(c). Table 8.8 further tabulates the measured load values at the end of each load parcel. As with the 50mm diameter case, a continuous reduction in the mobilised skin friction at the tension end of each cycle was observed. Table 8.9 expresses this reduction in terms of a degradation factor for each loading parcel. Again, more degradation is observed for the larger cyclic displacement amplitude loading parcel (see parcel A in Table 8.9 and Fig. 8.21). The subsequent parcel B further reduces the degradation factor, particularly for the test with a smaller cyclic displacement amplitude in parcel A (Fig. 8.20 and Table 8.9). It may be noted that, even though only 10 cycles were managed for parcel B in Test B3, negligible degradation was expected within parcel B since most degradation would have had occurred in parcel A (Fig. 8.20c). By extrapolating the normalised tension load values for Tests B2 and B3

(Figs. 8.20b and 8.20c), it is found that the limiting normalised values (i.e limiting degradation factor values) for both tests are in reasonably good agreement. This limiting degradation factor value (average of about 0.10) is slightly lower than that obtained for the 50mm diameter case (average of about 0.18), which in experimental terms can be considered as fair.

For the response at the compression end of the cyclic loading sequence, a similar observation to that for the 50mm diameter case was evident. For parcel A of Test B1 (Fig. 8.20a), with ρ_c/d of ±0.025, a continuous decrease in the measured pile head compression load (except for the slight increase between cycles 30 and 40) was observed. For cyclic displacements ρ_c/d greater than ±0.025, a gradual increase (following an initial reduction) in the measured pile head compressive load was obtained. Thus, both the 50mm and 100mm diameter test results indicate a threshold value ρ_c/d of ±0.025, above which an increase in the pile tip compression load can be expected with increasing cycles (see Fig. 8.22). Table 8.10 further tabulates this response in terms of a pile tip "magnification" factor for each load parcel. As evident, more significant increase in the mobilised pile tip compression load is obtained for larger cyclic displacement amplitudes (see results for parcel A).

Figs. 8.23(a) and 8.23(b) show the variations of the average unit skin friction (over the embedded pile shaft) during the cyclic loading parcel A of Tests B1 and B3 respectively. The variations for Tests B1 and B3, with cyclic loading parcel A of ρ_c/d of ±0.025 and ±0.10 respectively, show a continuous degradation of the mobilised skin friction under tension loading. The degradation of skin friction is more severe for the test with a larger cyclic displacement amplitude (Test B3). The "dip" in the average unit skin friction during the compression phase of the cyclic loading, particularly for Test B3, is caused by the slower data acquisition sampling rate relative to the cyclic loading test rate adopted. The average skin friction is calculated based on the difference between the pile head and pile tip load cells readings. As shown in Fig. 8.16(c) (Test B3), the pile head compression load (and hence, the pile tip load since the mobilised shaft friction is small in comparison) is mobilised quickly as the pile approaches the mean position (of the cyclic displacement loop) on the compression phase. The above factors are thought to have contributed to the "dip" observed in the average unit skin friction towards the mean position (on compression phase) of the cyclic displacement loop of Test B3. This "dip" is less evident for Test B1 (see Fig. 8.23a) where a continuous reduction of the mobilised compression pile head load (and hence, the pile tip load) is obtained for parcel A (see Fig. 8.16a). In any case, the important point to be noted from Fig. 8.23 is the clear indication of the continuous degradation of the average unit skin friction (from the tension loading phase).

Table 8.11 tabulates the measured initial static capacities and post-cyclic static capacities for the three 100mm diameter tests. The post-cyclic static capacities after parcel A indicate that for Tests B2 and B3, with ρ_c/d values greater than ±0.025, a greater post-cyclic static capacity (as compared to the initial static capacity) is attainable as a result of an increase in the pile tip resistance. No direct comparison of the final static capacity values (after parcel B) for Tests B2 and B3 (with cyclic loading details reverse of each other) can be made since in both tests only part of loading parcel B was completed. However, by extrapolating the measured results for Tests B2 and B3 (see Figs. 8.16b and 8.16c), assuming the total 50 cycles of loading parcel B were completed, the final estimated static capacity values for both tests (of about 45 kN) seem to be in agreement. The present results (Tests B2 and B3) and the 50mm diameter results (Tests A2 and A3) therefore appear to suggest that the final post-cyclic static capacity (after parcel B) is independent of the order of occurrence of the displacement-controlled loading parcels.

A comparison of the pile "penetrometer" results obtained after the completion (without applied overburden pressure) of Test A3 (50mm diameter) and Test B3 (100mm diameter) is shown in Fig. 8.24. The greater compaction of the sand mass caused by the installation and cyclic testing of the 100mm diameter model pile is clearly evident. It may be noted that the pile "penetrometer" positions for the present "after test" response are identical to the positions utilised to assess the consistency of the initial placed sand. It is of interest to note that the penetration responses shown generally indicate that, for depths below the embedded pile tip level (about 800mm depth), the measured resistance for Test B3 is about twice that of Test A3.

8.5 SUMMARISED COMPARISONS OF TEST RESULTS

In this section, summarised comparisons of the results obtained from the present series of tests with the 50mm and 100mm diameter model piles are presented and discussed. As noted by Lee and Poulos (1991), the results of model grouted pile tests seem to suggest that the degradation of skin friction capacity is governed by the relative (to diameter) value of the cyclic slip displacement, ρ_{cs} (see section 4.3.4). Therefore, an attempt is made in this section to further clarify this point regarding the degradation of skin friction capacity under cyclic loading conditions.

Fig. 8.25(a) shows the degradation factor D_τ as a function of the absolute cyclic displacement magnitude for the two pile diameter sizes. It is observed that for a given cyclic displacement magnitude, the degradation factor is lower (i.e more degradation) for the smaller 50mm diameter pile. Conversely, for a given degradation factor, a larger cyclic displacement amplitude is required for the larger diameter pile to initiate that amount of degradation. By extrapolating both curves, the results appear to indicate that there exists a critical cyclic displacement amplitude (about 1.2mm for both curves) below which no significant degradation in skin friction is obtained. This observation is in agreement with, and reinforces further, the results reported by Lee and Poulos (1991), and suggests the "cyclic slip displacement" model (see section 4.3.4) to be a more appropriate model (as compared to the "absolute cyclic displacement" model) governing the degradation response. This "cyclic slip displacement" degradation model will be referred to in more detail in the next section. The variation of D_τ with the normalised (to diameter) value of the absolute cyclic displacement amplitude (ρ_c/d) is further shown in Fig. 8.25(b). The normalised plot shows that for a given ρ_c/d value, a lower degradation factor is obtained for the larger pile.

As mentioned earlier, the results presented in Fig. 8.25(a) and those of Lee and Poulos (1991) strongly indicate that the "cyclic slip displacement" model is the appropriate model for skin friction degradation. The "cyclic slip displacement" (ρ_{cs}) is defined as the cylic displacement amplitude (ρ_c) less the displacement required to cause full static slip of the pile shaft (ρ_{fs}). Therefore, in this model, severe degradation of the skin friction only occurs when the cyclic displacement amplitude exceeds a certain value, in this case the displacement to cause static slip ρ_{fs}. It may be noted that this "cyclic slip displacement" model is conceptually similar to the "reverse-slip" numerical model of Matlock and Foo (1980). The question then that needs to be addressed is whether the degradation is governed by the absolute or normalised (to diameter) value of the cyclic slip displacement. Results presented by Lee (1988) (also Lee and Poulos, 1991) indicate the normalised value of the cyclic slip displacement to be the appropriate degradation model.

Fig. 8.26(a) expresses the degradation factor D_τ in terms of the cyclic slip displacement. The ρ_{fs} values for the 50mm and 100mm diameter model piles were taken as 1.5mm and 2.0mm respectively. These values were adopted based on the initial static loading results presented in Figs. 8.7 and 8.17. It may be noted that both ρ_{fs} values are greater than the "critical" cyclic displacement value of about 1.2mm obtained by extrapolating (to D_τ = 1.0) the curves of Fig. 8.25(a). The plot in Fig. 8.26(a) shows that, for a given value of the cyclic slip displacement $\pm\rho_{cs}$, less degradation (i.e larger D_τ value) is obtained for the larger diameter pile. The practical implication of this observation suggests that, for a given cyclic displacement amplitude $\pm\rho_c$, larger diameter piles are expected to undergo less severe degradation of the skin friction capacity than smaller diameter piles. The present results and the model grouted pile results of Lee (1988) (see also Poulos, 1988a) therefore indicate, for a given cyclic slip displacement, the significant influence of the pile diameter in affecting the D_τ value.

The results of Fig. 8.26(a) are replotted in terms of the normalised (to diameter) value of the cyclic slip displacement (ρ_{cs}/d) in Fig. 8.26(b). The normalised plot seems to suggest that D_τ is practically independent of the pile diameter. Also shown are the model jacked pile test results obtained by Poulos and Chan (1986) (see also Chan, 1986) and Al-Douri (1992). The results of Poulos and Chan (1986) were obtained using 20mm diameter model aluminium piles in "Bass Strait" calcareous sand while Al-Douri (1992) utilised a 25mm diameter model aluminium pile in "North Rankin" calcareous sand. It may be noted that the calcareous sand used for the present study was obtained from Bass Strait, Australia, and is therefore also classified as "Bass Strait" calcareous sand. Some physical characteristics and properties of these two different calcareous sands have been reported by Lee and Poulos (1987). The results of Poulos and Chan (1986), for 10 cycles of loading and applied overburden pressure of 138 kPa, are found to be in good agreement to the fitted curve for the present results. It may be noted that the results of Poulos and Chan (1986) also show that there is no significant difference between the degradation factors for 10 and 100 cycles. The results of Al-Douri (1992) however show less agreement, generally indicating less degradation (i.e larger D_τ value) for similar normalised cyclic slip displacement ratios. Indeed, model pile test results reported by Lee and Poulos (1987) tend to show that "North Rankin" calcareous sand is less susceptible to cyclic degradation than "Bass Strait" calcareous sand. This explains the larger degradation factor values obtained for the model tests of Al-Douri (1992). It should be noted that the curve shown in Fig. 8.26(b) is valid only for a given number of cycles of loading, a given applied overburden pressure and a given soil type. Therefore, a series of such curves is required to fully describe the cyclic degradation characteristics of a pile-soil system. The present model jacked pile results therefore reinforce the initial conclusion of Lee (1988) (see also Lee and Poulos, 1991), obtained from model grouted pile tests, that the normalised (to diameter) "cyclic slip displacement" model is the appropriate model governing the degradation of skin friction capacity under cyclic loading conditions.

8.6 COMPARISON BETWEEN THEORY AND MEASURED EXPERIMENTAL RESULTS

It is essential that the performance of any numerical analysis approach be assessed against experimental and/or field tests measurements. Only then can the accuracy and restrictions (if any) of the analysis approach be appreciated. In this section, comparisons between theoretical and measured results are presented for the initial static loading responses obtained for the 50mm and 100mm diameter model pile tests conducted in the present study. The theoretical solutions were obtained using the static analysis programs SPILE1 (elastic-plastic continuum analysis), SPILE2 (nonlinear hyperbolic continuum analysis) and SPILE3 (nonlinear hyperbolic "t-z" analysis), which were described in detail in Chapter 4. Due to the present lack of data on the empirical parameters necessary for a cyclic loading analysis (and also as no load-controlled test was conducted in the present study), no attempt is made in the present section to assess the cyclic loading response. It is hoped that future work will be directed towards obtaining and increasing the present limited data-base of the cyclic empirical parameters necessary for an assessment of the cyclic loading analysis approaches described in the present study (see Chapter 4).

In predicting the load-settlement response of an axially loaded pile, the single most significant input parameter required is the deformation property of the soil, characterised by the Young's (or shear) modulus of the soil. The Poisson's ratio of the soil is generally of less significance affecting the computed response. The approach adopted for the present comparison is to "match" the static loading response of the 50mm diameter test, in order to back-figure the Young's modulus of the soil. This back-figured Young's modulus of the soil is then utilised to obtain the theoretical predictions for the 100mm diameter model pile. In a nonlinear analysis, the limiting shaft and base capacities also have to be specified for each pile shaft element and pile base element. These limiting capacity values can be obtained from the present model test results (see Tables 8.2 and 8.7; the shaft capacity is assumed to be uniformly distributed over the pile shaft). Although the vertical stress distribution, due to the applied overburden pressure, decreased with depth from the top of the test chamber (see section 7.6.1), it was assumed for the present analysis that the soil could be characterised by an average constant Young's modulus value. The Poisson's ratio for calcareous sediments is generally low (0 to 0.2; see Poulos, 1988a), and a value of 0.2 was adopted for the present analysis. The equivalent Young's modulus of the pile shaft for the 50mm and 100mm aluminium model piles was taken as 12210 MPa and 7600 MPa respectively.

Fig. 8.27(a) compares the theoretical solutions (with no installation residual stresses taken into account), obtained from the elastic-plastic continuum program SPILE1, with the measured load-settlement response of Test A1. The significant influence of the adopted value for the soil Young's modulus is clearly evident. The theory tends to predict a "stiffer" (i.e less settlement) response (for the range of soil Young's modulus value shown) for applied loads of less than about 1 kN. Beyond this load value, a "softer" response is obtained since the pile shaft capacity has been fully mobilised. In this load range (i.e greater than about 1 kN), the pile response is governed solely by the (still) elastic response of the pile base (until the limiting base capacity is reached). Although the soil modulus value of 10 MPa gave a better prediction of the static displacement just prior to "failure" (i.e full mobilisation of pile capacity), it however resulted in an over-prediction of the pile displacement for load values greater than about 1 kN. The back-figured soil Young's modulus value of 25 MPa was adopted as the "representative" soil modulus value for the present case. Theoretical solutions were then obtained using programs SPILE2 and SPILE3 with this soil Young's modulus value of 25 MPa, the results of which are presented below. It may be noted that, by adopting an average effective overburden pressure of 80 kPa (i.e. 0.08 MPa) over the embedded pile shaft, the ratio of the Young's modulus value of 25 MPa to the average overburden pressure of 0.08 MPa equals 312.5. This value of 312.5 is slightly greater than the upper end of the tentative range ($[100-250]\sigma'_{vo}$ where σ'_{vo} is the effective overburden pressure in MPa) recommended by Poulos (1988a) for the Young's modulus of driven piles in uncemented calcareous sediments.

Fig. 8.27(b) shows the theoretical solutions obtained using the nonlinear hyperbolic continuum program SPILE2 for different values of the hyperbolic constant, R_{fb} , for the pile base. The hyperbolic constant for the pile shaft elements, R_{fs}, was taken as 0.5 and would not have a significant effect on the computed response since the pile shaft capacity formed only a small proportion of the total pile capacity. The significant influence of the hyperbolic constant R_{fb} in affecting the computed response, beyond a load of about 1 kN, is clearly evident. A more nonlinear computed load-settlement response is obtained when the pile base response is modelled as a more nonlinear response with a larger R_{fb} value. Earlier deviation from the measured load-settlement response occurs for the larger (i.e more nonlinear) R_{fb} value of 0.9. The developed pile tip load versus displacement responses from the experimental tests (see Fig. 8.8b) seem to indicate no significant nonlinearity, and suggest that an elastic-plastic idealization may represent a reasonable model for the pile tip response. For the present nonlinear hyperbolic program SPILE2, a value of R_{fb} = 0.1 was adopted corresponding to a small degree of nonlinearity for the pile tip response. This "representative" value of R_{fb} gave reasonably good prediction of the measured results, except for load values approaching the "failure" load where smaller displacements were computed.

Theoretical solutions obtained using the nonlinear hyperbolic t-z program SPILE3 are shown in Fig. 8.27(c) for different values of the hyperbolic constant R_{fb}. As compared to the corresponding solutions obtained from program SPILE2 (i.e with the same R_{fb} value), a "softer" response is obtained from the t-z program SPILE3 for load values greater than about 1 kN (i.e the shaft load capacity). The importance of proper modelling of the pile tip response in this case is again evident. It has been suggested by Randolph and Wroth (1978) that once the pile shaft capacity has been fully mobilised, the response of the pile tip to further load application is similar to that of a plate at the bottom of a borehole. In such a situation, the writers have suggested that the "rigid punch" solution (see equation 4.8) be multiplied by a factor of 0.85, resulting in an increased pile base stiffness (obtained from the reciprocal of equation 4.8). Curve (4) in Fig. 8.27(c), with R_{fb} = 0.1 (similar to that for curve 3), shows the computed solutions obtained using the increased base stiffness (a factor of 1/0.85 = 1.176) after full mobilisation of the shaft capacity. As expected, a stiffer response is obtained as compared to that of curve (3).

Table 8.12 tabulates the back-figured soil parameters from the 50mm diameter model pile Test A1. Comparisons between the three solutions, using the back-figured soil parameter values, for Tests A2 and A3 (with slightly larger static capacity values) are further shown in Figs. 8.28(a) and 8.28(b). The corresponding limiting capacity values for Tests A2 and A3 can be obtained from Table 8.2.

Using the back-figured soil parameters, theoretical solutions for the 100mm diameter model pile were obtained using the three programs. Since the measured static capacities for the three 100mm diameter tests were in excellent agreement (see Table 8.7), average values, from the three tests, for the limiting shaft and base capacities were utilised for the theoretical predictions. Fig. 8.29 compares the theoretical solutions with the measured results of Test B1. All three theoretical solutions predicted "softer" responses than the measured results, particularly for load values greater than about 3 kN (i.e after full mobilisation of shaft capacity). The SPILE3 solutions gave greater displacements than the solutions from programs SPILE1 and SPILE2. The slightly "softer" computed response of program SPILE2, as compared to the computed response of program SPILE1, was a result of the low nonlinearity (R_{fb} = 0.1) adopted for the pile tip response. It may be noted that the measured pile tip responses (see Fig. 8.18b) from the 100mm diameter model tests show a low degree of nonlinearity, as with the 50mm diameter model tests. It has been assumed for the present comparison that the back-figured soil Young's modulus from the 50mm diameter model pile is equally applicable to the 100mm diameter model pile. This assumption therefore ignores the effect of installation of the model pile, which in the case of the 100mm diameter pile would result in a higher effective stress state in the soil (hence, a stiffer soil). This could have contributed to the stiffer measured response of the 100mm diameter pile test results. It is also worthy to note that the "constant rate of penetration" testing (as utilised in the present study to obtain the "static" response of the model pile) generally results in a stiffer response (and larger load capacity too) as compared to the more commonly adopted "maintained load" test (Whitaker and Cooke, 1961). In view of the factors mentioned above, the theoretical solutions for the 100mm diameter model pile (see Fig. 8.29) can be considered as fair, even though the experimental results are not matched precisely.

In an attempt to further improve on the predictions obtained for the 100mm diameter model pile, the following factors were considered:

(i) the consideration of the installation residual stresses in the static pile analysis;

(ii) the use of a higher soil Young's modulus value for the pile tip response.

It has been suggested by, for example, Poulos (1972) and Leonards and Darrag (1989), that the use of a higher soil modulus value (than along the pile shaft) at the pile tip for driven piles is appropriate to reflect the densification and prestressing beneath the pile tip. Values of the ratio E_b/E_s between 5 and 10 (E_b = pile tip modulus, E_s = the average constant modulus along the pile shaft) have been suggested by Poulos (1972).

Figs. 8.30(a) and 8.30(b) compare the theoretical residual load distribution and the measured values for the 50mm and 100mm diameter model piles respectively. It may be noted that, for the theoretical residual load distribution profiles, identical results were computed using the three static analysis programs SPILE1, SPILE2 and SPILE3. In both cases, the theoretical solutions show complete pile-soil tensile slip (using limiting unit average tensile skin friction values of 4.9

kPa and 10.7 kPa for the 50mm and 100mm diameter model piles respectively) along the pile shaft. It was also found that the computed solutions were identical for the case of $E_b/E_s = 1$ and 5 (using E_s for the shaft of 25 MPa).

Fig. 8.31 show the improved predictions for the 100mm diameter model pile obtained using programs SPILE1, SPILE2 and SPILE3. The influence of a larger soil Young's modulus value for the pile tip response, in reducing the computed pile settlements, is clearly evident. For $E_b/E_s = 5$ (with E_s = 25 MPa for the pile shaft), "stiffer" computed solutions than the measured results are obtained from the three programs. Based on the "after test" pile "penetrometer" results shown in Fig. 8.24, it is reasonable to assume that the soil Young's modulus value at the pile tip for the 100mm diameter pile is twice that for the 50mm diameter pile. The computed solutions obtained using $E_b/E_s = 2$ show closer agreement to the measured results than the case using $E_b/E_s = 1$ (i.e computed solutions for a constant Young's modulus profile as shown in Fig. 8.29). The incorporation of the theoretical installation residual stress distribution for the 100mm diameter model pile (with $E_b/E_s = 2$) results in further improvement to the computed solutions. The theoretical solutions from the elastic-plastic continuum program SPILE1 show the best agreement between the predicted and measured results.

The important point to be noted from the prediction above is that the predicted load-settlement response by using a constant soil modulus profile, for the case of driven (or jacked) piles where significant compaction and densification of the soil near the pile tip can occur as a result of the installation process, is not realistic. This is so particularly for the case of short driven piles where the pile tip response is of major importance. For such a case, the use of a larger soil modulus value for the pile tip response leads to better agreement between the predicted and measured results. The incorporation of the installation residual stresses (rather than assuming an initially stress-free pile) further improves the predicted solutions.

8.7 SUMMARY

The results of a series of model jacked pile tests in calcareous sediments conducted in the present study have been presented in this chapter. The following main conclusions can be drawn from the test results reported herein:

1 The influence of the "rigid boundary" effect, due to the rigid side wall of the test chamber, was found to be relatively insignificant (under the present test applied overburden pressure of 100 kPa) during the installation of the 50mm diameter model pile. This "rigid boundary" effect was however of greater significance during the installation of the 100mm diameter model pile.

2 Both the 50mm and 100mm diameter model piles showed a decrease in the developed average unit skin friction with increasing pile penetration depth during the installation stage. Values of between 9 kPa and 14 kPa were obtained at final penetration for the 50mm and 100mm diameter model piles respectively. The larger value for the 100mm diameter model pile could have been caused by the larger effective confining stresses in the sand mass as a result of the installation process.

3 The static compressive capacity for the 50mm diameter model pile was found to vary between 4.8 kN and 5.4 kN, with the shaft capacity constituting only between 18% and 23% of the static compressive capacity. The corresponding value for the 100mm diameter model pile was 26.3 kN to 26.8 kN, with the shaft capacity forming a smaller percentage of between 11.9% and 12.5% of the static compressive capacity.

4 The static displacement required to fully mobilise the shaft capacity was found to be practically independent of the pile diameter. This displacement was found to be on the order of about 2mm for both the 50mm and 100mm diameter model piles. On the other hand, a larger displacement was required to fully mobilise the end-bearing capacity. This movement was found to to be about 7% and 5% of the corresponding pile diameter, for the 50mm and 100mm diameter model piles respectively.

5 It had been observed from model grouted pile tests (Lee, 1988; Lee and Poulos, 1991) in calcareous sediment that the developed maximum unit static skin friction decreased as the pile diameter increased. The present jacked pile test results indicated values of between 6.8 kPa and 10 kPa, and between 12.7 kPa and 13.5 kPa for the 50mm and 100mm diameter model

piles respectively. The larger value obtained for the 100mm diameter model pile could be attributed to the greater effective confining stresses in the sand mass (under the present test conditions) caused by the installation process. Thus, the present jacked pile test results are considered "insufficient" to confirm (or contradict) the reported trend observed from the model grouted pile tests, which excludes the "rigid boundary" effect during its installation stage.

6 For the displacement-controlled cyclic loading tests, the amount of degradation of the skin friction capacity was found to be dependent on the magnitude of the cyclic displacement amplitude. More skin friction degradation was observed for the larger cyclic displacement amplitude tests. The test results also indicated that significant degradation of skin friction capacity occurred when the cyclic displacement amplitude exceeded a threshold displacement value. This threshold displacement value was found to be on the order of that required to fully mobilise the shaft capacity.

7 For the sequence of displacement-controlled cyclic loading parcels, test results suggested the presence of a minimum (or limiting) degradation factor (for skin friction) corresponding to maximum possible degradation for the pile-soil system. This total degradation in skin friction appeared to be independent of the order of occurrence of the displacement-controlled loading parcels.

8 The present model jacked pile test results indicated that the normalised (to diameter) "cyclic slip displacement" model was the appropriate model governing the skin friction degradation. This conclusion is consistent with that suggested by Lee (1988) (see also Lee and Poulos, 1991) based on the results of model grouted pile tests.

9 Both the 50mm and 100mm diameter model pile test results indicated a threshold value ρ_c/d of ±0.025, above which an increase in the pile tip compression load could be expected with increasing cycles. This phenomenon occurring at the pile tip in turn contributed to an increase in the measured post-cyclic static compressive capacity, which reflected the corresponding increase in the end-bearing capacity.

10 Finally, comparison between theoretical solutions and the measured initial static load-settlement response for the 100mm diameter model pile showed fair agreement, even though the theoretical solutions tended to generally over-predict the pile settlements. It was shown that the use of a larger soil modulus value for the pile tip response, and the consideration of the installation residual stresses, resulted in better agreement between the predicted and measured results.

ADDENDUM

For the series of tests that were carried out, it is not possible to relate the degradation factor D_τ to such soil properties as ϕ (the friction angle), C_c (crushability coefficient) and the carbonate content. It is hoped that future tests can be directed toward this correlation.

Table 8.1 Details of model jacked pile test program for the present study

Loading stage	50mm diameter			100mm diameter		
	Test no.			Test no.		
	A1	A2	A3	B1	B2	B3
Initial static compression loading (mm)	6.5	6.5	6.5	13.0	13.0	13.0
Cyclic loading (parcel A) $\pm \rho_c/d$ values	0.025	0.050	0.10	0.025	0.050	0.10
Post-cyclic static compression loading (mm)	6.5	9.7	9.7	13.0	14.3	17.0
Cyclic loading (parcel B) $\pm \rho_c/d$ values	0.050	0.10	0.050	0.050	0.10	0.050
Cyclic loading (parcel C) $\pm \rho_c/d$ values	0.10	—	—	—	—	—
Post-cyclic static compression loading (mm)	13.0	13.0	13.0	17.0	17.0	17.0

ρ_c = cyclic displacement amplitude

N = 50 cycles for all parcels (unless otherwise specified)

Table 8.2 Summarised results during the initial static loading stage for 50mm diameter model pile tests.

Test No.	Total static capacity (kN)	End bearing capacity (kN)	shaft capacity (kN)	End bearing pressure (MPa)	Average skin friction (kPa)
A1	4.80	3.94	0.86	2.007	6.84
A2	5.18	4.15	1.03	2.114	8.19
A3	5.38	4.13	1.25	2.103	9.95

Table 8.3 Pile head load values at tension and compression ends of cyclic loading parcels for 50mm diameter model pile.

Test No.	Load parcel A				Load parcel B				Load parcel C			
	N = 1		N = 50		N = 51		N = 100		N = 101		N = 150	
	(a)	(b)	(a)	(b)	(a)	(b)	(a)	(b)	(a)	(b)	(a)	(b)
A1	-0.490	3.571	-0.418	0.881	-0.494	3.538	-0.329	3.656	-0.445	4.821	-0.306	7.157
A2	-0.665	4.514	-0.289	4.176	-0.382	5.695	-0.123	8.399	—	—	—	—
A3	-0.613	4.929	-0.134	7.955	-0.148	7.302	-0.108	5.999	—	—	—	—

(a) tension end of cycle

(b) compression end of cycle

All load values in kN

Note that a static load test performed after parcel A (prior to parcel B), and after parcel B (or parcel C for Test A1).

Table 8.4 Skin friction degradation factor for each displacement-controlled loading parcel (50mm diameter model pile).

Test No.	Displacement-controlled parcel		
	A	B	C
A1	0.853 [0.025]	0.666 [0.050]	0.688 [0.10]
A2	0.435 [0.050]	0.322 [0.10]	—
A3	0.219 [0.10]	0.729 [0.050]	—

Values in [ ] indicate ρ_c/d value relevant to each load parcel for each test.

Note: degradation factor obtained as ratio of measured tension pile head load values for last cycle to the first cycle within each loading parcel.

Table 8.5 Pile tip resistance magnification factor for each displacement-controlled loading parcel (50mm diameter model pile).

Test No.	Displacement-controlled parcel		
	A	B	C
A1	0.176 [0.025]	1.054 [0.050]	1.497 [0.10]
A2	1.011 [0.050]	1.531 [0.10]	—
A3	1.718 [0.10]	0.873 [0.050]	—

Values in [ ] indicate ρ_c/d value relevant to each load parcel for each test.

Note: "magnification" factor obtained as ratio of measured pile tip compression load values for last cycle to the first cycle within each loading parcel.

Table 8.6 Initial and post-cyclic static capacities for 50mm diameter model pile tests.

Test No.	Initial static capacity	Post-cyclic capacity	
		after parcel A	after parcel B
A1	4.80 [3.94]	3.83 [3.39]	7.71 [6.87]
A2	5.18 [4.15]	5.58 [4.81]	8.69 [7.87]
A3	5.38 [4.13]	7.98 [6.75]	8.67 [7.56]

All load values in kN
Value in [ ] indicate measured pile tip load

Table 8.7 Summarised results during the initial static loading stage for 100mm diameter model pile tests.

Test No.	Total static capacity (kN)	End bearing capacity (kN)	shaft capacity (kN)	End bearing pressure (MPa)	Average skin friction (kPa)
B1	26.29	23.01	3.28	2.929	13.05
B2	26.84	23.46	3.38	2.987	13.45
B3	26.56	23.39	3.17	2.978	12.61

Table 8.8 Pile head load values at tension and compression ends of cyclic loading parcels for 100mm diameter model pile.

Test No.	Load parcel A				Load parcel B			
	N = 1		N = 50		N = 51		N = 100*	
	(a)	(b)	(a)	(b)	(a)	(b)	(a)	(b)
B1	-2.342	20.970	-1.474	6.418	-1.934	23.146	-0.724	26.374
B2	-2.628	23.573	-1.101	28.019	-1.095	33.083	-0.683	43.173
B3	-2.839	25.288	-0.316	42.880	-0.234	36.814	-0.163	29.787

* N = 100 for Test B1, N = 75 for Test B2 (i.e. only 25 cycles for load parcel B), and N = 60 for Test B3 (i.e. only 10 cycles for load parcel B).

(a) tension end of cycle

(b) compression end of cycle

All load values in kN

Note that a static load test performed after parcel A (prior to parcel B), and after parcel B.

Table 8.9 Skin friction degradation factor for each displacement-controlled loading parcel (100mm diameter model pile).

Test No.	Displacement-controlled parcel			
	A		B	
B1	0.629	[0.025]	0.374	[0.050]
B2	0.419	[0.050]	0.624*	[0.10]
B3	0.111	[0.10]	0.697**	[0.050]

* Only 25 cycles of parcel B managed in Test B2

** Only 10 cycles of parcel B managed in Test B3

Values in [ ] indicate ρ_c/d value relevant to each load parcel for each test.

Note: degradation factor obtained as ratio of measured tension pile head load values for last cycle to the first cycle within each loading parcel.

Table 8.10 Pile tip resistance magnification factor for each displacement-controlled loading parcel (100mm diameter model pile).

Test No.	Displacement-controlled parcel			
	A		B	
B1	0.234	[0.025]	1.195	[0.050]
B2	1.211	[0.050]	1.303*	[0.10]
B3	1.753	[0.10]	0.833**	[0.050]

* Only 25 cycles of parcel B managed in Test B2

** Only 10 cycles of parcel B managed in Test B3

Values in [ ] indicate ρ_c/d value relevant to each load parcel for each test.

Note: "magnification" factor obtained as ratio of measured pile tip compression load values for last cycle to the first cycle within each loading parcel.

Table 8.11 Initial and post-cyclic static capacities for 100mm diameter model pile tests.

Test No.	Initial static capacity		Post-cyclic capacity			
			after parcel A		after parcel B	
B1	26.29	[23.01]	23.25	[20.36]	31.59	[29.16]
B2	26.84	[23.46]	31.68	[28.55]	41.17	[37.31]
B3	26.56	[23.39]	41.97	[38.99]	42.40	[39.17]

All load values in kN
Value in [ ] indicate measured pile tip load

Table 8.12 Back-figured soil parameters (from 50mm diameter model pile test results) utilised for 100mm diameter predictions

Program name	Adopted soil model	Soil parameters
SPILE1	elastic-plastic continuum model	$E_s = 25$ MPa, $\nu = 0.2$
SPILE2	nonlinear hyperbolic continuum model	$E_s = 25$ MPa, $\nu = 0.2$ $R_{fs} = 0.5$, $R_{fb} = 0.1$
SPILE3	nonlinear hyperbolic "t-z" model*	$E_s = 25$ MPa, $\nu = 0.2$ $R_{fs} = 0.5$, $R_{fb} = 0.1$

* For present comparison (program SPILE3), the "rigid punch" solution (see equation 4.8) is multiplied by 0.85 for load increments after full mobilisation of shaft capacity

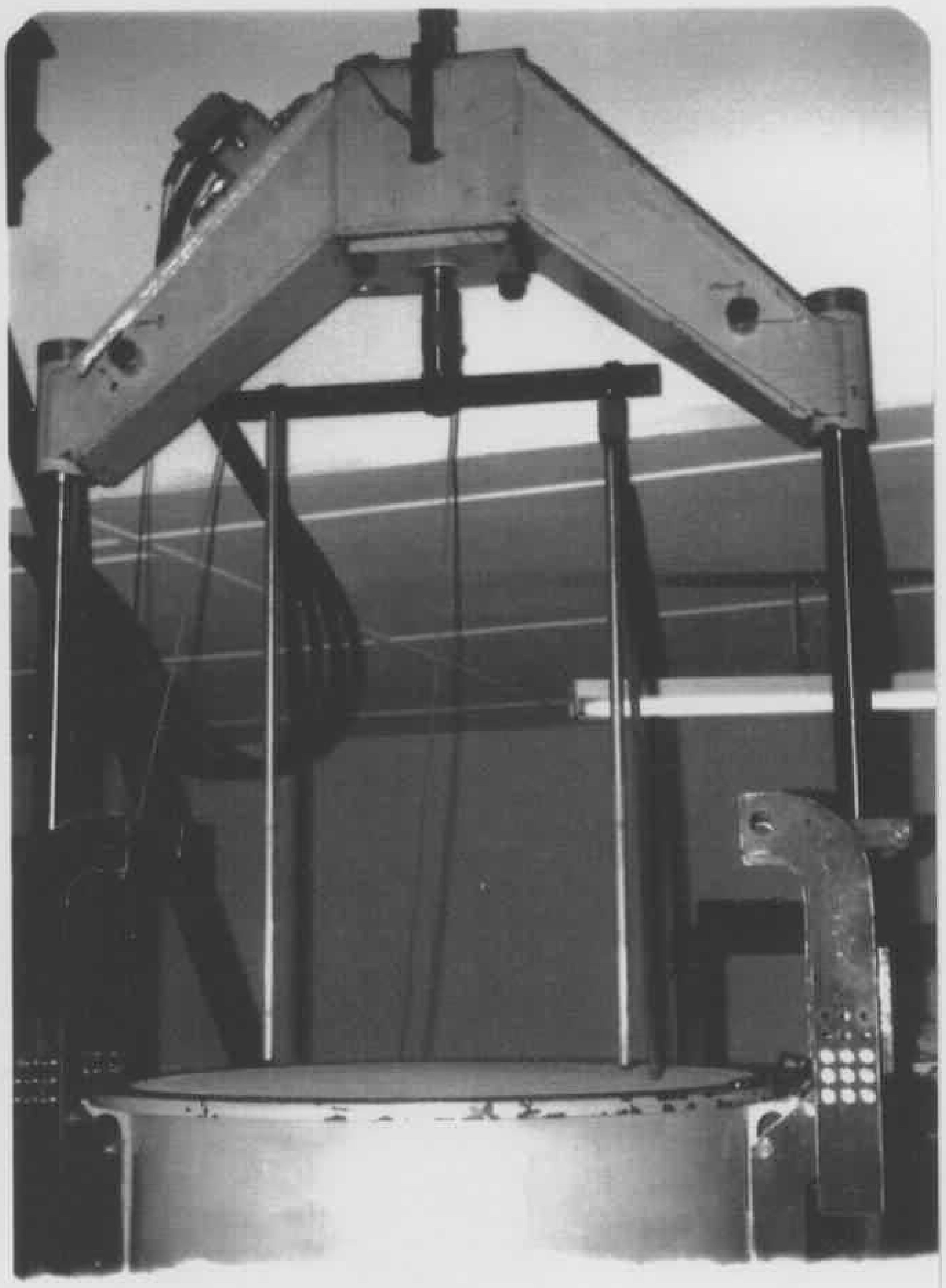

Plate 8.1 Pile "penetrometers" prior to installation into the prepared sand bed

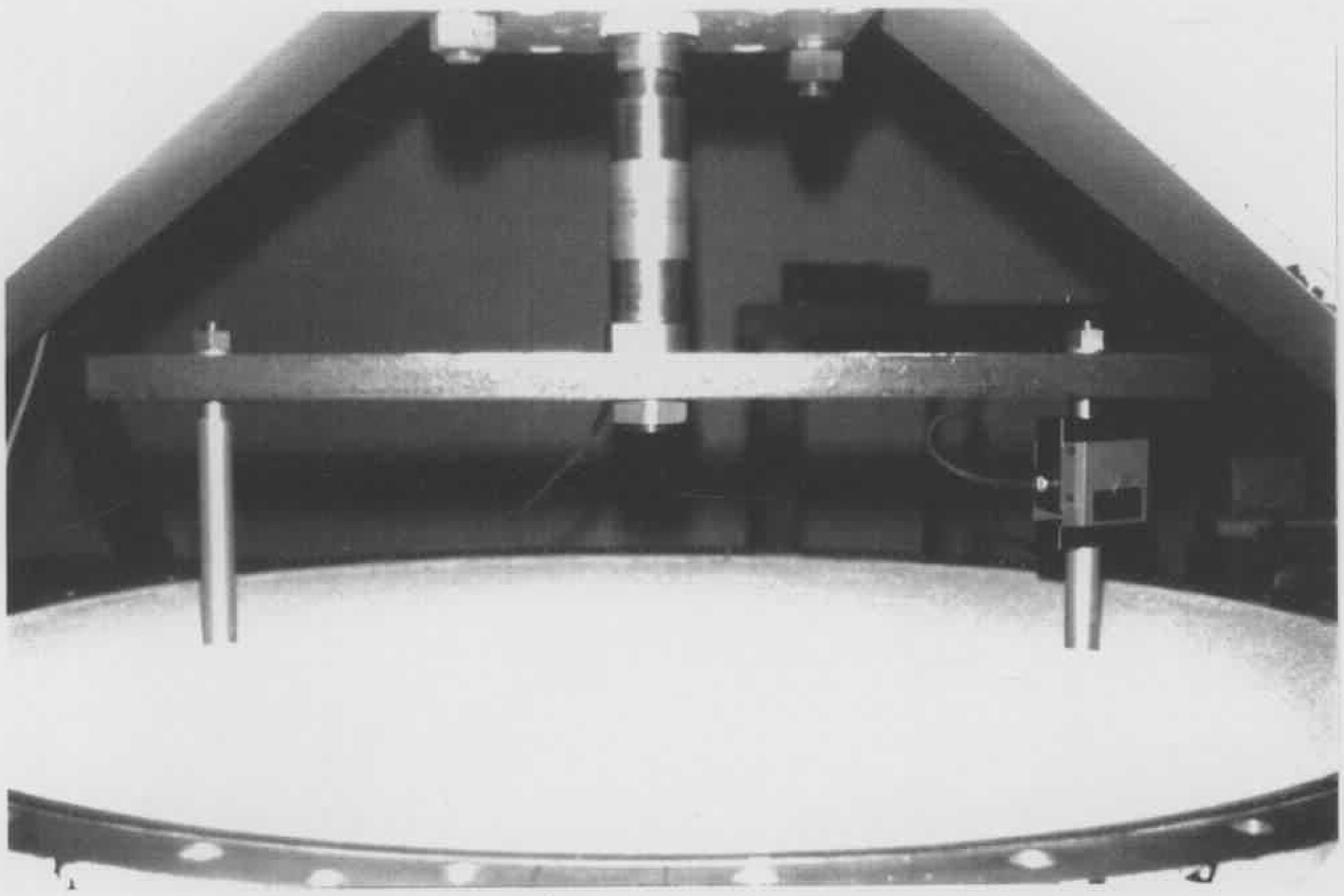

Plate 8.2 Pile "penetrometers" after installation into the prepared sand bed

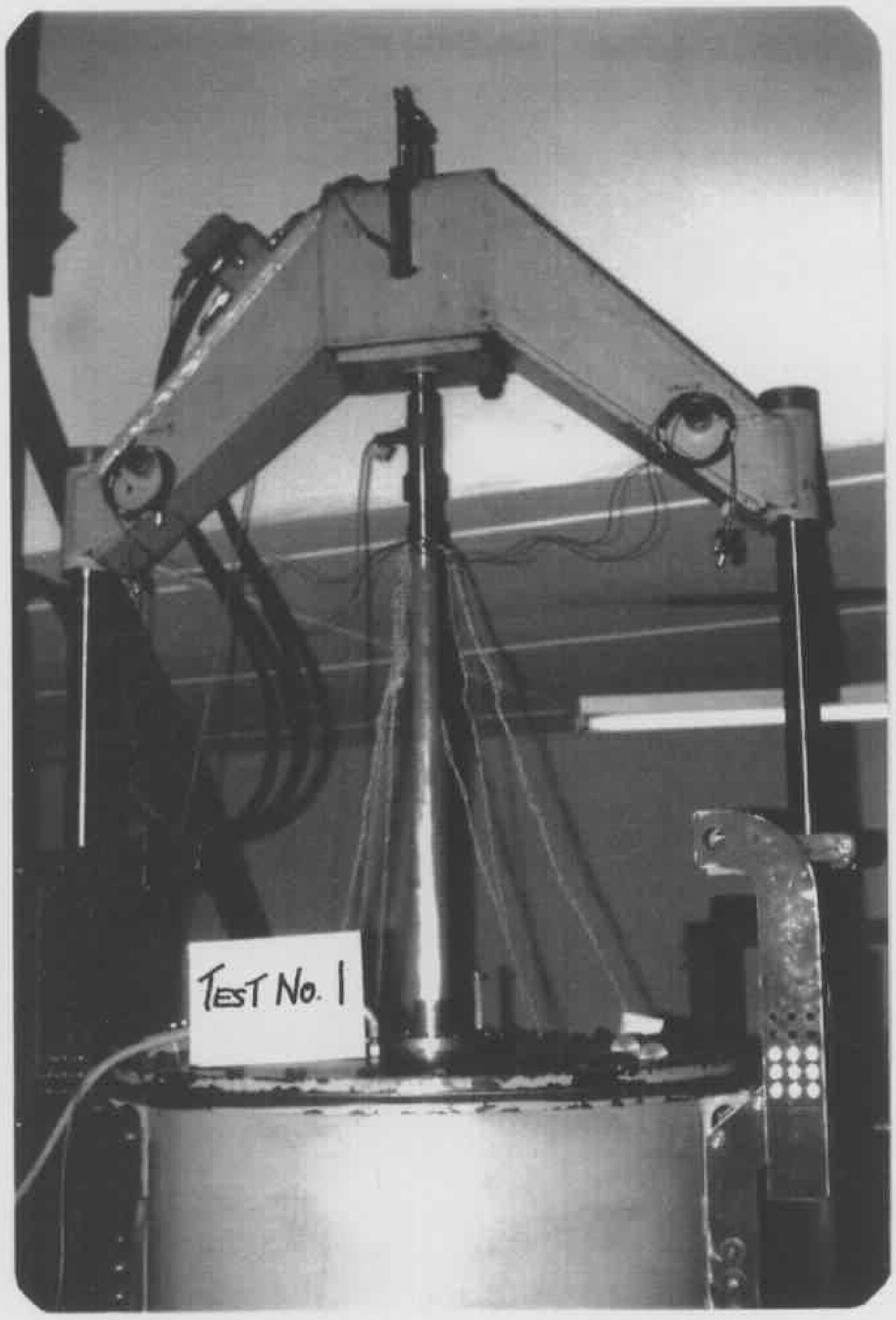

Plate 8.3 -

50mm diameter instrumented model pile prior to installation into the sand bed

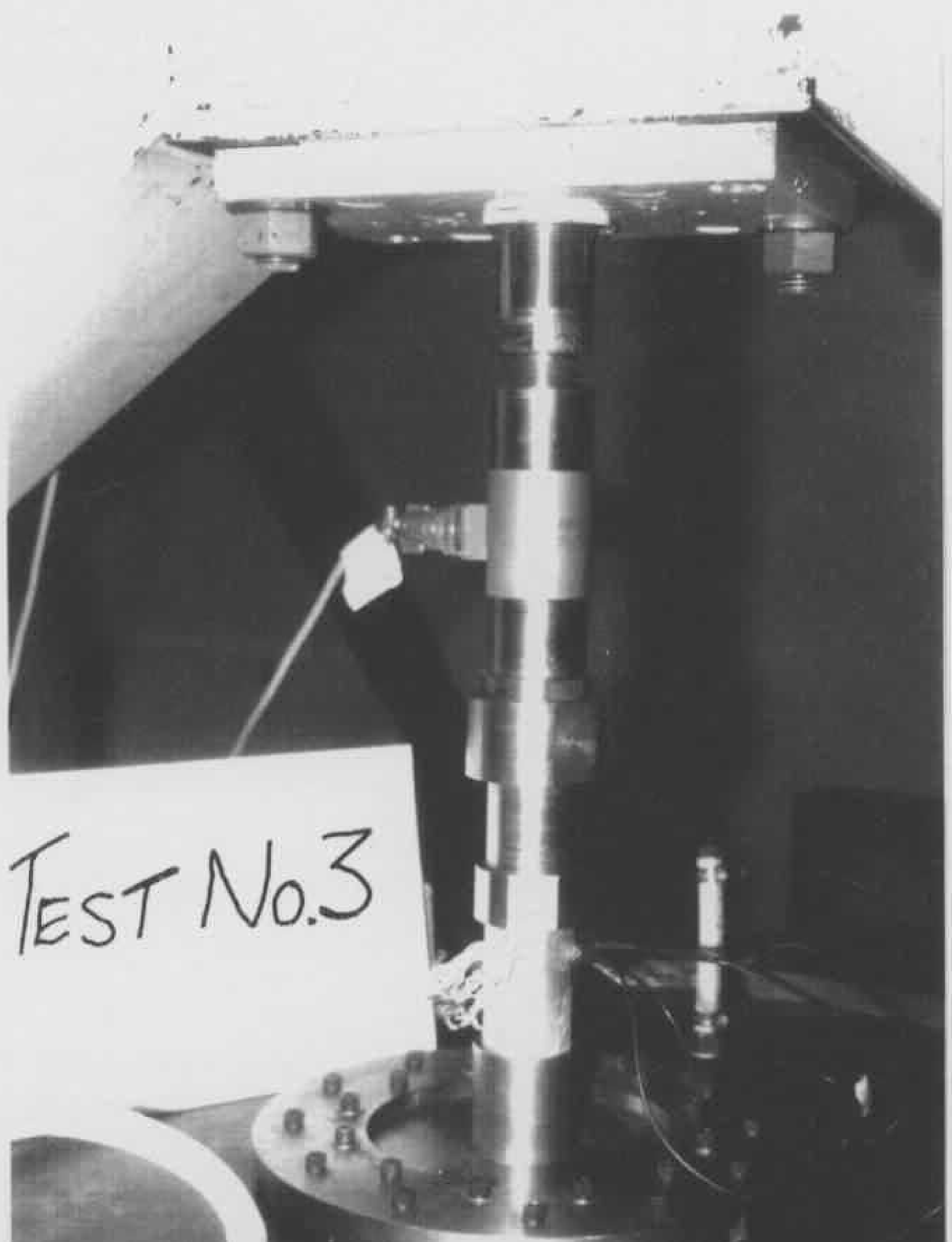

Plate 8.4 -

50mm diameter instrumented model pile after installation into the sand bed

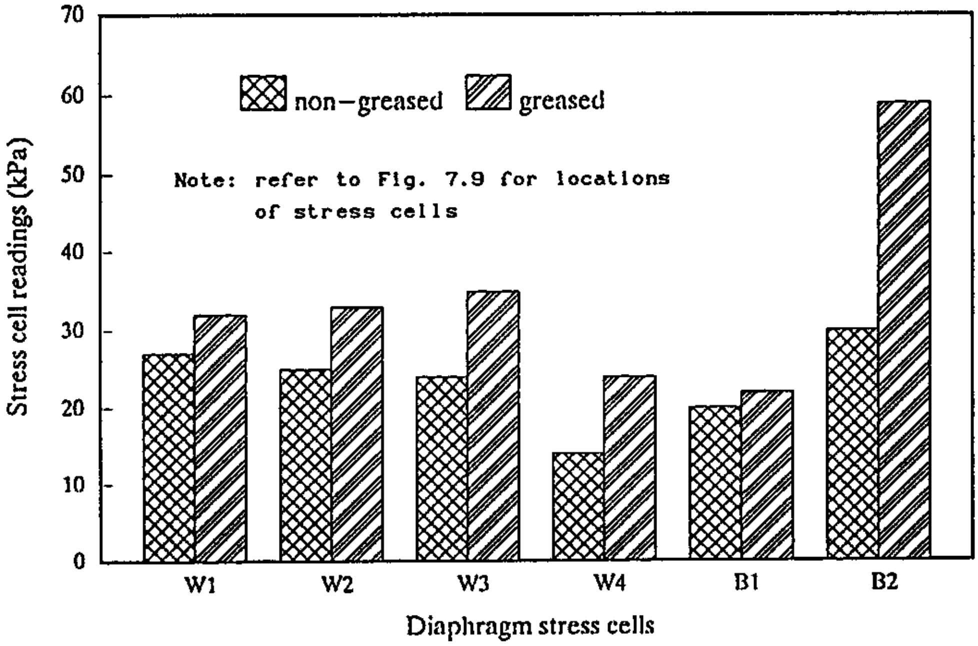

Fig. 8.1(a) Diaphragm stress cell responses after application of overburden pressure of 100 kPa

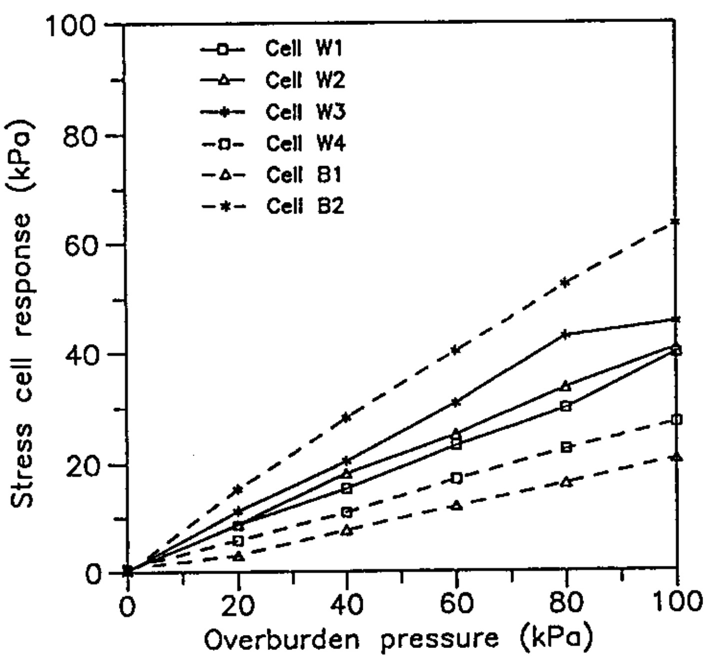

Fig. 8.1(b) Incremental responses of the diaphragm stress cells during application of overburden pressure of 100 kPa

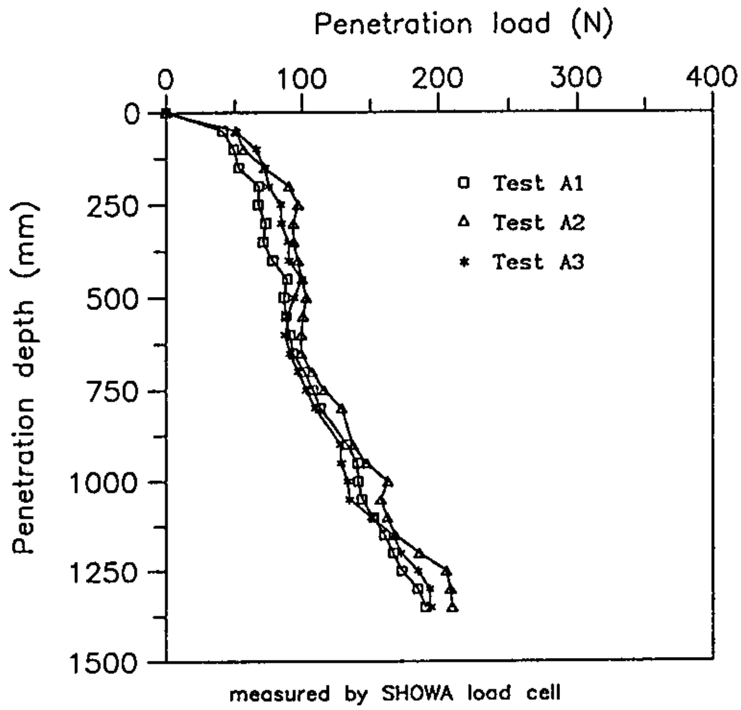

Fig. 8.2 Pile "penetrometer" results to gauge the consistency of the sand placement procedure

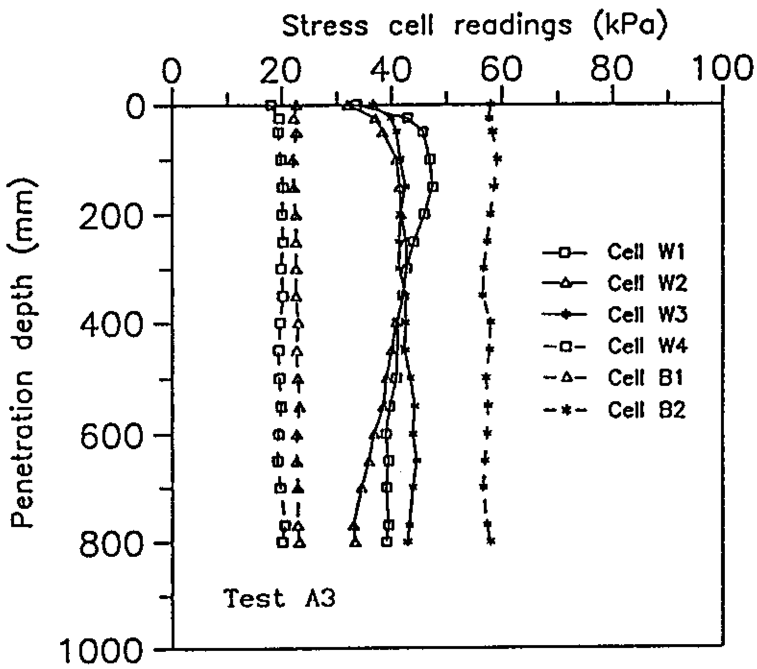

Fig. 8.3 Diaphragm stress cell responses during installation of the 50mm diameter instrumented model pile

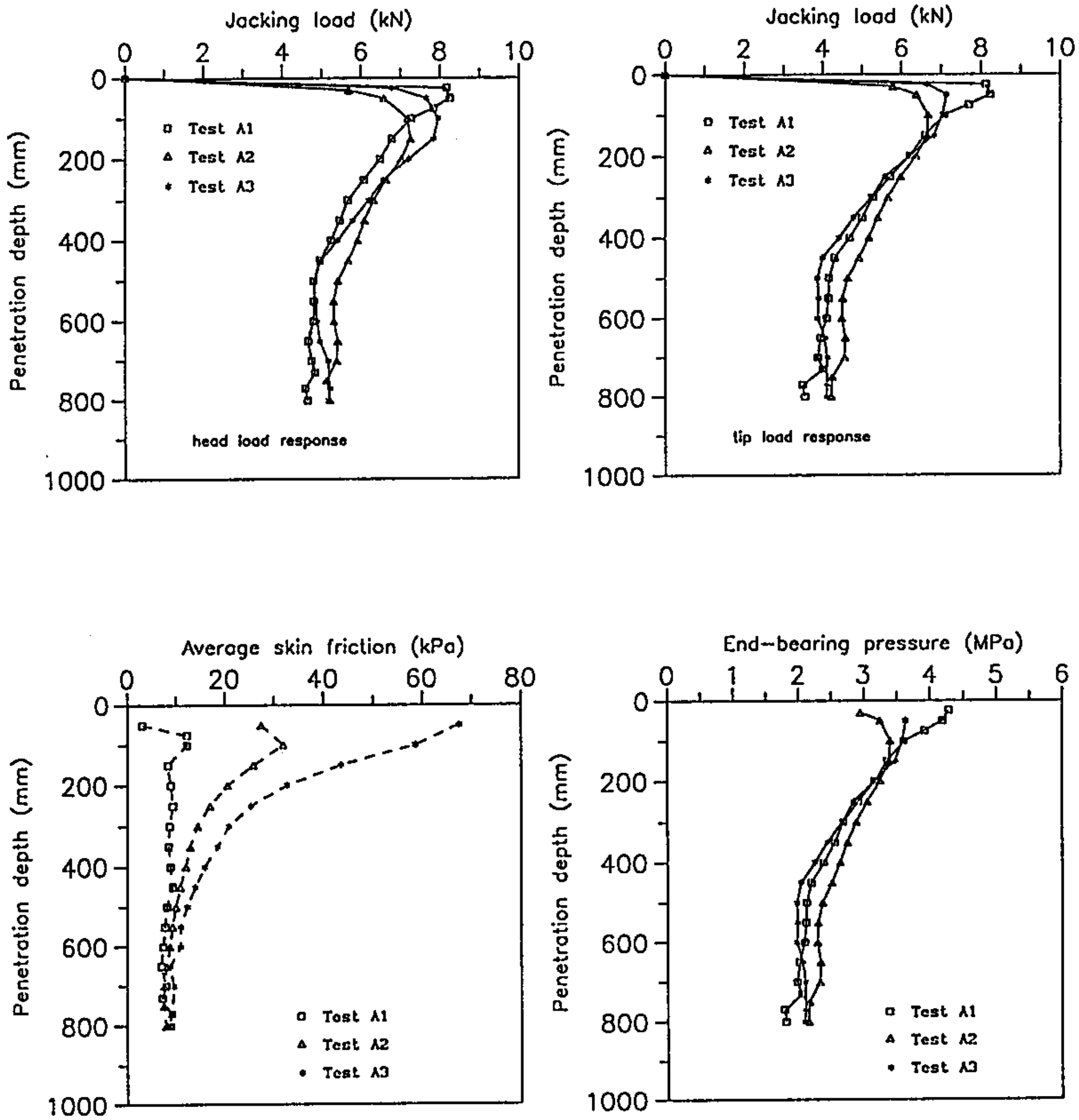

Fig. 8.4 Installation response of the 50mm diameter instrumented model pile: (a) head load response; (b) tip load response; (c) developed average skin friction; (d) developed end-bearing pressure

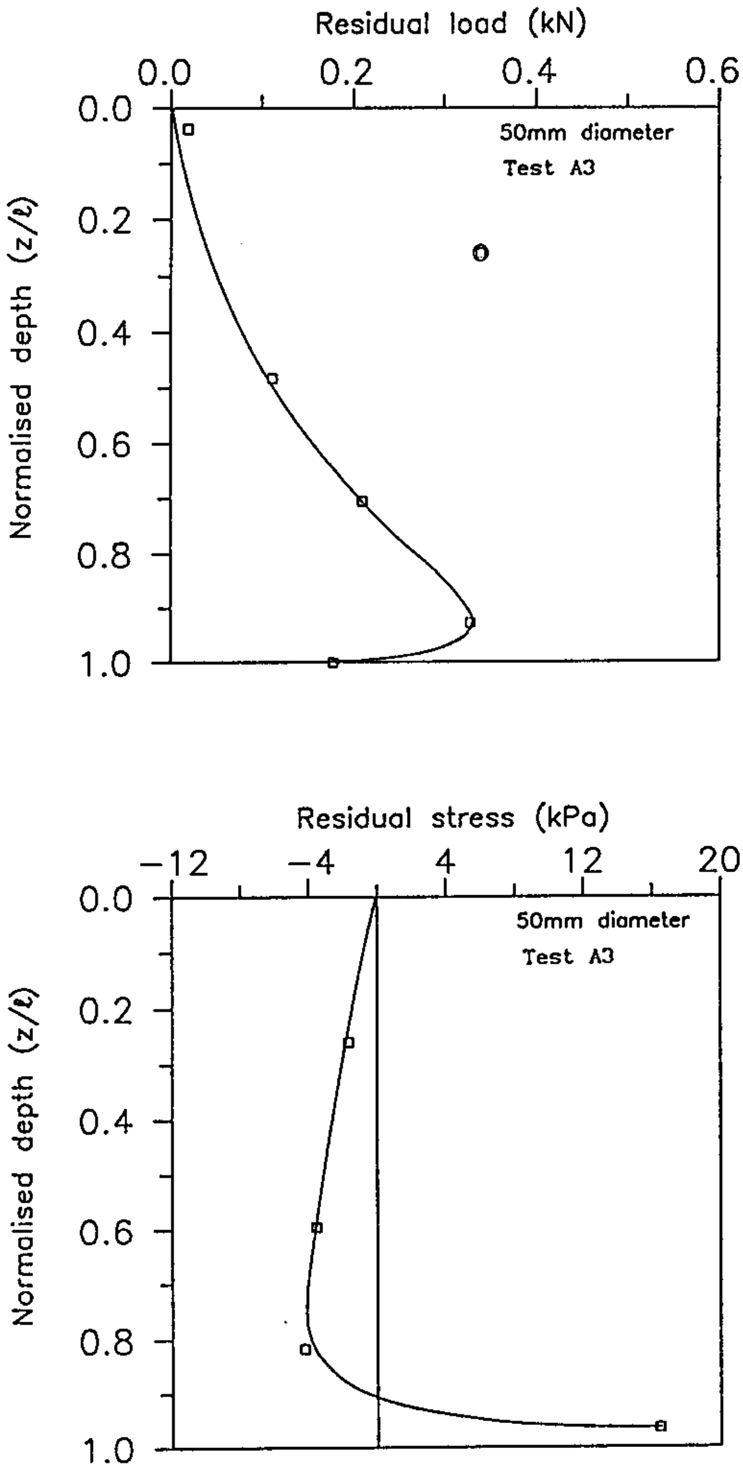

Fig. 8.5 (a) Residual load distribution after installation of 50mm diameter model pile; (b) corresponding residual stress distribution

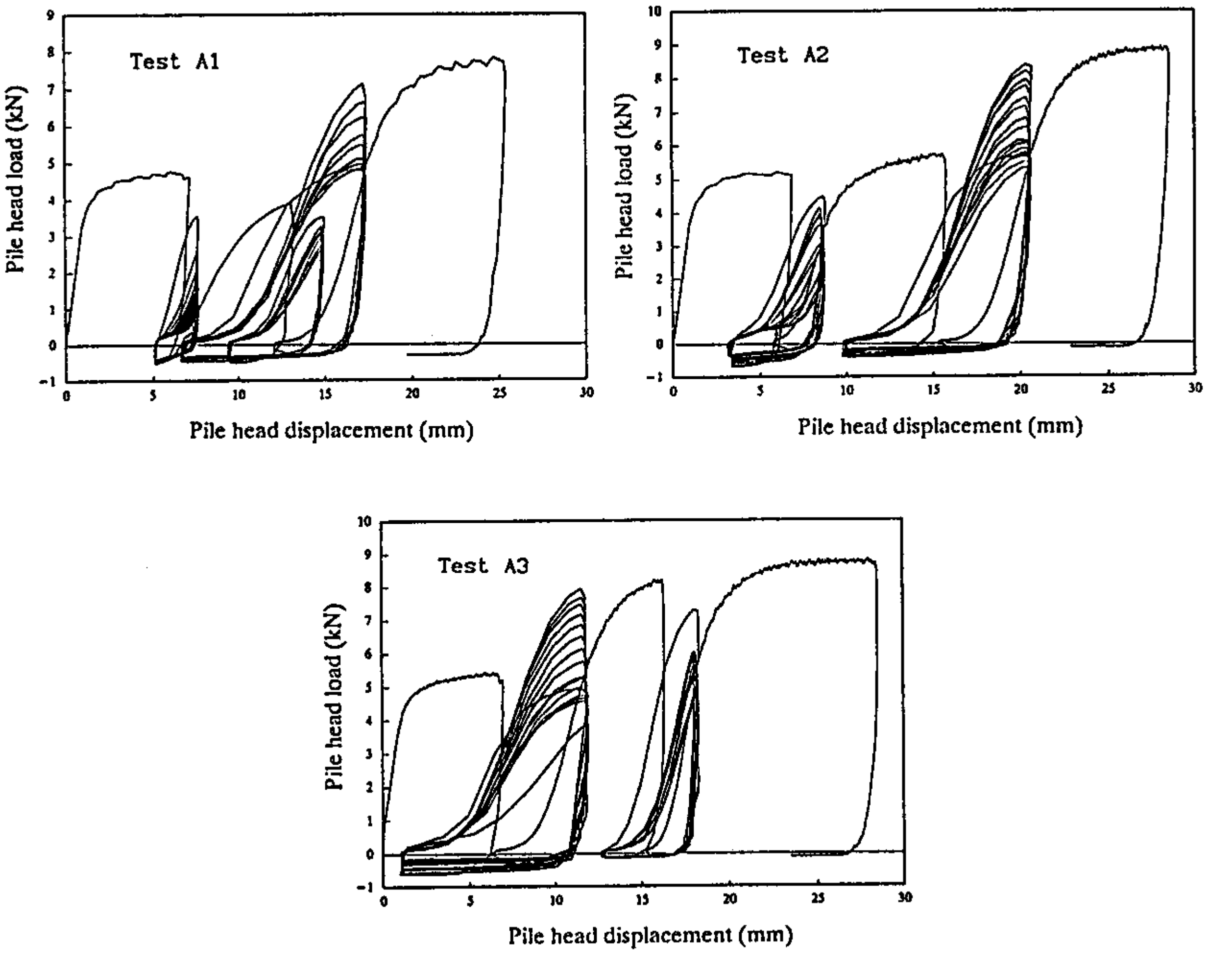

Fig. 8.6 Complete load-settlement responses for the three 50mm diameter model tests: (a) Test A1; (b) Test A2; (c) Test A3

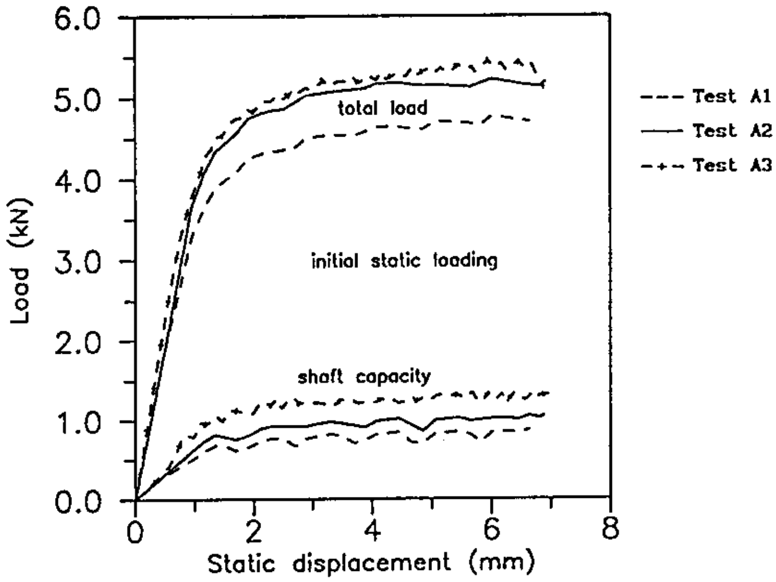

Fig. 8.7 Initial static load-settlement responses for the three 50mm diameter model tests

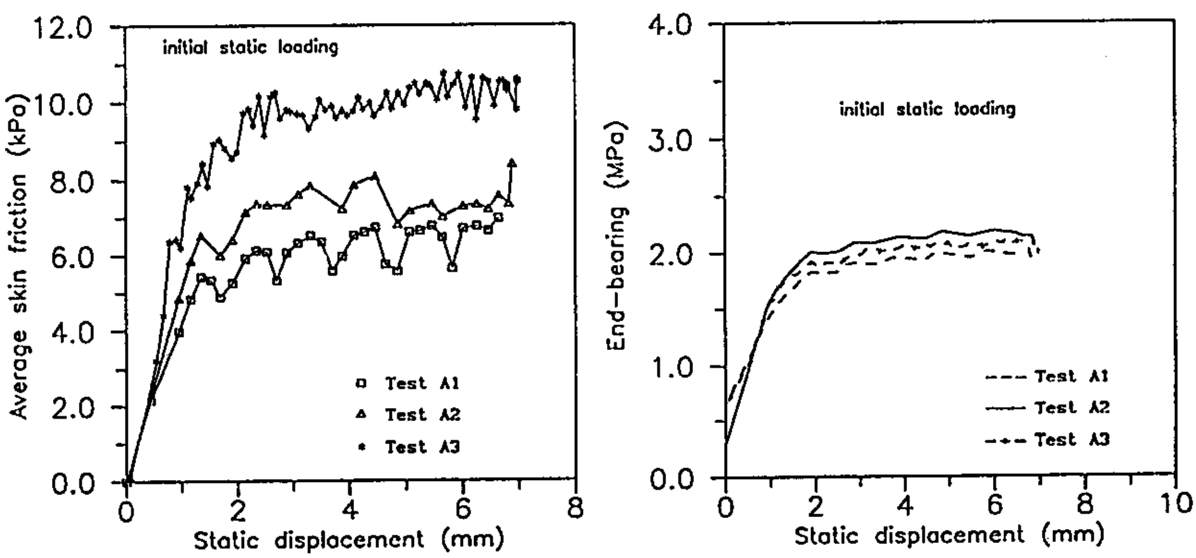

Fig. 8.8 Initial static loading responses for the three 50mm diameter model tests: (a) developed average skin friction; (b) developed end-bearing pressure

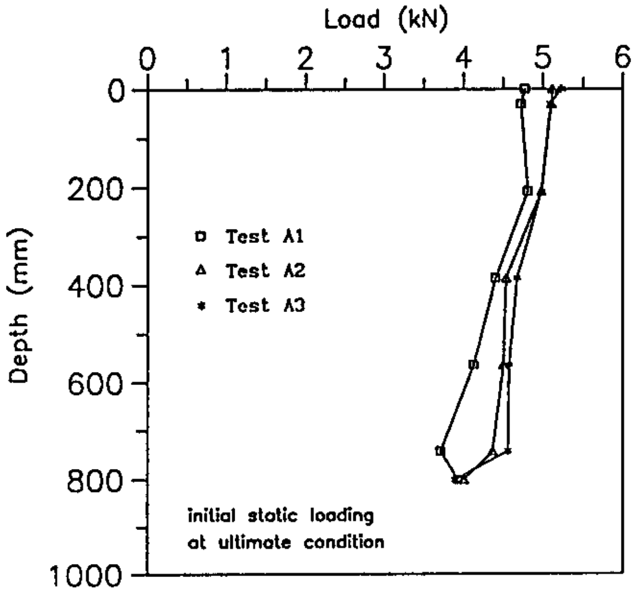

Fig. 8.9 Initial static load distributions for the three 50mm diameter model tests

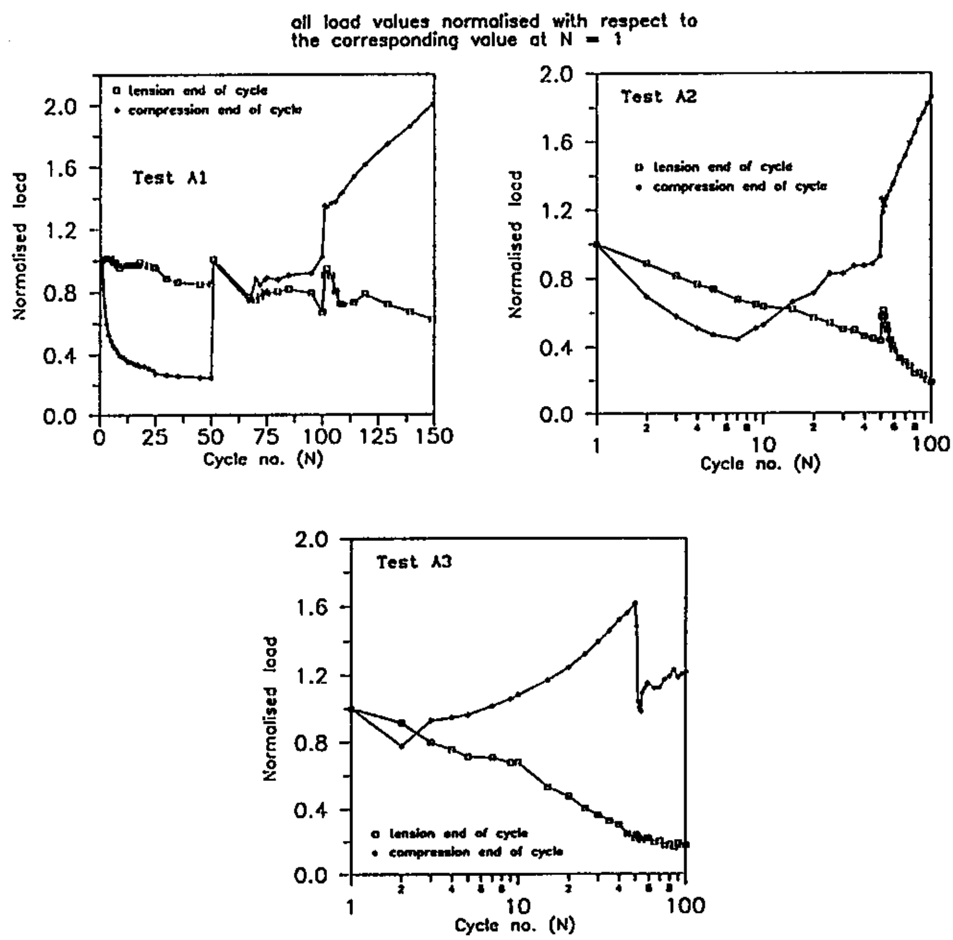

Fig. 8.10 Normalised distributions of the tension and compression pile head load values during cycling (50mm diameter model tests)

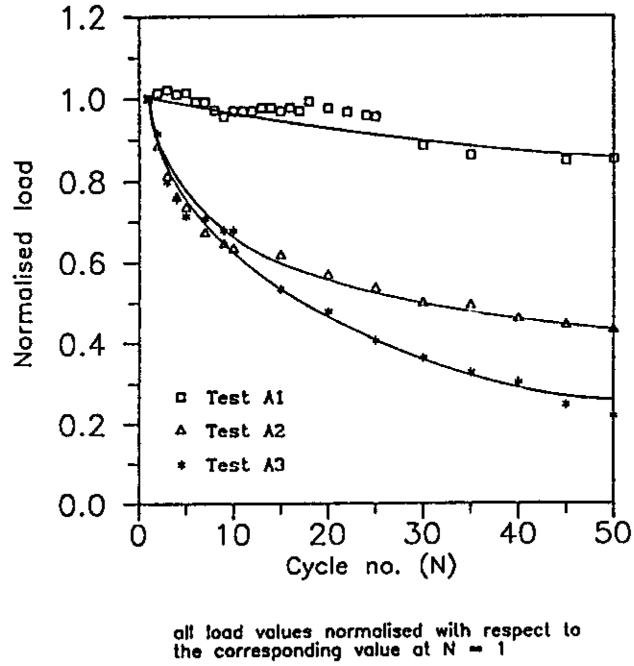

Fig. 8.11 Variation of the normalised pile head tension load values for the primary loading parcel A (50mm diameter model tests)

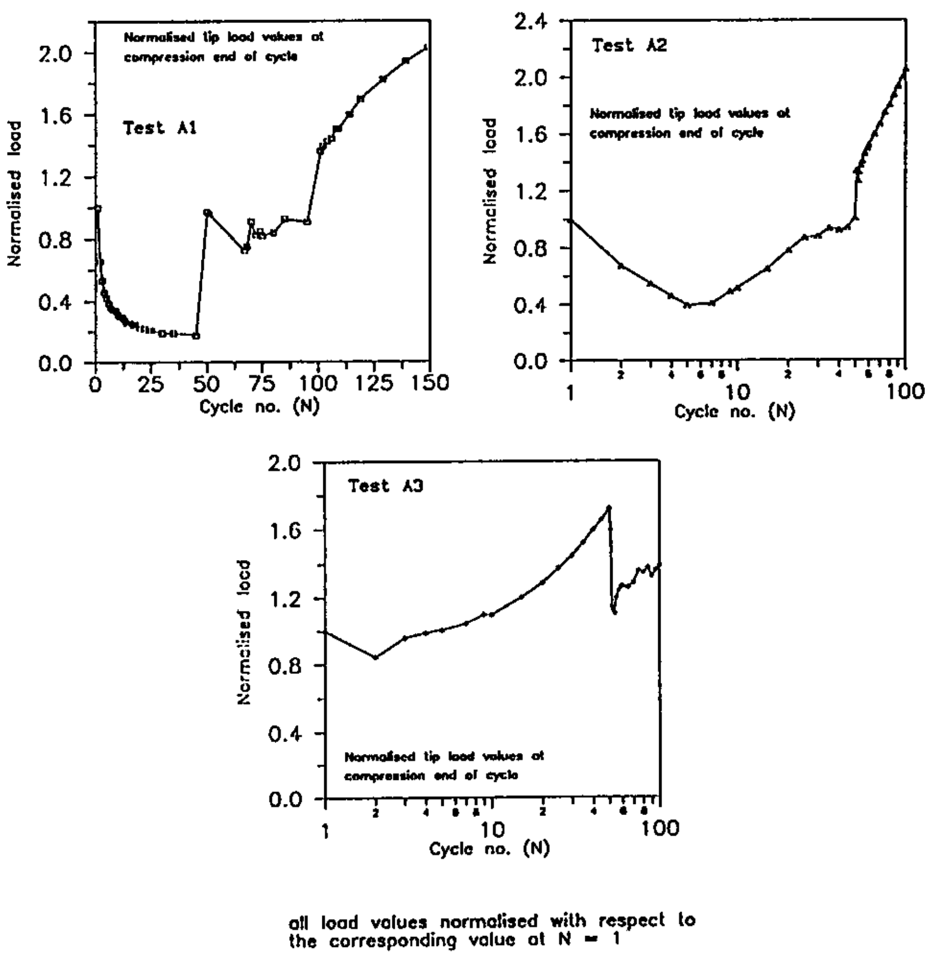

Fig. 8.12 Normalised distributions of the pile tip compression load values during cycling (50mm diameter model tests)

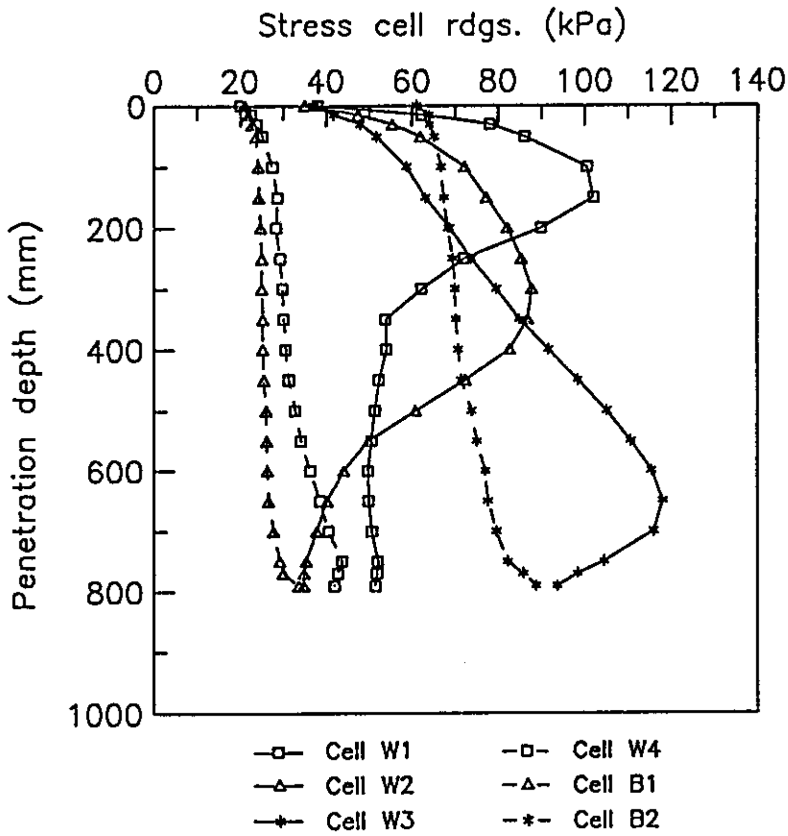

Fig. 8.13 Diaphragm stress cell responses during installation of the 100mm diameter instrumented model pile

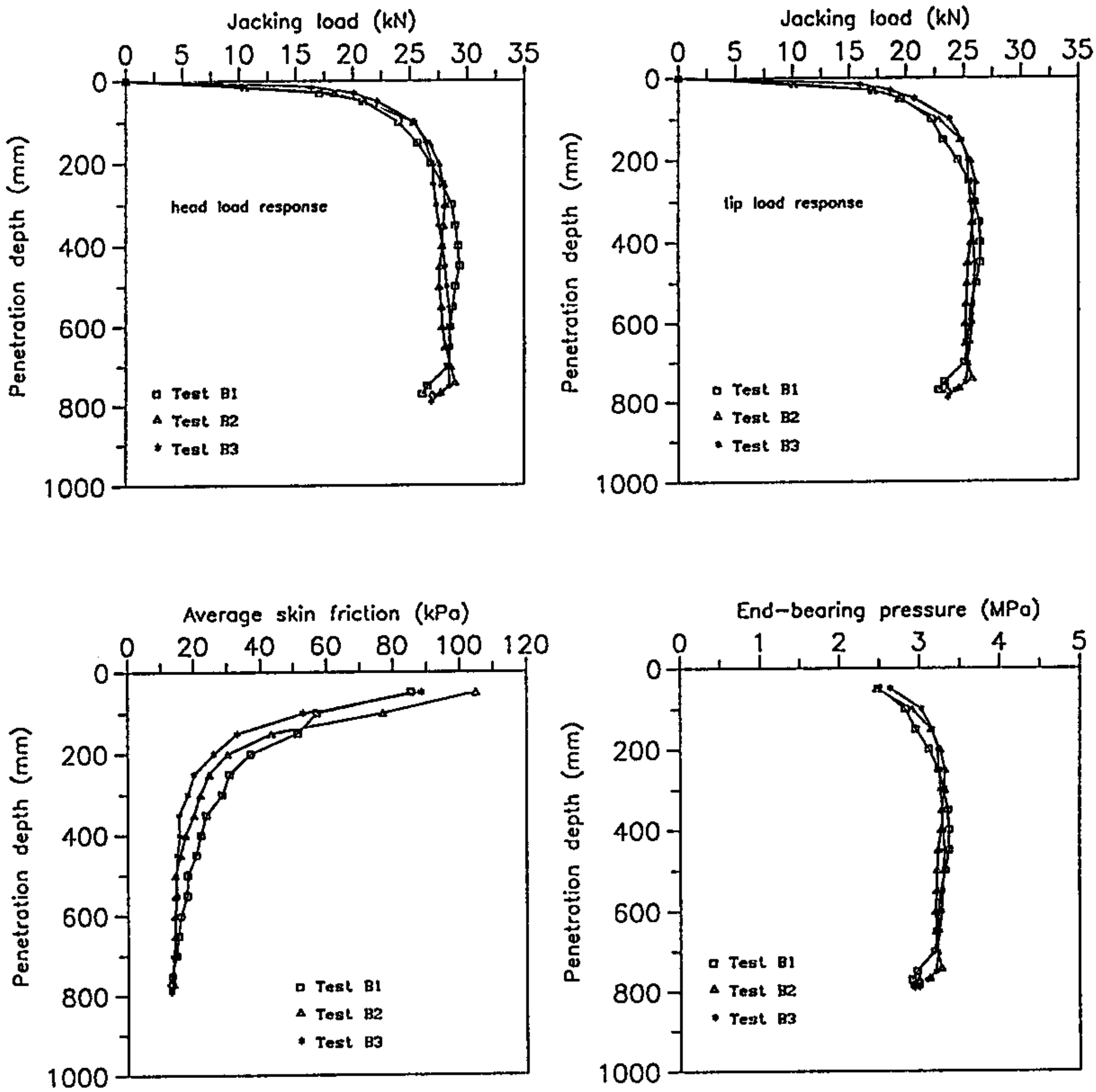

Fig. 8.14 Installation response of the 100mm diameter instrumented model pile: (a) head load response; (b) tip load response; (c) developed average skin friction; (d) developed end-bearing pressure

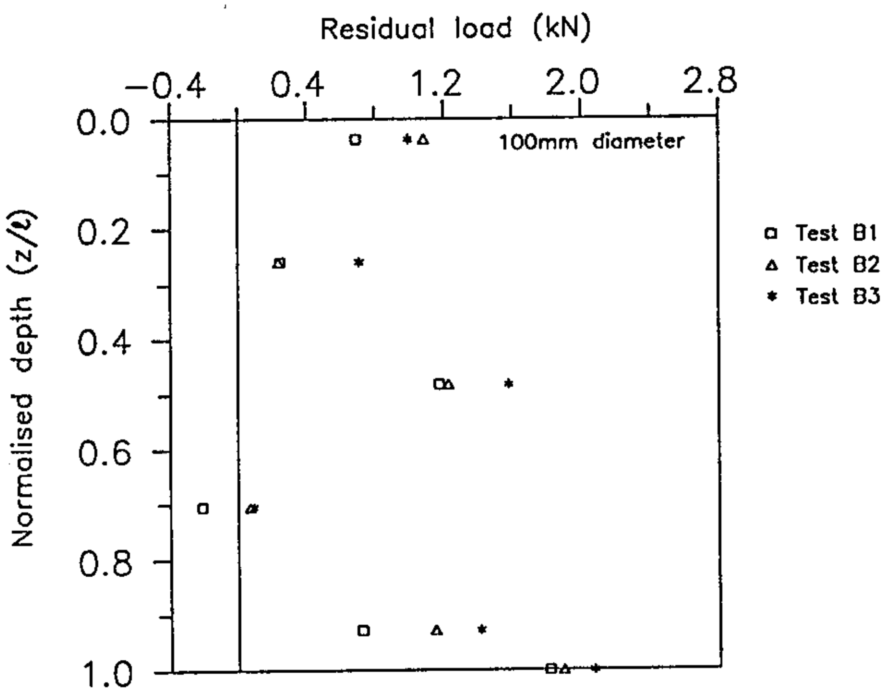

Fig. 8.15 Residual load values after installation for the three 100mm diameter model tests

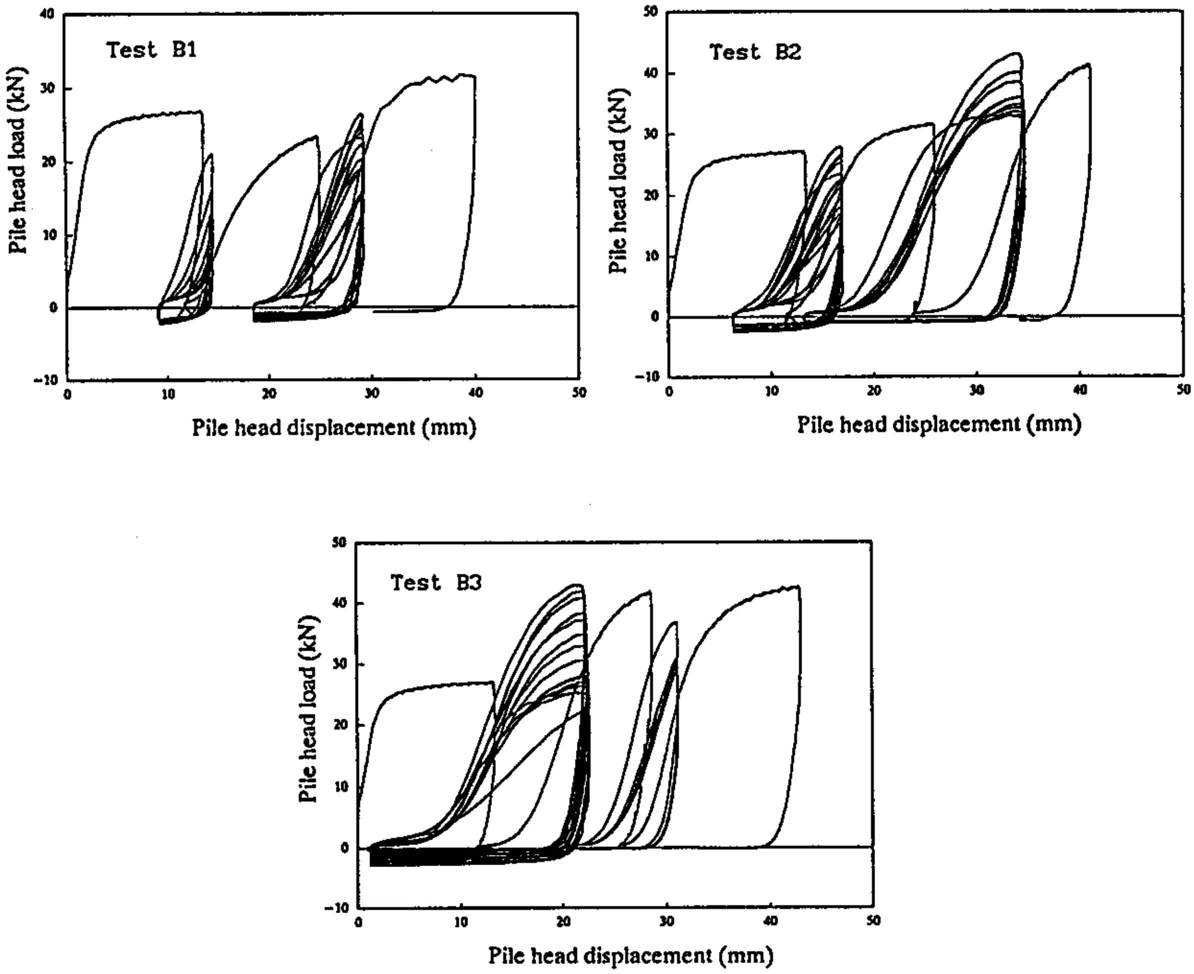

Fig. 8.16 Complete load-settlement responses for the three 100mm diameter model tests: (a) Test B1; (b) Test B2; (c) Test B3

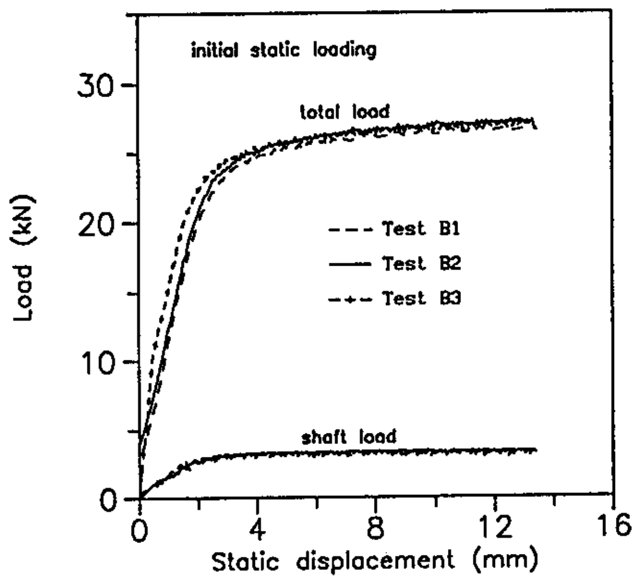

Fig. 8.17 Initial static load-settlement responses for the three 100mm diameter model tests

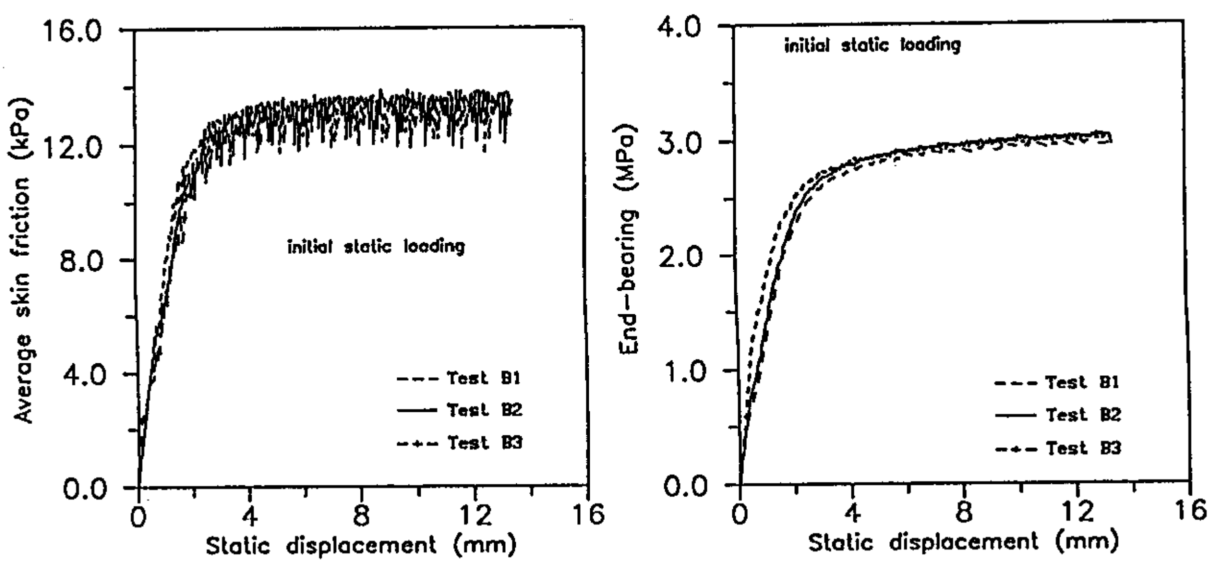

Fig. 8.18 Initial static loading responses for the three 100mm diameter model tests: (a) developed average skin friction; (b) developed end-bearing pressure

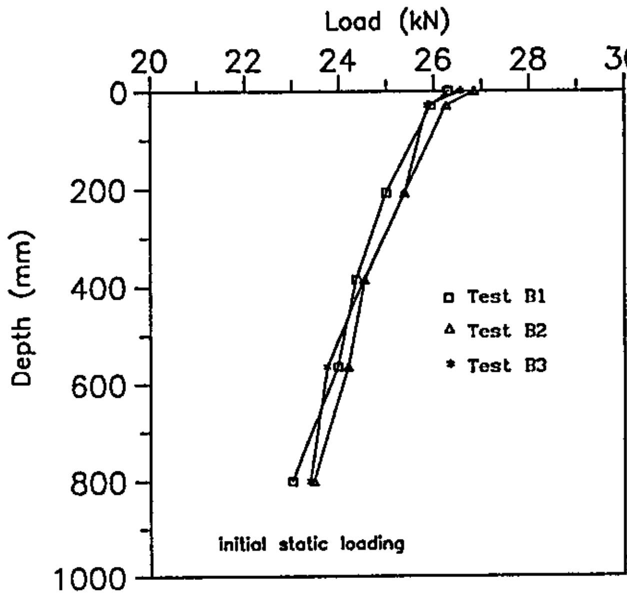

Fig. 8.19 Initial static load distributions for the three 100mm diameter model tests

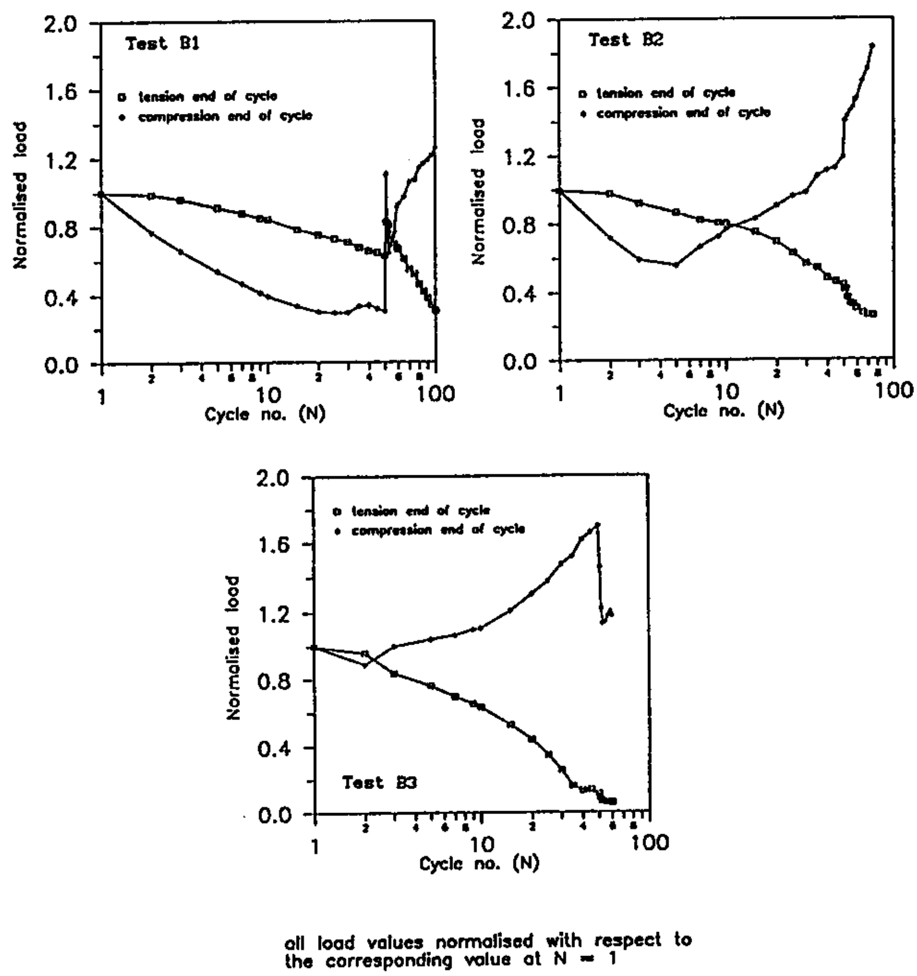

Fig. 8.20 Normalised distributions of the tension and compression pile head load values during cycling (100mm diameter model tests)

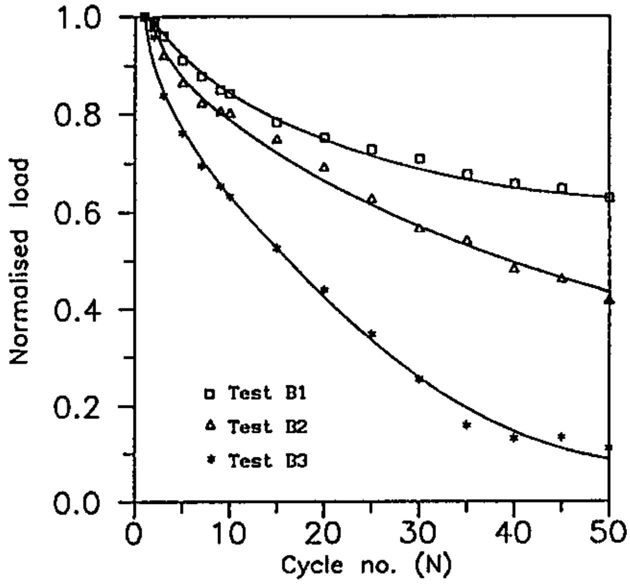

all load values normalised with respect to the corresponding value at N = 1

Fig. 8.21 Variation of the normalised pile head tension load values for the primary loading parcel A (100mm diameter model tests)

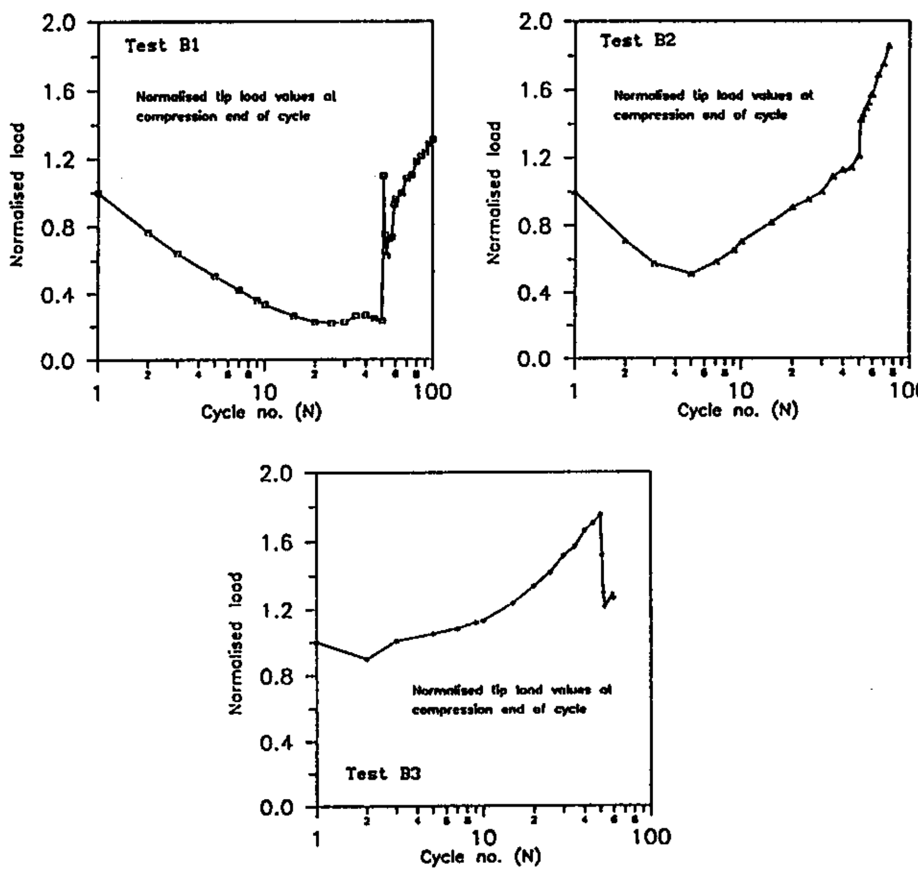

all load values normalised with respect to the corresponding value at N = 1

Fig. 8.22 Normalised distributions of the pile tip compression load values during cycling (100mm diameter model tests)

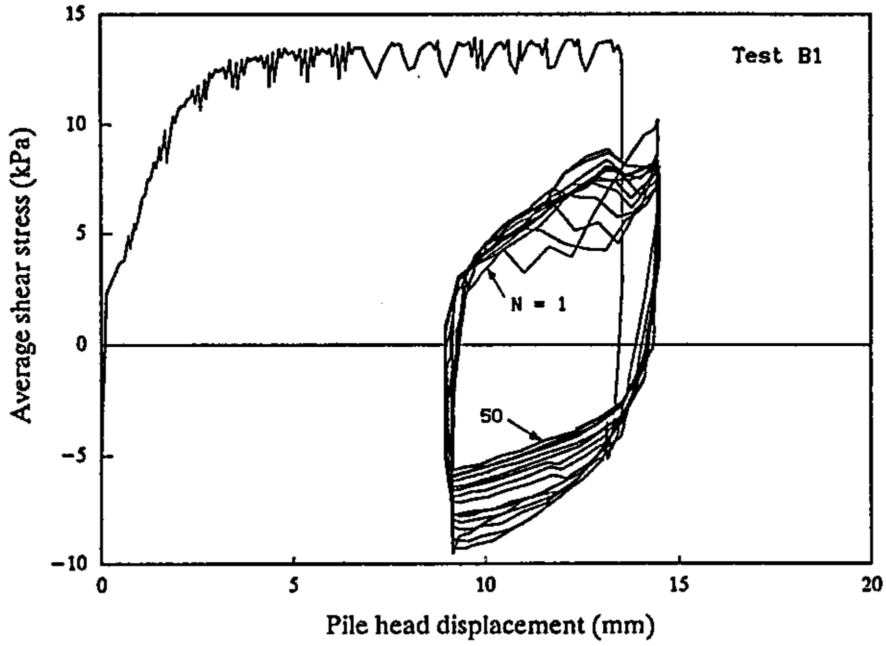

(a)

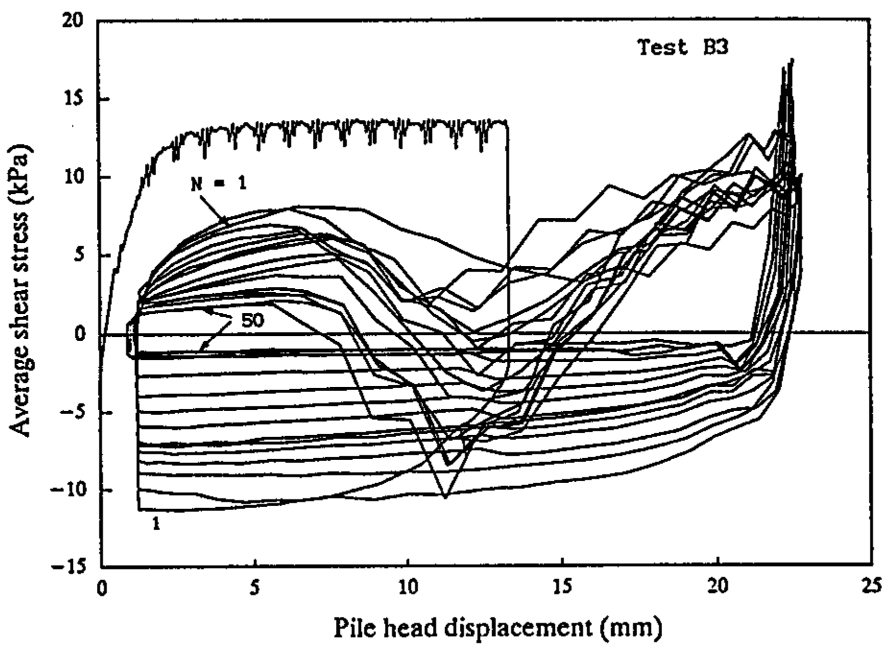

(b)

Fig. 8.23 Variation of average pile-soil shear stress during cyclic loading parcel A for (a) Test B1; (b) Test B3

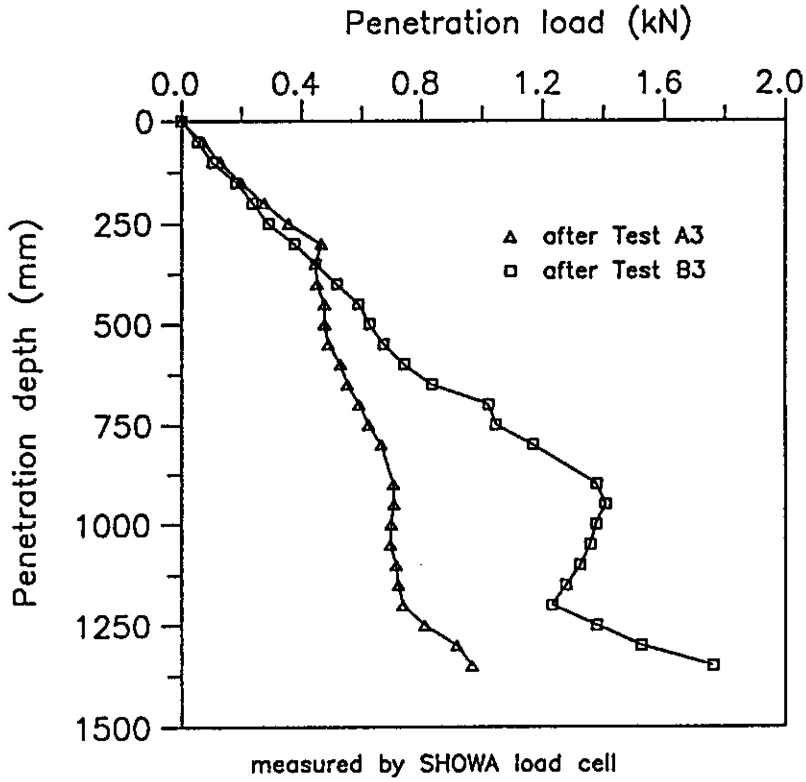

Fig. 8.24 "After test" pile "penetrometer" responses for Test A3 (50mm diameter) and Test B3 (100mm diameter)

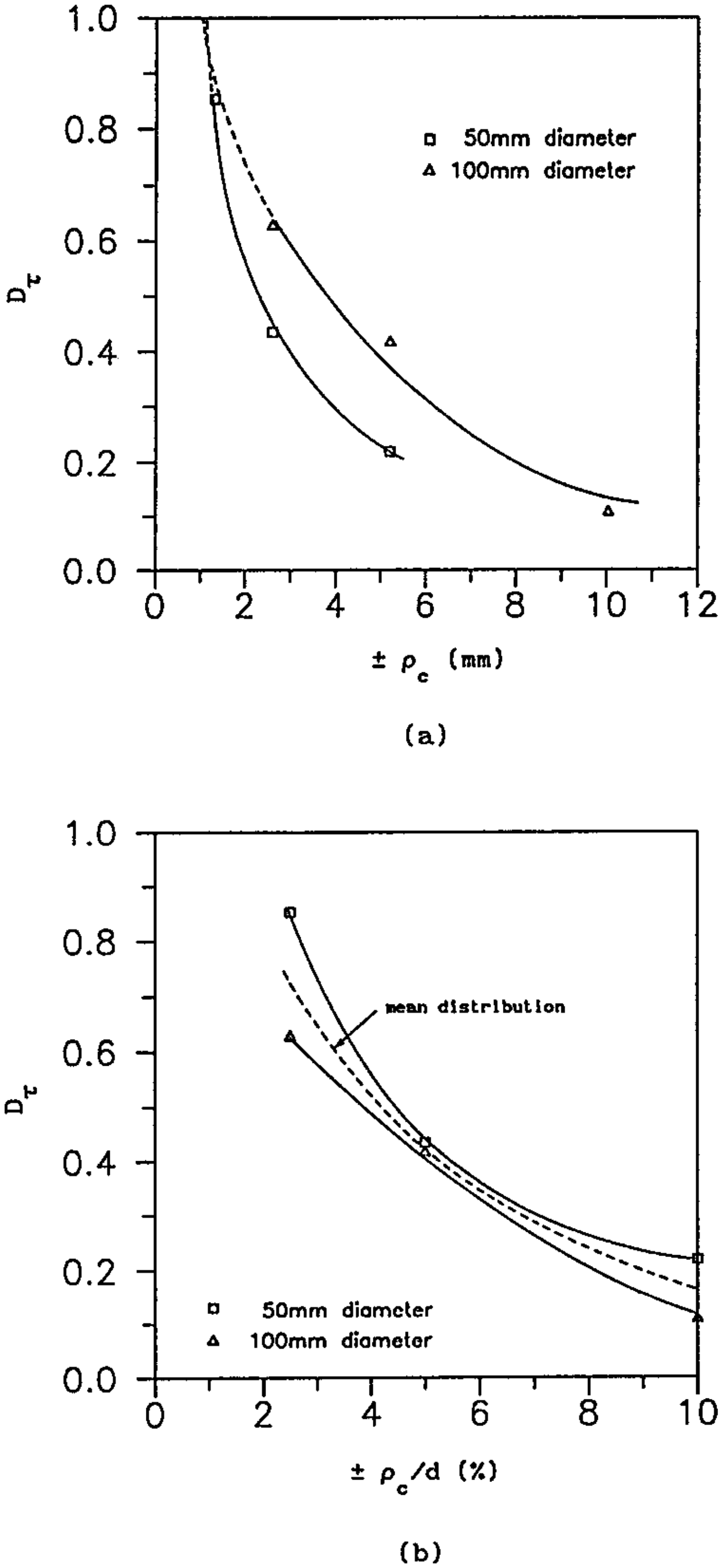

Fig. 8.25 Variation of skin friction degradation factor with (a) absolute cyclic displacement amplitude (ρ_c); (b) normalised cyclic displacement amplitude (ρ_c/d)

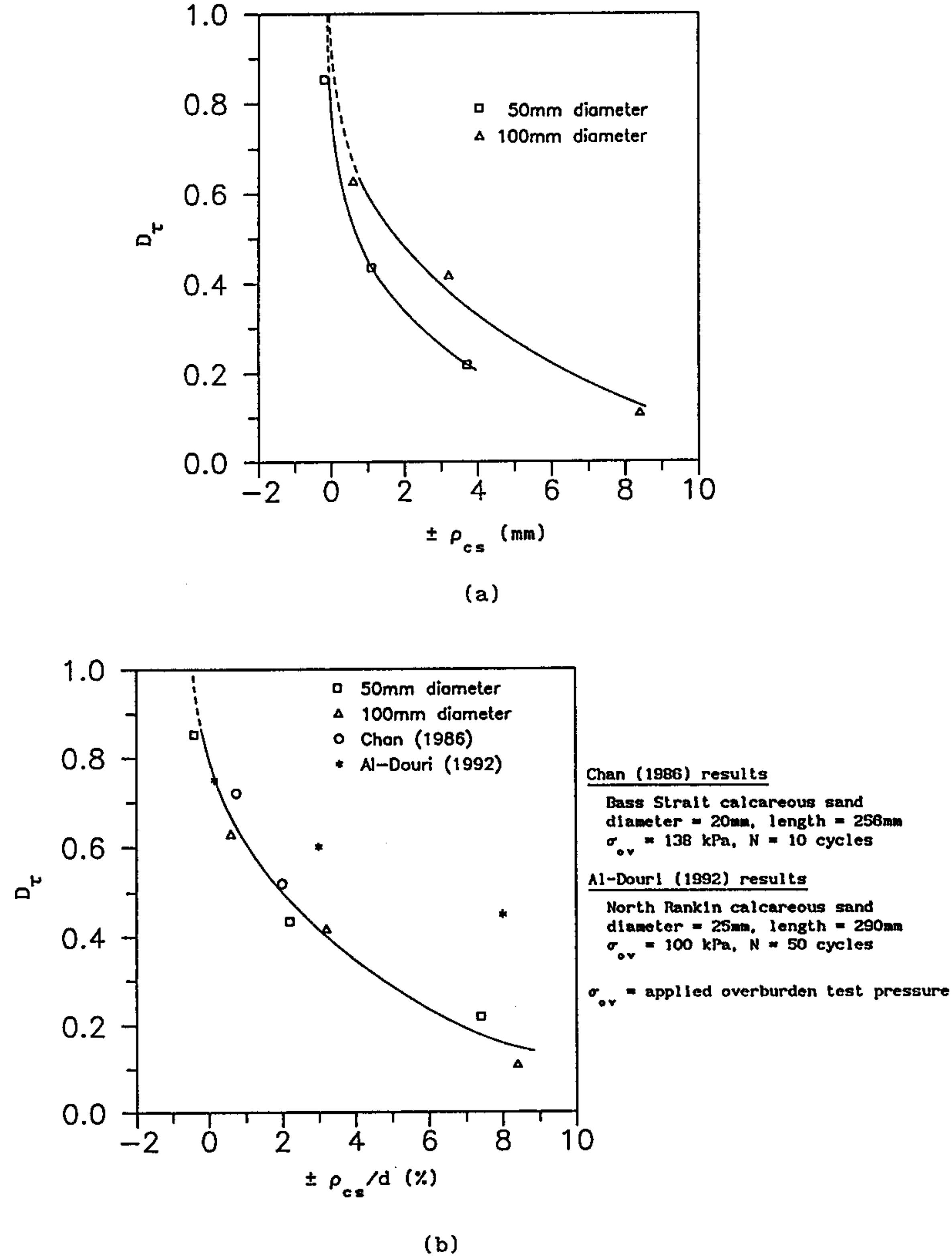

Fig. 8.26 Variation of skin friction degradation factor with (a) absolute cyclic slip displacement value (ρ_{cs}); (b) normalised cyclic slip displacement value (ρ_{cs}/d)

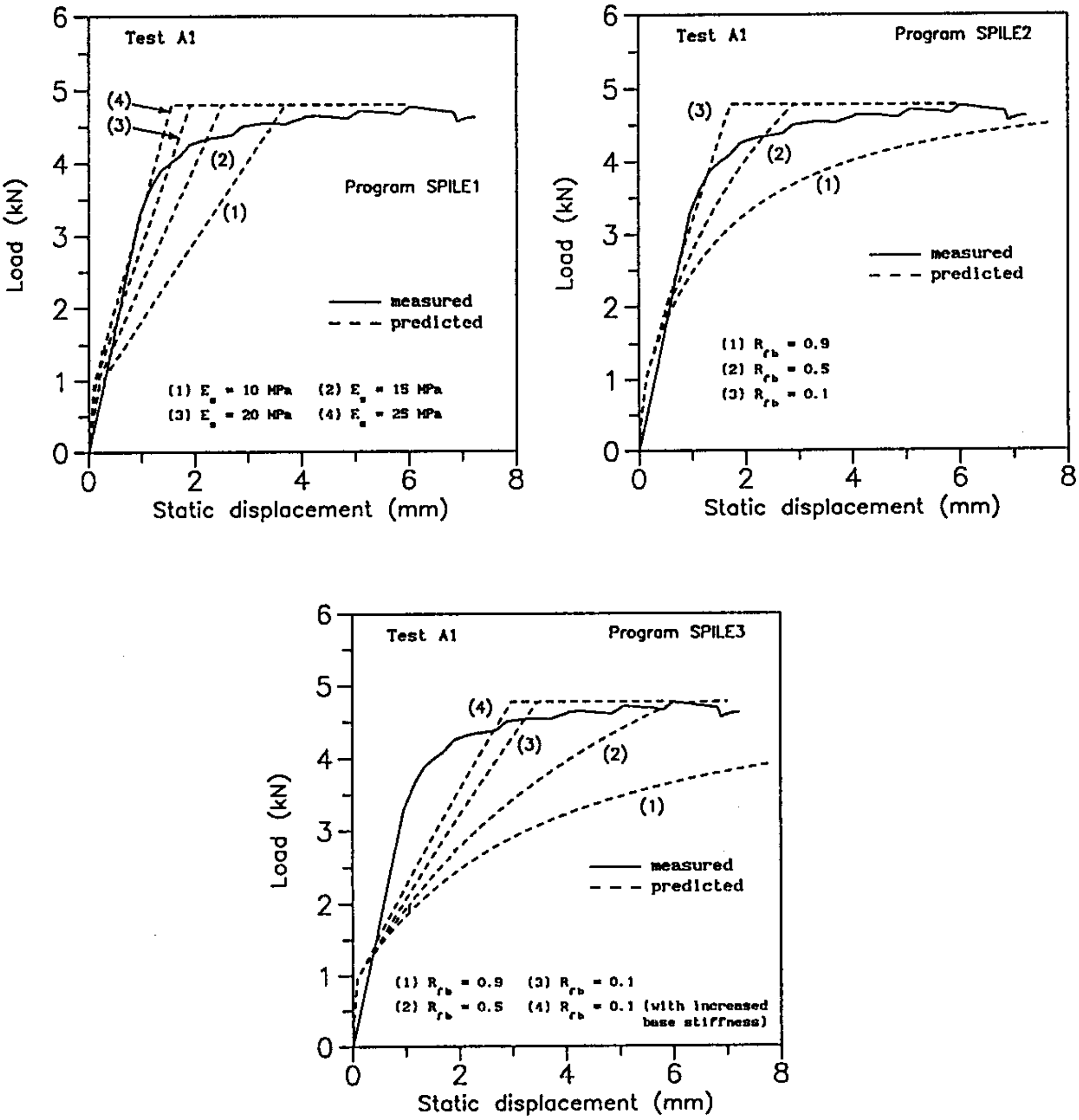

Fig. 8.27 Comparisons between predicted and measured initial static loading response of Test A1 utilised to back-figure the soil parameter values: using program (a) SPILE1; (b) SPILE2; (c) SPILE3

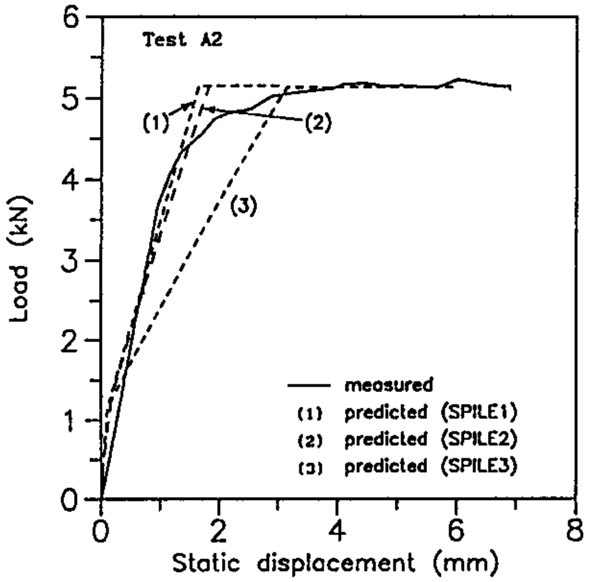

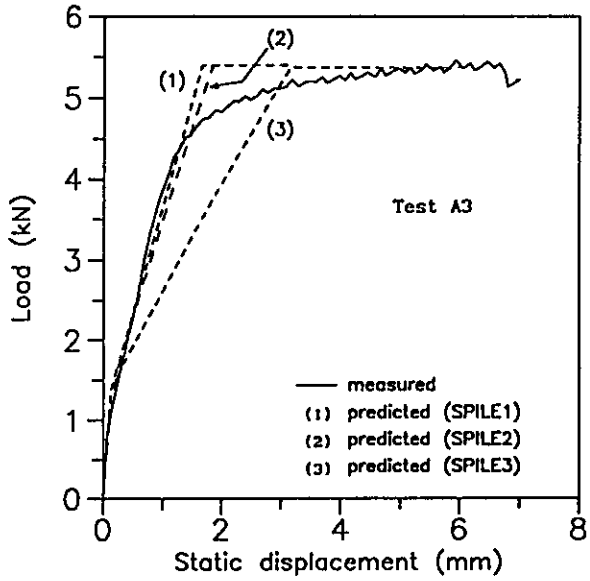

Fig. 8.28 Comparisons between predicted and measured initial static loading responses for Tests A2 and A3 using programs SPILE1, SPILE2 and SPILE3

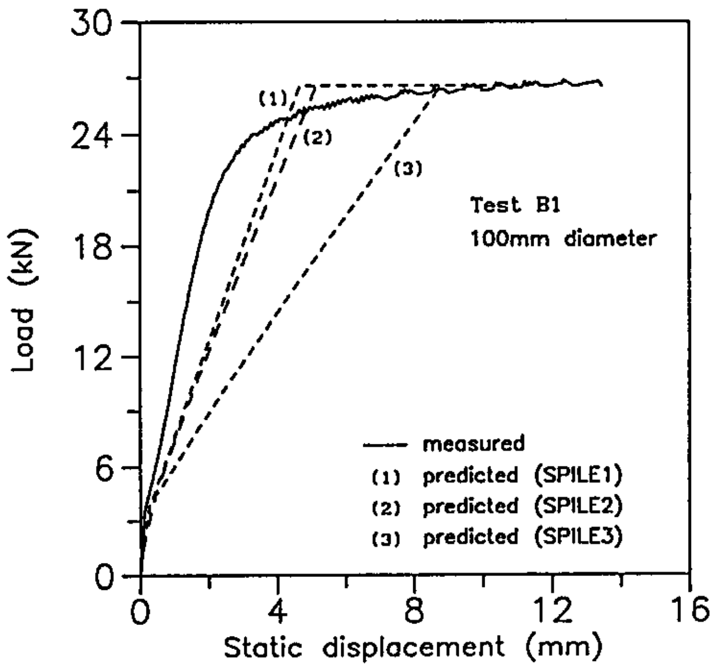

Fig. 8.29 Comparison between predicted and measured initial static loading response for the 100mm diameter model pile using programs SPILE1, SPILE2 and SPILE3

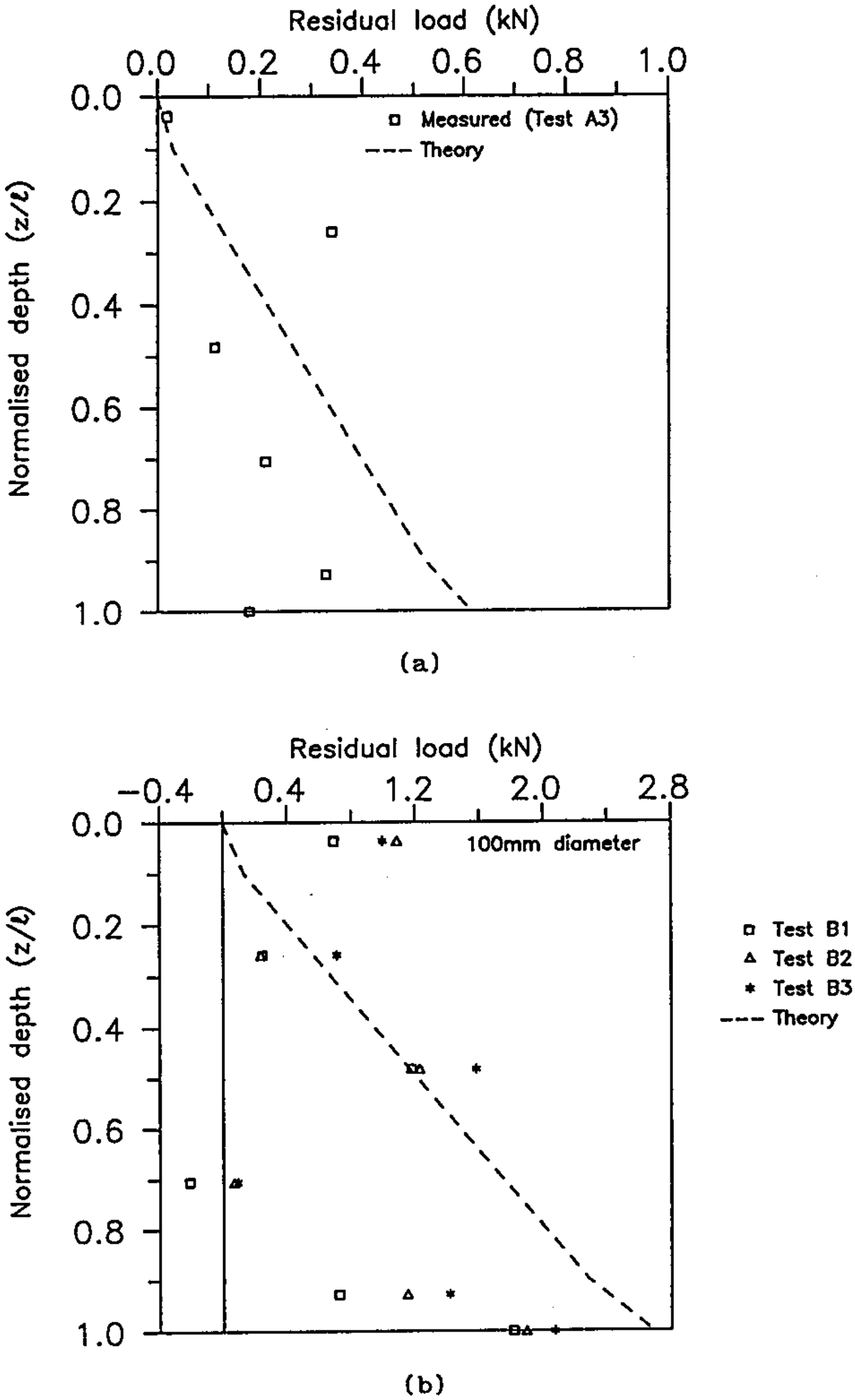

Fig. 8.30 Theoretical installation residual load profiles for (a) 50mm diameter model pile; (b) 100mm diameter model pile

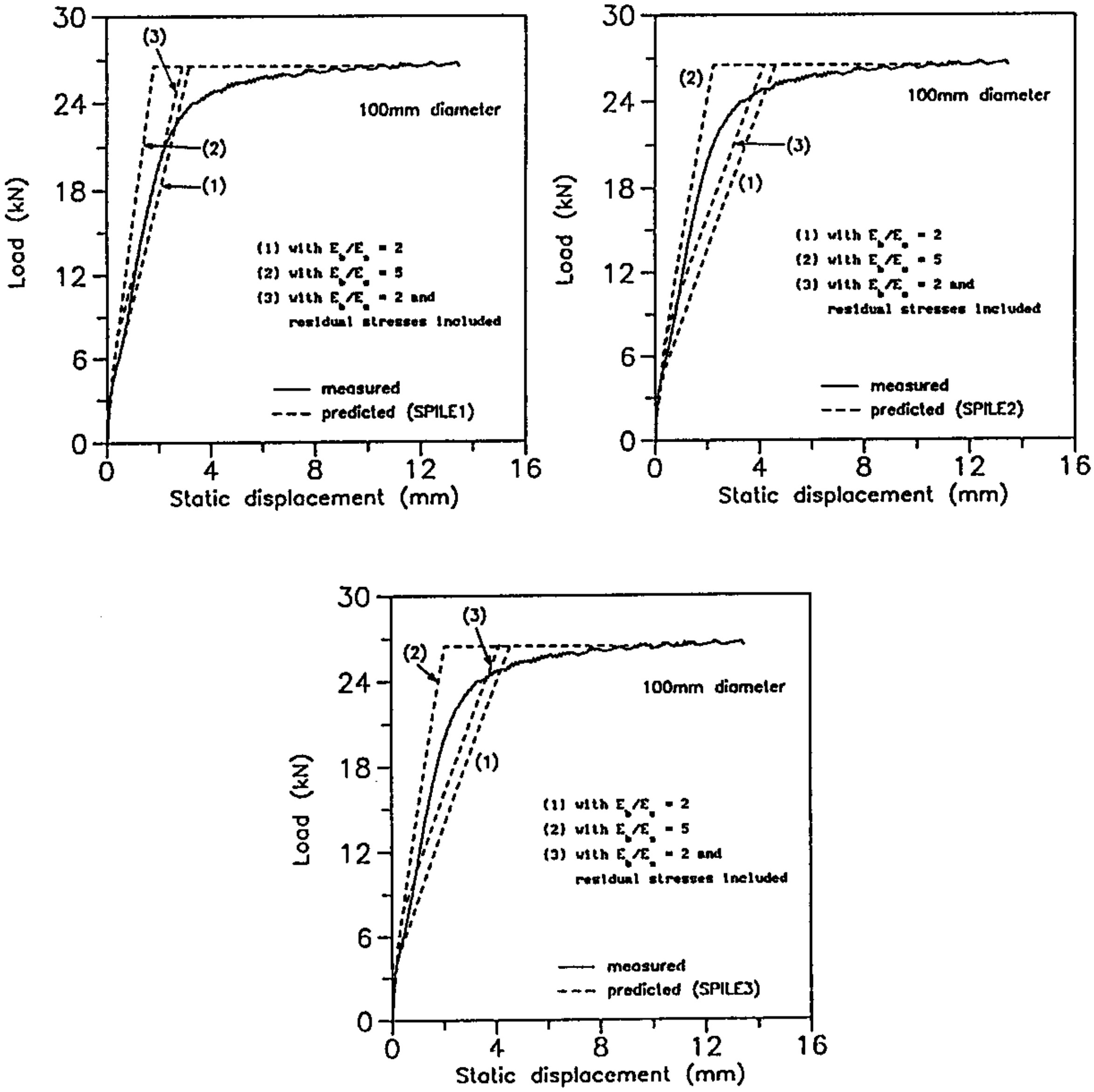

Fig. 8.31 Improved predictions for 100mm diameter model pile using programs SPILE1, SPILE2 and SPILE3

CHAPTER 9

CONCLUSIONS

CHAPTER 9

CONCLUSIONS

9.1 MAIN FINDINGS

In this chapter, the main conclusions from both the experimental and numerical parts of the work undertaken in the present study are summarised.

For the experimental part:

1 The series of model pile tests indicate low unit skin friction values of less than 15 kPa for piles in calcareous sediments consolidated under 100 kPa overburden pressure. This observation is in accord with other reported laboratory and field tests results. The static compressive capacity of the model piles (under the present test conditions) are contributed mainly by the developed end-bearing capacities, which form between 80% and 90% of the total static compressive capacity of the pile. The displacement required to fully mobilise the shaft capacity is found to be practically independent of the pile diameter.

2 No significant degradation of skin friction capacity occurs unless the cyclic displacement amplitude exceeds a displacement value on the order of that required to mobilise the full shaft capacity. Furthermore, the degradation of skin friction capacity under cyclic loading conditions is shown to be governed by the normalised (to diameter) value of the cyclic slip displacement. Thus, the present model jacked pile test results, together with the model grouted pile test results reported by Lee (1988) (see also Lee and Poulos, 1991), strongly confirm the normalised "cyclic slip displacement" model to be the appropriate model for skin friction degradation. There also appears to be a limiting degradation factor, corresponding to maximum possible degradation, for a given pile-soil system.

3 The test results also indicate that for cyclic displacement amplitude ρ_c/d greater than ±0.025, an increase in the mobilised pile tip compression load can be expected with increasing cycles. This increase in the mobilised pile tip load is a result of compaction occurring in the vicinity of the pile tip. For such a

situation, a corresponding increase in the post-cyclic static compressive capacity can be expected.

The conclusion reached that the degradation of skin friction capacity is governed by the normalised (to diameter) value of the cyclic slip displacement can thus, in future, be more confidently adopted in the numerical analysis approach described for modelling the degradation of skin friction capacity.

For the numerical part:

1 For static loading, the choice of the adopted soil model (elastic-plastic continuum model, nonlinear hyperbolic continuum model, nonlinear hyperbolic "t-z" model) is shown to have no significant influence within the working load range. Beyond the working load range, the adopted soil model may have a significant influence on the computed response. In situations where the total shaft capacity or pile base capacity forms a major proportion of the total pile capacity, proper modelling of the corresponding nonlinear pile shaft or pile base response is necessary in order to obtain a more "correct" response beyond the working load range. The efficiency and accuracy of the static "t-z" program SPILE3 for both single piles and pile groups analysis have also been demonstrated. The comparison between the predicted solutions and the measured static load-settlement response of the 100mm diameter model pile indicate that, a better agreement between predicted and measured results can be obtained if a larger soil modulus value is utilised for the pile tip response as well as the incorporation of the installation residual stresses in the pile analysis.

2 For cyclic loading, the numerical results presented show that the computed response is influenced by several parameters. The important parameters affecting the computed post-cyclic pile capacity and the accumulated permanent pile displacement have also been identified. In particular, for the "t-z" program SCPIL3 ("degrading secant modulus" approach) the importance of the accumulation rate parameter ψ in affecting the computed accumulated pile displacement is demonstrated. For pile groups, some results presented show that the choice of the capacity degradation model can lead to either a more severe or less severe computed degradation response as compared to the corresponding single pile solution. The results of a comparative study further highlight the

inconsistent prediction responses that can be obtained from different cyclic axial loading analysis programs. Finally, a comparison between numerical solutions and a field cyclic pile load test measurements shows general consistency between predicted and measured results.

In general, it can be concluded that our present ability to model the static axial response of both single piles and pile groups is generally satisfactory. Under cyclic loading conditions, however, our predictive ability is far less satisfactory, in particular, with regard to the predicted accumulated pile displacement. For pile groups, much less is known of the influence of pile-soil-pile interaction on the cyclic response.

9.2 SUGGESTIONS FOR FUTURE WORK

The series of displacement-controlled cyclic loading tests conducted in the present study has served to identify the appropriate model governing the degradation of skin friction capacity. Of equal importance also is the possible accumulation of permanent displacement under a load-controlled cyclic loading condition. It is therefore suggested that future work could be directed at conducting load-controlled tests using the present test facility. These load-controlled tests should be capable of providing the necessary empirical parameters required for an assessment of the cyclic loading analysis approach described in the present study. The influence of a "storm-loading" condition, consisting of a number of different load-controlled loading parcels, should also be investigated.

It may be recalled that the simplified approach adopted in the present study to deduce the normal pile-soil interface stress was not successful in the actual model pile tests. Therefore, future attempts could be made to instrument the model pile with the more complicated Cambridge-type contact stress cells to measure more reliably the normal pile-soil interface stress.

Some "wet" soil tests could also be conducted using the present model piles of 50mm and 100mm diameters. These "wet" soil tests represent a more realistic simulation of the saturated condition of the soil in the offshore environment. The development of excess pore-water pressures along offshore piles, as a result of cyclic loading, can lead to a momentary or short-term reduction of the pile capacity. This reduction (or degradation) in pile capacity may be in addition to the degradation occurring as a result of physical changes to the soil structure. It is recognised that for small scale laboratory piles in sand, any developed excess pore-water pressure would be dissipated quite rapidly (for a given height of the test chamber, the rate of dissipation can be taken as inversely proportional to the square of the pile diameter). Nevertheless, it would be of interest to compare the responses of both the present 50mm and 100mm diameter model piles under "wet" and "dry" soil conditions.

REFERENCES

REFERENCES

Abbs, A.F. and Needham, A.D. (1985), "Grouted piles in weak carbonate rocks", Proc. 17th. Offshore Tech. Conf., OTC No. 4852, vol.1, pp.105-112.

Abbs, A.F., Bell, R.A., Khorshid, M.S. and Jewell, R.J. (1988), "Evaluation of pile friction from conductor load tests", Proc. Int. Conf. on Calcareous Sediments, Perth, vol.2, pp.607-616.

Abendroth, R.E. and Greimann, L.F. (1990), "Pile behaviour established from model tests", Jnl. of Geot. Engrg. Div., ASCE, vol.116, No.4, pp.571-588.

Agarwal, S.L., Malhotra, A.K. and Banerjee, R. (1977), "Engineering properties of calcareous soils affecting the design of deep penetration piles for offshore structures", Proc. 9th. Offshore Tech. Conf., OTC No. 2792, vol.1, pp.503-512.

Airey, D.W., Randolph, M.F. and Hyden, A.M. (1988), "The strength and stiffness of two calcareous sands", Proc. Int. Conf. on Calcareous Sediments, Perth, vol.1, pp.43-50.

Al-Douri (1991), *private communication*

Al-Douri (1992), *The behaviour of jacked piles in calcareous sand*, forthcoming PhD Thesis, The University of Sydney, Australia.

Allman, M.A. and Poulos, H.G. (1988), "Stress-strain behaviour of an artificially cemented calcareous soil", Proc. Int. Conf. on Calcareous Sediments, Perth, vol.1, pp.51-60.

Allman, M.A., Lee, C.Y. and Poulos, H.G. (1988), "Behaviour of model grouted piles in cemented and uncemented calcareous soils", Proc. Behaviour of Offshore Structures (BOSS), vol.1, pp.379-391.

American Petroleum Institute (1987), *Recommended practice for planning, designing and constructing fixed offshore platforms* (RP2A), 17th. Edition.

Angemeer, J., Carlson, E.D. and Klick, J.H. (1973), "Techniques and results of offshore pile load testing in calcareous soils", Proc. 5th. Offshore Tech. Conf., OTC No. 1894, vol.2, pp.677-692.

Angemeer, J., Carlson, E.D., Stroud, S. and Kurzeme, M. (1975), "Pile load tests in calcareous soils conducted in 400 feet of water from a semi-submersible exploration rig", Proc. 7th. Offshore Tech. Conf., OTC No. 2311, vol.2, pp.657-670.

Armaleh, S. and Desai, C.S. (1987), "Load-deformation response of axially loaded piles", Jnl. of Geot. Engrg. Div., ASCE, vol.113, No.12, pp.1483-1500.

Arthur, J.R.F. and Roscoe, K.H. (1961), "An earth pressure cell for the measurement of normal and shear stresses", Civil Engrg. and Public Works Review, vol.56, No.659, pp.765-780.

ASTM D1143 (1981), *Standard method of testing: Piles under static axial compressive load.*

Australian Standard AS1289 (1977), *Methods of testing soil for engineering purposes,* Standards Association of Australia.

Baligh, M.M. (1984), "The simple-pile approach to pile installation in clays", Proc. Analysis and Design of Pile Foundations, San Francisco, pp.310-330.

Baligh, M.M., Martin, R.T., Azzouz, A.S. and Morrison, M.J. (1985), "The piezo-lateral stress cell", Proc. 11th. Int. Conf. on Soil Mechs. and Found. Engrg., San Francisco, vol.2, pp.841-844.

Banerjee, P.K. (1976), "Integral equation methods for analysis of piece-wise nonhomogeneous three-dimensional elastic solids of arbitrary shape", Int. Jnl. Mechanical Science, vol.18, No.6, pp.293-303.

Banerjee, P.K. (1978), "Analysis of axially and laterally loaded pile groups", *Developments in Soil Mechanics,* Ed. by Scott, C.R., Applied Science Publishers, U.K.

Banerjee, P.K. and Davies, T.G. (1977), "Analysis of pile groups embedded in Gibson soil", Proc. 9th. Int. Conf. on Soil Mech. and Found. Engrg., Tokyo, vol.1, pp.381-386.

Banerjee, P.K. and Davies, T.G. (1978), "The behaviour of axially and laterally loaded single piles embedded in nonhomogeneous soils", Geotechnique, vol.28, No.3, pp.309-326.

Banerjee, P.K. and Davies, T.G. (1980), "Analysis of some reported case histories of laterally loaded pile groups", Proc. Num. mtds. in Offshore Piling, ICE, London, pp.101-108.

Barthelemy, H., Bustamante, M., Gouvenot, D. and Martin, R. (1986), "Pressure grouted piles: a solution to offshore foundation problems", Proc. 3rd. Int. Conf. on Num. mtds. in Offshore Piling, Nantes, pp.481-494.

Barthelemy, H., Martin, R., LeTirant, P., Nauroy, J.F. and Cipriano de Meideres, J. (1987), "Grouted driven piles: an economic and safe alternate for pile foundations", Proc. 19th. Offshore Tech. Conf., OTC No. 5409, vol.1, pp.427-436.

Bea, R.G. (1992), "Pile capacity for axial cyclic loading", Jnl. of Geot. Engrg. Div., ASCE, vol.118, No.2, pp.34-50.

Bea, R.G., Litton, R.W., Nour-Omid, S. and Chang, J.Y. (1984), "A specialized design and research tool for the modelling of near-field pile-soil interactions", Proc. 16th. Offshore Tech. Conf., OTC No.4806, vol.3, pp.249-264.

Bellotti, R., Bizzi, G. and Ghionna, V. (1982), "Design, construction and use of a calibration chamber", Proc. 2nd. Europ. Symp. on Penetration Testing, Amsterdam, vol.2, pp.439-446.

Beringen, F.L., Kolk, H.J. and Windle, D. (1982), "Cone penetration and laboratory testing in marine calcareous sediments", Proc. Geotechnical Properties, Behaviour and Performance of Calcareous Soils, ASTM STP 777, pp.179-209.

Bieganousky, W.A. and Marcuson, III, W.F. (1976), "Uniform placement of sand", Jnl. of Geot. Engrg. Div., ASCE, vol.102, No.3, pp.229-233.

Boey, C.F. and Carter, J.P. (1988), "Mechanical testing of an artificially cemented carbonate soil", Proc. 5th. ANZ Conf. on Geomechs., Sydney, pp.145-149.

Bogard, J.D. and Matlock, H. (1990a), "In-situ pile segment model experiments at Empire, Louisiana", Proc. 22nd. Offshore Tech. Conf., OTC No. 6323, vol.2, pp.459-467.

Bogard, J.D. and Matlock, H. (1990b), "In-situ pile segment model experiments at Harvey, Louisiana", Proc. 22nd. Offshore Tech. Conf., OTC No. 6324, vol.2, pp.469-477.

Bogard, J.D., Matlock, H., Audibert, J.M.E. and Bamford, S.R. (1985), "Three years experience with model pile segment tool tests", Proc. 17th. Offshore Tech. Conf., OTC No. 4848, vol.1, pp.65-72.

Bond, A.J. and Jardine, R.J. (1989), "Instruments for measuring the effective stresses acting on a pile jacked into overconsolidated clay", Proc. Conf. on Geotechnical Instrumentation in Practice, ICE, pp.583-605.

Bond, A.J. and Jardine, R.J. (1991), "Effects of installing displacement piles in a high OCR clay", Geotechnique, vol.41, No.3, pp.341-363.

Booker, J.R., Rahman, M.S. and Seed, H.B. (1976), "GADFLEA - A computer program for the analysis of pore pressure generation and dissipation during cyclic or earthquake loading", Earthquake Engrg. Research Centre, Univ. of California, Berkeley, C.A., Report No. EERC 76-24.

Booker, J.R., Carter, J.P., Small, J.C., Brown, P.T. and Poulos, H.G. (1989), "Some recent applications of numerical methods to geotechnical analysis", Computers and Structures, vol.31, No.1, pp.81-92.

Boulon, M. and Foray, P. (1986), "Physical and numerical simulation of lateral shaft friction along offshore piles in sand", Proc. 3rd. Int. Conf. on Num. mtds. in Offshore Piling, Nantes, pp.127-147.

Boulon, M., Desrues, J., Foray, P. and Forgue, M. (1980), "Numerical model for foundation under cyclic loading: application to piles", Proc. Int. Symp. on Soils under Cyclic and Transient Loading, Swansea, pp.681-694.

Bransby, P.L. (1973), "Cambridge contact stress transducers", Cambridge Univ. Engrg. Dept., Rep. No. CUED/C-SOILS/LN2.

Briaud, J.L. and Felio, G.Y. (1986), "Analysis of existing cyclic vertical load tests for piles in clay", Proc. 18th. Offshore Tech. Conf., OTC No.5224, vol.3, pp.31-37.

Briaud, J.L. and Tucker, L. (1984), "Piles in sand: A method including residual stresses", Jnl. of Geot. Engrg. Div., ASCE, vol.110, No.11, pp.1666-1680.

Butterfield, R. and Banerjee, P.K. (1971a), "The elastic analysis of compressible piles and pile groups", Geotechnique, vol.21, No.1, pp.43-60.

Butterfield, R. and Banerjee, P.K. (1971b), "The problem of pile group-pile cap interaction", Geotechnique, vol.21, No.2, pp.135-142.

Butterfield, R. and Douglas, R.A. (1981), "Flexibility coefficients for the design of piles and pile groups", CIRIA Technical Note No.108, 79pp.

Butterfield, R. and Johnston, I.W. (1973), "The stress acting on a continuously penetrating pile", Proc. 8th. Int. Conf. on Soil Mechs. and Found. Engrg., Moscow, vol.2, pp.39-45.

Carter, J.P., Booker, J.R. and Wroth, C.P. (1982), "A critical state soil model for cyclic loading", Soil Mechs. - Transient and Cyclic

Loads, Eds. Pande, G.N. and Zienkiewicz, O.C., pp.219-252.

Chan, S.F. (1976), *The behaviour of piles subjected to static and repeated loads*, PhD Thesis, The University of Sheffield.

Chan, K.F. (1986), *Behaviour of model piles in calcareous sand*, M.EngSc Thesis, The University of Sydney, Australia.

Chan, S.F. and Hanna, T.H. (1980), "Repeated loading on single piles in sand", Jnl. of Geot. Engrg. Div., ASCE, vol.106, No.2, pp.171-188.

Chan, K.S., Karasudhi, P. and Lee, S.L. (1974), "Force at a point in the interior of a layered elastic half-space", Int. Jnl. Solids Struct., vol.10, No.11, pp.1179-1199.

Chandler, R.J. and Martins, J.P. (1982), "An experimental study of skin friction around piles in clay", Geotechnique, vol.32, No.2, pp.119-132.

Chaney, R.C., Slonim, S.M. and Slonim, S.S. (1982), "Determination of calcium carbonate content in soils", ASTM Special Tech. Publ. STP 777, pp.3-15.

Cheung, Y.K., Tham, L.G. and Guo, D.J. (1988), "Analysis of pile group by infinite layer method", Geotechnique, vol.38, No.3, pp.415-431.

Chin, J.T. (1988), *Analysis of piles and pile groups embedded in a layered half-space*, M.Eng. Thesis, National Univ. of Singapore.

Chin, J.T., Chow, Y.K. and Poulos, H.G. (1990), "Numerical analysis of axially loaded vertical piles and pile groups", Computers and Geotechnics, vol.9, No.4, pp.273-290.

Chow, Y.K. (1984), "Analysis of axially loaded piles in layered soil", Jnl. Inst. Engrs., Malaysia, No.35, pp.56-63.

Chow, Y.K. (1986a), "Analysis of vertically loaded pile groups", Int. Jnl. for Num. and Analytical mtds. in Geomechs., vol.10, No.1, pp.59-72.

Chow, Y.K. (1986b), "Behaviour of pile groups under axial loads", Proc. 3rd. Int. Conf. on Num. mtds. in Offshore Piling, Nantes, pp.237-251.

Chow, Y.K. (1986c), "Discrete element analysis of settlement of pile groups", Computers and Structures, vol.24, No.1, pp.157-166.

Chow, Y.K. (1987), "Iterative analysis of pile-soil-pile interaction", Geotechnique, vol.37, No.3, pp.321-333.

Chow, Y.K. (1989), "Axially loaded piles and pile groups embedded in a cross-anisotropic soil", Geotechnique, vol.39, No.2, pp.203-211.

Chow, Y.K. and Teh, C.I. (1991), "Pile cap - pile group interaction in nonhomogeneous soil", Jnl. of Geot. Engrg. Div., ASCE, vol.117, No.11, pp.1655-1668.

Chow, Y.K., Chin, J.T., Kog, Y.C. and Lee, S.L. (1990), "Settlement analysis of socketed pile groups", Jnl. of Geot. Engrg. Div., ASCE, vol.116, No.8, pp.1171-1184.

Chua, E.W. (1983), *Bearing capacity of shallow foundations in calcareous sand*, MEngSc. Thesis, University of Sydney, Australia.

Clark, A.R. and Walker, B.F. (1977), "A proposed scheme for the classification and nomenclature for use in the engineering description of middle eastern sedimentary rocks", Geotechnique, vol.27, No.1, pp.93-99.

Cole, K.W. and Stroud, M.A. (1977), "Rock socket piles at Coventry Point, Market Way, Coventry", Symp. on Piles in Weak Rock, ICE, London, pp.47-62.

Cooke, R.W. and Price, G. (1973), "Strains and displacements around friction piles", Proc. 8th. Int. Conf. on Soil Mechs. and Found. Engrg., Moscow, vol.2, pp.53-60.

Cooke, R.W., Price, G. and Tarr, K. (1980), "Jacked piles in London Clay: interaction and group behaviour under working conditions", Geotechnique, vol.30, No.2, pp.97-136.

Coop, M.R. (1990), "The mechanics of uncemented carbonate sands", Geotechnique, vol.40, No.4, pp.607-626.

Coop, M.R. and Wroth, C.P. (1989), "Field studies of an instrumented model pile in clay", Geotechnique, vol.39, No.4, pp.679-696.

Coyle, H.M. and Reese, L.C. (1966), "Load transfer for axially loaded piles in clay", Jnl. of Soil Mech. and Found. Engrg. Div., ASCE, vol.92, No.2, pp.1-26.

Coyle, H.M. and Sulaiman, I.H. (1967), "Skin friction for steel piles in sand", Jnl. of Soil Mechs. and Found. Engrg., ASCE, vol.93, No.6, pp.261-278.

Datta, M., Gulhati, S.K. and Rao, G.V. (1979a), "Crushing of calcareous sands during shear", Proc. 11th. Offshore Tech. Conf., OTC No. 3525, vol.3, pp.1459-1467.

Datta, M., Gulhati, S.K. and Rao, G.V. (1979b), "Undrained shear behaviour of calcareous sands", Indian Geot. Jnl., vol.9, No.4, pp.365-380.

Datta, M., Rao, G.V. and Gulhati, S.K. (1980a), "Development of pore - water pressures in a dense calcareous sand under repeated compressive stress cycles", Proc. Int. Symp. on Soils under Cyclic and Transient Loading, Swansea, pp.33-47.

Datta, M., Gulhati, S.K. and Rao, G.V. (1980b), "An appraisal of the existing practice of determining the axial load capacity of deep penetration piles in calcareous sands", Proc. 12th. Offshore Tech. Conf., OTC No. 3867, vol.4, pp.119-130.

Datta, M., Gulhati, S.K. and Rao, G.V. (1982), "Engineering behaviour of carbonate soils of India and some observations on classification of such soils", Proc. Geotechnical Properties, Behaviour and Performance of Calcareous Soils, ASTM, STP 777, pp.113-140.

Deane, R.B., Shade, D.S., Schrier, W. and Williams, A.F. (1988), "Development and implementation of grouted section tests", Proc. Int. Conf. on Calcareous Sediments, Perth, vol.2, pp.485-491.

Demars, K.R., Nacci, V.A., Kelly, W.E. and Wang, M.C. (1976), "Carbonate content: An index property for ocean sediments", Proc. 8th. Offshore Tech. Conf., OTC No. 2627, vol.3, pp.97-106.

Desai, C.S. (1974), "Numerical design-analysis for piles in sands", Jnl. of Geot. Engrg. Div., ASCE, vol.100, No.6, pp.613-635.

Desai, C.S., Zaman, M.M. Lightmer, J.G. and Siriwardane, H.J. (1984), "Thin-layer element for interfaces and joint", Int. Jnl. for Num. and Analytical mtds. in Geomechs., vol.8, No.1, pp.19-43.

Diyaljee, V.A. and Raymond, G.P. (1982), "Repetitive load deformation of cohesionless soil", Jnl. of Geot. Engrg. Div., ASCE, vol.108, No.10, pp.1215-1229.

Dobry, R., Ng, T., Ladd, R.S., and Reese, L.C. (1988), "Modelling of pore pressures and shear moduli in calcareous soils by strain-controlled cyclic triaxial testing", Proc. Int. Conf. on Calcareous Sediments, Perth, vol.2, pp.531-539.

Duncan, J.M. and Chang, C.Y. (1970), "Nonlinear analysis of stress and strain in soils", Jnl. of Soil Mechs. and Found. Engrg., ASCE, vol.96, No.5, pp.1629-1653.

Dunnavant, T.W., Clukey, E.C. and Murff, J.D. (1990), "Effects of cyclic loading and pile flexibility on axial pile capacities in clay", Proc. 22nd. Offshore Tech. Conf., OTC No.6378, vol.3, pp.289-298.

Dutt, R.N. and Cheng, A.P. (1984), "Frictional response of piles in calcareous deposits", Proc. 16th. Offshore Tech. Conf., OTC No. 4838, vol.4, pp.527-534.

Dutt, R.N. and Ingram, W.B. (1990), "Discussion to Classification of marine sediments, Noorany, I.", Jnl. of Geot. Engrg. Div., ASCE, vol.116, No.8, pp.1288-1289.

Dutt, R.N. and Ingram, W.B. (1991), "Significance of in-situ and laboratory tests for design of foundations in granular carbonate soils", Proc. 23rd. Offshore Tech. Conf., OTC No. 6515, vol.1, pp.155-163.

Dutt, R.N., Moore, J.E., Mudd, R.W. and Rees, T.E. (1985), "Behaviour of piles in granular carbonate sediments from offshore Philippines", Proc. 17th. Offshore Tech. Conf., OTC No. 4849, vol.1, pp.73-82.

Dutt, R.N., Doyle, E.H., Nandlal, S. and Ingram, W.B. (1986), "Frictional characteristics of calcareous sands from offshore Florida", Proc. 18th. Offshore Tech. Conf., OTC No. 5149, vol.1, pp.589-600.

Ebelhar, R.J., Young, A.G. and Stieben, G.P. (1988), "Cone penetrometer and conductor pullout tests in carbonate soils offshore Africa", Proc. Int. Conf. on Calcareous Sediments, Perth, vol.1, pp.155-163.

El-Sharnouby, B. and Novak, M. (1985), "Static and low frequency response of pile groups", Can. Geot. Jnl., vol.22, No.1, pp.79-94.

Evans, K.M. (1987), *A model study of the end-bearing capacity of piles in layered calcareous soils,* PhD Thesis, Univ. of Oxford.

Felio, G.Y. and Briaud, J.L. (1986), "Cyclic t-z curves for clay based on simple shear tests", Proc. 3rd. Int. Conf. on Num. mtds. in Offshore Piling, Nantes, pp.149-164.

Finn, W.D.L., Lee, K.W. and Martin, G.R. (1977), "An effective stress model for liquefaction", Jnl. of Geot. Engrg. Div., ASCE, vol.103, No.6, pp.517-533.

Fookes, P.G. and Higginbottom, I.E. (1975), "The classification and description of near-shore carbonate sediments for engineering purposes", Geotechnique, vol.25, No.2, pp.406-411.

Frydman, S., Hendron, D., Horn, H., Steinbach, J., Baker, R. and Shaal, B. (1980), "Liquefaction study of cemented sand", Jnl. of Geot. Engrg. Div., ASCE, vol.106, No.3, pp.275-297.

Ghaboussi, J. and Momen, H. (1982), "Modelling and analysis of cyclic behaviour of sands", Soil Mechanics - Transient and Cyclic Loads, Eds. Pande, G.N. and Zienkiewicz, O.C., pp.313-342.

Golightly, C.R. and Hyde, A.F.L. (1988), "Some fundamental properties of carbonate sands", Proc. Int. Conf. on Calcareous Sediments, Perth, vol.1, pp.69-78.

Golightly, C.R. and Nauroy, J.F. (1990), "End-bearing capacity of piles in calcareous sands", Proc. 22nd. Offshore Tech. Conf., OTC No.6239, vol.1, pp.345-356.

Goulois, A.M. (1982), *Contribution to the study of tension piles*, PhD Thesis, Massachusetts Inst. of Tech., USA.

Grosch, J.J. and Reese, L.C. (1980), "Field tests of small-scale pile segments in a soft clay deposit under repeated axial loading", Proc. 12th. Offshore Tech. Conf., No.3869, vol.4, pp.143-151.

Gudehus, G. and Hettler, A. (1981), "Cyclic and monotonous model tests in sand", Proc. 10th. ICSMFE, Stockholm, vol.3, pp.211-214.

Guo, D.J., Tham, L.G. and Cheung, Y.K. (1987), "Infinite layer for the analysis of a single pile", Computers and Geotechnics, vol.3, No.4, pp.229-249.

Hagenaar, J. (1982), "The use and interpretation of SPT results for the determination of axial bearing capacities of piles driven into carbonate soils and coral", Proc. 2nd. European Symp. on Penetration Testing, Amsterdam, pp.51-55.

Hansen, S.B., Solheim, K. and Norum, P. (1990), "Instrumentation of driven model test piles for determination of capacity of cyclically loaded offshore piles", Proc. Int. Conf. on Geot. Instrumentation in Practice, Nottingham, pp.749-768.

Hermann, L.R. (1978), "Finite element analysis of contact problems", Jnl. of Engrg. Mechs. Div., ASCE, vol.104, No.5, pp.1043-1057.

Hermann, H.G. and Houston, W.N. (1976), "Response of seafloor soils to combined static and cyclic loading", Proc. 8th. Offshore Tech. Conf., OTC No. 2428, vol.1, pp.53-60.

Hewitt, C.M. (1988), *Cyclic response of offshore pile groups*, PhD Thesis, The University of Sydney, Australia.

Hewitt, C.M. and Poulos, H.G. (1988), "Cyclic axial response of model pile groups in clay", Proc. 5th. ANZ Conf. on Geomechs., Sydney, pp.521-525.

Holloway, D.M., Clough, G.W. and Vesic, A.S. (1978), "The effects of residual driving stresses on pile performance under axial loads", Proc. 10th. Offshore Tech. Conf., No. 3306, pp.2225-2236.

Holmquist, D.V. and Matlock, H. (1976), "Resistance-displacement relationships for axially-loaded piles in soft clay", Proc. 8th. Offshore Tech. Conf., OTC No. 2474, vol.1, pp.553-569.

Houlsby, G.T., Evans, K.M. and Sweeney, M.A. (1988), "End-bearing capacity of model piles in layered carbonate soils", Proc. Int. Conf. on Calcareous Sediments, Perth, vol.1, pp.209-214.

Hull, T.S., Poulos, H.G. and Alehossein, H. (1988), "The static behaviour of various calcareous sediments", Proc. Int. Conf. on Calcareous Sediments, Perth, vol.1, pp.87-96.

Hunter, A.H. and Davisson, M.T. (1969), "Measurements of pile load transfer", ASTM Spec. Tech. Pub. STP 444, pp.106-117.

Huntsman, S.R., Mitchell, J.K., Klejbuk, Jr., L.W. and Shinde, S.B. (1986), "Lateral stress measurement during cone penetration", Proc. Use of In-situ Tests in Geot. Engrg., Blacksburg, pp.617-634.

Hyden, A.M., Hulett, J.M., Murff, J.D. and Abbs, A.F. (1988), "Design practice for grouted piles in Bass Strait calcareous soils", Proc. Int. Conf. on Calcareous Sediments, Perth, vol.1, pp.297-304.

Idriss, I.M., Dobry, R., Doyle, E.H. and Singh, R.D. (1976), "Behaviour of soft clays under earthquake loading conditions", Proc. 8th. Offshore Tech. Conf., OTC No. 2671, vol.3, pp.605-616.

Idriss, I.M., Dobry, R. and Singh, R.D. (1978), "Nonlinear behaviour of soft clays during cyclic loading", Jnl. of Geot. Engrg. Div., ASCE, vol.104, No.12, pp.1427-1447.

Ishihara, K., Yoshida, N. and Tsujino, S. (1985), "Modelling of stress-strain relations for soils in cyclic loading", Proc. 5th. Int. Conf. on Num. mtds. in Geomechs., Nagoya, vol.1, pp.373-380.

Ismael, N.F. (1989), "Skin friction of driven piles in calcareous sands", Jnl. of Geot. Engrg. Div., ASCE, vol.115, No.1, pp.135-139.

Ismael, N.F. and Al-Sanad, H.A. (1986), "Uplift capacity of bored piles in calcareous soils", Jnl. of Geot. Engrg. Div., ASCE, vol.112, No.10, pp.928-940.

ISSMFE Subcommittee on Field and Laboratory Testing (1985), "Axial pile loading test - Part 1: Static loading", Geotechnical Testing Jnl. (ASTM), vol.8, No.2, pp.79-90.

Jardine, R.J., Potts, D.M., Fourie, A.B. and Burland, J.B. (1986), "Studies of the influence of non - linear stress - strain characteristics in soil-structure interaction", Geotechnique, vol.36, No.3, pp.377-396.

Jennings, P.C. (1965), "Earthquake response of a yielding structure", Jnl. of Engrg. Mech. Div., ASCE, vol.91, No.4, pp.41-68.

Johnston, I.W. (1983), "A pressure cell for shear and normal stress measurement in piles", Proc. Int. Symp. on Field Measurements in Geomechs., Zurich, vol.1, pp.483-492.

Johnston, I.W., Carter, J.P., Novello, E.A. and Ooi, L.H. (1988), "Constant normal stiffness direct shear testing of calcarenite", Proc. Int. Conf. on Calcareous Sediments, Perth, vol.2, pp.541-553.

Kaggwa, W.S., Booker, J.R. and Carter, J.P. (1990), "Residual strains in calcareous sand due to irregular cyclic loading", Res. Report No.R613, Sch. of Civil and Mining Engrg., Univ. of Sydney.

Kaggwa, W.S., Poulos, H.G. and Carter, J.P. (1988), "Response of carbonate sediments under cyclic triaxial test conditions", Proc. Int. Conf. on Calcareous Sediments, Perth, vol.1, pp.97-107.

Karlsrud, K. and Haugen, T. (1985), "Behaviour of piles in clay under cyclic axial loading - results of field model tests", Proc. 4th. Int. Conf. on Beh. of Offshore Struct. (BOSS), Delft, pp.589-600.

Karlsrud, K., Nadim, F. and Haugen, T. (1986), "Piles in clay under cyclic axial loading; field tests and computational modelling", Proc. 3rd. Int. Conf. on Num. mtds. in Offshore Piling, Nantes, pp.165-190.

Khorshid, M.S., Haggerty, B.C. and Male, R. (1988), "Development of geotechnical aspects of the investigation programme (North Rankin 'A' platform)", Proc. Int. Conf. on Calcareous Sediments, Perth, vol.2, pp.377-385.

King, R.W., Van Haydonk, W.R., Kolk, H.F. and Windle, D. (1980), "Geotechnical investigations of calcareous soils on the North-West Shelf, Australia", Proc. 12th. Offshore Tech. Conf., OTC No. 3772, vol.2, pp.303-313.

Kiousis, P.D. and Elansary, A.S. (1987), "Load-settlement relation for axially loaded piles", Jnl. of Geot. Engrg. Div., ASCE, vol.113, No.6, pp.655-661.

Komaromy, S.W.M., Bromley, V., Mitchell, J.S. and Prifti, P.W. (1987), "A simplified way of modelling non-linear behaviour of pile groups supporting offshore structures", Proc. 19th. Offshore Tech. Conf., OTC No. 5394, vol.1, pp.315-327.

Kondner, R.L. (1963), "Hyperbolic stress-strain response: cohesive soils", Jnl. of Soil Mechs. and Found. Engrg. Div., ASCE, vol.89, No.1, pp.115-143.

Kondner, R.L. and Zelasko, J.S. (1963), "A hyperbolic stress-strain formulation for sands", Proc. 2nd. Pan-American Conf. on Soil Mechs. and Found. Engrg., Brazil, vol.1, pp.289-324.

Kraft, L.M., Jr., (1991a), "Computing axial pile capacity in sands for offshore conditions", Marine Geotechnology, vol.9, No.1, pp.61-92.

Kraft, L.M., Jr., (1991b), "Performance of axially loaded pipe piles in sand", Jnl. of Geot. Engrg. Div., ASCE, vol.117, No.2, pp.272-296.

Kraft, L.M., Jr., Ray, R.P. and Kagawa, T. (1981a), "Theoretical t-z curves", Jnl. of Geot. Engrg. Div., ASCE, vol.107, No.11, pp.1543-1561.

Kraft, L.M., Jr., Cox, W.R. and Verner, E.A. (1981b), "Pile load tests: cyclic loads and varying load rates", Jnl. of Geot. Engrg. Div., ASCE, vol.107, No.1, pp.1-19.

Kraft, L.M., Jr., Focht, J.A., Jr., and Amerasinghe, S.F. (1981c), "Friction capacity of piles driven into clay", Jnl. of Geot Engrg. Div., ASCE, vol.107, No.11, pp.1521-1541.

Krizek, R.J., Farzin, M.H., Wissa, A.E.Z. and Martin, R.T. (1974), "Evaluation of stress cell performance", Jnl. of Geot. Engrg. Div., ASCE, vol.100, No.12, pp.1275-1295.

Kulhawy, F.H. (1989), "Limiting tip and side resistance: fact or fallacy?", Proc. Analysis and Design of Pile Foundations, San Francisco, pp.80-98.

Lade, P.V., Jessberger, H.L., Makowski, E. and Jordan, P. (1981), "Modeling of deep shafts in centrifuge tests", Proc. 10th. Int. Conf. on Soil Mechs. and Found. Engrg., Stockholm, vol.1, pp.683-691.

Lam, T.S.K. and Johnston, I.W. (1982), "A constant normal stiffness direct shear machine", Proc. 7th. South-east Asian Geot. Conf., Hong Kong, pp.805-820.

Lambson, M.D. and Craig, W.H. (1988), "Behaviour of piles under axial cyclic loading", Proc. 20th. Offshore Tech. Conf., OTC No. 5760, vol.3, pp.129-138.

Lee, C.Y. (1988), *The behaviour of grouted piles in offshore foundations*, PhD Thesis, The University of Sydney, Australia.

Lee, K.L. and Farhoomand, I. (1967), "Compressibility and crushing of granular soil in anisotropic triaxial compression", Canadian Geot. Jnl., vol.4, No.1, pp.68-100.

Lee, C.Y. and Poulos, H.G. (1987), "Jacked model pile shafts in offshore calcareous soils", Marine Geotechnology, vol.7, pp.247-274.

Lee, C.Y. and Poulos, H.G. (1988a), "Effective stress dependence of pile shaft capacity in calcareous sand", Jnl. of Geot. Engrg. Div., ASCE, vol.114, No.10, pp.1189-1193.

Lee, C.Y. and Poulos, H.G. (1988b), "Influence of excess pore pressures on axial offshore pile response", Geot. Engrg., vol.19, No.1, pp.73-93.

Lee, C.Y. and Poulos, H.G. (1990), "Axial response analysis of piles in vertically and horizontally non-homogeneous soils", Computers and Geotechnics, vol.9, No.3, pp.133-148.

Lee, C.Y. and Poulos, H.G. (1991), "Tests on model instrumented grouted piles in offshore calcareous soil", Jnl. of Geot. Engrg. Div., ASCE, vol.117, No.11, pp.1738-1753.

Lee, C.Y. and Poulos, H.G. (1992), "Cyclic analysis of axially loaded piles in calcareous soil", under review

Lee, C.Y. and Small, J.C. (1991), "Finite layer analysis of axially loaded piles", Jnl. of Geot. Engrg. Div., ASCE, vol.117, No.11, pp.1706-1722.

Lee, C.Y., Allman, M.A. and Poulos, H.G. (1989), "Static behaviour of piles in cemented calcareous sands", Proc. Found. Engrg.: current principles and practices, Illinois, Ed. Kulhawy, F.H., vol.1, pp.485-499.

Lee, S.L., Kog, Y.C. and Karunaratne, G.P. (1987), "Axially loaded piles in layered soils", Jnl. of Geot. Engrg. Div., ASCE, vol.113, No.4, pp.366-381.

Leonards, G.A. and Darrag, A.A. (1989), "Discussion to Analysis of residual stress effects in piles, Poulos, H.G.", Jnl. of Geot. Engrg. Div., ASCE, vol.115, No.4, pp.589-596.

Lu, B.T.D. (1986), "Axial behaviour and capacity of driven piles in calcareous sands", Proc. 18th. Offshore Tech. Conf., OTC No. 5148, vol.1, pp.579-588.

Lu, B.T.D. (1988), "Effects of grain crushing on axial behaviour of driven piles in calcareous sand", Proc. Int. Conf. on Calcareous Sediments, Perth, vol.1, pp.231-238.

Maddocks, D.V. (1983), "A transducer to measure the radial effective soil stress and the pore-water pressure acting on the surface of a driven, steel pile", Cambridge Univ. Engrg. Dept., Rep. No. CUED/D-SOILS/TR131.

Masing, G. (1926), "Eigenspannungen und Verfestigung beim Messing", Proc. 2nd. Int. Congress of Applied Mechanics, pp.332-335.

Matlock, H. and Foo, S.H.C. (1980), "Axial analysis of piles using a hysteretic and degrading soil model", Proc. Num mtds. in Offshore Piling, ICE, London, pp.127-133.

Matlock, H., Bogard, D. and Cheang, L.C. (1982), "A laboratory study of axially loaded piles and pile groups including pore-pressure measurements", Proc. 3rd. Int. Conf. on Beh. of Offshore Struct., MIT, vol.1, pp.105-121.

Mattes, N.S. (1969), "The influence of radial displacement compatibility on pile settlements", Geotechnique, vol.19, No.1, pp.157-159.

Matthews, M.C. (1988), "The engineering application of direct and simple shear testing", Ground Engrg., Vol.21, No.2, pp.13,15-16,18-19,21.

McAnoy, R.P.L., Cashman, A.C. and Purvis, D. (1982), "Cyclic tensile testing of a pile in glacial till", Proc. 2nd. Int. Conf. on Num. mtds. in Offshore Piling, Austin, pp.257-291.

McCarel, S.C. and Beard, R.M. (1984), "Laboratory investigation on piles in calcareous sediments", Tech. Note TN No.N-1714, Naval Civil Engrg. Lab., Port Hueneme, California.

McClelland, B. (1974), "Design of deep penetration piles for ocean structures", 9th. Terzaghi Lecture, Jnl. of Geot. Engrg. Div., ASCE, vol.100, No.7, pp.709-747.

McClelland, B. (1988), "Calcareous sediments: an engineering enigma", Proc. Int. Conf. on Calcareous Sediments, Perth, vol.2, pp.777-784.

McClelland, B., Focht, J.A. and Emrich, W.J. (1969), "Problems in design and installation of offshore piles", Jnl. of Soil Mech. and Found. Engrg. Div., ASCE, vol.95, No.6, pp.1491-1514.

Meyer, P.L., Holmquist, D.V. and Matlock, H. (1975), "Computer predictions for axially loaded piles with nonlinear supports", Proc. 7th. Offshore Tech. Conf., OTC No. 2186, vol.1, pp.375-387.

Meyerhof, G.G. (1983), "Scale effects of ultimate pile capacity", Jnl. of Geot. Engrg. Div., ASCE, vol.109, No.6, pp.797-806.

Mindlin, R.D. (1936), "Force at a point in the interior of a semi-infinite solid", Physics, vol.7, pp.195-202.

Miner, A.M. (1945), "Cumulative damage in fatique", Trans. of ASME, vol.67, pp.1159-1164.

Mohan, D., Jain, G.S. and Jain, M.P. (1967), "A new approach to load tests", Geotechnique, vol.17, pp.274-283.

Murff, J.D. (1980), "Pile capacity in a softening soil", Int. Jnl. for Num. and Analytical mtds. in Geomechs., vol.4, No.2, pp.185-189.

Murff, J.D. (1987), "Pile capacity in calcareous sands", Jnl. of Geot. Engrg. Div., ASCE, vol.113, No.5, pp.490-507.

Nadim, F., Gabr, M. and Hansen, B. (1989), "Sensitivity study of the cyclic axial capacity of a single pile", Proc. Found. Engrg.: current principles and practices, Illinois, Ed. Kulhawy, F.H., vol.2, pp.1473-1485.

Nauroy, J.F. and LeTirant, P. (1983), "Model tests of piles in calcareous sands", Proc. Conf. on Geot. Practice in Offshore Engrg., Austin, pp.356-369.

Nauroy, J.F. and LeTirant, P. (1985), "Driven piles and drilled and grouted piles in calcareous sands", Proc. 17th. Offshore Tech. Conf., OTC No. 4850, vol.1, pp.83-91.

Nauroy, J.F., Brucy, F. and LeTirant, P. (1985), "Static and cyclic load tests on a drilled and grouted pile in calcareous sand", Proc. Behaviour of Offshore Structures (BOSS), Amsterdam, pp.577-587.

Nauroy, J.F., Brucy, F. and LeTirant, P. (1988), "Skin friction of piles in calcareous sands", Proc. Int. Conf. on Calcareous Sediments, Perth, vol.1, pp.239-244.

Nauroy, J.F., Brucy, F., LeTirant, P. and Kervadec, J.P. (1986), "Design and installation of piles in calcareous formations", Proc. 3rd. Int. Conf. on Num. mtds. in Offshore Piling, Nantes, pp.461-480.

Newmark, N.M. and Rosenblueth, E. (1971), 'Fundamentals of earthquake engineering', Prentice-Hall, Inc., Eaglewood Cliffs, N.J.

Noorany, I. (1985), "Skin friction of piles in calcareous sands", Proc. 11th. ICSMFE, San Francisco, vol.3, pp.1611-1614.

Noorany, I. (1989), "Classification of marine sediments", Jnl. of Geot. Engrg. Div., ASCE, vol.115, No.1, pp.23-37.

Noorany, I. and Gizienski, S.F. (1970), "Engineering properties of submarine soils: state of the art review", Jnl. of Soil Mech. and Found. Engrg. Div., ASCE, vol.96, No.5, pp.1735-1762.

O'Neill, M.W. (1983), "Group action in offshore piles", Proc. Spec. Conf. on Geot. Practice in Offshore Engrg., Austin, pp.25-64.

O'Neill, M.W. and Raines, R.D. (1991), "Load transfer for pipe piles in highly pressured dense sand", Jnl. of Geot. Engrg. Div., ASCE, vol.117, No.8, pp.1208-1226.

O'Neill, M.W., Ghazzaly, O.I. and Ha, H.B. (1977), "Analysis of three-dimensional pile groups with non-linear soil response and pile-soil-pile interaction", Proc. 9th. Offshore Tech. Conf., OTC No. 2838, vol.1, pp.245-256.

O'Neill, M.W., Hawkins, R.A. and Audibert, J.M.E. (1982a), "Installation of pile group in overconsolidated clay", Jnl. of Geot. Engrg. Div., ASCE, vol.108, No.12, pp.1605-1623.

O'Neill, M.W., Hawkins, R.A. and Mahar, L.J. (1982b), "Load transfer mechanisms in piles and pile groups", Jnl. of Geot. Engrg. Div., ASCE, vol.108, No.12, pp.1605-1623.

Ooi, L.H. and Carter, J.P. (1987), "A constant normal stiffness direct shear device for static and cyclic loading", Geot. Testing Jnl., ASTM, vol.10, pp.3-12.

Ooi, L.H., Boey, C.F. and Carter, J.P. (1989), "Modified load transfer analysis of axially loaded piles", Proc. PILETALK Conf., Kuala Lumpur, pp.217-233.

Ooi, L.H., Carter, J.P. and Boey, C.F. (1988), "Modelling the cyclic loading behaviour of calcarenite interfaces", Proc. Int. Conf. on Calcareous Sediments, Perth, vol.1, pp.119-127.

Ottaviani, M. (1975), "Three-dimensional finite element analysis of vertically loaded pile groups", Geotechnique, vol.25, No.2, pp.159-174.

Parkin, A.K., Yee, Y.W., Tan, C.P. and Willoughby, D.R. (1990), "Driven model piles tested in calcareous sand in a large calibration chamber", Proc. 22nd. Offshore Tech. Conf., OTC No.6242, vol.1, pp.389-397.

Ponniah, D.A. (1989), "Instrumentation of a jacked in pile", Proc. Conf. on Geotechnical Instrumentation in Practice, ICE, pp.357-370.

Poulos, H.G. (1968), "Analysis of the settlement of pile groups", Geotechnique, vol.18, No.4, pp.449-471.

Poulos, H.G. (1972), "Load-settlement prediction for piles and piers", Jnl. of Soil Mechs. and Found. Engrg. Div., ASCE, vol.98, No.9, pp.879-897.

Poulos, H.G. (1974), "Theoretical analysis of pile behaviour", *Soil Mechanics - New Horizons,* Ed. by Lee, I.K., (Butterworths, U.K.).

Poulos, H.G. (1979a), "Development of an analysis for cyclic axial loading of piles", Proc. 3rd. Int. Conf. on Num. mtds. in Geomechs., Aachen, pp.1513-1530.

Poulos, H.G. (1979b), "Settlement of single piles in non-homogeneous soil", Jnl. of Geot. Engrg. Div., ASCE, vol.105, No.5, pp.627-641.

Poulos, H.G. (1980), "A review of the behaviour and engineering properties of carbonate soils", Res. rep. No. R381, School of Civil and Mining Engrg., Univ. of Sydney, Australia.

Poulos, H.G. (1981), "Cyclic axial response of single pile", Jnl. of Geot. Engrg. Div., ASCE, vol.107, No.1, pp.41-58.

Poulos, H.G. (1982a), "Influence of cyclic loading on axial pile response", Proc. 2nd. Int. Conf. on Num. mtds. in Offshore Piling, Austin, pp.419-440.

Poulos, H.G. (1982b), "The influence of shaft length on pile load capacity in clays", Geotechnique, vol.32, No.2, pp.145-148.

Poulos, H.G. (1983), "Cyclic axial pile response - Alternative analyses", Proc. ASCE Specialty Conf. on Geot. Practice in Offshore Engrg., Austin, pp.403-421.

Poulos, H.G. (1984), "Cyclic degradation of pile performance in calcareous soils", Proc. Symp. on Analysis and Design of Pile Foundations, pp.99-118.

Poulos, H.G. (1985), "Engineering Properties of Bass Strait Sediments", Proc. Symp. on Recent Sediments in Eastern Australia, pp.77-85.

Poulos, H.G. (1986), "Program AXCYC - Cyclic Axial Response of Piles", Users Guide, School of Civil and Mining Engrg., Univ. of Sydney, Australia.

Poulos, H.G. (1987), "Analysis of residual stress effects in piles", Jnl. of Geot. Engrg. Div., ASCE, vol.113, No.3, pp.216-229.

Poulos, H.G. (1988a), "The mechanics of calcareous sediments", J.C. Jaeger Memorial Lecture, Proc. 5th. ANZ Conf. on Geomechs., Sydney, pp.8-41.

Poulos, H.G. (1988b), "Cyclic stability diagram for axially loaded piles", Jnl. of Geot. Engrg. Div., ASCE, vol.114, No.8, pp.877-895.

Poulos, H.G. (1988c), "Evaluation of long-term load capacity of pile foundations for Goodwyn Platform", Investigation Rep. No. S661, School of Civil and Mining Engrg., Univ. of Sydney, Australia.

Poulos, H.G. (1988d), *Marine Geotechnics*, Unwin Hyman, London.

Poulos, H.G. (1988e), "Evaluation of grouted pile friction from grouted section tests", Proc. Int. Conf. on Calcareous Sediments, Perth, vol.2, pp. 627-637.

Poulos, H.G. (1989a), "Cyclic axial loading analysis of piles in sand", Jnl. of Geot. Engrg. Div., ASCE, vol.115, No.6, pp.836-852.

Poulos, H.G. (1989b), "Pile behaviour - theory and application", 29th. Rankine Lecture, Geotechnique, vol.39, No.3, pp.365-415.

Poulos, H.G. (1989c), "Program SCARP - Static and Cyclic Axial Response of Piles", Users Guide, School of Civil and Mining Engrg., Univ. of Sydney, Australia.

Poulos, H.G. (1989d), Closure to discussion by Leonards and Darrag (1989) on "Analysis of residual stress effects in piles", Jnl. of Geot. Engrg. Div., ASCE, vol.115, No.4, pp.593-596.

Poulos, H.G. and Al-Douri, R.H. (1992), "Influence of soil density on pile skin friction in calcareous sediments", Proc. 6th. ANZ Conf. on Geomechs., Christchurch, New Zealand, pp.375-380.

Poulos, H.G. and Chan, K.F. (1986), "Laboratory study of pile skin friction in calcareous sand", Geot. Engrg., vol.17, No.2, pp.235-257.

Poulos, H.G. and Chan, K.F. (1988), "Tests on model instrumented piles in calcareous soil", Proc. Int. Conf. on Calcareous Sediments, Perth, vol.1, pp.245-253.

Poulos, H.G. and Chua, E.W. (1985), "Bearing capacity of foundations on calcareous sand", Proc. 11th. Int. Conf. on Soil Mechs. and Found. Engrg., San Francisco, vol.3, pp.1619-1622.

Poulos, H.G. and Davis, E.H. (1968), "The settlement behaviour of single axially loaded incompressible piles and piers", Geotechnique, vol.18, No.3, pp.351-371.

Poulos, H.G. and Davis, E.H. (1972), "The development of negative friction with time in end-bearing piles", Aust. Geomechs. Jnl., vol.C2, No.1, pp.11-20.

Poulos, H.G. and Davis, E.H. (1980), *Pile foundation analysis and design*, John Wiley and Sons, New York.

Poulos, H.G. and Lee, C.Y. (1988), "Model tests on grouted piles in calcareous sediments", Proc. Int. Conf. on Calcareous Sediments, Perth, vol.1, pp.255-260.

Poulos, H.G. and Mattes, N.S. (1969), "The behaviour of axially loaded end-bearing piles", Geotechnique, vol.19, No.2, pp.285-300.

Poulos, H.G., Uesugi, M. and Young, G.S. (1982), "Strength and deformation properties of Bass Strait carbonate sands", Geot. Engrg., vol.13, No.2, pp.189-211.

Poulos, H.G., Randolph, M.F. and Semple, R.M. (1988), "Evaluation of pile friction from conductor tests", Proc. Int. Conf. on Calcareous Sediments, Perth, vol.2, pp. 599-605.

Pressley, J.S. and Poulos, H.G. (1986), "Finite element analysis of mechanisms of pile group behaviour", Int. Jnl. for Num. and Analytical mtds. in Geomechs., vol.10, No.2, pp.213-221.

Prevost, J.H. (1977), "Mathematical modelling of monotonic and cyclic undrained clay behaviour", Int. Jnl. for Num. and Analytical mtds. in Geomechs., vol.1, No.2, pp.195-216.

Procter, D.C. and Khaffaf, J.H. (1987), "Cyclic axial displacement tests on model piles in clay", Geotechnique, vol.37, No.4, pp.505-509.

Puech, A. and Jezequel, J.F. (1980), "The effects of long time cyclic loadings on the behaviour of a tension pile", Proc. 12th. Offshore Tech. Conf., OTC No.3870, vol.4, pp.153-162.

Puech, A., Boulon, M. and Meimon, Y. (1982), "Tension piles: field data and numerical modelling", Proc. 2nd. Int. Conf. on Num. mtds. in Offshore Piling, Austin, pp.293-312.

Puyuelo, J.G., Sastre, J. and Soriano, A. (1983), "Driven piles in a granular calcareous deposit", Proc. Int. Conf. on Geot. Practice in Offshore Engrg., Austin, pp.440-456.

Pyke, R. (1979), "Nonlinear soil models for irregular cyclic loadings", Jnl. of Geot. Engrg. Div., ASCE, vol.105, No.6, pp.715-727.

Randolph, M.F. (1977), *A theoretical study of the performance of piles,* PhD Thesis, Cambridge University.

Randolph, M.F. (1983a), "Design considerations for offshore piles", Proc. Int. Conf. on Geot. Practice in Offshore Engrg., Austin, pp.422-439.

Randolph, M.F. (1983b), "Settlement considerations in the design of axially loaded piles", Ground Engrg., vol.16, No.4, pp.28-32.

Randolph, M.F. (1986), "RATZ - Load transfer analysis of axially loaded piles", Rep. Geo 86033, Dept. of Civil Engrg., Univ. of Western Australia, Australia.

Randolph, M.F. (1988), "The axial capacity of deep foundations in calcareous sands", Proc. Int. Conf. on Calcareous Sediments, Perth, vol.2, pp.837-857.

Randolph, M.F. and Jewell, R.J. (1989), "Load transfer model for piles in calcareous soil", Proc. 12th. Int. Conf. on Soil Mechs. and Found. Engrg., Rio de Janeiro, vol.1, pp.479-484.

Randolph, M.F. and Wroth, C.P. (1978), "Analysis of the deformation of vertically loaded piles", Jnl. of Geot. Engrg. Div., ASCE, vol.104, No.12, pp.1465-1488.

Randolph, M.F. and Wroth, C.P. (1979a), "A simple approach to pile design and the evaluation of pile tests", ASTM STP 670, pp.484-499.

Randolph, M.F. and Wroth, C.P. (1979b), "An analysis of the vertical deformation of pile groups", Geotechnique, vol.29, No.4, pp.423-439.

Rickman, J.P. and Barthelemy, H.C. (1988), "Offshore construction of grouted driven pile foundations", Proc. Int. Conf. on Calcareous Sediments, Perth, vol.1, pp.313-319.

Rieke, R.D. and Crowser, J.C. (1987), "Interpretation of pile load test considering residual stresses", Jnl. of Geot. Engrg. Div., ASCE, vol.113, No.4, pp.320-334.

Robinsky, E.I. and Morrison, C.F. (1964), "Sand displacement and compaction around model friction piles", Can. Geot. Jnl., vol.1, No.2, pp.81-93.

Rodgers, J. (1957), "Distribution of marine carbonate sediments", Regional Aspects of Carbonate Deposition, Society of Economic and Paleontologists and Mineralogists, Special Publ. No.5, pp.2-14.

Rotter, J.M. (private communication), "Program AXIP - Axisymmetric isoparametric finite element analysis", School of Civil and Mining Engrg., The University of Sydney, Australia.

Rowlands, G.O., Delpak, R. and Wersching, S.N. (1989), "A transducer for measuring normal and shear stresses", Proc. Conf. on Geot. Instrumentation in Practice, ICE, pp.629-648.

Sangrey, D.A. (1977), "Response of offshore piles to cyclic loading", Proc. 9th. Offshore Tech. Conf., OTC No.2944, vol.2, pp.507-512.

Seed, H.B., Idriss, I.M., Makdisi, F. and Banerjee, N. (1975), "Representation of irregular stress time histories by equivalent uniform stress series in liquefaction analyses", Earthquake Engrg. Res. Centre, Univ. of California, Berkeley, C.A., Rep. No. EERC 75-29.

Selig, E.T. (1980), "Soil stress gage calibration", Geot. Testing Jnl., vol.3, No.4, pp.153-158.

Semple, R.M. (1987), "Foundation design for calcareous soils", Civil College Tech. Rep., Inst. of Engrs., Australia, pp.1-5.

Semple, R.M. (1988), "The mechanical properties of carbonate soils", Proc. Int. Conf. on Calcareous Sediments, Perth, vol.2, pp.807-836.

Semple, R.M. and Rigden, W.J. (1986), "Shaft capacity of driven pipe piles in clay", Ground Engrg., vol.19, No.1, pp.11-16,19.

Shinners, C.D., Edwardes, R.J., Lloyd, J.R. and Grill, J.M. (1988), "Structural upgrading of original Bass Strait Platforms", Proc. 20th. Offshore Tech. Conf., OTC No.5701, vol.2, pp.181-191.

Singh, A. and Mitchell, J.K. (1968), "General stress-strain-time function for soils", Jnl. of Soil Mech. and Found. Engrg. Div., ASCE, vol.94, No.1, pp.21-46.

Smith, I.M. (1982), 'Programming the finite element method, with applications to geomechanics', John Wiley and Sons, Chichester.

Smits, F.P. (1982), "Cone penetration tests in dry sand", Proc. 2nd. Europ. Symp. on Penetration Testing, Amsterdam, vol.2, pp.877-881.

Steenfelt, J.S., Randolph, M.F. and Wroth, C.P. (1981), "Instrumented model piles jacked into clay", Proc. 10th. Int. Conf. on Soil Mechs. and Found. Engrg., Stockholm, vol.2, pp.857-864.

Steinbrenner, W. (1934), *Theoretical Soil Mechanics,* John Wiley and Sons, New York.

Swane, I.C. and Poulos, H.G. (1982), "A theoretical study of the cyclic shakedown of laterally loaded piles", Proc. 5th. Int. Conf. on Num. mtds. in Geomechs., Edmonton, vol.2, pp.853-864.

Sweeney, B.P. and Clough, G.W. (1990), "Design of a large calibration chamber", Geot. Testing Jnl., vol.13, No.1, pp.36-44.

Swinianski, J. and Sawicki, A. (1991), "A model of soil-pile interaction owing to cyclic loading", Canadian Geot. Jnl., vol.28, No.1, pp.11-19.

The Earth Technology Corporation (1983), "Conceptual piling systems for use in calcareous sediments", Rep. to Naval Const. Battalion Centre, Port Hueneme, California.

Trochanis, A.M., Bielak, J. and Christiano, P.P. (1987), "Hysteretic dissipation of piles under cyclic axial load", Jnl. of Geot. Engrg.

Div., ASCE, vol.113, No.4, pp.335-350.

Trochanis, A.M., Bielak, J. and Christiano, P.P. (1991), "Three-dimensional nonlinear study of piles", Jnl. of Geot. Engrg. Div., ASCE, vol.117, No.3, pp.429-447.

Trollope, D.H. and Lee, I.K. (1957), "The performance of a laboratory earth pressure cell", Australian Jnl. of Applied Science, vol.8, No.2, pp.84-97.

Trollope, D.H. and Lee, I.K. (1961), "The measurement of soil pressures", Proc. 5th. Int. Conf. on Soil Mechs. and Found. Engrg., Paris, vol.2, pp.493-499.

Turner, J.P. and Kulhawy, F.H. (1987), "Experimental analysis of drilled shaft foundations subjected to repeated axial loads under drained conditions", Report EL-5325, Electric Power Research Inst., Palo Alto, California.

Turner, J.P. and Kulhawy, F.H. (1989), "Load transfer in deep foundations under repeated axial loading", Proc. Found. Engrg.: Current Principles and Practices, Illinois, vol.1, pp.511-525.

U.S. Waterways Experimental Station (1944), "Soil pressure cell investigations", Tech. Memo. No.210, U.S. Waterways Experimental Station, Vicksburg, Miss.

Valliappan, S., Lee, I.K. and Boonlualohr, P. (1974), "Settlement analysis of piles in layered soil", Proc. 7th. Conf. of the Aust. Road Res. Board, vol.7, Part 7, pp.144-153.

Van Eekelen, H.A.M. (1977), "Single-parameter models for progressive weakening of soils by cyclic loading", Geotechnique, vol.27, No.3, pp.357-368.

Van Eekelen, H.A.M. and Potts, D.M. (1978), "The behaviour of Drammen Clay under cyclic loading", Geotechnique, vol.28, No.2, pp.173-196.

Vesic, A.S. (1963), "Bearing capacity of deep foundations in sand", National Academy of Sciences, National Research Council, Highway Research Record, No.39, pp.112-153.

Vesic, A.S. (1970), "Tests on instrumented piles: Ogeechee River site", Jnl. of Soil Mechs. and Found. Engrg., ASCE, vol.96, No.2, pp.561-584.

Vesic, A.S. (1977), "On significance of residual loads for load response of piles", Proc. 9th. Int. Conf. on Soil Mechs. and Found. Engrg., vol.3, Tokyo, pp.374-380.

Vipulanandan, C., Wong, D., Ochoa, M. and O'Neill, M.W. (1989), "Modelling of displacement piles in sand using a pressure chamber", Proc. Foundation Engrg.: Current principles and practice, ASCE, vol.1, Ed. Kulhawy, F.H., pp.526-541.

Weiler, Jr., W.A. and Kulhawy, F.H. (1978), "Behaviour of stress cells in soil", Geot. Engrg. Rep. 78-2, Cornell Univ. Sch. of Civil and Environmental Engrg., Ithaca, N.Y.

Weiler, Jr., W.A. and Kulhawy, F.H. (1982), "Factors affecting stress cell measurements in soil", Jnl. of Geot. Engrg. Div., ASCE, vol.108, No.12, pp.1529-1548.

Whitaker, T. (1970), *The design of piled foundations,* Oxford: Pergamon.

Whitaker, T. and Cooke, R.W. (1961), "A new approach to pile testing", Proc. 5th. Int. Conf. on Soil Mechs. and Found. Engrg., Paris, vol.2, pp.171-176.

Williams, D.J. (1979), *The behaviour of model piles in dense sand under vertical and horizontal loading*, PhD Thesis, Cambridge Univ.

Williams, A.F. and Van der Zwaag, G.L. (1988), "Analysis and evaluation of grouted section tests", Proc. Int. Conf. on Calcareous Sediments, Perth, vol.2, pp. 493-502.

Withers, N.J., Kolk, H.T., Lewis, W.M. and Hyden, A.M. (1986), "Grouted section tests in calcareous soils", Proc. 18th. Offshore Tech. Conf., OTC No. 5328, vol.4, pp.333-339.

Yamashita, K., Tomono, M. and Kakurai, M., (1987), "A method for estimating immediate settlement of piles and pile groups", Soils and Founds., vol.27, No.1, pp.61-76.

Yazdanbod, A., O'Neill, M.W. and Aurora, R.P. (1984), "Phenomenological study of model piles in sand", Geot. testing Jnl., vol.7, No.3, pp.135-144.

Young, G.S. (1983), *Investigation of axial cyclic loading of model piles in calcareous sand*, M.EngSc Thesis, University of Sydney, Australia.

Zienkiewicz, O.C. (1977), *The finite element method*, 4th. Edition, McGraw Hill, London.